

https://dspace.org/

The underground central deposits of the Sterkfontein Caves, South Africa

Stratford, Dominic Justin

2012-05-21
http://hdl.handle.net/10539/11470

Downloaded from a DSpace repository. https://dspace.org/

The underground central deposits of the Sterkfontein Caves, South Africa

By

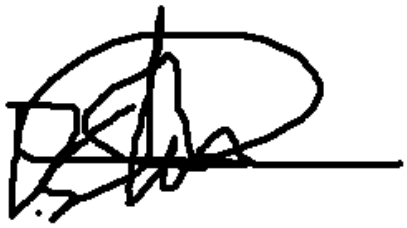
Dominic J Stratford

A thesis submitted to the Faculty of Science, University of the Witwatersrand, Johannesburg, in fulfilment of the requirements for the degree of Doctor of Philosophy.

Johannesburg, 2011

Declaration

I declare that this thesis is my own unaided work. It is being submitted for the degree of Doctor of Philosophy at the University of the Witwatersrand, Johannesburg. It has not been submitted before for any degree or examination in any other university.



_____

(Signature of candidate)

Date: 05.10.11

Abstract

Work on Sterkfontein cave deposits has generally focussed on clarifying the life histories of interned hominin remains. Less attention has been paid to the depositional context of the fossils and the specific stratigraphic processes involved in the formation of deposits, and their interaction within the cave system. Also lacking is an understanding of the complex processes influencing the distribution and integrity of the faunal and artefact assemblages. This research applied a broad-spectrum multidisciplinary approach to investigate a previously unexamined area of the caves with a particularly rich depositional history. The underground central deposits represent several infills of important fossil and artefact-bearing sediments. These sediments have accumulated into one of the deepest central areas of the Sterkfontein cave system creating a confluence area with a complex formation history. Three excavations (STK-MH1, STK-MH2 and STK-EC1) uncovered seven deposits. These deposits document a depositional history ranging from the earliest introduction of allogenic sediments (STK-MH1 T4), to the commercial exploitation of the caves through mining and tourism (STK-MH1 T1, STK-MH2). The stratigraphic sequence for the underground central deposits exhibits multiple formation processes including deposition (through numerous processes), erosion, collapse, diagenetic modification, deformation and displacement. The detailed stratigraphic history of these deposits was elucidated utilising sedimentological, fabric, stratigraphic, taphonomic and taxonomic analyses.

As well as deciphering the complex formation history of this important area, this research attempted to identify the influence of cave sedimentation processes on faunal distribution and assemblage integrity. Faunal assemblages are prone to extensive modification caused by sedimentation and re-sedimentation processes mixing and distributing deposits through the caves. Varying sedimentological properties within fossil-bearing sediment gravity flows can cause the destruction of primary context taphonomic evidence, the concentration of fossils representing

multiple stratigraphically distinct facies, and deposit-wide fossil distributions based on element size and shape. In addition to these processes, it was found that different skeletal elements change shape in different ways through breakage, thereby changing the specific mobility of the fossils and their potential distribution through the sediment body. Not identifying or not accounting for these post-depositional processes can lead to non-representative sampling, and to the misinterpretation of taphonomic and taxonomic data.

Acknowledgements

I wish to thank my supervisors Dr. Kathy Kuman and Professor Ron Clarke for their guidance and generous support throughout this research project and my time at Wits. I would like to thank Laurent Bruxelles for affording me the opportunity to learn so much from him. I'd also like to thank the Soils Laboratory in the Department of Geology at the University of Kwazulu-Natal and Professor Wilson at the University of the Witwatersrand School of Earth Sciences for the XRF data. My thanks also go to Dr. Travis Pickering for help with the taphonomic analysis. Many thanks go to the Sterkfontein technicians, without whose help, all the material would still be in the caves. They were always patient and generous with their help. Inexpressible gratitude goes to my parents, without their unwavering support and encouragement throughout my entire life, I may never have found or realised my passion for dirt and science. To Juliet, your presence, understanding and help mean the world to me, I could never ask for a more wonderful steadying hand. This project was sponsored by the University of the Witwatersrand through the Postgraduate Merit Award bursary, Palaeoanthropology Scientific Trust (PAST) and National Research Foundation (NRF) Grantholders bursary to Dr. Kathleen Kuman. Thanks for their financial support.

Contents

Declaration i

Abstract ii

Acknowledgements iv

List of Figures xi

List of Tables xix

List of Abbreviations xxii

Chapter 1 Introduction 1

1.1 Hypotheses 11

Chapter 2 Background 13

2.1 Sterkfontein Location and History 13

2.1.1 Sterkfontein palaeontological finds 15

2.1.2 Sterkfontein archaeology 18

2.2 Sterkfontein Geological Context 21

2.3 Current Stratigraphic Interpretations 28

2.4 Review of the Relevant Deposits 35

2.4.1 Member 4 deposit 36

2.4.2 Member 5 deposit 39

2.4.3 Silberberg Grotto M2 deposit 41

2.4.4 Name Chamber deposits 47

2.4.5 Lincoln Cave 50

2.5 Stratigraphic Complications Relating to Cave Deposits 51

2.5.1 Formation complications 54

2.5.2 Interpretative complications 63

2.6 Detailed Patterns of Formation Processes and Sediment Dynamics 65

2.6.1 Sediment gravity flow dynamics 66

2.7 Summary 70

Chapter 3 Methodology 72

3.1 Excavation Methods 74

3.2 Stratigraphic Representation 80

3.3 Sedimentological Analysis 82

3.4 Fabric Analysis 86

3.4.1 Basic particle measurements 87

3.4.2 Particle shape models 90

3.4.3 Skeletal elements and particle shape models 92

3.5 Faunal Analysis 98

3.5.1 Measurements taken from identifiable or *in situ* skeletal elements 99

3.5.2 Bone breakage attributes 102

3.5.3 Bone attributes taken from T1 deposit unidentifiable component & *ex situ* skeletal elements 104

3.6 Taxonomy 104

3.7 Taphonomy 105

3.7.1 Bone surface modification attributes 107

Chapter 4 RESULTS: FAUNAL PARTICLE SHAPE 108

4.1 Skeletal Element Type vs. Shape 109

4.2 Skeletal Element Type vs. Sphericity 110

4.3 Skeletal Element Elongation vs. Sphericity 112

4.4 Sphericity & Elongation Ratio vs. Number of Breaks 113

4.5 Faunal Particle Shape Discussion 118

Chapter 5 RESULTS: STK-MH1 119

5.1 T1 121

5.1.1 T1 stratigraphy 121

5.1.2 T1 fabric analysis 126

5.1.3 T1 faunal and artefact assemblage profile 130

5.1.4 T1 archaeology 131

5.1.5 T1 faunal analysis 135

5.1.6 T1 taxonomy 145

5.1.7 T1 taphonomy 146

5.1.8 T1 discussions 148

5.2 T2 150

5.2.1 T2 stratigraphy 151

5.2.2 T2 sedimentology 156

5.2.3 T2 fabric analysis 162

5.2.4 T2 particle shape 165

5.2.5 T2 faunal and artefact assemblage profile 169

5.2.6 T2 archaeology 171

5.2.7 T2 faunal analysis 174

5.2.8 T2 taxonomy 180

5.2.9 T2 taphonomy 181

5.2.10 T2 discussions 182

5.3 T3 183

5.3.1 T3 stratigraphy 184

5.3.2 T3 sedimentology 194

5.3.3 T3 fabric analysis 204

5.3.4 T3 particle shape 209

5.3.5 T3 faunal assemblage profile 212

5.3.6 T3 faunal analysis 215

5.3.7 T3 taxonomy 223

5.3.8 T3 taphonomy 224

5.3.9 T3 discussions 225

5.4 T4 229

5.4.1 T4 stratigraphy 230

5.4.2 T4 sedimentology 234

5.4.3 T4 discussions 239

5.5 STK-MH1 Comparisons 241

5.5.1 Sedimentology 244

5.5.2 Fabric analysis 248

5.5.3 Particle shape 250

5.5.4 Assemblage profile 254

5.5.5 Faunal analysis 256

5.5.6 Taxonomy and taphonomy 261

5.6 STK-MH1 Conclusions 262

Chapter 6 RESULTS: STK-EC1 265

6.1 Secondary Talus (S.T.) 271

6.1.1 Secondary Talus stratigraphy 272

6.1.2 Secondary Talus sedimentology 279

6.1.3 Secondary Talus fabric analysis 284

6.1.4 Secondary Talus particle shape 287

6.1.5 Secondary Talus faunal and artefact assemblage profile 290

6.1.6 Secondary Talus archaeology 292

6.1.7 Secondary Talus faunal analysis 294

6.1.8 Secondary Talus taxonomy 302

6.1.9 Secondary Talus taphonomy 303

6.1.10 Secondary Talus discussions 305

6.2 Primary Talus (P.T.) 306

6.2.1 Primary Talus stratigraphy 308

6.2.2 Primary Talus sedimentology 315

6.2.3 Primary Talus discussions 320

6.3 STK-EC1 Conclusions 322

Chapter 7 RESULTS: STK-MH2 324

7.1 STK-MH2 Stratigraphy 327

7.2 The Primary Infill Stratigraphy 330

7.2.1 Primary infill sedimentology 337

7.2.2 Primary infill particle shape 341

7.2.3 Primary infill faunal assemblage profile 346

7.2.4 Primary infill faunal analysis 350

7.2.5 Primary infill taxonomy 359

7.2.6 Primary infill taphonomy 360

7.3 The Secondary Infill Stratigraphy 363

7.4 STK-MH2 Conclusions 366

Chapter 8 SUMMARY AND DISCUSSION 370

8.1 The Eastern Milner Hall 370

8.2 STK-MH2 376

8.3 Final Discussion 377

References 381

Appendix 1 413

Appendix 2 426

List of Figures

Figure 1 Schematic plan of the Sterkfontein central underground area and positions of relevant chambers. 6

Figure 2.1 Gauteng Province showing the location of the Sterkfontein site in relation to Johannesburg. 14

Figure 2.2 Geological map of the Cradle of Humankind world heritage site. 21

Figure 2.3 Clarke's Sterkfontein stratigraphy. 30

Figure 2.4 Core samples from re-examined coring project originally conducted by Partridge and Watt (1991), and Partridge *et al*. (2000). 31

Figure 2.5 Present understanding of the horizontal spatial distribution of Members 4, 5 and StW 53 deposit as exposed in the current surface excavation. 41

Figure 2.6 The M2 hanging remnant. 46

Figure 2.7 Schematic plan of the Sterkfontein central underground area and positions of relevant chambers. 48

Figure 2.8 Common influences on the development of primary and secondary sedimentation cave deposits as discussed in the text. 55

Figure 2.9 A typical talus deposit formed under a vertical opening. 57

Figure 2.10 Schematic diagram illustrating the movement of a fan or tongue-shaped deposit during development through progressive infilling events or sedimentation episodes. 58

Figure 2.11 Classification of slope processes. 67

Figure 2.12 Microstructure of the basal sole of a grain flow deposit in Belesten, France. 69

Figure 3.1 STK-MH1 square plan and 3D schematic of excavation. 78

Figure 3.2 STK-EC1 3D excavation plan. 79

Figure 3.3 MH2b excavation plan. 80

Figure 3.4 The Harris Matrix three recognised stratigraphic relationships. 82

Figure 3.5 Example of the presentation of particle orientation and dip data used in this research. 90

Figure 3.6 Examples of MPS vs. DRI, Sneed & Folk and Zingg shape diagrams used in this research. 92

Figure 3.7 Sphericity vs. MPS for the control sample of complete skeletal elements. 95

Figure 3.8 Sneed & Folk diagrams for the complete skeletal elements from the comparative control collection. 98

Figure 3.9 Bone division categories used in this research. 100

Figure 3.10 Bone breakage attributes. 103

Figure 4.1 Sneed & Folk diagrams for fifty random skeletal elements from each element type class from the excavated fauna 110

Figure 4.2 Relative distribution of different elements across sphericity classes. 111

Figure 4.3 Element elongation plotted against element sphericity. 113

Figure 4.4 Sphericity plotted against number of breaks within specific skeletal element types. 117

Figure 4.5 Mean elongation ratio plotted against number of breaks within specific skeletal element types. 117

Figure 5.1 Profile of the STK-MH1 talus with the MH1 excavation and the deposits discovered and analysed in the text. 119

Figure 5.2 STK-MH1southern wall stratigraphic profile. 120

Figure 5.3 STK-MH1 eastern wall stratigraphic profile. 120

Figure 5.4 Stratigraphic profile of the southern wall of the T1 deposit. 123

Figure 5.5 Plan view schematic of the STK-MH1 site with plotted dolomitic boulders deposited during the initial blasting phase. 125

Figure 5.6 T1 particle shape indices. 128

Figure 5.7 T1 Voorhies groups. 129

Figure 5.8 T1 skeletal element type distributions. 137

Figure 5.9 T1 numbers of broken edges on fossil material. 140

Figure 5.10 T1 bone fracture types. 143

Figure 5.11 T1 bone fracture angles. 143

Figure 5.12 T1 fossil condition. 145

Figure 5.13 MH1 excavation with T2 surface slope cleared for excavation. 151

Figure 5.14 MH1 Southern wall and main body of the T2 deposit '*Facies I*' in the MH1 sequence. 154

Figure 5.15 T2 fossil concentration C. 155

Figure 5.16 T2 particle size distribution curves for three samples taken at the surface, middle and base of the T2 deposit. 160

Figure 5.17 T2 combined particle size distribution curves. 161

Figure 5.18 T2 fabric analysis models. 165

Figure 5.19 T2 particle shape indices. 167

Figure 5.20 T2 Voorhies groups. 168

Figure 5.21 T2 skeletal element type distribution. 175

Figure 5.22 T2 numbers of broken edges on fossil material. 177

Figure 5.23 T2 bone fracture types. 178

Figure 5.24 T2 bone fracture angles. 179

Figure 5.25 T2 fossil condition. 180

Figure 5.26 T3 deposit with the 1st *Facies III* stratum surface exposed across the deposit. 188

Figure 5.27 T3 deposit morphology. 189

Figure 5.28 STK-MH1 eastern wall profile of T2, T3 and T4. 191

Figure 5.29 Northern wall of STK-MH1. 193

Figure 5.30 Two examples of *in situ* bone breakage found within the T3 sediments. 194

Figure 5.31 T3 particle size distribution curves for three samples taken at the surface, middle and base of the T3 deposit. 202

Figure 5.32 T3 combined particle size distribution curves. 203

Figure 5.33 T3 fabric analysis models. 206

Figure 5.34 T3 orientation data plotted against elongation ratios for the same elements. 207

Figure 5.35 T3 particle shape indices. 211

Figure 5.36 T3 Voorhies groups. 211

Figure 5.37 T3 fossil yield through deposit depth in relation to spit depth and facies distribution. 214

Figure 5.38 T3 skeletal element type distribution. 217

Figure 5.39 T3 numbers of broken edges on fossil material. 220

Figure 5.40 T3 bone fracture types. 221

Figure 5.41 T3 bone fracture angles. 221

Figure 5.42 T3 fossil condition. 222

Figure 5.43 T4 floor at 135cm below datum, 10cm below surface. 232

Figure 5.44 T4 southern wall profile. 233

Figure 5.45 T4 particle size distribution curves for two samples taken at the surface and lowest point reached in the T4 deposit. 238

Figure 5.46 T4 combined particle size distribution curves. 239

Figure 5.47 MH1 major particle size fractions across the T2, T3 and T4 deposits. 245

Figure 5.48 MH1 chemical composition. 247

Figure 5.49 MH1 Fabric analysis models. 249

Figure 5.50 T2 and T3 orientation data. 250

Figure 5.51 MH1 particle shape indices for the deposits yielding clastic and faunal material large enough to analysis. 252

Figure 5.52 Relative proportions of Sneed & Folk shape classes within the three bone-bearing deposits. 253

Figure 5.53 MH1 Voorhies groups. 254

Figure 5.54 Fossil assemblage size profile for all MH1 bone-bearing deposits. 255

Figure 5.55 MH1 skeletal element type representation across the bone-bearing deposits. 257

Figure 5.56 T2 and T3 skeletal portion summary. 258

Figure 5.57 MH1 numbers of broken edges on fossil material. 259

Figure 5.58 T2 and T3 bone fracture types. 260

Figure 5.59 T2 and T3 bone fracture angles. 260

Figure 5.60 Harris Matrix representation of the MH1 stratigraphic sequence. 264

Figure 6.1 STK-EC1 LP talus slope surface prior to excavation, looking eastwards upslope. 266

Figure 6.2 STK-EC1 slope profile. 267

Figure 6.3 Schematic plan view of the Silberberg Grotto sediments exiting the Silberberg Grotto chamber into the EC1 passage, forming two false floor breccia bodies. 268

Figure 6.4 Eastern wall profile of the EC1 excavation. 270

Figure 6.5 S.T. eastern wall excavation profile. 275

Figure 6.6 STK-EC1 Secondary Talus southern wall excavation profile. 276

Figure 6.7 Artefact and fossil scatter plot. 277

Figure 6.8 S.T. particle size distribution curves for two samples taken at upper and base of the matrix supported sediments in the Secondary Talus deposit. 283

Figure 6.9 S.T. combined particle size distribution curves. 284

Figure 6.10 S.T. fabric analysis models. 286

Figure 6.11 S.T. particle shape indices. 288

Figure 6.12 S.T. Voorhies groups. 290

Figure 6.13 S.T. skeletal element type distribution. 295

Figure 6.14 S.T. numbers of broken edges on fossil material. 297

Figure 6.15 S.T. bone fracture types. 298

Figure 6.16 S.T. bone fracture angles. 300

Figure 6.17 S.T. bone condition. 302

Figure 6.18 P.T. exposed surface. 309

Figure 6.19 P.T. eastern wall excavation profile. 311

Figure 6.20 P.T. particle size distribution curves for two samples taken at top of the deposit and base of the excavation. 319

Figure 6.21 P.T. combined particle size distribution curves. 320

Figure 6.22 Harris Matrix representation of the EC1 stratigraphic sequence. 323

Figure 7.1 Schematic plan of the STK-MH2 location and immediate vicinity. 326

Figure 7.2 Primary Infill excavation point MH2a. 330

Figure 7.3 Transverse section of a proximal portion of a talus slope developed under an aven-type opening. 331

Figure 7.4 Schematic diagram of the vertical face of the Primary Infill. 336

Figure 7.5 Primary Infill basic particle size classes for the STK-MH2 site profile. 340

Figure 7.6 Primary Infill particle shape indices from excavation MH2b. 343

Figure 7.7 Primary Infill particle shape indices from excavation MH2a. 344

Figure 7.8 Voorhies groups for the MH2b and MH2a assemblages. 345

Figure 7.9 Assemblage size profiles for both Primary Infill excavation sites. 348

Figure 7.10 Skeletal element type representation for Primary Infill. 351

Figure 7.11 Numbers of broken edges on Primary Infill fossil material. 355

Figure 7.12 Break types for the Primary Infill. 357

Figure 7.13 Break angles for the Primary Infill. 357

Figure 7.14 Bone condition for the Primary Infill. 359

Figure 7.15 STK-MH2 truncated profile showing the western medial facies, the Primary Infill surface and the Secondary Infill boundaries. 365

Figure 8.1 Schematic plan of the Sterkfontein central underground area, positions of relevant chambers, and investigated areas. 372

Figure 8.2 Harris Matrix representation of the eastern Milner Hall stratigraphic sequence. 376

List of Tables

Table 2.1 Sterkfontein Oldowan assemblage including the Name Chamber component. 19

Table 2.2 Sterkfontein Early Acheulean assemblage. 20

Table 2.3 Particle size profiles for Phase I and Phase II sediments as described by Brain (1958). 59

Table 3.1 Correlation tests for particle size variables vs. utilised shape indices. 96

Table 4.1 Mean elongation ratio and sphericity figures plotted against number of breaks within specific skeletal element types. 115

Table 5.1 T1 faunal and artefact assemblage summary and size profile. 131

Table 5.2 T1 archaeological assemblage size profile. 134

Table 5.3 T1 flake attributes. 134

Table 5.4 T1 skeletal portion summary of identifiable component. 138

Table 5.5 T1 skeletal element representation of bovid taxa. 148

Table 5.6 T2 sedimentological summary. 156

Table 5.7 T2 XRF results. 158

Table 5.8 A selection of percentage bulk chemical compositions from limestone and dolomite karst-bearing rocks. 158

Table 5.9 Sterkfontein dolomitic limestone major oxide composition. 159

Table 5.10 T2 relative constituent Gaussian curve volumes. 162

Table 5.11 T2 faunal and artefact assemblage summary and size profile. 170
Table 5.12 T2 artefact summary. 173
Table 5.13 T2 artefact technological attributes. 173
Table 5.14 T2 skeletal portion distribution summary. 175
Table 5.15 T2 skeletal element representation of bovid taxa. 182
Table 5.16 T3 sedimentological summary. 195
Table 5.17 T3 XRF results. 198
Table 5.18 T3 relative constituent Gaussian curve volumes. 203
Table 5.19 T3 faunal and artefact assemblage summary and size profile. 213
Table 5.20 T3 skeletal portion distribution summary. 217
Table 5.21 T3 skeletal element representation of bovid taxa. 225
Table 5.22 T4 Sedimentological summary. 235
Table 5.23 T4 XRF results. 236
Table 5.24 MH1 sedimentological summary. 245
Table 5.25 Fossil assemblage size profile for all MH1 bone-bearing deposits. 255
Table 5.26 MH1 bone-bearing deposit faunal particle size statistics. 256
Table 6.1 EC1 Secondary Talus sedimentological summary. 280
Table 6.2 S.T. XRF results. 281
Table 6.3 S.T. relative constituent Gaussian curve volumes. 284

Table 6.4 S.T. faunal and artefact assemblage summary and size profile. 291

Table 6.5 S.T. skeletal portion distribution summary. 296

Table 6.6 S.T. skeletal element representation of bovid taxa. 305

Table 6.7 EC1 Primary Talus sedimentological summary. 315

Table 6.8 EC1 Primary Talus XRF result. 317

Table 6.9 P.T. relative constituent Gaussian curve volumes. 320

Table 7.1 Primary infill sedimentological summary. 339

Table 7.2 Primary infill faunal assemblage size profiles for both excavation sites. 347

Table 7.3 MH2b skeletal portion distribution summary. 352

Table 7.4 MH2a skeletal portion distribution summary. 352

Table 7.5 Combined skeletal portion distribution summary for the Primary Infill 353

Table 7.6 Primary infill MH2b site skeletal element representation of bovid taxa. 361

Table 7.7 Primary infill MH2a site skeletal element representation of bovid taxa. 363

List of Abbreviations

CSI	Corey Shape Index
DRI	Disk Rod Index
EC1 LP	Elephant Chamber Lower Passage
FWT	Far Western Talus
Ga	Billions of years ago
Indet.	Indeterminate
MPS	Maximum Projected Sphericity
Ma	Millions of years ago
M1- M6	Members 1 to 6
M5E	Member 5 East
M5W	Member 5 West
N.C.	Name Chamber
Pers. Comm.	Personal Communication
Pers. Obs.	Personal Observation
P.T.	Primary Talus
S.T.	Secondary Talus
StdDev	Standard Deviation
STK-EC1	Sterkfontein Elephant Chamber site 1
STK-MH1	Sterkfontein Milner Hall site 1
STK-MH2	Sterkfontein Milner Hall site 2
U-Pb	Uranium-Lead
U-Th	Uranium-Thorium
XRF	X-ray Fluorescence

CHAPTER 1 INTRODUCTION

Sterkfontein, one of the single richest hominin sites in the world, has a considerable amount of information to offer on the lifeways of hominin species. The fossil and artefact-bearing sediments are all found within a karst deposit context. These deposits have formed within a spatially confined dolomitic limestone karst system through a variety of sediment gravity flow processes. The fauna has been accumulated via a number of processes generally related to the morphology of the respective cave opening. Understanding of the formation and movement of fossiliferous deposits within cave systems is of key importance to the interpretation the primary 'surface' contexts and associations of the fossil remains, and the validation of hypotheses regarding human evolution. Understanding deposit formation and the influence of geogenic processes on fossil assemblages can assist in providing a far more accurate explanation of recovered data. Conventionally, the fossil-bearing deposits have been studied by various specialists with specific perspectives and goals. The Sterkfontein cave complex as a repository of bone and artefact-bearing deposits has been researched by a relatively small group of scientists of varying disciplines, including palaeontology, taphonomy, anatomy, palaeoanthropology and archaeology. The goal of the researchers has been to study the fossils, artefacts, and contexts of those specimens recovered from *in situ* and *ex situ* deposits.

Following the recovery of fossil monkeys from Sterkfontein by Trevor Jones in 1935, intense research started at Sterkfontein in 1936 after the discovery of TM1511 the first adult *Australopithecus* type specimen for *Australopithecus transvaalensis* (Broom 1936). The first stratigraphic interpretation of the fossil-bearing breccia body was published by Cooke (1938) two years later. Since then stratigraphic interpretations have been proposed by several researchers (Robinson 1957, 1962; Brain 1958; Wilkinson 1973, 1983, 1985; Partridge 1978; Partridge & Watt 1991; Clarke 1994a, 2006). Most stratigraphic studies have focussed on providing a context for the hominin fossils and associated fauna that have been excavated from the *in situ* breccia. These stratigraphic interpretations have

concentrated on the macro-level formation of deposits. The overall trend of these interpretations has been an increasing appreciation of the complexities of cave stratigraphy and the complex depositional sequences that characterise cave deposits. Studies of the infills themselves from a formation point of view, including assessment of the influence of deposit formation dynamics on fossil assemblages, has been limited. Kuman & Clarke's (2000) stratigraphic interpretation of the Member 5 deposits effectively utilised a facies approach to the artefact-bearing deposit and R. Pickering & Kramers (2010) have recently used facies found in some talus deposits (proximal, medial and distal sediment attributes) to more clearly identify deposit sections exposed on the surface, attempting to link them to Partridge's core samples. R. Pickering & Kramers then used U-Pb and U-Th dating on some of the flowstones that they considered to be associated with the sediments.

The research presented in this thesis examines cave deposit formation and modification, and the influence these processes have on fossil and archaeological material within the underground central deposits of the Sterkfontein caves. Gillieson (1996) points out, with regards to cave-based investigations, "a great deal of research has been carried out on the material deposited with clastic sediments (bones, pollen, archaeology) as a means of elucidating environmental or human histories. Less research has been undertaken on the processes by which clastic sediments are produced, transported and deposited within the cave system." (pp. 143). In cave environments like Sterkfontein, deposits of sediments can be accumulated, calcified, decalcified and redistributed through a number of processes around the cave environment. Farrand (2001) notes that "an understanding of the gamut of possible processes that contributed to the cave sediment is essential for deciphering the sedimentary and environmental history of the site." (pp. 543). These processes, and the associated deposit modification, can be regarded as highly variable both spatially and in terms of degree affected. The constantly changing structure of dolomitic limestone caves causes deposits to develop different morphologies and sedimentological patterns, thereby also affecting the distribution and preservation of faunal material within the deposit. For instance, the shape, position and height of the chamber opening or sediment

source can affect all characteristics of the developing deposit. Most previous research attempting to clarify the stratigraphy of the Sterkfontein deposits has focussed on a single aspect of the deposit or faunal assemblage. Examples of such approaches include a detailed sedimentological analysis (Brain 1958), the taphonomic analysis of a single member (T. Pickering 1999), and the examination of the ungulates (Kibii 2000). The exception to this tendency is Clarke (1994a) and Kuman & Clarke (2000). Both works approach the stratigraphy of the Member 5 area of the surface excavation. The former (Clarke 1994a) utilised faunal and sedimentological information and the latter, Kuman & Clarke (2000) utilised faunal, sedimentological and archaeological information.

This thesis is the first to focus on the formation and movement of a number of cave deposits at Sterkfontein using a multi-disciplinary approach. Identification and description of post-depositional sediment movement within the cave system is invaluable for accurate interpretations of the excavated fossil assemblages and identification of sediment sources. This research will illustrate the merit of the approach used and hopefully encourage similar methods to be used on other deposits and sites. A combination of stratigraphic, sedimentological, fabric, taphonomic and taxonomic analyses has been used in this study to decipher the formation histories of three previously un-sampled talus deposits that have accumulated in a central area of the cave complex called the 'underground central deposits'. The underground central deposits in Sterkfontein have been formed in highly complex depositional sequences that have resulted from the convergence of several deposits of significant age, archaeological and palaeontological importance. This area includes sediments deriving from the subterranean chambers of the Silberberg Grotto, Name Chamber, Milner Hall, and numerous intersecting passages that relate to upper, surface exposed deposits from Members 4 and 5, and the Lincoln Cave. Each parent deposit has distinct taphonomic, faunal or archaeological characteristics which may be identifiable within the deposits investigated. The central subterranean area, in which the central subterranean deposits are contained, is shown in Figure 1 together with the location of the three sites chosen for excavation.

The primary goal of this research is to decipher the formation history of the underground central deposits occupying the eastern Milner Hall and to relate that history to the greater Sterkfontein sequence. The secondary goal of this research is to add clarity to the understanding of deposit accumulation processes, and the influence of those processes on fossil and artefact-bearing sediments. The long term intention of this work is to develop less reliance on the more rigid member-based interpretation of the stratigraphy towards a more fluid model of the Sterkfontein deposits (and their fossils and archaeological assemblages), by establishing excavation methods and analytical approaches that may be applied to all areas of the cave. Until further extensive work is carried out on the intra- and inter-deposit sedimentological description and facies identification, the member system will be used to refer to the major depositional units established by Partridge (1978). This convention is upheld in this thesis.

Thus far, the focus of excavations and research at Sterkfontein has revolved primarily around the recovery and interpretation of hominin fossils. Applications of various disciplines, such as archaeology, botany, tooth wear analysis, locomotion studies and neuro-anatomy, have been employed to build an understanding of the life histories of the hominins found in the deposits. As well as the more classical study of hominin morphology, much work has been done in establishing an ecological framework into which the hominins fit, as well as how the hominins and the associated fauna within the deposits came to be buried (taphonomy). What has been accomplished to a much lesser degree, however, is an understanding of the formation processes of the deposits and the post-depositional influences on bones and teeth. In addition to this, approaches to stratigraphy from an intra- and inter-deposit perspective, and at the micro-level before considering the macro-level, have also been lacking. Accurate taphonomic and taxonomic interpretations are based on assemblages that are representative of a particular deposit, facies or strata. Assemblage completeness, distribution and representation are a direct result of the formation processes at work. It therefore follows that understanding the processes of sediment and fossil movement during and after deposition enables more reliable taphonomic and taxonomic interpretations to be made.

Research within the major disciplines (palaeontology and palaeoanthropology and archaeology) has shed some light on the chronological context of the deposits studied through the building of a biostratigraphic sequence (Broom 1945a; Cooke 1974; Vrba 1975, 1982, 1995; Partridge 1982; Kibii 2004), through the study of the associated archaeological material (Kuman 1994a, b, 1996, 1997,1998, 2003, 2007; Kuman & Clarke 2000), and through the application of various dating methods (Schwarcz *et al.* 1994; Partridge *et al.* 2000, 2003; Berger *et al.* 2002; Clarke 2002; Partridge 2002, 2005; Walker *et al.* 2004; R. Pickering *et al.* 2006; Walker *et al*. 2006; R. Pickering & Kramers 2010; R. Pickering *et al.* 2010)

There has also been a considerable amount of work attempting to clarify the context of the life assemblages, i.e. the environmental condition on the landscape during the development of the primary deposit. This has been assessed though the application of a taphonomic analysis (Brain 1974; T. Pickering 1999; T. Pickering *et al*. 2000, 2004a, b; Kibii 2004) and through the interpretation of palaeoecological information (Vrba 1974, 1985, 1995; McKee 1991; Sillen *et al.* 1998; Bamford 1999; Carrión & Scott 1999; Avery 2001; Luyt 2001; Luyt & Lee-Thorp 2003; Sponheimer *et al*. 2003; van der Merwe *et al*. 2003; Avery *et al.* 2010).

Early geological work on the Sterkfontein cave sediments and deposits was initiated by Basil Cooke (1938), and Robinson (1962), before Partridge dedicated much of his time and passion working as a consultant to the then Palaeoanthropology Research Unit (Brink & Partridge 1965; Partridge 1978, Partridge *et al*. 2000; Partridge & Watt 1991). Wilkinson (Wilkinson 1973, 1983, 1985) and more recently Martini *et al*. (2003) have carried out speleological investigations on the subterranean chambers of the cave system. These studies have endeavoured to increase our understanding of the formation of the caves and identify the relative positions, chronology and the nature of the fossil-bearing sediments.

The excavations for this research were designated STK-EC1 (Sterkfontein Elephant Chamber - The Elephant Chamber represents the south-east area of the Milner Hall), STK-MH1 (Sterkfontein Milner Hall 1) and STK-MH2 (Milner Hall

2). STK-EC1 and STK-MH1 (shown in Figure 1) have both been located to sample the convergence area of the Silberberg Grotto and Name Chamber deposits, which is located in the far eastern Milner Hall. This area is particularly important due to its proximity to the Name Chamber, which contains examples of the earliest archaeological material found at Sterkfontein, and the Silberberg Grotto, which contains the specimen of an almost complete early *Australopithecus* skeleton (StW 573) in sediments classified as Member 2. This area may also have accumulated some of the earliest sediments to have entered the cave system prior to the deposition of the current deposits found in Silberberg (Member 2 and Member 3) and the upper members exposed in the surface excavation (Member 4, Member 5 and Member 6).

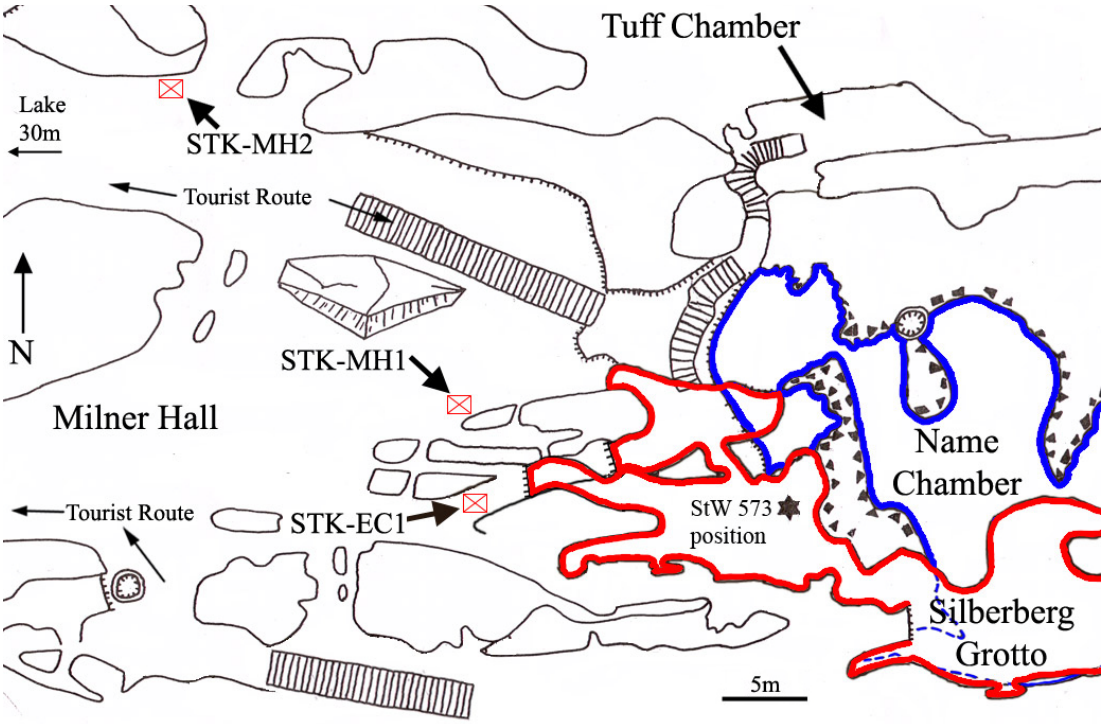


Figure 1 Schematic plan of the Sterkfontein central underground area and positions of relevant chambers. The positions of each excavation site in also indicated. The red line represents the limit of the current Silberberg Grotto deposits. The blue line represents the limit of the current Name Chamber deposits. Adapted from Martini *et al.* (2003).

STK-MH1

STK-MH1 has been placed at the base of a large talus deposit that has formed at the eastern end of the Milner Hall and spreads in a steep fan 25m westwards, radiating away from the contact area of the Name Chamber and Silberberg Grotto. The current tourist route is directed east from the lake (approximately 30m west of STK-MH2 and indicated in Figure 1) up the MH1 talus stairs to the eastern most part of the Milner Hall (the central contact area and focus of this research) before turning north and descending into the Tuff Chamber (route can be seen in Figure 1). The stairs and barriers supporting this part of the tourist route were built on top of the MH1 talus. Heavily calcified sediments exiting the Silberberg Grotto can be seen on the southern wall and ceiling of the eastern Milner Hall above the apex of the MH1 talus. The Name Chamber deposits have been truncated and disturbed by the mining and tourist activities and must have previously extended into the MH1 talus. The mining of a large stalactite from the roof above the top of the MH1 talus, combined with many years of tourist activities have tumultuously redistributed sediments from the Name Chamber and Silberberg Grotto on to the surface sediments of the MH1 talus. The placement of the MH1 excavation was chosen based on the hypothesis that the depositional activity would be preserved with greater integrity a little distance down slope of the main confluence of the central underground deposits. Four deposits were excavated and analysed. Each deposit has a distinct depositional history which fits into the main sequence of the area. The MH1 deposits are named T1 (Talus 1) through to T4 based on order of deposition. Each deposit is examined individually before a comparative analysis is presented.

STK-EC1

Site STK-EC1 has been positioned at the base of a long talus deposit which has formed inside a narrow passage leading from directly underneath the main contact area of the Silberberg Grotto and the Name Chamber. The relatively isolated nature of the passage containing the talus provided potentially greater protection

from damage caused by the lime mining operations carried out in the vicinity of the eastern opening. The sediments contained are not calcified which allowed meticulous excavation methodologies to be utilised, enabling a full spectrum of *in situ* analysis to be carried out. Two deposits were discovered and excavated within the EC1 talus. The upper deposit has been called the Secondary Talus (S.T.) and the lower deposit has been called the Primary Talus (P.T.). Each deposit has been accumulated through a distinct depositional history that is examined individually before a comparative analysis is presented.

STK-MH2

The STK-MH2 excavations have been placed to sample a large, fossil-rich truncated talus which has formed in the north-western area of the Milner Hall just above the lake (see Figure 1). This deposit represents an unknown entity in terms of its contents, age and formation in relation to the other Sterkfontein deposits. The deposit has entered the Milner Hall through an opening almost directly above the current truncated talus vertical face and is a considerable distance from the other deposits filling the Milner Hall. Previous to mining operations and tourist activities, this talus extended across the large E-W running passage (named 'Gallery A' by Wilkinson 1983), as demonstrated by the remnants seen on the wall opposite the remaining deposit. The truncated deposit is represented by a wide, rough profile face, running transverse to the sediment flow, of one to five metres in height and a network of small sediment filled passages behind the northern wall of the Milner Hall. The area exposed constitutes a long transverse profile, including the medial and both lateral portions of the deposit, with one well-preserved lateral termination. Two areas were sampled. MH2a has sampled the well-preserved eastern lateral termination of the talus and is capped by a 10cm thick flowstone. MH2b is a geo-trench style excavation running vertically up the maximum exposed medial profile of the deposit in order to yield a spatially broad sample of fossils and sediments and provide a clean stratigraphic section for as much of the deposit as possible.

This thesis is split into eight chapters. Chapter 2 – Background, is written to equip the reader with the knowledge needed to understand the Sterkfontein site, from its importance as a hominin and artefact-bearing site, to the intricacies and complications of sediment gravity flow dynamics. A brief history of the recognition of the site and the initial phases of work is presented. The palaeoanthropological value of Sterkfontein is well-known and this research, although inextricably linked to the fossil and artefact assemblages of Sterkfontein, is not a strictly a palaeontological or archaeological work. The weighting of Chapter 2 is, therefore, towards the description of the physical processes and complications of cave stratigraphy more than the discussion of the debates around the hominin and archaeological assemblages. However, for background, a brief description of the major palaeontological finds and archaeological assemblages yielded from Sterkfontein is presented. A detailed description of the geological context of the caves and the local area is then given. Establishing a geological setting early is necessary to assist understanding of the more detailed discussions of current stratigraphic interpretations, stratigraphic theory and the complications of cave depositional environments that follow. This is followed by a detailed discussion of the most recent stratigraphic interpretations (Clarke 2006, R. Pickering & Kramers 2010). A detailed description of the research conducted on each of the relevant deposits is then presented to provide the reader with an understanding of the comparative framework used for inter-deposit analysis. The final section of Chapter 2 addresses the physical processes affecting the formation, movement and preservation of cave deposits from the macro scale, describing the various influences over the deposition of entire deposits through to the micro scale, describing the sedimentological characteristics of the different sediment gravity flow types regularly found in caves. The indicators used for the identification of the depositional processes are also described. This final section also discusses the interpretive issues associated with working with assemblages yielded from cave deposits.

Chapter 3 – Methodology, presents the various analytical procedures used in this research. The multidisciplinary approach of the research first requires the terminology to be defined. A number of the terms used in this research have

different nuances in different fields so a basic vocabulary needs to be established before in-depth discussions commence. Each excavation sampled a broad range of sedimentary contexts with varying faunal and artefactual conditions. This unpredictability required the planning and execution of a fluid, adaptable and yet accurate set of excavation methods and techniques. A description of each of the excavations and the various methodologies utilised for each site is then presented. The data collection, analysis and presentation method for each discipline is then presented. When describing each methodology the key works establishing the methods utilised are discussed. The non-faunal analysis includes sedimentological and fabric analysis. Sedimentological data included XRF chemical composition, particle size distribution, hydrology, and sediment colour. These analyses were chosen to allow identification of deposit boundaries and possibly sediment source. Fabric analysis, including all of the relevant particle measurements, dimensional ratios and data presentation and interpretation, is discussed with reference to similar applications and formative works. The faunal analysis is split into two categories, taxonomic faunal analysis for stratigraphic indicators and taphonomic analysis. The methodologies for both are discussed in the penultimate section of Chapter 3.

Chapter 4 presents a set of analyses carried out on the excavated faunal assemblage to assess the more general changes in element shape and elongation through breakage. Deposit specific patterns are discussed in the deposit analyses. Modification of shape is an important factor in the transport of faunal material within assemblages that have been graded based on particle shape and size. Using the conventional Sneed & Folk shape diagram (1958), a selection of complete bones from a control group was compared to the entire excavated faunal assemblage to assess the change in shape through varying levels of breakage caused by deposition. The Krumbein sphericity equation (Krumbein 1941) was also used to examine the relationship between element elongation ratio and sphericity in different skeletal elements through different stages of breakage.

Chapter 5 presents the analysis and results for the STK-MH1 deposit. Chapter 6 presents the analysis and results for STK-EC1 and Chapter 7 presents the analysis

and results for the STK-MH2 deposit. Where comparisons are needed to demonstrate deposit boundaries and relationships they are presented at the end of each analytical chapter. Chapter 8 – Summary and Discussion, brings the individual site interpretations together to produce a stratigraphic sequence for central underground deposits and presents a concluding discussion of the those processes identified as influencing taxonomic and taphonomic interpretations. The final paragraph of the thesis discusses the merit of this approach, pertinent questions raised, future approaches and research directions to bring further clarity to fossil and artefact-bearing cave deposits.

1.1 Hypotheses

MH1

From the pre-excavated deposit position, morphology and literature a tentative hypothesis can be proposed for the MH1 talus and the eastern Milner Hall area. The placement of the MH1 excavation site should provide the greatest potential for preservation of the deposit infilling events occurring at the confluence point above the excavation site. The proximity of the M2 Hanging Remnant, and the proximity to the truncated Name Chamber Far Western Talus makes it probable that previously these deposits accumulated into the sample area and, if preserved, would document the sequence of infilling. The Silberberg Grotto represents a significantly older deposit than the Name Chamber Far Western Talus and can be proposed to have entered the Milner Hall at an earlier time to the Name Chamber sediments. This, however, is subject to the stratigraphic complications inherent in cave stratigraphy. From this information and initial observation of the site, I would propose to find, if preserved, the mining accumulated sediments on top of an infill deriving from the Name Chamber, which itself is accumulated on top of a distal representative of the M2 deposit.

EC1

The narrowness of the EC1 passage restricts the number of possible sediment sources to the Silberberg Grotto and the Name Chamber. The proximity of the opening of the passage to the Name Chamber suggests that this deposit would have contributed to the development of the EC1 talus, although it is unclear when during the accumulation of the Name Chamber Far Western Talus sediments would have entered the EC1 passage. The connection between the two areas has been cut by the mining and tourist activity. The proximity of the Silberberg Grotto openings out of which sediments have accumulated also suggests a probable previous connection. The false floors appear to be stratigraphically associated with the M2 Hanging Remnant and may represent a previous infilling event accumulating into the EC1 passage.

MH2

The MH2 deposit lies a significant distance from the far eastern Milner Hall focus area, and no present or previous stratigraphic connections can be found. The respective immediate sources are certainly distinct. It cannot be ascertained whether the M4 deposit reaches far enough west to be able to accumulate sediments into both the Name Chamber and into the north western Milner Hall. The nearest fossiliferous breccia to the north west of the surface exposed deposits is the Lincoln Cave system. The depth of the Lincoln Cave deposits is presently unknown. The MH2 area may represent a large deposit formed through a previously active connection between the subterranean chambers and one of the western-most Lincoln Cave chambers. If the opening has now filled, identification of the specific upper chamber in the Lincoln Cave may prove difficult.

CHAPTER 2 BACKGROUND

Section 2.1 presents a brief history of the Sterkfontein site together with the major palaeontological finds and archaeological assemblages. This is followed by a detailed description of the geological context of the Sterkfontein site (Section 2.2). Section 2.3 discusses the most current stratigraphic interpretations, by Clarke (2006) and R. Pickering & Kramers (2010). Section 2.4 describes the central underground deposits and the relevant surface deposits in greater detail, i.e. the Silberberg Grotto, the Name Chamber, surface Members 4 and 5 and the Lincoln Cave. Section 2.5 addresses the physical processes affecting the formation, movement and preservation of cave deposits, including an overview of some of the variables that affect the shape, size and distribution of deposits as they accumulate. Section 2.6 discusses more detailed patterns of deposit development. The common types of sediment gravity flow types encountered in caves are discussed together with the influences these processes imbue on particle properties and facies. The methods of analysis and the research that influenced the analytical methods used in this research are discussed in Chapter 3. The six conventional major deposit names established by Partridge & Watt (1991) for the Sterkfontein sequence (also referred to as the Sterkfontein Formation), Members 1 through 6, are abbreviated in the text to M1 through M6.

2.1 Sterkfontein Location and History

The Sterkfontein cave complex lies about 50km to the north-west of Johannesburg within the Cradle of Humankind World Heritage Site (Figure 2.1). The Sterkfontein site was first brought to the attention of scientists in 1895 by David Draper of the Geological Society of South Africa (GSSA). Draper (1898) described the outcropping cave sediments within the Transvaal Dolomite at the first meeting of the GSSA. The GSSA took steps to try and preserve the pristine cave system for the public following the opening of the subterranean chambers by Guglielmo Martinaglia during the mining of a large surface exposed calcite

flowstone in 1896 (Martini *et al*. 2003). The mining activities also revealed large portions of the breccias that were exposed to the surface through erosion of the cave roof and upper deposits. Despite the great effort of the GSSA to preserve the caves, a personal lease dispute resulted in initial blasting of the breccia and calcite flowstone inside the caves in 1918, and a change in the land lease saw mining of the calcite flowstone within the caves start in 1920 (Martini *et al.* 2003). Mining continued until 1939 and despite causing extraordinary damage to the caves and deposits, it facilitated the exposure of the fossil-bearing sediments, allowing the discovery of the earliest hominin specimens and *in situ* investigations to commence.

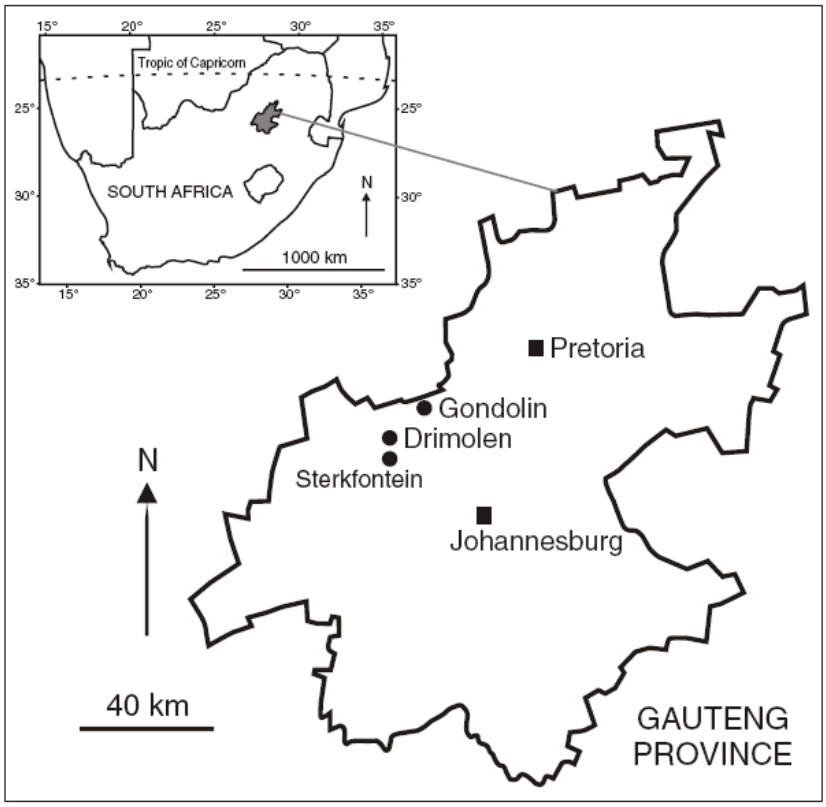


Figure 2.1 Gauteng Province showing the location of the Sterkfontein site in relation to Johannesburg.

2.1.1 Sterkfontein palaeontological finds

The large breccia dumps created by the mining process have yielded thousands of Plio-Pleistocene faunal specimens, and hundreds of hominin remains and archaeological specimens. These mining dumps were partially investigated between 1936 and 1966 and are still being processed today. The quarried breccia provided Robert Broom with the first adult hominin find from the site, the specimen TM 1511. On his first visit to Sterkfontein on the 9th of August 1936, Broom had asked the quarry manager, Mr Barlow, if he had ever seen or could save for him anything resembling the Taung Child. On Broom's third visit to the site on the 17th of August 1936, Broom was handed a remarkably preserved brain endocast. Upon a search of the nearby blasted out breccia heaps, Broom found other parts of the skull and teeth of the same specimen, as well as the top of the skull still embedded in the *in situ* exposed breccia. Despite being severely crushed, the specimen was the first adult *Australopithecus* type specimen and Broom named it as a new species, *Australopithecus transvaalensis* (*A. transvaalensis*) (Broom 1936). Later, the specimen was placed into the new genus, *Plesianthropus* by Broom (Broom 1947) but has now been classified as *Australopithecus africanus*.

On the 18th of April 1947, the discovery of Sts 5 (Mrs. Ples), at that point the most complete adult hominin cranium found at Sterkfontein, (Broom *et al.* 1950; Robinson 1997) secured Sterkfontein's place as a site of great importance for the study of human evolution. Since then hundreds of fragments of over 87 *Australopithecus* individuals (T. Pickering *et al.* 2004b) have been yielded from the Sterkfontein surface exposed deposits, representing two different species of *Australopithecus* (Clarke 1988, 1989, 1994b, 2008). StW 252, StW 505 and Sts 71 are considered by Clarke to represent young male, mature male and mature female specimens, of a second *Australopithecus* species (Clarke 1988, 1989, 1994b, 2008). Other hominin species represented include, *Homo ergaster* (Clarke 1994a) and *Paranthropus robustus* (Kuman & Clarke 2000). The more significant specimens that have been recovered from *in situ* excavations from the surface exposed member deposits (M4 and M5) include TM 1511 (parts of which were

excavated from *in situ* breccia), Mrs Ples (Sts 5), Sts 431 (partial skeleton), Sts 14 (pelvis), StW 252 (partial cranium), StW 505 (partial cranium), Sts 71 (partial cranium), StW 13 (partial cranium), and StW 53 (partial cranium). The StW 53 specimen, discovered by Hughes in August, 1977 (Hughes & Tobias 1977; Tobias 1978) has been considered by some to be a member of the *Homo habilis* species (Hughes & Tobias 1977; Tobias 1978; Howell 1978; Curnoe 2002; Curnoe & Tobias 2006). Based on the morphology, of the specimen, it has since been demonstrated that StW 53 represents an *Australopithecus africanus* (Wolpoff 1996; Kuman & Clarke 2000; Clarke 2008). The placement of StW 53 within the *Australopithecus* genus and derivation of the specimen from a deposit with no associated archaeological material does give cause to question T. Pickering *et al.*'s (2000) interpretation of the 'cut marks' as representative of "the earliest unambiguous evidence that hominins disarticulated the remains of one another" (pp. 579). Clarke (Pers. Comm. and in press) suggests that the feint cut marks were undoubtedly made by a sharp-edged chert block forced against the bone in the moving talus slope. Such a block was found in the zygomatic arch region when the specimen was found and there are many more such blocks in the breccia around the cranium.

Comparably, a small number of hominin specimens has been excavated from *in situ* subterranean breccias, including 11 *Australopithecus* fragments from the Jakovec Cavern (Partridge *et al.* 2003) and the most complete *Australopithecus* specimen yet found in the world, the StW 573 specimen from the Silberberg Grotto (Clarke 1998). The relatively small number of subterranean discoveries is due to a number of reasons. Firstly, not many of the fossil-bearing underground breccia bodies have yet been sampled. The Silberberg Grotto is special because of the extensive mining of a stalagmite that produced the dump material which provided both the interesting *Chasmaporthetes* specimen and inspired Tobias' early interest (Tobias 1979), and produced the foot bones that led to the discovery of the StW 573 specimen (Clarke 1998). Without the contribution of the mining, the deposits within the Silberberg Grotto could probably never have been sampled due to the massive stalagmite sealing in the M2 fossiliferous and basal breccia

bodies. Generally, there is a focus on those deposits which have produced temporally significant fauna or hominins already. Secondly, there is a taphonomic difference between the hominin-rich M4 deposit and the Silberberg Grotto, which has enabled deposition and preservation of significantly fewer hominins (Clarke 2008). Thirdly, there are significant logistical issues surrounding underground excavation, i.e. many of the fossil-bearing deposits are located in small chambers, form steep or vertical slopes or are heavily calcified making the work to recover fossils very difficult. Member 3, for example, has not yet been sampled but is fossiliferous and spans a depositional period between the M2 and the M4 deposit (Clarke 2006) but is exposed only on an inaccessible vertical face. The StW 573 specimen and the Jakovec Cavern specimens do, however, attest to the potential of finding rich and significant fossil-bearing deposits within the subterranean chambers.

Along with the wealth of hominin fossils yielded from seven decades of work at Sterkfontein, a very large number of stratigraphically associated faunal remains has also been excavated. Vertebrate faunal remains have been used to clarify a broad spectrum of deposit contextual information (for examples see Freedman 1957; Brain 1974; Vrba 1974, 1985, 1995; Eisenhart 1974; Delson 1984; Turner 1987, 1997; McKee 1991; Sillen *et al.* 1998; Carrión & Scott 1999; T. Pickering 1999; Elton 2000, 2001; T. Pickering *et al*. 2000, 2004a, b, c, 2008; Avery 2001; Luyt 2001; Luyt & Lee-Thorp 2003; Sponheimer *et al*. 2003, 2005; Kibii 2004; Heaton 2006; Avery *et al.* 2010). They have also provided the earliest dating method applicable to the hominin-bearing deposits. Referred to as biostratigraphy, this relative dating method remains an important inter-deposit and inter-site comparative method (Broom 1945a; Cooke 1974; Vrba 1975, 1982, 1995; Partridge 1982; Kibii 2004), and is applied to many of the fossil-bearing deposits where absolute dating methods are still problematic (Partridge 2005).

2.1.2 Sterkfontein archaeology

Sterkfontein has also yielded a number of important stone tool assemblages, including the oldest and largest example of the Oldowan techno-complex identified in southern Africa (Kuman *et al*. 2005). Stone artefacts have been recovered from various contexts at Sterkfontein and been worked on by a number of researchers (Robinson 1957; Mason 1957; 1962a, b, 1976; Stiles & Partridge 1979; Clarke 1985; Kuman 1994a, b; Kuman 1996, 1998; Field 1999; Kuman & Clarke 2000; Kuman & Field 2009). Traditionally, it was thought the Oldowan assemblage was restricted to the deeper portions of the Member 5 East (M5E) area of the surface deposits (Kuman 1994b; Kuman & Clarke 2000). More recently, the Oldowan assemblage has been enlarged through excavations within the Name Chamber (Stratford 2008), a subterranean chamber lying beneath the M5 area and connected by a 12m vertical shaft (Clarke 1994a). Oldowan artefacts from M5, originally estimated at about 1.7 to 2Ma by Kuman & Clarke (2000) have now been dated by the cosmogenic nuclide burial method to about 2Ma (Gibbon, R. Pers. Comm.). The Oldowan is characterised by: an expedient use of local quartz; an evident positive selection of river cobble quartz over vein quartz; a large proportion of <20mm small flaking debris; a dominance of polyhedral core forms demonstrating practice of a ‘simple’ core reduction strategy and correspondingly small sized flakes; (±35mm) (Kuman 1996; Field 1999; Kuman 2007; Kuman & Field 2009). Table 2.1 shows the summary profile for the Oldowan assemblage.

Artefact Types	**Quartz**	**Chert**	**Quartzite**	**Other**	**Total**	%
Small Flaking Debris <20mm	3644	256	14	0	**3914**	85.8
Complete flakes ≥20mm	66	16	23	0	**105**	2.3
Incomplete flakes ≥20mm	255	48	43	0	**346**	7.6
Chunks	121	2	11	0	**134**	2.9
Retouched pieces	5	1	1	0	**7**	0.2
Core tools	0	0	1	0	**1**	0.0
Cores	17	1	8	0	**26**	0.6
Core fragments	3	1	2	0	**6**	0.1
Manuports	2	1	8	1	**12**	0.3
Indeterminate	8	1	2	0	**11**	0.2
TOTAL	**4121**	**327**	**113**	**1**	**4562**	100.0
%	90.3	7.2	2.5	0.0	100.0	

Table 2.1 Sterkfontein Oldowan assemblage including the Name Chamber component, after Stratford (2008).

Above the Oldowan assemblage in M5E and in Member 5 West (M5W) an assemblage of 701 pieces of Early Acheulean (EA) technology has been yielded (Kuman 1994a, b) and analysed most recently by Field (1999). The Early Acheulean assemblage is estimated to date between 1.7 – 1.4Ma based on the stratigraphic relationship of the 'upper' area of M5W (Kuman & Clarke 2000). The Early Acheulean assemblage is characterised by: a positive selection of quartzite, sourced from the nearby river gravels; a high proportion of radially flaked bifacial pieces (discoidal cores); a high proportion of manuports; flakes measuring >100mm in maximum length; very low proportion of <20mm small flaking debris perhaps due to on site winnowing; a general but subtle move towards Large Cutting Tools (LCT's) (Kuman 1998; Field 1999; Kuman 2007). Table 2.2 shows the summary profile for the Early Acheulean assemblage. Unfortunately, most of the typologically diagnostic EA artefacts have been recovered *ex situ* from mining dumps or areas of deposit that have experienced some level of sediment mixing through infiltration of solution cavities and so

cannot be definitively associated with a solid M5W context. The problem of sediment mixing is endemic to karst cave deposits and identification of mixing is obviously of great importance when conducting archaeological analysis. The Early Acheulean sample was recently increased when a previously undiscovered miner's dump (named Dump 21) was found. The dump material contained 35 artefacts, the analysis of which revealed a considerable technological correlation to the Early Acheulean (Stratford 2008). The lack of another Acheulean assemblage from another part of the site also allowed an elementary stratigraphic relationship to be inferred. Two 'uncontentious' bifaces were excavated from the M5W deposit, one of which was directly associated with the StW 80 mandible of *H.ergaster* (Kuman & Clarke 2000). For full details of these assemblages refer to Field (1999), Kuman (2007) and Kuman & Field (2009).

Artefact Types	**Quartz**	**Chert**	**Quartzite**	**Total**	**%**
Small flaking debris <20mm	18	-	1	**19**	2.5
Chunks <20mm	44	14	54	**112**	15.0
Incomplete flakes ≥20mm	23	2	9	**34**	4.6
Complete flakes≥20mm	13	1	12	**26**	3.5
Retouch Pieces	1	-	2	**3**	0.4
Core Fragments	4	-	7	**11**	1.5
Flaked Flakes	1	-	4	**5**	0.7
Core Maintenance Flakes	0	-	2	**2**	0.3
Cores	78	9	196	**283**	37.9
Irregularly Fractured Cobble	7	-	21	**28**	3.8
Core tools	-	-	8	**8**	1.1
Utilised Cobbles	-	-	2	**2**	0.3
Manuports	17	21	171	**209**	28.0
Uncertain types	-	2	2	**4**	0.5
Total	**206**	**49**	**491**	**746**	100.0
%	27.6	6.6	65.8	100%	

Table 2.2 Sterkfontein Early Acheulean assemblage, after Stratford (2008).

2.2 Sterkfontein Geological Context

This section provides a review of the main points of the geological and geomorphological context of the area in order to establish an understanding of the formation of the caves, how the formation processes have influenced the morphology of the caves, and subsequently the depositional patterns found within the caves. Figure 2.2 shows the geological setting of the Sterkfontein caves within the Cradle of Humankind boundaries. Martini *et al.* (2003) have produced the latest contribution to the geological and geomorphological understanding of the Sterkfontein cave system.

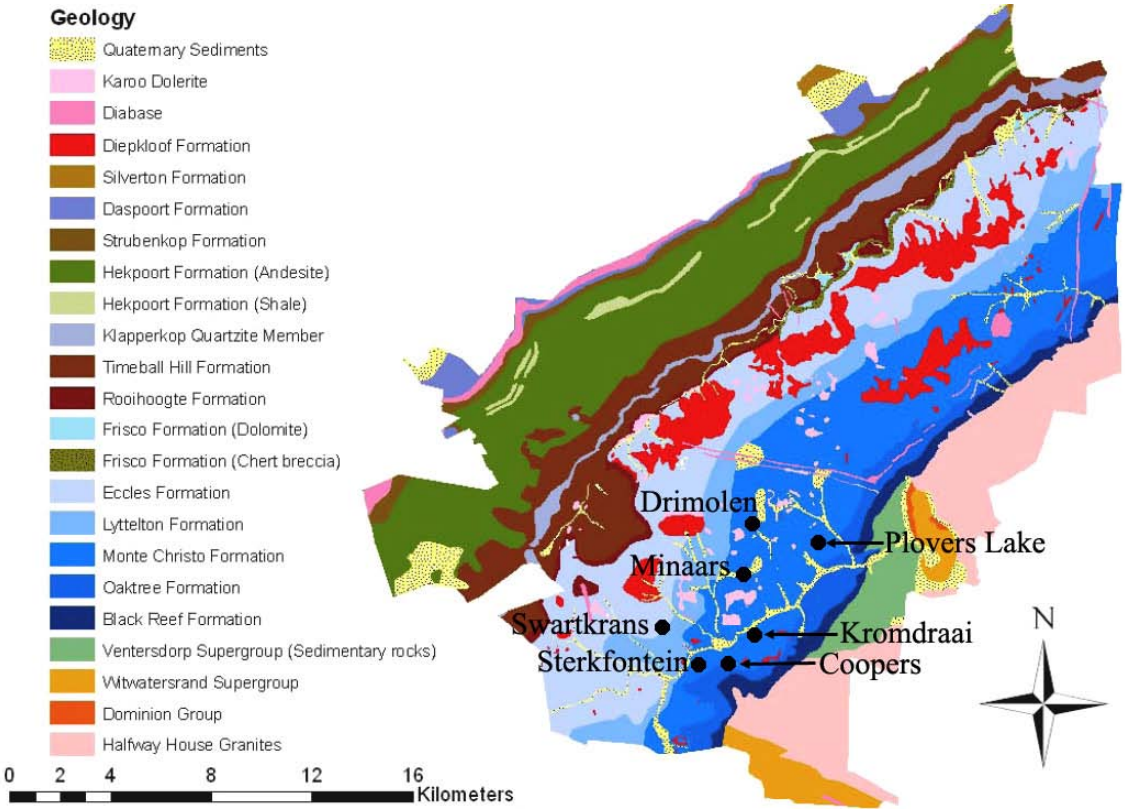


Figure 2.2 Geological map of the Cradle of Humankind world heritage site with some of the southern-most palaeoanthropological sites. Adapted from Leyland *et al.* (2008).

The Sterkfontein cave system has formed within a stromatolitic dolomitic limestone which was laid down as sedimentary rock during the Late Archaean age (2.5-2.6Ga years ago) (Martini *et al.* 2003). At this time, a shallow sea occupied the Transvaal Basin depositing the limestone and chert beds. The shallow marine dolomitic limestone of the Malmani Subgroup is a calcium magnesium carbonate, rich in iron and manganese. Secondary dolomitisation of the original limestone has removed many of the intricate varying sedimentary forms often seen in limestone beds (Bruxelles Pers. Comm.). The Sterkfontein cave system occupies the boundary between two subdivisions of the Malmani Subgroup, named the Oaktree Formation and the Monte Christo Formation. The Lincoln Cave system, running to the NNE of the Sterkfontein system, occupies the Monte Christo Formation, whereas the Sterkfontein caves straddle both formations. The Oaktree Formation is characterised by low proportions of chert, and high, narrow passages are often formed. It is in the Oaktree Formation that most of the Sterkfontein chambers have formed. In contrast, in the Monte Christo Formation, which is rich in chert beds, passages are often low and broad, 'stacked' into multiple levels on single fissure passages, separated by thick chert beds. The presence or absence of insoluble chert veins influences the movement of water through the host rock, thereby affecting the pattern of passage and chamber dissolution. Passage position is governed by vertical faults in the host rock, lower proportions of chert will allow high narrow passages to develop along these faults. Areas rich in chert veins will restrict the movement of water to between the veins, focussing the dissolution into short, broad, stacked passages. Both formations have varying interstratified chert beds, which have influenced the dissolution of the dolomitic limestone and thus the shape of the cave system (Martini *et al*. 2003).

The dolomitic limestone host rock dips at a 30° angle to the north-west. The outcrop of the dolomitic limestone in the Cradle area represents one of the margins of the basin formerly occupied by the shallow inland sea 2.5Ga years ago. Another margin of this sea outcrops at Makapansgat in the Limpopo Province where there is also an important *Australopithecus*-bearing site (Dart 1948, 1955, 1959; Clarke 1988, 1994b; Tobias 1997a, b). The host rock has been extensively overlain by intrusive igneous and metamorphic rocks. Erosion has

exposed the upper, marginal area of the dolomitic limestone basin to the shallower depths of ground water and facilitated cave development.

The development of the Sterkfontein cave system is restricted to an area 200 x 250 x 50m (Martini *et al.* 2003) by the formation of dolerite and syenite dykes, and silicified faults, as identified to the east of the cave system (Wilkinson 1973, 1983). The upper gallery which is now exposed on the landscape surface is characterised by one large chamber, with no visible network of passages, a characteristic of the lower subterranean area. This absence of passages in the upper gallery may be due to the dissolution of a particularly chert-poor area forming a single large chamber. A similar situation is seen in the Elephant Chamber.

The majority of the cave system was formed by the exposure of soluble minerals within the host rock to ground water during the phreatic (underwater) phase. Within dolomitic limestone, the calcium carbonate ($CaCO_3$) is the more soluble component, leaving the manganese and iron behind to oxidise into secondary minerals. Chert is high in silica and insoluble, so restricts water movement to the dolomitic limestone component of the host rock and forms natural boundaries and barriers to passage and chamber development. The position, thickness and joints of the interstratifying chert beds influence the direction and size of the forming system. This can influence cave development on a macro or micro level, influencing the direction or shape of passages or creating weaknesses prone to later collapse. Passages and chambers have developed following subvertical joints within the host rock and through focussed dissolution of chert-poor areas.

The dominant joint within the Sterkfontein system runs W-E with the subordinate jointing running N-S. Larger more influential joints may have formed due to large scale geological processes. Some of these faults can be traced in cracked chert beds that can be found in various areas of the caves. It has been suggested that the majority of the faults occurred during the tensional event associated with the flood basalt volcanism during the Early Jurassic (Kavalieris & Martini 1976). The influence of these joints can be seen in the pattern of passages developed. The static or very slow moving nature of the ground water has enabled this pattern to

be followed. In systems where ground water is moving more quickly, dissolution often develops a number of large conduit passages in the direction of flow and limits development of perpendicular passages. The movement of water is greatest within the upper 10m of the ground water level. This area represents the zone of maximum dissolution and most cave development occurs as the water-table drops and exposes dolomitic limestone to this zone.

The dissolution process during the phreatic phase (under water) has led to the development of multiple levels of small, interconnected networks of passages with occasional larger chambers. Where passage separating walls have been dissolved away due to prolonged exposure to ground water, larger chambers have been created. This is exemplified in the Elephant Chamber where the remnants of the separating walls can be seen truncated and suspended from the roof. The same process may account for the absence of passages found in the upper gallery (now exposed on the surface). Other larger chambers have been formed through collapse during the vadose (above water) phase, which follows a lowering of the water-table. In systems with slow-moving or stationary ground water, movement of non-soluble minerals is minimal allowing secondary minerals to form *in situ* and on undisturbed cave floors. Continued dropping of the water-table allows the upper chambers to fill with air and removes the buoyant support necessary for cave stability. The subsequent internal collapse caused by the readjustment of the cave's structure is controlled by existing subvertical joints and fissures present in the dolomitic limestone. This collapse is continuous as the water-table fluctuates and vadose zone volumes change. Collapse along these faults causes development of larger chambers and an increase in passage height and in some cases, the development of openings to the surface allowing externally derived sediment to enter and be deposited into the caves.

There are several types of cave opening found at Sterkfontein. Most openings are small vertical and sub-vertical shafts, characterised by a >15m drop into the caves below. Other openings are enlarged by localised dissolution and collapse of the exposed dolomitic limestone from surface water. In the latter cases, deep, wider shafts can open into chambers below the ground level. Where surface erosion has

intersected with the uppermost passages or the roof has collapsed due to surface erosion, long deep gullies are opened. Many openings are very steep sided and represent a serious natural trap danger to animals, and thus 'death trap' assemblages represent a common bone accumulation agent. Access to the water-table encourages large trees to grow in and around the openings, attracting a host of carnivores, primates and hominins and leading to a number of carnivore accumulation scenarios first described by C.K. Brain at Swartkrans (Brain 1958, 1981; see T. Pickering *et al.* (2004c) for a good account of multiple carnivore accumulations). The steep sided and deep nature of most of the cave openings prevented the use of the caves as resting or living places by hominins or most other animals apart from bats. It is most likely that hominins and primates used the increased vegetation density close to the cave openings as shelter (Brain 1981). Use of caves in general as resting areas by more nimble primates like baboons (Marais 1939; Simons 1966; Gow 1973; Wells 1973; Barrett *et al.* 2004), *Papio ssp.* (see McGrew *et al.* 2003 for review of the sightings) and chimpanzee (*Pan troglodytes*) (Pruetz 2001) has been observed. The possibility of the use of caves by primates within the Cradle sites has been suggested based on the age spectrum and articulated nature of primate fossils (Brain 1981, pp. 271). Actualistic studies are revealing interesting carcass assemblages within known primate resting sites (C. Menter Pers. Comm.; Pers. Obs.). In circumstances where the openings are not vertical this may well have been possible. Interpretation of the fossil accumulation at Malapa, another Cradle site, suggests a use of the trees by primates and hominins to access the water-table below in times of ecological stress (Dirks *et al.* 2010), with the steep sided opening contributing to the death of those animals attempting access (L. Berger Pers. Comm.). Caves can become shallow when accumulation of sediments fills the available receptacle space. Hyaena denning activities and accumulations of fauna related to hyaenas living in shallow cave openings has been suggested for the M5W deposit (T. Pickering 1999). The deposits sampled by the surface excavations represent the infills of the upper gallery chambers of the system. The original openings to the upper chambers would have been governed by the same influences and manifested the same structures.

The change of the cave environment from a phreatic to vadose system also initiated the growth of speleothems. Speleothems can form through two main processes. Stalactites, stalagmites and flowstones form as $CaCO_3$ precipitates out of a $CaCO_3$ rich solution, filtering through fissures in the dolomitic limestone. Evaporite speleothems form as 'popcorn' and aragonite crystals on the walls and require the movement of air. The high frequencies of aragonite also relate to the high concentrations of manganese in the ground water (Martini & Kavalieris 1978, Martini *et al*. 2003). Uptake of other minerals like uranium from the ground water by speleothems has allowed U-Pb and U-Th dating techniques to be applied to various flowstones in the Sterkfontein system (Walker *et al.* 2006; R. Pickering *et al*. 2006; R. Pickering *et al.* 2010; R. Pickering & Kramers 2010). A continuing problem with the supposed dating of sediments using speleothems is that speleothems can develop, re-crystallise, be removed completely, and grow in new fissures or gaps caused by collapse at any point in time. This presents a significant stratigraphic concern given that the sediments themselves are proving very difficult to date (Partridge 2005). This situation is perfectly demonstrated by the StW 573 specimen. Clarke's stratigraphic interpretation is that collapse of the deposit enclosing the specimen, within the Silberberg Grotto, caused the central part of the skeleton to subside into a lower cavity. The gaps formed by the collapse were filled by a flowstone at a much later date. This flowstone has subsequently been dated and produced results significantly younger than those indicated by biostratigraphic and stratigraphic analysis (Clarke 2006).

Speleothems have also been used at Sterkfontein to reconstruct previous cave environmental conditions and water-table levels (Wilkinson 1973). The tracking of speleothems is an important practice for the consideration of deposition timings. Fluctuating water-table levels can cause the erosion and movement of sediments. Dissolution of stalactites can be tracked up to 12m above the current water-table level within the Milner Hall (Wilkinson 1973). Dissolution of inactive speleothems within the Fossil Chamber about 20m above the current water-table level may also be due to previous high water-table levels (Martini *et al.* 2003). It has been suggested from the formation of botryoidal stalagmites and shelfstone that the water-table previously rose to submerge the lower portion of the

Silberberg Grotto, about 22m above current water-table levels (Partridge 1978; Clarke 2006). Fluctuations of the water-table in the order of tens of metres are, however, difficult to justify given the lack of evidence of such rises in the local river level. The geological evidence suggests a consistent lowering of the water-table with the cutting of the river into the valley floor. The evidence of partially dissolved flowstone remnants identified in the Milner Hall by Wilkinson (1973) are likely to be very old remnants of dissolved speleothem forms as the water-table fluctuated whilst dropping through that particular level of the cave system. Wilkinson (1973, 1983), importantly, did not propose a relative chronology for the water-table levels. Similar partially dissolved speleothem forms can be seen on the walls within a few metres of the current water-table and the water-table can be seen to fluctuate by up to 2m seasonally (Pers. Obs.). The existence of water-dependant speleothem forms, shelfstones and rimstones in currently relatively high chambers (like the Silberberg Grotto) is more likely to be a result of the blocking of chamber exits with speleothems causing the localised pooling of water rich enough in $CaCO_3$ to allow underwater speleothem growth. Generally, the low $CaCO_3$ quantity at the water-table facilitates only the dissolution of speleothems.

Historically, absolute dating techniques applied to Sterkfontein have been fraught with complications. Techniques are limited due to the lack of radioactive volcanic material within sediments. Use of oxygen isotope data from speleothems can provide correlations with established oxygen isotope stages and useful information on past karst and environmental conditions (Henning *et al.* 1983; Quinif *et al.* 1994; Bar-Matthews *et al.* 1996, 1997; Sancho *et al.* 2004). Recent advances in techniques like palaeomagnetic dating, cosmogenic nuclide dating and isotope decay analysis promise encouraging results in future using a combination of techniques (Partridge 2005). Given the complications inherent to the dating of karst cave sediments, combinations of techniques are needed to attain the most accurate interpretation of dates and stratigraphic relationships at Sterkfontein. Examples of multidisciplinary approaches to dating have started to appear (Muzikar & Granger 2006; Herries *et al.* 2009) but increased resolution

can only be achieved with a detailed understanding of the stratigraphic sequences forming the current deposit morphologies.

2.3 Current Stratigraphic Interpretations

The two most recent interpretations of the stratigraphic history of the fossil-bearing deposits at Sterkfontein have been made by Clarke (2006) and R. Pickering & Kramers (2010). Figure 2.3 illustrates Clarke's interpretation and is based partly on the depositional sequence established by Partridge & Watt (1991). Partridge and Watt's stratigraphic interpretation was based on sedimentological samples from a coring programme that sank 5 cores through strategic areas at the surface (Partridge & Watt 1991). Clarke's sequence presents 6 depositional units based on the remnants of infills exposed at the surface and connecting subterranean chambers. Currently these deposits are labelled Members 1 through 6 (M1-M6). The use of the member system is discussed in Section 2.5 and needs some level of adjustment as stratigraphic investigations continue. Collapses over time have moved some sediments into deeper areas of the cave allowing the infilling of vacant areas with younger sediments or other ancient collapse material. As one can see from the schematic section, it has been proposed that M2 and M3 filled from a different opening to that of the younger M4, M5 and M6 deposits. Deposition into chambers from multiple openings is a common process in cave systems like Sterkfontein. Most passages and chambers are connected, until they become choked with sediments, allowing the collection of sediments in central areas from various sources. Each source potentially provides sediments with differing faunal and sediment properties based on the respective opening shape. Sediment flow direction can be tested with the application of fabric analysis. If M2 and M3 have originated from a different opening to the subsequently deposited sediments (M4 through M6), then it should be evident in the sediments. As of yet no *in situ* investigations have been carried out on M3 and this deposit is currently represented by a vertical face in the upper eastern end of the Silberberg Grotto (on the descent into the Silberberg Grotto via the wooden stairway). Fossils can be seen within the breccia face of M3 as well as the

impression and remnants of the extensive stalagmite boss which filled this area of the chamber before it was subsequently mined out (Clarke 2006). This mining produced the breccia dump which extended across the floor of the Silberberg. The dump material contained the StW 573 foot bones, but also mixed with breccia containing M3 fossils. M3 has not yet yielded any hominin fossils. So far, M2 and M3 have produced only a single hominin specimen. Clarke has suggested this is due to taphonomic processes (Clarke 2008), although it could be said that given the size of the proposed M3, a representative sample of the deposit has not yet been recovered. Partridge and Watt (1991) have suggested that M3 represents an approximately eight meter thick infill that was deposited on top of the enormous stalagmite that covered M2 and was subsequently buried under M4. The lack of analysis of the M3 sediments makes it difficult to suggest associations between M3 and M4 or to make interpretations of the contents.

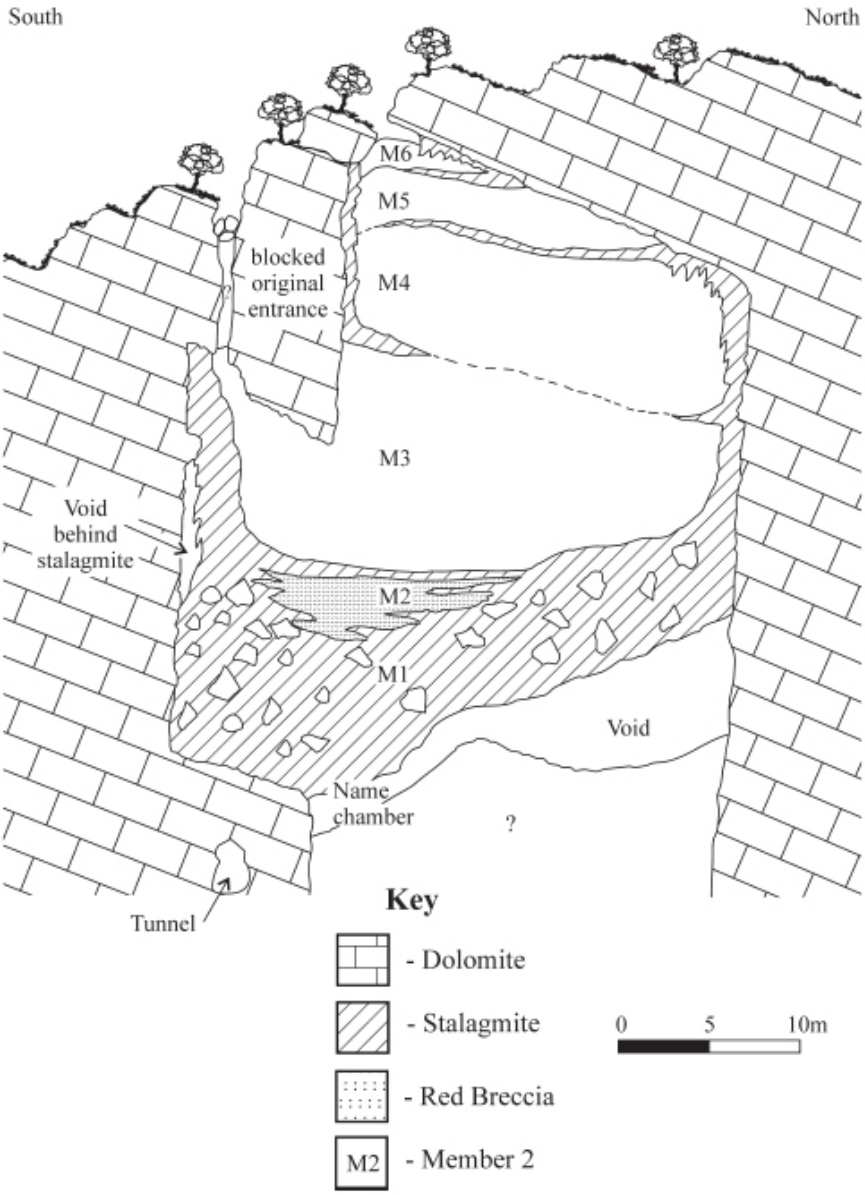


Figure 2.3 Clarke's Sterkfontein stratigraphy. Schematic north-south section of Sterkfontein to show general relationship of breccias with suggested original openings and possible surface topography. From Clarke (2006).

Partridge and Watt's diamond coring samples were re-analysed and updated in R. Pickering & Kramers (2010). In this study, they applied facies descriptions to the sediments in the core samples and to sediments exposed at the main surface excavation. They use these descriptions to correlate sediment patterns across the site in an effort to understand sediment boundaries. R. Pickering & Kramers focus

on the placement of sections of breccia that have been separated by major flowstones into larger depositional units, then correlate them with the existing member system. R. Pickering & Kramers propose an adjustment in the interpretation of major depositional units and propose joining M3 to M4, based on the facies represented in the core samples with M3 being interpreted as a distal portion of M4 (R. Pickering & Kramers 2010). The sediment logs used by R. Pickering & Kramers are shown in Figure 2.4. This hypothesis is plausible and the use of sedimentary facies is a step in the right direction. However, there are some issues with their approach and stratigraphic interpretations based solely on sediment cores. Although this work is not a critique of the investigation, I have briefly outlined some of the associated stratigraphic issues to demonstrate some of the caveats required in stratigraphic interpretations.

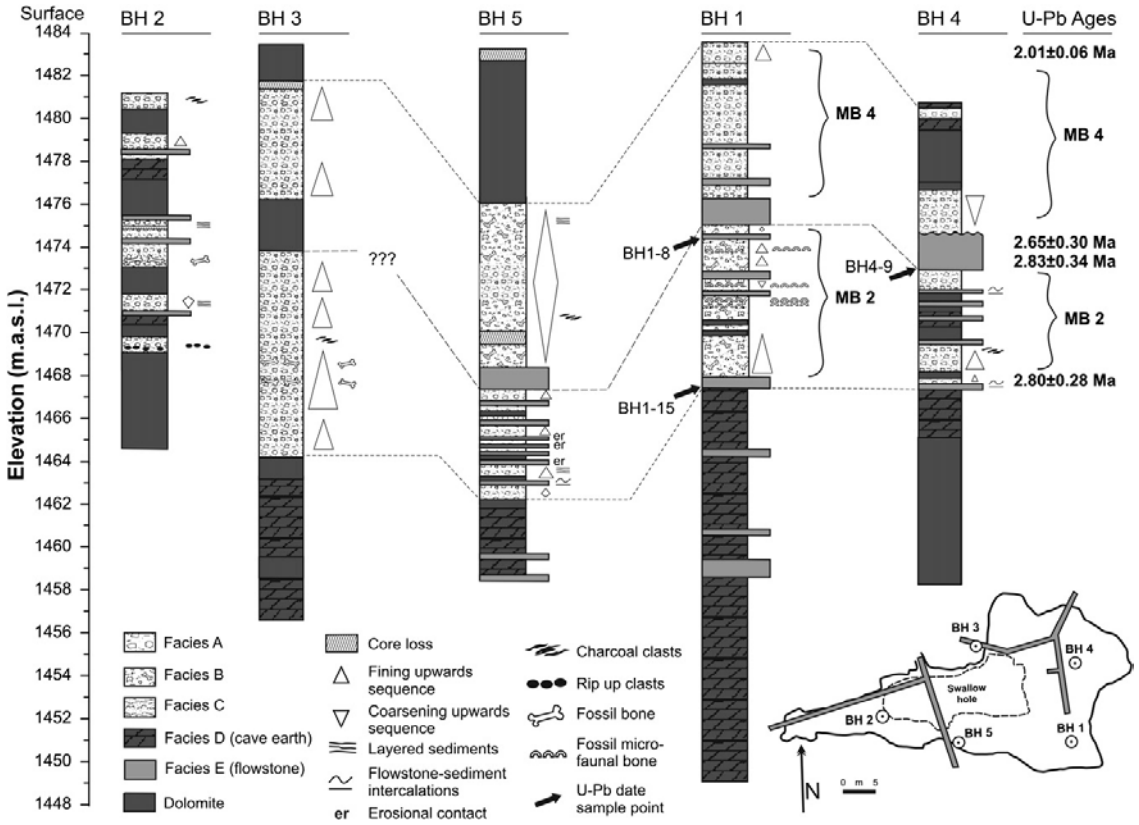


Figure 2.4 Core samples from re-examined coring project originally conducted by Partridge and Watt (1991), and Partridge *et al.* (2000) (R. Pickering & Kramers 2010).

1. Primary and secondary sedimentation processes and mixing of sediments are very difficult to identify in core samples. As can be seen in the sedimentary logs there is great variability on the identification of 'sedimentary packages'. Some divisions show four different grading sequences (e.g. lower unit in BH3), others show none (upper units in BH1). There is little control over identification and quantification of localised sediment mixing. Classifying deposit relationships should be done with caution when based on facies properties only, as isolated samples of facies from core samples may represent mixed sediments.

2. Sediment properties can vary greatly throughout the depositional history of one infill. Opening shape and depth, surface vegetation and climate all contribute to the properties of the sediments deposited. Any of the sedimentary facies indentified by R. Pickering & Kramers can be deposited at any time depending on the above variables. In deposits such as M4 that represent long accumulation times, coarser and finer sediments can be deposited as the landscape variables change. What appear to be distal facies may just represent a period of reduced soil erosion and finer sediments being deposited. Categorising sediments from cores as lateral or vertical facies of the same unit may be optimistic, given the depositional conditions are unknown. The inconsistency of the stratigraphic units between core samples suggests many discontinuous strata or terminating distal or lateral facies representing numbers of deposits originating from numbers of sources may have been sampled, a situation predicted by Wilkinson (1983). The cores also demonstrate the potential for inter-deposit stratigraphic variability.

3. Flow direction is a key variable for tracking sediment source and assessing the contribution of sediments from more than one source. Flow direction cannot be determined from core samples, due to the insufficient quantity of sediment sampled. Large chambers often have numerous openings and connecting feeding passages, and as such, sediment flow direction provides a vital deposit differentiating indicator.

4. Cave deposits are very rarely deposited in horizontal strata. Tracking lateral facies across a deposit surface is a valid analytical procedure for tracking broad patterns in flow direction and flow dynamics. However, in order to accomplish the desired results, one first needs to be confident that the exposed

surface represents the surface of a single depositional horizon. In non-stratigraphically sensitive excavations, excavation surfaces may cut through more than one sedimentary horizon thus sampling facies representing vertical changes, lateral changes or a different depositional unit. The existing M4 surface represents the excavated surface only, not the deposit's stratigraphic morphology. A good example of this is seen at the western end of the surface excavation where the M4 deposit has collapsed and the spaces are filled with M5. The horizontal excavations cut through the interfingered deposits (Clarke 1994a).

5. Identification of flowstone form is integral to the accurate interpretation of the absolute dating results. The restrictive representation of borehole samples presents significant difficulties in recognition of particular flowstone form. Those flowstones that have formed through the filling of existing gaps created by erosion, collapse or faulting may be incorrectly interpreted as capping flowstones based solely on borehole samples.

Both Clarke's and R. Pickering & Kramers' stratigraphic hypotheses regarding M3 are testable in the future. Until M3 is sampled and analysed using all tests available, relationships between subterranean and surface deposits can only be regarded as hypotheses.

What is noteworthy from the core samples is the number of identifiable grading sequences, each grading sequence representing a different infilling episode. The sediment sections of BH3 provide an opportunity to identify some of the intra-deposit episodes in areas of deposits that may otherwise be inaccessible. In the case of the lower BH3 section, infilling episodes are represented by four regularly graded strata. Identification and tracking of graded strata can be useful for stratigraphic interpretations, as they can indicate certain sediment flow types and prevalent depositional conditions. The intricacies of sediment grading and the stratigraphic benefits are discussed in Section 2.6.

In more recent years, the stratigraphic investigations carried out at Sterkfontein have tried to deal with the association between the exposed surface deposits and the subterranean deposits (Partridge & Watt 1991). Unfortunately, those deposits exposed on the surface are not similarly exposed in the subterranean chambers, so

identification of vertical boundaries remains the greatest problem. These problems are addressed in Section 2.5. Partridge and Watt's solution for the disassociation between M4 and the subterranean deposits was to name the unknown intermediate entity M3, the sediment body assumed to have been deposited before M4 and after M2. Only the lower portion of M3 is exposed in the Silberberg Grotto and estimates of the size of M3 made by Partridge and Watt remain unconfirmed. Although recent excavations in the deepest portions of M4 may be close to sampling the upper M3 portions (Clarke Pers. Comm.). Associations between the surface deposits and the subterranean deposits are still unclear.

The Jakovec Cavern which has yielded 11 *Australopithecus* specimens, is a good example of the disparity between the subterranean and the surface exposed deposits. Partridge and Watt suggested the sediments infilling the Jakovec area represent deposits unrelated to the main Sterkfontein sequence (Partridge & Watt 1991), which have entered the cave via an entrance in the far eastern end of the Jakovec (Partridge *et al.* 2003). A date of around 4Ma has been suggested for both the 'orange' (upper) fossil-bearing breccia and the StW 573-bearing breccia, based on cosmogenic Aluminium-26 and Beryllium-10 dates, indicating the two deposits (although representing distinct entities originating from different sediment sources) formed at a similar point in time (Partridge *et al.* 2003). Clarke has supported this interpretation based on morphological analysis of the *Australopithecus* specimens (Clarke 2006). It seems likely that the Jakovec Cavern represents another central accumulation area, similar to the eastern Milner Hall, where a number of deposits originating from a number of sediment sources, not necessarily associated, have accumulated into a deeper part of the cave system. In the ceiling of the eastern area of the Jakovec cavern, several blocked entrances are visible and have contributed material. In the western end of the cavern there are talus deposits spreading in an easterly direction from the direction of the main Sterkfontein subterranean deposits. The proximity of the western end of the Jakovec Cavern to the Name Chamber and associated passages suggests a previous connection (Pers. Obs.; Bruxelles Pers. Comm.). Until further analysis is carried out the Jakovec Cavern remains stratigraphically isolated from the recognised main deposits (Partridge *et al.* 2003).

Work by Stratford (2008) has made positive correlations between the surface exposed deposits and the subterranean Name Chamber deposits based on an approach combining excavation, stratigraphic analysis, archaeological and microfaunal taxonomic representation (Stratford 2008; Avery *et al.* 2010; Stratford *et al.* in prep). Taphonomic and taxonomic investigations of the excavated fauna are ongoing and will provide further correlations with established surface deposits.

2.4 Review of the Relevant Deposits

The central subterranean area of the caves, briefly described in the introduction, consists of an area fed by sediments from a number of important deposits found elsewhere in the caves. In this section the most likely source deposits are described by location, content and current accumulation interpretations. I have made no attempt to order the deposits in terms of chronology of original deposition or date. This approach is taken due to the irregular and unpredictable nature of cave depositional processes, where significantly older or younger deposits can be found in a jumbled stratigraphic position. The deposits sampled have potentially been through several phases of re-sedimentation, progressively depositing them deeper into the cave system. Therefore, the original date of sediment deposition into the cave (primary sedimentation) may differ greatly from the date of re-sedimentation into the sampled area. This issue of primary sedimentation and re-sedimentation (secondary sedimentation) is of key importance for understanding the different processes of deposit formation and will be discussed in the following section. In this research the member system is used to refer to the recognised major depositional units (M1 – M6), as established by Partridge (1978). This system is not ideal for the identification of mixed or secondary sedimentation deposits with broken stratigraphic connections but it does allow associations to be made to those deposits with a more familiar literature foundation. As stratigraphic investigations continue and intra- and inter-deposit relationships become clearer with greater sedimentological and facies resolution, the Member system will need to be adjusted in a move away from the

more rigid to more fluid interpretations of the stratigraphy. Until this point, the conventions established for the identification of the major bodies of sediment recognised at Sterkfontein are upheld. The following section addresses the surface deposits first, before describing the relevant, researched, subterranean deposits.

2.4.1 Member 4 deposit

The Member 4 deposit (M4) is possibly the most well known of the Sterkfontein deposits, being the main repository of *A. africanus* specimens, as well as a second species of *Australopithecus* (Clarke 1988, 1989, 1994b, 2008). The second species has been preliminarily associated with the species *Australopithecus prometheus*, the first Australopithecus species named by Dart (1948) from Makapansgat (Clarke 2008). The M4 deposit has also yielded the only fossil wood to be recovered from the site, providing a more conclusive indication of the environmental conditions during the deposition of at least some of the deposit (Bamford 1999). The M4 deposit is very large and represents a significant time span. Estimates for the accumulation time of the M4 deposit range from 500,000 years (Cooke 1974) to 600,000 years (R. Pickering & Kramers 2010). Although estimated depositional dates for M4 differ it is agreed that the deposit accumulated over a very long period of time, which presents significant difficulties when trying to identify deposit indicators. These difficulties, which are encountered in a number of Sterkfontein deposits, will be discussed in Section 2.5. Very long depositional times also create issues of time-averaging, especially when sampling in a non-stratigraphically sensitive fashion. Time-averaging influences all palaeoenvironmental and taphonomic interpretations and should be borne in mind (O'Regan & Reynolds 2009). Yielding any useful level of temporal resolution from time-averaged deposits is problematic. It is also difficult to assess deposit accumulation rates without suitable datable interstratifying flowstone formations.

M4 occupies the largest volume of the currently excavated Sterkfontein deposits and its stratigraphic boundaries are the subject of some debate. R. Pickering & Kramers (2010) have joined the M4 and M3 units together claiming that M3

represents a distal portion of M4. Wilkinson (1983) suggested that the M3-M4 boundary may represent a number of cones filling from a number of sediment sources and the contacts may be complex. Clarke's interpretation is different, claiming M4 has formed up against M3 with both members representing distinct depositional units that entered the cave system from different openings (Clarke 2006). Clarke's assessment of M3 and M4 support the suggestions of Partridge & Watt (1991), in that M3 represents a large, distinct deposit based on core samples BH3 and BH5. Cases can be made for all arguments, but without detailed analysis of M3 using a host of different disciplines, associations with other depositional units cannot be made.

The western boundaries of M4 at the contact with M5 have been made based on the presence or absence of certain taxa that are associated with different environments. In M4, the absence of stone tools, *Equus*, *Pedetes* and *Struthio* and the contrasting presence of fossil wood, *Parapapio, Colobus, Australopithecus* and other older more tropical faunal indicators common to the site have been used to identify the contact point of M4, M5 and the StW 53 infill (Kuman & Clarke 2000). Robinson (1962) identified a localised contamination of M5 with blocks of M4 breccia. The blocks of M4 sediment found within M5 are likely remnants of calcified M4 sediments that collapsed into eastern portion of the M5 area, prior to the opening and commencement of deposition of the M5 sediments.
Unfortunately, the M4 and M5 depositional indicators that are now used to suggest deposit boundaries have only been identified relatively recently. Early excavations, by Alun Hughes, in the western area of M4 did not concentrate on the stratigraphic boundaries of M4/M5, and because no obvious boundary could be seen, no potential contacts were noted. Fossils specimens are sourced to square and level (in feet and inches) accuracy with very little non-faunal data provided. This now provides a problem when attempting to provenance fossil remains excavated from the area between grid lines 49 through 65 and M through X. Attributing fossils to stratigraphic units based on stratigraphic extrapolation from current deposit exposures and other non-stratigraphically sensitive faunal material is not ideal.

A great deal of research has been carried out on the formation and accumulation of fauna of M4. The taxonomic list is extensive and suggests a predominantly closed environment of gallery forest prevailed, as indicated by large numbers of *Parapapio*, some *Cercopithecoides*, and *Makapania broomi* as well as taxa of antelope associated with more open woodland environments (Vrba 1976; Reed 1997; Luyt & Lee-Thorp 2003). There does seem to be some proximity to more open areas during the accumulation of the sediments based on the presence of some open environment species like *Antidorcas bondi* (Luyt & Lee-Thorp 2003). Member 4 has also yielded the only fossil wood, much of which has been identified as *Dichapetalum mombuttense*, a vine found to grow only on large well established trees found currently in tropical gallery forests of western and central Africa (Bamford 1999). Bamford (1999) suggests the wood indicates a "refugia of dense, humid forest-type vegetation occurred at Sterkfontein during the Pliocene" (Bamford 1999, pp. 231). The reconstruction of the M4 palaeoenvironment is complex and the time-averaging issues require consideration as localized or widespread sediment mixing can also mix interpretations based on faunal representation. The best way to describe the environment during the accumulation of much of the fauna is as a mosaic. The taphonomic work conducted by Kibii (2004) suggests a number of faunal accumulation agents have contributed to M4. Kibii (2004) identified the prevalent taphonomic accumulation agents as leopard (*Panthera pardus*), spotted hyaena (*Crocuta crocuta*) and death trap accumulations, as well as the contribution of bone entering the cave through slope wash. Some hominin specimens also seem to represent victims of a carnivore accumulator (T. Pickering *et al.* 2004b), although the small sample size precludes identification of a specific carnivore type. This is to be expected given the great time represented by the deposit, as well as the changing nature of the cave over time. The variety of taphonomic agents involved in the accumulation of fauna does provide problems when trying to identify taphonomic indicators specific to M4 fossils and correlating them to secondary deposits.

The StW 53 infill is regarded here as representing a late M4 infill (following Ogola 2009) closely preceding the deposition of M5 on the basis of an absence of

moist, closed environment taxonomic indicators, a lack of stone tools and dissimilarity in sedimentology to the M5 deposit. This issue is discussed in detail in Kuman & Clarke (2000).

2.4.2 Member 5 deposit

Member 5 has formed unconformably against the M4 talus in the western area of the type site and has been split into excavation areas, M5E (Member 5 East) and M5W (Member 5 West). M5W represents a more westerly extension excavated by Robinson (1962). Member 5 contains the only ESA (Earlier Stone Age) artefacts within the Sterkfontein system and is split stratigraphically into 2 infills, the M5 Oldowan and the M5 Early Acheulean. The M5 Oldowan is restricted to the lower levels (below 22 feet below datum) of the M5E deposit. The Member 5 Early Acheulean spreads across the upper levels (above 22 feet below datum) of M5E and into the M5W area. The Oldowan Infill has a few fragmentary fossils of *Paranthropus robustus* while the Early Acheulean tools are found in association with fragmentary fossils of *Homo ergaster* (Kuman & Clarke 2000). M5 contains three important faunal indicators of a more open savannah landscape, *Equus*, *Pedetes* and *Struthio* (Kuman & Clarke 2000). As discussed in the archaeology section, although the whole M5 deposit suggests a more open environment to M4, there are differences between the two M5 infills with a drier environment indicated in the Early Acheulean breccia than in the Oldowan sediments. Partridge suggested the substantial proportions of clay in the M5 Oldowan sediment indicate a more stable environment with less surface erosion than is seen in M4 (Tobias *et al.* 1993). The fauna from the Oldowan deposit also suggests a dryer environment than M4, but with the presence of some tree cover (Bishop *et al.* 1999). This change has been supported by isotopic analysis of teeth from the deposits. Research by Luyt (2001) and Luyt & Lee-Thorp (2003) found that the teeth of 40% of the faunal species sampled from the M5 Oldowan deposit were eating vegetation that was rich in C_4 carbon. Hence 40% of the faunal species sampled were living in more open grassland environments close enough to the cave openings to contribute significantly to the M5 deposit. The Early Acheulean

deposit has been accumulated during a more open environment than the M5 Oldowan with the fauna indicating an open wooded-grassland or open savannah (Vrba 1975; McKee 1991; Reed 1997). Taphonomic data indicates M5 Oldowan fauna was accumulated mostly via a death-trap scenario with an opening to the chamber high in the roof (T. Pickering 1999). This is a similar taphonomic pattern to that found in the Silberberg Grotto and can be considered a frequent accumulation process in the cradle cave sites (Cooke 1991). Figure 2.5 shows the latest interpretation of the surface exposed deposit distribution.



Figure 2.5 Present understanding of the horizontal spatial distribution of Members 4, 5 and StW 53 deposit as exposed in the current surface excavation. From Kuman & Clarke (2000).

2.4.3 Silberberg Grotto M2 deposit

The potential of the Silberberg Grotto deposit has been recognised for over thirty years (Tobias 1979). This potential was realised with the discovery of StW 573

(Clarke 1998) within the M2 talus deposit contained within the Silberberg Grotto. StW 573 provides an ideal opportunity for accurate interpretations of a nearly complete, articulated hominin specimen, found stratigraphically associated with autochthonous mammal species, and demonstrates clearly the preservation potential of cave deposits. Since the discovery of the StW 573 *Australopithecus* skeleton, much work has been done to place it in a firm stratigraphic, temporal and associative context. The most comprehensive stratigraphic interpretation can be found in Clarke (2006, 2008) (for an alternative interpretation see R. Pickering & Kramers 2010). The faunal analysis has taken the form of macro-faunal taxonomic representation (McKee 1996; Turner 1997; T. Pickering *et al.* 2004a) and taphonomic analysis (T. Pickering *et al.* 2004a). The taxonomic list produced in T. Pickering *et al.* (2004a) is the first to have been compiled from excavated fauna. Previous studies of M2 fauna were based on *ex situ* lime miner's rubble from the floor of the Silberberg Grotto, which was a mixture of M2 and M3 breccia. From this context came the remains of a partial face of a primitive hyaena *Chasmaporthetes silberbergi* (Broom 1945b; Broom & Schepers 1946). It should be noted that no deliberate sampling of the M3 deposit has been undertaken. The faunal analysis has been augmented by ongoing sedimentological analysis (Bruxelles & Clarke in prep) and trace element analysis (ICP-MS) (F. Thackeray *et al.* in progress), as well as the application of several absolute dating techniques (Partridge *et al.* 1999, 2003; Muzikar & Granger 2006; R. Pickering *et al.* 2006; Walker *et al.* 2006). Dating of the specimen remains contentious and estimates vary from 3.5Ma (Partridge *et al.* 2000, 2003) to 2.15Ma (Berger *et al.* 2002; for reply see Clarke 2002).

The newest work on the dating of the Silberberg deposits (R. Pickering & Kramers 2010), although useful, does not change the interpretation of the accumulation or history of the deposit. The M2 talus deposit has formed through the accumulation of sediment and fauna as it entered from a high aven-type opening in the roof of the chamber that was connected to the landscape surface.

The deposition of sediments formed a large talus deposit with two distinct sedimentary facies. The bone-rich breccia which contains the StW 573 specimen

(in this research called the M2 upper facies) is characterised by heavily calcified sediment with large proportions of variably sized dolomite and chert blocks. The intra-facies lateral faunal distribution pattern is due to the accumulation of mainly disarticulated, and some partially articulated, un-associated elements by water towards the eastern end of the talus (Clarke 2008). During excavation of the StW 573 specimen, faunal density increased with depth from a "noticeable near-absence of fossils" (Clarke 2008, pp. 444) around the StW 573 specimen. Clarke (2008) attributes the completeness of the skeleton, a state not shared by any other faunal specimens from the deposit, to the skeleton falling into the chamber close to the end of the deposition of sediments through this particular opening. The formation of a pure flowstone over the skeleton also facilitated the specimen's preservation. The M2 upper facies sediments seem to have been accumulated more steadily than the lower facies, perhaps due to an enlargement of the opening. At some time after the deposition of the StW 573 skeleton, the washing out of sediments below the skeleton caused part of the specimen to collapse into the available space (Clarke 2008). The gaps between the upper *in situ* and lower, collapsed skeleton, were filled with a flowstone (Clarke 2008). Modification of the Silberberg Grotto deposits through mining is extensive, and while the mining dumps have provided a considerable number of specimens, many fossils have potentially been lost through mining or collection by tourists (Broom 1945a, b).

T. Pickering's taphonomic interpretation of the M2 upper facies describes the entry of primates and carnivores - ("animals with climbing proclivities" (T. Pickering *et al*. 2004a, pp. 279)) - either by accident or intention into the cave, where they were then trapped and died. This is demonstrated by high numbers of primates and carnivores, large numbers of articulating skeletal elements, all skeletal elements represented and very low quantities of carnivore or pre-depositional modification. The palaeoenvironmental reconstruction based on the taxonomic representation suggests a riverine gallery forest with surrounding bushland and occasional open areas. The presence of *Panthera pardus* and *Alcelaphini* suggest the possibility of standing water nearby, most likely at the bottom of the valley. T. Pickering does, however, caution against the soundness of

environmental reconstructions based on taxonomically biased accumulations (T. Pickering *et al.* 2004a).

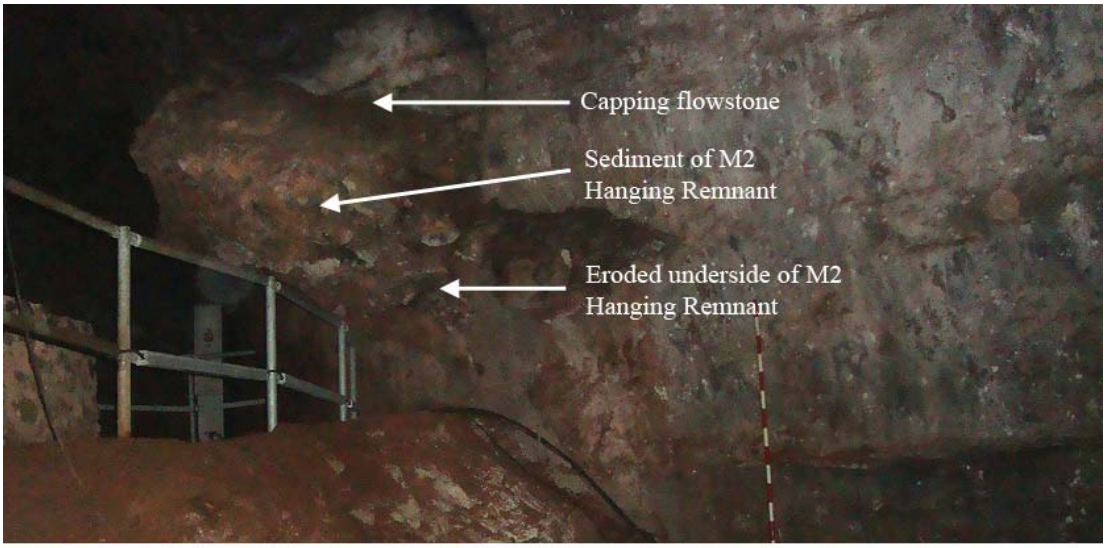
Beneath the M2 upper facies lays a bone-poor, loosely calcified talus with reddish sediment inter-bedded with many calcite layers and dark-brown calcified mudstone layers. These sediments are referred to in this research the M2 lower facies. Deposition of the earlier sediments seems to have been intervallic (periodically interrupted sedimentation) and Clarke suggests it formed prior to significant opening to the surface (Clarke 2006). Beneath this talus, lies the jumbled pile of collapsed roof blocks cemented with flowstone and the dark-sediment characteristic of Member 1 (M1).

The sediments that have formed the Silberberg Grotto M2 upper facies originally exited the Silberberg chamber in the upper reaches of the far eastern end of the Milner Hall as noted by Wilkinson (1983). Wilkinson (1983) originally described the sediments cemented to the southern wall of the eastern Milner Hall as "the original surface of the cone [that can be traced northwards from the Grotto into the eastern end of Gallery A in the tourist Cave (now known as the Milner Hall)] preserved as a hard flowstone carapace" (pp. 524). The remnants of the sediments exiting the Silberberg Grotto can be found cemented to the walls and ceiling in the eastern Milner Hall and are referred to as the M2 Hanging Remnant in this research. The entire roof of the far eastern Milner Hall is covered in breccia cemented by the flowstone that can be stratigraphically associated to that covering the StW 573 skeleton. These exiting sediments are important to the reconstruction of the depositional history of this part of the caves and so are described in detail. They are particularly important because of their relationship with the MH1 T3 deposit. The M2 Hanging Remnant preserves the upper levels and flowstone capped talus surface of the original medial portion of the M2 upper facies exiting the Silberberg Grotto. Wilkinson continues to describe the deposit lying beneath the M2 Hanging Remnant (the MH1 talus and location for the MH1 excavation) as:

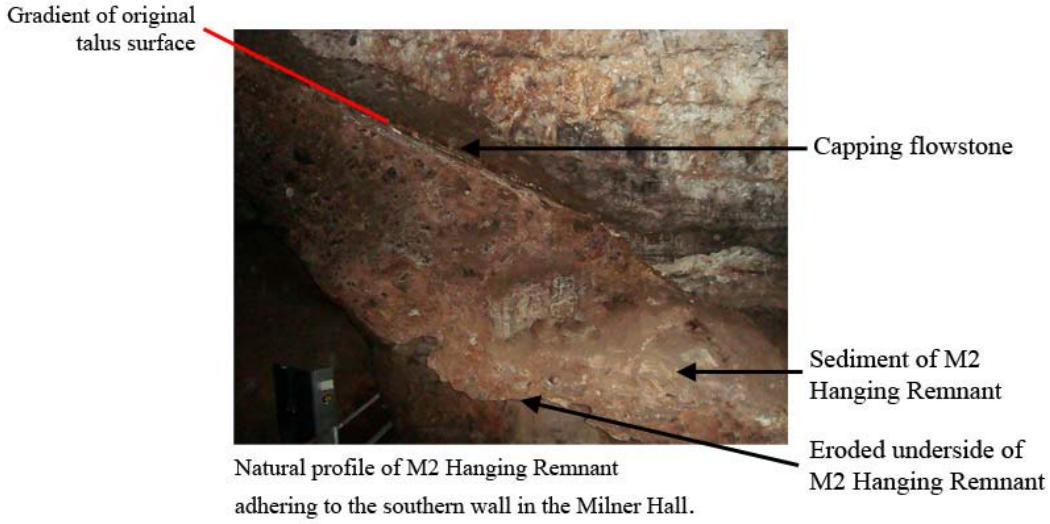
"a large cone of younger, unconsolidated, externally derived material [that] *debouches into gallery A, evidently from the same entry shaft as sections of the*

older remnant. Its surface slope is therefore analogous in dip and direction to that of the remnant. This younger cone extends down onto the east end floor of gallery A ten metres below the older cone remnants. There is little doubt that the cemented remnants are the upper parts of an older debris cone which also rested on the floor of gallery A, of proportions similar to those of the younger cone. That the mid-upper level Silberberg Grotto deposits once extended down to the lowest levels at this point in the cave system, seems inescapable." (pp. 525).

Although Wilkinson's initial assessment of this area is fairly accurate, the intricacies of the stratigraphy are significantly more complex as will be proven in the analyses of these deposits. The "cone of younger material" actually represents sediments deriving from a different entry point and will be described later. Sedimentologically, the M2 Hanging Remnant correlates closely to the StW 573 deposit M2 upper facies, characterised by heavily calcified matrix with a large proportion of jumbled variably sized non-decayed dolomite and chert blocks. Faunal material is present but in lower frequency than has been found during the excavation of StW 573. No fauna has been removed from the M2 Hanging Remnant to date. No evidence of the M2 lower facies or the M1 material, identified in the Silberberg, can be found in the M2 Hanging Remnant sediments. The underside of the M2 Hanging Remnant displays clear signs of water erosion and many of the protruding clasts on the underside of the remnant show decay indicative of exposure to water. It is apparent that the majority of the M2 upper facies deposit, which exited the Silberberg Grotto and filled into the eastern Milner Hall, has been undercut by extensive water erosion, leaving just the heavily calcified remnants adhering to the walls and ceiling of the eastern Milner Hall, and a portion below the capping flowstone (the M2 Hanging Remnant). Figure 2.6 shows a part of the M2 Hanging Remnant adhering to the southern wall.



South western aspect of the far eastern Milner Hall. The tourist route (indicated by barrier), runs along the top of T1 and under the M2 Hanging Remnant seen in the centre of the picture adhering to the southern wall.



Natural profile of M2 Hanging Remnant adhering to the southern wall in the Milner Hall.

Figure 2.6 The M2 Hanging Remnant. Notice the sediment flow trend in the upper picture as the deposit formed along the southern wall. The same tourist barrier seen in the upper picture can be seen in the bottom left corner of the bottom picture along with the electrical box. To the left of both pictures lies the Name Chamber Far Western Talus. The STK-MH1 excavation lies down slope to the right of both pictures. The range staff segments measure 10cm.

2.4.4 Name Chamber deposits

The most recent work conducted on the Name Chamber was by Stratford (2008). The research utilised stratigraphic, archaeological and microfauna analyses to decipher the formation history of the deposits found within and exiting the Name Chamber. A detailed account of the stratigraphic and archaeological findings can be found in Stratford *et al.* (in prep), for the interpretation of the microfauna analyses refer to Avery *et al.* (2010). Below brief overview has been given of the deposits that can be found in the Name Chamber. Figure 2.7 shows a schematic plan of the extent and location of the current relevant underground deposits, including the Name Chamber (blue outline). The arrows show the dominant sediment flow patterns. The externally derived deposits within the Name Chamber contain sediments from recognised surface deposits. The presence of archaeological material and the comparative analysis of the microfauna indicates the majority of the sediments derived from M5E. Minor contributions from other areas of the surface exposed deposits cannot be ruled out. The specific formation processes that formed the Name Chamber deposits are complex. Essentially, it can be described as a multi-phase re-deposition of sediments from an upper chamber into three areas of a lower chamber, through a long articulating vertical shaft (the Feeding Shaft) during and after the formation of the upper deposits.

The deposits can be separated into three sediment accumulation events. The first accumulation was that of M1 material, characterised by an ungraded mass of dolomite and chert blocks, jumbled and calcified within a matrix of fine, manganese-rich sediment with an absence of fossil material. This is typical of internally derived sediments formed during the early vadose period and prior to any major opening to the surface. Remnants of M1 can be found in all of the subterranean chambers (Clarke 2006).

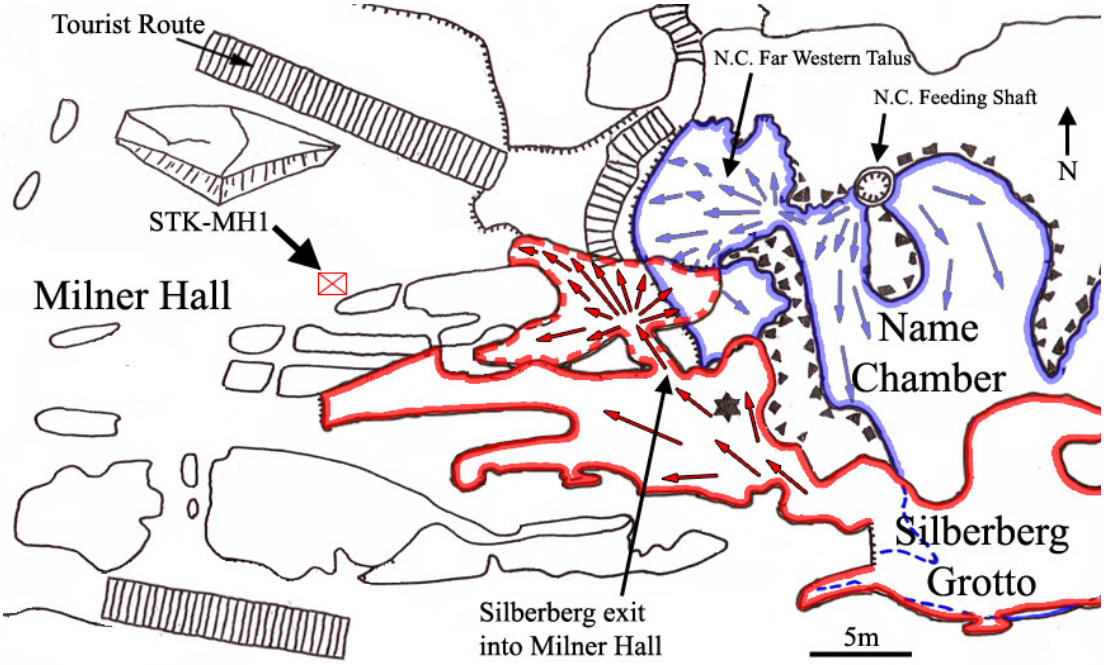


Figure 2.7 Schematic plan of the Sterkfontein central underground area and positions of relevant chambers. The red line represents the outline of the current M2 Silberberg Grotto deposits. The red dashed line represents the extent and location of the M2 Hanging Remnant exiting the Silberberg into the Milner Hall. The blue line represents the outline of the current Name Chamber (N.C.) deposits. The respective arrows represent the sediment flow patterns in the deposits. The star represents the location of the StW 573 specimen. Adjusted from Martini *et al.* (2003).

The second deposit, named the Older Brecciated deposit, was accumulated subsequent to the decalcification and erosion of the majority of the M1 material. This deposit has not been sampled as it remains at the heart of the Name Chamber talus and has not been reached by current excavations. Remnants of the deposit can be seen preserved on the walls and ceiling at the highest infill level of the deposit where it is cemented by a thick flowstone. The deposit is characterised by colluvially sorted, unconsolidated, coarse red sediment, bedded at approximately 35° with thick horizons (20-30cm) of randomly orientated, unsorted blocks of dolomite, chert and fragmented flowstone (≤100mm maximum dimension). Occasional blocks of more consolidated breccia are also found. The sediments are rich in both micro and macro fauna fossils, but unfortunately an adequate analytical sample could not be recovered from the available exposures. This

deposit probably formed from the rapid re-deposition of pre- or early M4 material through the Feeding Shaft when it opened at a pre-M5 time period. It is likely that large quantities of earlier material lie at the base of the Name Chamber talus. A thick flowstone then developed on top of the Old Brecciated deposit, indicating a hiatus in sedimentation before a significant portion of the deposit was eroded away to lower levels of the cave. This process left room for the deposition of the sediments that currently fill the chamber.

The final deposit, called the Younger 'Soft Deposit', has been accumulated more gradually through the Feeding Shaft. The sediments deposited during this phase of infilling originated in the lower levels of the M5E deposit, where the Feeding Shaft currently articulates with the surface deposits. The sediments of this deposit have not yet calcified, perhaps due to the consistent disturbance of the surface sediments, and an absence of calcareous precipitation in this chamber at this time. The changing internal structure of the shaft has influenced the size profile of particles deposited and led to the alternating distribution of sediments into the chamber, forming three talus deposits. Two of these talus deposits are contained within the Name Chamber. The most westerly (named the Far Western Talus (FWT)) exits the Name Chamber, just under the Feeding Shaft opening, flowing directly into the far eastern Milner Hall. A finely stratified profile of the Far Western Talus is found within the eastern end of the Milner Hall that derives from the Name Chamber. The Far Western Talus is most pertinent to this study as it has contributed to the confluence of the underground central deposit area (indicated in Figure 2.7). The alternating sediment filtration processes active in the Feeding Shaft are demonstrated by the particle size profile of the accumulated sediments. When the sediments were being deposited into the eastern part of the Name Chamber, larger particles≥100mm) were deposited due to a lower degree of filtration acting upon those sediments. Conversely, when sedimentation occurred within the western portion of the Name Chamber (and into the eastern Milner Hall) higher degrees of filtration within the Feeding Shaft restricted the particle size to <50mm.

The excavation of Oldowan material from the Name Chamber indicates a definite relationship with the M5E deposit and suggests the Name Chamber received sediments from this area during the formation and before the calcification of M5E. This re-sedimentation has led to the preferential deposition or winnowing of the smallest component (<20mm) of the archaeological material from the Oldowan-bearing M5E deposit into the Name Chamber. Significant similarities can be seen between the excavated Name Chamber artefacts and the M5E Oldowan in terms of raw material proportions, flake proportions and reduction strategy. This association is corroborated by the analysis of the microfauna by Avery *et al.* (2010) who found strong correlations between the microfauna taxa within the Name Chamber and the M5E Oldowan.

2.4.5 Lincoln Cave

The upper deposits exposed in the Lincoln Cave represent a mix of sediments from two sources and accumulation agents. Reynolds *et al.* (2007) describe two infills within the westerly portion of the cave system. Uranium series dating of the speleothems has placed the maximum age of the deposits at 265ka and yet the sediments certainly contain fauna and artefacts significantly older than the date given. The issues recently highlighted regarding the differences between filling and capping flowstones may necessitate a re-assessment of the speleothems in the Lincoln Cave. If the speleothem dates are accurate, the representation of older fauna indicates sediment mixing has significantly influenced the sediments. The presence of water-dependant taxa, particularly hippopotamus (*Hippopotamus amphibius*), indicates a significantly wetter environment in the later Pleistocene around Sterkfontein, a condition not found at any other point during the Sterkfontein deposition. Mixing of larger carnivore fossils (e.g. *Dinofelis barlowi*), Early Acheulean artefacts, *Homo ergaster* with MSA artefacts, and later taxa, has been interpreted as representing cycles of erosion and movement of material from the nearby M5W deposit through the L/63 area into the Lincoln Cave. The material that did not move through this area into the Lincoln Cave was washed in from a localised catchment area around the cave opening. The presence

of *Crocuta crocuta* may indicate a shallow cave entrance capable of sustaining denning activities. Reynolds has suggested that the Member 6 deposit (M6) in the Sterkfontein cave (accumulating in the L/63 area) and the later Lincoln Cave sediments were accumulated contemporaneously, while the proximity of the openings may have aided in the similarity of sediments, artefacts and fauna deposited (Reynolds *et al.* 2007). The deposits beneath the sediments sampled by Reynolds *et al*. (2007) are difficult to associate within the Sterkfontein stratigraphic sequence as they have not been sampled. In terms of relative spatial position to the Sterkfontein subterranean system, the Lincoln cave stretches from just above the Milner Hall, west to a position almost over the current lake. It is possible that the deepest sediments of the Lincoln Cave may have contributed to the Milner Hall deposits, although openings and routes for sediment movement have not yet been discovered.

2.5 Stratigraphic Complications Relating to Cave Deposits

The variability in deposit structure, history and properties, creates the potential for developing misleading interpretations of the associations and contexts of fossil and artefact material. Focus on one facet of a deposit with limited consideration of any of the highlighted complexities will unfortunately lead to inaccurate interpretations of fossil context. The problems surrounding the interpretation of the fossil deposits at Sterkfontein revolve around a lack of understanding and quantification of the processes influencing deposit development and post-depositional modification of sediments. These factors are paramount to the accurate placement of fauna and artefacts into respective stratigraphically secure facies. By ensuring the stratigraphic integrity of the material evidence, accurate interpretations and hypotheses can be tested regarding the primary contexts and associations of fossil species.

The complexities of Sterkfontein stratigraphy are demonstrated by the number of interpretations and refinements to the Sterkfontein site formation over the years (Cooke 1938; Brain 1958; Robinson 1962; Wilkinson 1973; Partridge 1978;

Partridge & Watt 1991; Clarke 1994a, 2006; R. Pickering & Kramers 2010). Each study has proposed a progressively more complex scenario than the preceding interpretation. The exception is R. Pickering & Kramers (2010) who attempted to simplify the member system through the identification of lateral margins of deposits and apply uranium series dates to those deposits. Previous stratigraphic investigations have sought to identify different macro-scale depositional units and place those units into a relative infilling chronology to provide a relative temporal context to the fossils found within them. This has been done largely through observation of deposit trends in terms of fossil taxa, artefacts and sediment properties from relatively small exposures, a practice which produces issues of representativeness of sample size in deposits of unknown size and distribution. Harris (Harris 1979a, b), originally warned of the dangers of recognition of strata exclusively through its contents instead of the dedicated study of the strata itself.

The deep and spatially widespread nature of the Sterkfontein deposits has provided many problems to the identification of deposit boundaries, which creates an obvious problem when determining spatial or temporal relationships. Member 4 for example, has been securely placed within the surface deposit stratigraphy as preceding M5 and M6, but the vertical boundary is not clear and its relationship with M3 remains to be clarified. As studies have progressed, the major depositional units have been split into increasing numbers of sub-deposits as more attention is given to the intra-deposit patterns. These sub-deposits (essentially depositional facies), are usually based on faunal content and sediment properties, the lateral and vertical margins of which are also unknown and identified from limited lateral or vertical exposures. Deposits can vary greatly laterally and vertically in terms of lithology, particle size distribution, sediment grading levels and type, fossil concentrations, fossil preservation levels, and fossil element distribution. The above factors are determined by the sediment source shape, taphonomy, receptacle morphology, deposit development patterns, diagenic processes and post-depositional sediment movement.

The objective of determining deposit boundaries on a macro-deposit scale may eventually produce an absolute chronology for the macro-depositional history.

This is however, somewhat secondary to the investigation of inter and intra-deposit stratigraphy. The goal of a stratigraphic interpretation of a deposit should be the identification of the processes involved in accumulation of all deposited components. This includes the identification of patterns and processes of development, modification of sediments and the extent to which these processes influence all components of the deposit in question. Together with identification and quantification of sediment mixing, identification of which is of the highest importance when attempting to attain accurate contextual information for hominin remains.

The member system as it is currently applied to the Sterkfontein formation, identifies depositional units based upon relative position and sediment source. The member system considers each deposit as a fixed entity formed from the deposition of sediment either through a different opening or at a different time to the other units. Generally, the more accessible, heavily calcified, surface exposed deposits have a more secure stratigraphic position. The surface exposed deposits, M4, M5 and M6 have all filled into different areas of an upper chamber from different openings in a roughly sequential order. M5 and M6 have both filled partially into erosion spaces formed in the western end of the large M4 deposit (Kuman & Clarke 2000; Ogola 2009). M6 has filled a smaller erosion cavity between M5E and M5W and some space remaining between the M5 capping flowstone and the cave roof (Ogola 2009).

In contrast, the underground deposits, with the exception of the Silberberg Grotto deposits, have largely been ignored, or considered as un-related to the main infilling history. M2 and M3 have unknown sources but have filled deeper portions of the cave beneath M4 and so have been presumed to precede the deposition of M4. Member 2 has received a great deal of attention and through bio-stratigraphic analysis is considered to have formed preceding the deposition of M4 (Clarke 2002). As mentioned in the geological background, the closed network of passages with occasional chambers that characterise the lower galleries is dissimilar to the upper gallery, which is represented by a single vertically and laterally expansive chamber (the M2, M3, M4, M5, M6 receptacle).

This dissimilarity affects the depositional processes as sediments move deeper into the cave.

The factors contributing to the stratigraphic complexities recognised in cave deposits can be regarded in two ways, at the deposit formation level and at the deposit interpretation level.

2.5.1 Formation complications

Formation level complications include all formation processes acting upon deposits, including the sediments, artefacts and faunal remains. I have classified formation level complications by separating them into primary and secondary sedimentation processes.

A. Primary sedimentation describes the initial development of the deposit into its original receptacle prior to any major diagenic influences.
B. Secondary sedimentation describes the re-working or movement of sediments around the karst environment through collapse, erosion or both, in varying degrees and includes all diagenic processes.

It is important to note that the processes involved are spatially and temporally variable. Change and re-working of sediments is an endemic, ongoing process. The variable nature of the processes means that several transitional phases are possible between the primary sedimentation deposit and the sampled sediment body. The descriptions below cover the principal forms of the processes at work and demonstrate the factors to be considered in karst stratigraphic analysis. Sediment gravity flow processes which govern how sediments move and develop deposits are discussed in Section 2.6. Figure 2.8 illustrates the common influences on deposit formation and re-sedimentation, the details of which are discussed below.

The assemblages we find within primary sedimentation deposits have already been through many stages of modification. Clarke & Kietzke (1967) noted the modification stages of a taphonomic assemblage from the life assemblage,

through death, burial and fossilisation, to the point at which it is excavated. The excavated assemblage, even in primary contexts, has been through many episodes of modification from the original life assemblage representative of the ecology. Gifford (1981) described a similar but more theoretical process of 'element transformation' from the anatomical context through eleven steps to the observational data. Between the fluvial contexts of east Africa and the karst contexts of South Africa the palaeoanthropological assemblages have been through many modifications over their accumulation, dispersal and fossilisation before a minute assemblage is excavated. In karst systems these modifications are complicated more so by re-sedimentation and distribution around the karst environment, modifying the primary context characteristics and reducing the integrity of the assemblage even more so.

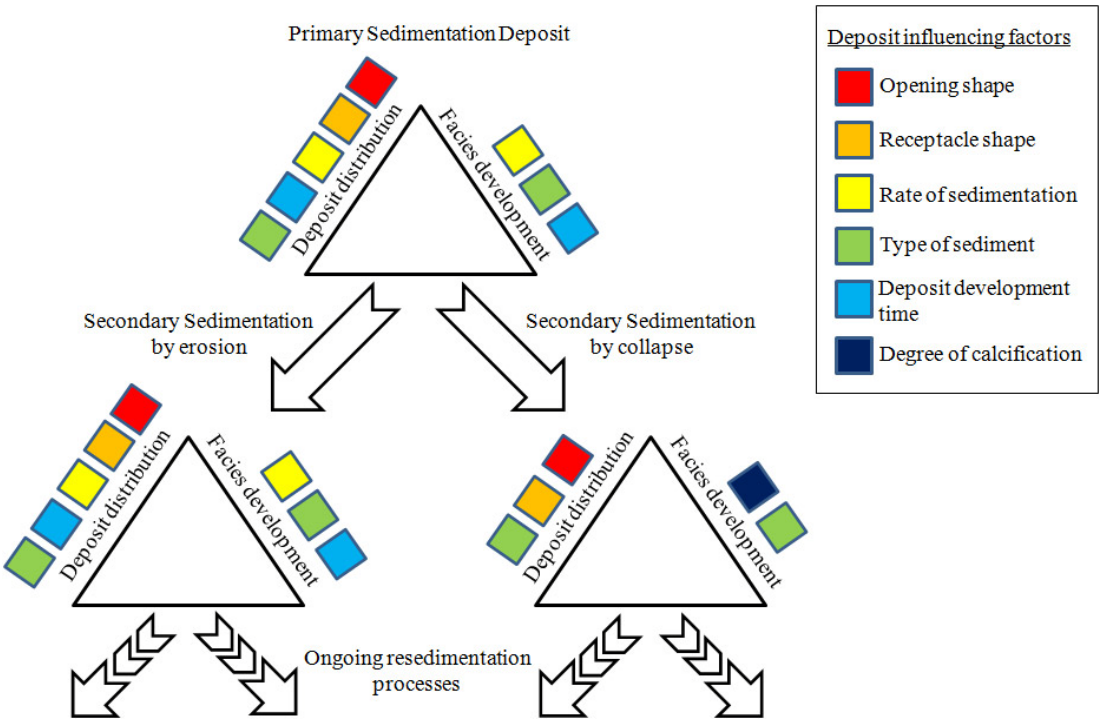


Figure 2.8 Common influences on the development of primary and secondary sedimentation cave deposits as discussed in the text. The two lower taluses represent the influences affecting deposits redistributed either by collapse or erosion.

Primary Sedimentation

The processes involved in the development of primary sedimentation deposits are influenced by a number of factors. These include: shape of the opening and the receptacle; sediment properties; rate of sedimentation and deposit development time. Below I have described the major factors influencing the development of a primary sedimentation deposit.

1. Opening shape: Throughout the development of a deposit, changes in opening shape can change the characteristics of the deposit. For instance, an opening that starts as an aperture in the roof high above the cave floor develops a talus cone shape with sediments radiating in all directions from the central accumulation point. The proximal area is characterised by a vertically ungraded mix of fallen roof blocks showing poor to slight longitudinal grading towards the distal margins. Interstitial gaps are common in proximal portions and these voids allow sediment to filter through the deposit, or speleothem forms to infiltrate the deposit. The proximal portions may have similar characteristics to rock-fall deposits (Bertran & Texier 1999). The distal portions may preserve stratified, graded sediments. Figure 2.9 shows a typical talus deposit accumulated under a high opening, several of the features identified in the text are indicated. Openings which facilitate long drop distances of particles will often produce high bone breakage proportions, due to the drop and due to crushing from following clastic material. As the deposit reaches near the roof, the opening shape may develop into a shallow passage such as is used by hyaenas for denning. This would produce a very different deposit, characterised by much finer stratified sediments, forming in a fan or tongue shape and building in a longitudinal direction. Tongue-shaped deposits often produce a high degree of longitudinal grading due to low sediment transport energies. As the fan or tongue-shaped deposit builds, the sediment flow direction may vary as it builds over previous lateral margins. Figure 2.10 demonstrates the movement of a developing tongue-shaped deposit. Multiple episodes of development into a single receptacle can occur within a primary or secondary sedimentation process. Notice that the culmination of the tongue-

shaped episodes creates a deposit that may be interpreted as a single infilling episode when internal stratigraphy is not considered.

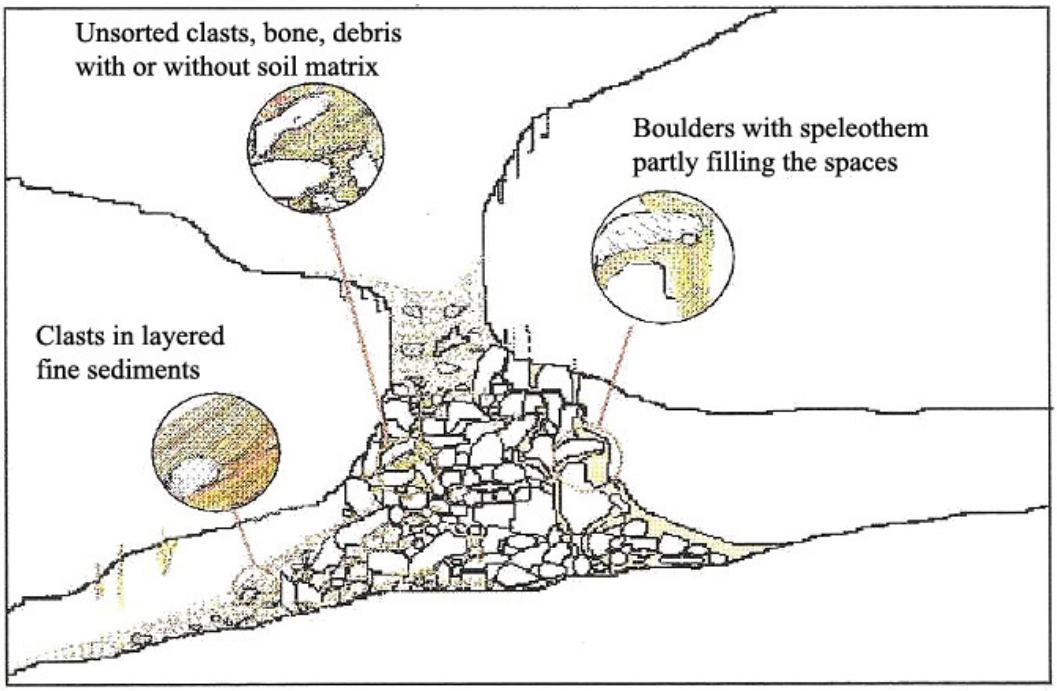


Figure 2.9 A typical talus deposit formed under a vertical opening. From Latham (1999).

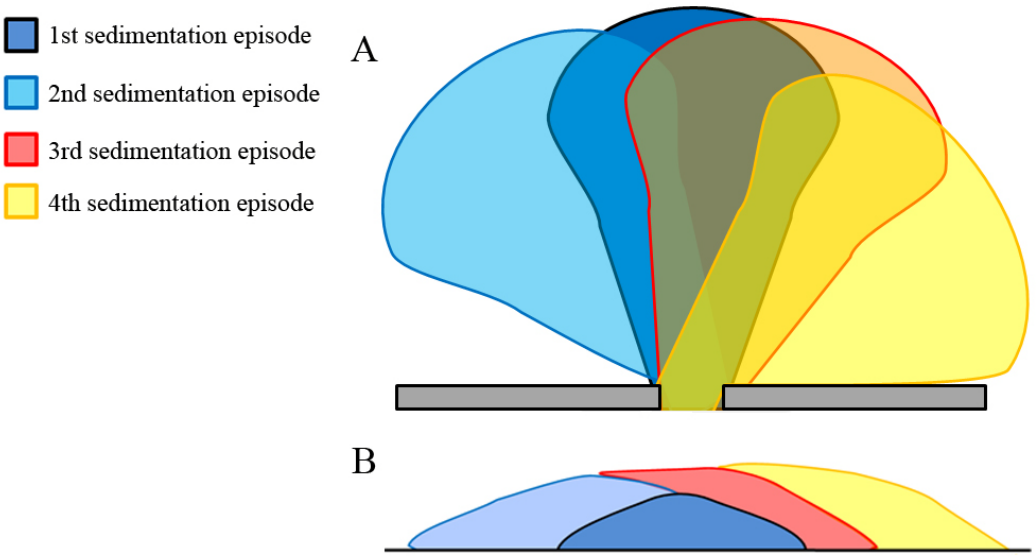


Figure 2.10 Schematic diagram illustrating the movement of a fan or tongue-shaped deposit during development and through progressive infilling events or sedimentation episodes. A, represents the plan aspect of the fan. B, represents the cross-section of the deposit snout. Each episode accumulates sediment that changes the receptacle topography thereby changing the morphology and direction of subsequent infilling episode.

2. Receptacle shape: Also described as the "topography of the depositional surface" (Kidwell *et al*. 1986, pp. 230). As Kidwell *et al*. (1986) point out; the receptacle shape is one of the most important factors in influencing the physical characteristics of the deposit. Essentially, the deposit morphology is defined by the shape of the receptacle into which the sediment accumulates. If the deposit is accumulated into a passage then sediment flow direction is restricted and travel distances may increase, affecting grading patterns and particle orientation. Receptacle shape can change in terms of dimensions and topography. Topography of the receptacle floors and walls is highly influenced by the geology of the cave system and morphology of any previous infills or erosion regimes. Major (1997), conducted a number of large flume experiments documenting this process.

3. Sediment properties: The sediments encountered in caves can vary in properties hugely, from unconsolidated aeolian sediments or colluvially accumulated allogenic (externally derived) and authigenic (internally derived) clays, to jumbled, fractured and heavily calcified, clast-supported authigenic and

allogenic collapse material. Anthropogenic sediments and artefacts and biogenic material may enter the cave at any point in time, mixing with both the allogenic, naturally accumulating sediments from the surface, and authigenic sediments, creating a cornucopia of possible combinations. Finer sediments will have more chance of developing good grading systems with strong fabric data and preserved stratigraphic horizons. Conversely, coarse sediments will often be poorly orientated with large interstitial voids and show poor grading patterns or develop post-depositional inverse grading patterns. Water content can influence grading processes and sediment travel distances. High water content within a fine matrix can create a hyperconcentrated flow with identifiable inversely graded horizons (Bertran *et al.* 1997; Bertran & Texier 1999). Accumulations of coarser sediments will frequently produce higher bone breakage levels. Sediments can be graded both horizontally and longitudinally. As a general rule, there is a drop in particle size with distance from source. Brain (1958) described two particle size profiles to determine mixed internally and externally derived sediments (Phase I) from the unmixed externally derived sediments (Phase II) (Table 2.3). He did not, however, consider sediment flow distance and the longitudinal grading possible in larger deposits.

	Phase I	Phase II
Clay	22.1	5.2
Silt	38.9	29.5
Fine sand	12.7	20.6
Sand	15.9	20.4
Coarse sand	8.3	13.6
Fine gravel	2.5	10.7

Table 2.3 Particle size profiles for Phase I and Phase II sediments as described by Brain (1958).

4. Rate of sediment deposition: Deposits that have been accumulated rapidly are often poorly graded, with weak particle orientation and often show little or no stratification. Depending on the particle size, large quantities of interstitial voids,

with a broad particle size range is a good indicator of quick deposition. Rapidly accumulated deposits are often unconsolidated and prone to post-depositional sediment settling and internal collapse. Post-depositional vertical movement of fauna and artefacts must be identified as associations and concentrations of material can develop that are not representative of the original primary context associations, and are intensely time-averaged. Speleothem may infiltrate the interstitial gaps and coat particles, a feature shown in Figure 2.9. In rapidly accumulated deposits, with similar clast proportions, bone breakage is much more prevalent. It should be noted that sediment properties and rate of sedimentation work in combination. Slow deposition can result in the formation of consolidated, stratified deposits with potentially well formed longitudinal and vertical grading and strong particle orientation. These deposits are less prone to post-depositional settling, and collapse is generally due to a radical change in the cave morphology or undercutting through erosion. The consolidated nature of the slowly accumulated primary sedimentation deposit allows more consistent calcification.

5. Deposit development time: The accumulation of the M4 deposit has been suggested to have taken as long as 500,000 to 600,000 years (Cooke 1974; R. Pickering & Kramers 2010). The accumulation of sediments over such a long period of time presents significant difficulties when trying to identify deposit indictors. Climate is perhaps the greatest factor influencing autochthonous taxa, rate of sedimentation, modes of fauna accumulation and pre-depositional bone surface modification. Climatic conditions may change significantly during the infilling of sediments through one opening, thereby contributing to differences within the same deposit. The representation of a number of climatic conditions within a single sediment body is common in the larger cave deposits. The variability of accumulated material within a single deposit can often produce misleading interpretations unless stratigraphically sensitive sampling is undertaken. Interpretive complications are discussed in Section 2.5.2.

Once the primary sedimentation has ceased due to a hiatus in deposition, calcification of the sediments may begin. Calcification may be sporadic and localised depending on the distribution of dripping $CaCO_3$ rich water, on the disturbance of surface sediments, and on the sedimentological properties of the

deposit. In ideal situations, the deposit is calcified and capped by a flowstone. Should sedimentation restart, the existing deposit is effectively sealed by the flowstone, allowing bracketing and potential dating of the contained deposits. Deposits with fine sediment surfaces can develop 'hard caps' which limits calcification of deeper areas of the deposit and promotes erosive undercutting at a later point (Latham 1999). The process of decalcification is as variable as the calcification process. Fresh water contacting the calcified sediments in various ways removes the $CaCO_3$ leaving 'soft' sediments which are easily eroded away. Sediment decalcification can affect entire deposits or spatially restricted areas of sediments. If the decalcified sediments are on the surface of the deposit then they can be eroded away, leaving a space for another generation of sediment accumulation. If the decalcified sediments are enclosed in the deposit then erosion may be delayed, leading to a deposit with isolated pockets of soft sediment within a harder surrounding breccia. When erosion of the decalcified sediments takes place, the spaces left are then liable to be filled by subsequently deposited sediments. When large quantities of fresh water are involved, such as in the rising of the water-table, speleothems can be re-dissolved and entire lower portions of deposits may be eroded away. It is worth noting that in cases where there is an absence of $CaCO_3$ rich water, calcification may not occur at all. In this case sediments will remain 'soft' and mineral uptake by bone may take longer. Modification of all components of a deposit through chemical alteration is regarded as diagenesis. Although work has been carried out on the diagenic modification of bone (Weiner *et al.* 1989; Hedges & Millard 1995; Sillen & Parkington 1996), the affects of diagenic change on artefacts remains limited.

Secondary Sedimentation

The onset of erosion of a primary sedimentation deposit can result in the distribution of sediments into a new space, lower in the cave system, or into a pre-existing void. Secondary sedimentation may affect sediments at any stage of diagenesis. There are two main secondary sedimentation processes. The first is the

re-distribution of sediments through collapse. The second is the re-distribution of sediments through erosion.

Collapse is an endemic process within dolomitic limestone karst systems (Brain 1981; Latham 1999). Where multiple galleries of chambers exist, as at Sterkfontein, the collapse of part of an upper chamber into a lower chamber or passage is common (Latham 1999). Collapse causes the instant re-distribution of part or all of a deposit to lower levels. Sediments can be in any stage of calcification, affecting the morphology and internal stratigraphy of the collapsed material in its new context. If the collapsed material is heavily calcified then non-graded, variably sized blocks of breccias mixed with the collapsed roof spall will be distributed in a limited fashion beneath the new opening. Collapse of partially or completely calcified material will often protect faunal material calcified within the blocks. In contrast if the collapsed material is 'soft' then the randomly orientated roof spall blocks will provide the core for a rapidly accumulated talus deposit. Secondary sedimentation deposits formed from collapse of 'soft' sediments will often take on characteristics similar to that of a rapidly formed primary sedimentation deposit. Receptacle characteristics will have a similar influence as is the case in primary sedimentation deposits.

Secondary sedimentation through erosion generally takes place on 'soft' sediments either prior to calcification or following decalcification and will move soft sediments in a predictable fashion, with the smallest particles moved first and furthest. Erosion of sediments can affect deposits on a localised or deposit-wide scale. Sediments will often first be affected by interaction with a fresh water source, with the movement of sediments facilitated by slope wash processes and gravitation. Secondary sedimentation deposits can often be affected more intensely by water than primary sedimentation deposits, given that sediments are deposited at progressively deeper levels of the cave with correspondingly increasing water contents. The strength of water flow or gradient of slope will determine the rate of sedimentation and the size of the particle moved. Ultimately, sediments may be deposited into a permanent water source. This is the suggested scenario for the Malapa site fossil-bearing sediments (Dirks *et al.* 2010). Deposits

accumulated by secondary sedimentation through erosion form similarly to primary sedimentation deposits, being affected by the same sediment gravity flow patterns and processual variables. These deposits can often create similar depositional facies as primary sedimentation deposits, as can be seen in the Name Chamber Far Western Talus (Stratford 2008). Indicators that may demonstrate the difference between a primary sedimentation deposit and secondary sedimentation formed through erosion may include: small blocks of breccia included within similarly sized dolomitic limestone and chert rock particles; exceptionally weathered bone; a high proportions of post-fossilisation bone breakage; host rock particles with speleothem coatings; broken speleothem particles, and sediments with higher $CaCO_3$ quantities than is found in non-calcified sediments.

The secondary sedimentation formation processes described above can take place in any order and be repeated many times before the deposit is investigated (Brain 1981). Inverted depositional sequences (older lying above younger) can be produced through repeated erosion episodes. Interactions between primary and secondary sedimentation deposits are exceptionally variable. Mixing and destroying of some of the available depositional indicators is to be expected. This further endorses the use of multidisciplinary approaches to maximise the recovery of associated information and produce accurate stratigraphic interpretations, which may allow the tracing of deposits and the reconstruction of primary stratigraphic associations.

2.5.2 Interpretative complications

The development of inaccurate interpretations is exacerbated further by inadequate sampling, unrecognised stratigraphic boundaries, unrecognised depositional indicators and practice of a single-discipline approach. Below, I have described a number of issues that influence interpretations of cave-derived palaeoanthropological material.

1. Sampling: In order for any accurate analysis to be made, a representative sample needs to be obtained. In the case of palaeoanthropological

material from Sterkfontein, most contextual data is taken from a collection of fossils excavated from *in situ* deposits, although on occasion *ex situ* deposits from lime miners dumps are processed. When most information is dependent on one type of evidence, sampling methods need to be carefully considered. Deposits within caves are rarely horizontally stratified and excavations need to be stratigraphically sensitive in order to provide a refined stratigraphic context prior to analysis. On a macro scale the problems compound, and sampling of multiple horizons may produce a variety of depositional, taphonomic and faunal indicators potentially producing unclear interpretations. Just as misleading is the sampling of only exposed or accessible sediments leading to the creation of deposit-wide interpretations. Excavation of seemingly massive deposits, like M4, where heavily calcified and 'soft' sediments are present in poorly stratified beds, ideally requires meticulous recording of sediments and provenance details to ensure stratigraphic patterns can be identified and stratigraphic integrity is ensured within the investigated assemblage. Due to the concrete-like nature of the calcified M4 sediments this has not been possible, and drilling has been the only way to extract faunal samples. Deposits vary vertically and longitudinally, affecting particle transport and deposition patterns. Skeletal elements act as geological particles in sediment gravity flow deposits (Frostick & Reid 1983) and are influenced by preferential transport. Sampling of proximal portions of a deposit may yield greater proportions of larger, less moveable skeletal elements thus influencing the taphonomic, palaeoenvironmental and possibly taxonomic interpretation if skeletal elements of smaller animals are moved away from the sample site.

2. Unrecognised depositional boundaries: Mixing of samples from different stratigraphic units is an obvious hazard when excavating through cave deposits with limited stratigraphic knowledge or observation. Associated deposits can be temporally distant, sometimes occurring in a stratigraphically inverted order, as well as having very different stratigraphic histories and associated fauna. It is possible that no obvious stratigraphic boundaries are visible between the deposits, leading to the assumption that they are a single depositional unit and inevitably to incorrect interpretations. In some cases sedimentological properties will indicate a facies or deposit 'boundary' where it is otherwise not visible.

Strategic particle size analysis may help identify internal stratigraphy. Unnoticed sediment displacement features may also produce inaccurate interpretations of taxonomic representation and assessment of faunal associations. Post-depositional movement and sediment displacement processes are common at Sterkfontein and they can cause the grouping of bones, artefacts and sediments from stratigraphically distinct facies.

3. Unrecognised depositional indicators: Stratigraphic indicators take the form of fossil breakage patterns, fossil condition, fossil shape and size, micro and macro fauna taxonomic representation and many sedimentological features. Deposits that are temporally and stratigraphically distinct may contain a suite of features that, when considered together, are diagnostic of a particular deposit. Many types of indicators form components of a number of disciplines but may not be recognised as stratigraphically important when considered in isolation. Sampling for all disciplines is integral to the identification and recognition of deposit-specific depositional trends.

4. Single discipline approach: The application of a single discipline to the investigation of a deposit has been a common practice at Sterkfontein. Generally, specialists concentrate on a particular field of expertise and trust that established stratigraphic interpretations are correct for the specific area of the site. This can produce significant problems both with the original analysis and with future analyses based upon that work. Deposit accumulation affects many aspects of the sediment contained within and all elements of a deposit act as geological particles enmeshed in a reactive depositional process. Looking at only one element of the deposit to interpret the convoluted depositional history is inappropriate.

2.6 Detailed Patterns of Formation Processes and Sediment Dynamics

This section will develop details from Section 2.5 with particular regard to the sedimentological processes that influence facies-level properties of deposits. The facies properties are of great importance for the identification of internal deposit structures and deposit boundaries. Facies properties represent complex products of

the deposit formation conditions. The formation conditions create patterns within the facies that can be identified and correlated with known sedimentological processes clarifying the histories of the deposit in question (Bertran & Texier 1999).

2.6.1 Sediment gravity flow dynamics

All deposits in the Sterkfontein system have been developed by the movement of sediments with varying properties through gravitation with differing influences of water. The development of colluvially accumulated sediments, known to as sediment gravity flows, creates slope deposits. Sediment gravity flow dynamics have received a great deal of attention from geologists and geographers and the processes of sediment movement remain the subject of much debate (Culling 1963; Lowe 1976, 1979, 1982; Albjar *et al*. 1979; Mills 1984; Akerman 1984; Costa 1984; Abrahams *et al.* 1985; Postma 1986; Abrahams *et al*. 1990; Mosher *et al.* 1994; Coussot & Meunier 1996; Bertran *et al.* 1997; Major 1997; Bertran & Texier 1999; Nemec & Kazanci 1999; Parsons *et al.* 2001; Obanawa & Matsukura 2006). Difficulties occur in the classification and terminology of different types of sediment gravity flow (for a review of conceptual problems see Dasgupta 2003). Some of the variables identified as affecting sediment gravity flow development include particle size profile, particle shape, water content, gradient of slope and height of sediment source. Betran & Texier (1999) do warn of the dangers of classifying sediment gravity flow types based on single variables, such as grading, as different parts of a single flow may produce different flow dynamics and resultant sedimentological characteristics. Major (1997) documents this variability within experimental debris flow deposits.

In this research, the terminology used follows Betran & Texier (1999). A table of slope formation process classification used in this research is illustrated below (Figure 2.11). For simplification purposes Bertran & Texier (1999) have classified each flow type as a product of sediment concentration and water content. Based on the above cited work and the geological and morphological context of the

Sterkfontein caves, three main types of sediment gravity flow are found: the hyperconcentrated flow; the grain flow; and the debris flow. Below, each type of flow is discussed and the characteristic fabric morphology is described from a number of researcher's works. The recognition and understanding of these characteristics are essential to any further analysis of deposits at Sterkfontein as they are potentially identifiable within the sedimentary facies analysed, provided adequate care is taken during excavation. It is important to remember that sediment gravity flows can inter-change between the three types during formation, based on the addition or removal of water or deposition of sediments of differing properties (Lowe 1982). Primary sedimentation facies are rarely preserved through secondary sedimentation processes. The degree of primary sedimentation facies preservation depends on the degree of calcification within the deposit during secondary sedimentation. In scenarios where more than one deposit is forming in the same area from multiple sources, accurate facies analysis and description, and fabric analysis, is vital.

<table>
<tr><td>Sediment concentration</td><td colspan="2">Low</td><td>Intermediate</td><td colspan="2">High</td></tr>
<tr><td>Main interstitial fluid</td><td>air</td><td>water</td><td>water + fines</td><td>air</td><td>water + fines</td></tr>
<tr><td rowspan="2">Process</td><td rowspan="2">Rockfall</td><td colspan="2">Runoff</td><td>Grain flow</td><td>Debris flow (liquefaction)</td></tr>
<tr><td>Streamflow</td><td>Hyperconcentrated Flow</td><td>Rock-avalanche (>103 m3)</td><td>Solifluction
Earth slide / flow (distinct sliding planes)</td></tr>
</table>

Figure 2.11 Classification of slope processes. From Bertran & Texier (1999).

Hyperconcentrated flows

A hyperconcentrated flow is a slurry-type mixture of water and mostly fine particles moved by gravity and a sediment saturating source of water, and is commonly found in cave deposits. The depositional morphology of a

hyperconcentrated flow is represented by a fan or tongue shape. Sediments may be transported further than grain or debris flows due to the higher water contents, creating an elongated front lobe (Major 1997). These flows often surge in the middle of the deposit, pushing material towards the lateral margins (Major 1997) (See Figure 2.10 for illustration of development model of fan or tongue-shaped deposits). Orientations of clasts are generally parallel to the flow direction in the central flow area. Depending on the grain size, hyperconcentrated flows can develop into faintly bedded thick cone deposits and regularly show inverse grading[1] (Bertran & Texier 1999). In deposits that have travelled greater distances, coarse particles travel more slowly creating more pronounced inverse grading systems and longitudinal sorting (Hand 1997). Lowe called these deposits "liquefied flows" describing them as grain-supported beds of laminar suspensions, with high proportions of fine sand and coarse silt (Lowe 1982, pp.280). These flows can often show water escape structures and post-depositional water erosion (Lowe 1982).

Grain flows

Bertran & Texier (1999) describe grain flows as flows of debris forming on steep talus slopes with little or no water presence. Grain flows can develop in many environmental conditions, altitudes and rheolological properties (for examples see Bones 1973; Albjar *et al*. 1979; Write & Anderson 1982; Abrahams *et al.* 1990; Sass & Krautblatter 2007; Parsons *et al.* 2001). Grain flows are perhaps the most well researched type of flow and represents the majority of deposit forms at Sterkfontein. In caves, regular introduction of enough water to mobilise sediments is rare, and most water in the caves is introduced via dripping from the ceiling. Grain flows develop through "the overloading and over-steepening at the talus apex by abundant debris supply" (Bertran *et al.* 1997, pp. 44). Grain flow deposits

[1] Inverse grading systems can be produced through depositional of post-depositional process and refers to the relative position of differently sized particles within a sediment body. In regularly graded sediments, the larger particles will be at the bottom of the deposit and particles will 'fine upwards'. In inversely graded deposits the opposite will be seen and the larger particles will be found in the upper levels of the deposit, suspended by progressively finer particles, it is also referred to as 'fining downwards'.

are characterised by stratified infills with high levels of clast imbrication and slope and flow direction parallel orientations (Hétu *et al.* 1995; Bertran *et al.* 1997). Grain flows often develop in surges of material, pushing previous material to the lateral margins and creating beds of inversely graded, well stratified deposits (Major 1997). These are often more intensely longitudinally graded and can have a larger collection of clasts at the snout (Parsons *et al.* 2001). The dry nature of the grain flow also often leaves interstitial voids between larger clasts. There is often a basal layer of large clasts which facilitate the suspension of the finer grained sediments. Grain flow deposits are often inversely graded due to post-depositional filtering of sediments to the base (Bertran & Texier 1999). Figure 2.12 presents an example of the microstructure of a grain flow deposit. The insert of Figure 2.12 shows a silt sand layer (black horizon) that has accumulated post-depositionally at the base of the grain flow strata.

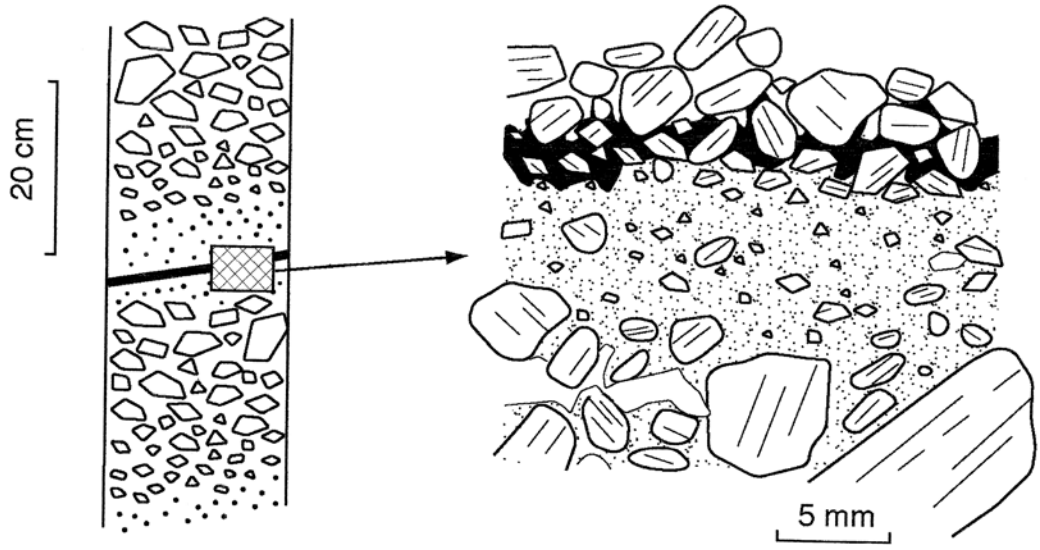


Figure 2.12 Microstructure of the basal sole of a grain flow deposit in Belesten, France. Dots correspond to the basal silty sand layer and black areas correspond to post-depositional silt accumulations (from Bertran & Texier 1999).

Debris Flows

A debris flow can be described essentially as a flow of sediments with a broad range of particle sizes in water that forms a tongue, fan or cone-shaped deposit. The inclusion of large clasts differentiates it from a hyperconcentrated flow and the presence of water differentiates it from the dry grain flow deposit (Bertran & Texier 1999). Debris flow deposits are usually crudely stratified with poorly orientated clasts. Stronger orientations are found in the lateral margins and frontal lobes of the deposit. Debris flow fabric is often characterised by coarse openwork lenses and is generally poorly sorted, with larger clasts potentially found within fine-grained matrix (Lowe 1982). Many debris flow deposits show a maximum dimension for supported large clasts, indicating that larger clasts settled to the bed of the deposit during deposition (Lowe 1982). As little as 5% water concentration can effectively create a debris flow with many angular clasts sliding down slope. Due to water content, debris flows have few and small interstitial pockets and can show either regularly graded, ungraded or inversely graded beds. Facies can look similar to those of a hyperconcentrated flow although a broader range of particle sizes is an indicator of a debris flow deposit (Lowe 1982). In the caves, debris flows are common but may be spatially localised due to isolated or localised flowing water sources.

2.7 Summary

The information in the first half of this chapter presented a synopsis of the history and geological context of the Sterkfontein site. The geological context has provided an interesting mix of influences over chamber formation and surface opening shape that have enabled a wide variety of sediment deposition processes and faunal accumulation agents to be active (Brain 1958; Brain 1981). This variety of processes, coupled with the time scales involved in accumulation, significantly complicates the contextual interpretation of the fossil and archaeological material. This research, along with past investigations, strives to

use the information preserved to identify both the formative processes and the original contextual indicators that provide valuable information for the study of the hominin and associated animal fossils. The second half of the chapter addressed the formation processes that influence the properties of the sediments as they are accumulated for the first time (primary sedimentation) and then when those sediments are moved around the cave environments through erosion or collapse (secondary sedimentation). The diagenic processes influencing the sediments and faunal material were also addressed. The number and variability of these processes makes the detailed examination of cave deposits absolutely necessary in order to identify and quantify the modification of those sediments from the pre-depositional condition through to the excavated assemblage. Within the processes discussed above, there are a number of poorly understood but potentially significant aspects particular to fossil-bearing cave sediments that should be addressed. For example, how do differing levels of element breakage influence element shape, and therefore transport potential? The multi-disciplinary approach to the data yielded from this research has allowed a number of those questions to be partially explored and are presented in Chapter 4. Chapter 3 presents the methodological framework utilised in the excavation and analysis of the focus deposits.

CHAPTER 3 METHODOLOGY

The methodological approaches discussed here include excavation, stratigraphy, sedimentology, fabric analysis, faunal analysis (including taxonomic and taphonomic analysis). All methods are consistent with the contemporary literature on each of the relevant disciplines. The multidisciplinary nature of the research conducted requires a basic description of the methodological approaches that have been established for each of the disciplines utilised.

Sedimentological analysis included particle size distribution, sediment colour (Munsell), sediment hydrology and chemical analysis (XRF). Facies, horizon and spot samples were carefully taken throughout excavation and analysed in order to establish inter- and intra-facies patterns. Fabric analysis methods used orientation, dip, particle shape, size and distribution to infer formation history. Natural clasts and skeletal elements were used as sedimentary particles (as used by Frostick & Reid 1983, Kidwell *et al.* 1986). Faunal analysis included taxonomic representation, which was supplemented by taphonomic information based on: skeletal element representation; bone breakage patterns; bone shape; bone dispersal patterns; and bone surface modification, all of which were all analysed either *in situ* or in the lab. A number of the terms used in this research have different nuances in different fields so a basic glossary is provided below. The terms below are taken from sedimentological or geological sources.

Fabric: The orientation of a particle of rock in a sediment or sedimentary rock (Longwell *et al*. 1969). The fabric can also be described as the geometric and spatial configuration of all elements within a specific facies.

Facies: A sedimentological unit of analysis within a deposit. A facies is characterised by a distinct set of sediment properties not shared by other parts of the deposit(s) or talus (Longwell *et al*. 1969). A facies can occur more than once within a deposit or talus when analogous depositional processes are prevalent. Facies can also represent features that are not

formed in the expected fashion, e.g. faulting cracks, causing the abrupt vertical displacement of a particular sediment type.

Clast: An individual piece of allogenic or authigenic rock (i.e. externally or internally derived). In the case of the Sterkfontein cave system clasts of dolomitic limestone and chert are often found within deposits. In clast-supported sediments, most individual clasts are in contact with each other.

Density: Density can be defined in two ways. As a degree of compactness of a substance, or as a number of objects in a given volume (Soanes & Stevenson, OED). Faunal analysis utilises the former definition to refer to the specific density of bone, which relates to the survivorship of different parts of bone through decomposition and deposition (Lyman 1984). Sedimentology utilises the latter definition to refer to the number of particles within a volume of sedimentary rock or deposit. To avoid confusion between disciplines, in this thesis density refers to the compactness of bones in relation to survivorship and 'fossil yield' is used to refer to the number of fossils contained within a given volume.

Deposit (synonym in a talus context: Infill): A unit of deposition characterised by the process of adding material to a landscape or receptacle (Longwell *et al*. 1969). A single infill may include many facies that illustrate the different phases of accumulation.

Matrix: The matrix refers to the small particles of a sediment or a sedimentary rock, which occupy the spaces between the larger particles that form the framework (Longwell *et al*. 1969). The collective term for background material in sedimentary rocks or deposits formed through sedimentation. In clast-supported sediments, if the matrix were flushed from the rock, the clasts would still be in contact supporting each other. In matrix-supported sediments, the individual clasts are held together by the matrix (i.e. they are not necessarily in contact with each other). The rock may appear disorganized without any clear internal structure. In this case, removing

the matrix will cause the larger clasts to collapse and become in contact with each other (Geol 243.3).

Particles: One variety of ultimate building block of the framework of a sedimentary deposit, refers to individuals that were transported as solids from their place of origin to their place of deposition. Particles may or may not be the products of the breakdown of pre-existing rocks. Particles not resulting from the breakdown of pre-existing rocks include whole or broken skeletal remains of organisms (Friedman & Sanders 1978).

Talus: An accumulation of sediments and rock debris in a slope or cone shape, formed by physical weathering processes (Longwell *et al*. 1969) and, within caves, collapses.

3.1 Excavation Methods

Excavations were undertaken regularly between the months of July 2008 to August 2009. All excavations were carried out by the author with site preparation and excavation of the MH1 T1 material conducted with the help of the Sterkfontein technicians. Excavation sites were located to most effectively sample the different deposits under investigation. The excavation methods used in this research followed the approach used by Kos (2001, 2003a, 2003b). In Kos' work, excavations were undertaken in a 'pitfall cave deposit' in Australia that is similar in depositional regime to the Sterkfontein deposits. Kos combines taphonomic, taxonomic and sedimentological facies description to interpret the influence of physical and chemical site formation processes on the patterns, condition and surface modification of fossil bone. In this research I have expanded Kos' methodology and added a number of extra analyses to help increase stratigraphic resolution and identify secondary sedimentation processes (identification of which was not necessary in Kos' work due to the young age of the infill).

One of the goals of this research was to clarify the stratigraphic pattern of the far eastern area of the Milner Hall, a locality in which a number of deposits converge.

Excavations were carried out in the most stratigraphically sensitive fashion possible to provide the greatest potential analytical resolution. Specific placement of the excavations was based on the maximum yield of stratigraphic data from minimal excavation. STK MH1 was positioned to sample the talus cone that has formed below the Silberberg Grotto M2 deposit and the Name Chamber Far Western Talus. STK-EC1 was positioned to attempt to isolate a sample deriving from the Silberberg Grotto M2 deposit within a narrow, protected passage. The STK-MH2 deposit was excavated in two places, MH2a sampled the eastern lateral distal termination of the truncated vertical face of the MH2 deposit. The excavation was the initial sampling point chosen to examine the sediment and fossil condition and to obtain a pilot sample. The MH2b excavation was located to provide further faunal and sedimentological samples from the already truncated STK-MH2 talus deposit preserved on the northern wall of the Milner Hall. Geological trench techniques were used on the truncated section of STK-MH2 to clean and develop the vertical face. The high degree of calcification of the STK-MH2 sediments required heavy-duty extraction methods to be employed and made excavation and recording of individual fossils impossible.

The upper deposit (T1) of the MH1 site was accumulated through the blasting activities of the lime-miners. The deposit was heavily disturbed with large quantities of fragmented travertine within the sediment. Fossils were abundant but deposited in a rapid, random distribution through the blasting activity and no contextual data was able to be recovered. Therefore excavations were conducted in 30cm spit depths. All material was then dry sieved through 2mm mesh and wet sieved through 5mm mesh. All≥20mm fossils were cleaned and individually numbered before analysis in the laboratory. All fossil and archaeological material <20mm was bagged by square and level. Due to the unconsolidated nature of the T1 sediments, collapse was a serious problem. Support squares (labelled ‘SS’) were excavated around the main grid. The ‘SS’ areas sampled only the T1 sediments. All materials from the ‘SS’ areas were processed as T1 material.

When decalcified sediments were exposed and excavated, as in the case of MH1 and EC1 sites, accurate mapping and *in situ* analysis could be conducted. All

contextual data was recorded from fossil material measuring≥20mm and archaeological material of any size prior to removal from the sediment. Paucity of light, coupled with cave topography prohibited the use of a theodolite or total station. Therefore distance, depth and bearing in relation to the site datum were taken using a Brunton Geological Compass (Brunton Geo 5010), protractor, measuring tapes and line levels. Artefact distribution diagrams can aid with the identification of natural grouping trends and dispersal influences. The methods for taking orientation and dip data and the presentation of this data are described in the 'Fabric Analysis' section below. Some natural clasts of appropriate elongation ratio were also plotted to provide added statistical resolution. Each fossil ≥20mm, and artefacts of any size, were bagged and labelled individually, while directly associated or broken fossils of the same element were labelled individually, then wrapped and bagged together and documented. Once artefacts had been removed from the sediment, they were cleaned, examined and analysed in the laboratory. All fossil material <20mm was dry sieved through 2mm mesh on site and bagged for context and subsequent microfauna analysis.

Excavations were carried out in accordance with the appearance of stratigraphic features. Identification and excavation of stratigraphic features were undertaken at the deposit-level then at the facies-level within a particular deposit. Within facies, 5cm levels ('spits') were dropped until the exposure of a different unit, at which point all squares were dropped until the next facies was exposed throughout the site. The excavated facies shape and slope was maintained throughout the excavation in order that artefacts could be positively identified to their corresponding facies and so that each facies could be exposed, mapped and excavated as an isolated unit. The excavation of stratigraphic features combined with accurate archaeological excavation techniques allowed greater facies identification, sampling and comparison of sediments and fossil contents. The MH1 and EC1 sites were gridded into squares and quadrants to aid mapping and site maintenance. When the deepest deposit of the MH1 talus, named T4 (Talus 4), was exposed and determined as sterile, the excavation was levelled to horizontal and excavated in 5cm spits until the cave floor was exposed.

Figures 3.1 and 3.2 show the excavation plans of the STK-MH1 and STK-EC1 sites and show the excavations in two perspectives. A square plan of the site is also presented. MH2b was the principle excavation of the STK-MH2 site and is presented in Figure 3.3.

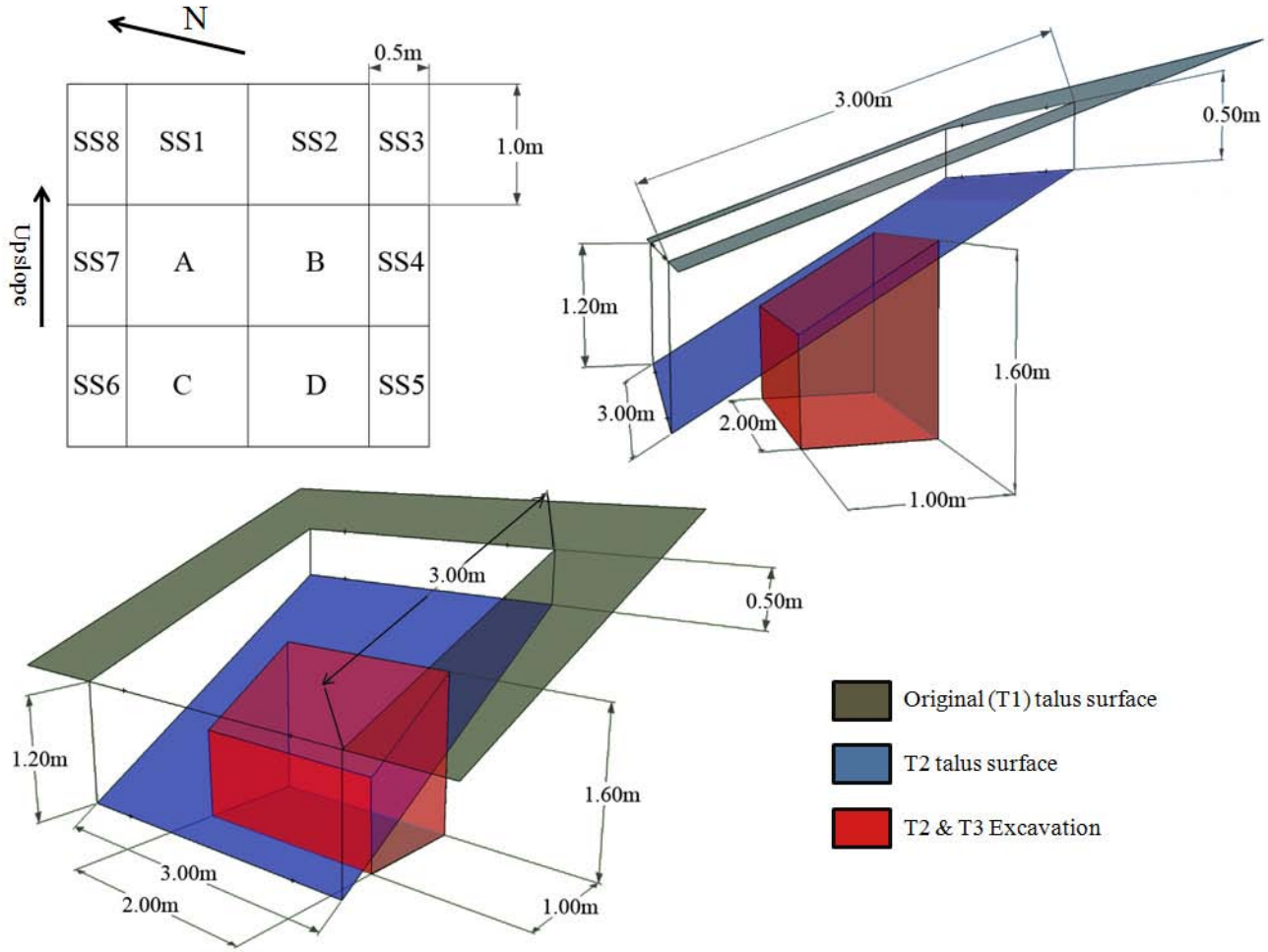


Figure 3.1 STK-MH1 square plan and 3D schematic of excavation. The talus slope angles are accurate. The T2 & T3 excavation dropped below the 160cm shown in the schematic, the 160cm represents the start of the horizontally deposited, sterile T4 deposit.

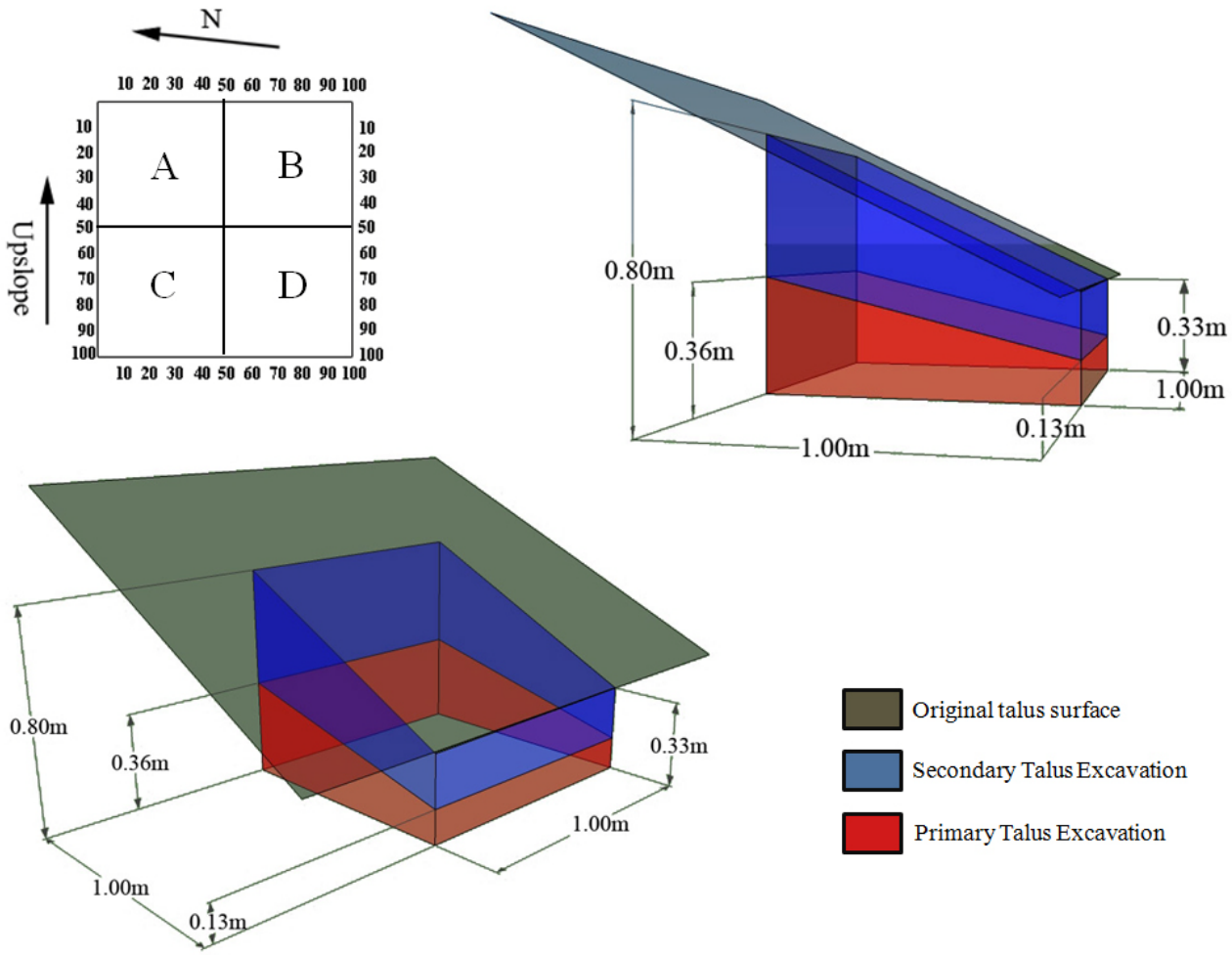


Figure 3.2 STK-EC1 square plan and 3D excavation plan.

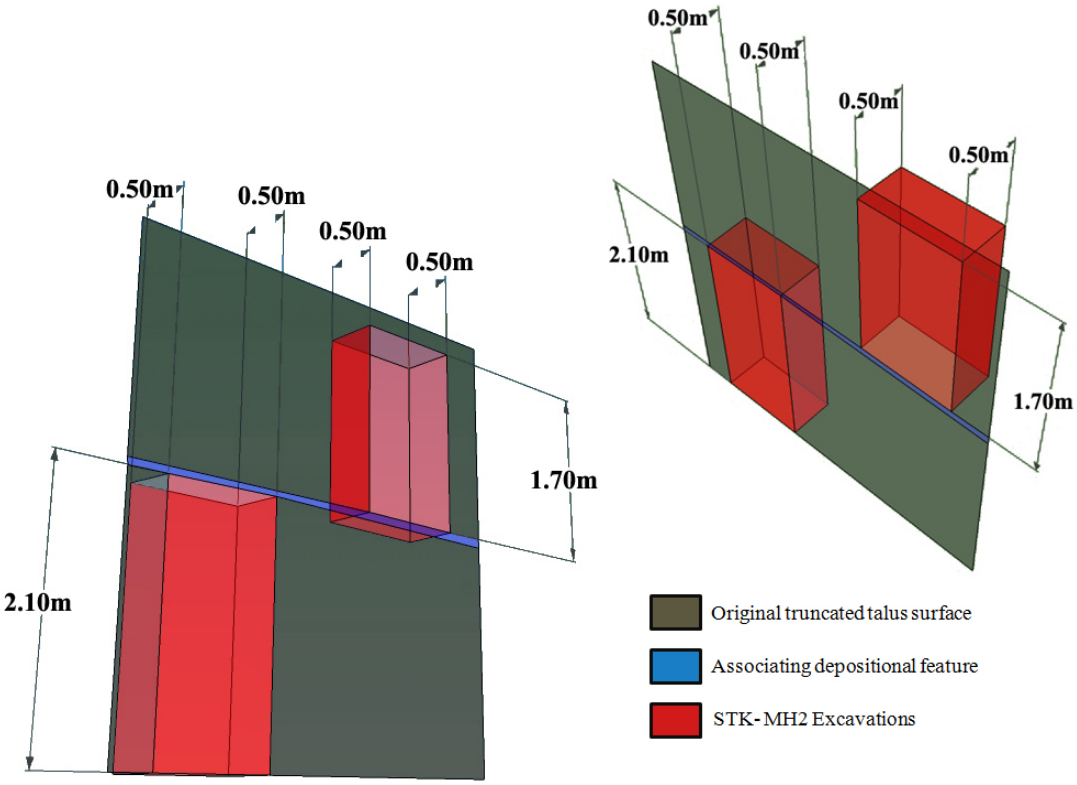


Figure 3.3 MH2b excavation plan. Excavations were made into the vertical face of the STK-MH2 truncated deposit. Due to the greatly differing degree of sediment consolidation and calcification the depositional feature was used to allow two smaller trenches to be excavated instead of one 4m high trench.

3.2 Stratigraphic Representation

At Sterkfontein, the deposits and the stratigraphy of those deposits have been represented by either a plan view of the surface of the deposit with the visible boundaries indicated (Cooke 1938, Kuman and Clarke 2000), or in a macro-scale section plan (usually N-S) of the cave with each identified breccia body placed in sequence of infilling within a general morphological representation of the cave (Robinson 1962, Wilkinson 1983, Partridge & Watt 1991, Clarke 2006). The representation of stratigraphic relationships in a clear and decipherable manner is problematic when dealing with multiple sources of sediments and possible mixing processes as well as unknown deposit boundaries. The temptation to represent as much information as possible and yet still admit to the gaps in data has the

potential to produce some confusing stratigraphic representations (e.g. Wilkinson 1983).

For work at the intra- and inter-deposit scale, where relationships between infills are the focus, another method is needed to illustrate stratigraphic sequences and provide perspectives on the relationships between contributing deposits. The Harris Matrix (invented by Edward Harris in 1973 and first published in 1975 (Harris 1975)) has become the most widely used tool for the representation of complex stratigraphy in archaeological sites. The method has also been used on cave sites to represent the stratigraphy (MacNeish & Libby 2003; Pleurdeau 2006). In this research the Harris Matrix is used to represent the stratigraphic relationships within and between the sites investigated.The benefit of the Harris Matrix is its ability to simplify stratigraphic relationships down to three possibilities based on the laws of archaeological stratigraphy established and described by Harris (Harris 1979a, b). The principles of archaeological stratigraphy vary in a number of ways from the principles of geological stratigraphy (Harris 1979a, b). Despite the differences, the three possible relationships between geological and archaeological strata hold fast. Caves, as accumulating agents, do provide a more dynamic system for the dispersal and accumulation of sediments than most geological or archaeological sites and the application of a tool enabling clear stratigraphic relationships to be represented is important for the interpretation and description of the stratigraphy. One of the potential issues with the reductionist philosophy of the Harris Matrix system and cave sediments is that some strata may not abide by the laws of superposition, i.e. due to calcification and erosion, younger strata may be found below a directly associated hanging remnant of an older strata. In such cases where a chronologically older stratum lies above a younger one the sequence must still be represented exactly as it appears but any discrepancy in the superposition law has to be noted on the representation. The Harris Matrix is a tool for the representation of a stratigraphic sequence regardless of accumulation history or contents - “the content of the deposit is irrelevant to arranging its place in the stratigraphic sequence, except of course that it is of a different nature that allows you to distinguish it as a separate unit of stratification” (Harris, Pers. Comm.).

Figure 3.4 shows the three possible stratigraphic relationships (A - C) and their representation within the Harris Matrix convention. In this research a two lines crossing the vertical superposition line denotes a stratigraphic unconformity and is demonstrated in 'D' of Figure 3.4. The unconformity symbol is then associated with an arrow denoting the relative age of the underlying deposit, either younger or older. The nature of the unconformity is not noted but is described in the deposit analysis. The additional restriction of the Harris Matrix is the absence of representation of the receptacle shape. This is a deliberate feature of the representation but in situations, like caves, where the deposit boundaries may be influenced by the physical constraints of the receptacle clear descriptions are required.

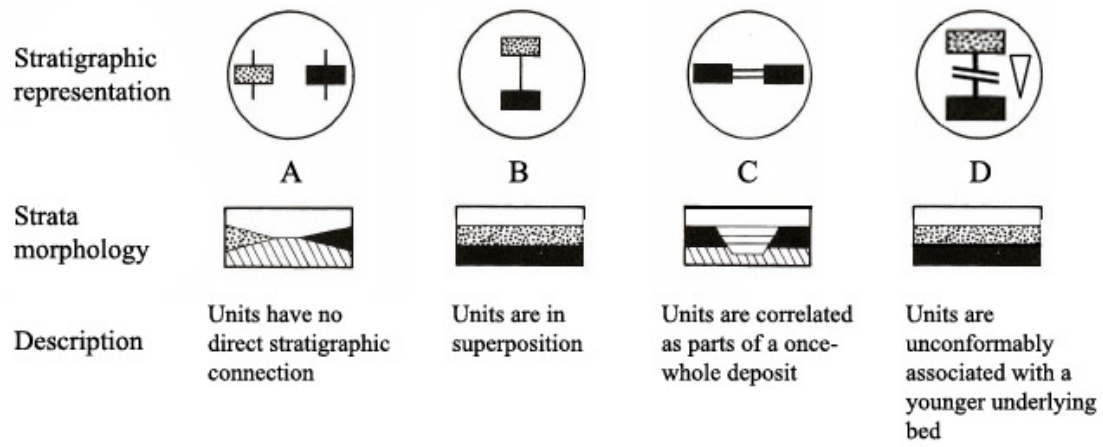


Figure 3.4 The Harris Matrix three recognised stratigraphic relationships. Adjusted from Harris (1979b).

3.3 Sedimentological Analysis

A number of sedimentological tests were carried out on the samples taken from systematic depth intervals, spot samples and facies samples for all excavations. All tests were carried out on each sample to provide as much comparable data as possible. Sediment colour, hydrology, particle size and chemical composition are relevant attributes that can help differentiate deposits and identify deposit or

facies boundaries. Diagenic processes can influence variables such as colour and pH, so more accurate differentiation of sediment sources and deposit/facies boundaries are provided by particle size analysis and major element analysis by XRF. Currently a mineralogical data set is being compiled for all the established Sterkfontein deposits (M. Sutton *work in progress*). Once compiled, this data will allow site-wide facies identification and comparisons to be made between subterranean and surface deposits.

Sediment colour was assessed on site. The methodology for the assessment of sediment colour follows the procedure recommended by the Munsell company. A Munsell Soil Colour Chart was used to establish the closest sediment colour match. Colour comparisons were carried out in natural light, out of the cave, and were prepared by wetting a 10g sediment sample with distilled water to create a paste-like consistency.

Particle size analysis and hydrological tests were carried out at the Soils Laboratory in the Department of Geology at the University of Kwazulu-Natal on a Mastersizer 2000. For facies sediments description, the sand, silt and clay proportions are assessed in relation to the 12 soil texture classes established by the U.S. Department of Agriculture. Particle size analysis has been successfully used to identify deposit boundaries on a number of archaeological and palaeontological karst sites (for examples see Farrand 1975; Tankard & Schweitzer 1976; Butzer 1981; Farrand & McMahon 1997; Woodward 1997a, b; Farrand 2000; Schuldenrein 2001; also see Farrand 2001 for a review of sedimentological techniques utilised in cave geoarchaeology). Brain (1958) used particle size profiles to identify Phase I vs. Phase II sediments deposited at Sterkfontein. A Phase I matrix represents a mix of 'cave earth' sediments (authigenic) and externally derived sediments (allogenic), and a Phase II matrix represents only allogenic sediments. The difference is a marked increase in the coarser particles and a reduction in the fines in Phase II sediments (Brain 1958). Brain did not, however, seem to consider transport of sediments over an extended distance underground, or the variability in particle size distribution associated longitudinal sediment sorting. Observation of grading processes and trends within the deposits

can allow identification of sedimentation cycles where macroscopic observation of sediment colour and stratigraphy are inconclusive. In this research particle size patterns are compared through the basic particle size classes (clay, silt and sand) and through the comparison of particle size distribution curves produced by the Mastersizer 2000. The curves are compared both descriptively and statistically. In order to allow a statistical comparison of the particle size distribution curves, each curve was de-convoluted into its constituent unconstrained Gaussian curves. Each major distribution curve was made up of four or five Gaussian curves. Each Gaussian curve represents the distribution of a particular grain size. The relative volumes of the Gaussian curves that make up a particular particle size distribution curve can then be compared to other distribution curves using Chi^2 test of significance. P-values <0.05 indicate the distributions and volumes of the Gaussian curves of one sample are significantly dissimilar to the distributions and volumes of the Gaussian curves of the comparative sample. P-values >0.05 indicate the distributions and volumes of the Gaussian curves are similar. The de-convoluted particle size distributions curves for each sediment sample are presented in Appendix 2.

Chemical property analysis (XRF) was carried by Professor Wilson out at the University of the Witwatersrand, School of Earth Sciences. Frisia & Borsato (2010) note that "research on Karst clastic sediments is limited with respect to the study of chemical and bio-mediated precipitates because of the difficulty of obtaining accurate dates and their complex stratigraphy" (pp. 275). Relatively few studies have been undertaken on the chemical composition and diagenesis of karst clastic deposits (Ford & Williams 2007, pp. 281). Those studies that have been carried out have focused on either calcified sediments (Osborne 2001) or mineral diagenesis in relatively recent archaeological cave infills (Karkanas *et al.* 1999, 2000). It should be noted that Karkanas *et al*. (1999, 2000) use a number of laboratory techniques not used in this research and so their interpretations are not necessarily applicable. For this research major element composition was deemed enough to indicate deposit boundaries and a similar approach was used by Pilo *et al.* (2005). Karkanas *et al*. (2000) warn that where diagenic reactions are ongoing or differed in the past, sediment chemical composition may have been quite

different. It stands to reason that the longer the depth of time between deposition and analysis the greater the potential influence of diagenic processes. These factors mean that caution should be taken when considering chemical or mineralogical data with respect to elucidating depositional conditions, palaeoenvironmental conditions, and sediment sources, based on chemical comparisons alone. Pilo *et al.* (2005) used a combination of sediment colour and chemical composition to characterise depositional facies. Differences in less abundant (rare) elements may be indicative of different sediment sources and several projects within the Cradle are exploring this avenue (M, Sutton; F, Garcia *work in progress*). Trace element analysis was not utilised in this research due to time constraints. The highly variable macro and micro-environmental conditions within the cave have unknown influences on intra-deposit chemical properties. Pilo *et al.* (2005) observed "a considerable chemical variation, sometimes even within the same facies" (pp. 758). For this research the major elements (listed below) are quantified as percentages of proportions within the total sample and normalised to reflect relative abundance differences between samples. The distribution of chemicals between deposits of facies can then be compared statistically using a Chi^2 test of significance. The following compounds were identified and quantified in the XRF analysis.

Chemical	Compound name
SiO2	Silicon dioxide
Al2O3	Aluminium Oxide
Fe2O3	Iron (III) Oxide
FeO	Iron Oxide
MnO	Manganese Oxide
MgO	Magnesium Oxide
CaO	Calcium Oxide
Na2O	Sodium Oxide
K2O	Potassium Oxide
TiO2	Titanium dioxide

P2O5	Phosphorus Pentoxide
Cr2O3	Chromium (III) Oxide
NiO	Nickel Oxide

Standard XRF sediment preparation procedures were carried out prior to the analysis. All data collection was performed on a PANalytical PW2404 WD XRF with a Rh (Rhodium) tube set at 50kV and 50mA an analysis time of 40 seconds per element and 20 seconds per background (backgrounds are measured for Si, Al, Mg, Na and P only).

3.4 Fabric Analysis

The Sterkfontein underground deposits provide an opportunity to investigate the influence of the geomorphological processes at work in the caves through the detailed study of the sedimentological particles. All deposits analysed demonstrate a number of identifiable patterns in particle orientation and arrangement. These patterns are analysed through the application of fabric analysis. Fabric analysis as a discipline concerns the quantification and modelling of several particle attribute variables, mainly the organisation, orientation, and dip values within a deposit. Fabric analysis has been shown by many researchers to be a powerful tool in the decipherment of sedimentological sources and movement of sediment within a depositional history (for examples see Clarke & McIntyre 1951; McSaveney 1972; Lisle 1976; Perez 1989; Abrahams *et al.* 1990; Tanner & Hubart 1991; Bertran *et al.* 1997).

Due to the abundance of fossils in the deposits excavated, the fossils themselves can be considered the most reliable form of sedimentological particle. The shape, size and condition of faunal remains make them potentially informative sedimentological entities in addition to their more conventional role as taxonomic and taphonomic indicators. Voorhies (1969) first investigated the different movement potentials of various skeletal elements in fluvial environments and the broader concepts of his element-determined transport potential have been referred

to in this research. The use of faunal remains as analytical particles in fabric analysis has been described by Kidwell *et al.* (1986). In their work Kidwell *et al.* (1986) describe the theory of 'biofabric' analysis, using skeletal element orientation, sorting by size and shape, and close packing as the variables to be analysed (Kidwell *et al.* 1986). This concept is followed in this research, with the exclusion of the close packing variable due to time constraints during excavation. Particle attributes were recorded prior to the removal of each fossil to provide maximum contextual data. Further particle attributes were measured under laboratory conditions. Frostick & Reid (1983) provided one of the first examples of the treatment of faunal remains as sedimentological particles in a sub-aerial slope environment and recognised the influence of skeletal element shape on transport processes and distribution, and the associated influence of element abundance on all subsequent faunal-based interpretations.

The specific fabric analysis techniques used in this research follow a number of previous works that have concentrated on the dynamics of colluvial sub-aerial slope deposits (Melton 1965; Mark 1973; Frostick & Reid 1983; Mills 1984; Abrahams *et al.* 1984, 1990; Perez 1989; Bertran *et al.* 1997; Kos 2001). Below I have listed the measurements and models used in the fabric analysis of the deposits investigated. The broader aspects of slope and talus development have already been discussed in the background section (Chapter 2).

3.4.1 Basic particle measurements

The following measurements were taken from all fossils excavated *in situ*. For the fossils excavated from the T1 deposit, fabric analysis was not relevant due to the highly disturbed, *ex situ* nature of the sediments and therefore not conducted. However, the T1 fossils were subjected to the faunal analysis, the details of which are discussed in Section 3.5.

Dimensions

- Max Length: (mm) expressed as L in fabric analysis models.
- Max, Min and Mid-point Breadth: (mm) - expressed as I in fabric analysis models.
- Max, Min and Mid-point Depth: (mm) - expressed as S in fabric analysis models.

In order that the axial ratios and models work correctly, breadth was chosen to be the intermediate (I) value in the axial measurements. Mean values were established for the breadth and depth to minimise the effects caused by changeable morphology found in skeletal elements.

Particle Attributes

Particle Size: Expressed as the mean of the L, I and S axes. Particle size is recognised as being the most important factor in the differential transport of particles by gravitational processes (Abrahams *et al.* 1984, 1985) and is a well understood process in fluvial environments.

Particle Volume: Expressed as the multiple of the L, I and S axes.

Elongation Ratio: Elongation ratio is generally recognised as being the most important dimensional attribute for the development of positive orientations in fossil-bearing deposits (Voorhies 1969; Behrensmeyer 1990; Bertran & Texier 1995; Lenoble & Bertran 2004), and is expressed as L/I. Particles possessing an elongation ratio of greater than 1.6:1 can be considered reliable indicator particles based on the minimum elongation value suggested by Bertran & Texier (1995). Cañón-Tapia & Chávez-Álvarez (2004), suggest an elongation ratio of greater than 1.7:1 will produce a stable and positive orientation parallel to the sediment flow. Due to the breakage patterns found in bone and the abundance of shaft fragments, most fossil particles have an elongation ratio well in excess of 1.6:1. Orientation data is represented using a conventional rose diagram displaying relative proportions of azimuth data. Software used for the representation is called

Rozetta and is available from a number of online geological recourses. Orientation values were also plotted on the x-axis of a histogram against proportion as a percentage, to more clearly represent relative magnitudes of azimuth values.

Dip/Plunge: taken as the angle of dip along the long axis of the particle with a Brunton Geological Compass with 0° being horizontal. Strike values were not taken as many particles were too narrow to allow consistent transverse axis measurements. Dip can either be measured as a vertical angular deviance of plunges of the particles from the dominant slope gradient (regarded as 0°) (as demonstrated by Perez & Yin, 1988) or by using the modal dip values to demonstrate the dominant deposit dip. The angle of a slope within a colluvial deposit changes with distance from source and through accumulation history. It follows that evaluating the dip of particles from different levels within a deposit will sample particles that have been deposited on the changing angles of the deposit surface. In order that the intermediate slope angles can be determined, and greater resolution provided on the gradual accumulation of sediment, the latter method has been applied in this research. Dip values were mapped using various models on a stereonet projection system. The models used include a standard scatter plot and two contouring methods, the first developed by Kamb (1959), and the second a 1% contouring plot. The modal values are also plotted to provide the dominant deposit dip and is plotted as an arch running through the projection. The advantage of the Kamb contour method is that it reduces the influence of sample size thereby allowing more accurate inter-deposit comparisons. Stereonet projections were mapped with the use of Stereonet v.6.3.3 developed by Rick Allmendinger of Cornell University and available as shareware (http://www.geo.cornell.edu/geology/faculty/RWA/programs.html). Figure 3.5 shows an example of the presentation of the fabric orientation and dip data.

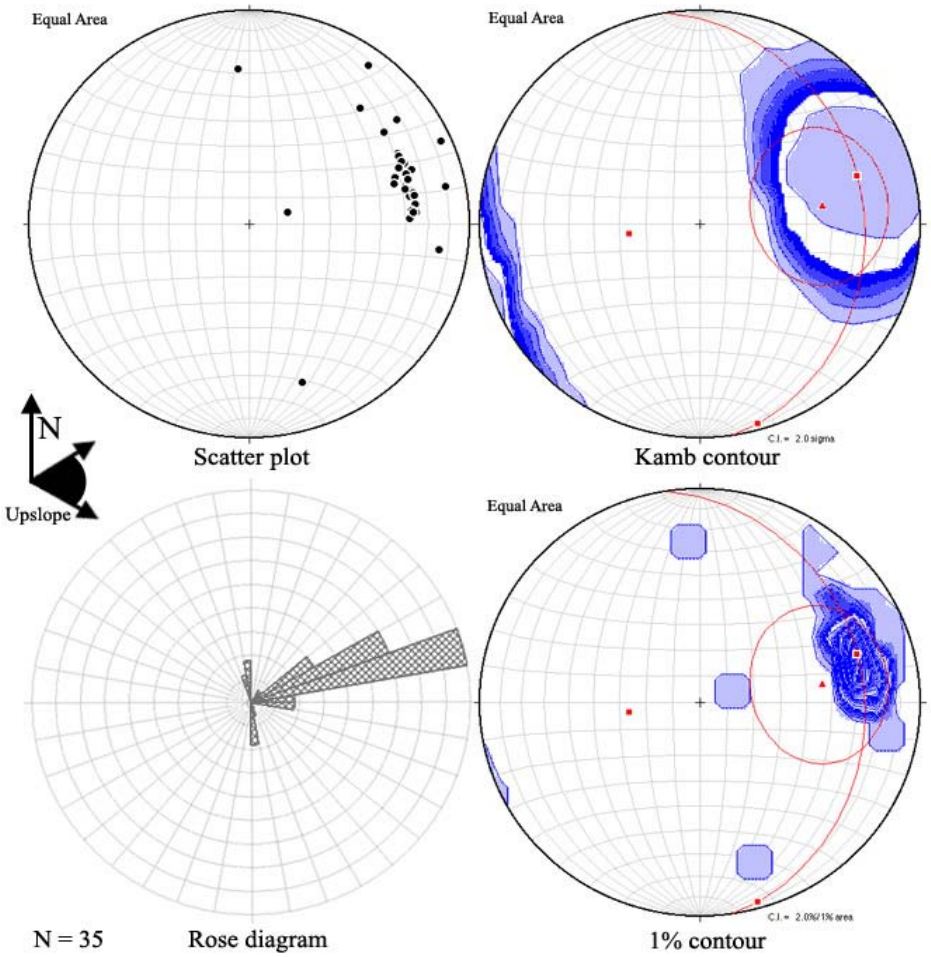


Figure 3.5 Example of the presentation of particle orientation and dip data used in this research. Stereonet projections are adjusted after mapping using Stereonet v.6.3.3 software.

3.4.2 Particle shape models

Particle shape has received a great deal of attention and is recognized as being a critical factor in the transport of sediments (e.g. Krumbein 1941, 1942; Sneed & Folk 1958), second only to particle size. It is generally agreed that within sediments of similarly sized particles, more spherically shaped particles possess higher transport potential and will be moved first and furthest within a colluvial deposit (Abrahams *et al.* 1984, 1985). A number of different models have been developed to measure and quantify the shape of particles. Most of the models used to evaluate shape and sphericity use equations based on the ratios established from

the three mutually perpendicular axes of the particle (Zingg 1935), named in this research the L, S and I axes. Shape classes have been established from the plotting of these ratios against one another in a standard scatter diagram or a ternary diagram following Illenberger (1991) and Benn & Ballantyne (1993). The general shape classes are: sphere, rod, disc, and blade. The four classes are seen to represent the major shapes that influence the movement of sedimentary particles.

In Frostick & Reid's work (1983), axial ratios are plotted as c/b vs b/a (axis originally named short (S), intermediate (I), and long (L) (Zingg 1935)). The Krumbein sphericity model (Krumbein 1941) developed from the same axial measurements, divides skeletal elements into general shape classes. Unfortunately, there has been little agreement on the best method of particle shape analysis (Oakey *et al.* 2005). As such, the most common forms of particle size analysis the Zingg ratios (1935), the Krumbein sphericity equation (Krumbein 1941) and the Sneed & Folk (1958) methods have been used in this research. As will be seen in the analyses, the different shape indices recognise fluctuations in particle dimension ratios in different ways, thereby classifying different proportions of shape classes within the same assemblage. Benn & Ballentine (1993) warn of the problems in selecting correlating shape class indices and suggest "indices should be chosen with reference to particular data distributions and specific research aims" (pp. 665), although the subjective choice of distribution based on desired results seems questionable. The relative merits and drawbacks of the models are discussed in Illenberger (1991) and Oakey *et al.* (2005). To combat biases inherent within the individual models, three methods have been used in conjunction with one another to provide greater scope for the identification of particle shape patterns. The models used, and their equations, are shown below. The presentation methods used for the evaluation of particle shape used in this research are presented in Figure 3.6. Figure 3.6 also shows the virtual spectrum of shape variation measured by each graph and the relative position of the shapes to the axes.

- Sphericity (Krumbein 1941) - expressed as $(SI/L^2)^{1/3}$
- Zingg Ratios (Zingg 1935) - expressed as S/I vs. I/L
- Disc-Rod Index (DRI) (Sneed & Folk 1958) - expressed as (L-I)/(L-S)
- Maximum Projected Sphericity (MPS) (Sneed & Folk 1958) - expressed as $(S^2/IL)^{1/3}$

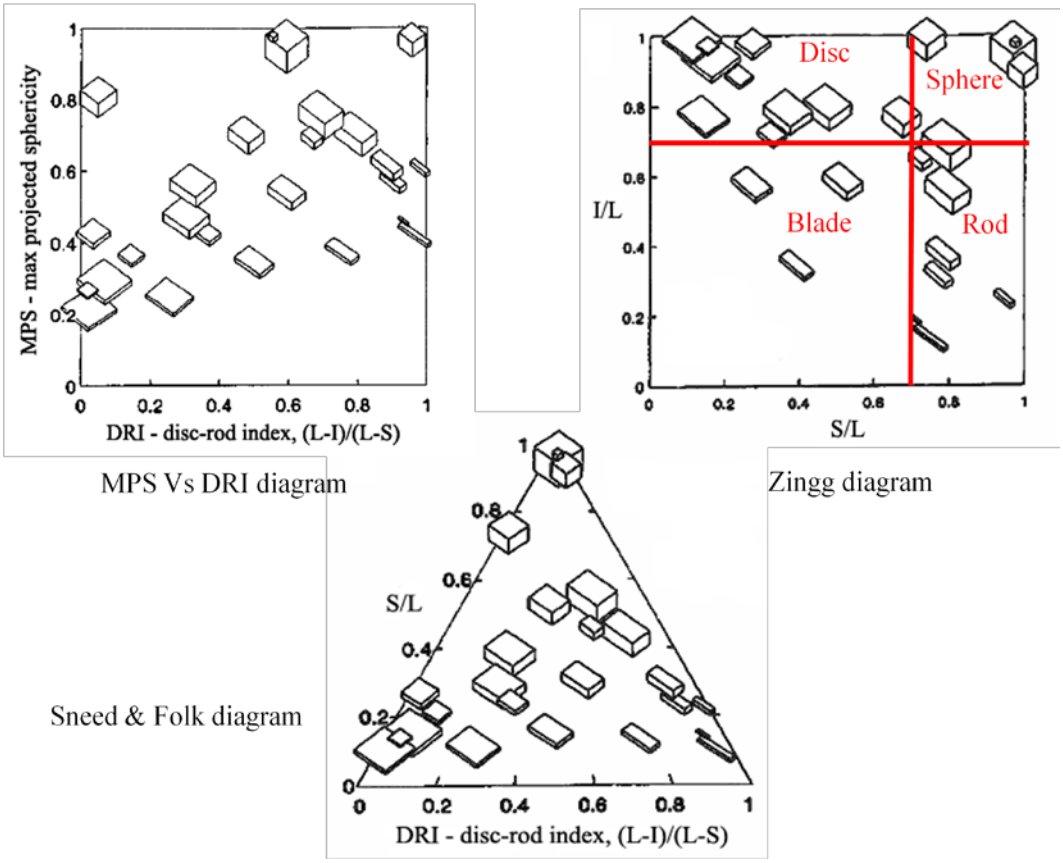


Figure 3.6 Examples of MPS vs. DRI, Sneed & Folk and Zingg shape diagrams used in this research. Adjusted from Illenberger (1991).

3.4.3 Skeletal elements and particle shape models

Particle shape is one of the key variables involved in the accumulation and potential sorting of fossils within sediment gravity flow deposits. The models used for the assessment of shape are described above, and as explained, the models will primarily be applied to the fossils excavated from *in situ* deposits. A number of researchers have recognised skeletal element shape as influencing fossil

distribution (Voorhies 1969; Frostick & Reid 1983; Kidwell *et al.* 1986). Particle movement patterns follow those trends recognised in geological contexts in that more spherical particles are moved first and furthest. Voorhies (1969) worked on faunal element transport within fluvially accumulated deposits, separating skeletal elements into three classes with five possible groups. Class I and I & II represent the most easily transported elements and include ribs, vertebra, sacrum and sternum, scapula, phalange and ulna. Class II and II & III represent larger, more gradually moved elements, and include the shaft elements and metapodial, pelvis, mandible and molar and incisor dental elements. The final group is the class III elements, the most immobile class which includes the skull and bovid mandible. Voorhies suggests the presence of class III elements would indicate a lag deposit (Voorhies 1969). As can be seen in Voorhies' experiments, the general trend shows smaller, more spherical elements being moved more easily.

Colluvial deposits are different in that the flow medium is sediment not flowing water, a difference that does influence the transport pattern. Frostick & Reid's work (1983) concentrated on the transport of skeletal elements on an arid sub-aerial slope deposit. They class elements in terms of their shape, using the Zingg ratio to assess the general shape of the element. They found that rod shaped elements moved the greatest distance followed by spherical elements. Disc and blade shaped elements were the slowest to move. Frostick & Reid made no mention of element size, but one can assume that relatively smaller elements will be transported first as is the case in geological contexts. More research needs to be carried out to fully understand the relationships between surface area, shape and size of elements in sediment flow environments. In this research the basic rules found in geological contexts are applied to fossil material, i.e. that the size and shape of particles are critical variables in the differential movement of particles in sediment gravity flows.

In this research all elements were plotted onto a Zingg scatter diagram (1935) and a Sneed & Folk (1958) ternary (triangular) diagram and an MPS vs. DRI scatter diagram (Illenberger 1991) to provide a distribution of skeletal element shapes within each deposit. CSI (Corey shape index) (Corey 1949) was not used in this

research due to its poor correlation with other indices, but should be noted as a further potential model. Interestingly, the Zingg shape model, as used by Frostick & Reid (1983) on skeletal element transport tests at Koobi Fora, has been found in this research to be particularly sensitive to bladed forms. This sensitivity creates distributions with a greater number of bladed forms than suggested by the other two models. This influences the interpretation of element transport potential negatively, as bladed forms are interpreted by Frostick & Reid to possess the lowest transport potential (together with disc-shaped forms) in contrast to Voorhies' placement of the blade-shaped ribs into Groups I and I & II. The difference in classification of transport potential of blade-shaped elements is considered here to be representative of the difference in transport dynamics in water versus sediment, although this suggestion needs to be tested experimentally. The other element shapes present in Groups I and I & II do follow the trends proposed by Frostick & Reid (1983). MPS (Maximum Projected Sphericity) has been recognised as being particularly sensitive to particle transport potential by Illenberger (1991) who found a strong correlation between MPS and particle settling and rolling velocity ($r = 0.97$ and $r = 0.86$ respectively (Illenberger 1991, pp. 759). To test this, MPS was plotted against particle sphericity (Krumbein 1941) using the complete skeletal elements of a bovid, carnivore and primate (this control sample is described in further detail in Chapter 4), the correlation coefficient was then determined from this graph. Of all the shape indices MPS showed the highest correlation coefficient to particle sphericity (0.93). Figure 3.7 shows the sphericity vs. MPS model.

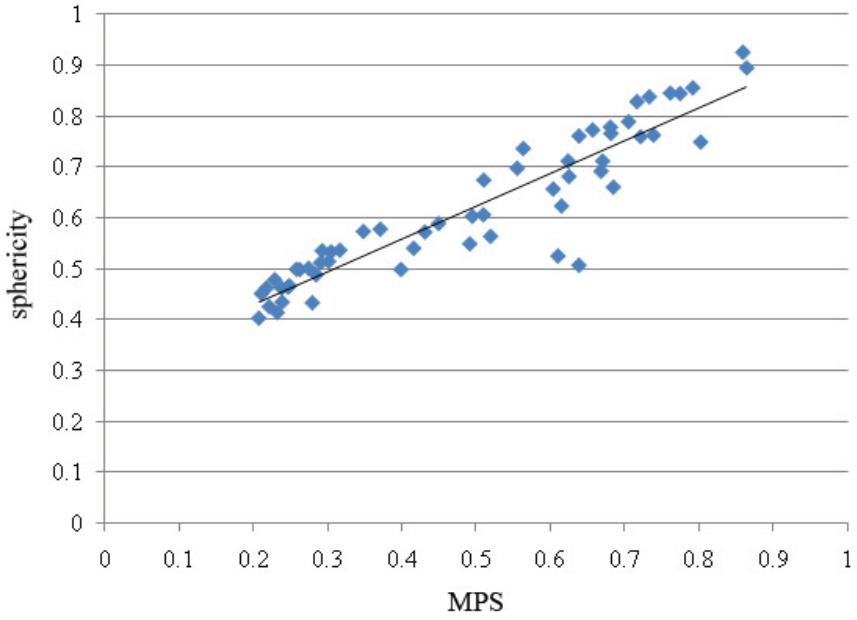


Figure 3.7 Sphericity vs. MPS for the control sample of complete skeletal elements.

The indices used in geological particle shape modelling have been designed to be applied to clastic material not faunal material, which possess a greater range of shape variation. The applicability of the indices on faunal particles, which possess an atypical shape in geological particle modelling, therefore requires testing. To establish the applicability of different shape indices on skeletal elements, the faunal control sample (described below) was used to run tests between the different particle shape indices. Table 3.1 shows that there are strong correlations between the particle shape indices used, and a strong correlation exists between particle size variables (size and volume) and the used shape indices. Those shape indices that correlated strongly with one another when applied to faunal material were preferred for this research.

	R squared	Df	F =	P =
Particle size vs. Particle Volume	0.829	57	268	<0.001
Sphericity vs. MPS	0.857	57	331.78	<0.001
Sphericity vs. DRI	0.348	57	29.39	<0.001
Sphericity vs. CSI	0.847	57	306	<0.001
CSI vs. DRI	0.0609	57	3.569	0.06
MPS vs. DRI	0.069	57	4.099	0.04

Table 3.1 Correlation tests for particle size variables vs. utilised shape indices. CSI (Corey shape index (Corey 1949) vs. DRI and MPS vs. DRI are indices with negative correlations.

A number of tests was also run to assess the impact of element attributes on sphericity through different stages of breakage. The results are presented in Chapter 4. Fifty randomly chosen specimens from the excavated fauna were compared to a control sample to assess the change in attributes through breakage. The results are useful for assessing how faunal particles change through breakage and how those changes affect the transport potential of elements and therefore where they may be found within a deposit. The control sample for these tests comprised a selection of complete elements from three commonly found species in the fossil deposits. The three species included, a modern bovid (*Aepyceros melampus*), a carnivore (*Panthera pardus*) and a primate (*Papio hamadryas*). Three long bone elements, three irregular bone elements and a compact bone element were chosen from each specimen for the analysis. The long bones included the humerus, femur and tibia. The three irregular bones included examples of a cervical, thoracic and lumbar vertebra from each species. The compact bone used was a metacarpal. This element was chosen as it changes shape significantly between species and is well represented in the fossil record. Four parts of the long bones and metapodial elements were measured. The basic particle measurements (outlined in Section 3.4.1) were taken from the proximal and distal metaphysis, the diaphysis and the complete bone and were all plotted

separately. The different parts relate to different densities within shaft elements and have been shown to possess different survivorship potentials (Lyman 1994). The control sample created a small but useful dataset of complete elements shapes and sizes. The comparative sample of complete elements was measured and plotted into Sneed & Folk ternary diagrams. Figure 3.8 presents the control sample measurements plotted onto the Sneed & Folks diagrams.

Figure 3.8 Sneed & Folk diagrams for the complete skeletal elements from the comparative control collection.

3.5 Faunal Analysis

In addition to the particle measurements described above, a number of quantitative measurements and qualitative observations was taken from each fossil. The full analysis was conducted on all fossils excavated *in situ* and all fossils identifiable to skeletal element in the T1 assemblage. The unidentifiable

fossils from the T1 deposit, of which there are 1528, were subject to a more concise analysis. Both analytical procedures are described below.

3.5.1 Measurements taken from identifiable or *in situ* skeletal elements

Cortical Thickness: Taken as the maximum thickness of cortical bone on an exposed cross-section from a fractured element.

Element Type: (1) Long (e.g. humerus); (2) Flat (e.g. rib); (3) Irregular (e.g. vertebra); (4) Compact (e.g. phalanx).

Element Completeness: <25%, 25-50%, 50-75%, 75-99%, 100%. Taken as an estimate of the recovered proportion of the original element.

Bone Type: (1) Cortical; (2) Cancellous; (3) Both. Can only be used on bone fragments where the preservation of cancellous bone can be observed. On complete elements, 3 will be the assessment.

Bone Portion: (1) Diaphysis; (2) Metaphysis; (3) Epiphysis; (4) All. Combinations of portions are likely to be preserved. It is impossible, however, to preserve 1 and 3 or vice versa. On complete elements all three areas will be preserved and will be recorded as 4.

Bone Division: (1) Proximal; (2) Medial (or Shaft); (3) Distal; (4) All. See Figure 3.9 for diagram.

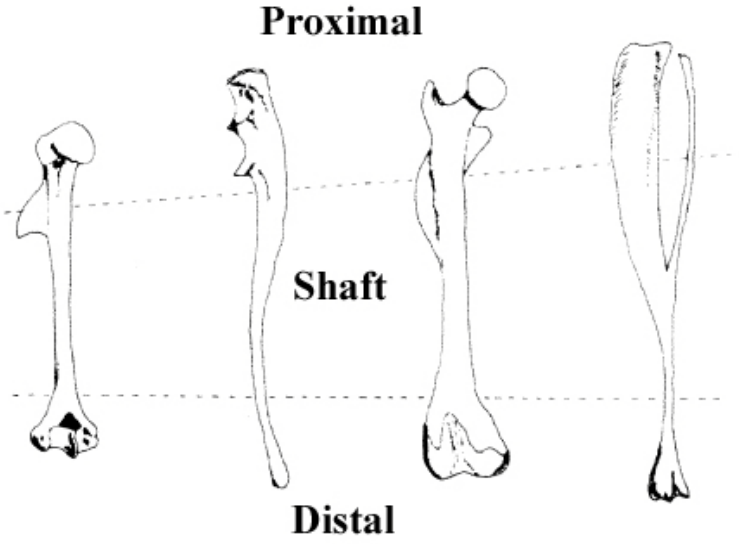


Figure 3.9 Bone division categories used in this research.

Condition: The condition of bone surface has been used to investigate ecological conditions prior to burial of a bone, and estimate a general time of exposure to these processes (Behrensmeyer 1978). It is agreed that in surficial deposits weathering processes slow after burial (Behrensmeyer 1978; Frison & Todd 1986; Behrensmeyer *et al.* 2000). Identification of pre-depositional and post-depositional bone surface damage has not been investigated in detail and it is currently assumed that subsurface weathering is insignificant (Lyman 1994). In caves, a similar trend cannot be assumed due to the influence of localised sediment movement, water erosion, and potentially localised chemical weathering. Bone assemblages can accumulate surface modification in the form of weathering attributes both pre- and post-depositionally. Exposure to post-depositional weathering processes may affect the bone much more than currently recognised, given the relative time spans involved between exposure on the landscape surface and burial and re-distribution within the cave. However, until focussed research is carried out on the identification and quantification of post-burial weathering processes on bone, specific to cave environments, Behrensmeyer's assessment remains the most applicable method. As indicated by Behrensmeyer (1978), the tempo of weathering stages depends largely on climate

and ecology and should be taken as rough guidelines. Gifford (1981), in particular, warns against the blind application of the interpreted exposure times and states that "absolute Time values are different to weathering stages" (pp. 418). Weathering stages as established by Behrensmeyer (1978) are useful for inter-site comparisons and for gauging the extent of bone surface damage. Broad inferences regarding burial time may be made on the basis of bone condition.

Bone condition is a subjective classification based on a relative spectrum. The attributes are separated into the following groups. For each condition the equivalent stage established by Behrensmeyer (1978) has been given. Due to the subjective nature of the analysis, both the author and Professor T. Pickering made bone condition assessments. Reference photographs can be found in Appendix 1.

Fresh (f) – Bone shows no abrasion or weathering evidence on shafts but may show some slight abrasion on the distal and protruding components. Fractures also may show slight abrasion damage but are mostly intact and free of further flaking from cortical bone. A visible sheen can be seen on the cortical bone surface. Fresh is recognised as being equivalent to Behrensmeyer's stages 0-1.

Slightly Weathered (sw) – Bone shows light to medium abrasion, small parallel cracks on shafts and distal portions, and more prominent abrasion and damage of protruding components. Some protruding components may be abraded to a point where cancellous bone is exposed. Flaking of cortical bone is minimal and reserved to fracture edges. This is recognised as being equivalent to Behrensmeyer's stages 2-3.

Weathered (w) – Bone surface is cracked in both parallel, subparallel and perpendicular routes. Cracking is more extensive, with cracks deep enough to reveal cancellous bone. Flaking of cortical bone is seen on the medial portion of bone shafts. Distal/fractured portions may be abraded severely. Pitting and exfoliation of cortical bone may be present. This is equivalent to Behrensmeyer's stage 4.

Very Weathered (vw) – Bone is very fragile and powders or fragments when touched. Larger pieces show extensive exfoliation of cortical bone over the entire

piece. Fractures are focal points of exfoliation. Cancellous bone is rare or very fragile. No bone surface modification is recognisable due to highly irregular and abraded surfaces. Equivalent to Behrensmeyer's stage 5.

3.5.2 Bone breakage attributes

A great deal of research has been carried out on bone fracture dynamics within various fields. From a taphonomic perspective the major works include Shipman *et al.* (1981), Johnson (1985), Marshall (1989), and Villa & Mahieu (1991), with notable critical works by Bunn (1982) and Lyman (1994). Collagen fibre patterns and decay of those collagen fibres provides some level of predictability of breakage patterns. The general trend established by these researchers allows the identification of the general state of the bone when the breakage occurred. Most researchers differentiate between 'green stick' or fresh, dry bone and fossilised bone states. Each bone state produces higher proportions of certain break types. Villa & Mahieu (1991) used Chi^2 analysis to compare fracture angle proportions between three assemblages and found the variable to be useful in distinguishing between bones broken when wet and dry. 'Green stick', or fresh bone fractures, are characterised by smooth or stepped break types and generally perpendicular or obtuse fracture angles. When the bone is 'wet' (fresh), the collagen fibres tend to snap directly across the longitudinal axis, or fractures travel parallel to the fibres. Dry bone tends to break with a combination of fractures depending on the decay of the bone. On dry bone, smooth fracture surfaces and perpendicular break angles are less common. Fossilised bone often breaks with a combination of fractures. Common break combinations are perpendicular and acute breaks with sawtooth break surfaces. If the bone is heavily mineralised then smooth fractures surfaces can occur. Identification of post-fossilisation breakage can be a useful depositional indicator and may suggest the presence or absence of re-sedimentation through collapse. Pre-fossilisation damage can suggest burial/exposure times of faunal material relating to opening shape, size and agent of accumulation. Kos' work (Kos 2003a, b) has most recently utilised pre- and post-fossilisation breakage patterns on a cave accumulated faunal assemblage.

The greatest problem with quantifying bone fractures is the analysis of different breaks types and textures on the same element (Bunn 1982). In this research, combination classes have been included so that more than one break can be identified on a single element. It is important to note, however, when considering bone breakage attributes that for elements with only a single type of break represented, the breakage data provides information only about the condition of the bone during the last major fracturing event, quantities of pre-fossilisation breakage are very difficult to assess as the breakage signature of the primary assemblage may have been destroyed by the subsequent episodes of re-sedimentation throughout the diagenic history of the bone.

Number of broken edges: The number of major broken edges on a single skeletal element. Maximum can be four. A bone fragment broken on all edges will have four main break axes. This is not influenced by break type.

Break Type: (1) Smooth fracture; (2) Step fracture; (3) Sawtooth fracture. See Figure 3.10 for examples.

Break Angle: (1) Perpendicular; (2) Acute; (3) Obtuse. Angle of breakage is taken as a relative qualitative assessment of the breakage plain angle in relation to the longitudinal axis of the bone. See Figure 3.10 for examples.

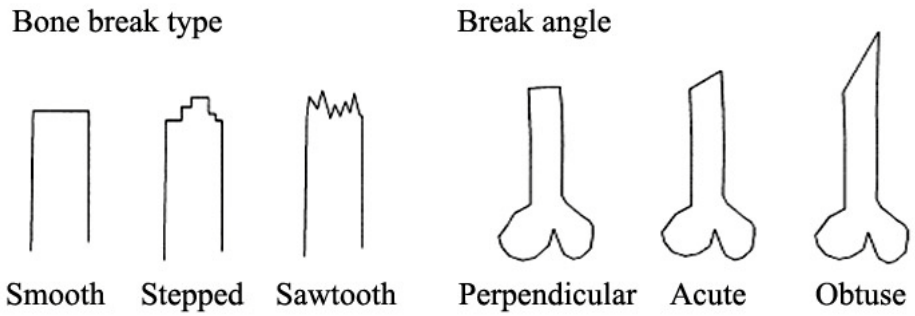


Figure 3.10 Bone breakage attributes.

3.5.3 Bone attributes taken from T1 deposit unidentifiable component & *ex situ* skeletal elements

Size class: Pieces were placed in the following size classes; <20mm; 20-29mm; 30-39mm; 40-49mm; 50-59mm; 60-69mm; 70-79mm; 80-89mm; 90-99mm; >100mm. The same size classes were used for all faunal material and faunal summary tables.

Number of breaks: See above.

Break types: See above.

Element types: See above.

Condition: See above.

Bone surface modification: Bones from T1 were analysed for the diagnostic anthropogenic and biogenic bone modification attributes, namely cut marks, tooth pitting and gnawing marks.

3.6 Taxonomy

Taxonomic evaluations were conducted by Professor Travis Pickering at the University of Wisconsin. The identification of specific species is an important process when attempting to identify sediments sources and mixing of sediments. Temporally distinct deposits can also contain temporally and climatologically distinct taxa. This principle forms the basis of biostratigraphic sequencing and its application to the Sterkfontein deposits has been discussed in Section 2.1.1. Those species that are considered to be temporally or climatologically distinct offer the greatest opportunity to source sediments as correlations in specific species across deposits suggest a similar age/climate and source deposit. The majority of fauna recovered, including the relatively small assemblages excavated during this research, do not represent temporally distinct species and can be found in a number of deposits, with the exception of *Equus*. *Equus* is one of the more important temporal indicators as it appears in East Africa 2.3Ma (Churcher &

Richardson 1978; Berger *et al*. 2002, Brugal *et al*. 2003) and in South Africa after. *Equus* is mostly found most noticeably in M5 and younger deposits (Pickering 1999; Ogola 2009), with some specimens possibly deriving from the later sediments within M4 (Kibii 2007). Outside Sterkfontein, equids are found in many deposits dating between 2ma and 1.5ma, including, Swartkrans Member 1 Lower Bank and Hanging Remnant, Swartkrans Members 2 and 3, Kromdraai A, Coopers D (de Ruiter *et al.* 2008) and Malapa (Dirks *et al*. 2010). Equids are also closely associated with more open environmental conditions along with many bovid species (de Ruiter *et al*. 2008). Environmental reconstructions are also based on the taxonomic representation. For each species identified from the respective deposits, a brief synopsis of the established palaeoenvironmental association is given.

3.7 Taphonomy

The taphonomic analysis was conducted by Professor Travis Pickering and Sarah Zwodeski of the University of Wisconsin. T. Pickering's work (1999, T. Pickering *et al*. 2004a) provides the most recent taphonomic study of Sterkfontein faunal remains deriving from deposits relevant to this research. His methods are utilised to aid comparisons and to help establish the consistency of data through multiple re-sedimentation phases. In primary sedimentation deposits, the goal of taphonomic analysis is to attempt to elucidate the environmental context during the accumulation of the original faunal assemblage, and to identify the potential faunal accumulation agents. The taphonomic interpretation should, in theory, support the stratigraphic analysis (which forms the basis for understanding the integrity of the assemblage). The goal of the taphonomic analysis of secondary sedimentation deposits is to attempt to elucidate the primary sedimentation environment during the accumulation of the original faunal assemblage, to identify possible mixing of sediments from different distinct deposits, and to identify time-averaging processes. The problem of reducing taphonomic assemblage integrity through the stages of assemblage development, from the life assemblage to excavated sample, was originally noted by Clarke & Kietzke

(1967). This process is compounded by the re-distribution of fossil assemblages around the karst environment, where successive generations of breakage eradicate primary diagnostic features. The methodology used by T. Pickering for these assemblages follows his PhD thesis (1999) methodology and is the standard for the Sterkfontein and Swartkrans sites. There are some issues that were brought up by the relatively small assemblages analysed in this research. The small samples limit the specimen abundance numbers, which also then limits the ability to clarify patterns of preferential deposition of certain taxa over others. The specific element representation data was useful for establishing consistencies and inconsistencies within deposits of a single site and between source deposit and investigated deposit. Element representation in primary sedimentation deposits also allows modes of accumulation to be inferred. Bone condition and bone surface modification assessment follows the system laid out in Section 3.5. The important terms and definitions particular to the taphonomic analysis are listed below:

1. LBS - long limb bone shaft fragment, a specimen $\geq$2 cm in maximum linear dimension that lacks its articular ends and can be classified as retaining (a) 100 % of its original diaphyseal circumference; (b) approximately 50 % of its original circumference; or (c) <50 % of its original circumference. For bovids, we consider metapodials as functional long limb bones, in addition to the functional (and anatomical) long limb bones: humeri and femora (collectively, upper limb bones); radioulnae and tibiae (collectively, intermediate limb bones).
2. Bone fragment - unidentifiable specimen <2 cm in maximum linear dimension. This type of specimen was examined for bone surface modifications; if none were diagnosed on a specimen, then it was excluded from all subsequent analyses.
3. Bone surface visibility - this is a subjective assessment of the amount of visible bone surface on a specimen (relevant to the identification of surficial taphonomic damage), expressed as a percentage (e.g., 100 % or 50 % visibility).
4. Bovid and mammal body size classes follow Brain's (1981) system.

3.7.1 Bone surface modification attributes

Bone surface modification analysis was undertaken by the author and Professor T. Pickering in order that pre and post-depositional modifications could be securely identified. Bone surface modification attributes were identified as: Indeterminate (indet); Splitting (s); Flaking (f); Small pitting (sp); Large pitting (lp); Tooth pitting (tp); Tooth gnawing (tg); Cut marks (ct). Each visible bone surface attribute was recorded and some fossils possessed a number of attributes. Classification of biotic bone surface modification is integral to establishing the pre-burial context and accumulation agent (Pickering 1999). Photographs were taken of elements displaying the bone surface attributes noted above, in order to enable consistent identification with a reference guide. These photographs were taken either at macro scale or under a microscope to provide the greatest resolution for recognition. The photographs can be found in Appendix 1.

CHAPTER 4 RESULTS: FAUNAL PARTICLE SHAPE

Particle shape is acknowledged to be a critical factor in the transport of particles within sediments (Krumbein 1941, 1942; Sneed & Folk 1958; Abrahams *et al.* 1984, 1985). Skeletal elements, as biological particles and proxies for geological particle in slope deposits, are equally influenced by their shape (Voorhies 1969; Frostick & Reid 1983; Kidwell *et al.* 1986). Many sediment gravity flow processes will fragment bones in primary sedimentation deposits and then further through secondary sedimentation. The fragmentation of elements during deposition will change their shape. This change in shape will affect the transport potential of those elements in subsequent sediment movements. In deposits that are assessed based on the relative abundance of specific skeletal elements regardless of completeness, it is useful to have an understanding of how certain elements change shape through breakage. The excavated faunal assemblage recovered during this research allowed the examination of fossils in a broad range of conditions. Analysis of all fossils regardless of completeness and depositional history allowed the broad patterns to be seen.

The following tests were run on the entire faunal sample to examine the relationships between element attributes and dimensional attributes. The patterns shown in the described analyses are important, but the tests themselves are considered supplementary to the focus of this research and should be reproduced through experimentation to confirm the patterns and to allow statistically supported conclusions to be made.

- Skeletal element type vs. shape
- Skeletal element type vs. sphericity
- Skeletal element elongation vs. sphericity
- Sphericity vs. number of breaks, within element types.
- Elongation ratio vs. number of breaks, within element types.

4.1 Skeletal Element Type vs. Shape

Element type is a useful, broad identification level based largely on patterns of element shape within a skeleton. Identification to element type is often possible when specific element cannot be recognized. Element type data can provide a useful analytical sample in assemblages with relatively few specimens identifiable to specific element and further to genus or species. All faunal elements change shape through breakage. The results presented in this section derive from a set of tests conceived to assess the change of element shape by comparing a collection of complete bones to the post-depositional, excavated, fossils recovered during this research. More investigation is needed but basic patterns can be seen in the shapes and therefore transport potentials of different complete skeletal elements. The control sample is described in Section 3.4.3. The results of the complete elements plotted into the Sneed & Folk diagram (1958) can be found in Figure 3.8. Fifty specimens including long, irregular and compact elements were taken at random from the excavated fauna and plotted into a Sneed & Folk diagram to provide a comparison to the complete elements. Figure 4.1 presents these Sneed & Folk diagrams.

The comparative sample taken from the excavated material represents elements with a broad range of breakage levels. The excavated sample does, however, contain very few complete elements, and so represents a heavily modified example of each element type. What can be seen from Figures 3.8 and 4.2 is a change in shape pattern within each element type when the bone is modified through breakage caused by depositional processes. Long bones maintain a highly elongate shape regardless of breakage levels. Irregular and compact bones tend to become more spherical with breakage and represent a wider range of shapes through modification. The patterns illustrated by the Sneed & Folk diagram support the element breakage experiments presented in Section 4.4.

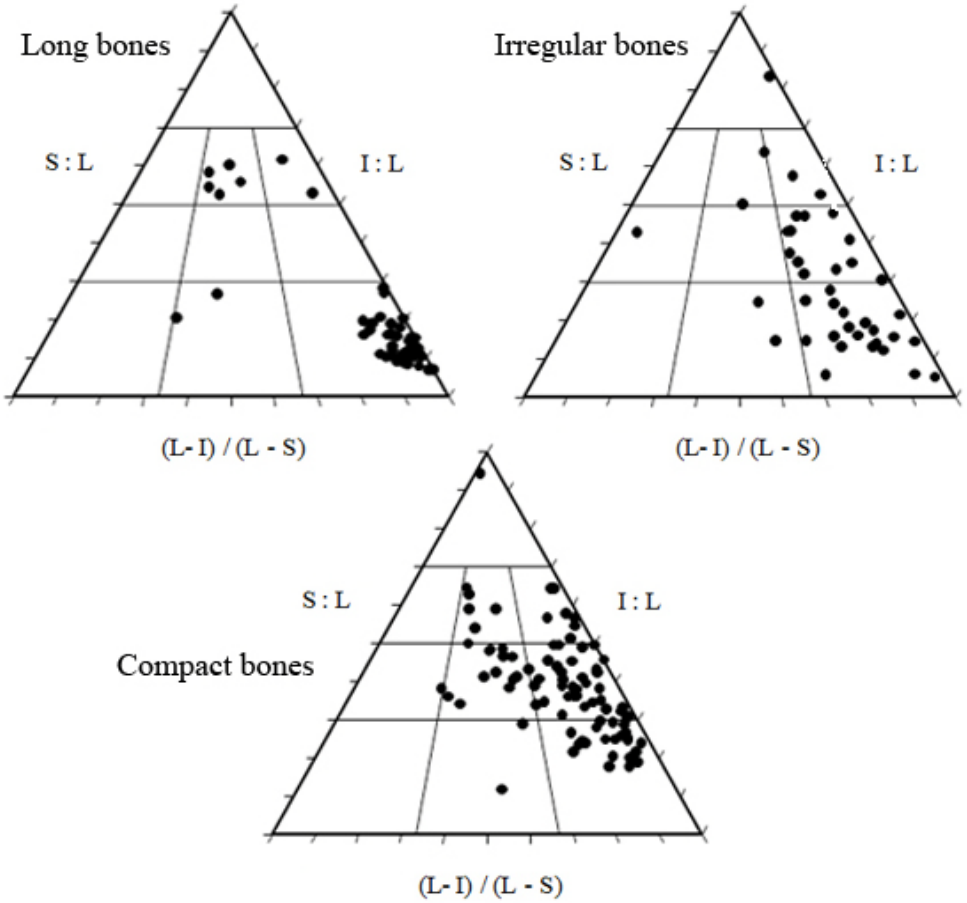


Figure 4.1 Sneed & Folk diagrams for fifty random skeletal elements from each element type class from the excavated fauna.

4.2 Skeletal Element Type vs. Sphericity

Element type classes were tested against sphericity (Krumbein 1941) to ascertain any basic trend in the sphericity of different element types regardless of breakage level. The test plotted the abundance of different skeletal element types in various sphericity classes across all the excavated faunal material. A general trend can be found for all skeletal element types. Linear trend lines were fitted to the gradients to represent the general patterns (Figure 4.2). Fossils deriving from long bones show a strong inverse gradient in representation vs. increasing sphericity. Long bone fossils, in all states of breakage, are presented most highly in low sphericity classes, representing between 55% and 79% of elements in the under 0.3 sphericity class. Fossils deriving from flat bones are also better represented in low

sphericity levels, up to 20% in the 0.3 to 0.39 sphericity class. No flat bones were found in the sphericity classes higher than 0.6. Dental elements show much the same pattern as ribs in that they are most highly represented in the low sphericity classes. Irregular and compact elements show the opposite trend, in that they are both better represented in the high sphericity classes. Regardless of breakage level, compact bones are not represented in sphericity classes lower than 0.3 and rise to a 50% representation in the 0.8 - 0.89 class. Irregular bones show a similar trend although to a lesser degree.

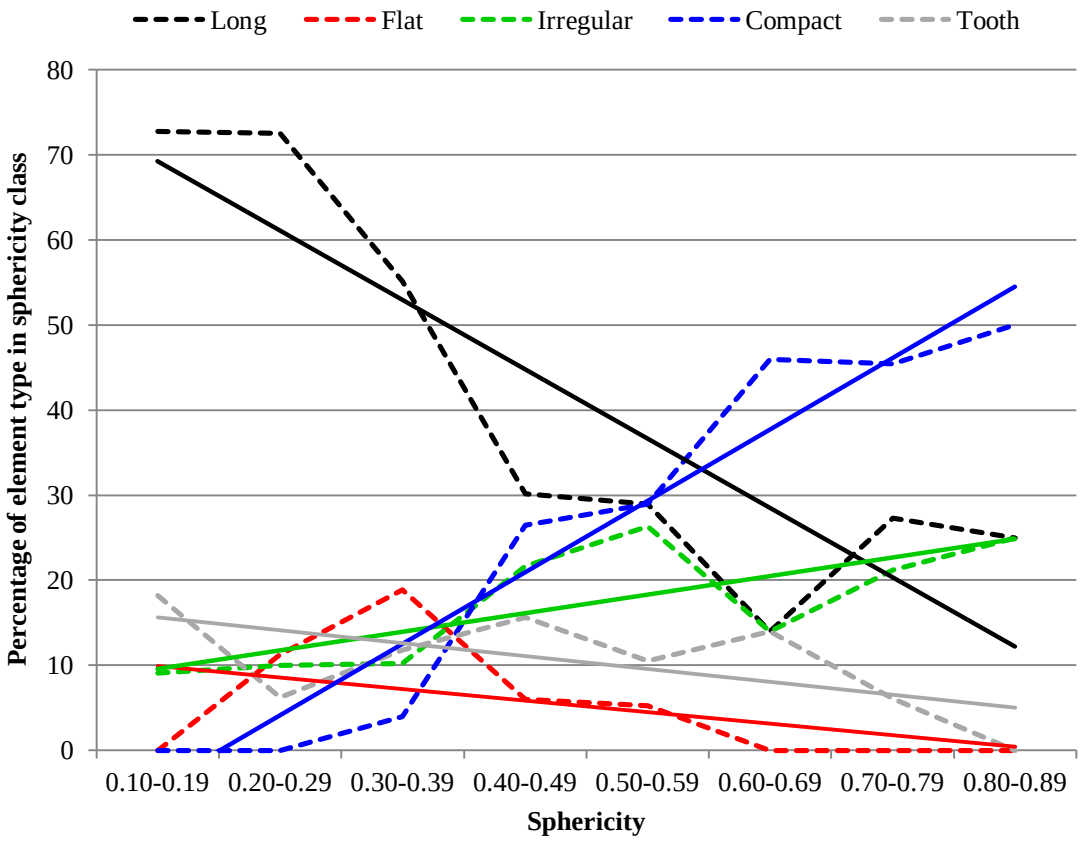


Figure 4.2 Relative proportions of different elements across sphericity classes. The dashed lines represent the actual data. The solid lines represent linear trend lines.

4.3 Skeletal Element Elongation vs. Sphericity

The above tests show a change in element shape from the original complete element to the excavated specimen. The change in shape affects the behaviour of those particles in a sedimentary environment. From a transport potential perspective, the more spherical particles get the more prone they are to movement. Particles are also used to indicate the sediment flow direction and gradient through deposits through fabric analysis. Fabric analysis requires particles to be a minimum elongation ratio to reliably orientate in sediment flows, a minimum of 1.6:1 length:breadth (L/I) is used in this research, following Bertran & Texier (1995). The following test was run to clarify the relationship between sphericity and elongation ratio across a fossil assemblage. Increasing elongation ratio was plotted against sphericity for 375 particles. Figure 4.3 shows that as elongation ratio increases sphericity decreases. In complete particle this would be entirely obvious but within a modified, broken assemblage it provides a clarification of a general relationship. If breakage is extremely heavy then particles will start to lose their suitability for fabric analysis. In the excavated assemblage, there are very few elements that fall under the minimum 1.6:1 elongation ratio. This is due to the morphology of shaft elements and the tendency of those elements to break into a large number of equally elongate fragments. This trend is illustrated in the following section.

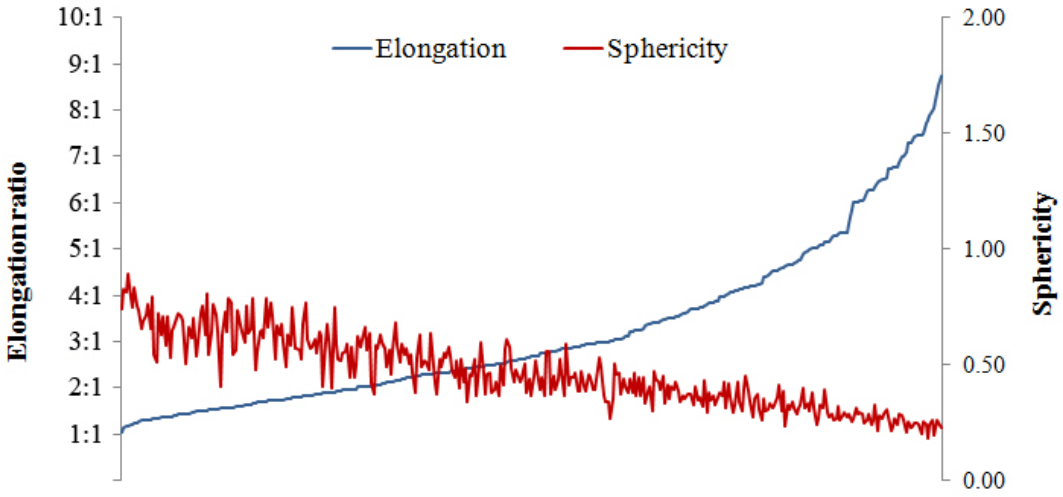


Figure 4.3 Element elongation plotted against element sphericity. All excavated faunal particles were used for the sample.

4.4 Sphericity & Elongation Ratio vs. Number of Breaks

This analysis attempted to assess changes in the levels of sphericity and elongation ratio in skeletal element types through increasing numbers of breaks. Element types were separated and placed in order of increasing number of breaks displayed on of the respective elements. The results are presented in Table 4.1. Mean sphericity numbers were taken for each break number category (e.g. for long bones with four breaks the mean sphericity was 0.37) (Figure 4.4). The same process was carried out to establish patterns of elongation ratio change with increasing levels of breakage across element types (Figure 4.5). Elongation ratio vs. number of breaks shows a similar trend to that seen in the sphericity tests. Elongation ratio is useful when used in conjunction with sphericity because it identifies the type of shape change during breakage, and distinguishes changes in shape the sphericity index is less sensitive too. The sphericity index was established to indicate changes in forms of natural clasts and is more sensitive to changes in shape of specimens with low elongation ratios like compact elements. The data indicate a general trend in how fossil element types change in terms of sphericity and elongation ratio through increasing breakage levels. This has implications for the transportation of elements with different preservation levels,

and can affect the distribution of specimens within a deposit or the representation of elements within a particular facies. These tests should be run under experimental conditions to confirm and statistically quantify the patterns seen here.

Long bones show a general decrease in elongation ratio with increasing levels of breakage. However, even those elements with a maximum number of breaks can still be classed as highly elongate forms with a mean elongation ratio of 3.50:1 (meaning the bone is 3.5 times longer than it is wide). Complete long bone elements, unsurprisingly, possess the highest elongation ratio. In terms of sphericity, an increase in sphericity (from 0.37 to 0.39) with increasing breakage is shown in the data. The degree of change is more slight than expected and indicates a low sensitivity of the sphericity index to changes within a range of highly elongated forms. Due to the relatively large size of complete shaft elements (mean particle size across complete long bones within the three control species = 89.9, in comparison to the mean particle size across the complete irregular or compact elements within the control species = 39.3), long bones have the potential to produce a much higher number of fragments, thereby increasing the relative abundance of this element type and disproportionately increasing the number of highly elongate pieces in the assemblage.

Flat bones show a general decrease in elongation ratio with breakage (from 4.9 to 3.3) and conversely an increase in sphericity (from 0.34 to 0.36). The spike in sphericity shown in flat elements with 3 breaks is mimicked by a sharp drop in elongation ratio. Again, as is the case with long bone elements, sphericity is not a sensitive index for detecting changes in highly elongate forms. Even flat bone elements showing maximum breakage have a mean elongation ratio of 3.3:1 and are classed as highly elongate forms.

Elongation Ratio

Element Type	Number of breaks				
	0	1	2	3	4
Long	6.4	4.8	4.5	3.2	3.5
Flat	N/A	4.9	3.8	2.7	3.3
Irregular	2.5	2.7	3.2	2.3	2.2
Compact	2.4	2.4	2.2	2.1	2.0
Tooth	3.0	2.2	2.6	2.9	4.6

Sphericity

Element Type	Number of breaks				
	0	1	2	3	4
Long	0.37	0.41	0.43	0.42	0.39
Flat	N/A	0.34	0.35	0.41	0.36
Irregular	0.54	0.49	0.50	0.52	0.49
Compact	0.58	0.58	0.58	0.60	0.64
Tooth	0.45	0.57	0.59	0.45	0.35

Table 4.1 Mean elongation ratio and sphericity figures plotted against number of breaks within specific skeletal element types.

Irregular bones show a generally stable elongation ratio with increasing breakage with a slight trend towards a lower elongation ratio (from 2.5:1 to 2.2:1). Interestingly, irregular elements also show a decrease in sphericity. The nature of this correlation cannot be inferred from this test data and requires further investigation. Irregular elements do represent a large variety of shapes that include the scapula, vertebra and mandible. It could be that the irregular element sample number (n = 80) in this test is insufficient to properly represent the variation of irregular element shapes. Further experiments would isolate the different irregular forms and test them individually. Vertebrae represent the largest component of the irregular element class, and as such were tested individually in the same fashion. In vertebrae, the elongation ratio increased slightly with breakage and sphericity decreased accordingly. The breaking off of the vertebral spinious and transverse processes during increased breakage creates a short, tubular form (Pers. Obs.). Unfortunately, time constraints precluded the running of further tests during this research.

Compact bones represent some of the most spherical elements in both complete and highly fractured condition. Elongation ratio decreased with increasing

breakage, as is expected (from 2.4:1 to 2:1), and there is a marked increase in sphericity (from 0.58 to 0.64). The increased relative change in sphericity (when compared to the change seen in long and flat bone elements, which show a relatively large change in elongation but little change in sphericity) can be interpreted as an increased sensitivity to shape change in less elongate forms.

Dental elements are the only example to show a marked increase in elongation ratio (from 3.0 to 4.6), and a correspondingly large decrease in sphericity (from 0.45 to 0.35) through breakage. Dental elements start as relatively spherical particles until broken, when the fracture dynamics of enamel creates many longitudinally fractured elongate pieces with high relative elongation ratios to the original complete tooth. Dental elements do show the largest change in shape and sphericity, which may heavily influence the depositional trends of differently fragmented dental elements.

These results do make logical sense when considering the pre-breakage shape, weaknesses, and collagen fibre patterns of the respective elements. Long bones fracture mostly parallel to the long axis of the bone, as do flat bones. Irregular bones, like vertebrae have more complex collagen fibre patterns and are more spherical in complete form. Breakage causes a reduction of that form. Compact bones, in complete form are also more spherical and collagen fibres are more complex but tend to break perpendicular to the long axis of the bone, creating a more spherical particle. The inverse relationship between elongation ratio and sphericity is well demonstrated by these data.

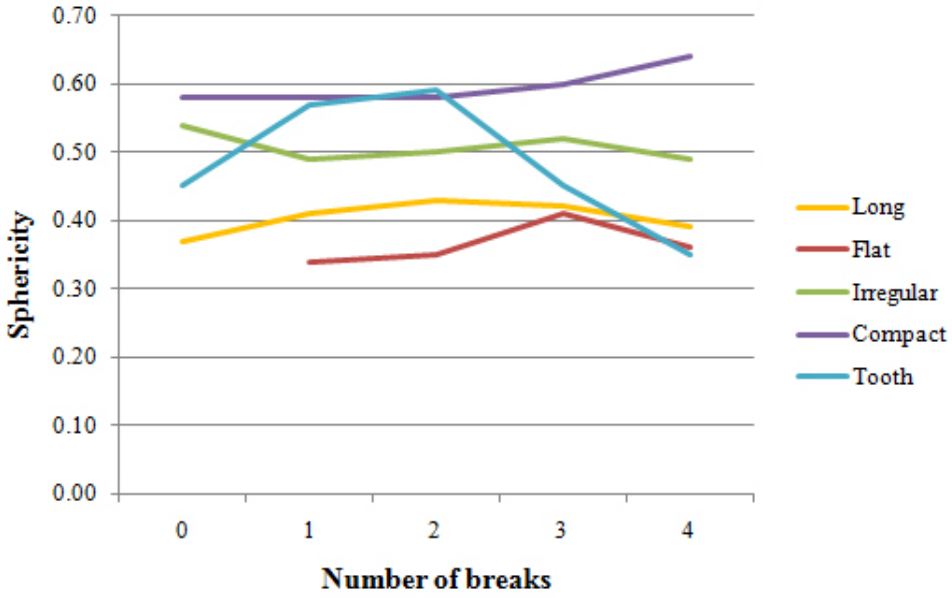


Figure 4.4 Sphericity plotted against number of breaks within specific skeletal element types. Sphericity and elongation ratio show an inverse relationship. The minor degree of variation in sphericity of long bones is a result of the low sensitivity of the sphericity index to highly elongated forms.

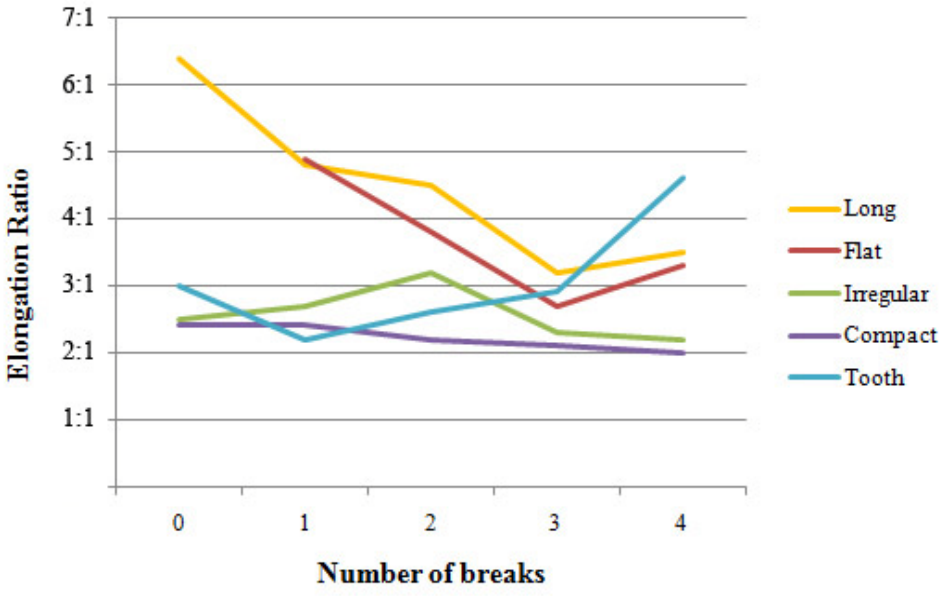


Figure 4.5 Mean elongation ratio plotted against number of breaks within specific skeletal element types. Sphericity and elongation ratio show an inverse relationship.

4.5 Faunal Particle Shape Discussion

The analyses presented above present a general perspective on the change in shape of faunal particles through breakage. The general trend shown is that bones decrease in elongation ratio and increase in sphericity. The question remains if these changes are significant enough to affect the transport and distribution of bones of varying levels of breakage, and therefore the relative abundance of the specimens in different parts of a deposit due to longitudinal grading processes. In the highly elongate forms, change in elongation ratio by 30%, perhaps isn't enough to affect the transport potential. This change, combined with the decrease in size associated with breakage, means fragments of long bones can be considered significantly more mobile than the complete long bone. The elements which, in a complete state, possess a more spherical form maintain that shape and will continue to be the more mobile particle. As breakage intensifies, through multiple sedimentation phases, and multiple generations of fragmentation are inflicted, all bones, with the exception of teeth, will become less elongate and more spherical. The intermediate stages of breakage are when element specific patterns may influence the distribution and transport of those elements through the deposit. In highly fragmented assemblages, the original transport potentials recognised for the represented elements may not be applicable as the elements are fragmented into more aggregate forms. To complicate matters more, different bones are prone to different rates of breakage. Long bones, due to their relative size and low density suffer greater levels of fragmentation (Lyman 1984), thereby producing a large number of fragments which may, due to their diminished size and shape, be transported with relatively complete compact or irregular elements. This situation is seen in the T3 deposit.

CHAPTER 5 RESULTS: STK-MH1

The location and intention of the MH1 excavation has been described briefly in the introduction (Figure 1) and the MH1 excavation plans have been illustrated in Chapter 3 (Figure 3.1). Four deposits have been excavated at the MH1 site. Named T1, T2, T3 and T4, these deposits represent progressively deeper infilling episodes. The sediments in each deposit derive from different sources and contain different sedimentary, archaeological and faunal material, all of which have accumulated through varying processes from the nearby area. Figure 5.1 shows a profile of the MH1 talus with the placement of the excavation. The MH1 talus is 17m long from apex to Milner Hall floor and drops 6.5m vertically. The floor of the Milner Hall and base of the MH1 talus currently lies 4m above the water-table. Figure 5.2 shows the stratigraphic profile of the southern wall of the MH1 site. Figure 5.3 shows the eastern wall of the MH1 site. Each deposit will be discussed in turn from T1 through T4. The final section of Chapter 5 (Section 5.5) brings the deposits together in a comparative analysis.

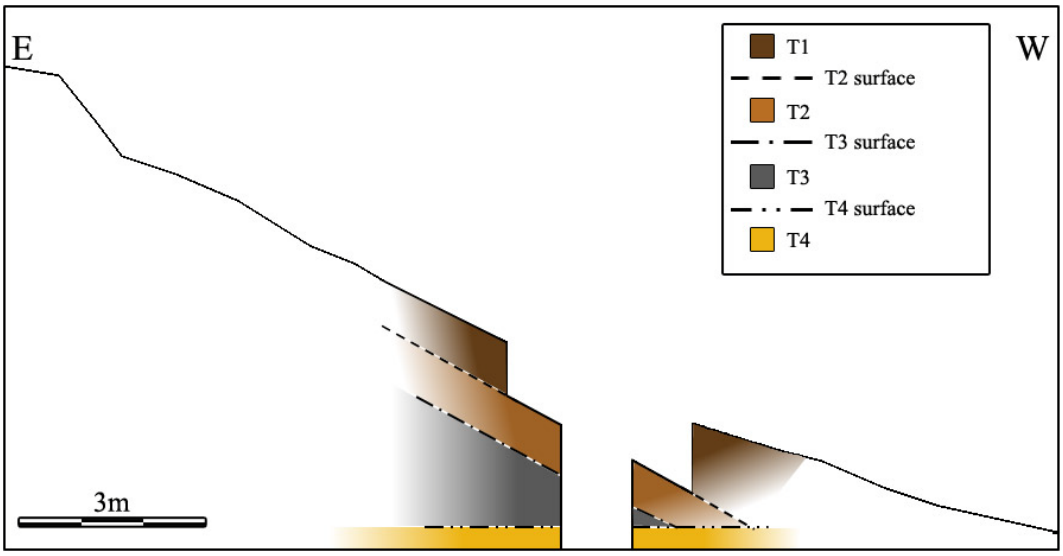


Figure 5.1 East-West profile of the STK-MH1 talus with the MH1 excavation and the deposits discovered and analysed in the text. Faded colour represents the decreasing knowledge of the deposit morphology. Dashed lines represent predicted talus surfaces based on exposed surfaces.

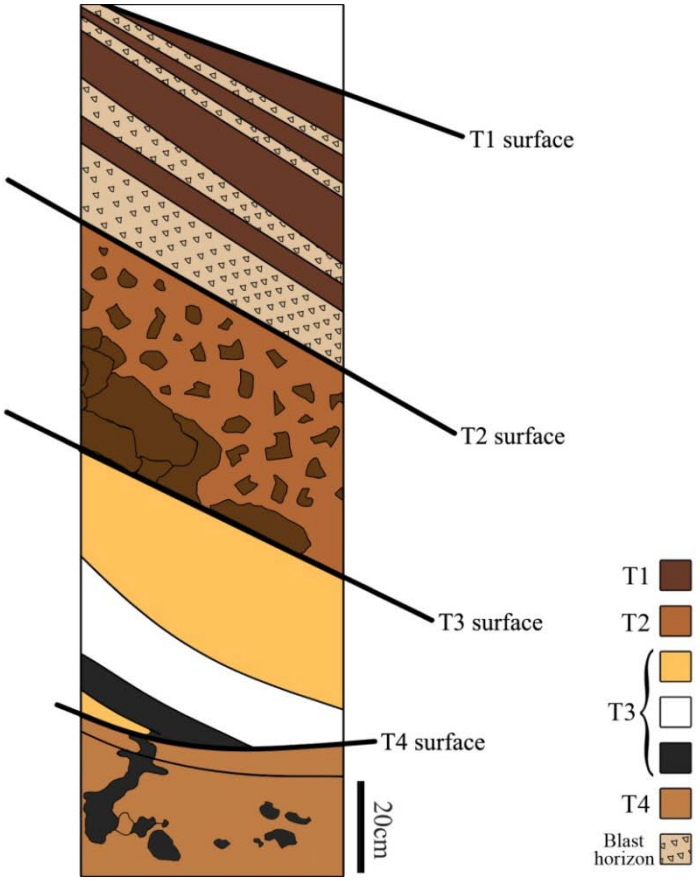


Figure 5.2 STK-MH1southern wall stratigraphic profile. T1 through T4 are displayed.

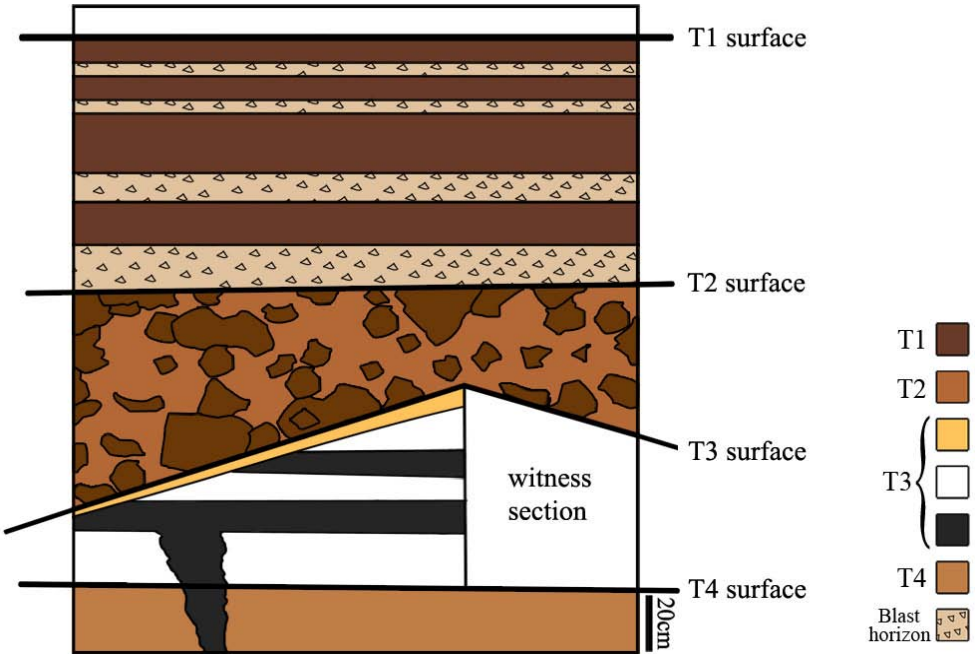


Figure 5.3 STK-MH1 eastern wall stratigraphic profile. T1 through T4 are displayed.

5.1. T1

The MH1 talus surface can be described as a mass of loose, shattered host rock and speleothem material with occasional bone fragments forming a slope running east to west from the far eastern corner of the Milner Hall. The talus surface represents the debris accumulation from extensive mining of a large stalactite that occupied the ceiling in the upper area of the far eastern end of the Milner Hall. The numerous drill holes and blast scars in the walls and ceiling attest to the intensity of the mining in this area. The sediments and fossils accumulated by this mining activity constitute the deposit named the T1 infill. The blasting redistributed sediments from the deposits in the vicinity of the large stalactite. The construction of the tourist path steps that ascend the MH1 talus has also added rubble to the talus surface. The route of the tourist path can be seen in Figure 1. The highly unconsolidated nature of these sediments created wall stability issues during excavation and so required extra squares to be extended around the main grid to allow the excavation of the deeper deposits. The support squares were labelled 'SS' and can be seen in the MH1 excavation plan illustrated in Figure 3.1.

5.1.1 T1 stratigraphy

The T1 deposit was accumulated in a short period of time during the mining of the above stalactite. Despite the quick deposition of these sediments, four separate infilling episodes can be distinguished within the T1 deposit. The relatively shallow angle of repose of the T1 slope (21°) is a result of the receptacle topography and the unconsolidated nature of the sediments which possess weaker shear strength and therefore encourage a shallower angle of repose (Verruijt 2010). The four intra-deposit strata repose at an increasing gradient with depth from the surface gradient of 21° until the basal strata, deposited directly upon the T2 surface, which shows a corresponding angle of repose of 28°. Two stratigraphic facies are identified within the T1 deposit, these facies are named *Facies AI* and *Facies AII*. Figure 5.4 shows the stratigraphic profile of the T1 deposit. Sediments within the T1 facies represent a mixture of material from a

combination of sources produced by anthropogenic activities and so are not placed within the main, naturally accumulated, stratigraphic sequence of the MH1 site. The mixed nature of the sediments makes the sedimentological properties non-diagnostic. The sediment chemical analysis (XRF) results are, however, informative when presented within the comparative framework of the entire MH1 sequence. As such, the XRF results are presented and interpreted in the comparative section at the end of the MH1 results (Section 5.5). Only *Facies AI* sediments were sampled for XRF. *Facies AII* sediments are made up entirely of highly fractured stalactite, with virtually no externally derived (allogenic) sediments, making XRF analysis pointless as it samples only internally derived (authigenic) material. The basal level of T1 is characterised by a thick (20-30cm) horizon of *Facies AII* material supporting a number of very large (>400mm^3) angular to sub-angular blocks of fractured dolomite. Both facies have developed in an alternating sequence, attesting to the episodic blasting that initiated deposit development.

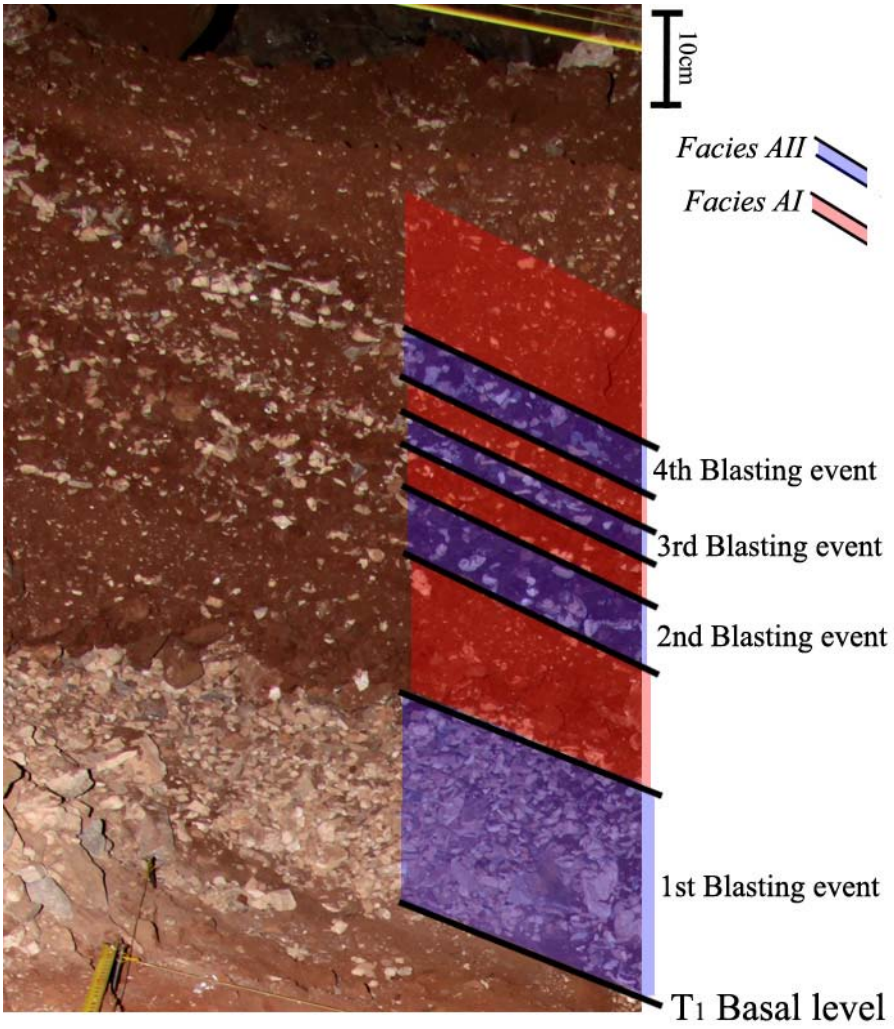


Figure 5.4 Stratigraphic profile of the southern wall of the T1 deposit. T1 basal level travertine stratum lies directly on the surface of T2.

The T1 facies can be described as follows:

Facies AI - Dark brown (2.5YR 2.5/2) loosely consolidated, unsorted, fossiliferous matrix-supported sediment inter-stratifying layers of *Facies AII* material. The dark brown matrix contains a high degree of clast size variability dominated by medium (100mm maximum dimensions) angular to sub-angular blocks of fragmented dolomite. Large interstitial voids are present throughout the dark brown strata. Fossils recovered from *Facies AI* are of a highly fragmented nature and generally have poor cortical preservation.

Facies AII – Unconsolidated, unsorted strata of highly fragmented travertine. The thickness of strata varies, with the basal stratum representing the thickest level, measuring between 20cm and 30cm. Speleothem particles are angular and measure no greater than 30mm in maximum dimensions. The travertine strata are reposed at progressively steeper gradients with depth. The basal *AII* stratum contains a large number of imbricated, boulder-sized dolomite blocks. *Facies AII* sediments contain no fossils as the material derives only from the blasted stalactite.

Each individual blasting event created and deposited a large quantity of shattered travertine directly onto the existing talus surface creating an *AII* stratum. The subsequently dislodged material from the local deposits then spread over the *AII* stratum forming an *AI* stratum, during the continued mining activities. This cycle took place four times. The thickest stratum of *AI* sediments corresponds with the thickest stratum of the *AII* material, suggesting a correlation exists between the magnitude of blasting event (depositing *AII* strata) and the quantity of disturbed sediments (constituting *AI*, fossiliferous, strata). The direct association of the basal travertine strata with the surface of T2 demonstrates the immediate impact of mining on the formation of these deposits and the cave environment.

The boulder-sized clasts of fragmented dolomite, supported by the basal travertine stratum, were accumulated during the initial blasting phase of the above stalactite. The rapid deposition of the blocks is indicated by the imbricated, randomly orientated nature of the clasts and the presence of large, unfilled interstitial voids. The position and pattern of deposition of the boulders corroborates the inferred location of the initial blasting phase. Figure 5.5 shows a schematic of plotted boulder position in the T1 deposit. It can be seen that the clasts have been deposited across the northern 'SS' squares and Squares A and C of the main grid. The absence of large clasts in the southern area of the excavation is caused by a shadow effect generated by the curvature of the southern wall. The relative position of the initial blasting is confirmed by the remnants of the stalactite that can be seen on the ceiling in the far eastern corner of the Milner Hall.

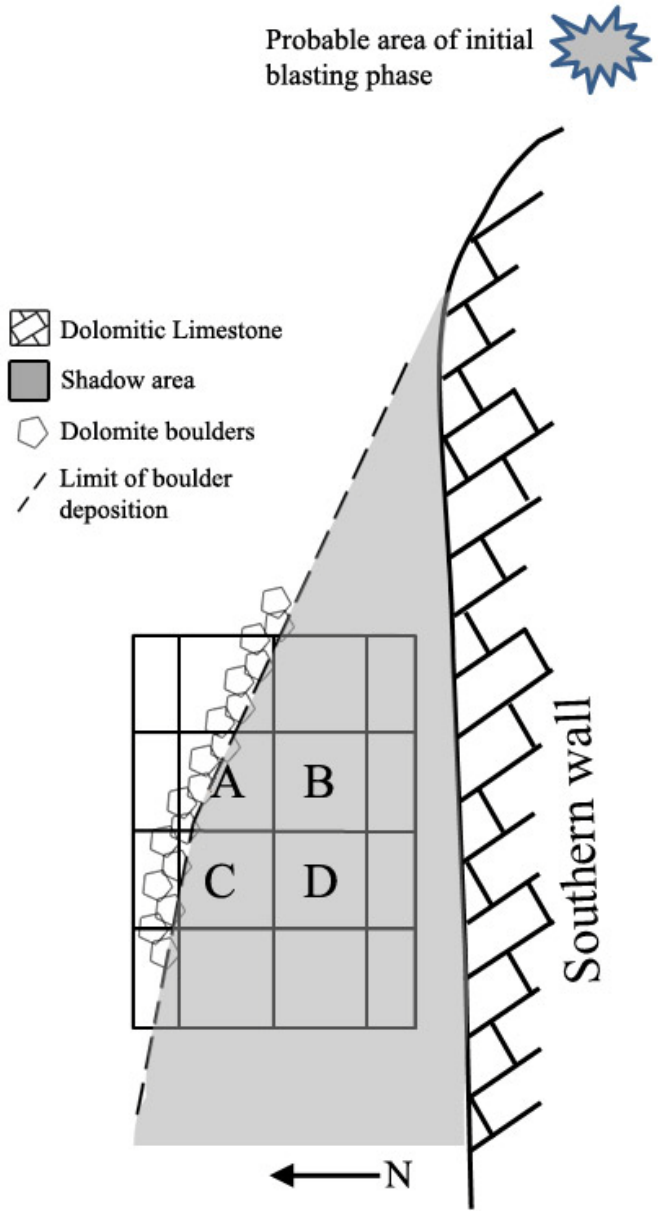


Figure 5.5 Plan view schematic of the STK-MH1 site with plotted dolomitic boulders deposited during the initial blasting phase. The area of initial blasting is indicated by the depositional pattern manifested by the fractured dolomite boulders.

The T1 deposit as a sediment gravity flow can be most closely compared to a rock-fall deposit. Bertran & Texier (1999) describe the accumulation of rock fall particles as "coming to a halt after rolling, bouncing and/or sliding onto the talus." (pp. 100). Characteristically, rock fall sediments have been described as "very

indistinctly bedded to typically unbedded, extremely poorly to very poorly sorted, with angular clasts and isotropic clast fabric." (Sanders *et al*. 2008, pp. 358). These facies are also characterised by an ungraded clast-supported matrix with large proportions of interstitial voids and a possible lack of finer sediments (Sanders *et al*. 2008). Regular internal collapse during settling causes further fragmentation of faunal material and may produce an inversely graded fine particle component once settled.

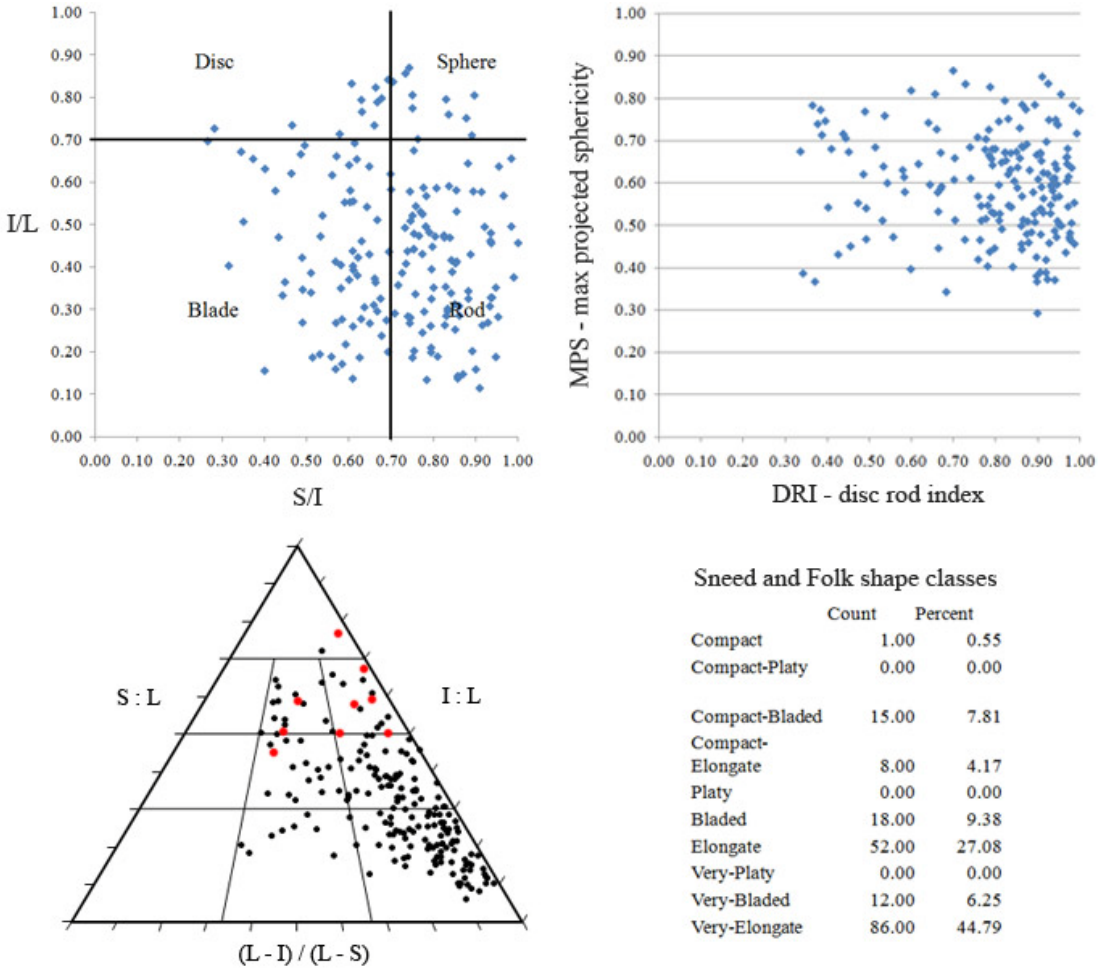
The highly fragmented nature of the fossils has probably been caused by a combination of processes associated with the mining activity. The bones that were blasted out were probably then subjected to trampling by the miners for the duration of the mining. The extensive fragmentation of the fossils prompted the splitting of the assemblage into two components, an identifiable and unidentifiable fraction. The identifiable component yielded a greater spectrum of data and was included in all analyses. The unidentifiable component was useful for only limited analyses. The interpretation of data from a subjectively selected subset requires a considered approach, given the inherent issue of sample representativeness. The heavily disturbed nature of the T1 deposit and its accumulation through mining activities qualifies the deposit as a secondary sedimentation deposit of anthropogenic origin. Positive correlations to probable sediment sources are unlikely as several deposits converge in the blasting area and would have contributed to the blast debris in different quantities depending on the exact location of each blasting event. The most probable sources are the Name Chamber and Silberberg Grotto.

5.1.2 T1 fabric analysis

The heavily disturbed nature of the T1 sediment limits the usefulness of formal fabric analysis. Any geomorphological indicators that may have been preserved within the original fabric of the source deposit(s) have been lost due to the blasting process. The blasting process as a re-sedimentation process eliminates more depositional indicators than natural re-sedimentation through collapse.

Essentially, the depositional history and area of origin of the T1 deposit is clear, and given that contextual data is limited to the analysis of yielded faunal and artefactual material, formal fabric analysis is unwarranted. In the case of T1, the natural clasts derive from blasting of the walls and ceiling through the mining process and re-distribution of those particles already contained within the original, local deposit(s). Faunal particles within the T1 deposit are highly fractured and have gone through more extensive breakage and atypical distribution to what would be expected in a natural collapse event. Particle shape and size profiles can, however, be used in conjunction with bone breakage data to exemplify the breakage intensity and poor assemblage integrity. The patterns that can be seen here support those patterns seen in the particles shape vs. breakage tests outlined in Chapter 4. The analysis of the T2 and T3 deposits provides a comparative framework for the T1 deposit.

The particle shape indices presented below sample only the identifiable component of the T1 assemblage because detailed dimensional attributes were only taken from the identifiable component. The unidentifiable faunal component was sorted into formal size classes based on maximum dimensions. The particle shape models in Figure 5.6 show a high proportion of elongated or rod-shaped forms. All indices show a similar proportion of elongated shapes. The Sneed & Folk shape categories show that 71% of all particles fit into either elongated or very elongated forms. The other 29% of the assemblage is made up of bladed or very bladed forms. When considering the proportion of fossils measuring below <30mm maximum dimensions, it is clear that the majority of the fossils in the T1 deposit have fractured to form elongated and very elongated faunal particles, a pattern seen in the breakage tests on long bone elements described in Chapter 4. Interestingly, the MPS (Maximum Projected Sphericity) vs. DRI (Disc-Rod Index) graph interprets the majority of T1 faunal elements into elongated to elongate-bladed forms. The trend seen in this research suggests that the MPS vs. DRI equation is more sensitive to spherical forms and produces representations with a higher proportion of spherical forms relative to the other shape indices.



Sneed and Folk shape classes

	Count	Percent
Compact	1.00	0.55
Compact-Platy	0.00	0.00
Compact-Bladed	15.00	7.81
Compact-Elongate	8.00	4.17
Platy	0.00	0.00
Bladed	18.00	9.38
Elongate	52.00	27.08
Very-Platy	0.00	0.00
Very-Bladed	12.00	6.25
Very-Elongate	86.00	44.79

Figure 5.6 T1 particle shape indices. It should be noted that only the identifiable bone component of the T1 faunal assemblage was used for the particle shape models. The red points on the Sneed & Folk diagram represent natural clasts collected during excavation. The natural clasts are not included in the shape class table.

The dominance of elongate, and to a lesser extent bladed forms, in the MPS vs. DRI graph indicates a very narrow particle shape profile within the assemblage. Shaft and flat element types produce disproportionately high quantities of elongate and bladed fragments due to their relative size and breakage tendencies. Compact element types represent 45% of the identifiable component and it is the presence and fracturing of these elements that has created the 12% of compact-combination shape forms recognised in the Sneed & Folks classes. T1 shows the highest proportion of compact shape forms (12.5%), a result of the increased

breakage inflicted on certain faunal elements types. Irregular and compact element (mostly axial bones and phalanges) often fracture into more spherical ‘compact’ forms. As fracture levels increase it seems all element types and fragments form more elongate and bladed forms. Clastic particles show a different fracturing pattern, as can be seen from the red points in the Sneed & Folk diagram in Figure 5.6. Chert and dolomite fracture into more compact or spherical forms that are less suitable for indication of sediment flow due to the low elongation ratio. Often, small, flat bulbs of percussion can be identified on fractured chert and look similar to small, archaeological incomplete flakes (Pers. Obs.).

The use of Voorhies groups as an interpretation of the transport potentials of the faunal material is not applicable for the T1 deposit due to the dominant sediment re-distribution process. Re-sedimentation through mining distributes sediments in an atypical manner and inhibits sediment flow, reducing the influence of particle shape on particle transport. Voorhies groups do, however, provide a form of element identification and classification and can be used as comparative data in inter-deposit analysis. The Voorhies groups of the T1 deposit are shown in Figure 5.7. Voorhies groups require a minimum level of skeletal element identification, and so only the identifiable component of the T1 assemblage could be used. Voorhies groups should be used with caution on assemblages that may be biased through subjective selection and non-representative sampling.

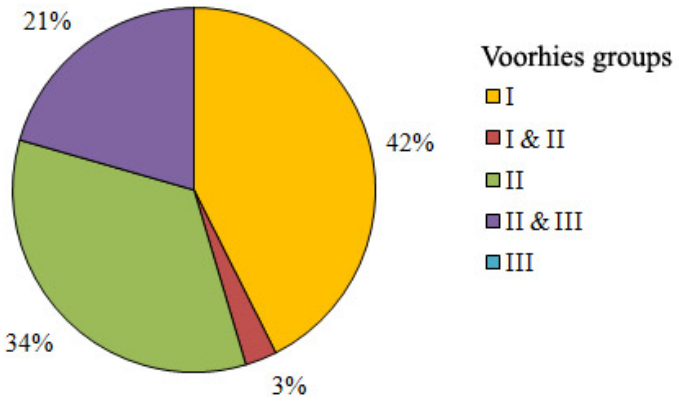


Figure 5.7 T1 Voorhies groups. For a description of the Voorhies groups see Section 3.3.

5.1.3 T1 faunal and artefact assemblage profile

The faunal assemblage has been split into two analytical components, the identifiable fossils and the unidentifiable fossils. The greatest amount of information can be yielded from the identifiable fossils as they can provide suitable data for the taphonomic analysis as well as taxonomic representation. This information is pertinent when attempting to identify potential source deposits, and to quantify the degree of mixing of sediments. The unidentifiable fossil component provides less information as a source deposit indicator, but is still useful for identification of fossil breakage patterns, element type representation, fossil condition and increasing the sample size for the identification of biogenic and anthropogenic bone surface modification attributes.

Table 5.1 presents the T1 assemblage profile. The high proportion of unidentifiable fossils can be considered significant in itself with over 88% of fossils excavated from the T1 deposit being unidentifiable to skeletal element or taxa. The assemblage size profile serves to demonstrate the highly fragmented nature of the assemblage with 91% of the entire T1 collection measuring <40mm maximum dimension, and 78.7% measuring <30mm maximum dimension. Within the identifiable component the mean maximum dimension of specimens is 31mm, with a modal value of 27mm, a median value of 29mm and a standard deviation of 13.5mm. In terms of particle size, a value calculated as the mean of the three dimensional axes L, I and S, the identifiable component shows a mean of 18, a mode of 12.4 and a median of 16.8 with a standard deviation of 6.2. The values of central tendency and standard deviation serve to illustrate the restricted size profile of the assemblage. The majority of the T1 fossils derive from species of size class two (23kg – 90kg (Brain 1981)). To place the T1 size profile in perspective, two commonly found species within the Sterkfontein deposits have humerus sizes in the range of 170mm to 200mm maximum dimension and femur sizes in the range of 220mm (taken from comparative specimens of impala (*Aepyceros melampus*) and leopard (*Panthera pardus*). Complete vertebrae from these species have a mean maximum dimension of 69mm (taken from cervical, thoracic and lumbar vertebra from the same species) with the smallest maximum

dimension, 44mm, represented by the carnivore cervical vertebra (particle size of 43.6) and a mean particle size of 45.3. The size profile clearly indicates that the majority of the T1 fossils have been extensively fragmented.

Max Length	Artefacts	Identifiable Fossils	Unidentifiable Fossils		
				Total	%
<19mm	2	28	593	623	36.1
20-29mm	0	68	667	735	42.6
30-39mm	2	56	164	222	12.9
40-49mm	2	22	76	100	5.8
50-59mm	0	5	18	23	1.3
60-69mm	0	8	6	14	0.8
70-79mm	0	3	3	6	0.3
80-89mm	0	1	1	2	0.1
90-99mm	0	1	0	1	<0.1
>100mm	0	0	0	0	0.0
Total	6	192	1528	1726	100.0
Total %	0.3	11.1	88.5	100.0	

Table 5.1 T1 faunal and artefact assemblage summary and size profile.

5.1.4 T1 archaeology

Six artefacts were excavated from the T1 deposit. The artefact details are shown in Table 5.2. Sourcing the T1 archaeological material is relatively simple. The only artefact-bearing deposit found in the vicinity of the blasting area, which accumulated the T1 deposit, is the Far Western Talus deriving from the Name Chamber. The Name Chamber deposits have been shown to have accumulated from the winnowing of sediments from the M5E Oldowan deposit and contained considerable quantities of Oldowan artefacts (Stratford 2008; Stratford *et al.* in prep). Given the proximity of the T1 deposit to the Name Chamber Far Western Talus, the inclusion of Oldowan material in the T1 deposit can therefore be expected, and the presence of archaeological material can be considered a strong stratigraphic indicator. With a larger archaeological assemblage from T1, one

would expect the raw materials, size profile and artefact type proportions to be comparable to the Name Chamber assemblage. Further sampling of the T1 deposit may indeed help enlarge the current Sterkfontein Oldowan, given the positive stratigraphic association between T1, the Name Chamber and M5E. Low concentrations of artefacts can also be expected within T1, as a result of the distance from the original artefact source (M5E), and the dispersion of the artefacts into the large, eastern Milner Hall area.

The excavation of only six pieces bearing diagnostic artefactual attributes restricts any broad technological interpretations. Of the six pieces, two measure <20mm and are considered small flaking debris (SFD). The technological attributes yielded from the four flakes are shown in Table 5.3. All six artefacts measure <50mm maximum dimension. The restriction of the artefact size may be considered a diagnostic trait of artefacts deriving from the Western and Far Western Talus deposits of the Name Chamber, where filtration within the Feeding Shaft has limited the deposition of particles to <50mm (Stratford 2008). The four flakes are represented by two quartz and two quartzite pieces. Photographs of the four flakes can be found in Appendix 1, Figures 1.18 – 1.21. Both the quartz and the quartzite artefacts are represented by an incomplete and a complete flake. The quartz artefacts both have some cortex preserved on the dorsal surface and can be interpreted as deriving from vein quartz outcropping on the landscape surface, as opposed to quartz deriving from river cobbles from the nearby Bloubank river. Kuman (1994a, b, 1997) has demonstrated a preferential utilisation of river cobble quartz in the Sterkfontein ESA assemblages due to the more predictable flaking properties of this raw material. The vein quartz found on the nearby landscape is often already highly fractured and very brittle (Pers. Obs.). Quartzite is not found on the nearby landscape and is only available in the form of cobbles within the river gravels of the Bloubank river. This allows positive identification of raw material source despite the absence of cortex. During the Oldowan at Sterkfontein, a pronounced preference for quartz has been demonstrated, although some quartzite and chert have been included in the assemblage. Subsequently a manifest move towards the utilisation of more quartzite is shown during the Early Acheulean (Kuman 1994a, b, 1997, 1998, 2007). The presence of quartzite within

the T1 assemblage cannot be used to imply any technological preference for raw materials because of the small sample size.

Artefact 244, a complete quartzite flake, has had all dorsal surface features eroded off, such features have been labelled indeterminate (indet.) in Table 5.3. The cause for such weathering is unknown and not typical of the Name Chamber, but could represent an artefact trapped in a particularly abrasive environment. A single artefact does not represent a pattern to be explored. Of particular interest is Artefact 283, which represents a probable quartz bipolar flake. The piece possesses the characteristic segment shape and shows, on the dorsal surface, three flake scars originating from opposing ends. One of the platforms has been split, leaving one measurable platform at the opposite end. On the split platform, crushing is found on both ventral and dorsal sides. The reduction of quartz using a bipolar flaking technique has been noted in the Sterkfontein Oldowan assemblage and bipolar cores represent a small (8%) but important component of the current Oldowan core collection (Kuman & Field 2009). Artefact 191, which represents a quartz complete flake, is particularly interesting as the entire ventral surface is covered in calcium carbonate, suggesting that this artefact has previously been in contact with localised speleothem growth. The artefact-bearing deposits within the Name Chamber are un-calcified and little to no flowstone growth can be currently seen in the Name Chamber. Similar conditions surround the Far Western Talus deposits entering the Milner Hall. It may be that the $CaCO_3$ found on Artefact 191 was formed on the artefact when it was in its original context (M5E) through localised contact with speleothem growth.

ART No.	R.M	Square	Spit Depth	Max length (mm)	WIDTH (mm)			DEPTH/thickness (mm)			Artefact type
					Max	Min	Midpoint	Max	Min	Midpoint	
158	Quartz	B	0-30	15	13	6	10.5	4	3.5	3.5	SFD
243	Quartz	D	0-30	19.5	10.5	7.5	9	7	4	6	SFD
244	Quartzite	D	0-30	33	16	10	16	4.5	4.5	4.5	complete flake
191	Quartz	C	0-30	42.5	25	11.5	23.5	10.5	6	9.5	complete flake
134	Quartzite	A	30-60	46	29.5	14	26.5	11	3	10.5	incomplete flake
283	Quartz	D	60-90	48	41.5	11.5	38	22.5	6.5	7.5	incomplete flake

Table 5.2 T1 archaeological assemblage size profile

Art No.	R.M	Artefact type	No. Flake scars (mm)	Length max scar (mm)	No. Step terminations	Remaining platforms	Platform thickness (mm)	Remaining cortex (%)	R.M source	Condition
244	Quartzite	complete flake	indet	indet	indet	0	3	0	cobble	w
191	Quartz	complete flake	1	28	0	0	5.5	50	vein	w
134	Quartzite	incomplete flake	2	41	0	0	9.5	0	cobble	f
283	Quartz	incomplete flake	3	37.5	1	0	10.5	25	vein	w

Table 5.3 T1 flake attributes

5.1.5 T1 faunal analysis

Unlike the artefacts from T1, the faunal material has two possible sources, the Name Chamber Far Western Talus and the Silberberg Grotto. Both deposits are found at the point where mining was most extensive in the eastern Milner Hall. The Name Chamber (by association the M5E) and Silberberg Grotto fossil assemblages are temporally different, and faunal representation may provide an indication of mixing of the two deposits. Unfortunately, the taphonomic analysis of the Name Chamber fauna has not yet been completed so no intermediate stage of re-sedimentation can be provided for comparison. The movement of sediments from M5E through the Name Chamber and into the Milner Hall provides an opportunity to study a known assemblage through multiple phases of sedimentation.

The T1 deposit yielded 1726 fossils. Of that assemblage, 192 fossils were identifiable to either skeletal element or further to taxa level. The measurements taken from both identifiable and unidentifiable components have been described in Chapter 3. The entire assemblage (1726 specimens) formed the dataset for the taphonomic analysis. For the remaining 1528 unidentifiable fossils, certain measurements were taken to recover as much depositional data as possible. Where data from both data sets could be used for certain analyses the results are provided for each dataset separately (referred to as T1 Identifiable and T1Unidentifiable), and in a combined form representative of the T1 deposit (referred to as T1 Total).

Skeletal element representation

Skeletal elements are split into long, flat, irregular bone, compact bones and tooth elements. This is the base level of skeletal element identification and includes both identifiable and unidentifiable components of the T1 assemblage. Element types are used in order to include all specimens even when fragmentation precludes positive identification to specific element or taxa. There is a significant difference in the element type representation between the identifiable and unidentifiable components. Positive identification to element type and all more

refined analyses are subject to the preservation of diagnostic attributes, but the quantity and nature of these attributes vary widely between element types and can bias information within either set. Compact bones, for example, represent a much greater proportion in the identifiable assemblage due to their relatively straightforward identification even in fragmented form. Conversely, long bones quickly lose element specific diagnostic attributes during fragmentation, producing large numbers of unidentifiable shaft fragments. Recognition of these potential data biases is important for accurate interpretation. Skeletal element representation, in terms of specimen abundance, is discussed in the taphonomic analysis in Section 5.1.7.

When combined, the T1 faunal assemblage shows a dominance of long bone elements representing nearly 70% of the entire collection. The next largest component is the indeterminate set representing 10% of the assemblage. All other skeletal elements make up the remaining 20%. As discussed in the methodology and demonstrated in the particle shape tests, long bones create large numbers of unidentifiable but similarly shaped particles (elongate and very elongate forms) when fragmented. The relatively large size of complete long bones provides a large potential yield of splinters and fragments.

The next level of skeletal element identification is the classification to appendicular, axial, podial and dental elements. This level only includes the identifiable fossils. Podial fossils are identified as any element distal to the tarsals/carpals, including the metapodials, and are not included in the appendicular count. The appendicular class includes the humerus, radius, ulna, femur, tibia and fibula elements. Podial elements represent nearly 40% of the assemblage with the next most highly represented skeletal portion being the appendicular elements at 22%. Both axial and dental elements represent under 20% of the fossils and suggest a relative dearth of cranial material. Non-dental cranial elements number eight in the T1 identifiable component (4%). These eight specimens consist of five bird skull fragments, two bovid horn cores and a bovid skull fragment. Metapodial elements in Bovidae are considered type 1 elements (long bones) and potentially yield a high number of small fragments as can be seen in the size

profile of the T1 podial component. Within the podial elements, twenty four (32%) of the fossils are presented by metapodial fragments. The remaining podial elements (n = 51, 68%) are represented by either phalanges or carpals and tarsals. Figure 5.8 and Table 5.4 show the representation of fossils with reference to either skeletal element or skeletal portions.

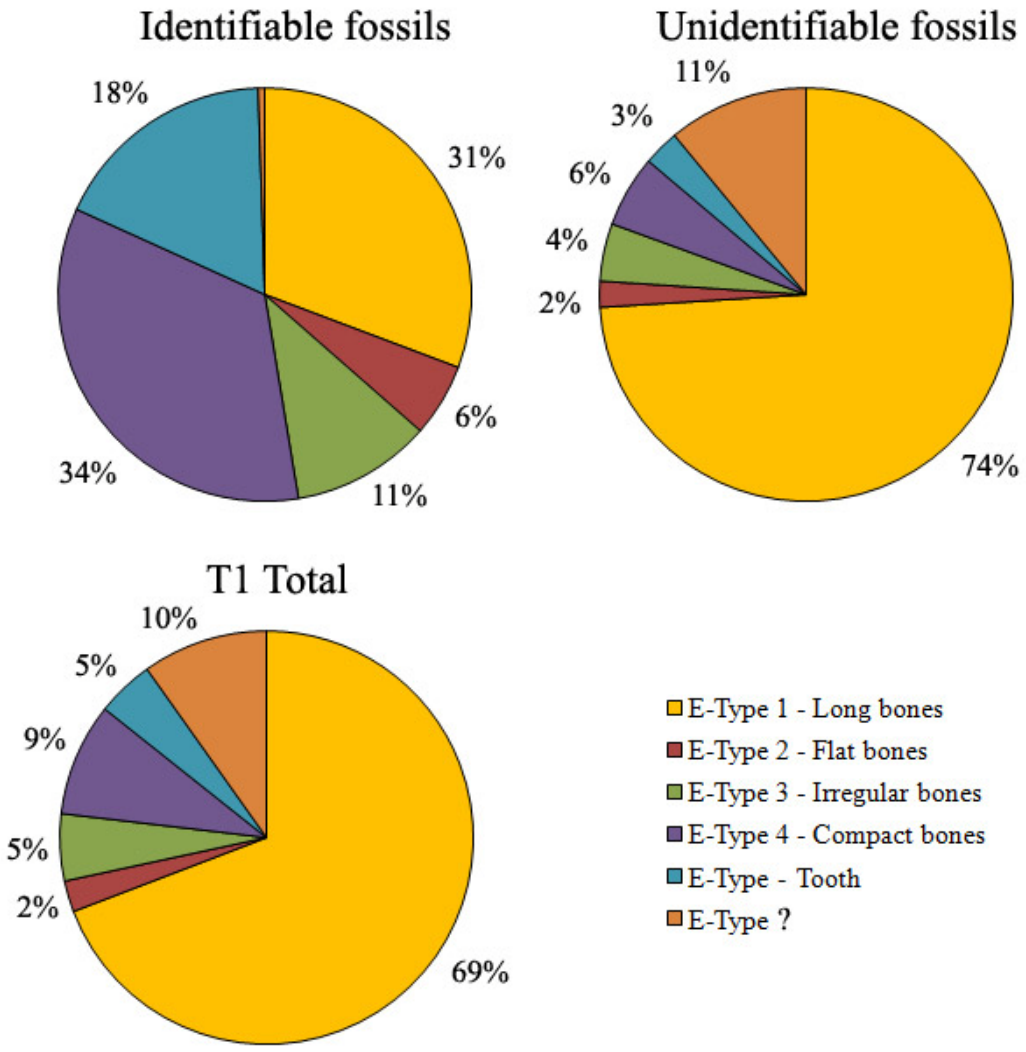


Figure 5.8 T1 skeletal element type distributions.

Max Length	Fossils						
	Appendicular	Axial	Podial	Tooth	?	Total	%
<10mm	0	0	0	0	0	0	0
<19.9mm	2	4	16	5	1	28.0	14.6
20-29.9mm	16	8	27	13	4	68.0	35.4
30-39.9mm	12	8	18	14	4	56.0	29.2
40-49.9mm	6	3	9	2	2	22.0	11.5
50-59.9mm	2	3	0	0	0	5.0	2.6
60-69.9mm	3	1	4	0	0	8.0	4.2
70-79.9mm	1	0	1	0	1	3.0	1.6
80-89.9mm	0	1	0	0	0	1.0	0.5
90-99.9mm	0	1	0	0	0	1.0	0.5
>100mm	0	0	0	0	0	0.0	0.0
Total	42	29	75	34	12	192.0	100.0
Total %	21.9	15.1	39.1	17.7	6.3	100.0	

Table 5.4 T1 skeletal portion summary of identifiable component.

Fossil survivorship

In highly disturbed and fragmented faunal assemblages like T1, bone survivorship can provide good corroborative information on the extent and nature of the breakage. Variable bone morphology and internal structure leads to biased patterns of element survivorship. Due to the explosive formation processes that formed the T1 deposit, breakage patterns and survivorship cannot be correlated to the assemblage source deposits.

The data presented below have been yielded from the T1 identifiable component of the assemblage. The bone breakage data presented below should be considered within the context of the broader T1 assemblage, as the T1 Identifiable component only represents 11% of the entire collection. The representation of the different parts of the bone (bone portion, bone division and bone completeness) can be considered specific to the identifiable assemblage and not representative of the entire T1 assemblage. For example, 53% (n = 102) of the T1 Identifiable component is represented by specimens with all proportions of the bone present, i.e. the diaphysis, metaphysis and epiphysis on a single specimen. This high

proportion is due to sample bias within the T1 Identifiable component. As will be demonstrated in the inter-deposit comparison, the identifiable fossil component is not representative of the whole assemblage. Use of the T1 Identifiable component as a representative of the original assemblage can produce similarities across deposits that are false a situation referred to as equifinality in taphonomy. It is important to note that preservation of all portions of bone does not equate to a complete element, but one that has been broken such a way that these parts remain. The preservation of these parts is what makes the specimen identifiable. The number of complete elements within the identifiable assemblage is just 35.

Bone breakage

The bone breakage numbers for the T1 deposit maintain the general pattern established by the previously described data. Basic breakage data are shown in Figure 5.9. There is a clear dominance of heavily broken faunal material with 86% of the total assemblage represented by fossils with the maximum number of breaks possible. That is 86% (n = 1484) show breakage of the circumference of the element at both ends. Within the T1 Total assemblage, only 11% of fossils possess fewer than three breaks. Only 2% (n = 35) of the T1 Total assemblage has no breaks and can be considered complete elements. Lyman (1994) describes the *intensity of fragmentation* as a measure of the extent of faunal fragmentation. The *intensity of fragmentation* is indicated from the size range of non-complete elements within an assemblage; the more intensely fragmented assemblages are represented by a larger proportion of smaller fragments, themselves represented by a lower mean maximum dimension. Contrastingly, less intensely fragmented assemblages will be represented by a collection dominated by larger fragments possessing a higher mean maximum dimension (Lyman 1994). Although some of the trend is seen in the T1 assemblage, in that small fragments clearly dominate the collection, the proposed mean size trend is not seen. The opposite is seen in T1, with the mean maximum dimension of the fossil fragments (33mm) being greater than mean maximum dimension of the complete bones (27mm). This trend may be a result of the gravity flow type accumulating the sediments. Larger bones

generally have lower density (Lyman 1984), higher volume and higher absolute surface area and are therefore more intensively fragmented in clast-rich, rapidly accumulated sediment flows, leaving the more compact and often smaller elements less prone to fragmentation. Lyman's *intensity of fragmentation* may, therefore, be inappropriate for application on assemblages accumulated by sediment gravity flows and is more applicable to fluvially accumulated assemblages. The high degree of fragmentation in the T1 assemblage is clearly demonstrated by the proportions of break numbers evident on the fossils.

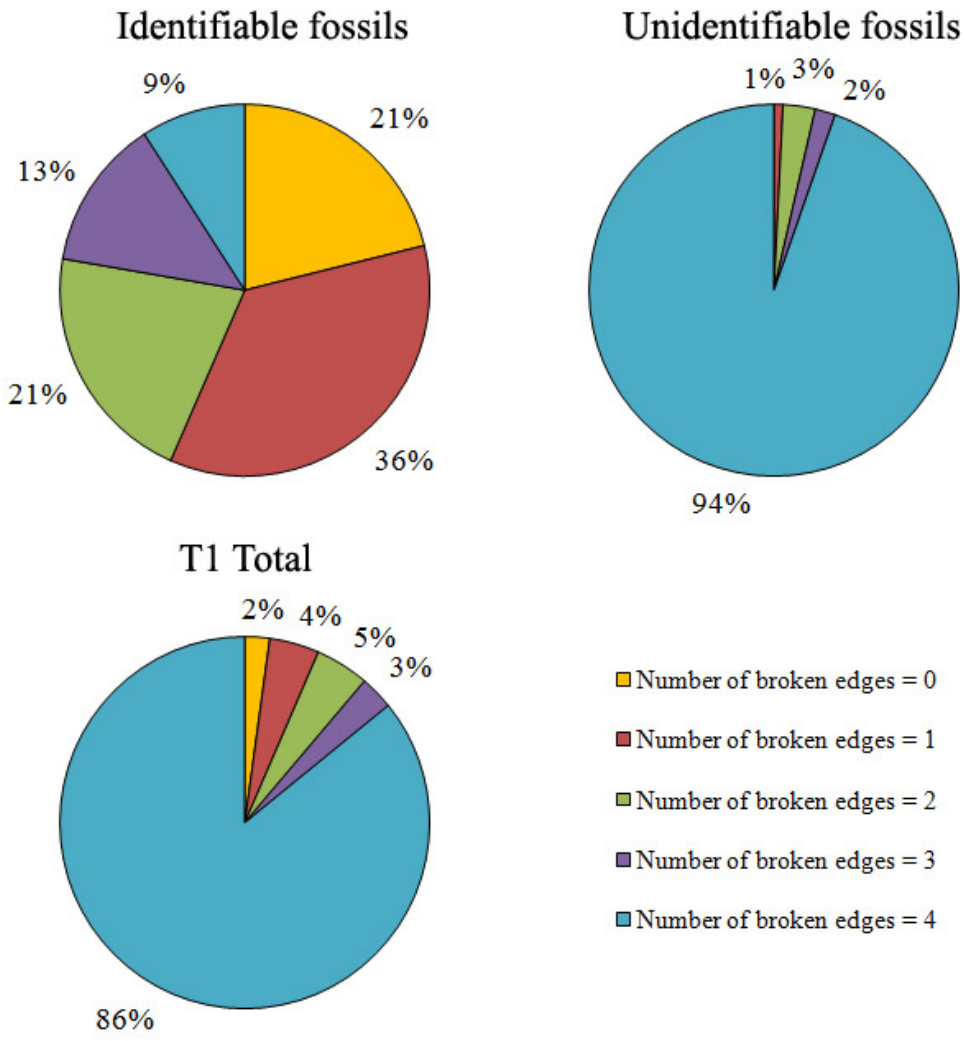


Figure 5.9 T1 numbers of broken edges on fossil material.

The T1 breakage data needs to be considered in isolation due to the destructive formation processes possibly significantly affecting the contributing deposit's breakage patterns during re-sedimentation. The distinction between the identifiable component and the unidentifiable component demonstrates the issue of sample biasing. The identifiable and unidentifiable component breakage level dichotomy is a broad indication of the limiting affect of breakage on element identification. Fossils are identifiable through the preservation of diagnostic morphology. The breakage proportions (number of fractures) for the identifiable component cannot be taken as an assemblage-wide representation of breakage levels, or representative of the source deposit.

Bone fracture type and angle are used to indicate when the breakage occurred relative to the diagenesis of the bone. The breakage types can be considered representative of the entire assemblage. The theory and previous work establishing breakage trend characteristics is discussed in Section 3.5.2. Breakage type proportions are given as a percentage of the broken fossil assemblage. Complete bones are included in the T1 Total assemblage data but not in the broken bone subset. Figure 5.10 illustrates the T1 break type proportions within the broken bones of the T1 Identifiable component.

The fracture analysis for the T1Unidentifiable component counted the dominant fracture type on each specimen and did not utilise combination categories. In the T1 Total assemblage 89% (n = 1359) show sawtooth fractures with 7.5% (n = 115) showing a dominance of smooth fracture surfaces. The remaining specimens (3.5%, n = 54) are dominated by stepped fracture surfaces. Within the T1 Identifiable component 46% (n = 72) of the broken fossils display only sawtooth fractures, with 60% (n = 94) specimens displaying at least one sawtooth fracture. 26% (n = 40) show only smooth fracture surfaces and 47% (n = 73) show at least one smooth fracture surface. Those specimens showing a stepped fracture type represent only 23% (n = 37) of the T1 Identifiable broken component. The dominance of sawtooth fractures throughout the assemblage attests to the majority of breakage occurring post-fossilisation.

Fracture angle has been demonstrated to be a valid indicator of breakage timing in relation to the diagensis of bone by Villa & Mahieu (1991). Fracture angle data was only yielded from the T1 Identifiable component. The majority of the breakages represented in the broken bones of the identifiable component are combination breaks i.e. there is more than a single fracture angle represented on one specimen. Of the 47% (n = 73) fossils with a combination of fracture angle the dominant combination is the perpendicular and acute. Fossils with at least one perpendicular fracture angle account for 77% (n = 120) of all broken bones. Fracture angle was not analysed for the unidentifiable component, but the data for the identifiable broken bones show a dominance of perpendicular breakage angles, followed by a combination of perpendicular and acute fracture angles. The fracture angle data for the T1 Identifiable component are illustrated in Figure 5.11. When considered together, the breakage patterns further support the T1 pattern. The dominance of perpendicularly broken, sawtooth textured fractures throughout the T1 Total assemblage indicates the majority of diagnostic bone breakage took place when the bones were already fossilised. The dominant post-depositional and post-fossilisation breakage would have replaced the majority of the primary depositional breakage patterns.

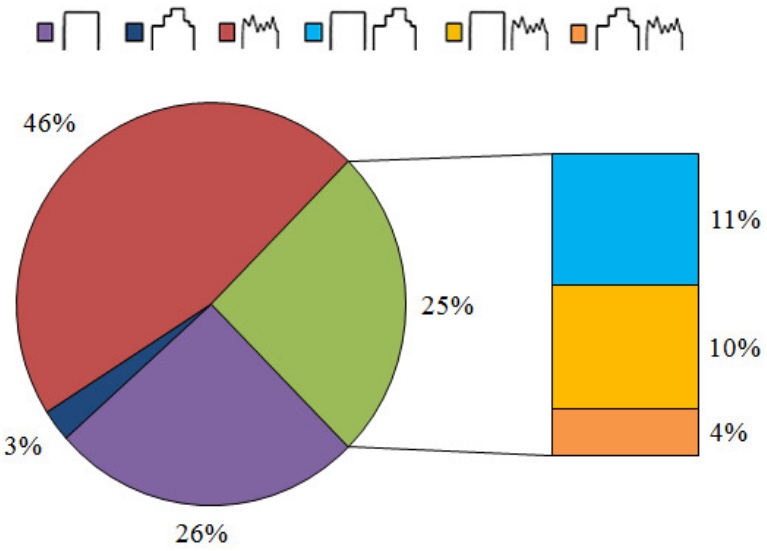


Figure 5.10 T1 bone fracture types. Proportions are taken from the identifiable component of the T1 assemblage. The green slice represents the proportion of bones with a combination of fracture types.

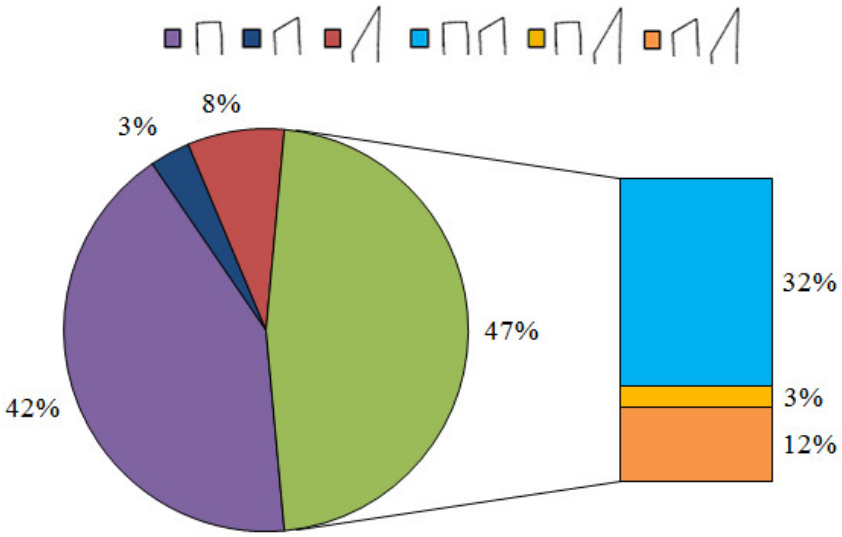


Figure 5.11 T1 bone fracture angles. Proportions are taken from the identifiable component of the T1 assemblage. The green slice represents the proportion of bones with a combination of fracture angles.

Bone condition

Non-biogenic bone surface damage has been used to gauge exposure times of faunal material prior to burial (Behrensmeyer 1978). The attributes identified as bone surface modification through geogenic processes have been described in Chapter 3. The problems with this system with reference to cave environments have also been discussed in Chapter 3. Figure 5.12 shows the bone condition data for all components of the T1 assemblage. There are clear differences between the T1 Identifiable and T1Unidentifiable component of the assemblage. It can be seen that 66% of pieces are slightly weathered (equivalent to Behrensmeyer's Stage 2-3) with the next largest fraction being of fresh condition. Behrensmeyer's stages 0-3 suggest a burial time of less than 6 years (Behrensmeyer 1978). The generally good condition of the fossil surface seems to contrast the highly fragmented nature of the assemblage and supports the idea that the assemblage was buried and fossilised relatively quickly. The relatively good bone surface condition contradicts the expectations of an assemblage affected by heavy levels of damage. It may be that the mineralised condition of the bone may have provided some protection to the bone surface from extensive damage, the majority of damage being focussed on the bone edges. Very weathered specimens (equivalent to stage 5) represent just 2% of the total.

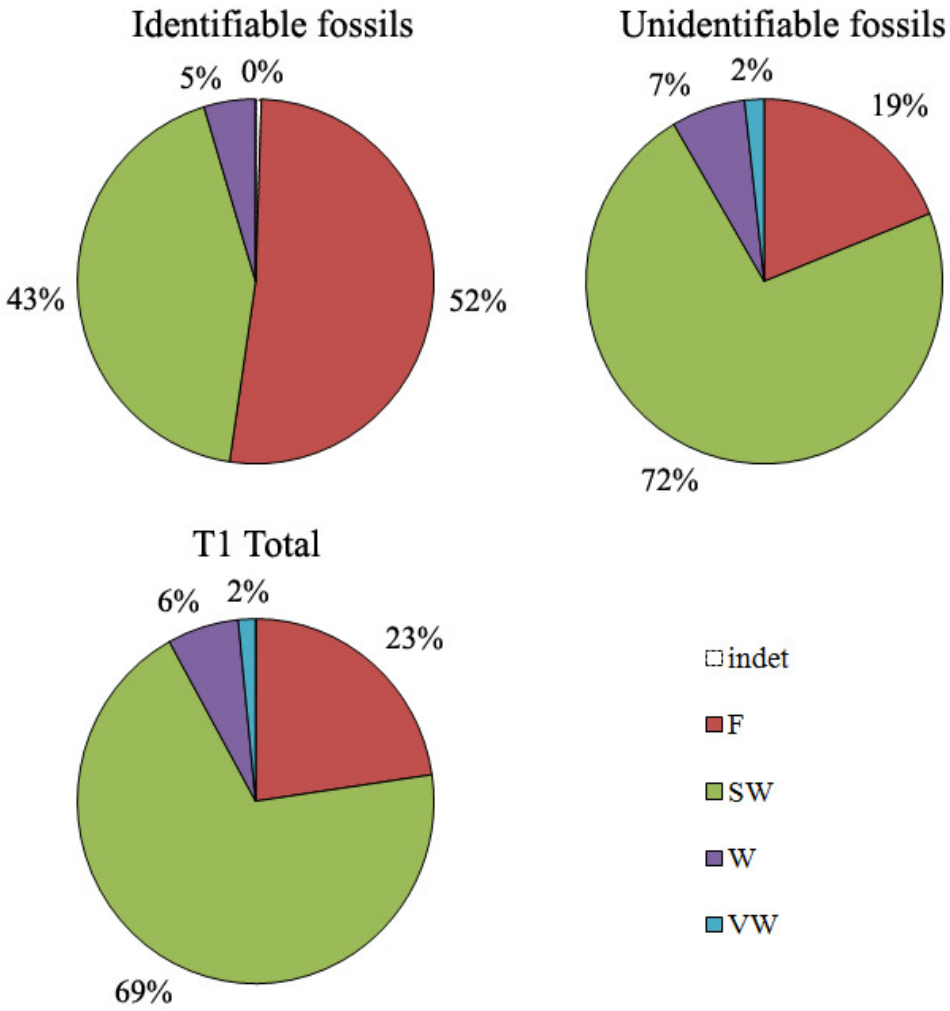


Figure 5.12 T1 fossil condition.

5.1.6 T1 taxonomy

The taxonomic results are difficult to interpret as they only represent faunal specimens located within the immediate area of the blasting activity. Temporally sensitive species would indicate the contribution of certain deposits but cannot quantify the level of contribution. The high fragmentation level, and bone condition quality, have allowed the positive identification of only three non-bovid mammals to species level, those being *Equus*, *Procavia antiqua* and the small felid *Caracal caracal*. The presence of these species is unremarkable for the Cradle sites. Caracal (*Caracal caracal*) are not uncommon in the Cradle sites and have been found within a temporally broad range of deposits. Within the

Sterkfontein site, the *Caracal caracal* is the most abundant cat in the M2 deposit (T. Pickering *et al.* 2004a) and also appears in the Jacovec Cavern (Kibii 2007). In other Cradle sites the caracal appears at Drimolen (O'Regan & Menter 2009) and Coopers D (Berger *et al.* 2003). The caracal is a small nocturnal cat that ranges over a broad spectrum of environments but prefers open rocky outcrops (Skinner & Chimimba 2005) and has been found near and within caves (B. Kuhn Pers. Comm). The significance of the presence of *Equus* is described in the Section 3.6. The *Equus* specimens must have come from the Name Chamber Far Western Talus, from the M5E deposit, as they are mostly found in this younger surface deposit (T. Pickering 1999) but are not found in the M2 fauna (T. Pickering *et al.* 2004a). The hyrax (*Procavia antiqua*) is unremarkable and appears both within Sterkfontein in M4 (Kibii 2007), M5E (T. Pickering 1999) and at the Coopers D site (Berger *et al.* 2003).

The presence of both only *Caracal caracal* and *Equus* precludes any palaeoenvironmental suggestions. Without larger samples, any singular species representation could represent time-averaging caused in the primary sedimentation deposit or by the mixing of sediments during re-sedimentation. In terms of bovids, two different Alcelaphini were identified, a small (size class one), *Damaliscus*-sized Alcelaphine and a medium (size class two), *Connochates*-sized Alcelaphine. A Tragelaphini (size class three bovid) was also identified based on a horn core fragment. The bovids identified are common throughout the Cradle sites and are represented in a temporally broad range of deposits and are not particularly useful as deposit diagnostic indicators.

5.1.7 T1 taphonomy

The T1 Total assemblage was used for the taphonomic analysis in order to allow the maximum resolution of bone surface modification features that may not have been well represented on the relatively small, T1 Identifiable sub-assemblage. The bone breakage and condition data for the T1 assemblage indicates the integrity of the assemblage is not good, and the residual, original depositional indicators may

have been removed during the re-sedimentation process and the violent re-distribution through blasting. This is, unfortunately, despite yielding the largest sample size of all the investigated deposits.

Table 5.5 presents the skeletal element representation within the bovid size classes. Size class one and size class two bovids provide the widest range of skeletal elements representing almost all body portions and multiple MNI (Minimum Number of Individuals). The smaller bovids clearly represent a greater proportion of the assemblage, both in terms of range of element representation, and number of individuals. The broad spectrum of element types and associated body portions represented by the size class one and two bovids does indicate that all elements from a number of animals must have been deposited. The bone surface modification data shows a low proportion of specimens with carnivore related damage. The number of specimens showing carnivore bone surface damage relative to the T1 Total assemblage is 10 (0.5%). This includes five pieces with one or more tooth scoring events, tooth pitting events on two bovid innominate fragments, one tooth pit on a midshaft fragment, and three probable tooth notching events on a bovid radius midshaft. Six pieces also display small rodent gnawing bone surface modification. Carnivore related damage cannot be considered a prominent taphonomic signal and although the presence of carnivore damage attests to the predation or scavenging of fauna prior to deposition, the proportion of carnivore damaged bones is too small to propose a significant amount of fauna was carnivore accumulated. The specimens displaying carnivore damage may also represent damage induced on those elements that were exposed on the surface for a longer period before burial. The bone condition data certainly suggests that a significant proportion of the specimens were possibly exposed to landscape surface weathering for up to six years (corresponding to Behrensmeyer's (1978) weathering stage 3). Non-biogenic bone surface features include notching (from natural percussion events) and randomly orientated and linear striations on protruding edges and cortical surfaces. These represent abrasions caused by movement of the specimen through clast-rich sediments or movement of clasts over the specimen. This kind of damage can be caused both pre- and post fossilisation.

Skeletal part	Antilopini	Size 1	Small Alcelaphini	Size 2	Medium Alcelaphini	Tragelaphini	Size 3
Skull	6/2/2		4/3/3	6/5/5	8/2/2	2/1/1	
Cervical				1/1/1			1/1/1
Thoracic		1/1/1		2/2/1			1/1/1
Lumbar							1/1/1
Indet.							1/1/1
Rib		2/2/1		1/1/1			2/2/1
Humerus		3/3/2		1/1/1			
Radius		2/1/1		2/2/1			1/1/1
Ulna		1/1/1					
Magnum		1/1/1		1/1/1			
Unciform				1/1/1			
Scaphoid				1/1/1			2/2/1
Cuneiform		1/1/1					1/1/1
Lunate							1/1/1
Metacarpal		1/1/1		3/2/2			
Innominate		1/1/1		2/2/1			
Femur				1/1/1			
Tibia		2/2/1		1/1/1			
Astragalus		2/2/2		1/1/1			
Navicular-cuboid		1/1/1					
Calcaneum				3/3/2			
External cuneiform		1/1/1					
Metatarsal		3/3/2		3/3/3			1/1/1
Phalanx I		9/7/2		3/3/2			1/1/1
Phalanx II		3/3/1		3/3/2			1/1/1
Phalanx III		3/3/2		2/2/2			
Sesamoid				1/1/1			1/1/1
Metapodial		10/5/3		10/5/3			5/2/1

Table 5.5 T1 skeletal element representation of bovid taxa. NISP/MNE/MNI data is given for each cell in columns two through seven. Bovid cranial elements include 23 dental elements, two horn cores and a skull fragment.

5.1.8 T1 discussions

The T1 deposit was created from the blasting of a large stalactite that occupied an area of the roof above the top of the MH1 talus, up slope and east of the MH1

excavation. The drill holes and blasting scars attest to the size of the speleothem and intensity of destructive activity. Each blasting event sent an immediate layer of shattered travertine (*Facies AII*) and a following layer of disturbed sediments (*Facies AI*) down slope, building an alternating sequence of strata documenting the mining of this area. The thickness of the strata of travertine and associated disturbed sediments is roughly proportional to the size of the blasting event. The first, and largest, blasting event distributed the thick basal fractured travertine horizon and dislodged a number of very large dolomite blocks which were sent tumbling down the talus to rest across the MH1 excavation site. The position of these large blocks attests to the position of the initial blasting area. The dislodged and re-distributed allogenic sediments that constitute *Facies AI* are highly fossiliferous and artefact-bearing. Despite providing the largest sample of fauna, the *Facies AI* faunal assemblage is characterised by a highly fragmented, extensively damaged collection. The vast majority of the damage is attributable to a post-fossilisation re-distribution process, most likely the violent blasting episodes and the associated rapid movement of sediments. Tracking the source deposit(s) of the allogenic sediments is difficult. The high levels of post-fossilisation fossil breakage reduce the preservation of faunal data and make quantification of mixing close to impossible. The most likely contributing deposits, based on proximity, are the Name Chamber, which was established to have derived from M5E, and the Silberberg Grotto M2. The heavily calcified nature of the M2 deposit makes it a less likely major contributor. The presence of *Equus* and archaeological material indicates at least a contingent of the T1 sediments derive from the Name Chamber Far Western Talus (and consequently M5E). The other taxa represented are not temporally sensitive and are found in a number of deposits in Sterkfontein and around the Cradle sites. It is most probable that the majority of sediments have derived from the Name Chamber. Unfortunately, the analysis of the Name Chamber fauna has not been completed so assessment of the intermediate stage of re-sedimentation between the M5E and the MH1 talus is not possible.

5.2 T2

The T2 deposit represents the infill directly underlying the T1 basal fractured travertine stratum. The T2 deposit surface represents the talus surface present in the eastern Milner Hall prior to the mining activity and is significant because of its natural accumulation. T2 was excavated in a 2m x 1m trench running north-south over Squares A and B (see Figure 3.1 for plan of the MH1 excavation squares). Excavations progressed following the morphology of the deposit. The T2 surface slopes at a 28° gradient running in an ENE-WSW direction, a steeper angle to that of the T1 surface of 21°. The angle of repose of the T2 deposit is significantly influenced by the topography of the underlying deposit surface. The angle of repose of the underlying deposit (T3) is 30° running ENE-WSW with two strike gradients, the first lies at 25° SW-NE, and the second at 21° in a NE-SW direction. The strike slopes of the T3 deposit form a ridge running in the dominant direction (ENE-WSW) of the main gradient of the slope. The morphology of the T3 surface is shown in Figure 5.3. The form of the T3 deposit is discussed in the T3 analysis (Section 5.3). A similar strike degree is not found in the T2 deposit. Both T1 and T2 have insignificant strike gradients. Due to the morphology of the underlying deposit, the T2 deposit varies in thickness by up to 40cm within the 2m long eastern wall profile. As an *in situ* secondary sedimentation deposit with numerous possible source deposits and good sediment sourcing potential, the T2 deposit was excavated using *in situ* techniques and methods (described in Chapter 3) with each fossil mapped and recorded prior to removal from the deposit. Figure 5.13 shows the T2 deposit surface before excavations were started.



Figure 5.13 MH1 excavation with T2 surface slope cleared for excavation. Notice the thick fractured travertine layer representing the basal stratum of T1 and the first blasting event. The range staff segments measure 10cm.

5.2.1 T2 stratigraphy

The MH1 excavation has sampled the medio-distal portion of the T2 deposit. Although the terminal portion was not sampled, the proximity of the cave floor and the termination of the underlying deposit suggest that the termination of the T2 deposit would occur within 2m down slope of the MH1 excavation (see Figure 5.1). The T2 deposit represents a single depositional facies and shows no grading of larger clasts although the particle size analysis does show an inverse grading process within the fine sediments. The post-depositional development of the inverse grading system is discussed in the following section. The T2 deposit can be classified as a grain flow deposit in the sense that the sediments have been redistributed colluvially, in a surge of sediment due to a collapse or over-steepening of the source deposit and a lack of influence of water (Bertran &

Texier 1999). The lack of internal stratigraphy is a result of the T2 deposit representing a single depositional surge, not recurrent surges that create multiple strata. Although grain flow deposits are often considered well stratified (Hétu *et al.* 1995; Bertran *et al.* 1997; Major 1997), stratigraphic resolution is usually limited to individual surges in sediment. In grain flows, it is common to find a basal level of highly imbricated larger clasts (Hétu *et al.* 1995; Bertran *et al.* 1997) and an accumulation of larger clasts at the snout of the deposit (Parsons *et al*. 2001). The rapid accumulation of the deposit is further suggested by the generally highly fragmented condition of the fossils. The T2 facies is labelled *Facies I* within the MH1 sequence and is described as follows:

Facies I - Dark brown red (ranging between 10R 3/3 and 10R 3/6) massive, clast-supported matrix. The *Facies I* bed ranges in depth from 40-80cm in the eastern wall profile, as dictated by the underlying T3 surface morphology. Clasts range in size from 50mm - 400mm maximum dimension. Clasts are made up of angular to sub-angular cobble sized blocks of fragmented dolomite, chert, fractured flowstone and occasional rounded blocks of heavily calcified, fossiliferous, fine-grained breccia characterised by different sedimentological properties to the surrounding 'soft' matrix. The basal level is dominated by the largest clasts and dips at the angle of repose of the underlying deposit. The suspended larger clasts show high levels of imbrication and an associated high proportion of interstitial voids. Interstitial sediments are loam to silt loam in texture and inversely graded. The matrix is unconsolidated, artefact-bearing and fossiliferous. Fossils are characterised by fragmented, exfoliating and crumbling white bone.

The breccia blocks found within the T2 deposit differed from the surrounding *Facies I* sediments in several ways. In terms of faunal content, the breccia blocks were highly fossiliferous and contained specimens that were generally more complete than was found in the surrounding *Facies I* sediments. Sedimentologically, the breccia blocks differed from *Facies I* in that the blocks contained a matrix that was a different colour (7.5YR 6/6-6/8) and were matrix-

supported with only small and infrequent dolomite and chert fragments. The source of these blocks is unknown and difficult to determine. The dissimilarity suggests they do not derive from the same deposit as the *Facies I* material and have probably contaminated the T2 deposit from a distinct, decalcifying or collapsing breccia body in stratigraphic contact with the *Facies I* source deposit(s). As a hypothesis I would suggest that the blocks derive from the Old Brecciated Deposit - the earliest fossiliferous and heavily calcified sediments found within the Name Chamber (Stratford 2008). The colour and contents found in the remnants of this deposit preserved on the walls of the Name Chamber bear a resemblance to the blocks found in the *Facies I* sediments. Unfortunately, the small size and infrequency of the contaminant blocks preclude a dedicated sampling and valid analysis of their contents. The presence of fractured flowstone in the *Facies I* sediments does support the inference that a component of *Facies I* has derived from sediments redistributed through collapse. Figure 5.14 shows the stratigraphic profile of the T2 southern wall.

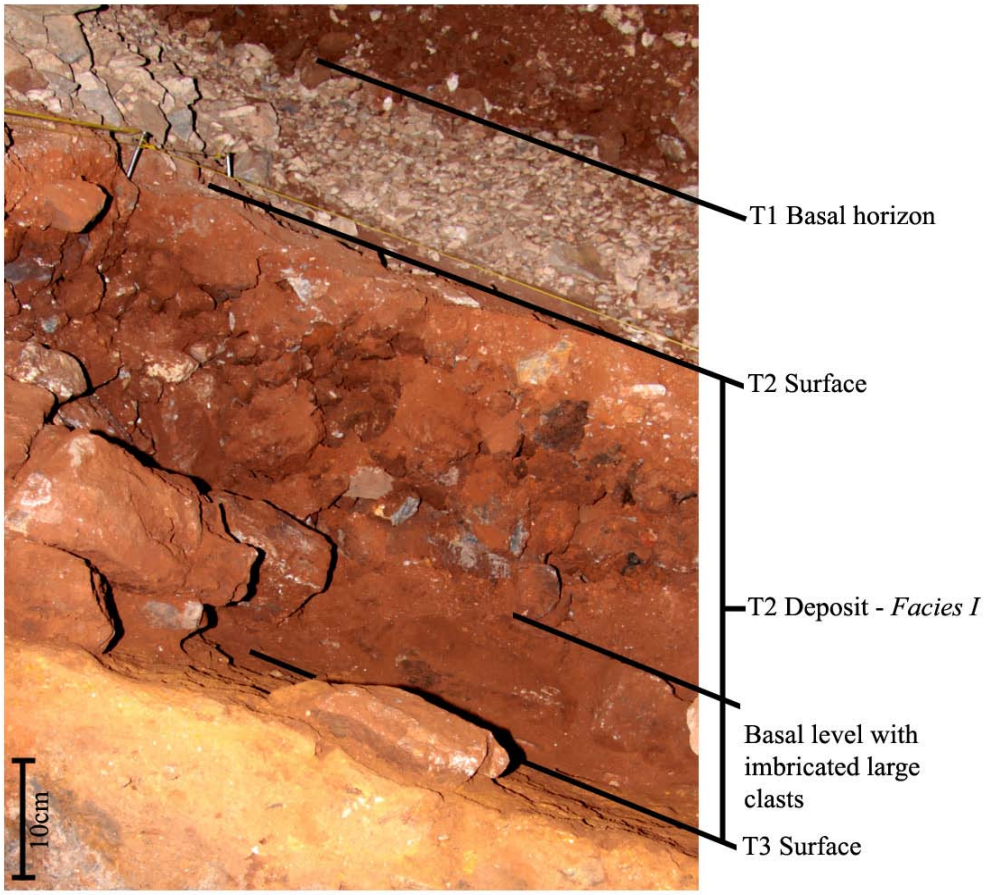


Figure 5.14 MH1 Southern wall and main body of the T2 deposit, '*Facies I*' in the MH1 sequence. T1 basal stratum is 1.5m from the camera and is 20cm thick. T2 deposit is 40cm thick on the southern wall.

A number of fossil concentrations were found within the T2 deposit. The concentrations contained similarly sized and associated fragments of the same element as well as pieces from differing body portions and taxa. The concentration of associated broken pieces of the same element indicates that the fossil material has been fragmented *in situ* during the accumulation and not moved since deposition. The concentration of pieces from a variety of elements (within a restricted maximum dimension), indicates the movement of fossils through interstitial pockets, settling into a relatively open area, after the main sediment surge. Evidence of both processes is found in 'Concentration C' (Figure 5.15), suggesting the small receptacle is relatively stable and has both preserved

pre-existing contents and accumulated vertically moving fossils. Secondary sedimentation fossil concentrations differ to concentrations developed during primary sedimentation in that multiple phases of breakage and sorting may have significantly altered the properties of the primary bone assemblage. Secondary re-sedimentation may also concentrate or mix specimens deriving from different deposits, or strata within the source deposit, creating non-representative associations. In primary sedimentation fossil concentrations, it is possible for skeletal elements (broken or complete) of the same individual to be found directly associated or even articulated, e.g. the StW 573 specimen. Figure 5.15 shows 'Concentration C', the densest of the T2 fossil concentrations.

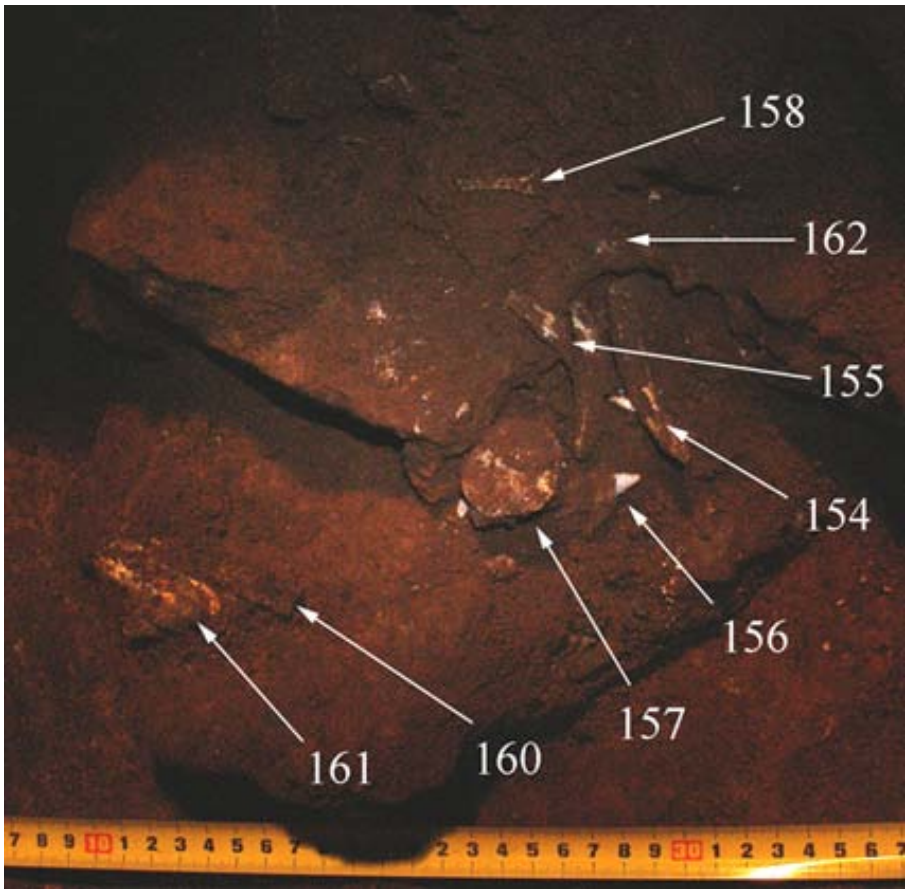


Figure 5.15 T2 fossil concentration C. Specimens 154,155,156 represent an *Equus* tooth broken *in situ*, with most of the fragments remaining in place. All other pieces represent pieces from a variety of skeletal elements from a variety of taxa that have accumulated in the same interstitial void.

5.2.2 T2 sedimentology

The natural accumulation of the T2 deposit necessitated a full range of sedimentological analyses to be applied to ascertain as much contextual information as possible. Particle size analysis, hydrology, XRF (chemical composition analysis) and *in situ* fabric analysis were all conducted on the *Facies I* sediments. A single sample was taken for the XRF analysis as a representative of the single depositional facies identified. The sedimentological summary for *Facies I* is shown in Table 5.6. The sediments within *Facies I* can be classed as a loam at the surface to a silt loam in the middle and lower sections of the deposit. Sediment samples were taken from the surface, middle and the base of the deposit for the particle size and hydrology to determine intra-deposit variation. The hydrological analysis shows a similarity between the surface and base of the deposit with a 50% drop in moisture content in the middle of the deposit. This pattern correlates with the drop in clay content also found in the middle of the deposit, and corresponds to a trait identified in grain flow deposits by Bertran & Texier (1999). The more unconsolidated sediments in the middle of the deposit have allowed water and clay sized particles to settle down into the lower levels of the deposit. The consolidated surface of the underlying deposit acted to trap the descending clays and hold higher proportions of water. The middle level of the deposit may be considered similar to an eluvial horizon (or E Horizon in soil science, which is characterised by a dearth of fines and water as they are leached downwards to the basal horizon, Coyne & Thompson 2006) with the basal level representing the B Horizon, which is characterised by the greatest proportion of clays and water and is identified in Bertran & Texier (1999).

				Particle Size		
Art No.	**Sample location**	**Munsell**	**Hydrology %**	**% Clay (<2µm)**	**% Silt (2µm - 63µm)**	**% Sand (> 63µm)**
102	T2 - 0-5 cm	2.5 YR 3/4	6.99	6.318	53.597	40.085
139	T2 - 30-40 cm	10 R 3/3	3.39	4.681	59.881	35.438
151	T2 - 50-60 cm	10 R 3/3	9.17	6.475	68.207	25.318

Table 5.6 T2 sedimentological summary.

XRF

The XRF chemical composition of the *Facies I* sediments is shown in Table 5.7 The MH1 inter-facies comparative XRF analyses are presented in Section 5.5.1. XRF samples were taken from basal levels of each deposit to avoid sampling leached sediments. Varying water movements in each depositional unit may cause leaching and concentration of heavy metals in different areas. These factors must be considered when planning sampling and comparing chemical components. The chemical composition of the *Facies I* sediments are consistent with what one would expect from a deposit composed of allogenic (externally derived) sediments. Distinction between sediments composed of authigenic sediments (internally derived) and allogenic sediments is relatively easy where mixing has not occurred. Primary minerals commonly found within dolomitic limestone include compounds based on Ca, Mg, K, Na, and distinctively low proportions of Si (Ford & Williams 2007). These primary minerals occur in varying amounts based on the depositional chemistry of the original sedimentary rock. Table 5.8 presents the major oxide components found in nine different limestone and dolomite karst systems. Table 5.9 shows the major oxide components found at Sterkfontein by Brain (1958). Secondary minerals (mostly clays), are formed from the decomposition of organic matter on the landscape surface and the weathering of allochthonous rock types. These make up the remaining proportion of the sediments in the form of Si, Al, P, Cr, Ni and Ti. The presence of these oxide forms in greater abundance than can be found in the host rock indicates an allogenic origin for the sediments. The chemical weathering process is complex and produces high degrees of variation within and between chemical compounds in the resultant sediments (Coyne & Thompson 2006). The presence and relative proportions of certain chemicals within sediments can be suggestive of the nature of the primary weathered rock generating the sediments and in some cases the weathering environment (e.g. kaolinite) (Coyne & Thompson 2006). What is clear from the data is that Fe and Al oxides do not represent over 2.5% in any of the sampled host carbonate rocks. SiO_2 is also restricted to below 14% through all carbonate rock samples. The comparative richness in Si, Fe and Al oxides of the *Facies I* sediments indicate they derive from allogenic sources of sediment, with

minimal mixing of host rock derived sediments. Due to the nature of T2 as a secondary sedimentation deposit and the potential for mixing of sediments from more than one source during the phases of accumulation and re-sedimentation, interpretation of the contributing mineralogy is impractical. Primary sedimentation deposits may allow such interpretations. Phosphates (P_2O_5) are generally found in raised proportions in bone-bearing deposits and sediments with bat guano components (Onac 2003, Ford & Williams 2007). In the case of T2, the presence of fossils suggests the former as the primary contributor but secondary additions through bat guano cannot be ruled out without XRD mineral analysis.

SiO2	Fe2O3	FeO	MnO	MgO	CaO
77.96	0.44	3.59	1.00	0.88	5.10

Al2O3	Na2O	K2O	TiO2	P2O5	Cr2O3	NiO
6.73	0.11	0.59	0.5034	3.09	0.0218	0.0075

TOTAL
100.02

Table 5.7 T2 XRF results.

	Sample							
	1	2	3	4	5	6	7	8
Oxides								
CaO	56.0	55.2	42.6	37.2	54.5	30.4	29.7	34.0
MgO	-	0.2	7.9	8.6	1.7	21.9	20.3	19.0
Fe, Al oxides	-	-	0.5	1.6	-	-	0.2	0.2
SiO2	-	0.2	5.2	8.1	0.2	-	1.5	-
CO2	44.0	44.0	41.6	43.0	41.8	47.7	46.8	46.8

1 - ideally pure limestone **2** - Holocene Coral, Bermuda **3** - average of 345 samples from Clarke (1924)
4 - Hostler limestone (Ordovician) **5** - Guilin limestones (Devonian) **6** - ideally pure dolomite
7 - Niagaran dolomite, Silurian **8** - Triassic dolomite, Budapest

Table 5.8 A selection of percentage bulk chemical compositions from limestone and dolomite karst-bearing rocks. Not the variation caused by localised original depositional chemistry (adjusted from Ford & Williams 2007).

Oxides	Concentration (weight %)
CaO	31.0
MgO	20.2
Fe2o3 + MnO	1.0
SiO2	1.1
Al2O3	0.3
CO2	46.1

Table 5.9 Sterkfontein dolomitic limestone major oxide composition. From Brain (1958)

The low calcium levels in *Facies I* (5.1%) indicate that the majority of the sediment contained within the T2 deposit has not been calcified. The presence of blocks of breccia within the sediments is not indicative of the calcification of the *Facies I* sediments, and they are considered contaminants from another deposit. The low calcium content fits with the interpretation of the Name Chamber Younger 'soft' Deposit that makes up the Far Western and Western Talus. These sediments have not been calcified and were deposited into the Name Chamber from M5E before the calcification of this surface deposit (Stratford 2008). In calcified sediments the range of calcium quantity is significantly higher than is found in the *Facies I* sediments. XRF samples taken from various areas of the M2 deposit and M4, which are both considered heavily cemented, yield mean Ca proportions of 39% (n = 4, Std Dev 17.5) from two areas of M4 and 52% (n = 18, StdDev 5.8) from the M2 deposit (M. Sutton, work in progress). In Brain's (1958) work at Sterkfontein his sampling of the surface deposits (M4 and M5) yielded Ca proportions with an average of 71.1% by weight.

Particle size

Figure 5.16 shows the particle size curves for each sample. The samples are presented on the same axes in Figure 5.17. A reduction in the coarse grains with depth and a corresponding rise in silt sized proportions can be seen. In the case of T2, the inverse grading pattern is the result of post-depositional movement of water, silts and clays through the clast-supported matrix towards the base. A

common process in grain flow deposits (Bertran & Texier 1999). The method of statistical comparison of the particle size distribution curves is discussed in Section 3.3. The Chi^2 statistical comparison of the area occupied by the de-convoluted curves on each sample shows the surface and middle samples (T2 - 0-5cm; T2 - 30-40cm) are significantly similar ($p = 0.266$), whereas the deepest sample (T2 - 50-60cm) is significantly different to both middle and surface samples ($p = 0.028$).

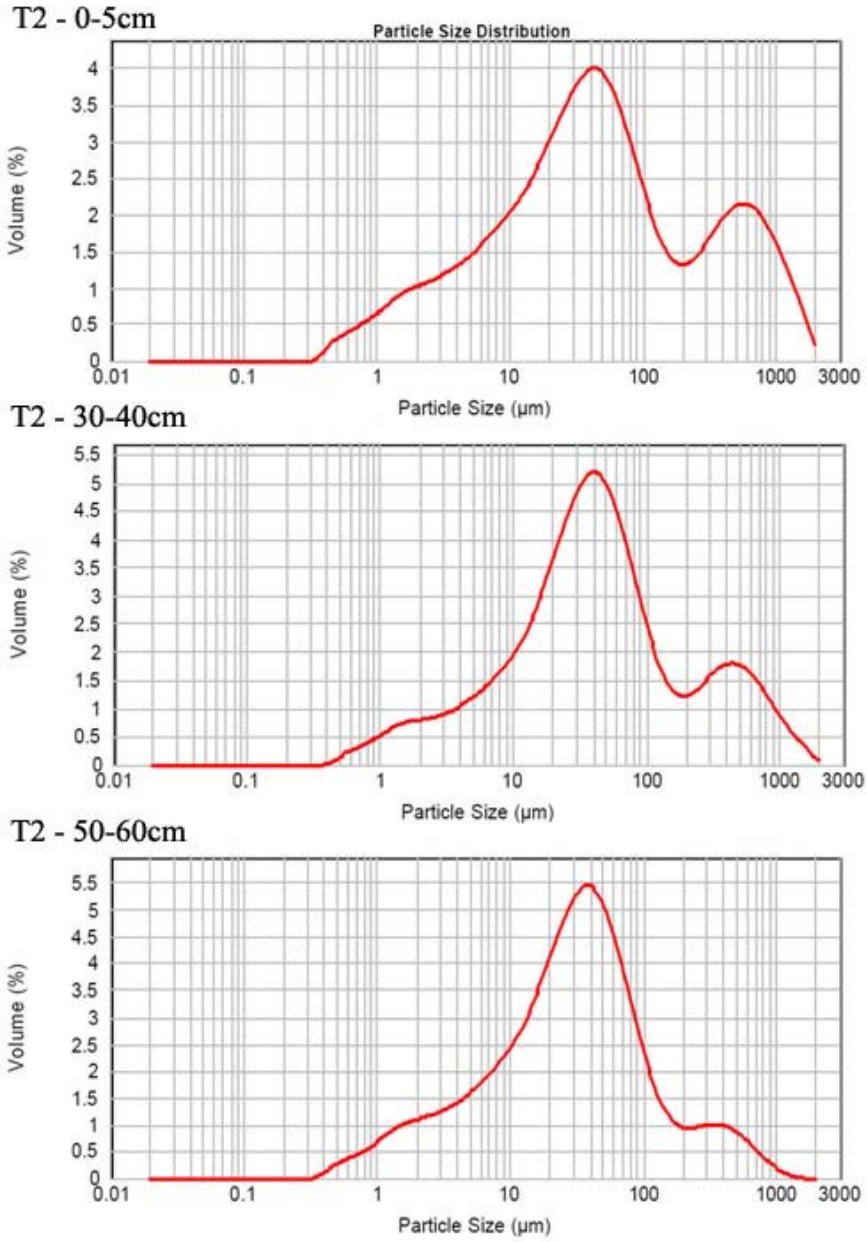


Figure 5.16 T2 particle size distribution curves for three samples taken at the surface, middle and base of the T2 deposit.

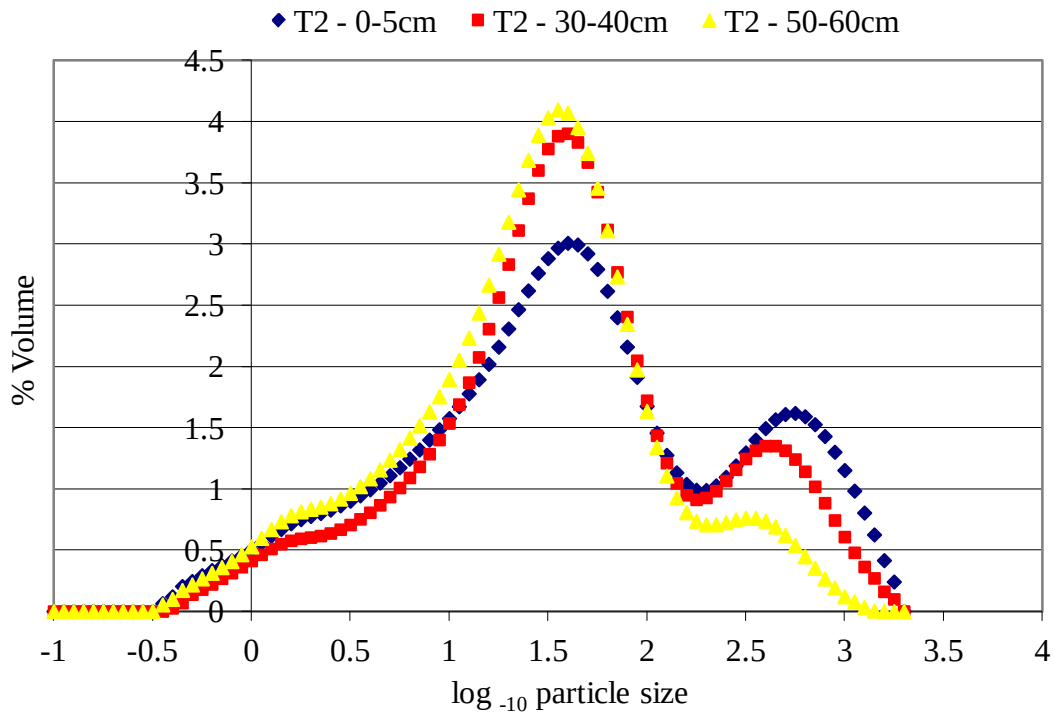


Figure 5.17 T2 combined particle size distribution curves. Stated sample depths are relative to deposit surface.

Table 5.10 presents the percentage volumes of each constituent Gaussian curve within the *Facies I* sediment samples. The associated particle size-distribution curve, with its constituent Gaussian curves is presented in Appendix 2. The comparison of these figures allows a quantitative analysis of the change in particle size proportions within different levels of the deposit. Starting with Curve 4, which represents the sand-sized particles, there is a drop in relative volume with depth from 23% to 9%, a total reduction of 14%. In contrast, Curve 3, which represents the coarser silt component (1/25mm; 40µm) (Wentworth scale), shows a 13% rise in representation with depth, with the greatest rise of 8% being shown between the upper and middle horizon. The basal level contains only 5% more coarse silt than the middle level. Curve 2, which represents the very fine silts (1/100mm; 10µm), shows a more stable level throughout the deposit showing a slight dip of 3% from top to basal layer with the lowest quantity found in the middle of the deposit. Curve 1, representing the clays (<1/256mm; <5µm) shows a similar pattern to Curve 3, in that the quantity of clays in the deposit is

proportional to depth. The difference between Curve 1 and Curve 3 is the location of the different proportions. The greatest rise in clay proportion in Curve 1 is shown between the middle and basal sample. These results suggest that the clays in the deposit are the first particles to have been redistributed during the post-depositional development of the inverse grading pattern. The coarser silts are still being graded and show the greatest vertical movement between the upper and middle levels, the basal level still receiving filtered silt fractions. Although *Facies I* demonstrates a clear inverse grading pattern, this process is ongoing and clearly is still to develop the distinctive silt/clay basal stratum documented by Betran & Texier (1999).

	Curve 1	Curve 2	Curve 3	Curve 4	Total
T2 - 0-5cm	2.990	25.911	47.835	23.265	100.0
T2 - 30-40cm	4.033	19.565	56.475	19.927	100.0
T2 - 50-60cm	7.114	22.766	60.979	9.141	100.0

Table 5.10 T2 relative constituent Gaussian curve volumes. The figures represent the volume as a percentage of the whole sample distribution curve. The T2 particle size distribution curves could be de-convoluted into four Gaussian curves.

5.2.3 T2 fabric analysis

The *in situ* fabric analysis yielded useful data regarding the orientations and dips of the faunal elements and indicates the prevalent sediment flow direction. Despite the clast-supported nature of the sediments, positive orientation data has been preserved in the faunal remains. Even fragmented faunal elements often have elongation ratios suitable for positive orientation to sediment flow direction. The sample has a modal and median orientation value of 74° from North with 67% of elements showing orientations between 60° and 80°. The narrow range of element orientation confirms that the *Facies I* sediments derived from an ENE direction. The excavated T2 surface covers an area 2m x 1m and does not, from the surface morphology, indicate a flow direction or sediment source other than the major

flow direction to the west (down slope). The particle orientation helps isolate the flow direction regardless of slope surface morphology, which may have been modified by post-depositional erosive processes. The orientation data suggest a sediment source in a more northerly direction than directly east, as most particles outside the major concentration of 60-80° have an azimuth to the north. All particles, bar four, have orientations north of due east and suggest that the majority of the sediments may have derived from the Name Chamber Far Western Talus, which lies in exactly that direction. Those four particles that do not fit within the narrow primary orientation concentration are orientated in an almost perpendicular direction and are orientated within a ten degree range, from 350-358°. Those four particles don't follow any distribution pattern within the sediments and thus do not represent an isolated sediment flow event contained within a discrete horizon. The appearance of perpendicularly orientated particles has been suggested by Voorhies (1969) to be a result of extreme particle elongation ratio. Although the geological literature does not necessarily support this, it may be a process limited to faunal elements in fluvial environments. Cañón-Tapia & Chávez-Álvarez (2004) don't test orientation potential within very elongate forms (>0.2; 5.0:1) but state that elongate forms of <0.5 (>2:1), including very elongate forms (0.2; 5.0:1), make reliable positively orientated particles. In any case, T2 does show a number of perpendicularly orientated particles (all faunal elements). The *Facies I* elongation ratio ranges from 1.6:1 to 14.3:1 with a mean elongation ratio of 4.0:1. Within the sample of those elements orientated to the primary direction, the mean elongation ratio is 3.5:1, with a range of 1.6:1 to 14.3:1. Within those four particles showing orientations perpendicular to the dominant concentration the mean elongation ratio is 5.0:1 with a range of 1.9:1 to 7.8:1. The sample size of perpendicularly orientated pieces needs to be larger in order to allow the statistical assessment of the significance of difference in elongation ratio. The relationship between settling behaviours of faunal elements with differing elongation ratios in different sedimentary flows requires experimental clarification.

The orientation data also confirms the absence of any other major contributor to the sediments from other sources. The presence of other sediment flow sources

would be indicated by a proportion of elements with a different orientation and would be expected to occupy a discrete horizon. The orientation data is consistent through all depths of the T2 deposit. In terms of dip values, 70% of the sample ranges between 20° and 30° with median and modal value of 26°. This value fits well with the angle of repose for the T2 surface which lies at 28°. The dip of the particles does not change with depth, as would be expected if the deposit were to form on a horizontal underlying surface. The consistency of dip through the depth of the deposit is a result of the underlying deposit surface gradient. Figure 5.18 shows the combined orientation data for the *Facies I* sediments.

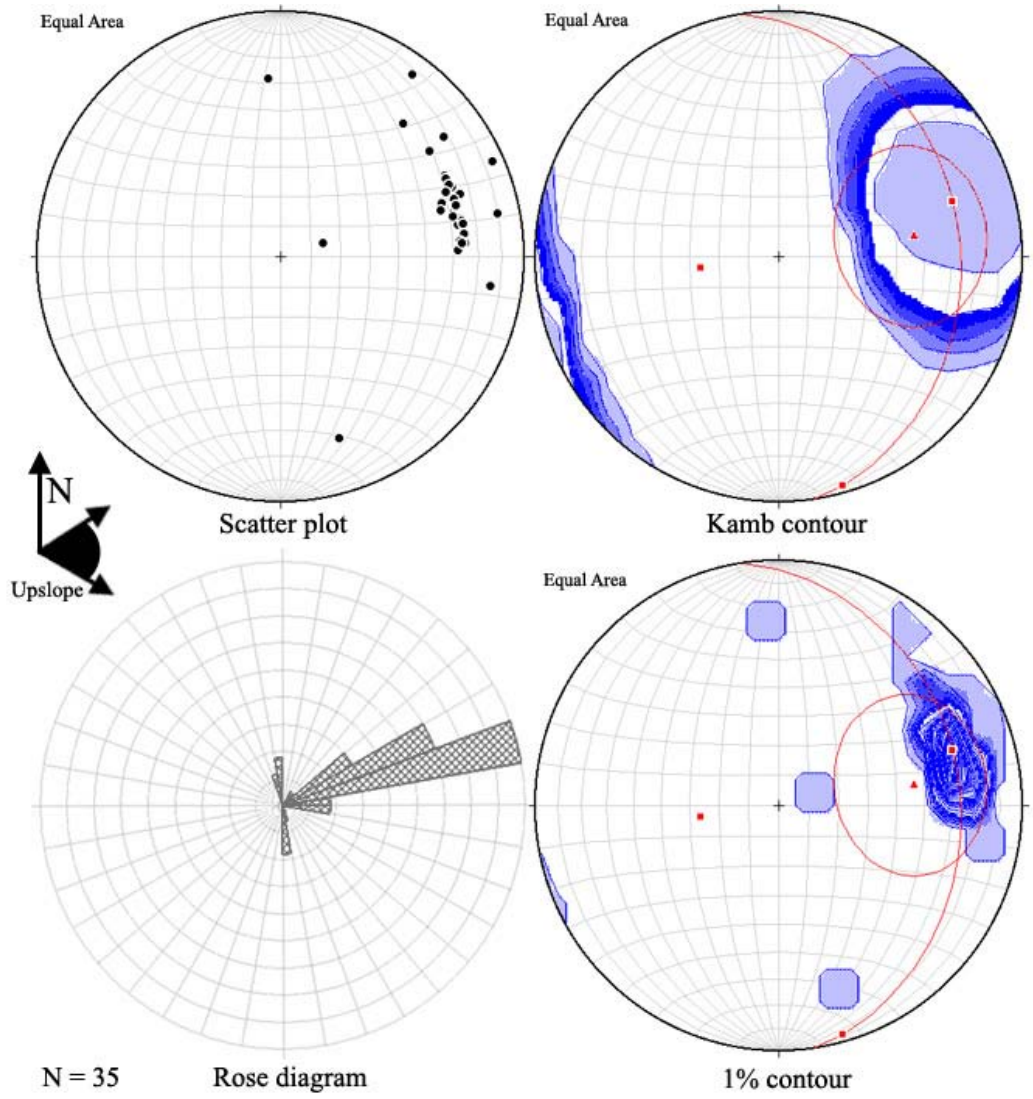


Figure 5.18 T2 fabric analysis models. Kamb contouring has a contour interval of 2.0 sigma. The 1% contour plot has a contour interval of 1%. Both the Kamb and 1% show best the best fit plain and cone. The rose diagram sections represent 10°.

5.2.4 T2 particle shape

The T2 faunal elements fall mostly into the elongate forms with very few spherical or compact-shaped pieces. As was demonstrated in the T1 analysis, the natural clasts that have undergone significant movement have been fractured into more spherical, compact shapes and are less suitable as orientation and slope indicators. The contrast between fractured clast shapes and fractured fossil

material can be seen in Figure 5.19. The red points represent the shape of ten natural clasts chosen randomly during excavation. T2 is a clast-rich deposit and the movement of the clasts has caused high levels of fossil breakage throughout the deposit. Within the Sneed & Folk shape classes 90% of the assemblage are classed as elongate or very-elongate forms with only 3% of the assemblage representing compact forms. *Facies I* shows a relatively low proportion of long bone elements (41.2%) in comparison to the T1 deposit (69%), but shows a comparatively high proportion of elongate forms. Long and flat bone elements tend to fracture into similarly elongate forms reducing in elongation with increasing breakage levels, but still falling into the elongate to very-elongate shape class. Dental element types tend to become more elongate with increasing levels of breakage (see Chapter 4 for discussion). Interestingly, it's the higher proportion of fractured dental elements (21.6%) combined with the long bone elements that produces the high elongate representation in the *Facies I* shape profile. Breakage profiles and element representation for *Facies I* are discussed in the following section. The Zingg diagram shows a higher proportion of bladed forms within *Facies I* despite the presence of only two rib fragments within the assemblage. The other bladed forms shown in the Zingg diagram represent the long bone elements that have been fractured longitudinally. The Zingg index is more sensitive to bladed forms than the Sneed & Folk. The MPS vs. DRI model shows a general trend toward sphere/disc-shaped elements, clearly contrasting with the T1 assemblage.

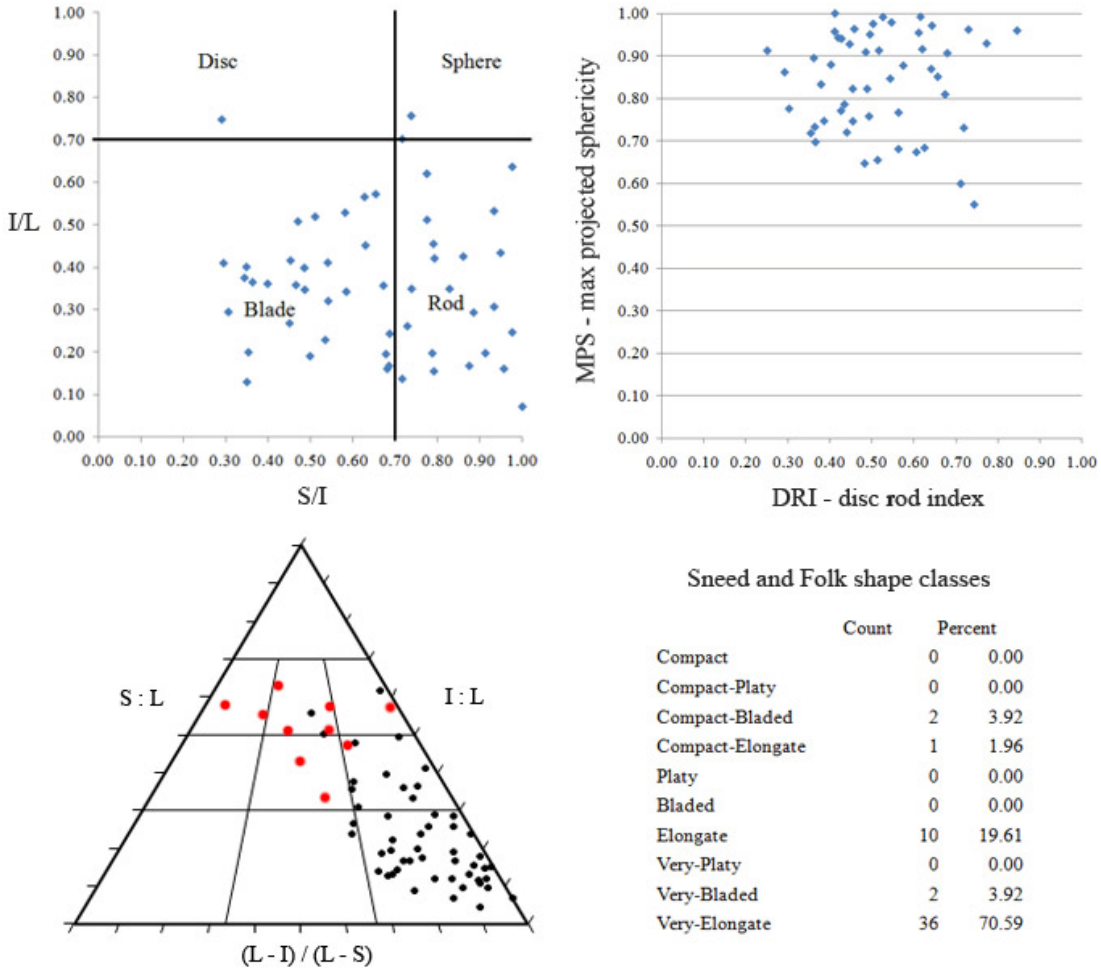


Figure 5.19 T2 particle shape indices. The red points on the Sneed & Folk diagram represent natural clasts excavated from the T2 deposit. The natural clasts are not included in the shape class table.

Figure 5.20 shows the Voorhies groups represented in the T2 faunal assemblage. Due to the high levels of fragmentation only 32 elements were sufficiently identifiable to element type to allow Voorhies groups to be assessed. Over 75% of the assemblage contains Group II elements, with almost 25% of the elements falling into Group II & III. Elements classed as Group II and Group II & III types are regarded by Voorhies as those elements that are particularly immobile and are moved by flows with greater energy (Voorhies 1969). In terms of faunal particle distribution, Group I and Group I & II element types are generally found towards the distal area of the deposit. The Voorhies data for *Facies I* shows a high

representation of Group II & III element types in a relatively distal portion of the talus. The representation of elements across the Voorhies groups in this area of the deposit indicates the sediments were not longitudinally sorted and remained mixed during the accumulation process. This pattern is a result of the particular sediment gravity flow processes at work during the accumulation of the sediments, which have produced a deposit with low levels of longitudinal sorting. Grain flows, in general, accumulate in relatively rapid surges of mixed sediments (Bertran *et al.* 1997; Major 1997). Parsons *et al.* (2001) noted that grain flow deposits often accumulate the largest clasts at the snout of the deposit. The same pattern may also be relevant for fossil particles and is proposed from EC1 deposit data. The T2 sediments, however, do not provide enough evidence to observe the same pattern due to the sampling point of the excavation. T2 has been sampled at the medio-distal portion of the talus and therefore sediment characteristics and related fossil accumulation dynamics found at the distal or terminal portions are not evident.

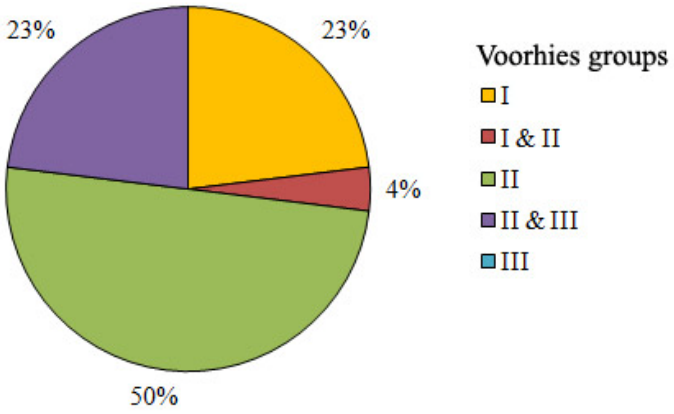


Figure 5.20 T2 Voorhies groups.

5.2.5 T2 faunal and artefact assemblage profile

The entire T2 assemblage is *in situ* so the fauna does not require the same separation as the T1 assemblage. Unidentifiable elements are included in all bone breakage assessments but are not included in element representation. The unidentifiable elements in the T2 assemblage are classified with a question mark (?).

The size profile for the T2 assemblage (Table 5.11) shows a similar pattern to that of the T1 assemblage, in that the majority of the fauna (54.7%) measures <30mm maximum dimension, and 75.5% of the assemblage measures <40mm. Mean maximum dimensions for all faunal elements is 33mm with a StdDev of 13.6. The mean particle size (expressed as the mean of axis L, I and S) is 17.4 with a StdDev of 7. This compares closely to T1, which yielded a mean particle size of 18 with a StdDev of 6.3. The largest and smallest specimens measure 69.5mm and 17mm respectively. The dominance of <50mm material within the size profile and the relatively low standard deviation can be considered both a result of fragmentation processes during re-sedimentation, or due to a residual primary sedimentation pattern. Analysis of the breakage data will help elucidate the timing of the majority of the fragmentation.

Facies I yielded a faunal assemblage of 51 fossils. The relatively small sample size reflects an accurate view of fossil yield (number of bones per predetermined volume) at this point in the deposit, and is not the result of preferential sorting or excavation methods. Fossil yield is a result of distance from source and fossil survivorship within the sedimentary environment. The *Facies I* sediments have travelled a significant distance, been through multiple sedimentation processes and contain a high proportion of clasts, facilitating bone fragmentation. Given this situation, one would expect fossil yield and bone completeness to diminish with distance from primary sediment source. Sampling of the upper portions of the same deposit may prove more fruitful in terms of fossil yield and size, and completeness of specimens.

It is clear that at least a significant proportion of T2 derives from the Name Chamber Far Western Talus as indicated by the fabric analysis and the presence of archaeological material (discussed in the following section). The natural clasts within T2 range in size up to 400mm maximum dimensions and may represent a period when differing filtration levels within the Feeding Shaft allowed larger material to pass into the Name Chamber. A stratum with similar clastic properties to T2 has been found at the base of the Far Western Talus and may represent proximal portion of the same facies. Unfortunately, this area could not be sampled due to time constraints, but, if related, the contents of the stratum should be comparable to the assemblage yielded from excavations undertaken within the Name Chamber. Taxonomic and taphonomic indicators may indicate similarities between the M5E (the Name Chamber source deposit) and the T2 assemblage.

Max	Summary					
Length	Artefacts	%	Fossils	%	Total	%
<10mm	0	0.0	0	0.0	0	0.0
<20mm	0	0.0	4	100.0	4	7.5
20-29mm	0	0.0	25	100.0	25	47.2
30-39mm	1	9.1	10	90.9	11	20.8
40-49mm	1	16.7	5	83.3	6	11.3
50-59mm	0	0.0	3	100.0	3	5.7
60-69mm	0	0.0	4	100.0	4	7.5
70-79mm	0	0.0	0	0.0	0	0.0
80-89mm	0	0.0	0	0.0	0	0.0
90-99mm	0	0.0	0	0.0	0	0.0
>100mm	0	0.0	0	0.0	0	0.0
Total	2	-	51	-	53	100.0
Total %	3.0	-	97.0	-	100.0	

Table 5.11 T2 faunal and artefact assemblage summary and size profile.

5.2.6 T2 archaeology

Only five artefacts were yielded from the T2 deposit, three of which were excavated from the surface of the T3 deposit and are considered contaminants of that deposit originating from the T2 sediments. The accumulation of fossil concentrations indicates that materials (sediments, fossils and artefacts) have been able to move down through the deposit post-depositionally via the large and frequent voids found in *Facies I*. All artefacts excavated from the T3 deposit derived from the top 5cm of the deposit. The first piece to be excavated from the T3 deposit was Artefact 101, a quartz flake fragment (Appendix Figure 1.23). As discussed in the analysis of the T1 artefacts, archaeological material found in this area can only derive from the Name Chamber. The small assemblage comprises a casual core and four flakes, including two complete flakes, an incomplete flake and a flake fragment. All pieces, except for the core, measure <50mm and fit within the same pattern as seen in the T1 collection and the Name Chamber Western and Far Western Talus. The core is larger than the fauna or other four archaeological pieces (maximum dimension = 83mm; particle size = 64.6) but fits well within the clast size spectrum found within the *Facies I* sediments. Although 83mm is larger than the more recent depositional trend found in the Western Talus of the Name Chamber, the presence of a single slightly larger piece cannot be considered diagnostic of an alternative sediment source. Previously, occasional larger artefacts have been found within the Name Chamber (Robinson 1962; Stratford 2008) and may be residual representatives of lower filtration levels active in the Feeding Shaft (Stratford 2008).

No significant technological or depositional trends can be suggested from the small current sample, and only a description of pertinent attributes is provided in this analysis. None of the five artefacts displays any diagnostic technological attributes that would place them outside the ESA techno-complexes. In terms of raw material representation, all artefacts are made from those raw materials used most prevalently in the Sterkfontein ESA, i.e. quartz and quartzite with minor contributions of chert. None of the quartz artefacts display enough dorsal cortex to allow positive identification of their source. The quartzite, however, must have

been brought to the site from the nearby river gravels as it is not found on the Sterkfontein hillside (Kuman 1998, 2007; Field 1999). Artefact 110 (Appendix Figure 1.22) is classed as a complete flake but has a small step fractured, convex distal-lateral edge that covers 25% of the total distal edge length. The predicted loss of material due to this breakage is <5%. The remaining distal edge terminates in a feather type. Artefact 124 (Appendix Figure 1.24) was excavated from the surface facies of the T3 deposit and represents a good example of a quartzite casual core. The definition of a casual core follows Stratford (2008) in order to maintain parallel analytical methods to those used on the Name Chamber assemblage. Quartzite cores are most commonly found in the Sterkfontein Early Acheulean (representing 24% of the Early Acheulean at Sterkfontein) (Kuman 2003, 2007) but do occur in the Oldowan levels of the M5E deposit, although in very small numbers (<1%). The presence of Early Acheulean material filtering into the Name Chamber has not been ruled out, although microfauna analysis (Avery *et al*. 2010) and technological analysis of the Name Chamber sample (Stratford 2008) suggest it is minimal. Either way, the casual core does serve as a further depositional indicator for sediments and artefacts deriving from the M5E Oldowan or Early Acheulean deposits travelling through the Feeding Shaft into the Name Chamber Far Western Talus which previously extended down the MH1 slope, forming T2. Table 5.12 shows the provenance and size attributes of the pieces. Table 5.13 shows the technological attributes yielded from each of the artefacts.

				Max	WIDTH (mm)			DEPTH/thickness (mm)			
ART No.	Square	Quad	Spit Depth	Length	Max	Min	Midpoint	Max	Min	Midpoint	Artefact type
110	A	B	10-15CM	45	42	25	34	13	5.5	11	complete flake
126	A	D	15-20CM	33	16	8.5	16	5	3	4	incomplete flake
101	B	A	0-5CM	34	30.5	16	24.5	12.5	5	11.5	split flake fragment
116	B	A	0-5CM	31	20	10.5	17	6	4.5	5.5	complete flake
124	A	B	0-5CM	83	78	39.5	73	50	44	48	casual core

Excavated from T3 *Facies II*

Table 5.12 T2 artefact summary

Art No.	R.M	Artefact type	No. Flake scars (mm)	Length max scar (mm)	Termination type	Remaining platforms	Platform thickness (mm)	Remaining cortex (%)	R.M source	Condition
110	quartz	complete flake	2	36	feather/step	0	12	<25	?	f
126	quartzite	incomplete flake	1	31	step	0	6	0	cobble	sw
101	quartz	flake fragment	1	11	step	0	na	0	?	f
116	chert	complete flake	0	na	hinge	0	split platform	0	?	sw
124	quartzite	casual core	3	32	all step	1	na	>75	cobble	w

Excavated from T3 *Facies II*

Table 5.13 T2 artefact technological attributes

5.2.7 T2 faunal analysis

The 51 fossils recovered during the excavation of the T2 deposit have been analysed for stratigraphic information in the same way as the T1 Identifiable component. The size profile of the faunal assemblage had already been discussed in the assemblage profile. Of the 51 fossils, only one specimen (2%) was not identifiable to element type. Element type is the most basic level of faunal identification and those specimens not identifiable at this level are classified as unidentifiable. The taxonomic and taphonomic analyses are presented below.

Skeletal element representation

Figure 5.21 and Table 5.14 show the distribution of skeletal element type and body portion representation respectively. Fossils deriving from long bone elements still represent the largest proportion of the assemblage (41%) but to a much smaller degree than was seen in the T1 Total assemblage. The next highest proportion is fossils deriving from irregular elements. Irregular bones include vertebra, scapula, most of the axial skeleton with the exception of ribs. The relatively high proportion of irregular bones within the assemblage is interesting, given the generally easily fragmented nature of irregular elements mostly due to their low density and therefore survivorship (Lyman 1984). There is a relatively low proportion of compact bones in the *Facies I* assemblage, representing only 4% (n = 2). This number is lower than expected given the relatively high survivorship of compact bones (Lyman 1984). The high representation of vulnerable elements in contrast to the poor representation of more durable elements within a clast-rich deposit suggests that, unlike T1, the *Facies I* faunal skeletal element distribution reflects an element abundance pattern in the source assemblage. Table 5.14 shows the same pattern as Figure 5.21 in that appendicular elements are most highly represented (45.1%) followed by axial (21.6%) and teeth (22%). In *Facies I*, the high proportion of teeth is a result of both a high durability (due to the protective qualities of enamel), and due to a high representation in the source assemblage.

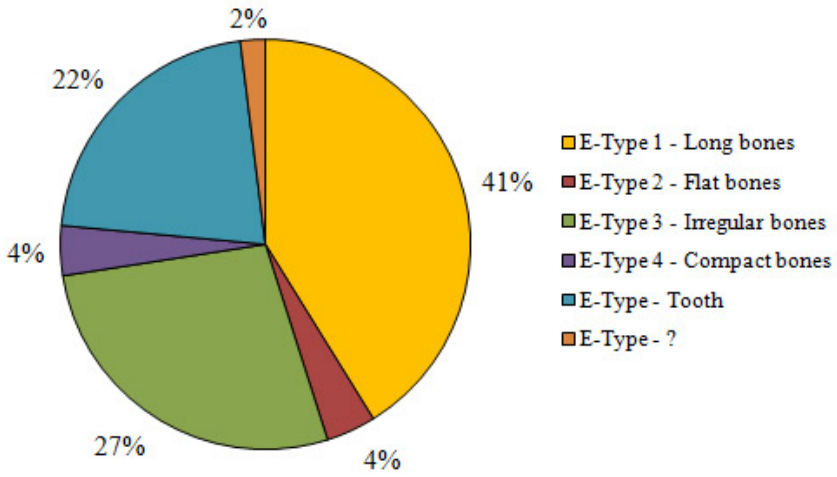


Figure 5.21 T2 skeletal element type distribution.

Max Length	Fossils						
	Appendicular	Axial	Podial	Tooth	?	Total	%
<10mm	0	0	0	0	0	0	0
<19.9mm	2	0	0	2	0	4.0	7.8
20-29.9mm	11	5	1	3	5	25.0	49.0
30-39.9mm	7	2	0	0	1	10.0	19.6
40-49.9mm	1	2	0	2	0	5.0	9.8
50-59.9mm	1	1	0	1	0	3.0	5.9
60-69.9mm	1	1	0	1	1	4.0	7.8
70-79.9mm	0	0	0	0	0	0.0	0.0
80-89.9mm	0	0	0	0	0	0.0	0.0
90-99.9mm	0	0	0	0	0	0.0	0.0
>100mm	0	0	0	0	0	0.0	0.0
Total	23	11	1	9	7	51.0	100.0
Total %	45.1	21.6	2.0	17.6	13.7	100.0	

Table 5.14 T2 skeletal portion distribution summary.

Bone breakage

The excavated fossils from the T2 deposit have been through multiple sedimentation episodes, progressively moving them further from the original primary sedimentation deposit and deeper into the caves. This movement within a clast-rich matrix has led to high levels of fragmentation during re-distribution.

Bone breakage data can indicate the timing of the majority of breakage but fossil completeness patterns will not be comparable to the primary deposit assemblage. Bone breakage, as a process, replaces previous generations of breakage information with the most recent generation of breakage. Figures 5.22 through 5.24 show the breakage data for the T2 assemblage. The data show that there are very few (4%, n = 2) specimens that are complete. 58% of the assemblage shows at least three broken edges with 33% showing the maximum number of breaks of four per specimen, the largest component in the assemblage. An inverse relationship can be seen between number of breaks and representative proportion. The low proportion of complete elements in the assemblage results in a negligible influence on the measures of central tendency for the fossil dimensions. The *intensity of fragmentation* (Lyman 1994) for the T2 assemblage is similarly inappropriate to the T1 faunal analysis, in that the mean maximum dimension of the non-complete specimens is 33mm, and the two complete elements posses maximum dimensions of <20mm, a reverse to what Lyman (1994) proposed. The complete specimens are a rodent tibia and a bovid premolar. Both these bones measure <20mm maximum dimension and have probably escaped fragmentation due to their small size. Larger elements, which possess a higher absolute volume, surface area and lower density, are fragmented more intensely. The high degree of fragmentation is adequately demonstrated by the proportions of break numbers within the assemblage.

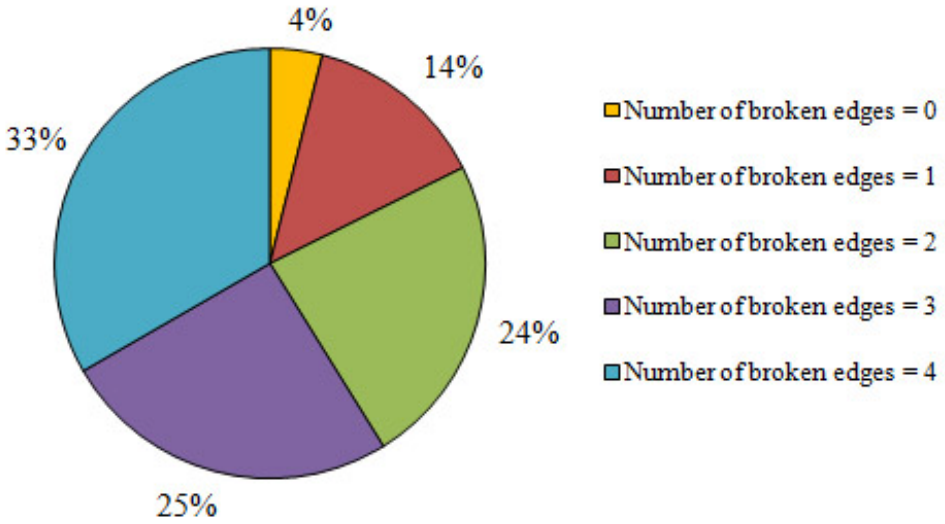


Figure 5.2.22 T2 numbers of broken edges on fossil material.

Figure 5.23 shows the fracture type proportions within the T2 assemblage. Those specimens showing only ‘green stick’ or smoothly fractured edges represent 47% (n = 23) of the assemblage. Specimens showing a combination of fractures represent 24% (n = 12). Elements showing only sawtooth breaks represent 23% of the fracture types. Those specimens showing at least one sawtooth fracture number 22 (45%) and specimens showing at least one smooth fracture number 28 (54%). Those specimens showing any step-shaped fractures number 11 (23%). Most specimens within the T2 assemblage display smooth fractures, with the remaining specimens displaying at least one sawtooth fracture. The fracture angle data shown in Figure 5.24 show a similar dominance of the perpendicular fracture angle to that seen in the T1 assemblage. 80% of specimens display at least a single perpendicular fracture angle, with the majority of the remaining 20% displaying acute fractures. Despite the similarity of the break angle data, the combination of break type and break angle data endorses a different interpretation. The data suggest a mix of major breakage events during the burial and distribution history of the specimens. The dominance of the ‘green stick’ fractures, characterised by smooth fracture surfaces and perpendicular or acute fracture angles, indicates a significant proportion of breakage of the T2 assemblage occurred whilst the bone

was in a pre-fossilised state. The bone was then fossilised and was fragmented during re-sedimentation, which is when the large number of sawtooth fractures occurred. It is interesting that, despite the relatively destructive processes that are characterised by clast-rich grain flows, and the generally high level of fragmentation found in the fauna, the early depositional breakage pattern has been preserved and remains the dominant breakage signal. The pattern of breakage timing fits the accumulation scenario proposed by T. Pickering (1999) for the M5E Oldowan deposit, where a high aven-type opening in the ceiling provided the dominant mode of death and accumulation for the fauna. Death-trap assemblages regularly display a broad range of skeletal element representation and potentially high levels of fresh bone breaks. The taphonomic and taxonomic analysis may further corroborate the stratigraphic interpretation of the faunal data presented above.

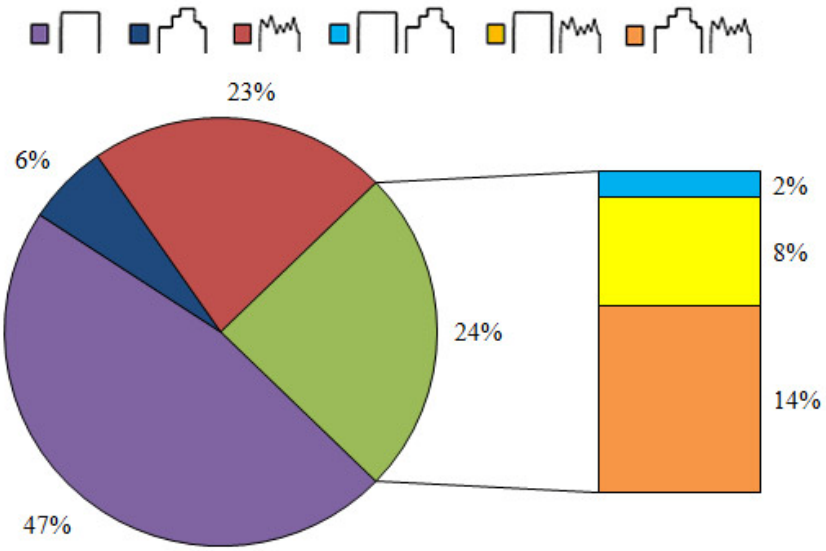


Figure 5.23 T2 bone fracture types. The green slice represents the proportion of bones with a combination of fracture types.

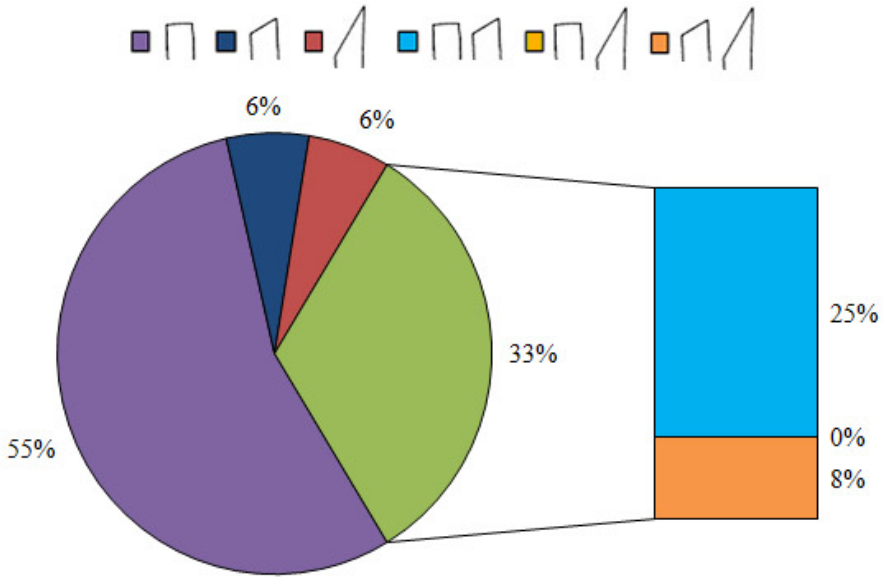


Figure 5.24 T2 bone fracture angles. The green slice represents the proportion of bones with a combination of fracture angles.

Bone condition

The bone condition data for the T2 fauna is shown in Figure 5.25. It is clear that the general condition of the bone is good with 84% of the assemblage classed as either fresh or slightly weathered (equivalent to Behrensmeyer's stages 0, 1, 2 and 3). There are no specimens that are classed as very weathered, and only 16% (n = 8) that can be classed as weathered (equivalent to Behrensmeyer's stage 4). The surface visibility is also regarded as good with over 70% of the assemblage possessing 100% surface visibility. This is a result of the generally fresh condition of the bone and makes recognition of bone surface damage feasible. The bone condition data further support the previous evidence that the majority of faunal specimens was deposited into the cave and buried relatively quickly without significant exposure to weathering processes on the surface. In the case of the T2 deposit, post-depositional bone surface weathering seems to have affected the bone to a small degree, preserving the condition of the bone surface through multiple re-sedimentation phases. Bearing in mind the recognised issues with the varied tempo at which the weathering processes work (Gifford 1981), it is prudent

to simply suggest that the T2 assemblage, dominated by fresh bones, was deposited quickly into the cave, in a fresh condition, and then fossilised quickly prior to the surface attritional affects of re-distribution. There is, however, a component of the T2 assemblage that suggests some bones may have entered the cave after a significant period of time exposed on the surface as indicated by the 16% of weathered elements.

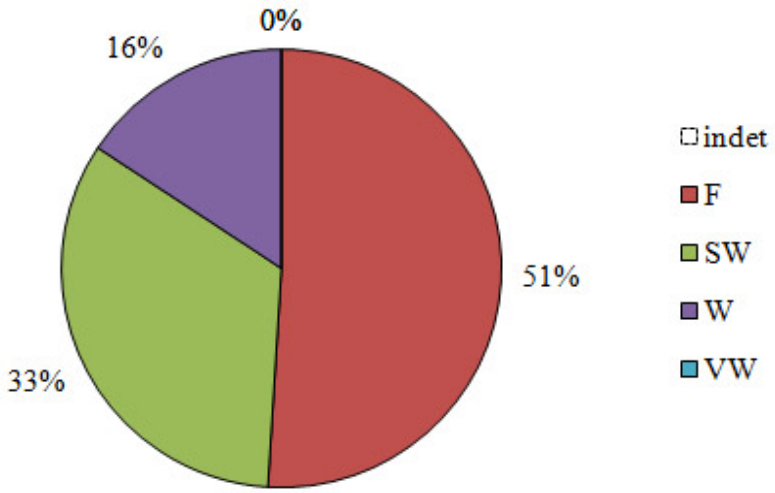


Figure 5.25 T2 fossil condition.

5.2.8 T2 taxonomy

The high levels of fragmentation in T2 create the low representation of taxonomically identifiable specimens, and make confident suggestions of source deposit based on taxonomic representation limited. *Equus* was the only specimen identifiable to species. The significance of the presence of *Equus* has been discussed in Section 3.6. One bovid specimen was identifiable to family level classification and was determined to be a *Damaliscus*-sized Alcelaphine. Small Alcelaphine's are common around the Cradle sites and are found at: Kromdraai A and B; Coopers D; Swartkrans Lower Bank, Hanging Remnant, Members 2 and 3 (de Ruiter *et al*. 2008) and Drimolen (Keyser *et al*. 2000). If the specimen is *Damaliscus*, then it is considered by de Ruiter *et al*. (2008) to be indicative of an

open, grassland environment and one could suggest that grassland would have been nearby at the time of death in order to support such species.

5.2.9 T2 taphonomy

The bone breakage data for the T2 assemblage indicates the integrity of the assemblage is relatively good with good proportions of the residual, original depositional indicators having been preserved during the re-sedimentation process, despite the affects of distribution within a clast-rich sediment flow. Without a greater sample size, interpretations on the palaeoenvironmental conditions at the time of primary sedimentation cannot be substantiated. Table 5.15 presents the skeletal element representation within the bovid size classes and shows all major body parts are represented from dental elements through to vertebrae and podial elements and include two examples of the humerus long bone element. Bovid representation could only be identified to size class. As can been seen from the MNI data, the abundance of these elements could only account for single specimen, a direct reflection of the small sample size. In terms of bone surface modification, the small sample size reduces the chances of finding taphonomically diagnostic biogenic bone surface modification features. There is, however, a number of specimens with tooth pitting and tooth scores, as well as a single puncture caused by a tooth on a size class two bovid thoracic centrum. The presence of carnivore-modified bone indicates at least a part of the assemblage has been either predated or scavenged and then deposited into the cave. Those elements that do show some carnivore modification are also classed as slightly weathered and indicate those particular elements may have suffered a longer exposure on the surface and been more vulnerable to carnivore damage.

Skeletal part	Small	Size 2	Size 3
Skull	1/1/1	1/1/1	
Cervical		1/1/1	1/1/1
Thoracic		1/1/1	
Lumbar		1/1/1	
Humerus		2/2/1	1/1/1
Radius		1/1/1	
Femur		1/1/1	
Phalanx II			1/1/1
Metapodial		1/1/1	1/1/1

Table 5.15 T2 skeletal element representation of bovid taxa. NISP/MNE/MNI data is given for each cell in columns two through four.

5.2.10 T2 discussions

The T2 deposit has accumulated from a single surge of sediments in a dry grain flow process from an area in the vicinity currently occupied by the Name Chamber Far Western Talus. The natural accumulation of the sediments allowed a full spectrum of analyses to be applied both during the excavation and in the lab. The sedimentological data, faunal and archaeological content support the hypothesis that the sediment largely derive from the Name Chamber. The preservation of the residual, primary breakage patterns and the taphonomic representation concurs with the proposed accumulation process for M5E faunal assemblage proposed by T. Pickering (1999). The sediments accumulated during a collapse or over-steepening of the sediments developing the Western or Far Western Talus causing a rapidly accumulated, clast-supported surge of material. The high energy flow process has created a longitudinally poorly sorted facies, with faunal particles of all shapes, sizes and types distributed throughout the deposit. Prior to the development of the mining platform at the top of the MH1 talus and the subsequent tourist infrastructure, the T2 deposit is likely to have been stratigraphically associated to the Far Western Talus. The sedimentology shows an ongoing vertical grading process, with a leaching of fines and water from the middle of the deposit to the base. Artefacts and faunal material has also

been prone to vertical movement through the large and frequent interstitial voids. The presence of *Equus* illustrates a younger age for the sediments than the nearby M2 and is found mostly within the M5 surface deposit, dating to younger than 2Ma. The T2 deposit represents an opportunity to assess the affect of re-sedimentation of assemblages and sediments through three known sedimentation phases. The majority of the T2 material has moved from the gradually accumulated primary sedimentation location in M5E, through the Feeding Shaft, into the gradually developing Name Chamber deposits and then through a rapid surge of sediments into the deeper areas of the Milner Hall. Completion of the faunal analysis of the Name Chamber assemblage would provide the data on the intermediate stage and present a full sequence of multi-stage sediment distribution. To clarify the association between M5E and the T2 sediments, a greater faunal sample would be useful as well as the analysis of the microfauna in a similar procedure to that applied to the Name Chamber assemblage in Avery *et al*. (2010).

5.3 T3

The T3 deposit represents the deepest fossiliferous deposit in the MH1 talus. Lying directly beneath T2, the T3 deposit is both the oldest fossil-bearing infill in the sequence and the most complex in depositional history. The significance of the T3 deposit lies in its nature as a very early *in situ*, primary sedimentation deposit that has never calcified. The fossil yield, condition and element completeness are all excellent, providing good data resolution for the sample size. Numerous examples of complete elements broken *in situ* and remaining directly associated have been found. T3 represents one of the only deposits of this nature and possibly one of the oldest fossil-bearing deposits accumulated in the deepest areas of the Sterkfontein caves. The full complement of *in situ* analyses was used for the T3 deposit in order to yield the greatest quantity of information. The T3 deposit has accumulated onto the horizontally stratified deposit named T4. Three stratigraphic profiles are described for the T3 deposit. Each of the three profiles illustrates a distinct soft sediment deformation process that occurred during the

formation of the deposit. T3 was sampled by a 1.5m x 1m trench running N-S, transverse to the direction of the sediment flow. The excavation extended down from the base of the T2 trench that exposed the T3 surface. The southern-most 50cm of the exposed T3 surface was not excavated in order to provide a witness section and potential area for future extension. The eastern wall profile (Figure 5.3) shows the witness section and the morphology of the T3 deposit. The excavation samples the very terminal portion of the T3 deposit. The sampling of this point provides a unique opportunity to study fabric form, shape and properties at the distal tip of a deposit. As briefly described in the previous chapter, the surface of T3 has two strike surfaces running away from a longitudinally orientated ridge, which itself runs at the main angle of repose (30° ENE-WSW). The first strike slope runs 25° SW-NE, and the second runs at 21° in a NE-SW direction.

5.3.1 T3 stratigraphy

The stratigraphy of the T3 deposit is particularly interesting and requires extensive explanation as its formation has shaped each of the following deposits, and therefore, the current cave environment in the eastern Milner Hall. The T3 deposit has accumulated over a prolonged period of time and represents the dominant occupying infill in this area of the Milner Hall for a long time before the T2 deposit was accumulated on top of it in a relatively rapid process. The T3 deposit was accumulated very close to, or in the margins of the water-table, as is indicated by the sedimentological and morphological evidence. T3 represents multiple phases of consistent primary sedimentation from a single, distant source in an unbroken formation sequence. These phases are represented by three sedimentological facies. Each facies is distinct, but fits into a deposit level depositional and sedimentological trend. The facies are labelled *Facies II*, *Facies III* and *Facies IV* and contribute the main depositional sequence of the MH1 talus. It should be noted that the facies number does not necessarily reflect the order of deposition. *Facies III* and *IV* are found as multiple, sometimes discontinuous strata. *Facies III* can be split into six depositional phases of the same sediment

composition indicating a recurring depositional regime. *Facies III* and *IV* are also found as deep intrusions into the T4 deposit through a number of sediment displacement/deformation processes that have affected both the T3 and T4 deposits. Each facies is described below:

Facies II – Yellow (2.5YR 4/4), consolidated, silt loam matrix-supported sediment with occasional coarser inclusions (small chert fragments <20mm) showing no particle sorting. Particle sizes ranges from <2mm – 5mm maximum dimensions. Internal strata slope at the longitudinal angle of repose (30° ENE-WSW). Transverse strata run horizontally. The internal lenses are characterised by very thin (<5mm) discontinuous dark strata representing decayed dolomite fragments. *Facies II* represents the upper, surface stratum of the T3 deposit. There is no evidence of flowstone development at the T2/T3 (*Facies I/II*) contact. The morphology of this facies has been shaped by post-depositional water erosion of the surface of the T3 deposit. To the south of the T3 ridge, *Facies II* forms a stratum 10-20cm thick. North of the ridge this stratum thins rapidly from 10cm - <1cm forming a capping stratum to the T3 deposit directly under T2 base. Vertical desiccation cracks in this facies displace sediments into the underlying *Facies III* and *Facies IV*. *Facies II* is fossiliferous, the faunal specimens often representing the largest particles. The facies shows lower fossil yield and slightly smaller faunal particle size range (15mm-66mm) than the deeper T3 facies.

Facies III - White and grey (7.5YR 4/3), highly consolidated, inversely graded silt loam matrix-supported sediment. Sediment particle size is restricted to <5mm and contains no clasts measuring >20mm. Faunal particle sizes range between 15mm and 144mm. Discontinuous strata and localised pockets of *Facies IV* are spread at random both horizontally and vertically through the layer. The transition from *Facies II* to *III* is gradual with a 2 - 3cm transitional horizon. *Facies III* makes up the majority of the T3 deposit with inter-stratifying layers of *Facies IV*. *Facies III* is highly fossiliferous with *in situ* bone representing complete or near-complete elements. Faunal material represents the largest particles within the sediments and all fossils from this bed are stained black. The internal strata of *Facies III* slope longitudinally at a decreasing gradient with

increasing depth in an ENE-WSW direction, and the transverse bedding is horizontal. Six separate strata of *Facies III* sediment can be seen. Vertical cracks open from multiple levels within this facies and inclusions of this sediment can be found infiltrating the T4 deposit.

Facies IV - Black (10R 2.5/1) unconsolidated, poorly sorted silt loam found interstratifying *Facies III* sediments. Like *Facies III*, all the sediments and faunal material has been stained black. *Facies IV* are found in layers matching the gradient and shape of the surrounding *Facies III* beds with the thickest of the *Facies IV* strata is represented by a 7 - 10cm thick continuous stratum. Discontinuous lenses are also found which indicate previous episodes of erosion of *Facies IV*. Infiltrating *Facies IV* material can be found in deeper cracks penetrating the T4 deposit. The sediments are highly fossiliferous with faunal material representing the largest particles, and microfauna specimens dominating the representation. Clastic particles range in size from <2mm to 50mm and faunal particle size range corresponds with *Facies III*. Heavily decayed, powdered, small (<50mm) and unsorted blocks of dolomite are also found.

One of the key features of the T3 facies is the restriction of sediment particle size and clast frequency. The faunal material represents by far the largest particles found in the T3 deposit. Because there is no evidence of post-depositional sorting or removal of clasts from the sediment, it can be suggested that the sampled area lies a significant distance from the sediment source. The longitudinal sorting found in many sediment gravity flows, including hyperconcentrated flows, shows sediment particle size (including clast frequency) is inversely proportional to the distance from sediment source (Bertran *et al*. 1997). Fines and very low clast frequencies/sizes are found at the distal tip of many long-travelled deposits, with the exception of grain flow deposits (Parsons *et al*. 2001) which, like the T2 and EC1 deposits have accumulated large clasts at the snout. The faunal material found in the T3 deposit represents elements that possess particularly high transport potential as will be discussed in the following analyses. Sampling the more proximal areas of the T3 deposit in the future would provide a very useful

analogy for the influence of longitudinal sorting processes on sediment/faunal particle size, clast frequency and faunal element representation in particular sediment gravity flow types.

The varying colours of the different facies contained within the T3 deposit (Figure 5.26) represent both primary depositional chemical composition and post-depositional accumulations of chemicals based on the sedimentological properties of the respective facies. The alumina (Al) in *Facies III* is a primary sedimentation chemical, which has not been heavily changed through diagenic processes due to the low porosity of the sediments. The significance of the Al content is discussed in the XRF analysis section. Oakley (1955) first recognised black staining caused by minerological processes at Makapansgat during investigations into burnt bones. The analogous chemical composition of the host rocks in both the Makapansgat and Sterkfontein system suggests similar processes may be responsible for both phenomena. The nature and cause of the staining black of *Facies IV* sediments and bone is discussed in the XRF section.



Figure 5.26 T3 deposit with the 1st *Facies III* stratum surface exposed across the deposit. The high contrast picture shows the drastic change is sediment colours and the white and black sediments of *Facies III* and *IV*. The dark brown/red sediment is that of the T2 deposit, *Facies I*. The orange/yellow sediment represents the *Facies II* stratum. The range stick segments measure 10cm.

The high fluid interaction is also indicated by the multiple erosion surfaces that can be seen in the profile of the eastern wall of the T3 excavation (see Figure 5.27 for a diagrammatic representation of the T3 morphology). The most extensive erosive episode shaped the surface of the T3 deposit and has resulted in the strike gradients described above. After the accumulation of the T3 deposit, in horizontal strata onto the isotropic, horizontally laid T4 deposit, two streams flowed down the T3 surface in an ENE-WSW (down slope) direction. One less intense stream flowed to the south, along the southern wall, and eroded the southerly strike slope. The other, more intense stream flowed to the north and eroded through *Facies II, III* and *IV*, reducing the thickness of the deposit by half at the northern most point of the excavation (the T3 deposit measures 70cm deep at the top of the ridge and 30cm at the northern most point of the east profile). Prior to the opening of the erosive channels, the T3 deposit may have spanned the width of the eastern

Milner Hall. A similar, less intensively erosive channel operated after the deposition of the lower *Facies IV* stratum, creating a tapering of the horizon to the north. Evidently small streams flowed intermittently during the deposition of the T3 sediments in a similar vicinity to the later more erosive stream that shaped the T3 surface.

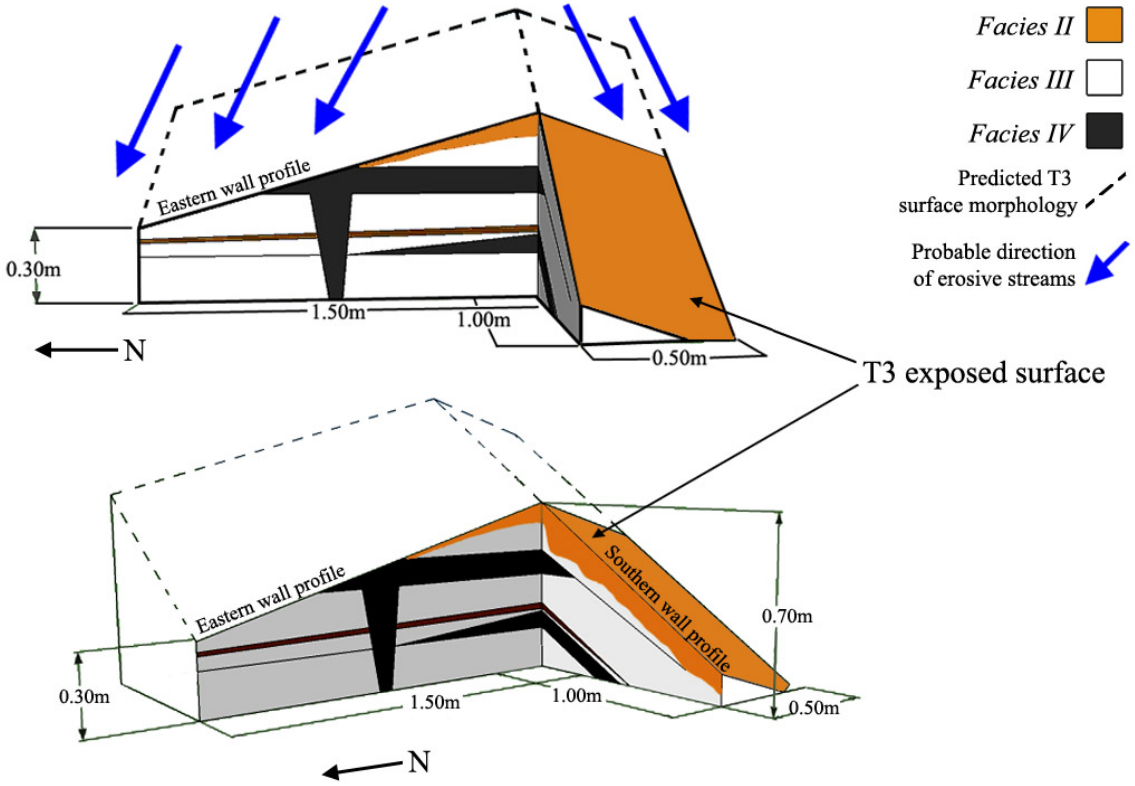


Figure 5.27 T3 deposit morphology. Notice the ridge and associated slopes running away from the ridge. Eastern and southern profiles are illustrated with the notable strata. The different facies are also illustrated. The dashed line represents the predicted shape of the T3 deposit upslope of the current excavation. The blue arrows represent the probable direction of the erosive streams. Also notice the tapering of the lower *Facies IV* bed in a similar nature to the T3 surface, indicating a similar previous erosion of the surface immediately after the deposition of that particular stratum.

The eastern wall profile shows a number of cracking events that have displaced sediments to lower levels (Figure 5.28). The order of the cracking and erosion events illustrate the cyclical phases of deposition, erosion and desiccation of the

sediments. During the deposition of T3, the water-table has evidently risen and receded, saturating and drying the sediments and forming cracks of varying sizes between different phases of deposition. The subsequent sediment flow would fill the open cracks, depositing sediments into deeper levels. Three such desiccation-deposition events can be seen in the eastern wall. Cracks C and B were formed after the desiccation of the lower main body of *Facies III*. The subsequent deposition of *Facies IV* has filled Crack B with characteristically black sediments. The same *Facies IV* accumulation filled the contemporary Crack C, depositing black sediments and fossils deep into the sterile T4 deposit. Crack A was formed by the desiccation of the deposit following the deposition of the second bed of *Facies III* material. *Facies II* sediments were then deposited and filled Crack A, depositing light-brown sediment almost to the base of the T3 deposit. The repeated cracking of *Facies III* sediments, to a greater extent than is seen in the other facies, may relate to the swell-shrink dynamics of the finer-grained sediments (Vogel *et al*. 2005a, b). It can be suggested that the cyclical phases of deposition, erosion and desiccation of sediments represent fluctuations of the water-table and the proximity of permanent and flowing water. Fluctuations in the water-table of metres occur over very long periods of time. The recording of multiple major fluctuations during the deposition of the T3 sediments demonstrates the very long accumulation time of this deposit. There are a number of unknown variables when considering the depositional accumulation times, such as infill development time and water-table fluctuation time. These unknown factors make correlations between climate, sediment chemical composition and water-table levels difficult to correlate and quantify.

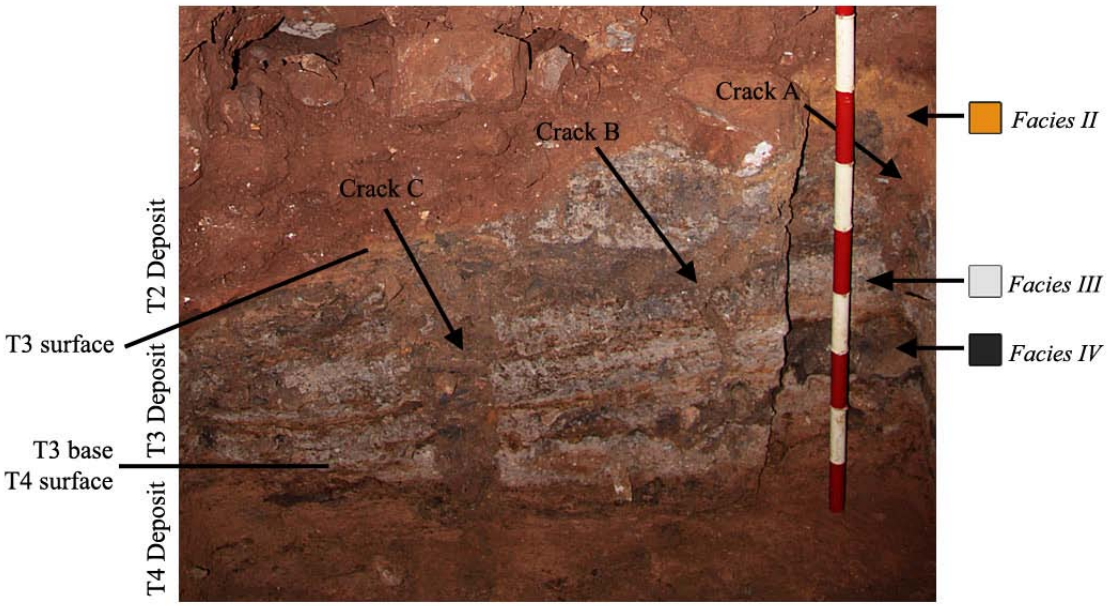


Figure 5.28 STK-MH1 eastern wall profile of T2, T3 and T4. The three main cracks A, B and C are labelled. The facies described in the text are also indicated. The segments on the range staff measure 10cm.

Fluctuating levels of sediment water content during and after the deposition of the T3 sediments is also indicated by a number of soft sediment deformation features found in the excavation profiles. In the southern wall of the excavation (Figure 5.2), the upper 30cm of the underlying T4 deposit has been warped into a concave form under the weight of the terminal portion of the T3 deposit during the deposition and settling of the T3 sediments. Thin black strata within the T4 deposit show decreasing levels of concave deformation with depth. The deformation is localised to areas where the receptacle sediments are hydroplastic and more prone to warping under localised loading. The increased water content of the accumulating T3 sediments at the termination also increases the load impressed on the receptacle sediment.

The sediment deformation/displacement process evident in the northern wall of the MH1 excavation (Figure 5.29) further demonstrates the fluctuation of the water-table after the deposition of T3. Sediment load-casting, also known as a water-escape feature, is a soft sediment deformation process caused by the fluidization and reduction of sediment strength to nearly zero (Lowe 1975). The

causes of these features include grain size differences between vertically associated layers, sediments packing and consolidation (Lowe 1975). The feature is, however, spontaneously developed through externally derived stresses (Lowe 1975). The pillar features originate on the underside of an overlying dense layer, which is superimposed on a less dense, hydroplastic layer (Reineck & Singh 1980; Postma 1983; Allen 1985; Nichols et al. 1994). The inverted density and particle size layering is essential for load casting to occur (Reineck & Singh 1980; Allen 1985). In Nichols et al.'s (1994) analysis of water escape structures, they describe the fluidization process of the basal layer in response to the increasing weight of an overlying layer (equivalent to Lowe's external stresses). They continue to suggest that the maximum force of the outbursting underlying material occurs when the basal layer contains sediments with a particle grain size 15% less than the upper layer.

In the case of the T3 and T4 sediments, silts show an increase of 12.1% in T4 and a 7% reduction of sands, clearly demonstrating an inverse gradient in particle size between the two beds. It can be seen that the deformation event took place after the deposition of the T3 sediments but prior to the T2 deposition. The T4 level represents the basal layer which undergoes fluidization under the increased weight during the deposition of the T3 layer. The external stress responsible for the sudden formation of the feature is likely to be a combined result of the cumulative weight of the developing T3 deposit onto T4, and a lowering in the water-table creating a more pronounced density difference between T3 and T4. The forceful casting process burst through the T3 deposit from within the T4 deposit, mixing and deforming material from all facies. The void left by the water was then filled with a mixture of all facies from T3, depositing fauna and sediments deep into T4.

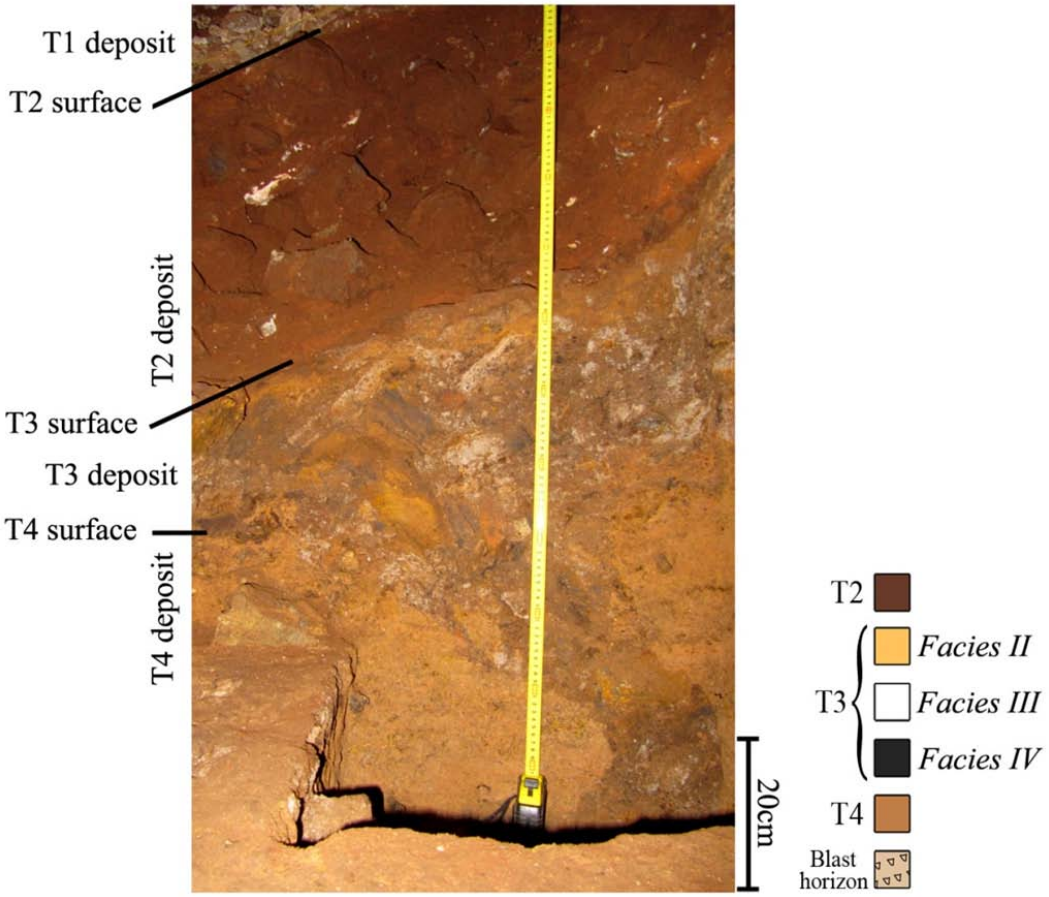


Figure 5.29 Northern wall of STK-MH1. The deformed, mixed sediments of all T3 facies can be seen in the load-cast soft sediment deformation process. Immediately after the load-casting event the mixed T3 sediments collapsed into the void deep within the T4 deposit.

The sediment displacement/deformation and erosional features found in the T3 deposit all indicate the strong influence of water during and after the deposition of the T3 sediments, which in turn can be used to suggest the type of sediment gravity flow operating during the sedimentation process. The dominance of fine-grained, finely stratified sediments, paucity of larger clasts, and strong presence of water during sedimentation qualifies the flow as a more hyperconcentrated flow than debris or grain flow. The inverse and longitudinal grading patterns found in T3 are also often found in hyperconcentrated flows and are a result of greater depositional transport distances, which are facilitated by the increased water content (Hand 1997).

The lack of post-depositional sediment movement is important for the evaluation of the contextual nature of the deposit and integrity of the faunal assemblage.

Evidence for an absence of post-depositional movement can be seen in numerous examples of bones that have been brought together during deposition and remained directly associated after deposition, or elements that have been broken after deposition but remained directly associated. In one particular example a small primate phalange (Art. 176) is directly associated with a broken rib (Art. 175). The two elements have remained in contact from deposition to excavation as is exemplified by the small impression made by the phalange on the rib during the fossilisation process. Figure 5.30 shows two examples of *in situ* breakage. In each example the bone has broken but maintained its original depositional position since breakage. It is notable that examples of *in situ* breakage are found in all levels of the deposit. In light of the numerous soft sediment deformation processes acting on the T3 sediments, it can be suggested that the majority of the breakage occurred after deposition, during the settling of the sediments, which also formed the concave deformation of the T4 sediments.



Figure 5.30 Two examples of *in situ* bone breakage found within the T3 sediments. In each example the bone has broken but maintained its original, directly associated depositional position since breakage.

5.3.2 T3 sedimentology

Table 5.16 presents the sedimentological summary for the T3 deposit. All the T3 sediments fit within the 'silt loam' texture classification (as defined by the US

Department of Agriculture). Samples were taken within the different facies but also represent the upper, middle and lower portions of the entire T3 depositional unit. The T3 sedimentological data shows that despite the three quite different chemical properties of the facies the unit can be considered as a single entity in terms of grading patterns and moisture content. The grading pattern will be explained in detail within the particle size analysis and relates to the sediment gravity flow type. The upper boundary of the T3 deposit is represented by a marked dip in moisture content from 9.17% at the base of *Facies I* (T2) to 7.32% at the surface of T3 (*Facies II*). This is followed by a gradual but clear increase in water content with depth to a moisture content value of nearly 10%. The consolidated surface of T3 has created a boundary for the movement of moisture down from the above deposit, thereby trapping the fines and moisture moving down through *Facies I* and accumulating them in the basal level of the T2 deposit. The comparatively high water content of the T3 sediments is to be expected given the dominance of stable, fine-grained particles and the depth of the deposit in relation to the cave system and the water-table (4m below the excavation floor). The current moisture content of the sediments cannot, however, be considered representative of the content during deposition. Fluctuations in sediment hydrology are influenced by many factors throughout the deposit history, including proximity to the water-table and movement of externally derived water through the cave. The stratigraphic features attest to the fluctuating levels of water in the immediate vicinity during and after deposition of the T3 sediments. The basic particle size classes show a general inverse grading of the deposit, with a reduction in sand proportion with depth and an associated increase in silt proportion. Inverse grading is a common characteristic of hyperconcentrated flows and flows that have travelled a significant distance from the source (for a description see Section 2.6.1 and Bertran & Texier 1999). Stable clay content throughout the deposit may be interpreted as an indicator of the paucity of post-depositional vertical movement of sediments. This, together with the intact fossil concentrations, suggests that the current sediment composition is an accurate representation of the primary context sediment composition. It follows that if the clay content remains stable and has not been altered by post-depositional

movement, then similarities in clay content may suggest an analogous source and distance for the three facies.

					Particle Size		
Art No.	Facies	Sample location	Munsell	Hydrology %	% Clay (<2µm)	% Silt (2µm - 63µm)	% Sand (> 63µm)
129	II	T3 - 5-10 cm	2.5YR 4/4	7.32	6.362	59.62	34.018
254	III	T3 - 40-50 cm	7.5YR 4/3	9.33	6.165	66.324	27.511
251	IV	T3 - to 125cm	10R 2.5/1	9.97	6.95	69.59	23.46

Table 5.16 T3 sedimentological summary.

XRF

The XRF results for the T3 facies are shown in Table 5.17. Analysis through the facies from upper to lower shows that *Facies II* (T3 surface) differs from *Facies I* (T2) chemical properties in a slight rise in Fe, a marked drop in Mn and a similar drop in Ca. These differences, together with the particle size data indicate an abrupt change in deposit, as is clearly indicated by the stratigraphy. The comparatively high quantity of Si, as well as the presence of recognised secondary minerals indicates the allogenic origin for the T3 sediments with minimal mixing of authigenic sediments. The pale colour of *Facies III* is due to the high alumina (Al_2O_3) and low iron oxide (both Fe_2O_3 and FeO) content. High alumina content in sediments can be a result of high levels of weathering and leaching of generally acidic rocks that have high Si and Al and low Fe proportions. Examples are silicate sedimentary rocks and low-grade metamorphic rocks, such as granites, granite gneisses, clays and shales (Schellmann 1994). This weathering process creates the mineral kaolinite, which in turn, decays into lateritic bauxite (Bárdossy 1982; Bárdossy & Aleva 1990; Schellmann 1994). The higher alumina content found in lateritic bauxite over normal laterite (Schellmann 1994) suggests that lateritic bauxite is the more likely mineral contributor to *Facies III*. The debate over alumina content and genesis in bauxites is not addressed here but a review can be found in (Gow & Lozej 1993). The creation of bauxites and laterites requires certain climatic conditions, namely consistently warm temperatures and

high annual rainfall (Price *et al*. 1997). Bauxites in particular, may require even higher levels of precipitation than are needed for laterite genesis (Schellmann 1994). The specific environmental conditions required for the creation of bauxite and Al-rich sediments provide an opportunity for past environmental inferences (for examples see Bárdossy & Aleva 1990; Tardy *et al*. 1991; Taylor *et al*. 1990). In a similar fashion, it may be suggested that the *Facies III* sediments derived from external sources during or closely following a local climate conducive to bauxite creation, i.e. tropical conditions.

Contributions of these types of sediments to the Swartkrans cave material (1km from Sterkfontein) were first described by Brain (1958, pp. 46). The current local surface mineralogy (<1km radius of Sterkfontein) is controlled by the dolomitic limestone and sporadic outcropping quartz veins. There are however, outcrops of shale beds 500m south-east and up slope to the current site, and metamorphic rocks can be found under 1km from Sterkfontein at a higher altitude than the current cave openings (Figure 2.2). In the past, when landscape surface levels and topography were significantly different (Dirks *et al*. 2010), local sedimentation may have been influenced by drainage from a wider area, thereby incorporating decay and weathering products of local shale and quartzite outcrops which lie within 1km from Sterkfontein. The current Sterkfontein valley surface sediments may not represent a sediment *catena* comparable to that during the deposition of T3 and T4 when landscape levels, climate and drainage differed. The proximity of rocks that decay into alumina-rich clays makes these likely contributors of the distinctly high alumina contents in T3 and T4. Pedogenic processes can take many thousands of years, so although sediment chemical composition can indicate soil creation in a tropical environment, the soils may be deposited into the cave for many thousands of years after the tropical climatic conditions have past.

	SiO2	Fe2O3	FeO	MnO	MgO	CaO
Facies II	80.67	0.49	3.97	0.44	0.71	3.35
Facies III	77.95	0.27	2.18	0.45	1.07	3.83
Facies IV	75.56	0.42	3.42	2.55	0.93	4.49

	Al2O3	Na2O	K2O	TiO2	P2O5	Cr2O3	NiO
Facies II	6.33	0.15	0.73	0.5156	2.54	0.0190	0.0020
Facies III	9.86	0.19	1.10	0.7024	2.43	0.0264	0.0061
Facies IV	7.46	0.24	0.87	0.4626	2.86	0.0222	0.0286

	TOTAL
Facies II	99.92
Facies III	100.07
Facies IV	99.31

Table 5.17 T3 XRF results.

Facies III does have a similar proportion of manganese as the *Facies II* (0.44%) and half the amount found in *Facies A* and *Facies I* (0.97% & 1.00% respectively). The fossils in *Facies AI, AII* and *Facies I* are not, however, stained black as is found exclusively in the T3 faunal remains. *Facies IV* which is characterised by blackened sediments and fauna has an expectedly high proportion of manganese, representing more than four times the proportion found in the other T3 facies. Two causes of black staining may be possible in the case of the T3 deposit. Following White (2007), the black staining of the *Facies IV* sediments may be a result of the accumulation of manganese (Mn) as a diagenic process caused by the movement of water through strata with greater sediment porosity, the porosity being representative of different primary depositional conditions. Although sediment porosity was not calculated for the different facies, *Facies IV* is obviously more porous than the other T3 facies by macroscopic observation. The relationship between porosity and hydraulic conductivity is complex but the general trend is towards a positive correlation (Morin 2006). When bounded by more consolidated, less porous strata, *Facies IV* would have provided a conduit for water moving through the deposit, depositing the manganese. The sediment staining evident in the opening *Facies III* stratum (Figure 5.26) suggests the sediments were saturated by water allowing the deposition of Mn into the coarser particle pockets within individual strata (White 2007). White (2007) states that the deposition of oxide coating on clasts must be

carried out under water because Mn^{2+} must be oxidised to Mn^{4+} in cave water before deposition can occur.

Alternatively, the staining of sediments and bone with manganese may be caused by manganese-oxidising bacterial activity under warm, moist cave conditions associated with the decay of organic material during the deposition of the *Facies IV* sediments (Shahack-Gross et al. 1997; Arroyo et al. 2008; Karkanas et al. 2008). Different studies have revealed slightly different prevailing environments encouraging the bacterial activity which facilitates the precipitation of the Mn, but most agree on the basic humid conditions and presence of organic matter (Arroyo et al. 2008; Karkanas et al. 2008). In Arroyo et al.'s (2008) study, bones were classified and spatially plotted according to the level of staining. The study found a direct correlation between occupation intensity and staining as a result of the increased quantity of organic matter available for the manganese-oxidising bacteria. Interestingly, higher levels of manganese could not always be detected in the sediments surrounding the bone (Arroyo et al. 2008). A positive gradient of staining was observed with distance from the main occupation area of the cave. The use of XRD mineralogy would be most useful in the decipherment of the original source of the manganese (Arroyo et al. 2008). This gradient is not observable in the T3 sediments and bones throughout the deposit are equally permeated by manganese.

Of particular significance is the staining black of all the osseous material within all T3 facies, with no exceptions. All fossils have been completely permeated by the manganese to the point that no unaffected parts can be found. When broken, the cortical and cancellous bone is black but often in an excellent state of preservation. The Mn staining is more intense than that found on the surface of many of the bones and artefacts found elsewhere at Sterkfontein (Pers. Obs.) and described by Cukrowska *et al*. (2005), Thackeray *et al*. (2005). The relatively high porosity of the faunal remains in relation to the surrounding sediments created a density gradient and by osmotic processes facilitated the absorption of the available manganese (Arroyo et al. 2008). The role of bone porosity in the preferential uptake of certain minerals during fossilisation has also been suggested

by Kuczumowa *et al*. (2010). As White (2007) attests, the time required for manganese to completely impregnate fossil bone is significant and suggests that the sediments of all facies were saturated by standing water as well as by water moving through the coarser grained strata.

The absence of large quantities of organic matter found in the caves and the significant levels of naturally occurring manganese in the host rock suggest that this is the source of the mineral and staining. It is most likely, in light of the relative position of the deposit to permanent water, the evidence of water moving through the sediments, and the uniform levels of staining throughout the T3 bone, that the manganese deposited into the fossils and particularly into *Facies IV* derives from the host rock and has been concentrated by water moving through a more porous matrix and bone where sediments are close to saturated near the water-table. During the deposition of T3, the sediments would have occupied one of the deepest parts of the cave, close to the water-table, and the majority of vadose dolomitic breakdown would have occurred in higher parts of the system (see Osborne 2002 with regards to the vadose weathering process). The flow of water down to the water-table facilitated the concentration of the decaying minerals into the deepest fine-grained deposits.

The low Ca proportions, increasing steadily with depth from 3.35% to 4.49%, indicate that the deposit has never been calcified. In calcified and decalcified sediments the Ca level is significantly higher. Section 5.2.2 describes the differences in Ca proportions between calcified, and non-calcified sediments. Silty clay sediments often do not calcify due to low matrix permeability (Ford & Williams 2007) and sometimes create hard caps limiting the calcification process. The hard capping process would be recognisable as higher proportion of Ca isolated in the surface sediments of T3.

Particle Size

Figure 5.31 shows the particle size curves for each sample taken from the T3 deposit. The sample curves are presented on the same axes in Figure 5.32. The

sampling of the upper, middle and bottom of the deposit shows a clear deposit-level inverse grading trend, regardless of individual facies' sediment grading. In the case of T3 the inverse grading is a result of the accumulation of multiple hyperconcentrated sediment gravity flows during deposition. The proximity to water, particle size attributes and evidence of water during deposition support the classification of each strata as a hyperconcentrated flow (Bertran & Texier 1999). Hyperconcentrated flows can develop both regularly graded and inversely graded sediments depending on sampling location and distance from sediment source (Bertran & Texier 1999; Hand 1997). Consequently, although T3 may show an inverse grading trend, typically found within hyperconcentrated flows, at the sample point the individual facies may have developed a regular grading pattern. Further testing needs to be carried out to clarify the grading patterns of the individual facies in order to show how their particle size distribution contributes to the deposit level inverse grading pattern. Due to time and financial constraints intra-facies samples could not be analysed although the samples were taken during excavation.

From the basic particle size class volumes presented in Table 5.16, sand proportions dip radically from 34% at the surface to 23% at the base of the deposit. Silt proportions steadily rise with depth from 59% at the surface to 69% at the base. Clay proportions drop slightly in the middle of the deposit and then rise to the highest level at the base of T3. Despite slight fluctuations, the clay proportion stays within the 6% bracket throughout the deposit. The trend of the deposit is a reduction in the coarse grains with depth and a corresponding rise in silt sized sediments. The Chi^2 statistical comparison of the area occupied by the de-convoluted curves on each sample shows the surface and middle samples (T3 – 5-10cm; T3 – 40-50cm) are significantly dissimilar ($p = 0.0$) and the surface and deepest sample (T3 – 5-10cm; T3 -125cm) are also significantly different to both middle and surface samples ($p = 0.0$). The middle and deeper samples are, however, statistically similar with $p = 0.791$. This is an expected pattern, given that the greatest degree of change is found between the upper and middle samples. Table 5.18 presents the relative volumes for each of the constituent curves which

make up the particle size distribution curves shown for each particle size sample. The de-convoluted curves from each sample are presented in Appendix 2.

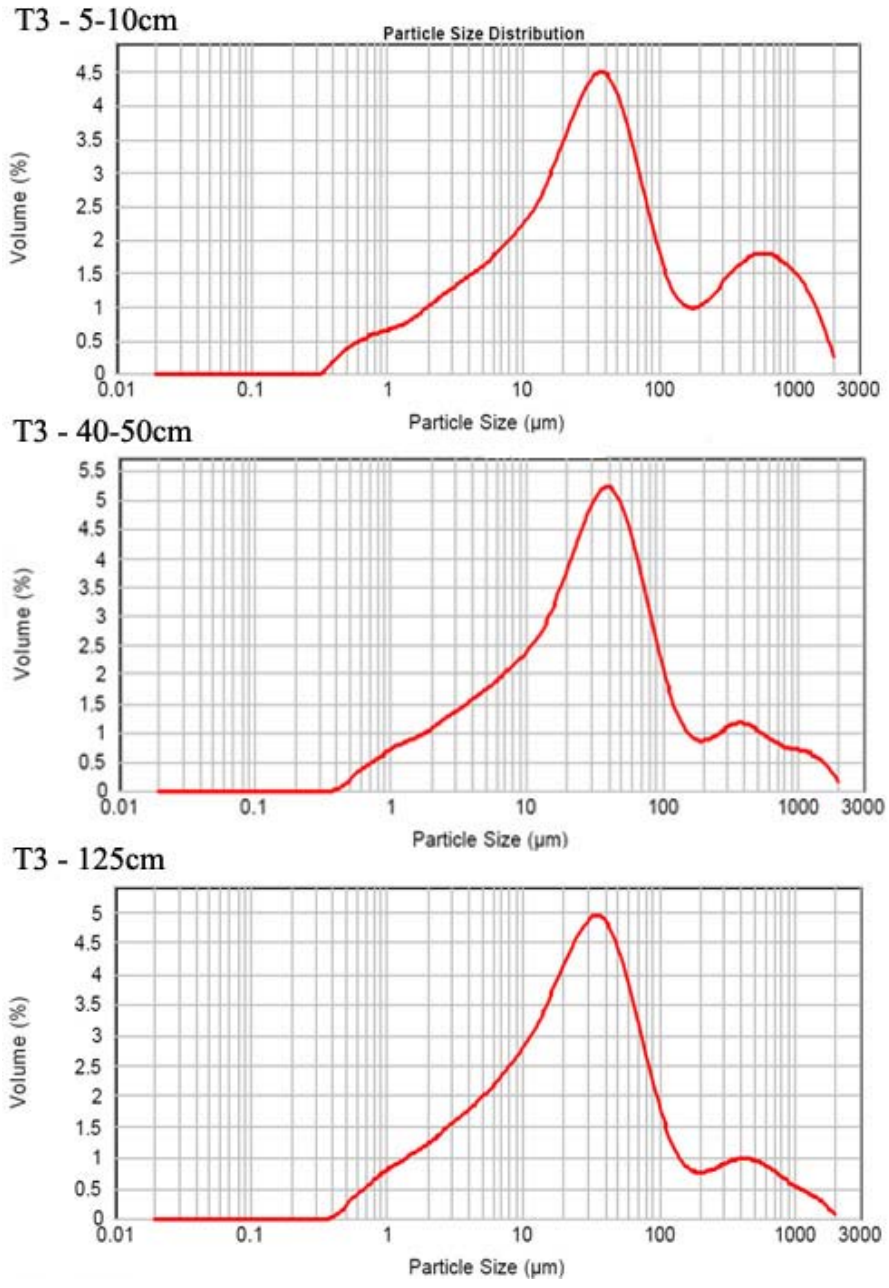


Figure 5.31 T3 particle size distribution curves for three samples taken at the surface, middle and base of the T3 deposit.

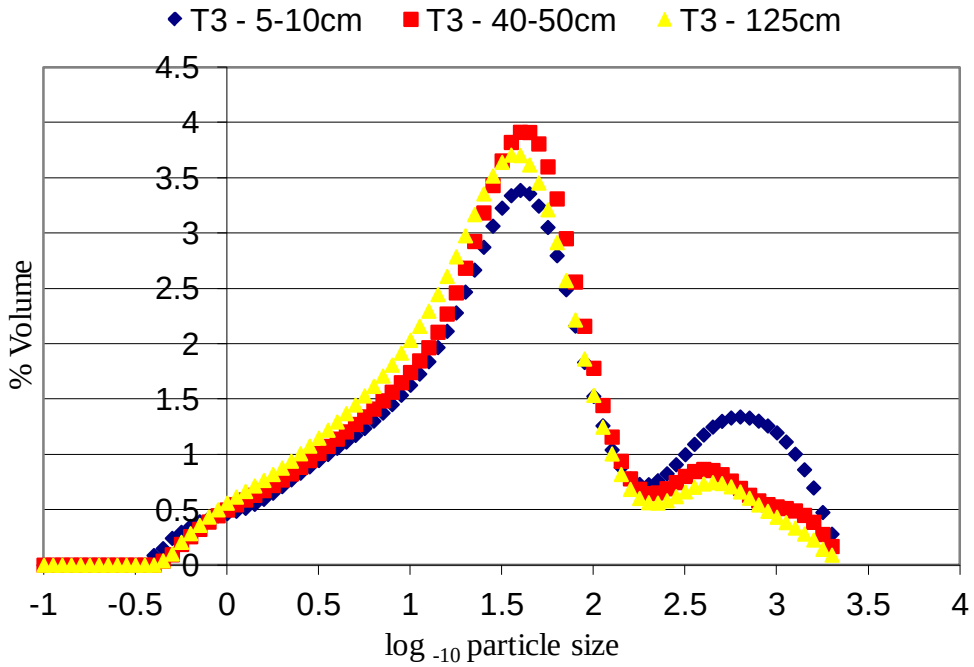


Figure 5.32T3 combined particle size distribution curves. Stated sample depths are relative to deposit surface.

	Curve 1	Curve 2	Curve 3	Curve 4	Curve 5	Total
T3 - 5-10cm	3.149	36.407	38.375	22.050	0.020	100.0
T3 - 30-40cm	3.319	35.147	49.791	8.004	3.738	100.0
T3 - 125cm	3.292	39.913	46.898	7.975	1.921	100.0

Table 5.18 T3 relative constituent Gaussian curve volumes. The figures represent the volume as a percentage of the whole sample distribution curve. The T3 particle size distribution curves could be de-convoluted into five Gaussian curves.

The basic particle size class proportions show a very simple and clear picture of the inverse grading trend within the T3 sediments. The relative volumes of the five constituent Gaussian curves provide a more detailed view of the relative proportions within and between the basic particle size classes. The absence of obvious post-depositional movement of sediments implies that the slight variations in the distribution of particle sizes seen in Table 5.18 may relate to the depositional particle suspension dynamics acting within the hyperconcentrated

flows. Alternatively, a minor quantity of vertical movement of silts has occurred during the settling of the deposit aided by the fluctuating moisture levels. Curve 1, which represents the smallest component, <1µm, correlates with the basic particle size class data for the clays in that there is very little change through the T3 deposit, regardless of facies. The difference between the basic particle size class clay distribution and the Curve 1 distribution is that Curve 1 focuses on the relative volume of the smallest particle found which, in the case of T3, is≤1µm or 1/1000mm. Curve 1, therefore, represents the finer half of the clay component and shows an even more restricted distribution of just 0.170% compared to 0.78% in the <2µm clay class. Curve 2 represents the coarser clay and fine silt component of the sediment, and shows a slight dip (1.26%) in the middle of the deposit before rising rapidly at the base. Despite this discrepancy, in the middle of the deposit within this particle size component Curve 2 still shows an increase with depth and supports the inverse grading pattern found in the T3 sediments. Curve 3, representing the coarser silts, shows a rapid rise of 11.46% from the upper to middle of the deposit before dropping 2.9% at the base but still maintaining the general inverse grading trend where silts increase in proportion from the upper levels down. Curve 4 represents the sand sized component and shows an expected clear drop in proportion with increasing depth. The greatest area of change is from the upper to middle level showing a drop of 14%. Curve 5 represents the coarsest component with sand grains measuring >1mm (classified as very coarse sand using the Wentworth scale). This component shows an increase in representation from the upper to middle level and then a small dip to around 2% at the base of the deposits.

5.3.3 T3 fabric analysis

The *in situ* nature of the T3 sediments combined with the absence of post-depositional movement of the sampled particles allowed a good opportunity for detailed fabric analysis to be conducted on the sediments. Within the T3 deposit, there is a lack of clastic material suitable for fabric assessment. The faunal material, however, represents the largest and most frequent particle, which

possess shapes conducive to positive orientation to flow direction. Figure 5.33 shows the fabric data for the T3 deposit. The dominant gradient for the T3 particles is 26° as demonstrated by a best fit plane (red line) on the stereographic projections in Figure 5.33. This dip figure is slightly less than the 30° dip of the T3 deposit surface, but it can be explained as a result of the progressively shallower gradient of the deposit with depth. The deepest faunal specimens from the T3 deposit, excavated from the basal levels (in the bottom 20cm), have a mean dip of just 6°. The middle and upper levels show a gradient mean of 28°. The changing faunal gradients in different levels supports the observations made on the internal stratigraphy of the T3 deposit. The pattern demonstrates the importance of receptacle morphology to the development of deposits. T1, for example, becomes progressively steeper with depth as it builds on top of the relatively steep surface of T2. The opposite can be seen in T3 with the first sediments being laid down on the horizontal T4 deposit and building gradually into a steeply sloped talus deposit.

The rose diagram and 1% contour stereographic projection (Figure 5.33) show two major fabric orientations represented in the fabric. Within the rose diagram and 1% stereograph, the primary fabric orientation is between 120-130° and the secondary fabric orientation is between 70-80°. The Kamb contour stereographic projection (Figure 5.33) and the best fit cone groups both concentrations into a single orientation trend in the 70-130° bracket. The presence of two fabric orientation concentrations suggests the recording of two directions of sediment flow within the deposit. One may expect elements orientated to the secondary concentration to be contained within a distinct horizon indicating a different sediment flow direction during a specific depositional process. This is not the case, however, as elements orientated to the secondary concentration are found sporadically in all levels of the deposit and in all facies. Alternatively, it could be proposed that those elements orientated to the secondary concentration may possess different dimensional attributes, thereby affecting their settling behaviour in the sediment flow.

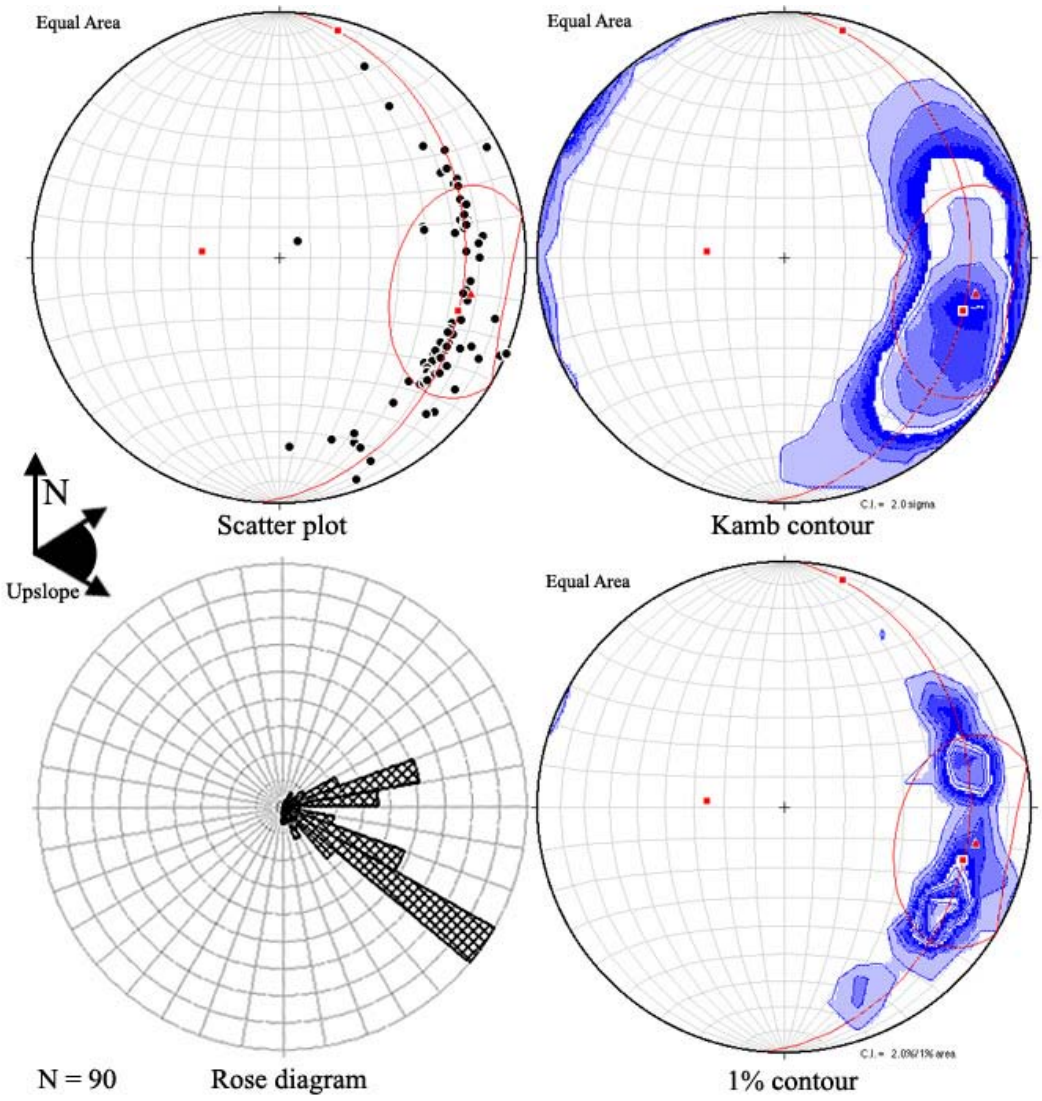


Figure 5.33 T3 fabric analysis models. Kamb contouring has a contour interval of 2.0 sigma. The 1% contour plot has a contour interval of 1%. All stereographic projections show best the best fit plain and cone. The rose diagram sections represent 10°.

To assess this, elongation ratio was plotted against the orientations on a histogram (Figure 5.34). The mean elongation ratio for the T3 elements is 4:1. Only 15 faunal elements have elongation ratios under 1.6:1, those elements were excluded from the fabric analysis. There is a slight rise in the mean elongation ratio of those

elements orientated to the secondary concentration compared to those orientated to the primary orientation, 4.7:1 compared to 3.9:1 respectively. This difference may be significant but without experimental research it is difficult to assess the influence on orientation of a 20% difference in elongation ratio on already highly elongated particles. Cañón-Tapia & Chávez-Álvarez (2004) don't test orientation potential within very elongate forms but state that elongate forms of <0.5 (>2:1) including very elongate forms (0.2, or 5:1) make reliable positively orientated particles. Following this assessment, the differences in elongation ratio are ruled out as the main cause of the secondary orientation concentration. No difference in associated sediment or faunal attributes was found relating to those elements orientated to the secondary concentration and so presence of an alternative contributing source is considered unlikely. The two orientation concentrations must then reflect a particular sediment flow pattern acting throughout the history of the deposit with a more dominant sediment flow moving down the southern wall and a minor sediment flow converging into the terminal portion of the deposit from a more northerly direction.

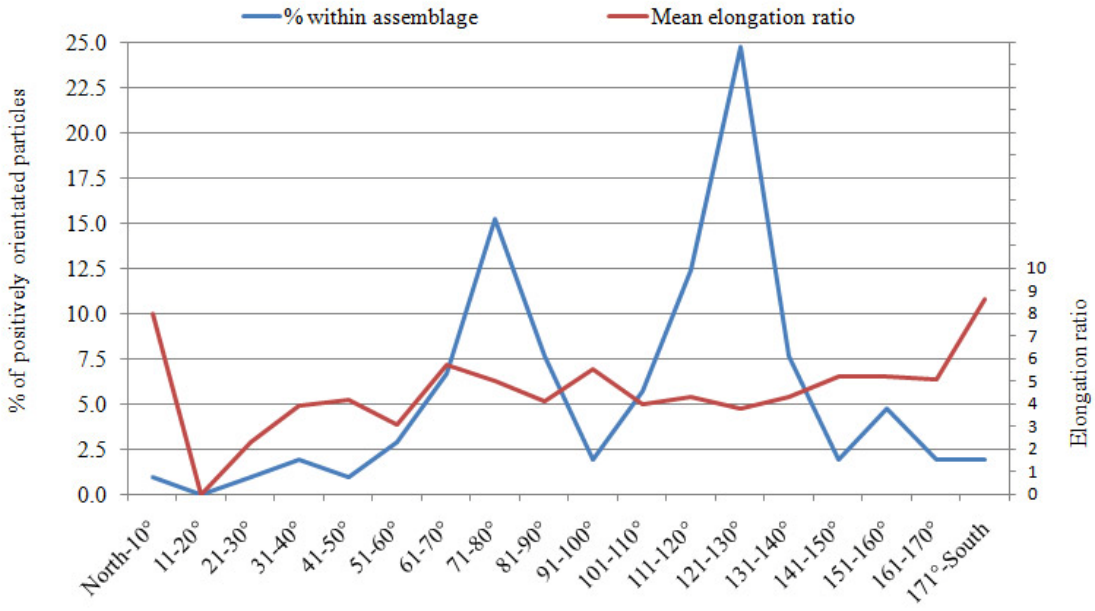


Figure 5.34 T3 orientation data plotted against elongation ratios for the same elements.

Despite the presence of a secondary orientation concentration, it is clear that the majority (55%, n = 58) of the sediments derived from a source in the direction of 110-130°, or from the south east (SE). This differs significantly from the T2 deposit, considered to have accumulated from sediments deriving from the Name Chamber (almost 70% of particles orientated between 60° and 90°). The Silberberg Grotto is the only deposit that has deposited sediments into the Milner Hall from a SE direction. Wilkinson (1983) had originally noted the development of sediments from the Silberberg Grotto into the Milner Hall. The residual body of sediments illustrating this connection is called the M2 Hanging Remnant and has been described in the Background Chapter. The M2 Hanging Remnant has entered the Milner Hall from the Silberberg Grotto to the SE and has been cemented to the southern wall. The M2 Hanging Remnant sediments have clearly developed in a talus flowing down the southern wall from a south-easterly direction (See Section 2.4, Figure 2.8 and 2.9 and for a description, diagrams and location of the M2 Hanging Remnant). The stratigraphic relationship between the M2 Hanging Remnant and the T3 deposit is discussed in the conclusion section of this chapter. Detailed inspection of the cave roof shows no other past or present openings into this area of the Milner Hall. From the above orientation data it can be proposed that the T3 sediments derived from the Silberberg Grotto.

The sampling of the terminal portion ('snout' or 'lobe') of a deposit provides an opportunity to assess the morphology of the deposit in this area. A number of studies have investigated sediment properties and fabric in different portions of sediment gravity flows (McSaveney 1971; Mills 1984; Francou 1990; Nieuwenhuijzen & Van Steijn 1990; Bertran *et al*. 1997; Major 1998; Parsons *et al*. 2001). The works mentioned cover a number of different sediment gravity flow types, including dry grain flows (Bertran *et al*. 1997), lahar flows[2] (Mills 1984; Bertran *et al*. 1997), rockfall deposits (Bertran *et al*. 1997), periglacial solifluction flows (Bertran *et al*. 1997), and debris flows from an experimental perspective (Major 1997) and from field analysis (Bertran *et al*. 1997). The general trend shown amongst most flow types covered above, with the exception

[2] "large scale debris flows on active volcano slopes" (Bertran *et al*. 1997, pp. 10)

of rockfall deposits, is a parallel clast orientation trend within the main body of the flow with the highest potential for transverse orientations being found at the lateral margins or in the frontal lobe (Bertran *et al*. 1997). The terminal portion of the T3 deposit does not show a significant number of transversely orientated particles. A lack of transversely orientated particles is not diagnostic of flow type, and Bertran *et al*. (1997) suggest "fabric characteristics reveal large overlaps of the fields representing different sedimentary processes" (pp. 12), thereby precluding the evaluation of past or present slope processes from particle orientation alone. Following this warning, particle shape, size and structure, water content and grading properties were used in this research to assess sediment gravity flow type.

5.3.4 T3 particle shape

The particle shape analysis is shown in Figure 5.35. The assemblage is again dominated by elongate forms, as mentioned in the section above. 71% of the assemblage is classed within the Sneed & Folk elongate or very elongate shape class with 65% of the assemblage classed as very elongate. Compact forms represent 5.6% of the assemblage. Interestingly, when comparing T3 to the other MH1 deposits, the greatest similarity is found between T3 and T1. In the Sneed & Folk classes, both deposits show a similar proportion of elongate, very elongate and compact forms. In the Zingg diagram (top left) both T3 and the T1 Identifiable component show a similar spread of points across the plot area, representing a larger proportion of disc-shaped and spherical forms, more so than seen in T2. From these diagrams the T3 and T1 Identifiable component look similar in shape representation despite the very different depositional histories. Different shape indices are sensitive to different particle dimension ratios. MPS (maximum projected sphericity) offers a different perspective on particle shape that can be useful for insinuating element transport potentials. The MPS vs. DRI diagram shows a clearer difference between the T3 and T1 assemblages. In the T1 assemblage the major concentration of points indicates a more rod-shaped form with a lesser representation of bladed forms. In the T3 assemblage most of the

particles qualify within the more spherical to disc-shaped classes. One would expect those elements found in the distal portion of a long-travelled talus to possess a greater transport potential, as suggested by Frostick & Reid's experimental work (1983). This pattern is supported in part by the MPS vs. DRI interpretation of the T3 particle dimensions in the identification of a more spherical trend to the particles. The Zingg and Sneed & Folk diagrams identify a dominance of elongated rod-shaped forms that also possess a high transport potential according to Frostick & Reid (1983). As found in the T2 particle shape analysis, the Zingg diagram is more sensitive to bladed forms and so presents a greater proportion of bladed forms than the other indices. This sensitivity influences fossil transport interpretations and must be taken into account when analysing *in situ*, well preserved sediments.

The trend implied by the MPS vs. DRI shape index is supported further by the Voorhies Group assessment of element representation in relation to transport potential. Figure 5.36 shows a dominance of Group I and Group I & II elements within the T3 deposit. Representing over 60% of the elements found within the deposit, elements that fall into Groups I and I & II are considered to be more prone to movement within a fluid or sediment. Group I, representing over 50% of the excavated elements, is considered to be the most easily moved and, therefore, most likely to be moved furthest (Voorhies 1969).The decreasing proportions of less moveable elements (26% of Group II and 12% of Group II & III elements) further support the process of longitudinal sorting that took place during the deposition of the T3 deposit. The relative proportions of Group II and Group II & III contrast quite starkly to the T1 and T2 deposits, where high energy, clast-rich flows (or in the case of T1, destructive re-sedimentation) moved all types and shapes of elements and produced a diamicton[3]. Longitudinal sorting must be taken into consideration when considering the skeletal element representation and specimen abundance data used for taphonomic analyses, a problem discussed in Section 2.5.2.

[3] A diamicton is a very poorly sorted deposit containing a wide range of particle sizes. Diamictons are often associated with slope deposits and glacial moraines.

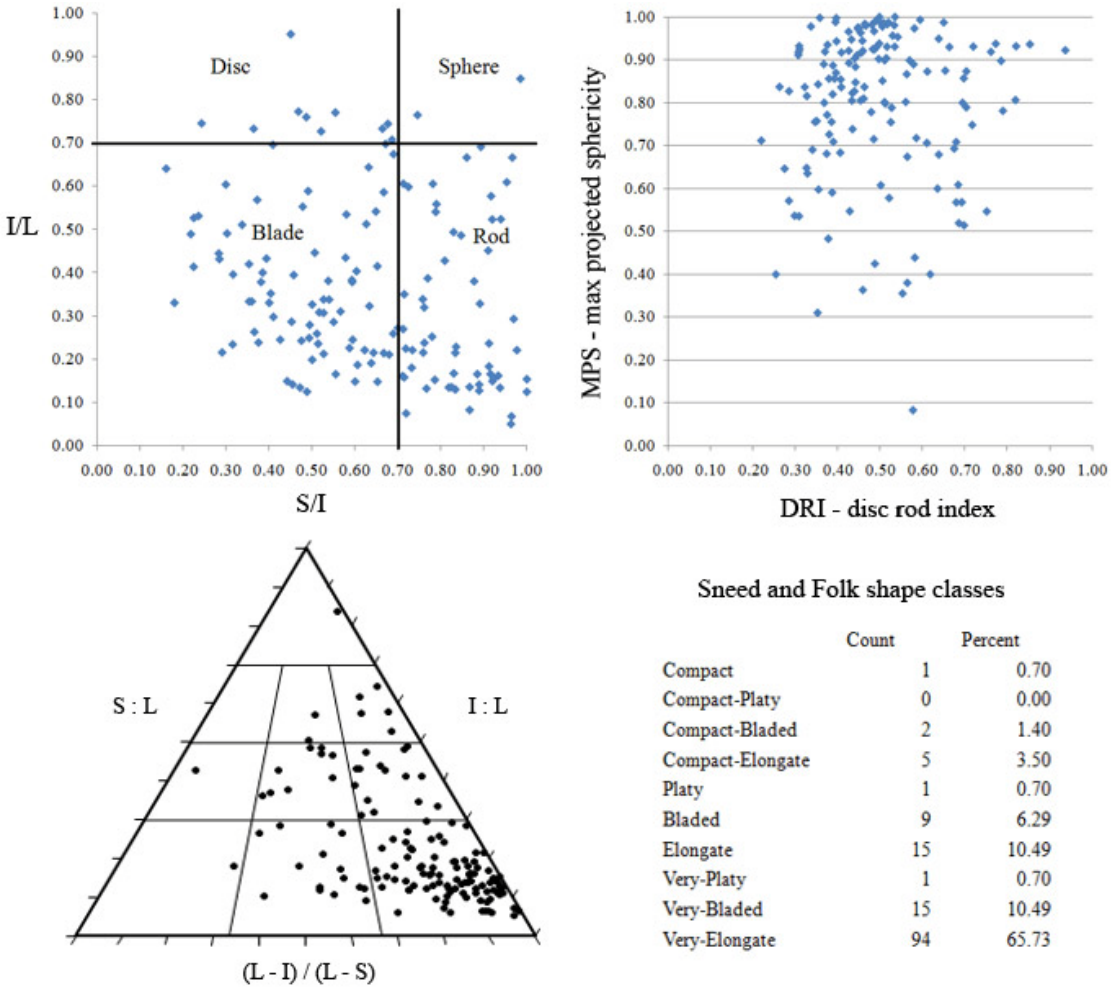


Figure 5.35 T3 particle shape indices.

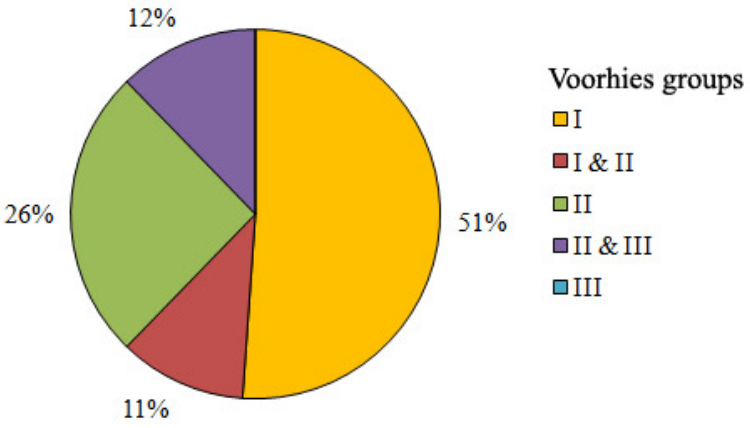


Figure 5.36 T3 Voorhies groups.

5.3.5 T3 faunal assemblage profile

The entire T3 assemblage (Table 5.19) was excavated *in situ* and is analysed in the same fashion as the T2 assemblage. Unidentifiable elements are included in all bone breakage assessments but not in element representation. The T3 deposit is not an artefact-bearing deposit as all artefacts were excavated from the surface level and represent contamination from the upper *Facies II* sediment from the basal levels of the artefact-bearing T2 deposit. Because the artefacts were excavated from T3 sediments, they are included in the T3 assemblage profile. These artefacts have, however, been included in the T2 archaeological analysis (Section 5.2.6).

The T3 assemblage shows a broader size profile than was found in either the T1 or the T2 deposit. The range of specimen sizes is a result of the relatively intact *in situ* primary deposit characteristics. The greater proportion of larger sized fossils does suggest a more evenly distributed assemblage composition and demonstrates a lower degree of pre or post-depositional fragmentation than is found in the other MH1 assemblages. This will be corroborated by the following faunal analysis. As can be seen in Table 5.19, the majority of the T3 assemblage measures >30mm (T2; 55% measures <30mm) with a mean maximum dimension of 44mm (largest = 144mm) and a StdDev of 23.6 (T2 has mean maximum dimension of 33mm (largest = 69.5mm) with a StdDev of 13.6). In terms of particle size (expressed as the mean of axis L, I and S), T3 shows a mean of 22.2 with a StdDev of 9.5, compared to T2 that has a mean particle size of 17.4 with a StdDev of 7. The higher standard deviation shown in the T3 particle dimensions is indicative of the broader range of sizes found within the assemblage in comparison to the more restricted size profiles of the T1 and T2 assemblages. The more restricted faunal size profile of T1 is a result of the increased breakage levels due to anthropogenic accumulation processes, and in the case of T2, a result of both depositional breakage and secondary filtration processes during re-sedimentation.

Max Length	Summary					
	Artefacts	%	Fossils	%	Total	%
<10mm	0	0	0	0	0	0
<19mm	0	0.0	2	100.0	2	1.4
20-29mm	0	0.0	42	100.0	42	28.8
30-39mm	2	5.4	35	94.6	37	25.3
40-49mm	0	0.0	25	100.0	25	17.1
50-59mm	0	0.0	15	100.0	15	10.3
60-69mm	0	0.0	8	100.0	8	5.5
70-79mm	0	0.0	5	100.0	5	3.4
80-89mm	1	50.0	1	50.0	2	1.4
90-99mm	0	0.0	4	100.0	4	2.7
>100mm	0	0.0	6	100.0	6	4.1
Total	3	-	143	-	146	100.0
Total %	2.0	-	97.9	-	100.0	

Table 5.19 T3 faunal and artefact assemblage summary and size profile.

A total of 143 faunal specimens was excavated from the T3 deposit. It should be noted that the faunal material infiltrating T4 through the sediment displacement processes was not excavated. Those specimens remain within the T4 deposit. Figure 5.37 presents the fossil yield data through the deposit in relation to spit depth (5cm slices excavated at the angle of repose) and facies distribution. Fossil yield shows a rise in yield from the surface levels and *Facies II* sediments into the main body which is made up of *Facies III* and *IV* sediments and measures in depth between 5cm and 55cm. Fossil yield continues to make a steady rise through the first body of *Facies III* and the main *Facies IV* stratum into the upper levels of the second *Facies III* bed, where at about 25cm depth throughout the deposit there is a rapid tailing off of fossil yield from 31 specimens at the 20-25cm spit to just three specimens in the 30-35cm spit just ten centimetres deeper. The bottom 20cm of the deposit yields under 10 fossils per 5cm spit. The mean maximum fossil dimensions are also plotted on the same graph. Mean particle size follows a similar trend to the mean maximum length albeit with less variation. The drastic spike in specimen dimension in the 30-35cm spit is due to the small

yield from this spit, only two fossils were recovered, one measuring 79mm and the other 98mm maximum dimension.

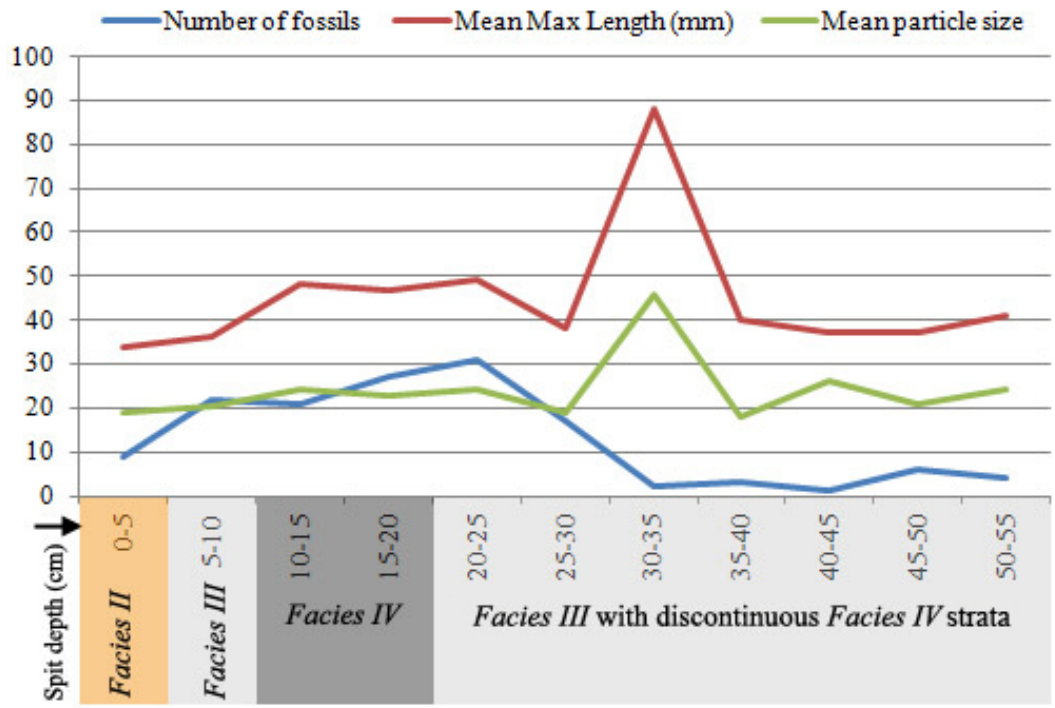


Figure 5.37 T3 fossil yield through deposit depth in relation to spit depth and facies distribution.

When considered within the depositional sequence (from base of T3 to the surface), the data indicates a fairly consistent fossil yield of under ten specimens/spit with a mean maximum length of 38mm for the first half of the sedimentation process (lower 25cm of deposit). This is followed by a pronounced rise in yield (up to 26 specimens/spit), and an associated rise in size of faunal specimens (mean maximum dimension of 48mm). Fossil yield and mean fossil size then gradually decrease from the deposition of the main *Facies IV* horizon through to the *Facies II* sediments at the surface (the upper 20cm of T3). The pattern presented in this data is significant and implies a varying pattern of fossil deposition during the history of the deposit. The relationship between fossil size and fossil yield within a primary sedimentation deposit is complex and relates to the taphonomic accumulation agent, faunal population density within the opening

catchment area, landscape surface sedimentation rates, and cave opening shape fluctuations. The taphonomic analysis (Section 5.3.8) may provide some idea of the agents of accumulation active during the T3 sedimentation and what affect those agents had on the faunal representation.

5.3.6 Faunal analysis

All 143 faunal specimens were analysed with the same procedure applied to the T2 assemblage. The taphonomic analysis, which focuses on the modes of accumulation of the fauna, is presented in the following section (see Chapter 2 for the methods for the Taphonomic analysis). The analysis for stratigraphic information is presented before the taphonomic analysis. Because T3 represents a primary sedimentation deposit the two analyses are particularly cohesive. Many of the attributes found in the T3 assemblage are representative of the original faunal accumulation agent. In primary sedimentation deposits, the integrity of the assemblage may be much greater than in secondary sedimentation deposits, allowing the faunal analysis to support the taphonomic data in the clarification of the accumulation agent. All elements from the T3 assemblage were at least identifiable to element type although 29 specimens were not identifiable to specific element.

Skeletal element representation

Figure 5.38 and Table 5.20 show the distribution of skeletal element type and body portion representation respectively. This data includes all specimens excavated from *Facies II*, *III* and *IV*. Those specimens deriving from *Facies II*, *III*, and *IV* that have contaminated *Facies V* were not excavated or analysed. There is no sub-assemblage of unidentifiable material that influences the data as seen in T1. Long bone elements dominate the assemblage (45%, n = 64), with irregular bones representing the next largest component (22%, n = 32). The richness in long bones is a result of the fragmentation characteristics of shaft elements, which

break into disproportionately high numbers of long fragments thereby increasing the relative abundance of the long bones. Long bones because of their relative size, surface area and density are also subject to greater exposure to breakage forces (Lyman 1984). To demonstrate this point, there are only two complete long bone elements and both belong to rodents. Irregular elements which include most of the axial skeleton, with exception of the ribs, represent a significant proportion of the T3 assemblage, and many of the specimens are more than 80% complete. From the relatively even distribution of elements it can be suggested that a broad range of elements representing most mammal body parts has been deposited. The relatively high proportion of near-complete irregular elements supports the suggestion that the T3 deposit was accumulated by a gradual, non-destructive process. These elements are considered to be more vulnerable to fragmentation and have lower survivorship rates (Lyman 1984). Breakage of bone within clast-rich deposits is mostly facilitated by interaction with clasts. In some cases fragmentation can be highly localised through the collapse of a block onto the end of a bone or the crushing of a single element. In long travelled deposits with low clast proportions attritional processes will inflict damage on protruding parts of bones. Table 5.20 presents the body portion representation within the T3 assemblage. Classification to body portion requires specific element identification which is not always possible on mid-shaft fragmented that can be easily identified as deriving from long bone elements. Within the body portion analysis, axial elements represent the greatest proportion of the assemblage (32.9%, n = 47) with appendicular elements following closely after (31.5%, n = 45). The third greatest proportion represents those elements unidentifiable to specific element by this researcher.

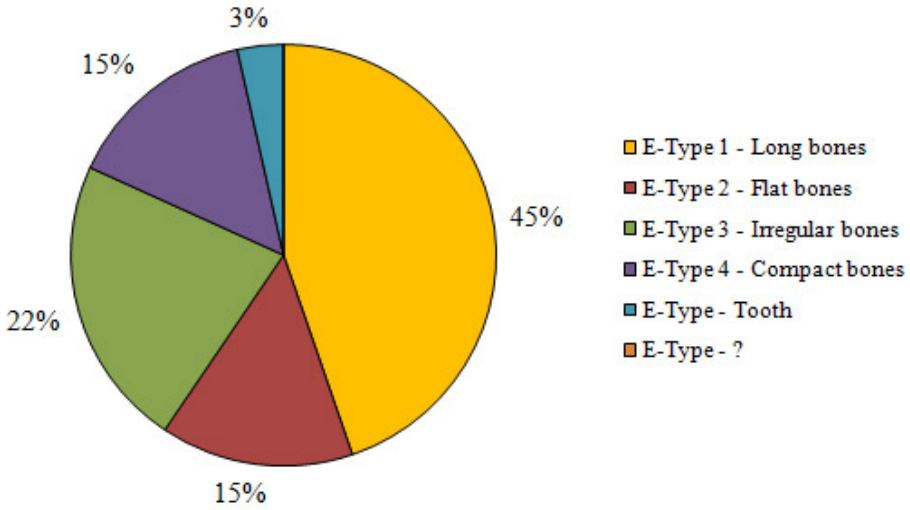


Figure 5.38 T3 skeletal element type distribution.

Max Length	Fossils						
	Appendicular	Axial	Podial	Tooth	?	Total	%
<10mm	0	0	0	0	0	0	0
<19.9mm	0	0	0	1	1	2.0	1.4
20-29.9mm	8	9	10	2	13	42.0	29.4
30-39.9mm	10	11	4	2	8	35.0	24.5
40-49.9mm	7	11	3	0	4	25.0	17.5
50-59.9mm	7	8	0	0	0	15.0	10.5
60-69.9mm	5	1	0	0	2	8.0	5.6
70-79.9mm	4	1	0	0	0	5.0	3.5
80-89.9mm	0	1	0	0	0	1.0	0.7
90-99.9mm	3	1	0	0	0	4.0	2.8
>100mm	1	4	0	0	1	6.0	4.2
Total	45	47	17	5	29	143.0	100.0
Total %	31.5	32.9	11.9	3.5	20.3	100.0	

Table 5.20 T3 skeletal portion distribution summary.

The proportions within this data provide an interesting analogy to the proportions found within naturally buried bone assemblages published by Behrensmeyer (1983) where axial elements represent a few percent more of the assemblage than appendicular elements in naturally buried faunal assemblages. A similar pattern would be present in a death trap assemblage as is suggested by T. Pickering *et al*.

(2004a, b) as the major accumulation process for the M2 deposit fauna. The faunal sample used for T. Pickering *et al.*'s analysis (2004a) derived from the more proximal and medial portions of the upper M2 deposit, and so may not have been affected by longitudinal sorting. The element proportion representation found in the distal portion of the T3 talus may differ significantly from the relative element proportions at the proximal or medial portion of the T3 deposit. The specific pattern of element representation at specific points of the deposit may be considered a false signal caused by the longitudinal sorting process, preferentially accumulating vertebrae and other more mobile elements. This signal was identified from the Voorhies group representation. Although the specific pattern of element representation may have been influenced by the longitudinal grading process, the elements represented must relate to the original assemblage. The T3 assemblage does represent all body portions and element types found in complete skeletons.

Fossil survivorship

In primary sedimentation deposits, fossil breakage data and completeness can be used to identify levels of post-depositional breakage. In T3, where the sampled portion of the talus is matrix-supported with very few clasts, one would expect there to be a relatively small level of post-depositional breakage with the majority of the primary depositional breakage signature still preserved on the fossils. The *in situ* fossil breakage in T3 caused by the deformation of sediments attests to the ability for *in situ* post-depositional breakage to occur in clast-poor sediments. As breakage levels increase through episodes of deposition, consecutive breakage generations eradicate previous breakage evidence. This can be seen in a number of the investigated deposits, like the Primary infill of the MH2 site. The sedimentological characteristics at the medial and proximal portions of the T3 deposit are unknown and clast size and proportions are probably significantly different to that seen in the distal portion. Higher clast proportions in the un-sampled sections of the talus may potentially inflict breakage on the specimens as they move to the more distal areas during the diagenic process. If the T3 deposit

does represent the terminal portion of a death trap assemblage then a strong pre-fossilisation breakage signature should be evident.

Bone breakage

Figure 5.39 presents the breakage numbers for the T3 deposit. Elements showing two or fewer breaks represent 68% of the assemblage with specimens showing no breaks, complete elements, representing 18%. This is the highest proportion of complete elements in any of the investigated deposits. The only other assemblage that shows as a higher representation of complete elements is the T1 Identifiable assemblage, which for reasons that have been discussed, is not representative of the T1 deposit. The T3 assemblage is representative of the distal portion of the deposit and breakage patterns can be considered representative of the entire assemblage in primary sedimentation contexts. The *intensity of fragmentation* (Lyman 1994) is not applicable to the T3 assemblage, in that the mean maximum dimension of the non-complete specimens within the assemblage is 47.1mm and the complete elements possess mean maximum dimensions of 31.8mm. In both primary and secondary deposits accumulated by sediment flows, larger elements seem to be fragmented more intensely due to the higher absolute surface area and volume. In the deposits accumulated by clast-rich sediment flows like T2, the larger particles were more prone to breakage than the small particles thus creating the same issues with Lyman's *intensity of fragmentation* (1994). In this case the method does not differentiate between a highly fragmented assemblage like T2 and T1 and a significantly less intensively fragmented assemblage like T3.

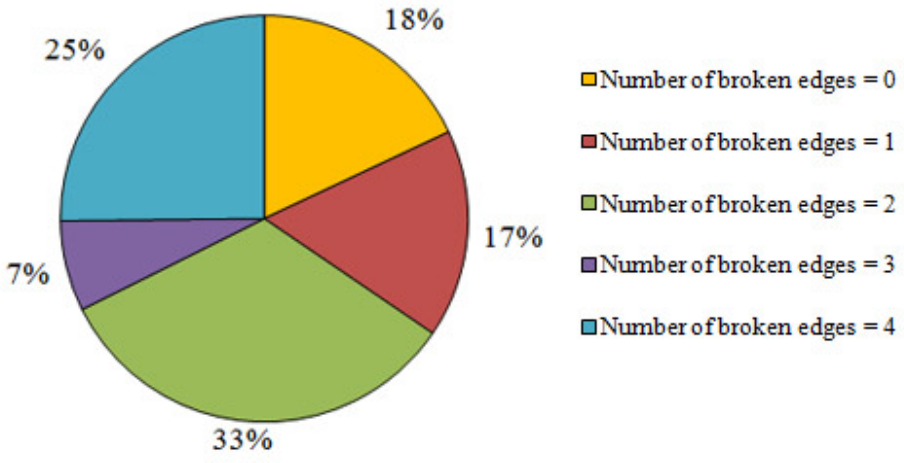


Figure 5.39 T3 numbers of broken edges on fossil material.

Figures 5.40 and 5.41 present the bone breakage type and angle for the T3 deposit, which provide a perspective on the timing of the breakage in relation to the diagenesis of the bone. Smooth break surfaces dominate the T3 assemblage, with 36% (n = 42) of the specimens showing only smooth breakage surfaces and over half of the assemblage (52%, n = 62) showing at least a single smooth fracture surface. Sawtooth breaks, which are generally considered to be indicative of post-fossilisation fracture, represent only 11% (n = 13) with 25% (n = 30) of elements showing at least a single sawtooth breakage surface. By comparison, the EC1 Secondary Deposit, which has been extensively fragmented whilst the bone has been fossilised, shows 58% of specimens with only sawtooth break surface textures, and 73% of all specimens show at least on sawtooth break. Perpendicular and acute break angles also dominate the assemblage, with only 12% (n = 14) of specimens showing only obtuse break angles and 35% (n = 42) with at least one obtuse break. The remaining 65% represent elements with either only perpendicular or acute breaks or a combination of the two. The breakage pattern shows a distinct dominance of fresh breaks on those elements that are not complete. The post-fossilisation breakage characterised by sawtooth break textures and obtuse break angles accounts for a small proportion of the assemblage, with fewer than a third of elements showing sawtooth break surface textures. It can be suggested that the majority of breakage occurred during the

primary accumulation process before fossilisation. The remaining post-fossilisation breakage proportion occurred either during the accumulation of the spatially extensive talus, or during the *in situ* settling and deformation processes seen in the T3 sediments.

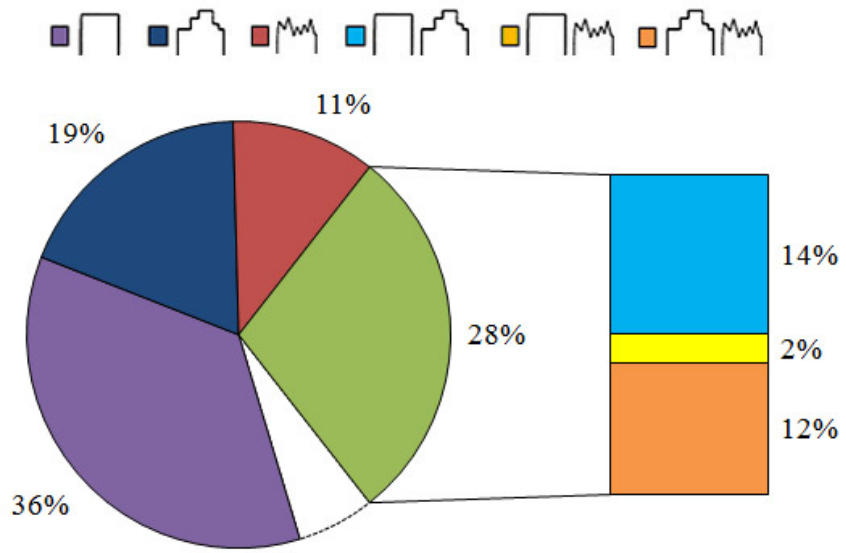


Figure 5.40 T3 bone fracture types. The green slice represents the proportion of bones with a combination of fracture types.

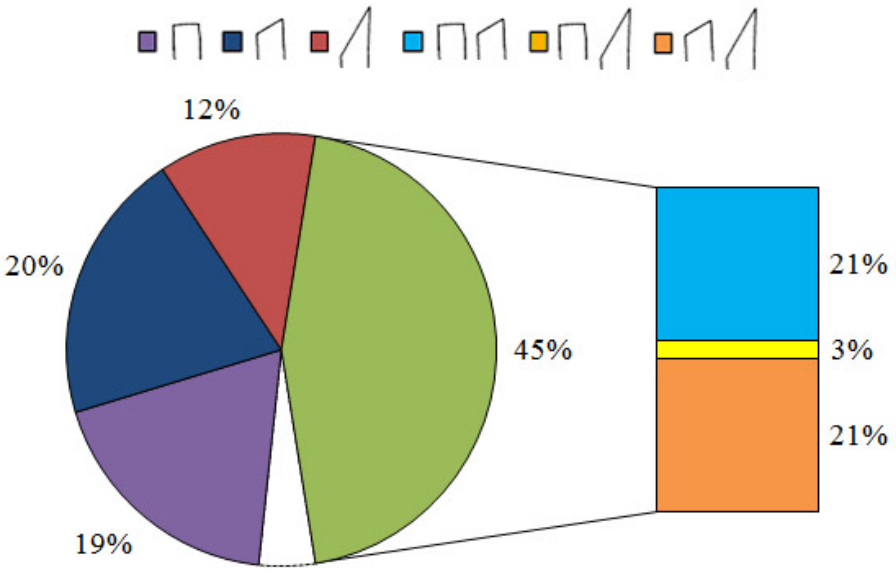


Figure 5.41 T3 bone fracture angles. The green slice represents the proportion of bones with a combination of fracture types.

Bone condition

The bone condition data for the T3 fauna is shown in Figure 5.42. It is clear that the general condition of the bone is good with 83% of the assemblage classed as either fresh or slightly weathered (equivalent to Behrensmeyer's stages 0, 1, 2 and 3). When the assemblage is classed specifically by weathering stage, 66% fall into Stage 0 and 87% of the assemblage are classed within Stage 0 and 1. Only 15% (n = 22) can be classed as weathered and 1% (n = 2) of the specimens are classed as very weathered. This pattern supports the previous evidence that the majority of faunal specimens was deposited into the cave and buried relatively quickly without much time exposed to weathering processes on the surface. In the case of the T2 deposit, post-depositional bone surface weathering seems to have affected the bone to a small degree, preserving the condition of the bone surface through multiple re-sedimentation phases. The T3 fauna was evidently deposited quickly into the cave in a fresh condition. There is, however, a component of the T3 assemblage that suggests some bones may have entered the cave after a more significant period of time exposed on the surface as indicated by the 16% of weathered and very weathered elements.

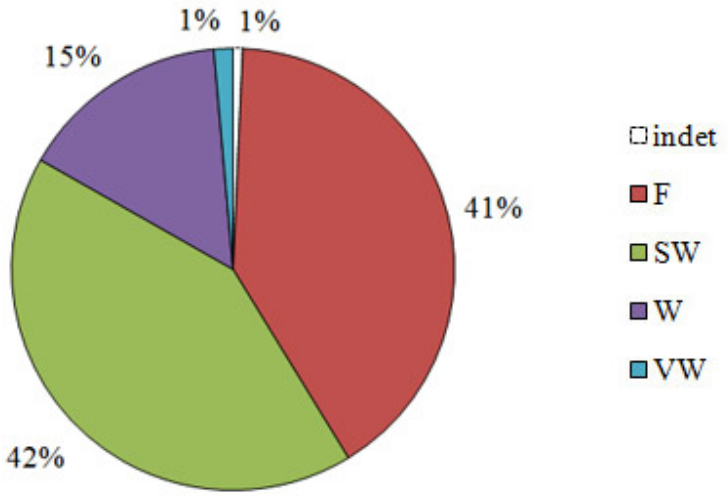


Figure 5.42 T3 fossil condition.

5.3.7 T3 taxonomy

In the T3 assemblage only two species could be identified, a *Carcacal caracal* and a *Panthera pardus* and one specimen to family level, a Cercopithecidae of a small size. *Caracal caracal* have already been discussed in the T1 taxonomic analysis. *Panthera pardus* is also a common but important species at Sterkfontein and within the Cradle sites. Since Brain's (1981) seminal work on the accumulation of the Swartkrans, Sterkfontein and Kromdraai primate collections, and the accumulating role of the leopard, *Panthera pardus* have been the focus of a great deal of research to clarify the role of the leopard in the accumulation of hominin remains (Simons 1966; de Ruiter & Berger 2000; Lee-Thorp *et al*. 2000; Carlson & T. Pickering 2003; T. Pickering *et al*. 2004a, b, c, 2008; O'Regan & Menter 2009; O'Regan & Reynolds 2009). The abundance of leopard in the Cradle sites is a result of the use of similar habitats. Leopards, baboons and monkeys all live around rocky outcrops with nearby tree cover. Leopards often use caves for shelter and often prey on small and medium-sized primates and hominins, but range over a wide spectrum of habitats (Brain 1981). At Sterkfontein, leopards have been found in most sampled members including M2 (T. Pickering *et al.* 2004a), M4 (Turner 1997, O'Regan & Reynolds 2009) and possibly M5E (O'Regan 2007) but not in any of the Lincoln Cave deposits (Reynolds *et al*. 2007). The Old World monkey (Cercopithecidae) may have been more terrestrial than contemporary monkeys and indicate a more open environment (Ungar & Teaford 1996; Elton 2000, 2001) in proximity to the cave opening at the time of burial. Numerous Cercopithecidae species appear in many of the Cradle sites but are not useful as environmental or temporal indicators as they are found in a temporally broad range of deposits. The use of caves by primates has already been discussed in Chapter 2. It can certainly be suggested that the presence of these species implies a proximity to a variety of closed and open environs at the time of burial. The small sample size reduces the statistical strength of the interpretations based on species abundance. Future expansion of the sample would allow more confident correlations to be made.

5.3.8 T3 taphonomy

The relatively small sample size means that the inferences made from the taphonomy alone would be tentative. When supported by the stratigraphic data presented above, the taphonomic interpretations can be more confidently proposed. The bone breakage data for the T3 assemblage indicates the integrity of the assemblage is good, and the residual, original depositional indicators are still evident on the fauna. The quality of the faunal preservation reflects in the bone surface visibility data where over 68% of the specimens have greater than 90% of the surface preserved.

Table 5.21 presents the skeletal element representation within the bovid size classes and shows all major body parts are represented in large size-classed bovids, from vertebrae and phalanges, to several specimens of the largest single elements in the body (femur and tibia). Bovid representation could only be identified to size class. The pattern seen correlates with the faunal analysis presented above, in that elements deriving from most body portions are found in the deposit. Notably, four of the excavated bovid specimens are represented by either epiphyses or shaft elements with missing epiphyses suggesting a number of juvenile specimens were deposited into the cave. The most widely represented bovid class size in terms of numbers of elements is the size class three animals. The relative size of these animals is significantly larger than the two predators and monkey, weighing between 130kg – 190kg. Tragelaphini are large bovids that can weigh up to 290kg and are commonly represented by the Kudu (*Tragelaphus strepsiceros*) in South Africa. The size class three bovids and the Tragelaphini are represented by browsers, grazers and mixed feeders and provide little information regarding the local environment at the time of death and burial. When all fauna for the T3 assemblage are considered it can be tentatively compared to the reconstruction proposed by T. Pickering (2004a) for M2, and suggests a similar species representation and taphonomic accumulation scenario for the two deposits. Elements within the bovid size class two also represent all body portions with skull, axial and appendicular elements present. In terms of bone surface modification, the T3 assemblage shows a general absence of biogenic

modification with just two specimens showing notches that may have been caused by teeth and a single specimen with a puncture mark. In a similar fashion to the M2 deposit, T3 is also greatly time-averaged and the species list may represent a significant amount of 'surface' time with changing climatic conditions.

Skeletal part	Antilopini	Size 1	Size 2	Tragelaphini	Size 3
Skull	1/1/1		3/1/1	1/1/1	1/1/1
Cervical					1/1/1
Thoracic			3/3/1		
Lumbar		1/1/1	4/2/1		
Caudal					1/1/1
Rib			9/4/1		1/1/1
Sternebra			1/1/1		
Humerus			4/1/1		2/1/1
Magnum					1/1/1
Lunate					1/1/1
Pisiform					1/1/1
Innominate		1/1/1			2/1/1
Femur			1/1/1		1/1/1
Tibia			1/1/1		1/1/1
Phalanx I					1/1/1
Phalanx II					3/3/1
Sesamoid					2/2/1
Intermediate					1/1/1
LBS			1/1/1		

Table 5.21 T3 skeletal element representation of bovid taxa. NISP/MNE/MNI data is given for each cell in columns two through six. LBS: Long Bone Shaft.

5.3.9 T3 discussions

The T3 deposit represents one of the oldest and deepest primary sedimentation fossil-bearing deposits at Sterkfontein. The T3 deposit developed in a slow, but consistent deposition of sediments in many hyperconcentrated flows very close to, or in the margins of, the ancient water-table. The stratigraphic and

sedimentological data indicates the regular presence of water during deposition with periods of desiccation and erosion followed by periods of deposition and saturation. The duration of these phases is impossible to tell. It can be assumed that the multiple soft sediment deformation processes as seen in the T3 sediments a the result of fluctuations in the water table and gradual but consistent fine sediment deposition, suggesting prolonged periods of deposition and producing a heavily time-averaged deposit. The soft sediment deformation processes have caused post-depositional *in situ* breakage and the introduction of younger fossil material into the older, underlying sterile T4 deposit. This process demonstrates the potential for contamination of younger material in older sediments and *vice versa*. Fossil assemblages collected from *ex situ* contexts, or excavated without sensitive excavation techniques may miss the sedimentological indicators of contamination. The result of this is a classification of stratigraphically distinct fossils or artefacts into one assemblage, and potential misinterpretation of the temporal, or cultural context of the deposit.

The role of water has proved integral to the shaping of the deposit and to the characteristic colouration of the sediments and faunal material. The distance of sediment transport from the source and the presence of water have developed a well stratified, vertically inversely graded and longitudinally well sorted silt dominated deposit. The absence of clasts >50mm and the dominance of more mobile skeletal elements can be considered a result of the great distance from the original opening. The fabric analysis indicates the dominant sediment flow derived from a SE direction to the excavation site. This correlates closely to the exit from the Silberberg Grotto, from which the M2 Hanging Remnant derives. The morphology of the M2 Hanging Remnant shows a similar developmental pattern, in that the sediments enter the Milner Hall from the SE and curve around and down the southern wall. The taxonomic representation, although small, matches that of the M2 upper facies, in a presence of cats, monkeys and larger bovids. The bone breakage and taphonomic data also support a comparable accumulation process, where, through a death-trap scenario most animals were deposited as whole bodies, the fall producing a number of fresh-bone breaks, but leaving a large number of mostly complete elements. The paucity of biogenic

bone surface modification and fresh condition of the bone also attests to the quick burial of most of the specimens. Furthermore, in a death trap assemblage scavengers are unable to access the carcasses. Hence, any limited biogenic modification relates to damage inflicted before the animals were deposited into the cave. If the T3 faunal assemblage represents mostly natural deaths and the deposition of whole carcasses, then the varying fossil yield through the deposit may closely relate to the varying opening size and shape, facilitating more or fewer accidental deaths. A greater sample size is needed to increase the confidence of the taxonomic and taphonomic interpretations and to allow correlations to be assessed between the original assemblage, the assemblage occupying the medial portions of the deposits (M2 upper facies), and the assemblage at the terminal portion of the deposit. The T3 deposit provides an opportunity to study the effects of distance from source on taphonomic and taxonomic representation in a primary sedimentation deposit. This would form the basis of interesting future research given a larger sample size.

The deposition of sediments deriving from the Silberberg Grotto into the deepest parts of the Milner Hall was proposed by Wilkinson (1983). The surface of the M2 upper facies entering the Milner Hall is represented by the Hanging Remnant and the associated capping flowstone. There are important stratigraphic differences between the two sediment bodies. The T3 deposit occupies a significantly deeper stratigraphic level than the M2 Hanging Remnant. The relative stratigraphic position of the T3 deposit can be extrapolated from the pattern and gradient of the M2 Hanging Remnant surface. When the surface of the Hanging Remnant is projected down the southern wall, at the gradient of the capping flowstone, the deposit extends 10m further west, and the surface lies 3m above the current T1 talus surface and 4.5m above the T3 deposit surface. The Hanging Remnant therefore represents a stratigraphically younger more medial portion of the same deposit, and provides a firm stratigraphic connection between the T3 and M2 upper facies. The T3 sediments were deposited via the same opening in much the same gradual consistent development as is noted for the upper facies of the M2 sediments (Clarke 2006). The removal of most of the M2

upper facies sediments occupying the Milner Hall, through water erosion, left just the upper surface, represented by the M2 Hanging Remnant, and the base, represented by the T3 deposit. The middle portions of the deposit were removed and replaced, in part, with much younger deposits from the Name Chamber. The specific characteristics of the Hanging Remnant have been described in detail in Section 2.4.3. The faunal assemblages of the M2 upper facies and T3 were also accumulated in much the same process, producing similar bone breakage and element representation data. The fauna also implies a similar, albeit tentative, environmental reconstruction. However, T. Pickering (2004a) warns with regard to the M2 upper facies assemblage (which is equally applicable to the T3 assemblage), that "the assemblage likely samples an evolving paleo-community over a substantial time span" (pp. 290).

It is apparent from the sampling of a terminal portion of a primary sedimentation deposit, that certain faunal attributes remain representative of the original faunal assemblage, despite the sorting process. Bone breakage and bone surface modification seem to be preserved but require a large sample size and minimal post-depositional damage to provide meaningful interpretations. Interpretations of accumulation process and palaeoenvironmental context based on representation and relative abundance of particular elements are vulnerable to biases caused by depositional trends. Element representation and proportions at time of burial may be significantly modified through the processes of distribution within the deposit. This process can be seen in the T3 deposit, and the distribution of element types can be described as a result of the breakage processes acting during deposition. At the most extreme level at the distal portion of a pristine assemblage, complete element types will be graded in terms of size and relative mobility (shape), creating sub-assemblages that are dominated by small and spherical elements. In the T3 assemblage complete elements at the distal portion of the deposit are represented by those pieces that are naturally small or spherical (vertebrae and podials).

Breakage in long-travelled assemblages in clast-poor sediments is different to that found in clast-rich deposits like T2 or M2 upper facies in the Silberberg Grotto. In these deposits breakage is characterised by localised crushing by clast-bone interaction. Instead, in T3, the breakage is more attritional, breaking off pieces that protrude or breaking edges of bones. Most elements become more mobile through attritional breakage, as the breakage process focuses on those areas hindering movement in the first place. The breakage process then reduces element specific transport potential and produces a more uniform mobility across element types thereby facilitating their representation in areas of a deposit generally reserved for highly mobile specimens. Long flat bones, for instance, are the least mobile elements and yet are most vulnerable to breakage and so, through the breakage process, increase in transport potential and are moved further. If the T3 assemblage were represented only by complete elements then the interpretation of the fauna would have been very different. As it happens, even the T3 deposit with its relatively good integrity has suffered enough breakage to facilitate the mobility of a representative range of element types.

5.4 T4

The T4 deposit represents a sterile body of sediment directly underlying the T3 infill. Figures 5.2 and 5.3 in Section 5.0 show the MH1 profiles and the T4 deposit within the MH1 sequence. Although externally derived, the sediment does not contain faunal material or any clasts large enough to allow fabric analysis. Only stratigraphic and sedimentological analysis could be carried out. Any and all faunal and clastic material large enough for analysis has entered the deposit from T3 through the sediment displacement processes discussed in the T3 analysis. The T4 deposit has been mentioned numerous times in the T3 analysis with reference to soft sediment deformation processes that have affected the underlying sediments during and after the deposition of the T3 sediments. The T4 sediments can be considered similar to the overlying T3 sediments in that they: are *in situ*; represent a primary deposit; have never calcified; were deposited into or very close to the margins of the water-table; and derive from an opening to the surface

a considerable distance from the sampled area. The soft sediment deformation processes that have affected the sediments relate to the fluctuating proximity of the water-table during the deposition of the upper deposit. The T4 deposit was sampled over the same area as the T3 deposit, via a 1 x 1.5m trench running N-S, transverse to the MH1 flow direction. Having exposed the surface sediments over the complete trench to map the surface, the sediments were excavated carefully to ascertain the nature of the deposit, and to track the infiltrating sediments from T3. Once the sterile nature of the deposit was clarified and the infiltrating sediments from T3 were identified and tracked, the non-contaminated areas were excavated to clarify the vertical extent of the T4 deposit to a maximum depth of 75cm below the T4 surface. The excavation was halted due to time constraints. The final excavation level reached the depth of the floor in the Milner Hall, 3m above the current water-table level.

5.4.1 T4 stratigraphy

The surface of T4 formed a very slightly undulating horizontal surface and contacts abruptly with the T3 lower *Facies III* bed. The deposit contact is sharp, with no transitional strata or mixed sediments present, indicating that at least the surface of the T4 deposit was well consolidated prior to the deposition of T3. A number of the stratigraphic features found in the upper T4 deposit have already been discussed in the T3 analysis due to their morphology being a result of the deposition and modification of the T3 sediments. Brief descriptions of those processes that have directly affected the T4 deposit are given below. The depositional interpretation of these features, however, remains the same so the reader should refer to Section 5.3.1 for the relevant process description. The sediments making up the T4 deposit form the basal facies (*Facies V*) of the MH1 sequence and can be described as follows:

Facies V – Reddish brown (7.5YR 4/4), horizontally deposited, and weakly graded, non-fossiliferous consolidated matrix-supported silt loam. Sediments are isotropic, with only intermittent internal stratigraphic indicators

preserved in the form of decayed dolomite. Maximum particle dimension of non-contaminated sediments is restricted to <4mm with infrequent inclusions of small (<20mm) chert and heavily decayed dolomite clasts. Three thin (<10mm) upper continuous strata and numerous discontinuous lenses conform to the sediment deformation morphology. Basal levels are unaffected by the deformation processes and no discernable deposit gradient is evident. No flow direction could be determined due to lack of non-contaminant clast inclusions.

Figure 5.43 shows the floor of the T4 excavation at a level 10cm below the T4 surface and 135cm below the MH1 surface datum level. The sediment displacement processes described below (and in the T3 section) are labelled on the figure. The eastern wall profile of the excavation shows a number of large cracking events caused by the desiccation of the T3 and T4 sediments at various stages during the deposition of the T3 deposit (discussed in detail in the T3 analysis and presented in Figure 5.28). In order for these cracks to have reached deep into the T4 deposit the T4 sediments would need to be well consolidated with enough tensile strength to maintain sharp sediment boundaries during and after the cracking event. No sediment mixing between the crack walls and infiltrating sediment is apparent. Cracks C and D have caused the introduction of T3 material deep into the T4 deposit, both events have deposited predominantly *Facies IV* sediments due to the cyclical pattern of desiccation of *Facies III* strata. The infiltration of predominantly *Facies IV* material into the T4 deposit is, however, relatively easy to identify given the characteristically dark nature of the sediments. The maximum dimension of infiltrating clasts is 50mm, mimicking the maximum clast dimension found within *Facies IV*. In the southern wall profile (Figure 5.44), a similar crack (Crack D) can be seen at the base of the convex terminal portion of the T3 deposit. Desiccation immediately prior to and during the deposition of the lower, discontinuous *Facies IV* stratum in T3 has introduced sediment, faunal material and clasts in a laterally and vertically extensive crack. One unusually large chert fragment (60mm maximum dimension) has been deposited into the deeper portions of this crack. Thin black discontinuous strata (described below) and small chert fragments can be seen in the southern wall of

T4 following the concave distortion of the deposit. The influence of this deformation on the internal stratigraphy of T4 reduces with increasing depth.

In the northern wall profile, the load-casting displacement process has introduced a mixture of all T3 facies sediment deep into the T4 deposit (see Figure 5.29). As can be seen in the photograph, the infiltrating sediments are easily identifiable and the sediment contact between infiltrating sediments and the *Facies V* sediments is sharp with no evidence of sediment mixing during or after the respective displacement processes.

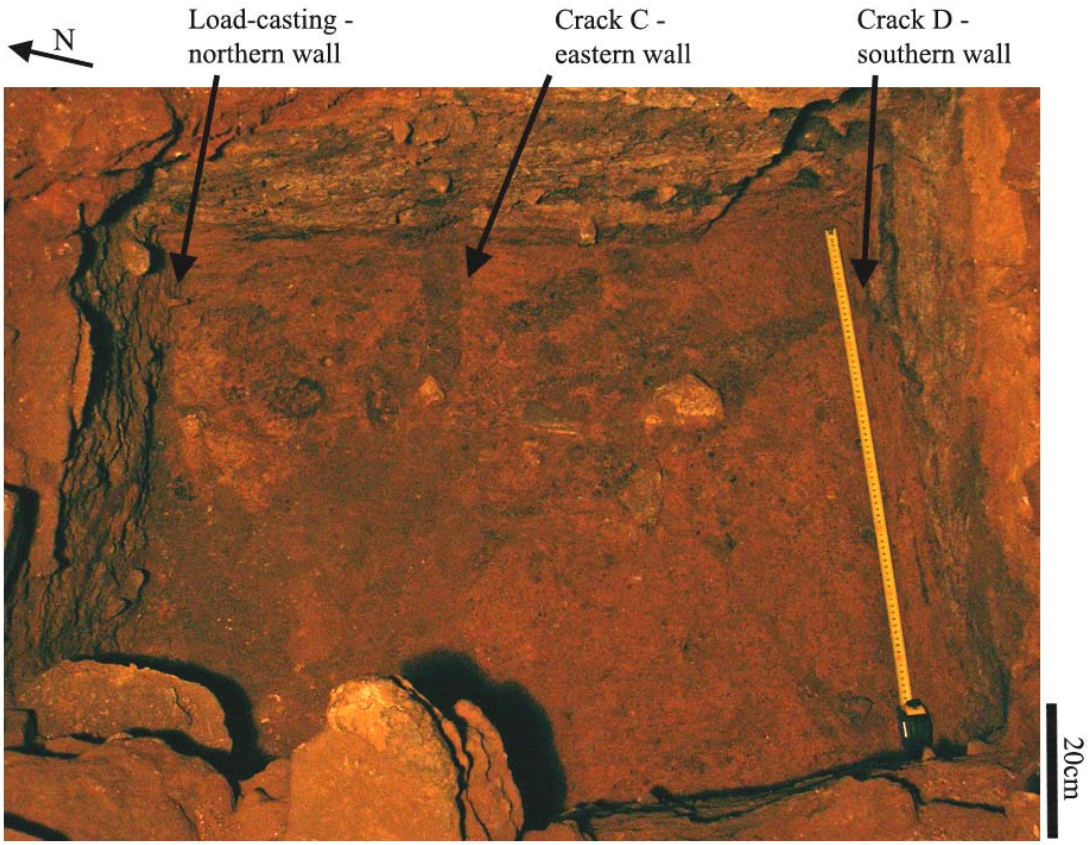


Figure 5.43 T4 floor at 135cm below datum, 10cm below surface. Infiltrating, darker sediments and larger clasts from deformation/displacement processes described in the T3 description and above are labelled and can clearly be seen spreading from T3 into the fine-grained, sterile *Facies V* sediments.

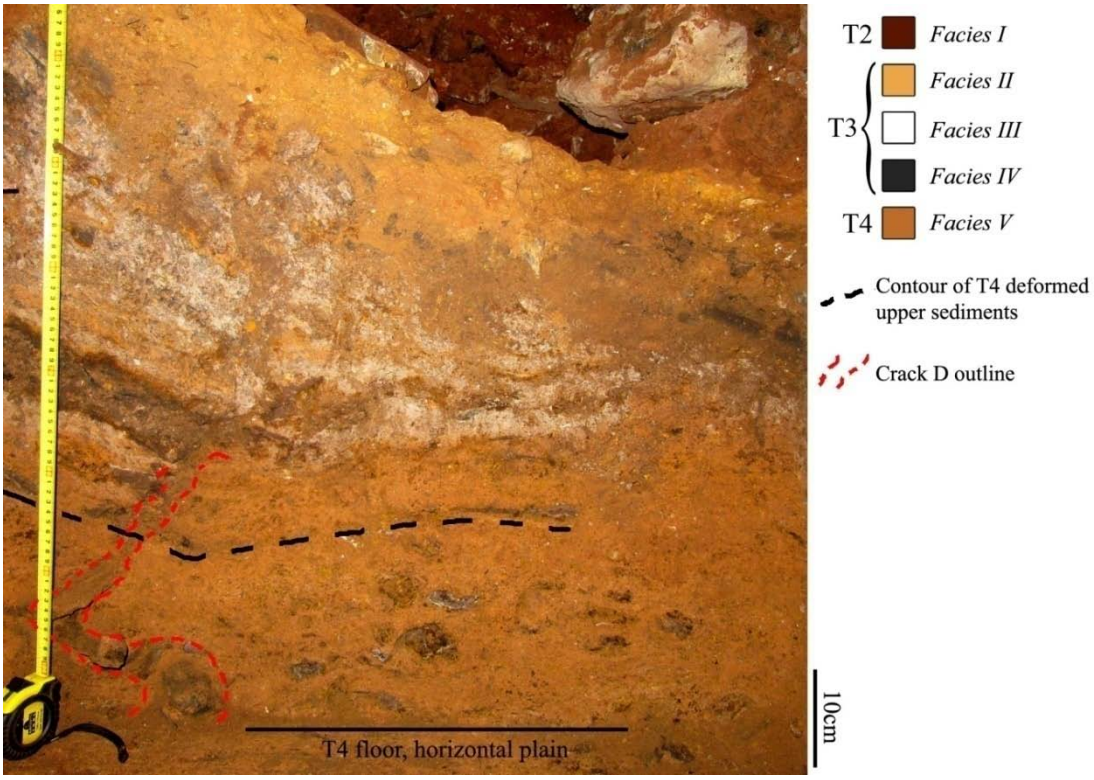


Figure 5.44 T4 southern wall profile. T4 surface is excavated to a horizontal plain 30cm below the T3/T4 contact.

The *in situ* decay of small dolomitic limestone pieces has left small, isolated, black powdery pockets and lenses randomly distributed throughout the infill. Generally high but fluctuating moisture levels during and after the deposition of *Facies V* would have increased the rate of decay of the soluble dolomitic limestone pieces. The narrow spatial distribution of the decay demonstrates that these pieces (and the containing sediments) have not moved since decay began. In the southern wall small chert fragments <20mm can also be found associated with the black pockets and lenses. Pieces of chert appear in a relatively fresh condition despite the extensive time of burial. The marine chert of Sterkfontein is composed of micro-quartz and chalcedony, which is highly siliceous and therefore not decayed by fresh water. The provenance of the chert and decayed dolomite is unlikely to be the same as the sediment origin given its infrequent and sporadic presence. It is more probable that most such clasts have fallen into the lake margins during accumulation of *Facies V* from the walls and ceiling. Each clast

has fallen onto the respective surface of the T4 deposit as it is accumulating, before being buried and contained in the same position. It follows then, that each of the black pockets and lenses represents a previous deposit surface. The dark lenses are the only internal stratigraphic features within the generally isotropic *Facies V* sediments. The dark lenses do suggest the original internal stratigraphy consisted of very thinly laminated (<10mm), horizontal strata spanning the width and depth of the deposit, characteristic of sediments laid down in water. Many of the lamination boundaries have been blurred by the fluctuating water levels, and cyclical saturation and drying the non-calcified sediments. Only those strata containing stained sediments are now evident. The homogeneity of the sediments suggests a slow but consistent accumulation of sediments from distal broad sheets of water flowing into shallow permanent water, depositing many thin horizons of fines.

5.4.2 T4 sedimentology

Table 5.22 presents the sedimentological summary for the T4 deposit. Only two sediment samples were analysed due to the homogeneity of the sediments. The first was taken at a depth of 10cm from the T4 surface to avoid any possible contamination from the basal T3 level. The second was taken from the deepest point reached by the T4 excavation, 75cm below the T4 surface. It should also be noted that sediment samples were taken from areas unaffected by the numerous sediment displacement processes contaminating the T4 deposit. The sedimentology indicates a homogeneous deposit with only a very slight change in hydrology and particle size distribution across a 60cm depth range. Despite some infrequent indications of past stratification within the deposit, the current sediments can be described as isotropic. Water content rises from 9.65% to over 10.41%, the highest of all the MH1 deposits but remains within a single percent of the lower facies of the T3 deposit (*Facies III* and *IV*). The differentiation between T3 and T4 is seen in the particle size distribution, which shows a distinct rise in silt in comparison to the T3 basal facies, 73.5% (T4) compared to 67%, and a drop in sand proportion, 19% in T4 compared to 23% at the base of T3. The deposit

then shows a weak regular grading pattern with a drop in clays with depth (from 7.1% at the surface to 5.8% at the base) and a corresponding rise in sands (from 19.3% at the surface to 20.6% at the base). The particle size is discussed in detail in the following section. Sediment colour, a useful supporting deposit differentiator, remains consistent throughout the uncontaminated sediments, and differs significantly (in Munsell classification) from the other MH1 facies. The homogeneity of the sediments supports the suggestion that the deposit was accumulated gradually and from a distant sediment source. This process has averaged any sporadic fluctuations in sediment properties.

					Particle Size		
Art No.	Facies	Sample location	Munsell	Hydrology %	% Clay (<2µm)	% Silt (2µm - 63µm)	% Sand (> 63µm)
267	V	T4 - 10cm	7.5 YR 4/4	9.65	7.103	73.555	19.341
270	V	T4 - 75cm	7.5 YR 4/4	10.41	5.834	73.577	20.589

Table 5.22 T4 Sedimentological summary.

XRF

Due to the homogeneity of the T4 deposit one XRF sample was analysed, as a representative of *Facies V*, to identify similarities and differences to the other MH1 facies. The T4 XRF sample was taken from an upper, uncontaminated point 10cm below the contact of the T3 and T4 deposits. The XRF results are presented below (Table 5.23). The results for the *Facies V* chemical composition fit with the pattern seen in the T3 facies but differ enough to indicate a distinct depositional unit. Similar to the other MH1 facies, *Facies V* is made up predominantly of allogenic sediments. The very high proportion of silica (Si) and low levels of manganese and magnesium are diagnostic of sediments deriving from external sources with minimal mixing of sediment deriving from the decomposition of the host rock (see section 5.2.2 for a description of allogenic vs. authigenic sediments and their relative chemical compositions). Notably, *Facies V* contains proportions of alumina (Al_2O_3) almost as high as *Facies III*, perhaps indicating a similar pedogenic origin for the sediments. The difference in colour between the two

alumina-rich facies is a result of the relative iron content, T3 having almost half the iron, producing a more white/grey sediment.

Also notable is the higher phosphate (P_2O_5) content. Phosphate minerals appear regularly in karst environments, and are generally attributed to either fresh or fossil bat guano deposits or bone rich breccias (Onac 2003, Onac & Veres 2003, Ford & Williams 2007). Unlike T2, which contains a similar proportion of P_2O_5 and high quantities of bone, T4 contains no bone and therefore suggests an organic origin for the phosphates in the form of bat guano. Chemical reactions between bat guano and limestone produce different mineral species under different depositional environments (wet or dry) (Onac & Veres, 2003). Particularly in the case of T4, XRD analysis may allow the identification of the specific species of phosphate and it's most likely origin and possibly the previaling depositional environment (Onac & Veres, 2003). Identification of brushite, in particular, would support the sedimentological evidence of the wet depositional conditions of the T4 sediments (Onac & Veres, 2003). All the sediments researched here would benefit from a dedicated XRD analysis to identify the source minerals. Unfortunately, XRD analysis was not available during this research.

SiO2	Fe2O3	FeO	MnO	MgO	CaO
74.93	0.48	3.89	0.43	1.18	4.80

TOTAL
100.39

Al2O3	Na2O	K2O	TiO2	P2O5	Cr2O3	NiO
9.68	0.08	1.15	0.6706	3.06	0.0376	0.0121

Table 5.23 T4 XRF results.

Particle size

Figure 5.45 shows the separate particle distribution curves for the two samples taken from the upper and lower parts of T4. From the particle size distribution, the two curves look similar. Statistically, however, the curves are significantly

different. The two distribution curves, which represent the two T4 sediment samples, can be de-convoluted into five constituent unconstrained Gaussian curves, the relative volumes of which are compared with the Chi^2 test. The de-convoluted curves for every sample taken are presented in Appendix 2. The Chi^2 test, shows $p = 0.000$. The difference, which is not obvious from the basic particle size class summary (Table 5.22) or the separate distribution curves (Figure 5.45), is evident in the proportions of the coarsest and finest particle size components. This can be more clearly seen when the two distribution curves are combined on the same graph (Figure 5.46). From Figure 5.46 it can be seen that the deeper level of T4 contains a greater range and volume of coarser particles. Conversely, it can be seen that the upper level of T4 shows higher volume of finer particles. This data shows the T4 deposit is weakly but definitely positively graded. The positive grading pattern seen in the data is a result of the influence of water during the deposition of *Facies V* sediments. It is most likely that the sediments were accumulated by broad streams in a fluvial process into the shallow water at the margin of the water-table.

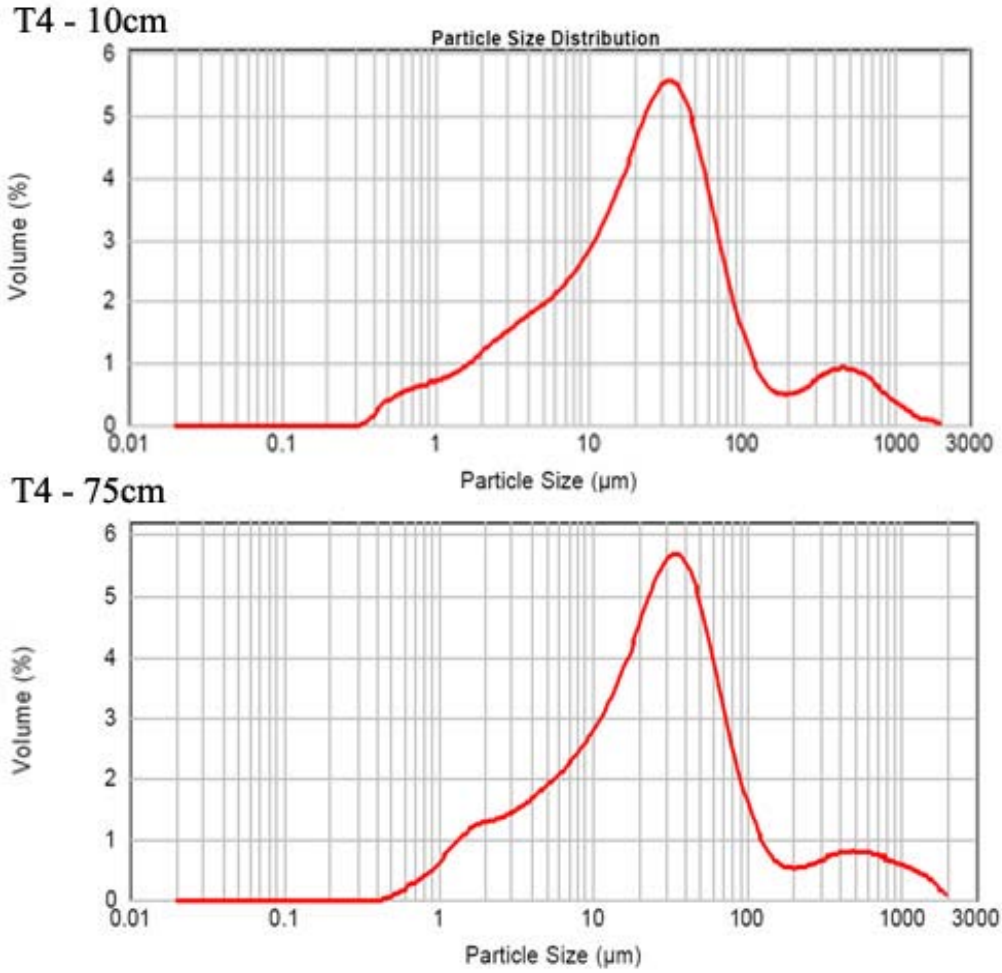


Figure 5.45 T4 particle size distribution curves for two samples taken at the surface and lowest point reached in the T4 deposit.

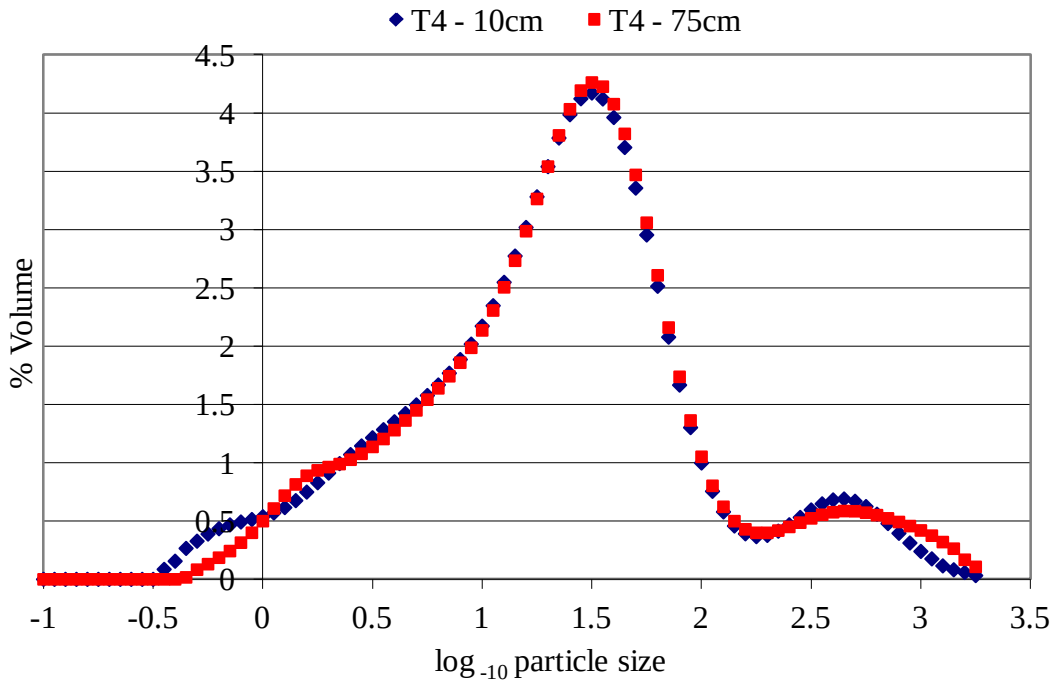


Figure 5.46 T4 combined particle size distribution curves. Stated sample depths are relative to deposit surface. The x-axis is a log scale.

5.4.3 T4 discussions

The lack of clasts or faunal material limits the options available for analysis of the T4 deposit, preventing fabric analysis and faunal analysis. Analyses are limited to stratigraphic observations and sedimentological procedures including XRF and particle size analysis. Despite the absence of other lines of investigation, the evidence available provides an adequate view of the accumulation history of the T4 sediments. The lack of clasts and faunal material can be considered stratigraphically significant in itself.

The T4 sediments represent unmixed fines dominated by silts (73%), then sands (20%) and clays with an obvious lack of particles larger than 10mm. The sediments are likely to have been accumulated gradually, over a very long period of time through repeated washing of fine sediments from a distant opening into the margins and shallows of a permanent body of water, most probably the water-table at the time. The deposition of sediments into water has created a weak

regular grading within the deposit and presumably within each original stratum. The thin laminations characteristic of sediments deposited in water are suggested by occasional, discontinuous stained lenses formed from the *in situ* decay of authigenic rock falling into the deposit from the walls and ceiling during sedimentation. The *in situ* decay of this material indicates the absence of post-depositional sediment movement. The fluctuating water-table during and after the deposition of T4 further consolidated the sediments and removed most internal stratigraphy. T4 was well consolidated when the T3 sediments were accumulated directly on top. During the accumulation of the distal portion of T3, T4 must have remained very close to water and hydroplastic enough to be warped under the weight of the building sediments, but consolidated enough to not form transitional mixed contacts during the cracking events. As T3 was building, fluctuations in the water-table periodically desiccated both deposits causing large cracks to open and introduce sediments deep into T4. Another significant drop in the water-table after the deposition of T3 but prior to T2 caused the load-casting displacement found in the northern wall. The fine-grained composition of T4 combined with regular periods of saturation prevented the deposit from being calcified.

Stratigraphically, T4 represents the deepest of the deposits found in the MH1 talus, one of the deepest externally derived *in situ* deposits yet found at Sterkfontein and the earliest externally derived sediments to enter this part of the cave system. T4 was deposited before the earliest Silberberg Grotto sediments accumulated as the T3 deposit. The sediments, therefore, accumulated when openings to the surface had just started to allow the introduction of allogenic sediments.T he absence of any faunal material within T4 is probably due to the very slow introduction of sediments through narrow ceiling fissures throughout the upper galleries, and the gradual washing of sediments into the water-table. The size of the active openings precluded the entry of micro-fossil accumulating agents such as owls, and the entry of larger bone specimens from the landscape surface. No suggestions of sediment source can be made due to the lack of suitable flow-sensitive particles. The chemical composition indicates an allogenic origin for the sediments, and an absence of mixing with host rock sediments or ‘cave earth’ sometimes found near cave floors. This may signify that although the

excavation reached the same level as the Milner Hall floor, the excavations did not yet sample the transitional level between cave floor and allogenic sediments.

5.5 STK-MH1 comparisons

The final section of this chapter brings together the data from the individual deposit analyses (Sections 5.1- 5.4) to compare the properties of the deposits contained within the MH1 talus. The comparison of all aspects of the deposits allows accurate broad spectrum interpretations to be made on the depositional history of the focus area. These comparisons also allow the identification of small but important distinguishing properties from an inter-deposit perspective that may be missed in a single disciplinary approach. As will be seen, there are a number of individual properties that are very similar between the described MH1 deposits, and only through comparative analyses are the differences apparent. The stratigraphic features of each deposit have already been described at length and do not require comparison as each unit occupies an exclusive position within the MH1 sequence. The final stratigraphic interpretation for the MH1 site and the eastern Milner Hall of the caves is made in the final section of this chapter. The facies for the MH1 sequence are, however presented below. All sedimentological, fabric, faunal and taphonomic data for the contributing deposits are presented together. It should be noted that in some analyses some deposits (mostly T1 and T4) are excluded because the relevant data did not exist within the sediments. Where deposits are not included, the reasons are discussed.

Facies AI - Dark brown (2.5YR 2.5/2) loosely consolidated, unsorted, fossiliferous matrix-supported sediment inter-stratifying layers of *Facies AII* material. The dark brown matrix contains a high degree of clast size variability dominated by medium (100mm maximum dimensions) angular to sub-angular blocks of fragmented dolomite. Large interstitial pockets are present throughout the dark brown strata. Fossils recovered from *Facies AI* are of a highly fragmented nature and generally have poor cortical preservation.

Facies AII – Unconsolidated, unsorted strata of highly fragmented travertine. Thickness of strata varies within and between stratum, the basal stratum represents the thickest level measuring between 20cm and 30cm. Speleothem particles are angular and measure no greater than 30mm in maximum dimensions. The travertine strata are reposed at progressively steeper gradients with depth. The basal *AII* stratum contains a large number of imbricated boulder-sized dolomite blocks.

Facies I - Dark brown red (ranging between 10R 3/3 and 10R 3/6) massive, clast-supported matrix. The *Facies I* bed ranges in depth from 40-80cm in the eastern wall profile as dictated by the underlying T3 surface morphology. Clasts range in size from 50mm - 400mm. Clasts are made up of angular to sub-angular cobble sized blocks of fragmented dolomite, chert, fractured flowstone and occasional rounded blocks of heavily calcified, fossiliferous, fine-grained breccia characterised by different sedimentological properties to the surrounding 'soft' matrix. The basal level is dominated by the largest clasts and dips at the angle of repose of the underlying deposit. The suspended larger clasts show high levels of imbrication and an associated high proportion of interstitial void space. Interstitial sediments are loam to silt loam in texture and inversely graded. The matrix is unconsolidated, artefact-bearing and fossiliferous. Fossils are characterised by fragmented, exfoliating and crumbling white bone.

Facies II – Yellow (2.5YR 4/4), consolidated, silt loam matrix-supported sediment with occasional coarser inclusions (small chert fragments <20mm) showing no particle sorting. Particle sizes ranges from <2mm – 5mm maximum dimensions. Internal strata slope at the longitudinal angle of repose (30° ENE-WSW). Transverse strata run horizontally. The internal lenses are characterised by very thin (<5mm) discontinuous dark strata representing decayed dolomite fragments. *Facies II* represents the upper, surface stratum of the T3 deposit. There is no evidence of flowstone development at the T2/T3 (*Facies I/II*) contact. Morphology of this facies has been shaped by post-depositional water erosion of the surface of the T3 deposit. To the south of the T3 ridge, *Facies II* forms a stratum 10-20cm thick. North of the ridge this stratum thins rapidly from 10cm -

<1cm forming a capping stratum to the T3 deposit directly under T2 base. Vertical desiccation cracks in this facies displace sediments into the underlying *Facies III* and *Facies IV*. *Facies II* is fossiliferous, the faunal specimens often representing the largest particles. The facies shows lower fossil yield and slightly smaller faunal particle size range (15mm-66mm) than the deeper T3 facies.

Facies III - White and grey (7.5YR 4/3), highly consolidated, inversely graded silt loam matrix-supported sediment. Sediment particle size is restricted to <5mm and contains no clasts measuring >20mm. Faunal particle sizes range between 15mm and 144mm. Discontinuous strata and localised pockets of *Facies IV* are spread at random both horizontally and vertically through the layer. The transition from *Facies II* to *III* is gradual with a 2 - 3cm transitional horizon. *Facies III* makes up the majority of the T3 deposit with inter-stratifying layers of *Facies IV*. Facies III is highly fossiliferous with *in situ* bone representing complete or near-complete elements. Faunal material represents the largest particles within the sediments and all fossils from this bed are stained black. The internal strata of *Facies III* slope at a decreasing gradient with increasing depth in an ENE-WSW direction and the transverse bedding is horizontal. Six separate lenses of *Facies III* sediment can be seen. Vertical cracks open from multiple levels within this facies and inclusions of this sediment can be found infiltrating the T4 deposit.

Facies IV - Black (10R 2.5/1) unconsolidated, poorly sorted silt loam found interstratifying *Facies III* sediments. Like *Facies III*, all the sediments and faunal material has been stained black. *Facies IV* are found in layers matching the gradient and direction of the surrounding *Facies III* beds with the thickest of the *Facies IV* strata is represented by a 7 - 10cm thick continuous stratum. Discontinuous lenses are also found which indicate previous episodes of erosion of *Facies IV*. Infiltrating *Facies IV* material can be found in deeper cracks penetrating the T4 deposit. The sediments are highly fossiliferous with faunal material representing the largest particles with microfauna specimens dominating the representation within *Facies IV* sediments. Clastic particles range in size from <2mm to 50mm and faunal particle size range corresponds with *Facies III*.

Heavily decayed, powdered, small (<50mm) and unsorted blocks of dolomite are also found.

Facies V – Reddish brown (7.5YR 4/4), horizontally deposited, weakly graded, non-fossiliferous, consolidated matrix-supported silt loam. Sediments are mostly massive, with only intermittent internal stratigraphic indicators preserved in the form of decayed dolomite. Maximum particle dimensions of non-contaminated sediments are restricted to <4mm with infrequent inclusions of small (<20mm) chert and heavily decayed dolomite clasts. Three thin (<10mm) upper continuous strata and numerous discontinuous lenses conform to the sediment deformation morphology. Basal levels are unaffected by the deformation processes and no discernable deposit gradient is evident. No flow direction could be determined due to lack of non-contaminant clast inclusions.

5.5.1 Sedimentology

Table 5.24 presents the sedimentological summary for the MH1 sequence. The T1 deposit (comprising *Facies AI* and *AII*) has been accumulated through destructive anthropogenic processes and contains an unquantifiable mixture of sediments potentially from a number of sources. The differentiation of the T1 facies is also clear. For this reason T1 is not included in the sedimentological analysis. Figure 5.47 presents the intra and inter-deposit particle size class data for the T2, T3 and T4 deposits. The intra-deposit patterns and boundaries can be clearly seen in the first two figures. Sediment colour can be a useful indicator of deposit boundary and each facies contact is indicated by a clear sediment colour change. As is demonstrated by *Facies IV*, sediment colour and chemistry can result from post-depositional diagenic processes and although useful, should be supported by both hydrological analysis and particle size to ensure accurate identification of deposit boundaries. The MH1 hydrological data follow a similar pattern to the particle size, with water content gradually rising with depth in each deposit with a marked drop at the surface of the underlying deposit. T4 lies at the base of the MH1

sequence and contains the highest moisture content and lies just 3m above the current water-table level.

					Particle Size		
Art No.	Facies	Sample location	Munsell	Hydrology %	% Clay (<2µm)	% Silt (2µm - 63µm)	% Sand (> 63µm)
102	I	T2 - 0-5 cm	2.5 YR 3/4	6.99	6.318	53.597	40.085
139	I	T2 - 30-40 cm	10 R 3/3	3.39	4.681	59.881	35.438
151	I	T2 - 50-60 cm	10 R 3/3	9.17	6.475	68.207	25.318
129	II	T3 - 5-10 cm	2.5YR 4/4	7.32	6.362	59.62	34.018
254	III	T3 - 40-50 cm	7.5YR 4/3	9.33	6.165	66.324	27.511
251	IV	T3 - to 125cm	10R 2.5/1	9.97	6.95	69.59	23.46
267	V	T4 - 10cm	7.5 YR 4/4	9.65	7.103	73.555	19.341
270	V	T4 - 75cm	7.5 YR 4/4	10.41	5.834	73.577	20.589

Table 5.24 MH1 sedimentological summary.

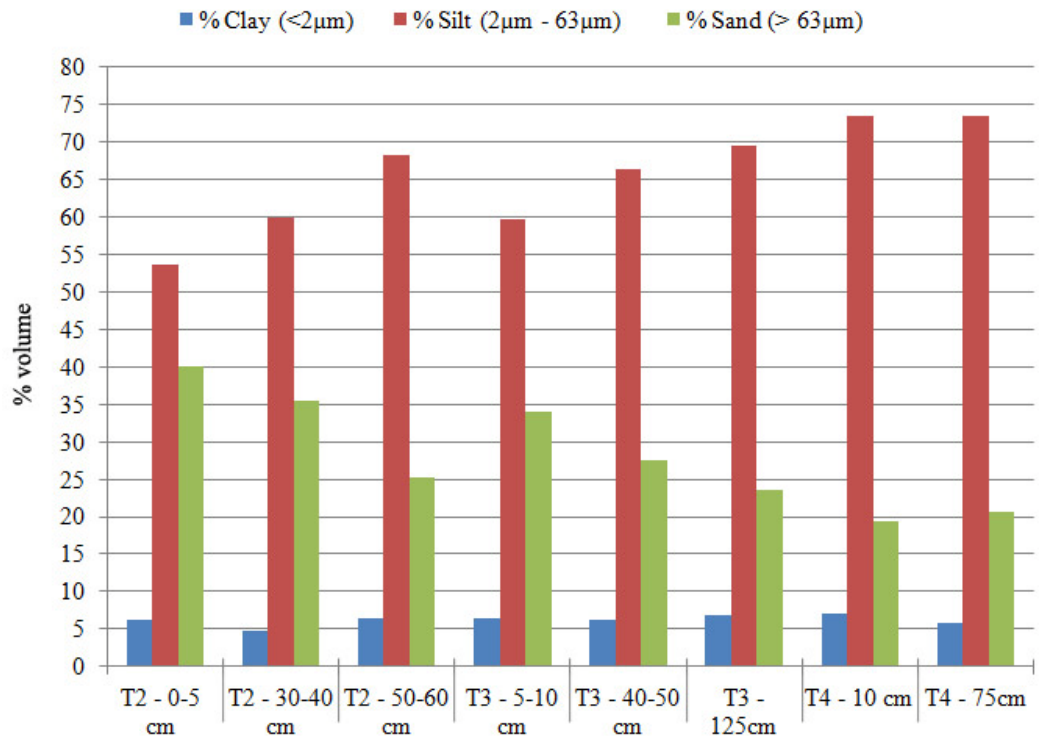


Figure 5.47 MH1 major particle size fractions across the T2, T3 and T4 deposits. Depth from excavation surface increases from left to right.

In terms of particle size distribution, T2 and T3 both show an inverse grading pattern but represent different inverse grading processes. The gradual increase in

silt and correlating decrease in sand proportions with depth within T2 and T3 can be seen together with a distinct 're-setting' of the pattern at the contact point of the two deposits. The inverse grading patterns of the T2 and T3 deposits are contrasted by the weak but clear regular grading pattern seen in T4, a result of deposition of sediments into water. When Chi^2 tests are applied to the constituent de-convoluted particle size distribution curves of the inter-deposit contact samples, the boundaries are supported in all but the T3/T4 boundary. The basal level of T2 and the upper level of T3 is significantly different in particle size ($p = 0.000$). However, the particle size of the basal level of T3 and the upper level of the T4 deposit shows that the two particle size distribution curves are statistically similar ($p = 0.736$). The similarity is due to the comparable depositional histories, T3 and T4 represent longitudinally graded sediments sampled at the distal or terminal portions of deposits which have accumulated from sources a significant distance away with an influence of water during deposition. In the case of T3 and T4 the different sediment grading patterns, fabric data, sediment colour and most significantly the presence of fossil and clastic material in T3 and a contrasting absence in T4 support the classification of T3 and T4 as two distinct depositional entities, despite the statistical similarities in particle size distribution.

Figure 5.48 presents the chemical composition data for the MH1 sequence including samples from *Facies AI, I, II, III, IV*. *Facies AII* was not included as it is represented by fragmented travertine strata and has negligible analytical value. The comparison also includes a flowstone sample from Sterkfontein (taken from a flowstone capping Member 1). The chemical composition from several forms of dolomite (values and sources can be found in Table 5.8 and Table 5.9) are also provided to demonstrate the differences between allogenic and authigenic sediments. The graph shows that all sediments from the MH1 sequence derive from sources outside the caves and show insignificant mixing of cave earth (low Ca, Mn and Mg oxides in the MH1 deposits). The high level of calcium (14%), in *Facies AI,* which is not rich in fractured travertine, is considered to be a result of contamination by calcium from the interstratifying *Facies AII* horizons. Chi^2 analysis run on the chemical distributions within the inter-deposit contact samples shows that all samples are statistically similar although p values range from 0.075

between T1 and T2 samples and 0.997 at the T2 and T3 contact to 0.478 for the T3 and T4 contact. This serves to demonstrate that the chemical composition of sediments deriving from a relatively small catchment area around cave openings will supply statistically similar sedimentary chemicals. The relative fluctuations in alumina and iron compounds are more significant when the limited scope for variation within the original chemical depositional environment is considered. The presence of alumina in the T3 and T4 sediments has already been discussed in Section 5.3.2. The raised phosphate content in the MH1 deposits can be suggested to be the result of the bone-bearing nature of the all the sediments, with the exception of T4. XRD analysis is needed to identify the mineralogical species and origin of the T4 P_2O_5. XRF major chemical composition is not particularly useful from a statistical perspective at identifying deposit boundaries in the MH1 sequence.

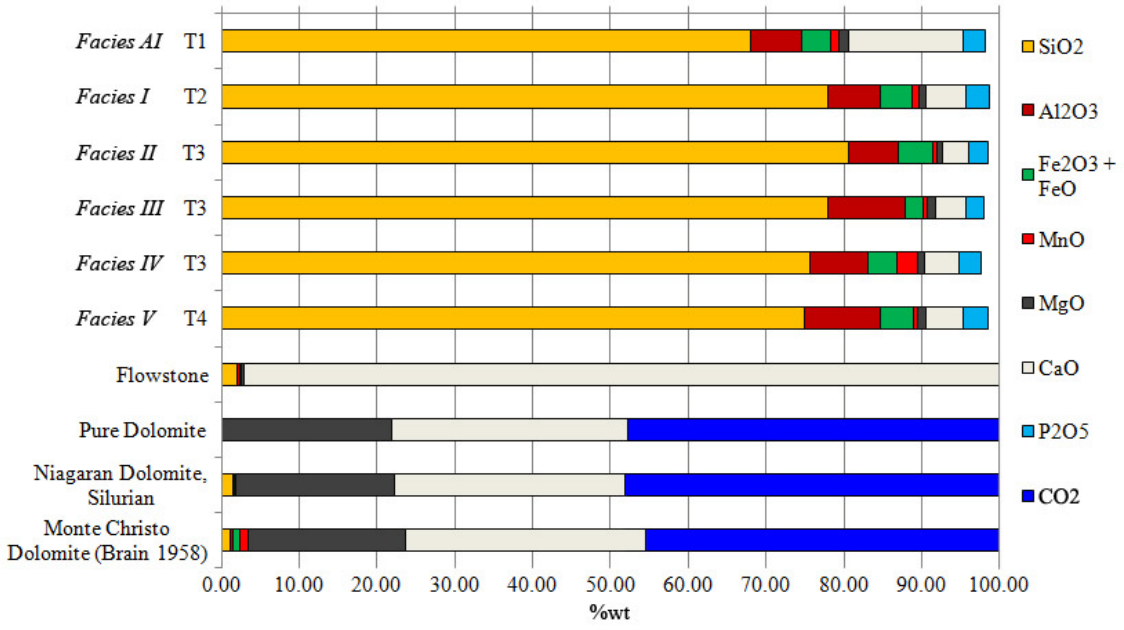


Figure 5.48 MH1 chemical composition. An example of the chemical composition of a flowstone and three forms of dolomite have also been presented to illustrate the difference between the MH1 allogenic sediments and the authigenic sediments of the host rock. The elements contributing less than 1% to the totals have been removed for clarity of the major patterns.

5.5.2 Fabric analysis

Within the MH1 sequence only T2 and T3 provided an appropriate sample for fabric analysis. T1 material is not appropriate for fabric analysis due to the destructive accumulation process, and T4 contained no faunal or clastic material of sufficient size or shape to allow fabric analysis. Figure 5.49 presents the comparative fabric analysis for the T2 and T3 deposits. For descriptions of the individual deposit interpretations the reader can refer to Sections 5.2.3 and 5.3.3 respectively. The Kamb contour and rose diagram representations have been chosen as comparative representations to illustrate the broader depositional patterns within each deposit. T2 orientation data shows 67% of particles have a positive orientation between 60° and 90° from north. In contrast, T3 shows over 55% of the T3 sample show orientations between 110 and 130 degrees from north. The Kamb contour stereonet projection shows a steeper mean gradient of dip in the T2 sample. This is due to a narrower range of particle gradient values which in itself is a result of the receptacle shape during deposition of T2. T2 was deposited directly onto the steep surface gradient of T3. In contrast, T3 was accumulated onto the horizontal T4, the deposit slope gradually building in gradient during accumulation as is indicated by the decreasing particle gradient with depth. This has produced a wider range of particle gradient values thus slightly skewing the best fit line and representation of the T3 particle gradient. A distinct difference between the T2 and T3 dominant fabric orientations is shown in the data. Figure 5.50 shows the T2 and T3 comparative orientation distributions plotted in a histogram. The representation further demonstrates the difference between the two deposit's fabric orientations. When the two orientation distributions are tested with Chi^2, they are found to be significantly different ($p = 0.000$), supporting the proposal that the two deposits derive from different sediment sources.

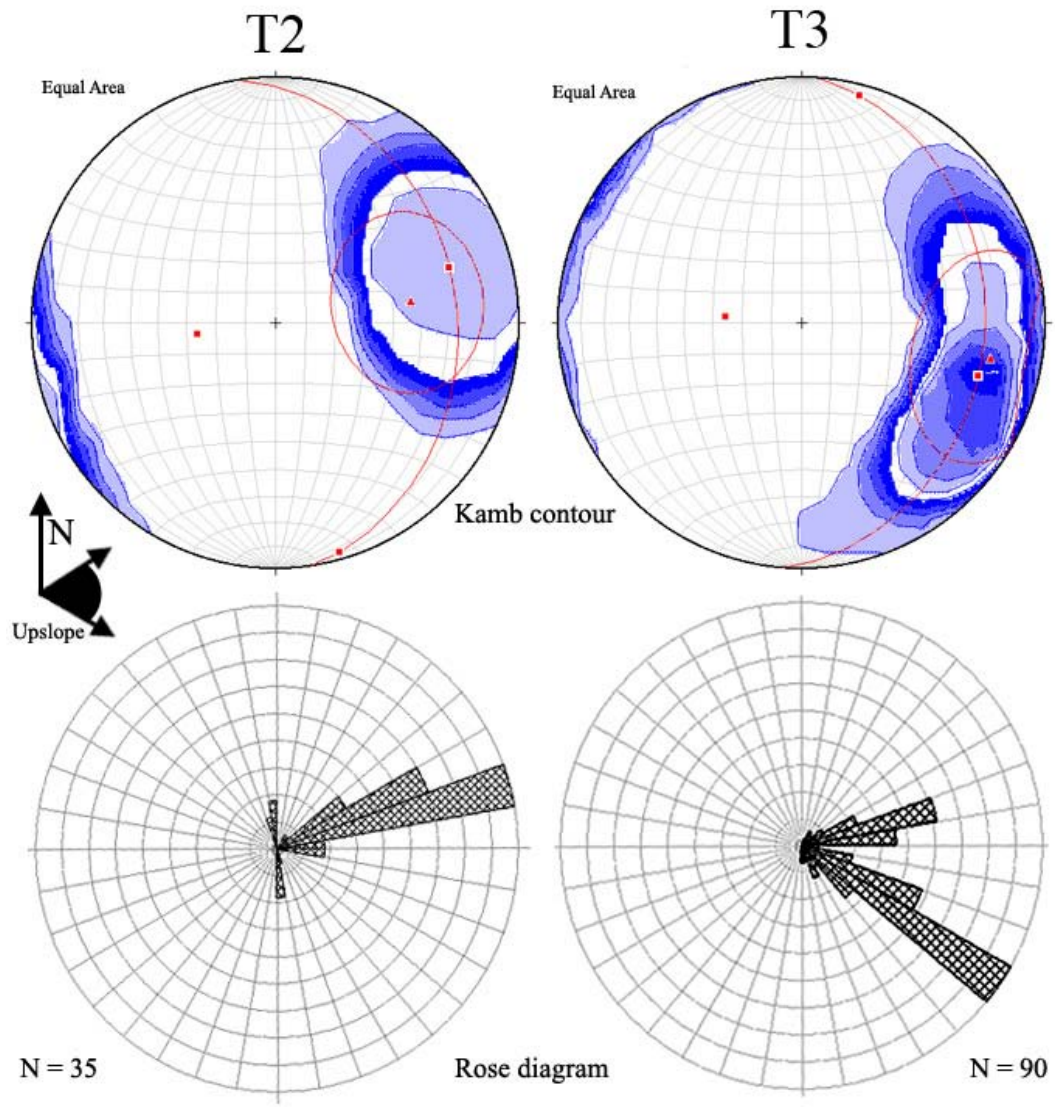


Figure 5.49 MH1 Fabric analysis models. Only T2 and T3 provided data for fabric analysis.

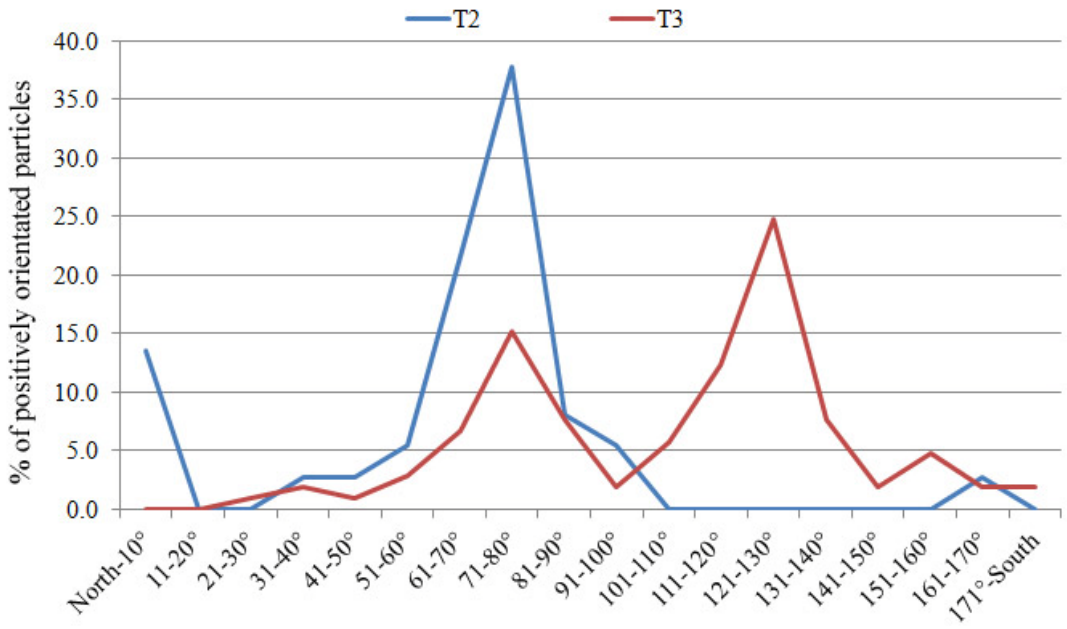


Figure 5.50 T2 and T3 orientation data.

5.5.3 Particle shape

Figure 5.51 presents the particle shape models for the three bone-bearing deposits found within the MH1 sequence. As discussed in Section 5.1.2, the T1 particle shape analysis has been conducted on the identifiable component of the assemblage. The T1 Identifiable component represents only 11% of the entire T1 assemblage. The other 88% of the assemblage is represented by elements that have been broken beyond possibility of identification. This produces fundamental issues with the representativeness of the fabric analysis. Despite these issues, the T1 Identifiable fossils do represent elements that had, before the mining re-distribution, accumulated in the vicinity of the far eastern Milner Hall. The T1 models are used here to demonstrate the differences in particle shape profile of the three different deposits. Each deposit shows a slightly different pattern of particle shape distribution within each particle shape model. Figure 5.52 presents the distribution of the MH1 bone-bearing deposits across the Sneed & Folk shape classes. Statistically, when the distribution of elements within the Sneed & Folk shape classes are compared, all the deposits are significantly different ($p = < 0.01$ for all Chi^2 inter-deposit comparisons). T3 shows the broadest distribution of

shapes through all the shape models, with elements ranging from highly elongate to more spherical forms. In the MPS vs. DRI scatter plot, T1 shows a definite concentration in the elongate area of the graph, despite the sensitivity to sphericity of this model. In comparison, T2 is dominated by elements that are classed as highly elongate. T2 shows the narrowest distribution across shape classes, with 90% of the elements classed within elongate or highly elongate classes. There is no overlap of the natural clast and faunal sample in the Sneed & Folk diagram. This has been interpreted as a result of the different affects of breakage on different components within the deposit. T2 is a clast-rich deposit and the movement of the sediments has caused high levels of breakage throughout the deposit. Clastic material tends to break into more rounded forms, whereas faunal material tends to break along collagen fibre direction into more elongate forms essentially creating two shape components within the assemblage. This process has been discussed in Chapter 4. The Zingg and the MPS vs. DRI shape models are sensitive to different dimension calculations and show slightly different trends to the Sneed & Folk diagram. The Zingg diagram has been shown to be sensitive to bladed forms in the individual analysis and this sensitivity can be clearly seen in the comparative analysis, where only 34 flat elements (naturally blade-shaped elements) have been yielded from all deposits, compared to over 70 particles classed as blade-shaped within T3 alone.

The data recovered from this research show that no other element type, apart from bladed forms, break into blade-shaped forms. T2 and T3 show a similarity in their distribution within the MPS vs. DRI model. T3's faunal particles show a broad distribution with a more general trend towards the sphere/disc shape. The relationship between the MPS vs. DRI model and particle transport has been discussed in Section 3.4.3. The similarities between the MPS vs. DRI distribution in T2 and T3 exemplify the issue of equifinality[4] identified in taphonomy, and due caution should be taken when considering secondary vs. primary sedimentation particle shape distribution. A particle shape distribution represented within a

[4] Equifinality, defined as the property of allowing or having the same effect or result from different events (Webster's Third International Unabridged Dictionary). In taphonomy euifinality is used to refer to two or more accumulation processes producing the same assemblage characteristics and features (Lyman 1994).

deposit is not necessarily the result of particle shape grading. In secondary sedimentation deposits, particularly with high clast proportions, like T2, breakage processes can create shape distributions that are similar to primary sedimentation shape distributions caused by longitudinal grading processes. Skeletal element representation provides a good discriminator between such assemblages.

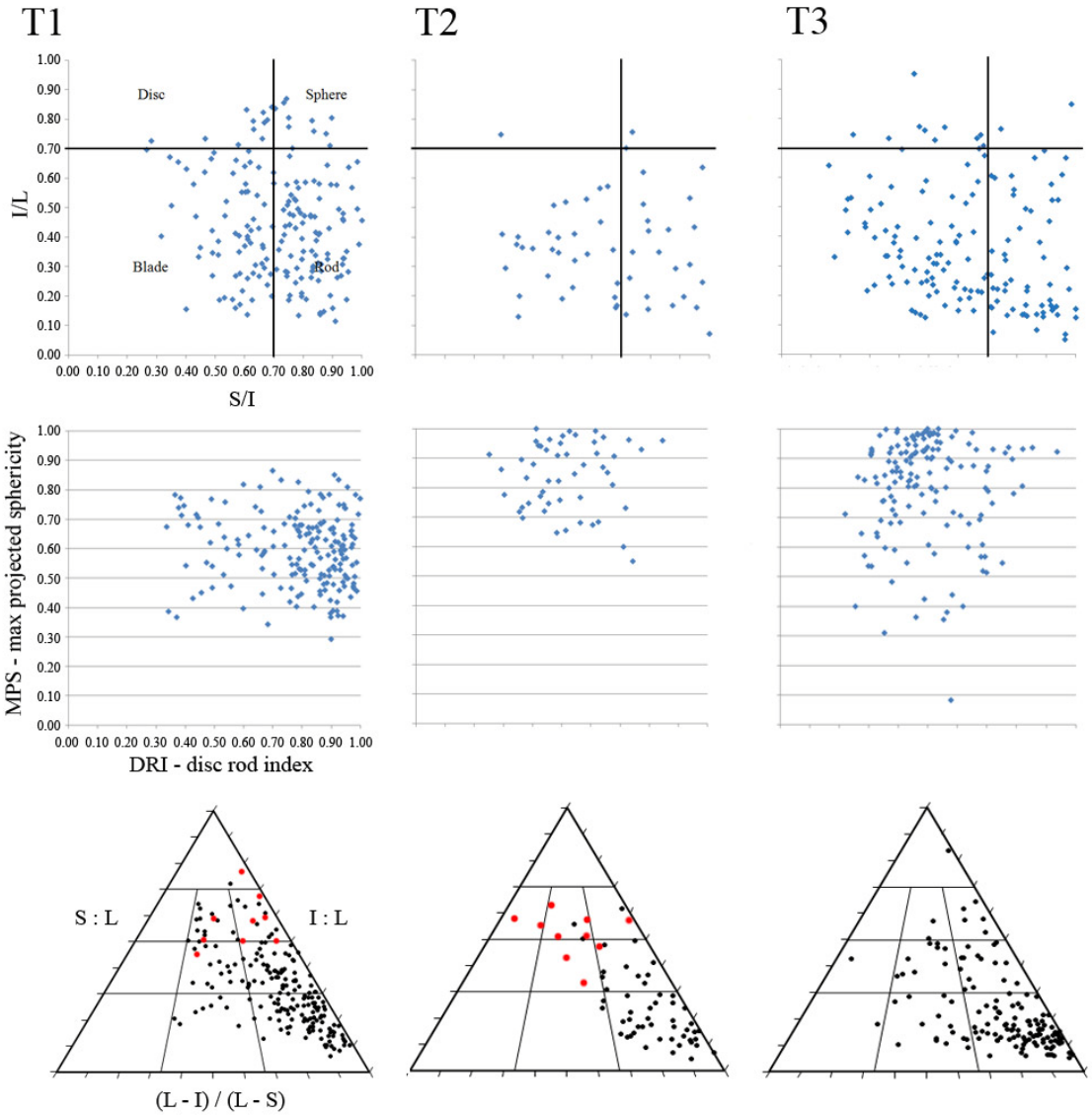


Figure 5.51 MH1 particle shape indices for the deposits yielding clastic and faunal material large enough to analysis. The red dots on the Sneed & Folk diagrams represent natural clasts excavated during excavation.

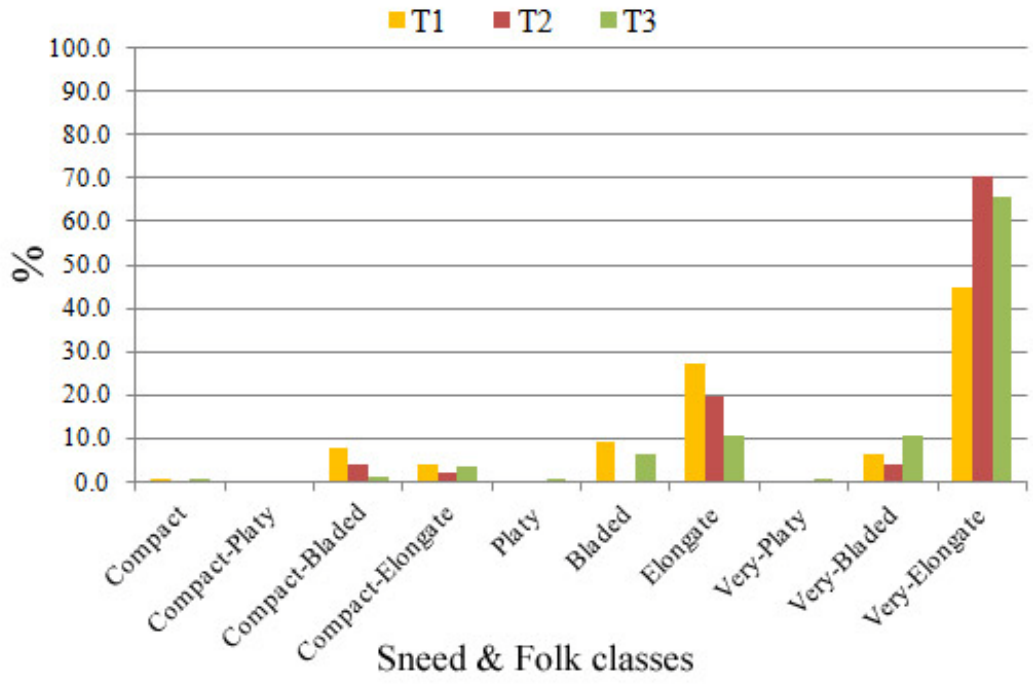


Figure 5.52 Relative proportions of Sneed & Folk shape classes within the three bone-bearing deposits. It should be noted that the T1 groups present only the identifiable component of the assemblage.

The Voorhies groups for each bone-bearing deposit (Figure 5.53) show three dissimilar profiles. The T1 Voorhies groups cannot be considered representative of the entire assemblage when using a sample based on the preservation of diagnostic skeletal element features and only 11% of the assemblage. T1 is shown to provide a comparative perspective, and an example of the possible interpretation issues caused by a non-representative sample. The T2 and T3 samples are representative and show quite different profiles. 73% of T2 is represented by Group II & III and Group III elements, in comparison to only 38% for the equivalent groups in T3. T2 also has less than half the Group I elements of T3. T3 differs from T2, in that the element representation supports the T3 particle shape models which are both supported by the T3 depositional processes.

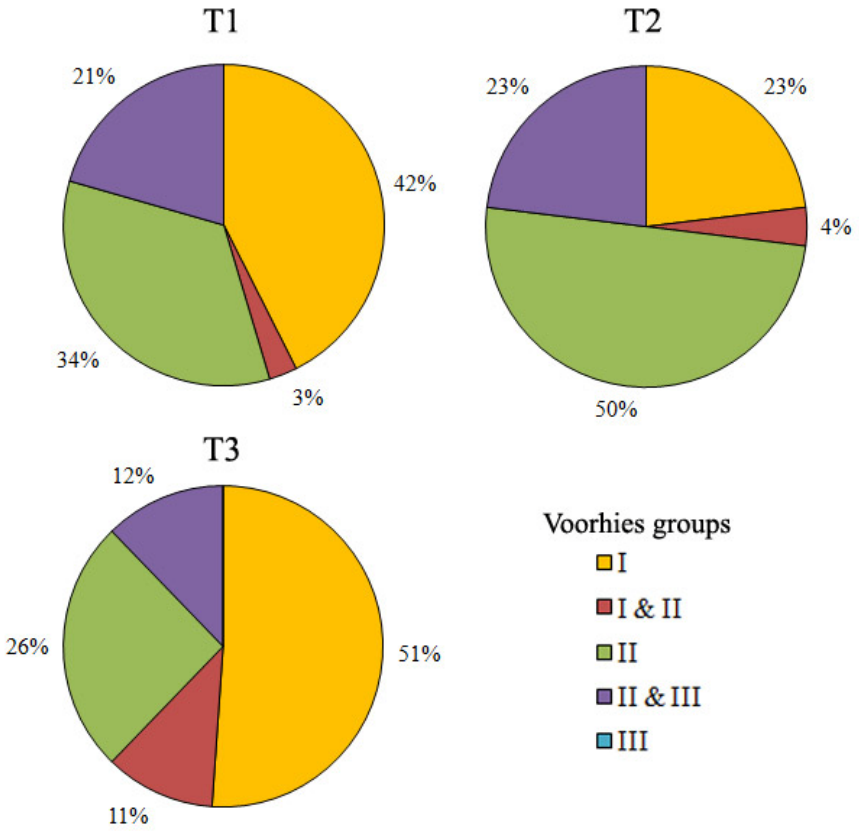


Figure 5.53 MH1 Voorhies groups. It should be noted that the T1 groups present only the identifiable component of the assemblage.

5.5.4 Assemblage profile

Table 5.25 and Figure 5.54 present the size profile data for the MH1 bone-bearing deposits. All assemblages show the same general pattern – a dominant representation of smaller (<40mm) particle sizes. These profiles have been created by the distinct depositional processes which formed each infill. The T1 Identifiable component is represented as a dashed line because the assemblage size profile is biased by the identification process, 'T1 Total' presents a more accurate perspective of the T1 size profile. The T1 Identifiable component is presented to provide an example of the difference in size profile between unbiased and biased sampling. T3 represents a broader range of fossil sizes in comparison to all the other deposits. Table 5.26 presents the basic statistics for the maximum dimensions and the particle size of the faunal particles in the bone-bearing MH1

deposits. The values of central tendency and the standard deviation of the particle size range support the preceding size profile data in that the T3 deposit has yielded the largest individual elements and the broadest range of faunal particle sizes.

Max Length	T1 Total		T1 Identifiable		T2		T3	
	Number	%	Number	%	Number	%	Number	%
<10mm	0	0.0	0	0.0	0	0.0	0	0.0
<19mm	621	36.1	28	14.6	4	7.5	2	1.4
20-29mm	735	42.6	68	35.4	25	47.2	42	28.8
30-39mm	220	12.9	56	29.2	11	20.8	37	25.3
40-49mm	98	5.8	22	11.5	6	11.3	25	17.1
50-59mm	23	1.3	5	2.6	3	5.7	15	10.3
60-69mm	14	0.8	8	4.2	4	7.5	8	5.5
70-79mm	6	0.3	3	1.6	0	0.0	5	3.4
80-89mm	2	0.1	1	0.5	0	0.0	2	1.4
90-99mm	1	<0.1	1	0.5	0	0.5	4	2.7
>100mm	0	0.0	0	0.0	0	0.0	6	4.1
Total	1720	100.0	192	100.0	53	100.0	146	100.0

Table 5.25 Fossil assemblage size profile for all MH1 bone-bearing deposits.

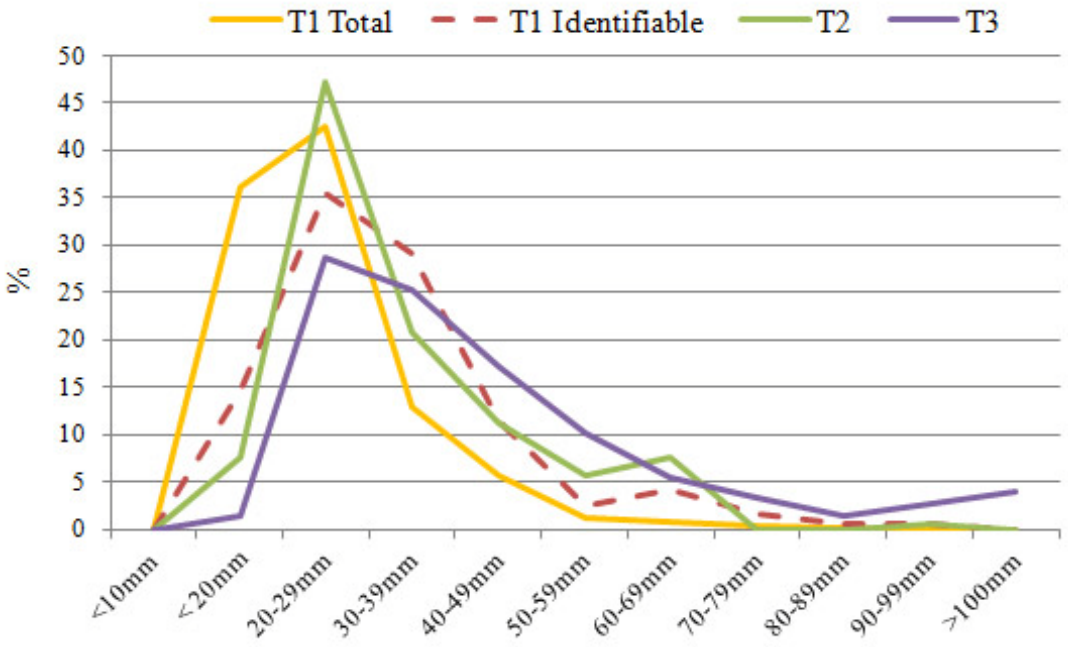


Figure 5.54 Fossil assemblage size profile for all MH1 bone-bearing deposits.

	T1	T2	T3
Min (mm)	11.5 : 8.6	17.0 : 7.2	15.0 : 7.9
Max (mm)	91.0 : 44.8	69.5 : 35.9	144.0 : 58.0
Mean	32.0 : 18.0	33.0 : 17.4	44.2 : 22.2
Mode	27.0 : 12.4	23.0 : 10.5	23.5 : 15.7
Median	29.0 : 16.9	28.0 : 15.9	37.0 : 20.1
Std Dev	13.5 : 6.2	13.6 : 7.1	23.6 : 9.5

Maximum dimension (mm) : Particle size

Table 5.26 MH1 bone-bearing deposit faunal particle size statistics.

5.5.5 Faunal analysis

The MH1 sequence yielded just under two thousand fossils from a range of depositional conditions. These depositional processes have been shown to have affected the particle size profiles and shape profiles of the faunal assemblages. They have also been shown to affect the distribution of certain element types through the respective deposits as demonstrated by the Voorhies Group representation. The faunal analysis below presents the data that has been described in the respective individual deposit analysis in a comparative framework. For the T1 assemblage, both the identifiable, non-identifiable and total assemblage data is given for the basic element type representation and breakage data. The evaluation of the effects of sample representativeness on assemblages is critical to being able to produce confident data interpretations. The presentation of the T1 data shows how extensive the non-representative subsample affects many aspects of the assemblage. The ‘T1 Total’ sample contains all specimens and is therefore most representative of the deposit assemblage.

Skeletal element representation

Figure 5.55 presents the basic element types represented in the different bone-bearing MH1 deposits. The similarities between the T1 Identifiable assemblage and *in situ* deposits are erroneous but useful reminders of the influences of data bias. The more accurate representation of the T1 assemblage is shown in the 'T1 Total' data, which shows a dominance of shaft fragments and a 10% component of indeterminate elements. This profile is a result of the fragmentation patterns of shaft elements. Figure 5.56 presents the skeletal portion representation for the T2 and T3 deposits. In fragmented and sorted deposits, the presence of a wide range of elements and body portions is more important than the proportions of those elements, which can be affected by the sorting and or breakage beyond the most basic level of identification. Both assemblages show a mix of all element types and body portions which enables taphonomic interpretations of both deposits to be suggested.

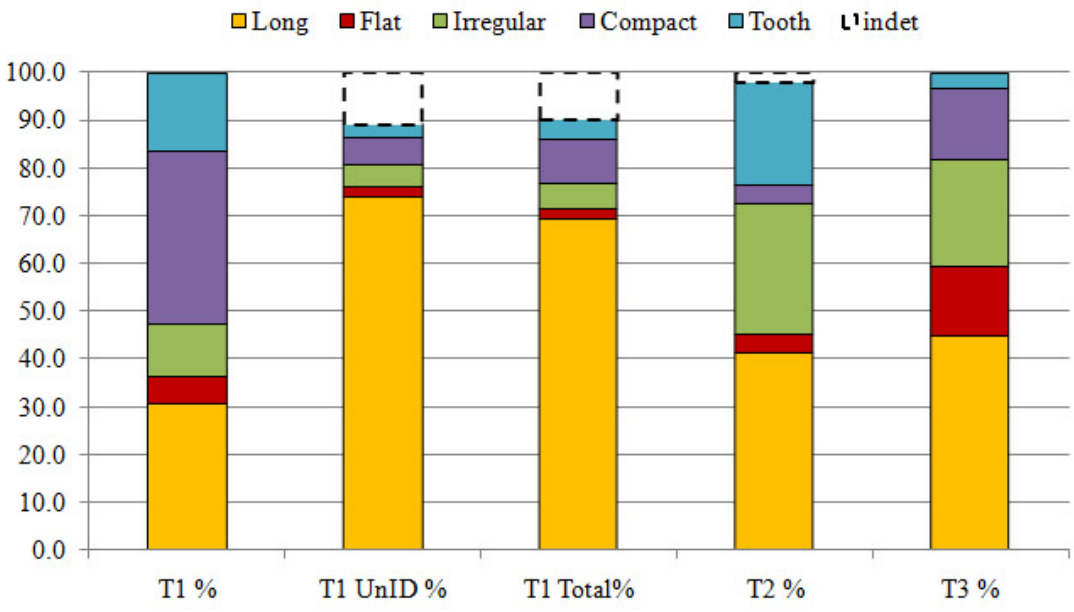


Figure 5.55 MH1 skeletal element type representation across the bone-bearing deposits.

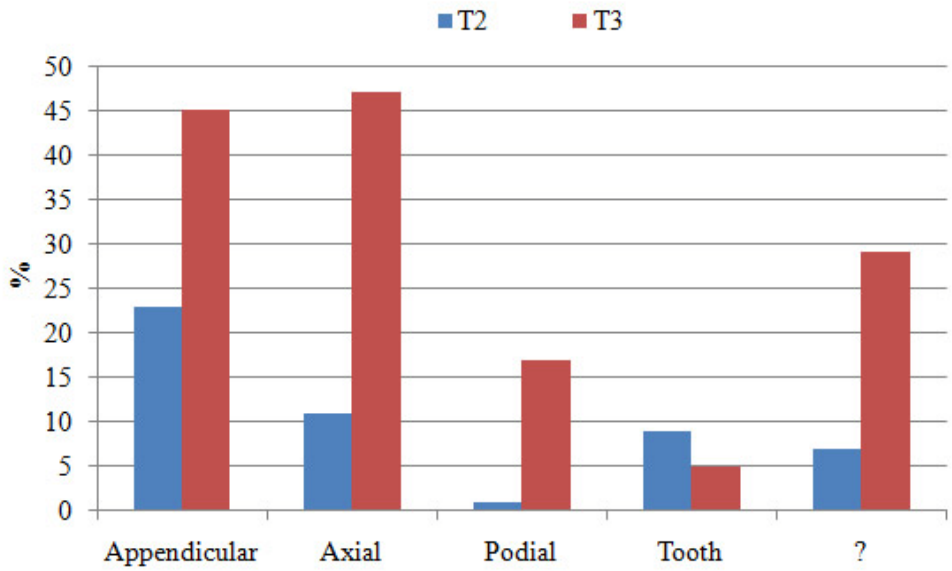


Figure 5.56 T2 and T3 skeletal portion summary.

Bone Breakage

Figure 5.57 presents the bone breakage numbers yielded by the different deposit assemblages. There are obvious differences between the extensive fracturing of the T1 Identifiable and 'T1 Total' assemblages. The T1 Identifiable subsample yields data indicating a good state of preservation with over 50% of the assemblage showing one or fewer broken edges. In the T1 analysis, it was seen that as breakage levels increase (here represented by number of broken edges), the preservation of element specific diagnostic features decrease. This creates a subsample assemblage dominated by the fossils retaining those features and a generally better state of preservation. 'The T1 Total' data is much more in line with what would be expected from the bone within a deposit developed through mining activity. Both the bone-bearing secondary sedimentation deposits show expectedly high levels of breakage. T3 shows the lowest quantity of breakage, as would be expected of a primary deposit which was more gradually accumulated by matrix-supported hyperconcentrated flows.

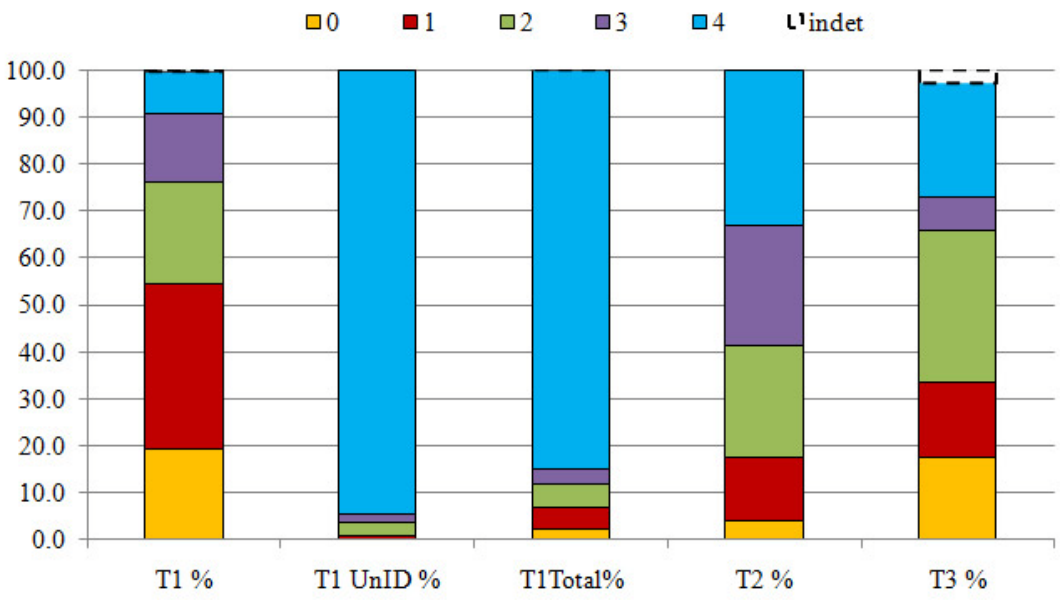


Figure 5.57 MH1 numbers of broken edges on fossil material.

Figures 5.58 and 5.59 present the bone breakage surface texture and breakage angle data for the T2 and T3 assemblages. The T1 assemblages are not included in the comparison as the breakage patterns do not represent natural accumulation processes and so are of limited comparative value. The T1 bone breakage data is discussed within the T1 analysis. The T2 and T3 assemblages show a number of similarities, despite the differences in accumulation history. Both assemblages show a relatively high state of preservation of the primary, pre-fossilisation, breakage pattern with a more minor contribution of post-fossilisation breakage. The T2 assemblage shows a higher proportion of sawtooth break surface textures both in the combination proportion and as specimens showing only sawtooth break surface textures. The relatively good preservation of pre-fossilisation breaks, generally good condition of the bone surface, and the high levels of surface clarity within both assemblages, demonstrates the relatively good integrity of the two deposits. High assemblage integrity can allow greater resolution on taphonomic interpretations regarding the primary sedimentation environment and faunal accumulation agent. It can be proposed that both assemblages have been through a number of phases of breakage, with the primary accumulation of the

fauna inflicting a significant portion prior to fossilisation. After fossilisation both assemblages have suffered some level of breakage, although T2 has suffered significantly greater breakage than T3. The low resolution of breakage timing identification precludes the recognition of multiple phases of post-fossilisation breakage. The stratigraphic information fills in these gaps in the data. In terms of fossil condition T2 and T3 show similar patterns, with the greatest proportion of bone in a fresh condition (equivalent to Behrensmeyer's (1978) weathering stage 0-1), followed by slightly weathered and then equally small proportion of weathered specimens.

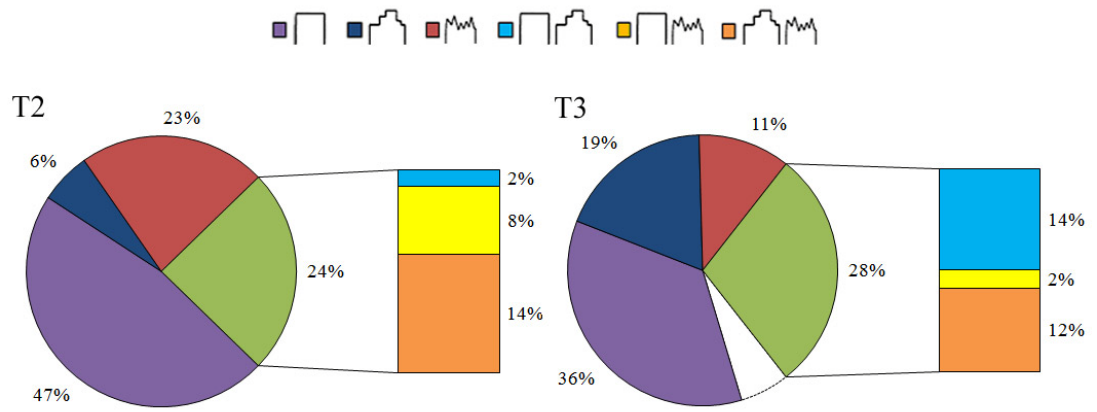


Figure 5.58 T2 and T3 bone fracture types. The green slice represents the proportion of bones with a combination of fracture types.

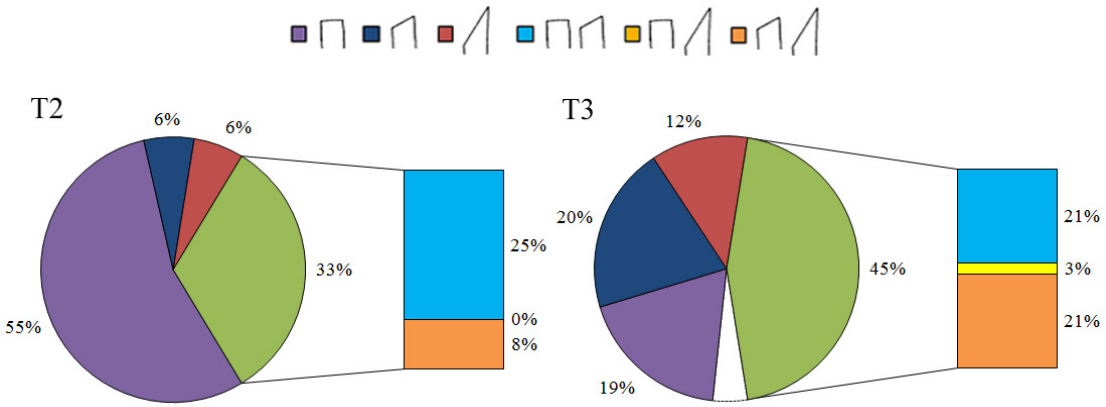


Figure 5.59 T2 and T3 bone fracture angles. The green slice represents the proportion of bones with a combination of fracture types.

5.5.6 Taxonomy and taphonomy

The taphonomic interpretations for each of the MH1 deposit are based on relatively small samples and so should be treated with considered caution. The primary objective of the taphonomic analysis is to provide added resolution for the stratigraphic interpretation, in that each naturally accumulated deposit derived from a distinct but recognised deposit in the Sterkfontein sequence and might contain distinguishing taphonomic features. The taphonomic analysis is not meant to provide extensive insight into the accumulation processes acting during the development of the respective primary sedimentation deposits. Instead, by comparing the taphonomic data of the known contributing deposits and taking into account the differing formation processes influencing the assemblage, discrepancies and biases related to the formation processes may be recognised. T1 is characterised by a wealth of bovid material representing a wide range of animal sizes; most body portions are represented and there is a low proportion of carnivore-inflicted bone surface damage. The presence of *Equus* can be considered a significant temporal and stratigraphic feature. The T2 faunal assemblage has also yielded an *Equus* specimen. The assemblage is very small but also provided evidence of different sized bovids being deposited. The presence of all body portions of size class two bovids suggests at least some animals may have been deposited whole. The bone surface is in a good condition and the dominant breakage signal is that of a pre-fossilisation type. There is a dearth of carnivore-inflicted damage but this is possibly influenced by the sample size. The T3 deposit also shares the same features, but with the noticeable absence of *Equus*. Elements from all body portions are represented, the bone surface is mostly fresh and undamaged by carnivores and breakage data indicates a dominant pre-fossilisation signal. T3 also contains a high proportion of complete elements. An equally wide range of bovid size classes is represented, and the same mix of non-bovid species as are represented in the M2 deposit was identified. All three assemblages share a similar set of taphonomic features. The presence of certain stratigraphic and temporal attributes distinguish between the T2 and T3 deposits and in a similar way the same shared attributes can be used to tie the T1 and T2 assemblages together. All three assemblages derive from fauna accumulations developed

through the same processes, which is why each deposit shares certain features. Death-trap accumulation processes have been proposed as the major mode of accumulation for both the M5E and M2 faunal material (T. Pickering 1999; T. Pickering *et al*. 2004a), although they represent significantly different time periods. T. Pickering (1999) describes a death-trap assemblage as a process that accumulates a large range of body parts with very little carnivore damage. Bone surfaces are usually fresh as surface exposure time is minimal if not absent. Taxonomic representation is highly variable depending on the landscape topography, climate and vegetation.

5.6 STK-MH1 Conclusions

Part of the goal of this research was to clarify the formation history of the far eastern area of the Milner Hall, an area where a number of deposits of significant age and importance come together. This area is known as the central underground deposits. The goal of the MH1 excavation was to explore and elucidate the nature of the large talus which spreads west from the far eastern area of the Milner Hall, beginning directly beneath the confluence of the central underground deposits. The proximity to the central underground deposits made the MH1 talus the most likely area to preserve a stratigraphic sequence documenting the depositional history of the area. The excavation of four deposits revealed a long and intricate sequence spanning the history of the caves from the earliest allogenic sediment deposition to the commercial exploitation of the caves. The MH1 sequence documents a variety of deposit types including those formed through anthropogenic destructive processes, natural secondary sedimentation processes and gradually accumulating primary sedimentation deposits formed in the margins of the ancient water-table. The deposits found within the MH1 site have been described in detail in this chapter and been shown to have distinct sedimentological and stratigraphic attributes that illustrate the formation history of each deposit within the development of the MH1 talus, and the infilling history of the eastern Milner Hall. The multidisciplinary analysis of the contents and sediments of the deposits has also allowed firm proposals to be made on the

sources of the sediments. A formation history for the MH1 site and the eastern Milner Hall can now be proposed. The stratigraphic sequence and proposed associations to source deposits are represented in Figure 5.60. In the case of the MH1 sequence, the stratigraphy is relatively simple in that the oldest deposit (T4) lies at the bottom and the other deposits are built on it in a typical chronological sequence, T3 through to T1.

The use of stratigraphically sensitive attributes like archaeological material and *Equus* have allowed firm associations between T1, T2, the Name Chamber and M5E to be made. The numerous re-sedimentation processes occurring between the deposition of the M5E deposit and the deposition of the T2 and T1 deposit have affected many aspects of the assemblage, including the fossil yield, fossil completeness, size profile, specimen shape and breakage patterns, but have also preserved enough data to provide correlations between the deposits. An inclusion of material from the M5W cannot be ruled out completely, but Avery *et al*. (2010) proposed the majority of sediments derived from M5E with minimal mixing from the M5W deposit. Stratigraphic analysis, including fabric analysis provided grounds for the hypothesised connection and the foundation upon which all other data rests. The association between the M2 upper facies and T3 was relatively simple once the M2 Hanging Remnant could be stratigraphically tied to both bodies. Wilkinson's (1983) observation of the Silberberg Grotto material being deposited deep into the Milner Hall has been proven correct. The significance of the T3 deposit lies in its position as perhaps the oldest and earliest *in situ* primary sedimentation fossil-bearing deposit yet found at Sterkfontein.

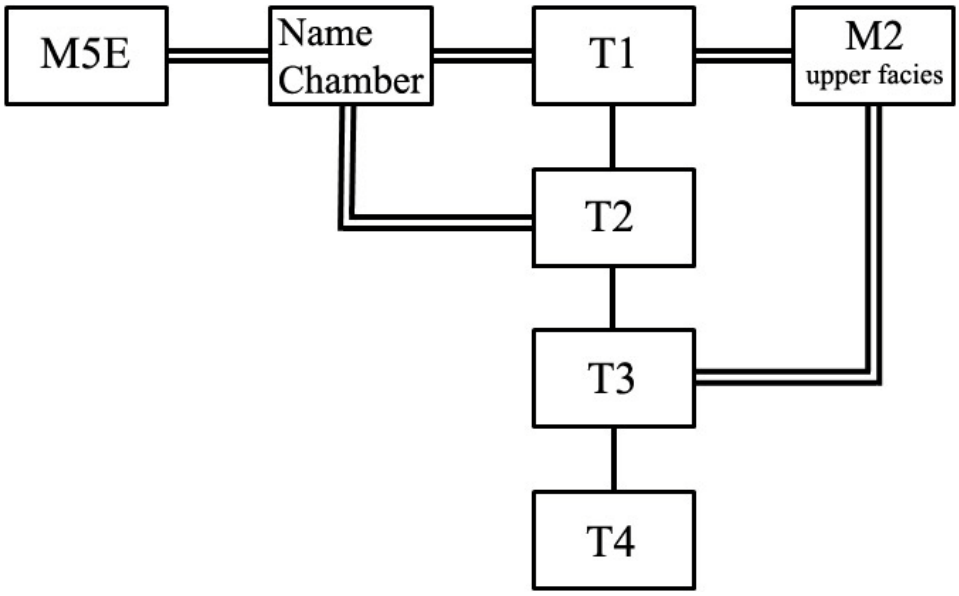


Figure 5.60 Harris Matrix representation of the MH1 stratigraphic sequence.

CHAPTER 6 RESULTS: STK-EC1

The location of the EC1 excavation has been indicated in Figure 1, and the rationale behind the choice of site has been briefly described in the Introduction Chapter. The EC1 site samples sediments that have been accumulated through a tall, narrow passage. The passage opens at the main contact area of the Silberberg Grotto and the Name Chamber Far Western Talus. Removal and re-distribution of sediments during the mining and subsequent tourist route construction near the passage opening has cut any direct stratigraphic connections between the most proximal part of the EC1 passage and the previously associated sediments. The passage exits into the southern extremity of the Milner Hall, an area commonly referred to as the Elephant Chamber. The EC1 excavation plans have been illustrated in Chapter 3 (Figure 3.3). Figure 6.1 shows the EC1 site prior to excavation looking east, up slope.

The passage feeding the EC1 site is split into two levels with a false floor separating an upper and lower gallery. The superimposition of sediments within tall, narrow passages is common in karst systems like Sterkfontein and can be found in a number of places (Martini *et al*. 2003). The false floor is composed of heavily calcified sediment, the remnant of a previous deposit filling the passage that was then undercut. The dolomitic limestone above and the protection afforded to sediments within these passages promotes heavy calcification and flowstone growth, which is often followed by undercutting through localised water flow into and through the passage. As discussed by Martini *et al.* (2003), the superimposition of passages creates difficulties in plan aspect representations of cave systems. In Martini *et al*. (2003) dashed lines are used to illustrate lower gallery levels, and the same method is used in the insert of Figure 6.1 to identify the position and shape of the lower passage.

Figure 6.2 shows the slope profile for the EC1 talus and the false floor of the upper passage. The shape of the EC1 passage is depicted above the slope profile (Diagram A, Figure 6.2) to provide a perspective on the relationship between

deposit morphology and receptacle shape. The limit of the sediments found accumulating at the EC1 site is also depicted.

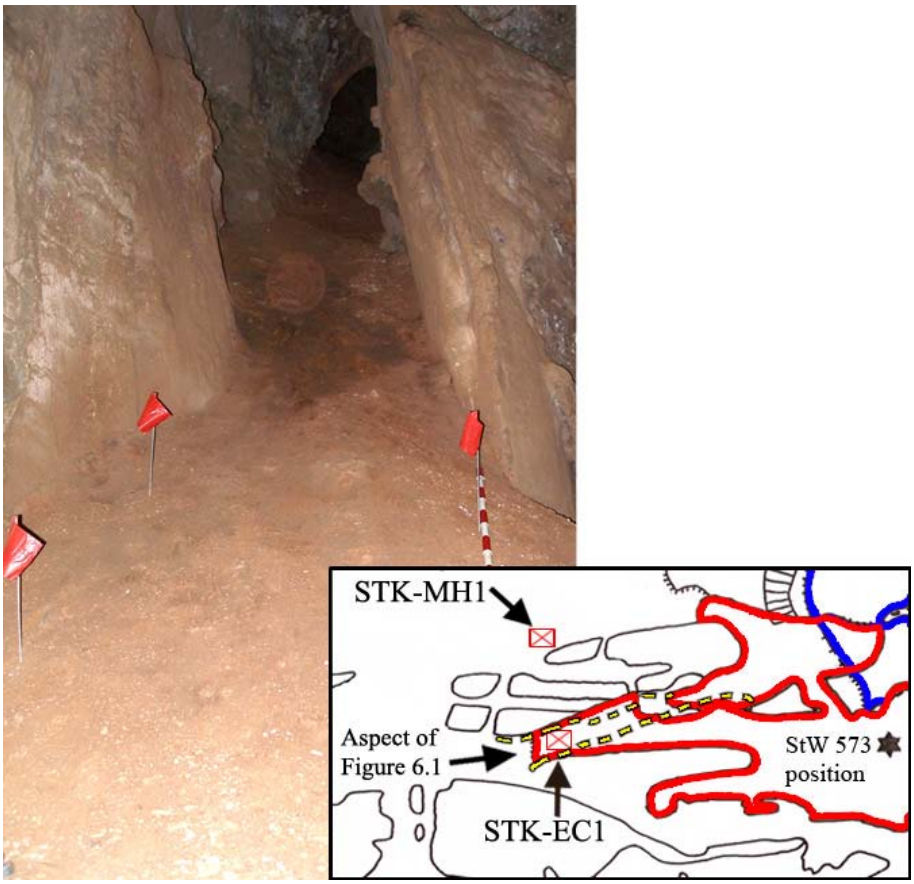


Figure 6.1 STK-EC1 LP talus slope surface prior to excavation, looking eastwards upslope. Within the insert the solid red line represents the upper passage and outline of the Silberberg Grotto deposits, and the dashed yellow line represents the path of the lower passage which is sampled by the EC1 excavation. Insert is adjusted from Martini *et al*. (2003), the expanded version is shown in Figure 1.

The false floor dividing the EC1 passage can be split into two breccia bodies named False Floor 1 and False Floor 2. False Floors 1 and 2 represent remnants of the primary sedimentation of Silberberg Grotto M2 deposit and the spread of this deposit into the EC1 passage. Both bodies derive from the upper facies of the M2 deposit (within the Silberberg Grotto) but exit the Silberberg Grotto from different apertures, then converge into the EC1 passage.

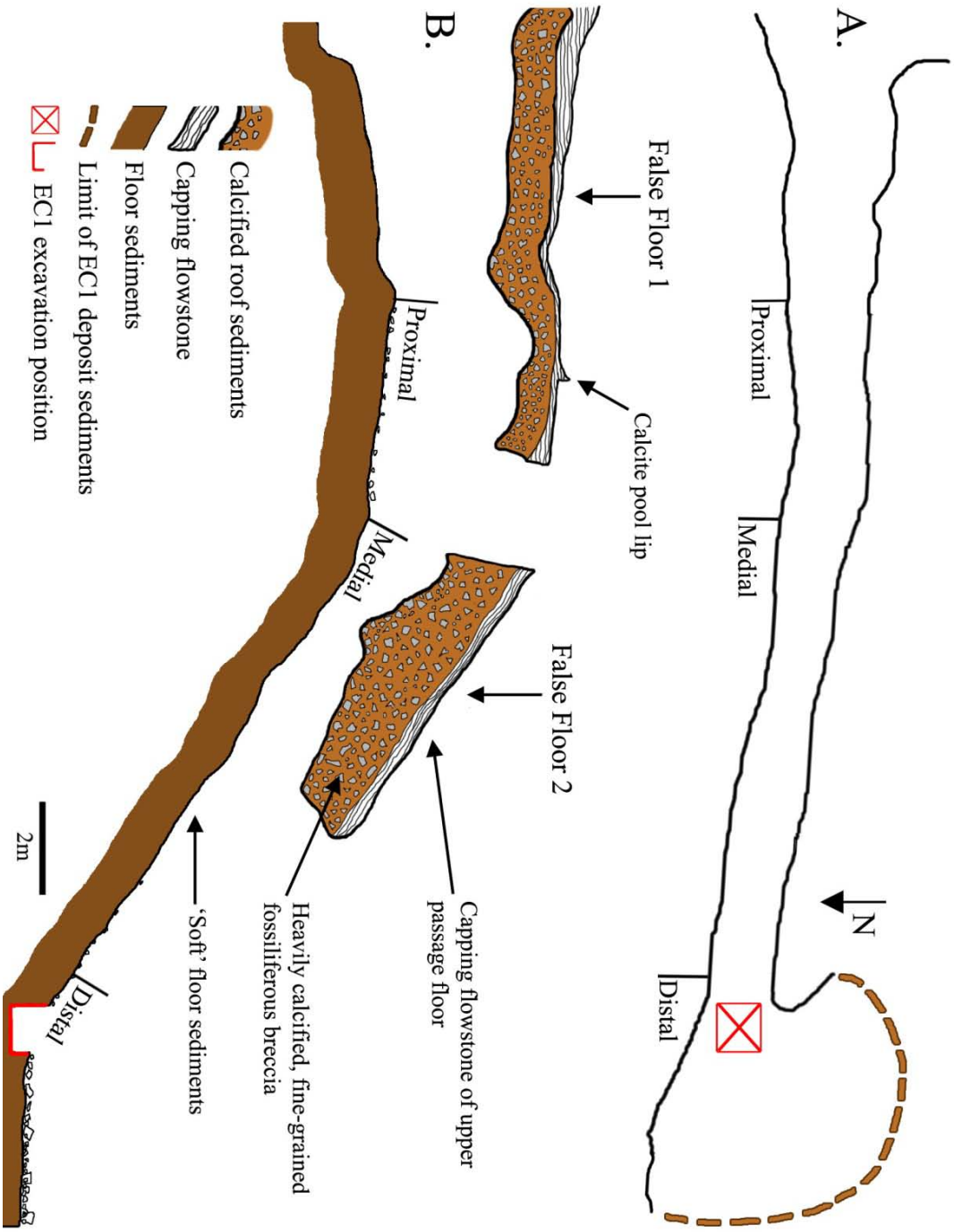


Figure 6.2 STK-EC1 slope profile. Diagram A represents a plan view of the lower passage direction, shape, placement of the EC1 excavation and limit of the EC1 lower passage sediments. Diagram B represents the slope and roof morphology. Both diagrams use the same scale.

Figure 6.3 shows a schematic plan view of the Silberberg Grotto in relation to the EC1 passage and the eastern Milner Hall. Both false floors are made up of stratified, fine-grained breccia with microfauna but with little representation of larger vertebrate material. The sediments forming both false floors have developed through relatively narrow apertures generating a level of filtration of the sediments. Both floors are capped by a thick flowstone which represents the previous infilling surface. This flowstone is the same calcite body that can be tracked back in to the Silberberg Grotto through each exit of the chamber and formed between parts of the StW 573 specimen, capping the M2 deposit.

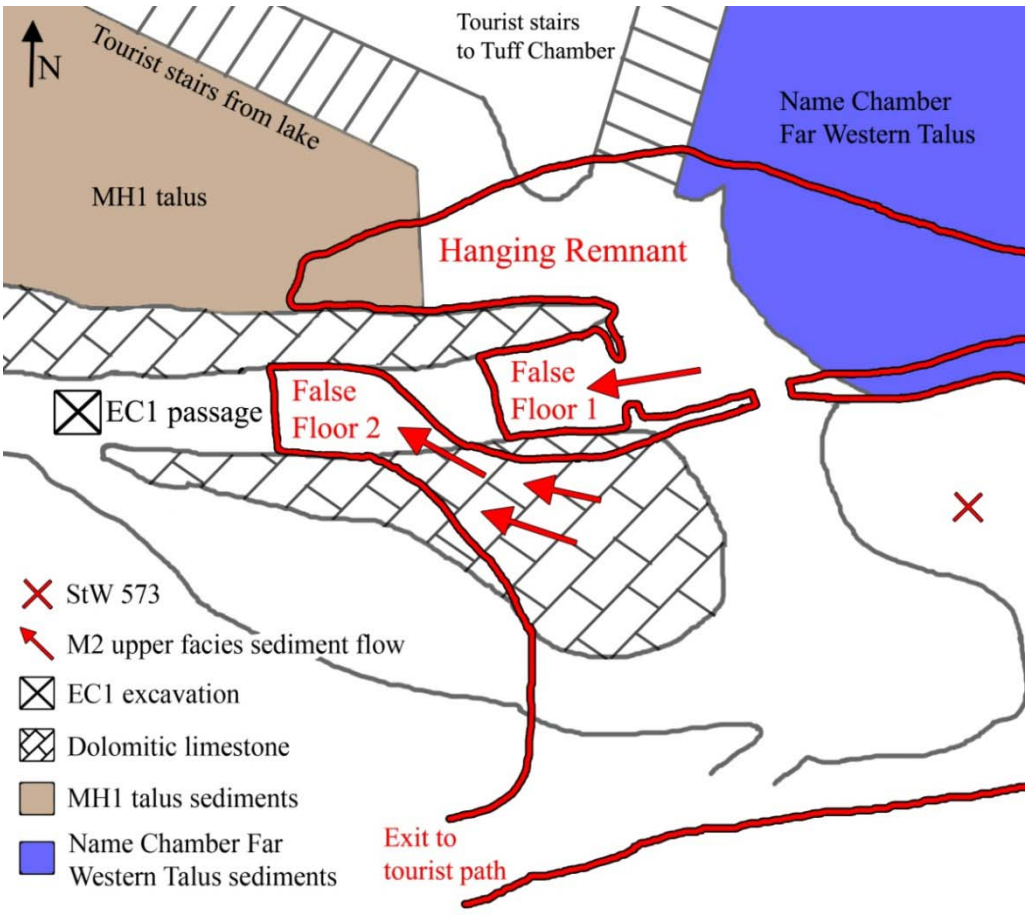


Figure 6.3 Schematic plan view of the Silberberg Grotto sediments exiting the Silberberg Grotto chamber into the EC1 passage, forming two false floor breccia bodies. The Red line represents the limits of the Silberberg Grotto and the current limits of the M2 sediments. The grey line represents the cave morphology of the underlying chambers and passages. The general sediment flow trend creating the false floors found in the EC1 passage is illustrated. Diagram is not to scale.

False Floor 1 is stratigraphically associated with the M2 Hanging Remnant but occupies a slightly deeper and lateral stratigraphic position to the main flow that accumulated the Hanging Remnant. It is probable that the fine-grained nature of the False Floor 1 matrix is a result of the relative position to the main flow, accumulating towards the lateral margin. Also present on the surface of False Floor 1 is a calcite lip (rimstone), evidence of long-term pooling of water in this part of the passage and suggestive of a closed system with little or no sedimentation for a long period of time.

False Floor 2 represents a distal portion of the M2 upper facies breccia body exiting the Silberberg Grotto in the far west of the chamber (Figure 6.3). The fine-grained nature of the False Floor 2 matrix is most likely due to the distance of the sediments from the source. False Floor 2 is stratigraphically associated to the M2 Hanging Remnant but only close to the source of the flowstone in the Silberberg Grotto before the sediments diverge through their respective exits. The flowstone capping False Floor 2 has a gradient of 32° and represents the talus surface morphology when it originally exited the Silberberg and filled into the EC1 passage in a steep talus slope.

The EC1 excavation sampled the distal portion of the lower passage, specifically where the sediments start to spread into the widening passage exit. The EC1 eastern wall stratigraphic profile is presented in Figure 6.4. The lower passage (EC1 LP) represents an undercutting channel which removed the M2 upper facies sediments that previously filled the EC1 passage. This erosive episode left only the false floors as evidence of the preceding deposit. The passage was then filled by other sediments creating the present talus slope. Unfortunately, sampling of the sediments within the false floors was not possible during this research, but stratigraphically the associations are clear. The EC1 LP opens from a platform on top of a collapsed roof block directly underneath the M2 Hanging Remnant within 3m of the Name Chamber Far Western Talus sediment limit and 1m from the highest point of the MH1 talus (Figure 6.3). The EC1 LP runs almost due east and opens in an abrupt downward turn to the south facilitating preferential sediment infilling in a southerly direction. The slope is just over 20m in length from start of

decline to sediment termination, and drops 8m vertical height to a level 2m above the floor of the Milner Hall and 5m above the current water-table.

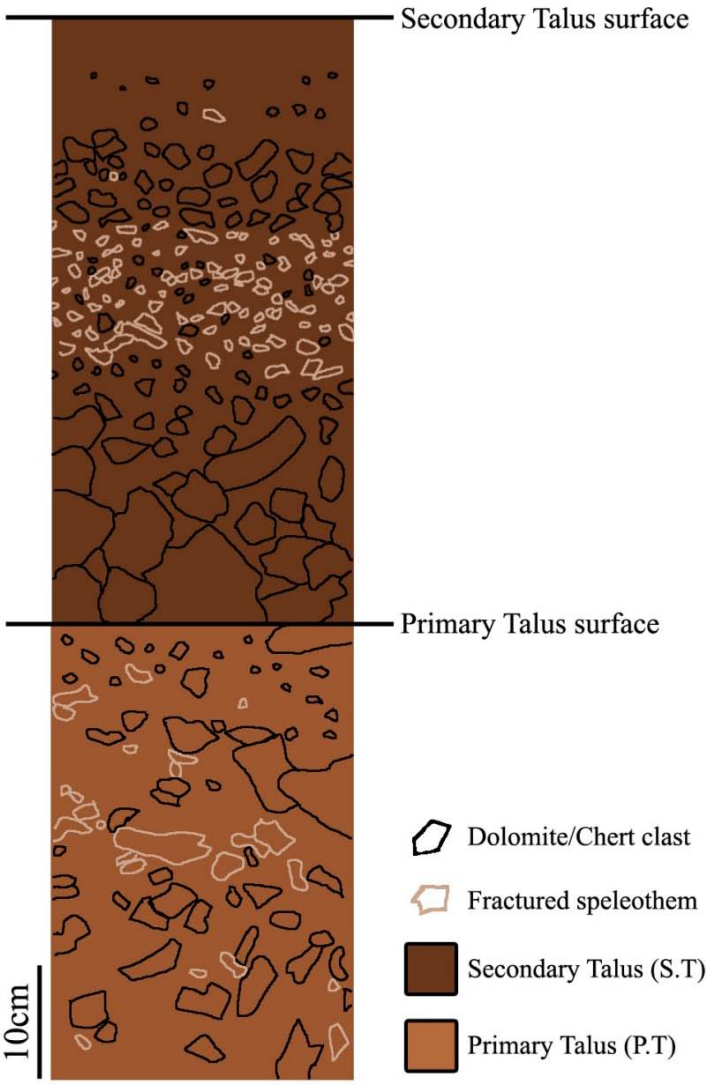


Figure 6.4 Eastern wall profile of the EC1 excavation.

The EC1 LP talus contains two deposits, both of which have accumulated into a narrow passage with a maximum width of 1.5m and a minimum width of 1m. The two deposits have been named the Primary Talus (P.T.) and the Secondary Talus (S.T.) in order of deposition. The Primary Talus is described in Section 6.2. The sediments within the P.T. and S.T. were 'soft' and allowed the full spectrum of

analyses to be conducted. Both deposits represent distinct depositional entities with different sediment properties and histories. As discussed in Chapter 2, tracing deposits through multiple phases of re-sedimentation becomes increasingly difficult with increasing stratigraphic disassociation through collapse and/or erosion and changes in cave morphology.

6.1 Secondary Talus

Figure 6.2 shows the profile of the EC1 slope deposit. The Secondary Talus (S.T.) represents the current surface of the EC1 LP talus. The S.T. surface is characterised by a dry, fine, loose matrix with similarly sized small (<30mm) fragments of fractured travertine, dolomite and chert, no faunal material was found on the deposit surface. The surface sediments at the proximal and medial portions of the talus are more consolidated with little or no >20mm material. At the distal portion of the talus the gradient shallows and sediments become progressively looser and larger (30mm - 100mm). The EC1 LP talus surface differs from the MH1 talus surface in that it represents a natural sediment accumulation relatively unaffected by mining activity. The burial of the naturally accumulated T2 deposit by T1, an anthropogenic accumulation, allowed the exposure of only 2m x 2m of the T2 deposit surface by excavation, thereby restricting investigation of the deposit surface morphology. The longitudinal morphology of the S.T. surface can be considered a straight, uniform slope, neither concave nor convex for the majority of the gradient. The talus surface can be split into three sections (see Figure 6.2 for representation). The proximal section measures from the point at which the positive decline starts to the point at which the gradient reaches the slope gradient average. The proximal section covers the first 6m of the slope. The medial section measures 10m, from 6m to 16m along the slope and represents the body of the slope that reposes at the average gradient. The angle of repose of the medial portion of the slope ranges from 33° to 35° with the mean being 34°. The maximum gradient is found 12m from the start of the positive decline, just over half way down the medial section. The majority of the medial section is contained within the narrowest portions of

the passage. Finally, the distal portion measures 4m, from 16m to 20m along the slope and represents the decrease from the mean angle of repose to the horizontal at the sediment termination. The mean angle of repose of the S.T. slope fits well with other observations of natural talus slope angles dominated by loose, sand to gravel-sized supporting material (Ward 1945; Chandler 1973; Sanders *et al*. 2008). It was suggested by Ward (1945) that due to the shearing resistance of loose material of this size, a relatively straight, 35° slope will be commonly formed. The EC1 excavation samples the distal section of the talus at a point where the talus gradient starts to shallow. At the point of excavation the EC1 LP talus surface has an angle of repose ranging from 26° at the more proximal eastern end to 24° at the distal, westerly end.

The transverse morphology of the proximal section of the S.T. surface is level and shows no strike angle. Within the narrowest sections of the passage, through the medial section, there is a slight (9° average) transverse north-south gradient (seen in Figure 6.1). As the talus enters the distal section and the passage opens up to the south, the transverse morphology is characterised by a convex shape where the sediments spread to fill a larger receptacle in an exaggerated tongue-shaped lobe that spreads mostly in a southerly direction. The internal stratigraphy is influenced by the spread of sediments into the larger receptacle as can be seen in Figure 6.2. This process is described in the following section.

6.1.1 Secondary Talus stratigraphy

Figure 6.4 shows the eastern wall stratigraphic profile of the EC1 Secondary Talus. The Secondary Talus can be split in to two strata, named Stratum 1 (lower) and Stratum 2 (upper) representing a single facies named, *Facies 1*. Despite the barely discernible contact of the two strata, two regular grading sequences distinguish the two strata. The absence of a consolidated Stratum 1 surface suggests a relatively short period of time separated the two infilling events. Sediments within the S.T. fit into a deposit-level regular grading pattern. Both strata have developed through dry grain flow sediment accumulation processes

which have re-distributed sediments from an area in the immediate proximity of the opening of the passage to the east. Grain flow deposits often develop good stratification based on multiple surges of sediment (Hétu *et al.* 1995; Bertran *et al.* 1997; Major 1997). Each S.T. stratum represents a surge in material from the same source. The regular grading pattern is a result of the sediment flow processes that often operate within dry grain flows, the basal clast-supported horizon facilitating the suspension of the finer grained sediments (Bertran & Texier 1999). A basal level of highly imbricated larger clasts (Hétu *et al.* 1995; Bertran *et al.* 1997) and an accumulation of larger clasts at the snout of the infill (Parsons *et al.* 2001) are typical characteristics of grain flow deposits, both of which are evident in the S.T. deposit. The lack of water during the deposition of the sediments is probably aided by the restricted size and shape of the passage opening. The S.T. differs from some grain flow deposits in that the sediments have not developed a post-depositional inverse grading pattern. This pattern is found in many grain flow deposits, and is found in the T2 deposit in the MH1 site. In the case of the Secondary Talus this process has not yet taken place and the sediments remain regularly graded with a basal stratum characterised by a high proportion of unfilled, interstitial pockets. The grain flow depositional process active in the accumulation of the S.T. sediments have produced a highly fragmented faunal assemblage, in a similar fashion to the *Facies I* (T2) sediments in the MH1 site. *Facies 1* which contains Stratum 1 and Stratum 2 can be described as follows.

Facies 1: Dark reddish brown (5YR 3/3) loosely consolidated, stratified, regularly graded matrix-supported silt loam with basal clast-supported horizon. Clasts in the matrix-supported levels show a restricted range in size with infrequent particles measuring >20mm. Interstitial voids are infrequent and the unconsolidated nature of the sediments is due to lack of sediment settling. Microfauna remains are abundant and macro-mammal fossils increase in yield with depth. A fractured travertine horizon is contained within an acutely transitional horizon 8-10cm thick, with an equally progressive transition above and below, and contains a 60% proportion of fractured travertine over dolomite and chert clasts. The original speleothem form is not identifiable from macroscopic observation. The basal clast-supported level has high numbers of imbricated clasts, large interstitial

pockets and very little fine sediment between clasts. Sizes of the basal, clast-supported, horizon range from 50mm to 200mm maximum dimensions. Clasts in the basal level are predominantly made up of broken dolomite blocks with smaller proportions of chert and are angular to sub-angular in shape.

Figure 6.5 shows the eastern profile of the S.T. deposit excavation profile. As can be seen in Figure 6.5, both S.T. stratum surfaces are convex in transverse surface morphology which is a characteristic of a tongue-shaped distal lobe of the deposit. The base of the lower, Stratum 1, is transversely horizontal and has formed abruptly on to the transversely horizontal, highly consolidated surface of the Primary Talus. The transverse convex nature of the surface of the Stratum 1 material is caused by the spreading of sediments into a wider receptacle at the distal end of the deposit. Conversely, the P.T. surface is horizontal, suggesting these sediments were not heavily influenced by the widening of the passage, this will be discussed in Section 6.2.1. The relatively thin horizon that constitutes Stratum 2 (10-12cm) can be considered to have followed the underlying dominant Stratum 1 longitudinal morphology as well as its transverse morphology. Firstly, the widening of the sediment receptacle to the south, at the distal portion, creates a tongue-shaped spread of sediments in a southerly direction. Secondly, the convex nature of the receptacle surface (surface of Stratum 1) has further exaggerated the spread of Stratum 2 sediments to the south and the transverse convex morphology. To illustrate this, it can be seen that the transverse apex of Stratum 2 lies further towards the south than the underlying Stratum 1 infill, the transverse apex of which is more central.

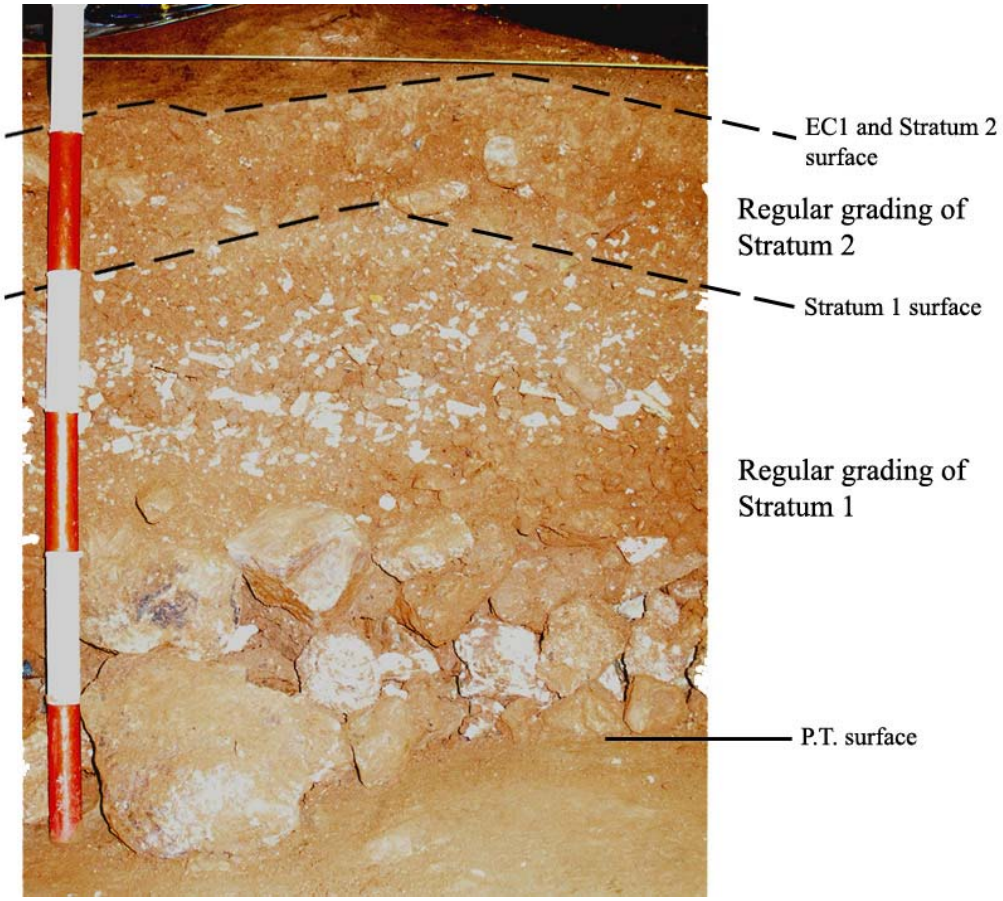


Figure 6.5 S.T. eastern wall excavation profile. The consolidated surface of the P.T. (*Facies 0*) can be seen at the base of the picture. The staff segments measure 10cm.

Figure 6.6 shows the southern profile of the S.T. excavation. Noteworthy is the increase in clast size and frequency within the clast-supported horizon towards the talus termination. The matrix-supported sediments taper off with increasing distance down slope as the whole deposit reduces in thickness towards the termination of the deposit. The basal, clast-supported level, however, shows an associated increase in thickness until the level intersects with the surface of the deposit, indicating the start of the deposit termination. The termination is characterised by a dominance of large, imbricated clasts, a common feature in dry grain flow deposits (Parsons *et al.* 2001).

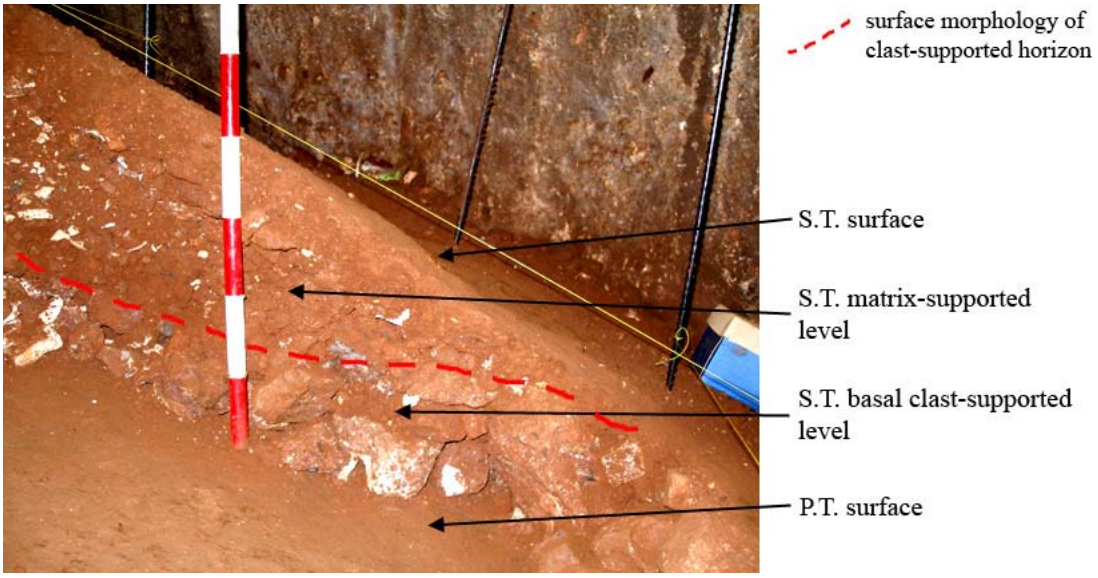


Figure 6.6 STK-EC1 Secondary Talus southern wall excavation profile. Notice the increase in clast size and clast frequency in the basal clast-supported level towards the distal portion of the talus. The staff segments measure 10cm.

Figure 6.7 presents the plotted fossil and artefact distributions throughout the S.T. deposit. All faunal material measuring >20mm and archaeological material of any size was plotted from a single, fixed datum point. Ninety six pieces were plotted prior to removal from the sediment. Eight pieces suffered precise context loss due to a partial collapse of the southern wall. The eight pieces were successfully assigned to Stratum (2) quad (A) and spit level (10-15cm) but could not be confidently plotted into the distribution. The seven fossils and single artefact have also been excluded from the fabric analysis. Significantly, only seven fossils/artefacts (6.7%[5]) were found within the basal clast-supported level. The remaining 97 pieces (93.7%), regardless of size, were only found in the matrix-supported sediments. The eight pieces with lost context also derive only from the matrix-supported sediments. This pattern can be seen in the YZ distribution plot, where the positions of the plotted pieces follow the morphology of the matrix-supported level. The large gaps in this distribution plot represent the morphology

[5] The eight pieces from the collapse can be assigned to Stratum 2 and the assemblage subset deriving from the matrix-supported sediments and therefore do not influence the assemblage total which is 104 fossils and artefacts deriving from the Secondary Talus.

of the basal clast-supported level. The morphology of the clast-supported basal level can also be seen in the southern wall profile (Figure 6.6).

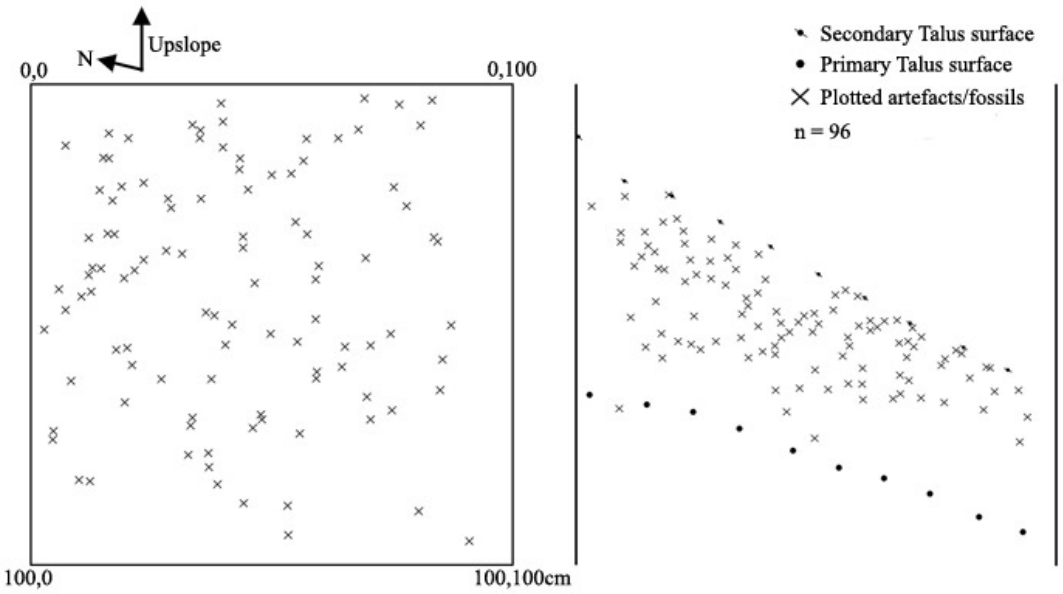


Figure 6.7 S.T. Artefact and fossil scatter plot. The left figure presents the XY (plan view) distribution, and the right figure presents the YZ distribution.

The XY fossil/artefact distribution plot shows a generally even distribution of fossils and artefacts across the $1m^2$ area of the excavation with a slight grouping of fossils/artefacts towards the northern wall of the excavation. This grouping is not a result of a concentration caused by flow around large clasts or channels of water concentrating fossils/artefacts in this area. Almost all fossils are found within the matrix-supported levels and so are not heavily influenced by flow of sediments around large clasts. Water is also not a great influencing factor in the deposition or post-depositional processes found within the S.T. deposit. The grouping is a result of the morphology of the receptacle. As the sediment grain flow slowed at the shallowing distal portions of the lower passage, the sediments compressed against the northern wall of the passage, creating a thicker matrix-supported level and a slight, but noticeable, concentration of fossils and artefacts. To the south of the excavation the opposite situation occurred. As sediments filled

the expanding passage to the south (Figure 6.2), specimens were distributed across a broader area, creating a thinner matrix-supported level and lower fossil/artefact yield.

The distribution of fossil yield by stratum shows a higher yield within Stratum 1 than Stratum 2. Within Stratum 1 there is a higher yield at the surface with 26 specimens per 5cm spit, this continues for three spits (15cm) before the fossil yield tapers off with the transition into the clast-supported, specimen-poor basal level. Stratum 2 has a mean fossil yield of five specimens in the opening spit, increasing to 14 specimens towards the base. The transition into Stratum 1 from Stratum 2 is marked by a distinct increase in fossil yield. In stratigraphically sensitive spits of 5cm, fossil yield through the whole S.T. deposit rises from five specimens in the opening spit through to 26 in the middle three spits before yield then tapers off with the transition into the clast-supported sediments representing the basal level. In terms of the XY fossil yield distribution, quadrant A shows the highest yield of bone by a significant quantity, producing 40 specimens. Quadrant C produced the next highest number of specimens with 24. Quadrant B and D (the southern quadrants) yielded the fewest specimens with 18 and 22 respectively. The relative richness of fossils in Quadrants A and C relates to the associated thickness of the matrix-supported strata and to the compression of sediments against the northern wall as described above.

During this research very little water was observed travelling through the passage or dripping on the sediments from above. The rate and quantity of water interaction both during and after deposition can have significant influences over the calcium content of the sediments, by depositing and removing it or by transporting the calcium already contained in the sediments in the forms of fractured speleothem material. The relatively sheltered nature of the EC1 LP has enabled the sediments to be mostly unchanged since deposition. The XRF analysis supports the interpretation that the sediments remain uncalcified and may closely represent the source deposit sediment conditions.

6.1.2 Secondary Talus sedimentology

Table 6.1 presents the sedimentological summary data for the EC1 Secondary Talus. Due to the late recognition of multiple internal strata, only two sediment samples were taken from the S.T. sediments. These samples incidentally sampled each stratum but are regarded as representing the S.T. deposit as a whole. One samples was taken from the upper 10cm level (Stratum 1) and one from the lowest of the matrix-supported level at 30cm depth (Stratum 2). For greater clarification of the stratum boundary and relationship at least three samples should taken from each stratum. The identification of two grading sequences was made through observation. The hydrological results show a slight dip in water content with depth (from 7.83% to 7.19%), which is associated with a slight rise in the sand proportions (from 27.5% to 33.2%). The decrease in water content with depth is expected given the lower water retention potential of coarser sand grains and the drainage of the lower levels into the interstitial pockets of the basal clast-supported level. The low moisture content in the S.T. sediments may not be representative of the primary deposit hydrological pattern, but a result of the lack of water in the immediate vicinity of the passage. The moisture content of the S.T. deposit is most comparable to the T2 deposit. However, within the T2 deposit there is a greater intra-deposit range, indicating a higher level of vertical water movement, facilitating the associated vertical movement of fine-grained sediments. The S.T. deposit does not show a similar level of intra-deposit water movement and evidently does not show the same level of vertical sediment movement. The differences in vertical water movement are most likely to be responsible for the inverse grading found in the T2 deposit and the regular grading, or lack of development of an inverse pattern, in the S.T. sediments. As the S.T. sediments settle and start to filter through the interstitial voids with the help of water passing through the matrix, the clays will accumulate towards the base of the deposit, eventually creating the inverse grading pattern found in many grain flow deposits (Bertran & Texier 1999) and the T2 deposit. The relatively unsettled nature of the S.T. deposit, in comparison to T2, does not imply a relatively young age, sediment settling rates and development of grading patterns

are determined primarily by exposure to enough water to move sediments vertically.

It will be shown in the XRF analysis to follow, that the lack of water may have helped protect the sediments from extensive post-depositional calcification, but some post-depositional chemical modification of the sediments is indicated by an increased level of calcium. The sediments from both samples remain rather similar, in terms of sediment hydrology, colour and faunal content, as each stratum represents a different surge of sediments from the same source. The basic particle size data show the deposit-level regular grading pattern of the S.T. sediments. The silt proportion shows the greatest decrease of the fine particles, dropping by a total of 4.5%, with the clay quantity only dropping by 1.2% and sand proportions rising by 5.7% with depth.

				Particle Size		
Art No.	**Sample location**	**Munsell**	**Hydrology %**	**% Clay (<2µm)**	**% Silt (2µm - 63µm)**	**% Sand (> 63µm)**
158	Stratum 1 - *10cm*	5YR 3/3	7.83	8.85	63.693	27.457
206	Stratum 2 - *30cm*	5YR 3/3	7.19	7.649	59.114	33.238

Table 6.1 EC1 Secondary Talus sedimentological summary. Depths are taken from the datum on the talus surface.

XRF

Table 6.2 presents the XRF chemical composition of the S.T. sediments. One sample was taken from the same location as the Stratum 1 samples, at 30cm depth from the talus surface datum. Due to financial constraints, only a single sample was taken. However, when the general homogeneity of the S.T. sediments is taken into account, with the inference that the strata derive from the same source, a single sample is considered sufficient for representation of the S.T. deposit. What is clear from the chemical composition is that the sediments are predominantly allogenic, with small inclusions of authigenic material in the form of fractured travertine. The S.T. sediments show a statistical similarity with all the MH1 facies chemical distribution (*Facies AI*, p = 0.995; *Facies I*, p = 0.827; *Facies II*, p =

0.992; *Facies III*, p = 0708; *Facies IV*, p = 0.814; *Facies V*, p = 0.891). All of the externally derived sediments follow the same pattern of chemical distribution, however, the T1 and EC1 deposit sediments are differentiated by significantly higher quantities of calcium (*Facies AI*, Ca = 14.72%; EC1 S.T., Ca = 12.33%). The higher calcium content in *Facies AI* (MH1 T1) was interpreted as post-depositional contamination of the sediments by the extensive and frequent horizons of fractured travertine (*Facies AII*) inter-stratifying the *Facies AI* beds. A similar interpretation is suggested for the S.T. sediments in that the horizon of fractured travertine (richer in calcium carbonate particles with a large surface area), in the upper part of the Stratum 1 sediments, has leached calcium down into the lower levels of the deposit (to the XRF sample point) creating a post-depositional accumulation of calcium. The absence of localised water activity in the passage reduces the probability that the calcium has been accumulated through infiltration from the surrounding dolomitic limestone in the same way that calcifies sediments and forms speleothems. The generally low proportion of Ca and the lack of fresh water in the passage to decalcify the sediments, suggest that the sediments in the S.T. deposit are representative of the source deposit in their absence of calcium. This fits with the interpretation of the Name Chamber Younger 'soft' Deposit that makes up the Far Western and Western Talus. These sediments have not been calcified and were deposited into the Name Chamber from M5E before the calcification of this surface deposit (Stratford 2008). Varying calcium quantities in calcified sediments from Sterkfontein have been discussed in Section 5.2.2.

SiO2	Fe2O3	FeO	MnO	MgO	CaO
70.01	0.43	3.45	1.00	1.26	12.33

TOTAL
99.48

Al2O3	Na2O	K2O	TiO2	P2O5	Cr2O3	NiO
6.68	0.09	0.62	0.505	3.07	0.0200	0.0070

Table 6.2 S.T. XRF results.

Particle size

Figure 6.8 presents the particle size distribution for the S.T. sediments. The samples derive from the same areas as the main sedimentological samples, i.e. one from the upper 10cm level (Stratum 1) and one from the lowest of the matrix-supported level at a depth of 30cm (Stratum 2). Figure 6.9 presents the combined particle size distribution curves for both samples represented on the same axes. As briefly discussed above, both strata fit into a deposit-wide regular grading trend, and both represent two regularly graded horizons. The significant rise in the coarser particles with depth is clear, with an associated drop in the silt and clay sized component. The particle size distributions were compared statistically using the method described in Section 3.3. The Chi^2 statistical comparison of the volume occupied by the de-convoluted curves on each sample show that the two S.T. samples are statistically similar, but with a low p value of 0.203. Table 6.3 shows the relative volume percentages of the four constituent curves from each of the S.T. samples. The de-convoluted curves for all samples are presented in Appendix 2. From these relative volumes it can be seen that Curve 4, representing the distribution curve for the coarsest particle range, shows a 5.5% increase with depth and Curve 3, which represents the silt sized fraction which shows a 6.8% decrease with depth. Interestingly, Curve 1, representing the clay sized particles (about 1μm), shows a relative volume of between 6.8% and 7.3% in both S.T. samples, more than double the mean relative volume of Curve 1 found in the MH1 samples (MH1 Curve 1 mean = 3.154%). Only one other sample has a similarly high relative volume of the finest particle and that is the basal T2 sample with a Curve 1 relative volume of 7.114%. The two deposits have different grading patterns, T2 being inversely graded and S.T. being regularly graded. This makes the statistical comparison between particle size distributions impossible.

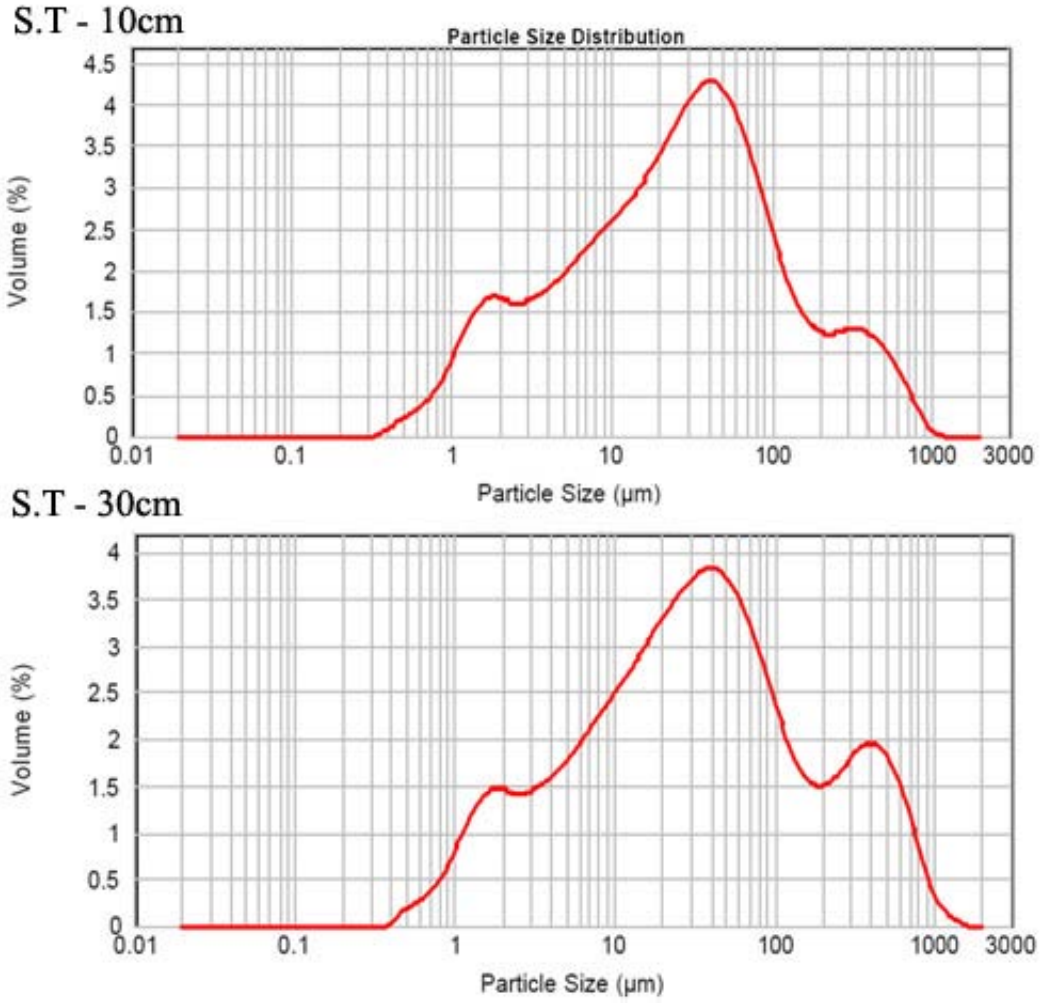


Figure 6.8 S.T. particle size distribution curves for two samples taken at upper and base of the matrix-supported sediments in the Secondary Talus deposit.

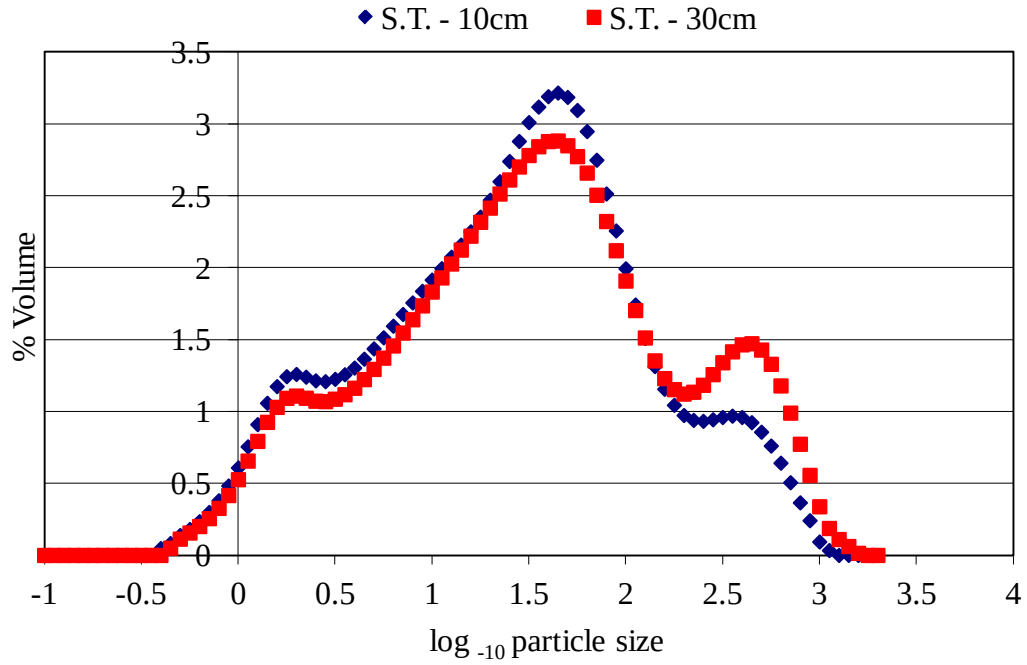


Figure 6.9 S.T. combined particle size distribution curves.

	Curve 1	Curve 2	Curve 3	Curve 4	Total
S.T. - 10cm	6.862	41.178	43.138	8.821	100.0
S.T. - 30cm	7.385	41.920	36.330	14.365	100.0

Table 6.3 S.T. relative constituent Gaussian curve volumes. The figures represent the volume as a percentage of the whole sample distribution curve. The Secondary Talus particle size distribution curves could be de-convoluted into four Gaussian curves.

6.1.3 Secondary Talus fabric analysis

Figure 6.10 presents the fabric analysis representations for the S.T. sediments. The pattern in the data fits with what would be expected given the accumulation of sediments through a restricted aperture. Ninety four pieces (90%) were eligible for fabric analysis. Of the remaining ten fossils and artefacts, eight were subject to context loss and have been mentioned in Section 6.1.1, and two fossil pieces possessed elongation ratios of under 1.6:1 and were deemed unreliable for positive orientation development based on Bertran & Texier (1995). 88% of the

specimens are oriented to between 60-100° representing the dominant flow direction. The mean elongation ratio for the S.T. fabric analysis assemblage is 3.3:1 with a maximum of 9.2:1. Eleven pieces (of the 94 total) (11.7%) are orientated between 350-20°, perpendicular to the sediment flow direction. The perpendicularly orientated pieces have a mean elongation ratio of 3.8:1 with a maximum of 6.4:1. The perpendicularly orientated pieces are spread throughout the matrix-supported deposit in both Stratum 1 and Stratum 2 and therefore cannot be assigned to a distinct stratum with differing sedimentological properties or accumulation processes that may have influenced the orientation process. The perpendicularly orientated pieces also represent a wide range of skeletal elements, from irregularly shaped bones (mandible) through to compact bones (phalanx). Eight of the eleven perpendicularly orientated pieces represent shaft elements. The seeming lack of shared characteristics between the perpendicularly orientated pieces precludes positive interpretation of the processes affecting their orientation. Skeletal elements possess the ability to orientate themselves perpendicular to flow direction, as noted by Voorhies (1969) although the S.T. perpendicularly orientated specimens do not show a marked increase in elongation ratio as Voorhies observed in fluvial contexts.

The dip values show an equally expected pattern with a mean dip value of 24° from horizontal (mode and median of 24°). This compares closely to the 26° to 25° angle of repose of the slope surface at the excavation point, where the talus starts to shallow from the medial slope. Bones found at all levels of the matrix-supported level show the same dip values. A similar dip pattern as seen in MH1 T2 is evident, where the form of the slope below, or receptacle gradient, has affected the dip of particles.

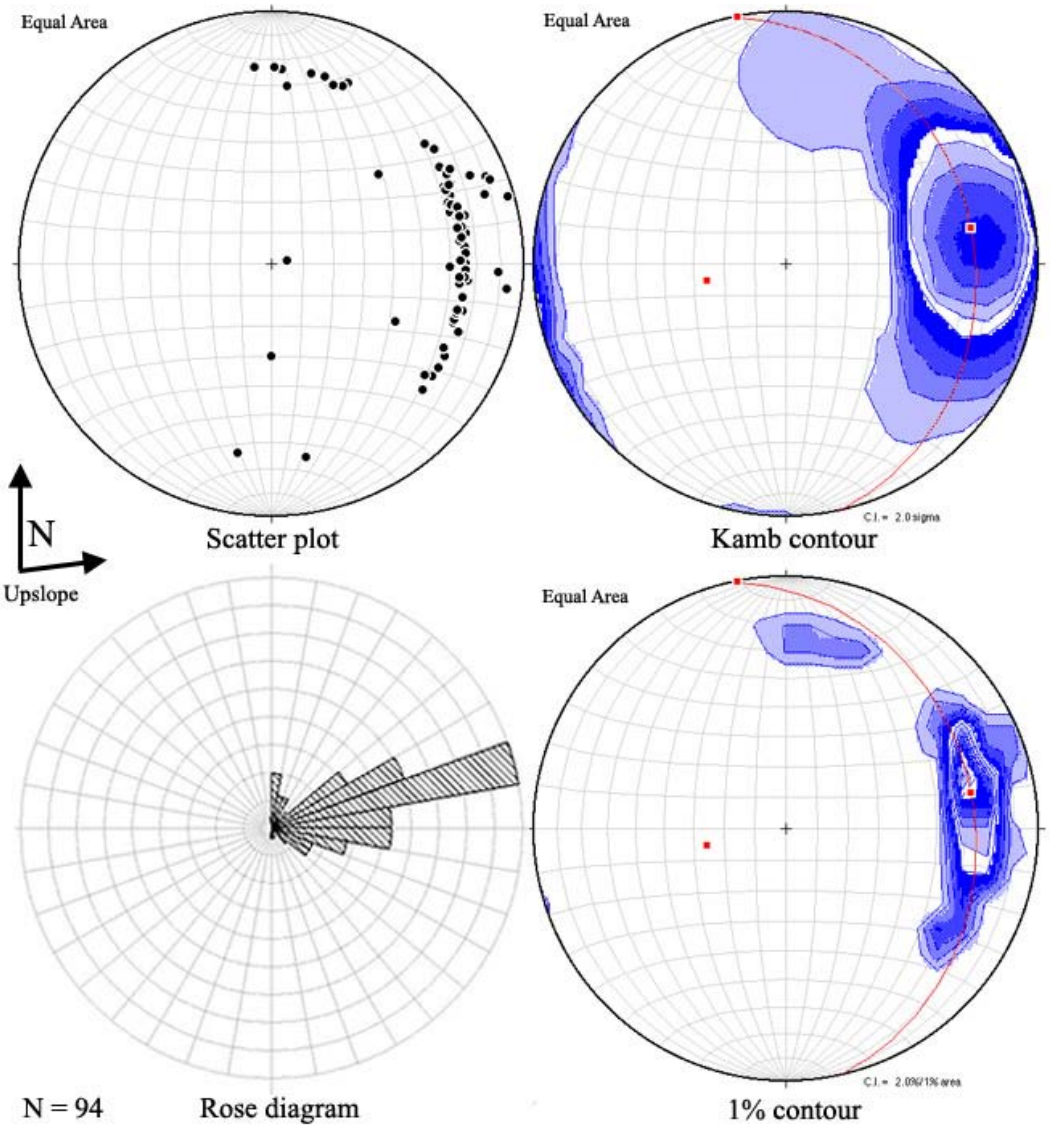
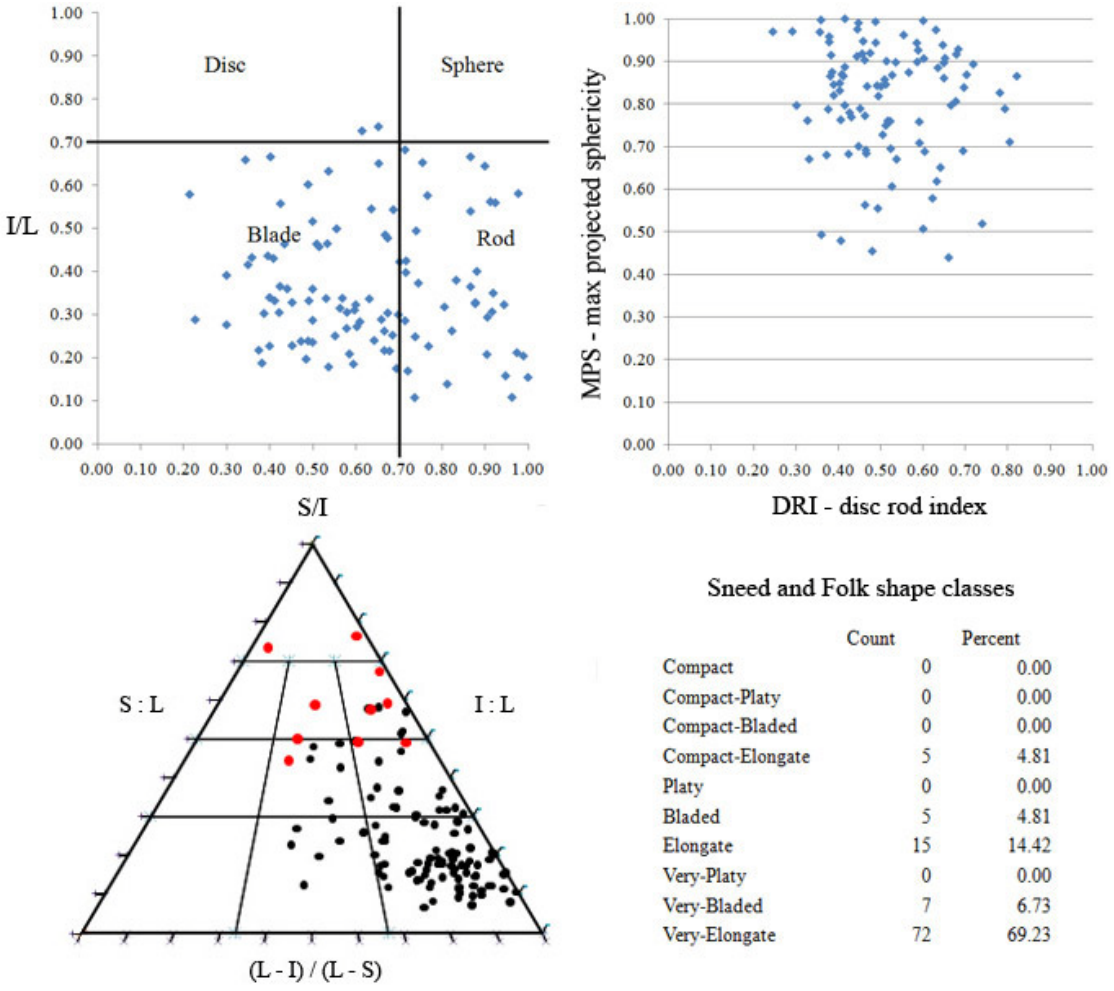


Figure 6.10 S.T. fabric analysis models. Kamb contouring has a contour interval of 2.0 sigma. The 1% contour plot has a contour interval of 1%. All stereographic projections show best the best fit plain and cone. The rose diagram sections represent 10°.

6.1.4 Secondary Talus particle shape

Figure 6.11 shows the particle shape indices for every excavated specimen from the S.T. deposit. Ten natural clasts were plotted into the Sneed & Folk (1958) ternary diagram and are represented by red points. The Sneed & Folk shape classes show a clear dominance of elongate forms (95%) with very elongate forms contributing the greatest (69%) and blade-shaped particles representing the only non-elongate forms in the assemblage. The assemblage particle shape profile resembles the MH1 T2 deposit in that the grain flow process of accumulation has led to significant levels of post-depositional breakage. Generally, the greater the degree of fragmentation the lower the possibility of positive identification to both element and taxa and the S.T. assemblage follows this pattern. The S.T. assemblage is characterised by a large number of long bone shaft fragments that are identifiable to element type and body portion but not to taxa. As found in the particle shape tests (discussed in Chapter 4), long bones break into large quantities of shaft and elongated cortical bone fragments, the relative size of long bones contributing to their disproportional representation in fragmented form. The similarity of the T2 and S.T. profiles may well imply more of a correlation than just the same accumulation processes producing the same particle shape profile.



Sneed and Folk shape classes

	Count	Percent
Compact	0	0.00
Compact-Platy	0	0.00
Compact-Bladed	0	0.00
Compact-Elongate	5	4.81
Platy	0	0.00
Bladed	5	4.81
Elongate	15	14.42
Very-Platy	0	0.00
Very-Bladed	7	6.73
Very-Elongate	72	69.23

Figure 6.11 S.T. particle shape indices. The red points on the Sneed & Folk diagram represent natural clasts collected during excavation. The natural clasts are not included in the shape class table.

It is possible that the contributing, faunal assemblages may well have had a similar element representation. Analysis and comparison of the bone breakage profiles and intensity of fragmentation may suggest how similar the fossil assemblages were prior to this stage of secondary sedimentation. As can be seen in the Zingg diagram the assemblage falls into the rod and bladed forms with the majority of elements spreading across into the blade-shaped particle area. The S.T. assemblage contains only eight rib fragments, elements that possess a naturally elongate blade-shape before breakage and continue to possess an elongate blade-shape through all levels of breakage. The high proportion of blade-

shaped particles within the S.T. assemblage is due to the sensitivity of the Zingg equation (1935) to bladed forms.

The MPS vs. DRI graph also follows the patterns seen in the other deposit analysis, which is a general trend towards more spherical forms than is recognised by the other particle shape models. Generally, fossil fragments do show an increase in relative sphericity with increasing levels of breakage, and different elements increase in sphericity at different rates during breakage (see Chapter 4 for discussion). Complete long bone elements (composed of tibia, humeri, and femur) from modern forms of genera well represented in the fossil record, a bovid (*Aepyceros melampus*), carnivore (*Panthera pardus*) and primate (*Papio hamadryas*), have an average MPS (maximum projected sphericity) of 0.47 with a maximum MPS of 0.54 (primate humerus) and minimum MPS of 0.40 (primate femur). By comparison, the mean MPS on shaft bone fragments from the S.T. assemblage is 0.53, with a maximum MPS of 0.74 and a minimum MPS of 0.30, despite being classed equally as very elongate forms by the Sneed & Folk model. The MPS vs. DRI graph may help indicate where breakage has caused increased particle sphericity and therefore increased transport potential.

Figure 6.12 presents the Voorhies Groups (1969) for the S.T. faunal assemblage. Due to the high levels of fragmentation found within the S.T. assemblage only 35 bones were sufficiently identifiable to specific element and thus applicable to Voorhies analysis. The small sample size is an issue, but the presence of elements can still be considered representative of the whole assemblage. As seen in the MH1 deposits fossil grading can influence the skeletal element representation and proportions within different parts of a deposit depending on the breakage levels incurred on the bones. Given the similarities in formation processes between the S.T. and T2 deposits, one may expect to see similarly low levels of longitudinal mixing. Almost half of the S.T. assemblage falls into Voorhies Group II and III, which represents particularly immobile elements. The S.T. deposit represents a sediment transport distance of over 20m from the original source deposit, an ample space for longitudinal grading to influence the transport of specimens. It is worth considering the possibility that the nature of the grain flow process, as well

as facilitating the deposition of the largest clasts at the snout (Parsons *et al*. 2001), also facilitates the preferential deposition of larger, less mobile elements to the snout. Examination of the S.T. assemblage distribution vs. element type potentially reveals such a pattern. Those elements found at the most distal portion of the S.T. deposit, where the largest clasts start to dominate the sediments, fall within Voorhies Groups II and III, and represent some of the single largest elements found in the deposit, including the largest (measuring 90mm maximum dimensions). The same pattern may be present in the T2 deposit. However, the excavation sampled the medio-distal portion of the talus and not the termination.

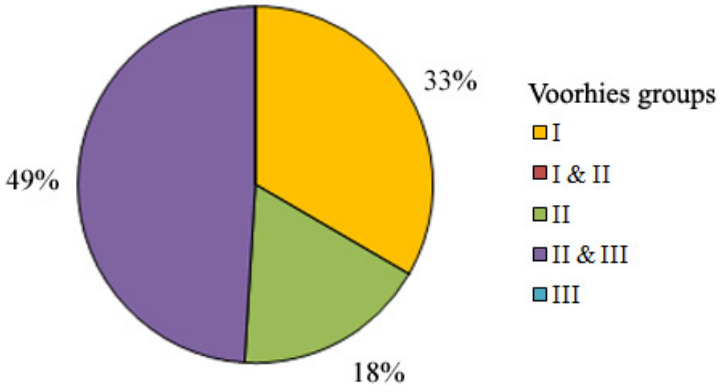


Figure 6.12 S.T. Voorhies groups.

6.1.5 Secondary Talus faunal and artefact assemblage profile

Table 6.4 presents the assemblage composition and size profile summary for the S.T. deposit. As can be seen only two artefacts were excavated from the sediments, both of which measure <20mm and would traditionally be considered small flaking debris (Andrefsky 2001). The significance of the artefacts as depositional indicators is discussed in the following section. The pattern shown in the size profile corresponds to that seen in most of the investigated deposits. Almost half the S.T. assemblage (49%) measures <30mm and just over 90% of the assemblage falls <50mm maximum dimension. Larger fossils, although poorly represented, are present within the assemblage, the largest of which measures

90mm (maximum dimension). This specimen represents a bovid hemi-mandible and is found at the most distal point of the sampled talus where the clast-supported horizon starts to dominate the sediments. The size profile of the S.T. deposit is comparable to that found in the MH1 T2 deposit where 55% of the assemblage measures <30mm maximum dimensions and a similar proportion of the assemblage is represented within in the <50mm bracket (87%). The T3 profile shows a greater spread of fossils into the larger size brackets, with 27.4% of the assemblage measuring >50mm maximum dimension (S.T. = 9.6% >50mm; T2 = 13.2% >50mm; T1 = 2.6% >50mm).

Max Length	Summary					
	Artefacts	%	Fossils	%	Total	%
<19mm	2	33.3	4	66.7	6	5.8
20-29mm	0	0.0	45	100.0	45	43.3
30-39mm	0	0.0	32	100.0	32	30.8
40-49mm	0	0.0	11	100.0	11	10.6
50-59mm	0	0.0	5	100.0	5	4.8
60-69mm	0	0.0	2	100.0	2	1.9
70-79mm	0	0.0	1	0.0	1	1.0
80-89mm	0	0.0	1	0.0	1	1.0
90-99mm	0	0.0	1	0.0	1	1.0
>100mm	0	0.0	0	0.0	0	0.0
Total	2	-	102	-	104	100.0
Total %	3.0	-	97.0	-	100.0	

Table 6.4 S.T. faunal and artefact assemblage summary and size profile.

The mean maximum dimension of fossil and artefact particles in the S.T. sediments is 33mm, with a mode of 25mm, median 30mm and a StdDev of 13.5mm. In terms of particle size data (taken from the mean value of the three axis), the mean value for the S.T. fossils and artefacts is 17.26 (maximum particle size = 45.61) with a mode of 14.4, a median of 15.6 and a StdDev of 6.3. This compares closely to the T2 assemblage in showing a mean particle size of 17.3

with a mode of 10.5 and a median of 15.8. By comparison the T3 assemblage has a mean particle size value of over 22 (mode of 15.7; median of 20.1). The size profile of the S.T. assemblage serves to illustrate the increased levels of breakage prevalent during the grain flow sedimentation processes. The condition of the assemblage prior to the S.T. phase of accumulation is unknown but it can be assumed that the physical processes active during the development of grain flow (relatively rapid surges of sediments with a broad range of sedimentological properties) cause a high level of breakage. Faunal size profiles alone cannot be used to to indicate pre-depositional assemblage condition or to imply stratigraphic associations as similar deposit accumulation processes may produce similar size profiles regardless of pre-depositional attributes. For archaeological assemblages, where breakage is less of a problem, size profiles may be correlated to source assemblages when potential sorting processes have been taken into account. In order to assess pre-depositional faunal condition, faunal, taphonomic and taxonomic analyses are required. The yield of bone, from approximately 400,000cm^3, is contained predominantly within the matrix-supported level which represents approximately half the volume of the excavated area. The S.T. fossil yield is relatively high, in comparison to the T2 assemblage which sampled an area twice as voluminous but produced half the number of fossils. The relatively high fossil yield may be a result of the funnelling processes at the opening and within the passage, concentrating the specimens.

6.1.6 Secondary Talus archaeology

As can be seen in Table 6.4, two artefacts have excavated from the S.T. deposit. Both fall into the small flaking debris category, in measuring <20mm maximum dimensions. A great deal of work has been carried out on the research potential of small flaking debris (Fladmark 1982; Stahle & Dunn 1982; Sullivan & Rozen 1985; Ahler 1989; Patterson 1990; Shott 1994; Austin 1999; Andrefsky 2001, 2006), and only a larger sample size may allow the application of these approaches. Previous to this research, analysis of small flaking debris has been used to successfully source winnowed material from the M5E Oldowan

assemblage through a secondary sedimentation process into the Name Chamber and its three talus deposits (Stratford 2008). The value of the archaeological material yielded from the S.T. deposit is, therefore, limited to its significance as a stratigraphic indicator. The use of archaeological material as a diagnostic indicator of sediment source is valid when all other sources can be ruled out. In the case of the Milner Hall, just one artefact-bearing source has been identified making the presence of artefacts within nearby deposits a diagnostic inclusion. In the MH1 T2 deposit, the presence of artefacts provided evidence supporting the stratigraphic interpretation that the majority of the deposit derived from the Name Chamber Far Western Talus prior to the stratigraphic disassociation of the deposit into two entities through mining and tourist activity. The presence of artefacts within the T1 deposit also indicated a contribution from the same source. Similarly, the presence of artefacts in the S.T. deposit regardless of quantity or size indicates at least a proportion of the sediments derive from an artefact-bearing deposit, in this case the Name Chamber Far Western Talus. The sediments from the Name Chamber Far Western Talus are currently accumulated against the large collapsed block that forms the base for the opening of the EC1 talus (see insert of Figure 6.1 for a diagram of the current deposit limits and EC1 passage location) and a previous stratigraphic association is not difficult to envisage.

Both pieces derive from the Stratum 2 sediments. The first piece found was a quartzite flake fragment (a flake which has only the medial and/or distal portions preserved) measuring 16mm maximum dimensions. The piece represents the distal termination of a flake that may have measured >30mm when complete. Quartzite, as a raw material, can only derive from the river gravels and the preferred utilisation over quartz in the M5W Early Acheulean assemblage has been interpreted as indicating a positive selection process (Kuman 1998, 2007; Field 1999). The second artefact is a piece of quartz small flaking debris (measuring 16mm maximum dimension), of similar nature to those found in abundance within the Name Chamber (Stratford 2008). The quartz appears fresh and is not obviously rolled or patinated, but this may be due to the relative hardness of quartz. It is currently unknown to what extent sediment diagenesis affects quartz and quartzite surfaces in cave environments. It is also unknown how

the re-distribution of sediments within the cave system, in a range of diagenic conditions, affects artefact condition and preservation. The absence of any larger artefacts correlates with the size profile of the Western Talus (and Far Western Talus) of the Name Chamber which shows a 91% dominance of <20mm material (Stratford 2008). One would not expect the size profile of an archaeological assemblage to be significantly affected by breakage.

6.1.7 Secondary Talus faunal analysis

A total of 102 fossils was excavated from the S.T. sediments and was analysed in the same fashion as the T2 and T3 assemblages. The taphonomic analysis was undertaken separately as slightly different goals called for a slightly different focus. The taphonomic analysis methodology is described in detail in Chapter 3. The size profile of the faunal assemblage has already been discussed in the assemblage profile. Of the 102 fossils, only one specimen (1%) was unidentifiable to element type.

Skeletal element representation

Figure 6.13 and Table 6.5 present the skeletal element representation for the S.T. deposit. Figure 6.13 presents the first level of identification and splits the body into element types. Quantifying relative body portion or element representation attempts to spot possible biases within the assemblage. In this section, the data is used to explain the biases found within the assemblage from a stratigraphic perspective, taking into account the influences of the different forms of depositional processes through multiple episodes of re-sedimentation.

Figure 6.13 shows a dominance of long bones, representing 63% of the assemblage. The relative size of long bones tends to lead to the production of a higher number of fragments per element than is seen in other smaller elements. In the MH1 T1 assemblage, long bones represent 69% of the total assemblage. T2 shows a significantly smaller proportion of long bones (41%). Irregular elements

represent the next largest component (14%), and within T2, irregular bones represent over a quarter of the assemblage and almost double the proportion of irregular bones in the S.T. deposit. Both assemblages are small and element representation should be treated with caution. The small sample sizes will allow similarities to be noted more than statistically firm conclusions to be made. If S.T. and T2 derive from the same source then the stratigraphic data will form the foundation for the association with support given by similarities in contents attributes. Based on the hypothesis that the S.T. deposit and T2 derive mostly from the Name Chamber Far Western Talus (founded on the stratigraphic data), the discrepancy in element representation may be due to a number of reasons: a) the sediments derive from different strata of the same deposit, with different element abundance; b) small differences in the distribution of fossils through the deposits during secondary deposition caused un-representative sampling; c) mixing of sediments and faunal specimens from a number of sources occurred and d) the small sample size of T2 precludes comparisons based on faunal representation.

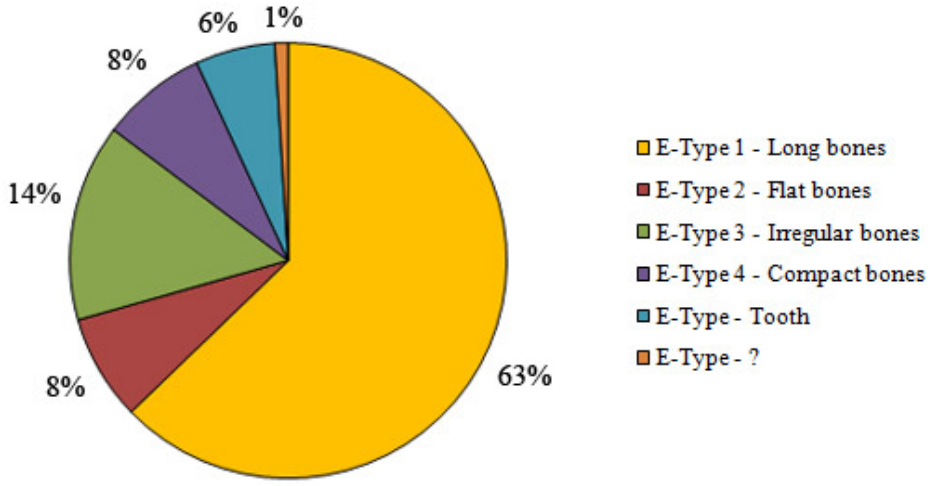


Figure 6.13 S.T. skeletal element type distribution.

Max Length	Fossils						
	Appendicular	Axial	Podial	Tooth	?	Total	%
<10mm	0	0	0	0	0	0	0
<19.9mm	2	1	0	1	0	4.0	3.9
20-29.9mm	28	9	5	2	1	45.0	44.1
30-39.9mm	22	4	4	2	0	32.0	31.4
40-49.9mm	6	2	2	1	0	11.0	10.8
50-59.9mm	4	1	0	0	0	5.0	4.9
60-69.9mm	1	1	0	0	0	2.0	2.0
70-79.9mm	1	0	0	0	0	1.0	1.0
80-89.9mm	1	0	0	0	0	1.0	1.0
90-99.9mm	0	1	0	0	0	1.0	1.0
>100mm	0	0	0	0	0	0.0	0.0
Total	65	19	11	6	1	102.0	100.0
Total %	63.7	18.6	10.8	5.9	1.0	100.0	

Table 6.5 S.T. skeletal portion distribution summary.

Bone breakage

The excavated fossils from the S.T. deposit may have travelled a significant distance from the original primary sedimentation deposit. This movement within a clast-rich matrix has led to high levels of fragmentation during re-distribution around the karst environment. Original patterns of skeletal element representation may be identified and correlated to the primary deposit through a single phase of re-sedimentation. However, within the S.T. assemblage where potentially multiple phases of re-distribution have affected the assemblage, fossil representation is harder to compare. Bone breakage data can indicate the timing of the majority of breakage but fossil completeness patterns will not be comparable to the primary deposit assemblage. Figures 6.14, 6.15 and 6.16 present the bone breakage data for the S.T. assemblage. The data demonstrate that there are very few specimens that are complete (5%; n = 5). 68% of the assemblage shows at least three broken edges with 57% showing the maximum number of breaks of four per specimen, which is by far the largest component of the assemblage. A general inverse relationship can be seen between number of breaks and representative proportion within the assemblage. Elements with a single break or less number eleven (11%). The five complete specimens are represented by two rodent tibia, a bovid

metatarsal distal epiphysis and a bovid phalanx. Apart from the microfauna fossils which can often escape fragmentation, all complete elements fall into the smaller, more compact bone elements or are teeth. In general, teeth and compact bones, such as epiphyses of long bones and phalanges, have a greater density which has been found to roughly correlate to survivorship (Lyman 1984). None of the complete fossils measures >50mm in maximum dimension. The *intensity of fragmentation* (Lyman 1994) for the S.T. assemblage is inappropriate for the demonstration of fragmentation level. The mean maximum dimension of the non-complete specimens within the assemblage is greater (33mm) than the mean maximum dimension of the complete elements (29mm). The same trend that was found in the T1 identifiable component and in T2 is found in the S.T. deposit in that the complete elements possess a lower mean maximum dimension than the fragmented specimens. The high degree of fragmentation is adequately demonstrated by the proportions of break numbers. Simply put, larger, more complete, bones have been broken into fragments (with increased number of breakage surfaces) in all three deposits. All three of the deposits showing this trend have been accumulated by rapid forceful sediment gravity flow types, which have evidently played a significant role in the fragmentation of different bone types.

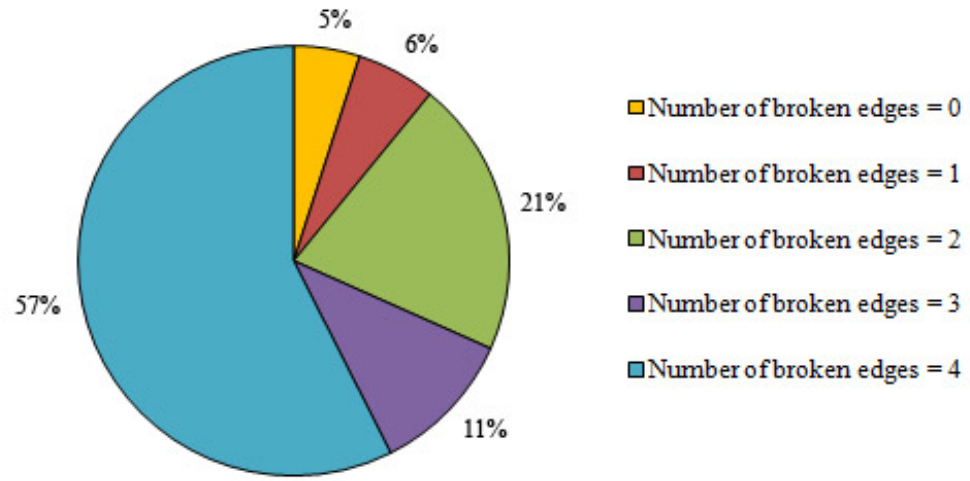


Figure 6.14 S.T. numbers of broken edges on fossil material.

Figure 6.15 presents the break type proportions for the S.T. assemblage. There is a clear dominance of those elements showing only sawtooth break surface textures (58%; n = 56) and the total number of elements showing at least one sawtooth break surface textures numbers 71 (69%). In contrast, the number of elements showing only 'greenstick' fractures is 15 (16%) and the number of elements showing at least one 'greenstick' fracture is 31 (30%). Relatively few elements show the step break surface texture and 23% of the assemblage shows a combination of break types. The fracture type data suggests a significant amount of breakage occurred post-fossilisation during the re-distribution of sediments through multiple stages. Despite the fact that the largest proportion of break types is typical of post-fossilisation bone fracture, it is impossible to say that post-fossilisation breakage has had the greatest influence over the element size. It is only possible to say that post-fossilisation breakage has contributed heavily to the current state of the bone in the S.T. deposit. It can also be suggested that from the number of greenstick fractures that at least 30% of the elements had suffered some level of breakage when the bone was fresh probably during the primary deposition.

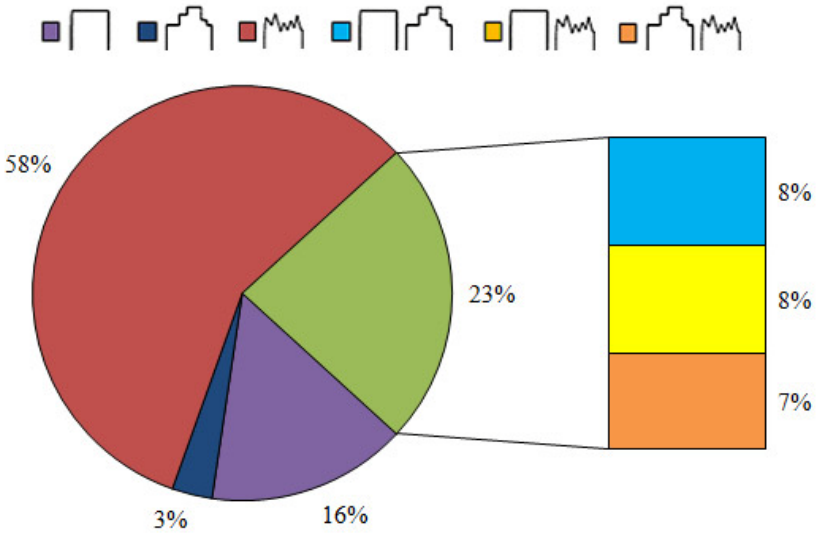


Figure 6.15 S.T. bone fracture types. The green slice represents the proportion of bones with a combination of fracture types.

The fracture angle data presented in Figure 6.16 show the majority of elements (67%; n = 65) has a combination of fracture angles. This is to be expected when different episodes of deposition and fragmentation occur throughout the diagenesis of the bone. Of those elements showing a single type of fracture angle, obtuse elements dominate, representing 17% (n = 16) of the assemblage. In total 35 elements (34%) show at least one obtuse fracture. 59% (n = 61) of the assemblage show at least one perpendicular break with only 12% (n = 12) of the fossils showing only perpendicular breaks. The fracture angle pattern supported the episodic breakage pattern indicated in the fracture type data, with a strong early depositional breakage signal followed by a large quantity of post-fossilisation breakage through re-sedimentation episodes. Of particular interest is the difference between the S.T. breakage data and the T2 breakage data. Both assemblages have developed through similar sediment distribution processes and yet have quite different breakage profiles. One would expect that during multiple re-sedimentation episodes the proportion of combination breaks would increase as breakage is inflicted on the bone during its mobilisation and diagenesis, up to a point when progressive post-fossilisation breakages start to replace all preceding breakage evidence. In the T2 deposit, the dominance of greenstick and perpendicular breaks, representative of early breakage, has been preserved to a far greater extent than in the S.T. assemblage.

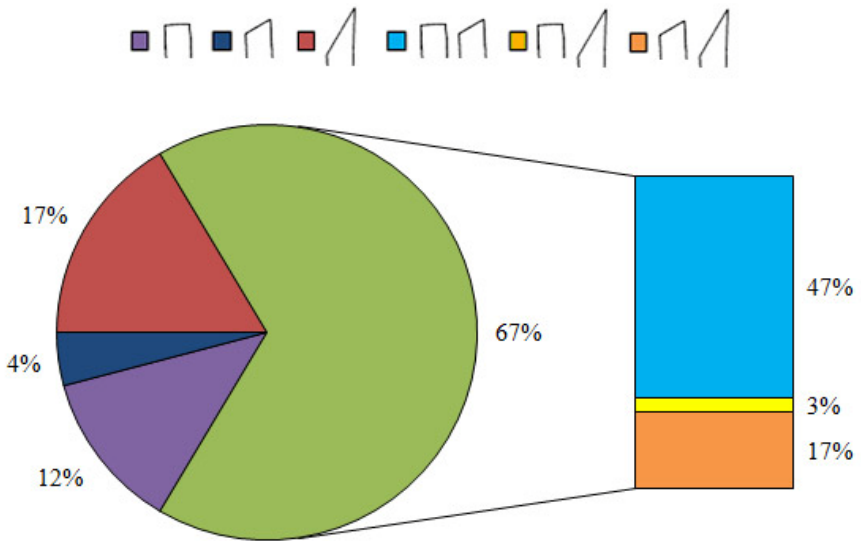


Figure 6.16 S.T. bone fracture angles. The green slice represents the proportion of bones with a combination of fracture angles.

Bone condition

The bone condition data for the S.T. fauna is shown in Figure 6.17. It is clear that the general condition of the bone is good with 83% (n = 85%) of the assemblage classed as either fresh or slightly weathered (equivalent to Behrensmeyer's stages 0, 1, 2 and 3). 79% of the assemblage can be classed within weathering stages o and 1. One specimen is classed as very weathered and 12% (n = 12) can be classed as weathered. Four elements are of indeterminate condition because the majority of the cortical surface is covered in calcified sediment. In a similar way to the T2 deposit, post-depositional bone surface weathering seems to have affected the bone surface to a small degree, preserving the condition of the bone despite multiple re-sedimentation phases and heavier breakage levels. According to Behrensmeyer, bones classes within stages 0-1 could have been exposed on the landscape for between 0-3 years before deposition. These timings are influenced greatly by climate and ecology as indicated by Behrensmeyer (1978). Bearing in mind the recognised issues with the tempo at which the weathering processes work, it is prudent to suggest that the S.T. assemblage, dominated by fresh bones,

was deposited quickly into the cave in a fresh condition and then fossilised prior to the attritional affects of re-distribution.

No work has yet been carried out investigating the relationship between fossil movement in karst environments, bone breakage and associated surface condition preservation. The proportion of heavily broken bones in a fresh condition does suggest that post-depositional movement does not necessarily advance bone surface weathering and attrition. It may be that certain karst environments (probably dryer conditions, e.g. S.T. sediments) inflict breakage but little or no change in bone surface condition. The S.T. bone surface condition proportions do show a similar pattern to T2, and may be representative of the primary source deposit. The Name Chamber, T2 and the S.T. assemblages have accumulated by dry grain flow processes with limited water exposure. The presence of a large proportion of fresh breakages would fit with the proposed accumulation of the M5E Oldowan assemblage which has been interpreted by T. Pickering (1999) to have entered the cave via a death-trap scenario, capturing much of the bone in a fresh condition. Both T2 and the S.T. assemblages do show a proportion of weathered elements that may represent specimens entering the cave via slope-wash, exposing those bones for a longer time on the surface. Alternatively, the weathered elements may represent a small proportion of bones that have been exposed to more intense sub-surface weathering processes, such as localised pooling of fresh water.

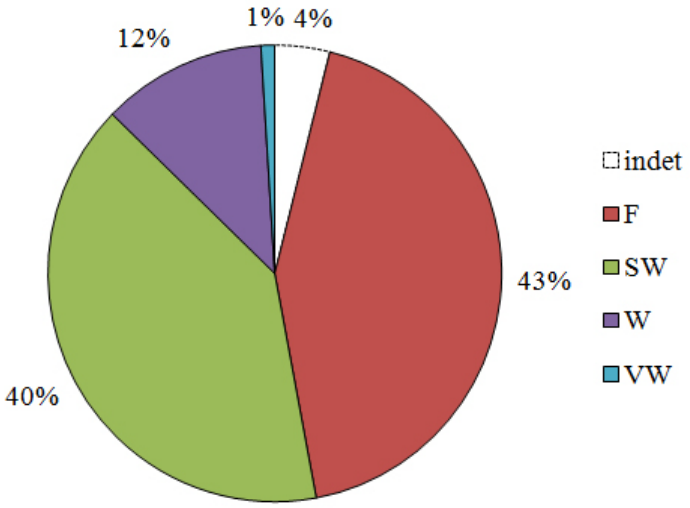


Figure 6.17 S.T. bone condition.

6.1.8 Secondary Talus taxonomy

In the S.T. assemblage only two species could be identified, a small Felid, *Carcacal caracal* and a large Felid *Panthera leo. Caracal caracal* has been found in the T1 and T3 deposits in the MH1 site and its significance has been discussed in the T1 taxonomy section. At Sterkfontein *Panthera leo* has been found in M5E (O'Regan 2007), M4 (Turner 1997; O'Regan & Reynolds 2009), possibly in M2 (T. Pickering *et al*. 2004a) but absent from the Lincoln Cave deposits (Reynolds *et al*. 2007). *Panthera leo,* has been found at a number of Cradle sites, including Coopers D (Berger *et al*. 2003), Swartkrans Member 1 (Brain 1993) Member 2 (Brain 1981) and Kromdraai A (Brain 1981). *Panthera leo* is found in a broad temporal range of deposits, making them uninformative as an environmental indicating species but does, on the basis of presence or absence in other deposits, allow suggestion of possibly associated deposits. *Panthera leo* is predominantly a nocturnal hunter with a wide habitat tolerance but are generally not found in forested areas. The most important environmental requisite for *Panthera leo* is an ample food supply in the form of medium to large Bovidae and access to shaded areas (Skinner & Chimimba 2005). They are generally found hunting in more open grasslands where prey species concentrate (K. Stratford Pers. Comm.).

Only one bovid specimen was identifiable to species, *Oreotragus* (commonly called the Klipspringer) and two specimens were identifiable to family level. *Oreotragus* are small (size class one) diurnal bovids that inhabit cliff faces and rocky outcrops and use them for shelter and sleeping. *Oreotragus* constitute the prey species to leopard (*Panthera pardus*), *Caracal caracal*, baboon (*Papio anubis*) and black eagles (*Ictinaetus malayensis*) (Skinner & Chimimba 2005). All these species are well represented in the Cradle area. The presence of *Oreotragus* is not surprising in assemblages accumulated by well known local carnivore species but also habitat rocky outcrops (near the cave openings) that may make them susceptible to accidental deaths. Without displaying diagnostic carnivore damage and a larger sample, no conclusions can be made as to the cause of death. At Sterkfontein *Oreotragus* appears in M5E (Vrba 1976) and M4 (Vrba 1976). In de Ruiter *et al.'s* work (2008) they suggest *Oreotragus* be associated with woodland environments. *Oreotragus* is found at a number of Cradle cave sites including Drimolen (Keyser *et al*. 2000), Malapa (Dirks *et al*. 2010) Motsetse (Berger & Lacruz 2003), Swartkrans Lower Bank, Hanging Remnant, Member 2 and Member 3 (Vrba 1976).

6.1.9 Secondary Talus taphonomy

The bone breakage data for the S.T. assemblage indicates that the integrity of the assemblage is mixed. On one hand the bones show extensive post-fossilisation breakage, removing primary breakage patterns, leaving only a small residual primary signal. On the other hand the surface clarity is good with over 55% of the assemblage possessing 100% surface clarity making recognition of bone surface damage more possible. Table 6.6 presents the skeletal element representation within the bovid size classes. It can be seen that most bovids are only represented by occasional elements, including three skull pieces from three different families of bovid. Size class two bovids are represented by the largest number and broadest range of elements representing axial, appendicular and podial elements. The small sample size only allows an MNI of one for all bovids. There is a general dominance of smaller size class two or smaller bovids. Inter-deposit comparisons

are difficult in small and heavily fragmented assemblages but one could suggest a tentative correlation with T2, in that size class two bovids are most abundant in number of elements and range of element types represented. T3, by comparison shows a dominance of size class three bovids. The presence of species associated with different habitats most likely represents time-averaging caused in the primary sedimentation deposit or by the mixing of sediments during re-sedimentation. Their presence cannot be considered a sound palaeoenvironmental indication. In terms of bone surface modification there is a general dearth in carnivore damage, with one specimen showing a tooth pit and another showing rodent gnawing damage. The general condition of the bone surface is good implying that preservation of carnivore damage wouldn't necessarily have been removed. The absence of biogenically modified bone does suggest a minimal influence of carnivores on the accumulation of the fauna. Non-biogenic surface modification includes minor striations and abrasion damage preserved on the edges of three pieces. Natural abrasion and attrition of specimens is to be expected given the distance of the deposit from the possible source within the M5E deposit.

Skeletal part	*Oreotragus*	Antilopini	Size 1	Small Alcelaphini	Size 2	Size 3
Skull	1/1/1	2/1/1		1/1/1		
Cervical						1/1/1
Lumbar						1/1/1
Indet. vertebra					1/1/1	
Rib			2/1/1		1/1/1	
Humerus					1/1/1	
Radius			1/1/1		1/1/1	
Metacarpal			1/1/1		2/1/1	
Innominate					2/2/1	
Femur					1/1/1	
Tibia					1/1/1	
Navicular-cuboid						1/1/1
Phalanx II						1/1/1
Upper LBS					4/2/1	
Intermediate LBS					5/3/1	
Metapodial			2/2/1			

Table 6.6 S.T. skeletal element representation of bovid taxa. NISP/MNE/MNI data is given for each cell in columns two through seven. LBS: Long Bone Shaft.

6.1.10 Secondary Talus discussions

The S.T. deposit represents a secondary sedimentation deposit formed from two surges in dry sediments into the EC1 Lower Passage. The first surge, Stratum 1, deposited a large quantity of fossil and artefact-bearing material directly onto the consolidated sediments of the Primary Talus. The grain flow developed in a typical fashion with a basal clast-supported level suspending the matrix-supported finer sediments. The second, lesser surge, Stratum 2, accumulated shortly afterwards onto an unconsolidated Stratum 1 surface. Stratum 1 and 2 both represent dry grain flow sediment surges from the same source deposit as indicated by the homogeneity of the sediment properties and contents throughout the deposit. The surges derive from the over-steepening and collapse within the source deposit. The XRF analysis indicates the S.T. sediments have remained

uncalcified throughout the history of deposition. An absence of significant quantities of water has protected the sediments from extensive diagenic modification and so can be considered in a similar condition to the source deposit. A lack of water has also restricted the settling of the deposit and the development of an inverse grading pattern, a feature found in many grain flow deposits including T2. Most features of the S.T. sediments including particle shape profile, particle size profile, breakage extent and breakage types correspond closely to the T2 deposit. The sharing of these features is a result of the analogous depositional processes responsible for the accumulation of both deposits. Suggesting a single source deposit for both assemblages, based only on features that are heavily affected by each sedimentation phase is problematic. Those features that are not influenced by the sedimentation process include skeletal element representation (in a suitably representative sample), species representation, bone surface condition and modification and artefact representation. The uncalcified condition of the sediment is significant when considering the heavily calcified nature of the next most proximal deposit, M2. When these features are considered, correlations can be proposed between the S.T. deposit and the M5E deposit, the Name Chamber and by mutual association the T2 deposit. The stratigraphic proximity of the Far Western Talus to the EC1 passage opening supports the probability of a previous connection before the stratigraphic association was cut by the mining and the tourist route development. The discrepancies seen between the T2 and S.T. deposits do suggest the two deposits may not derive from contemporaneous surges originating within the Far Western Talus but may represent different surges containing different material relating to different areas of the same primary source, M5E. The commencement of mining at the junction of the EC1 passage and Far Western Talus would have broken this connection and re-distributed the sediments down the MH1 slope contributing to the developing T1 deposit.

6.2 Primary Talus

The Primary Talus (P.T.) represents the infilling episode directly preceding the deposition of the Secondary Talus. The abrupt nature of the transition from the

Primary Talus to the Secondary Talus indicates the sediments are not mixed and the two represent distinct infilling events into the same receptacle. As described in the introduction to the EC1 site, the P.T. deposit yielded no fauna or artefacts. The absence of faunal or archaeological material can be considered significant, and contrasts the other externally derived deposits studies here. The dearth of fauna and artefacts is stratigraphically significant and does provide an indication of the possible source deposit. The lack of fauna or artefacts does, however, limit the potential to conduct comparative analysis between the P.T. and other deposits which are known predominantly through their faunal or archaeological composition (e.g. M4, M5). The EC1 slope profile and the stratigraphic profile of the eastern excavation wall can be found in Figures 6.2 and 6.4. The shape and random orientation of the clasts within the deposit also prohibited the use of formal fabric analysis. This is not considered a problem, however, given the obvious and restricted avenue of deposition for the sediments in that they have been deposited down the same narrow passage as the S.T. sediments. Of key importance, given the absence comparative material, is the identification of possible source deposit(s). The sedimentological analysis is considered to be sufficient when combined with the wealth of stratigraphic information available. Only two quadrants ($50cm^2$) were excavated and sampled the Primary Talus. Quads B and D (See Figure 3.2 for excavation plan) were chosen as initial sampling points for the P.T. sediments. When the deposit proved to be sterile of fauna and artefacts, and the yielded stratigraphic information was considered to be representative of the deposit, excavations were halted. Time constraints during the excavation phase of this research prevented a re-sampling of the deposit to determine the vertical boundaries. However, the P.T. deposit is considered the basal deposit of this site based on the internal stratigraphy of the deposit, which is discussed in the following section. Quads A and C were left as a witness section and representative of the P.T. surface.

6.2.1 Primary Talus stratigraphy

Upon first discovery of the P.T. surface approximately 46cm below the surface of the S.T. deposit, the contact was considered to be a very large slab of fallen chert or dolomite such was the hardness of the surface sediments. The extent of consolidation of the surface of the P.T. deposit suggests a long period of time may have separated the end of deposition of the Primary Talus and the commencement of deposition of the Secondary Talus. There is also a noticeable absence of any particles between the highly consolidated surface and the clast-rich basal S.T. strata. Figure 6.18 shows the exposed surface of the Primary Talus. Although the sediments of the P.T. surface are highly consolidated, they are 'soft' in that they are not cemented by calcium carbonate. The condition of the sediments is described in the XRF section. What is immediately noticeable is how flat and smooth the P.T. surface is (0° gradient transverse to flow direction). The smooth, highly consolidated fine sediments, with no transverse gradient, capping a clast-rich deposit, and a lack of loose sediment at the deposit contact all imply the role of water in the development of the surface. This suit of features suggests it represents an erosion surface. The prolonged washing of sheets of water through the passage would account for the deposition of fines into the uneven clast-rich upper surface and the compaction of upper surface fines. The absence of micro-laminations is a result of the predominantly erosionary process instead of a depositional process. The focussed movement of water through the passage would fit with the undercutting by water of the false floors when they originally overlaid the P.T deposit.

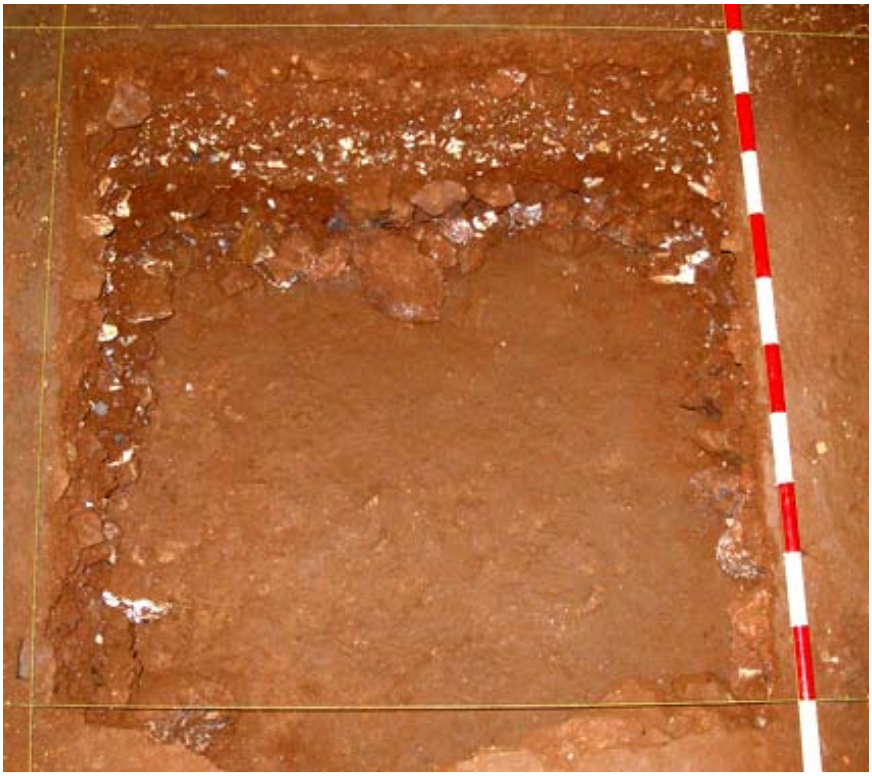


Figure 6.18 P.T. exposed surface. Notice the absence of transitional horizon and consolidated nature of the P.T. surface. The range staff segments measure 10cm.

The exposed surface of the P.T. slope shows a much lower angle of repose than is found in the above S.T. deposit. At the excavation point the P.T. deposit surface dips at only 19° with the slope direction determined by the narrow nature of the feeding passage, in exactly the same way as the above deposit. The low angle of repose found in the P.T. deposit is most likely to be due to the sampling point of the excavation. The excavation into the Primary Talus has sampled the distal-terminal portion of the talus, where the sediments are spreading and shallowing at the snout of the deposit. The morphological attributes of the receptacle, which have affected the shape and flow of the P.T. sediments, are identical to those affecting the S.T. deposit in that a long (20m), narrow, steep passage has concentrated the sediment accumulation until the passage exit, where the sediments abruptly spread into a fan shape preferentially flowing to the south, following the shape of the receptacle. A detailed description of the process has been discussed in Section 6.1 and illustrated in Figure 6.2. The relatively small

amount of the exposed P.T. surface limits the assessment of the original slope morphology. In the future, small test pits would ideally be excavated into the medial and proximal portions of the slope to compare the morphologies of the S.T. and P.T. deposits. Barring erosive episodes modifying the P.T. deposit surface, which are not indicated in the sediments, the medial slope morphology should be consistent with that seen in the S.T. deposit and fit within the approximate 35° angle of repose proposed for loosely consolidated, sand to gravel-supported fabrics (Ward 1945; Chandler 1973). This angle is mimicked in the False Floor 2 surface morphology. What is unknown is the shape of the basal receptacle into which the S.T. developed. If the passage base is flat then the P.T. has built in much the same fashion to the T3 deposit with an increasing gradient from the flat basal strata. If the passage base is, on the other hand, sloped then this will affect the internal stratigraphy of the developing P.T. talus. Only by exposing the passage base would this be clarified as no internal stratigraphy was obvious.

Figure 6.19 shows the stratigraphic profile of the P.T. deposit eastern wall. Some of the interesting inclusions have been indicated in the figure. It can be seen from the profile that the sediments of the P.T. represent a single massive matrix and a single depositional facies. The facies, named *Facies 0,* constitutes the basal and first facies of the EC1 talus. The facies is described below:

Facies 0 - Reddish brown (5YR 4/3) consolidated, poorly graded, matrix-supported diamicton. Matrix is made up of partially decalcified, partially crushed sandy loam sediments. Clasts range in size from 10mm to 100mm (maximum dimensions) and are made up of fractured blocks of dolomite, chert, mudstone and travertine. Several travertine forms are represented and flowstone forms frequently have adhering calcified sediment of the same sedimentological nature as the surrounding matrix. Breccia blocks representing a different sediment colour are also present, and these are well rounded and non-fossiliferous. Clasts are angular to sub-angular with rounded, battered edges, and these are orientated randomly throughout the deposit and are often directly associated or imbricated. Large quantities of small (10mm max dimensions) chert fragments are found

throughout the interstitial areas. Very little to no void space remains. At the base of the excavation a number of very large dolomite clasts (≥300mm maximum dimensions) was found.

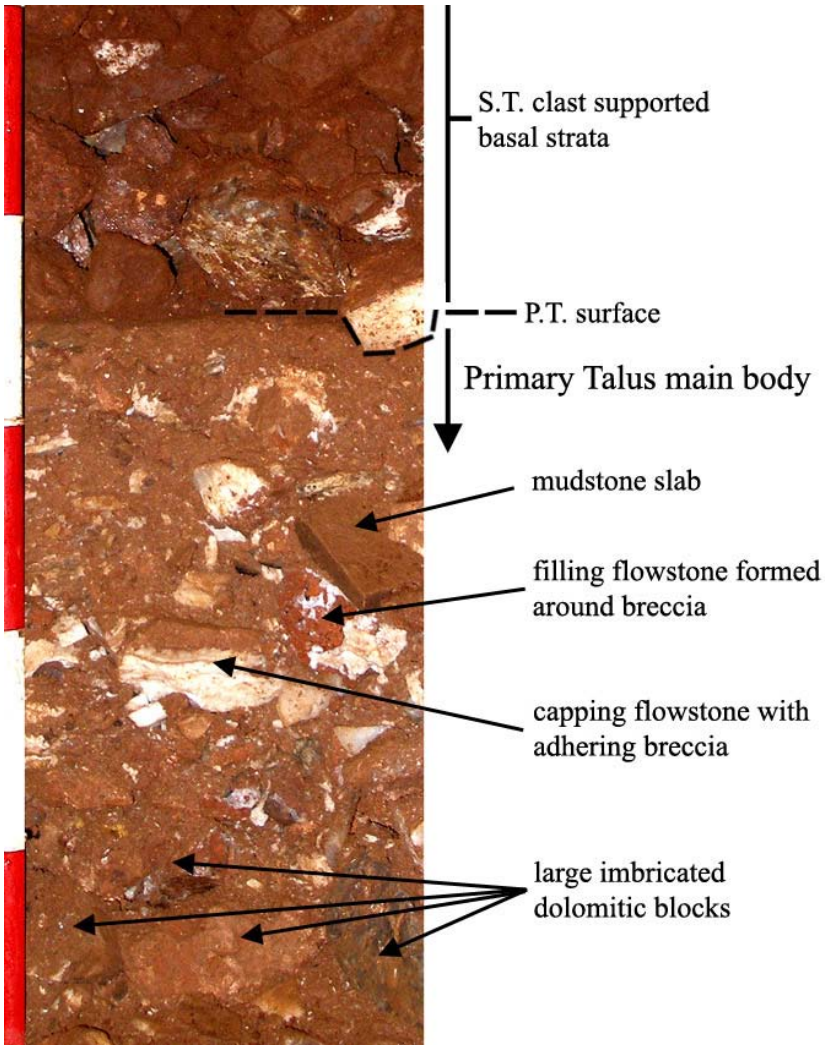


Figure 6.19 P.T. eastern wall excavation profile. Some of the features present in the sediments are indicated. The range stick segments measure 10cm.

The stratigraphic profile of the excavated P.T. eastern wall shows a number of noteworthy features which indicates the process of accumulation of the sediments and the condition of the sediment source. Firstly, no internal bedding structure is evident within the P.T. deposit suggesting the sediments accumulated in a single

surge event, mixing the clasts and creating a poorly graded, jumbled deposit. The influence of water as the main sedimentation medium is unlikely given the dryness of the sediments and the relative quantity of remaining original $CaCO_3$ deposits, which, in a water driven sediment flow (such as a hyperconcentrated flow or debris flow) may have suffered a noticeable level of dissolution damage. The preservation of calcified mudstone also suggests an absence of water during the deposition of the P.T deposit, with the major water interaction being an erosive process after deposition had stopped. This water movement through the passage created the present surface of the P.T. deposit. An absence of water involved in the accumulation of the P.T. deposit, indicates the sediment flow process was similar to that of the subsequent deposit, mainly a dry grain sediment gravity flow caused by a single collapse surge event, through the collapse or over-steepening of the source deposit. The high fragmentation of clasts and battering found on the edges of the deeper clasts indicates a rapid and turbulent accumulation, reducing the clasts to a sub-angular shape and producing large quantities of small chert fragments. In a similar manner to the S.T. facies, post-depositional water interaction also seems to have had little or no affect on the sediments and is probably a result of the shelter the passage has afforded on the sediments. From an observational perspective, the sediments contained within the P.T. are much dryer than the upper, S.T. facies. This is confirmed in the sedimentological analysis which is presented in the following section.

Despite the similarities in location and accumulating processes, there are significant differences between the S.T. facies and the P.T. facies. These differences will be discussed in turn and correlated to the stratigraphic indicators found in *Facies 0*. The absence of a faunal or archaeological component for inter-deposit comparative analyses necessitates the comprehensive analysis of the stratigraphic indicators available.

The presence of multiple forms of travertine (seen in the P.T. sediments in Figure 6.19), including broken stalactite and two forms of flowstone, attest to a collapse event supplying the majority of the *Facies 0* sediments. There are several pieces of capping flowstone in the *Facies 0* sediments. Some have calcified sediment

adhering to the upper surface suggesting the capping flowstone was sandwiched between two calcified sediment bodies and did not necessarily derive from the surface of a deposit. Capping flowstones are most likely to form on the top of a talus slope during a depositional hiatus. These forms are important as stratigraphic boundary indicators and subsequently form the basis for most speleothem-based dating techniques. Capping flowstones take the form of the underlying morphology of the talus slope, with the upper surface morphology being dictated by the flow of the $CaCO_3$, usually forming flat, laminated forms with smooth upper surface or occasionally more bulbous surface morphology (Pers. Obs.). The second type of flowstone represented in the *Facies 0* sediments is the filling flowstone. Filling flowstones can form in cracks and faults at any point in time depending on the formation of the fault and localised speleothem activity. It follows that recognition of the filling flowstone form is of the utmost importance if the speleothem in question is going to be considered for dating. Filling flowstones take the form of the fault or crack that they are infiltrating. They are commonly found filling interstitial pockets, but can form in cracks, holes and around clasts within breccia. They can also fill horizontal or vertical cracks that have resulted in the collapse of a body of breccia. The formation of filling flowstone around clasts but within hard breccia must postdate the deposition of the sediments (Latham 1999). In longitudinally extensive filling flowstones the internal laminations often butt up against changes in the morphology of the fault/crack and they often have no smooth upper surface. From a profile view, filling flowstones are relatively easily identified. The two flowstone forms mentioned above are not mutually exclusive and either form can develop from one another depending on the topography and nature of the receptacle. For example, a filling flowstone may develop through a fault and into a chamber, it then continues to form and caps whatever it develops over, in a typical capping flowstone form. Flowstones should be traced so that their origin can be clarified before dating is carried out. Both forms of flowstone are represented within the P.T. deposit and suggest that the material supplying the deposit derived from one or more heavily calcified deposits rich in speleothem growth and documenting a number of depositional episodes and possible faulting events.

The presence of two differently coloured calcified sediments in a single deposit can be interpreted as either representing a mix of sediment sources, or a mix of facies from a single source. Unfortunately, a lack of time precluded the analysis of the alternate breccia type. What can be said is that the alternate calcified sediment breccia blocks represent a minor contributor to the sediments. Most of the breccia blocks (80%) are breaking down and decalcifying *in situ*, filling the interstitial areas of the fabric with identical sediments. The very low void space throughout the P.T. deposit attests to the extended period of *in situ* breakdown and decalcification of the calcified sediments.

Facies 0 also contains large (60mm) pieces of calcified mudstone, a feature that has not been found in any of the other investigated deposits. Mudstone is created from the accumulation of fine particles (silts and clays) via slope wash. Mudstone can be found on and in a number of deposits in Sterkfontein, it is usually formed and found in primary sedimentation deposits where a direct connection to the surface has facilitated the accumulation of fine allogenic particles through slope wash. The proximity to an active opening is required to generate the abrupt deposition of the fines in single wash episodes. These mud horizons are then calcified. In secondary sedimentation deposits accumulated by water erosion, mudstone is the first sedimentary feature to be dissolved, fractured and mixed with the other sediments, effectively dispersing the deposited mud. Mudstone remnants survive more often in secondary deposits accumulated by dry sediment gravity flows and collapses. Increasing levels of aggressive accumulation rapidly break mudstone pieces down into small rounded fragments, which is the most common form found. The preservation of larger, slab or tabular-form mudstone suggests a restricted re-sedimentation distance, or a relatively gentle re-sedimentation process. Most of the sedimentary evidence suggests the accumulation of the P.T deposit was a particularly localised rapid, probably aggressive accumulation process. Therefore, it can be suggested that the presence of fractured but angular slab-form mudstone, indicates that the source of the P.T. sediments was probably a primary sedimentation deposit in close proximity to the current P.T. sediments.

The presence of many large, imbricated dolomite and chert blocks at the base of the P.T. excavation most likely represents the transition and surface level of the clast-rich basal strata often found in grain flow deposits (Hétu *et al.* 1995; Bertran *et al.* 1997). The same feature is seen at the base of the Secondary Talus. In the case of the P.T. the interstitial spaces have been filled through *in situ* decalcification and breakdown of breccia blocks as discussed above, the filling process has not, however, created an inversely graded deposit, as is regularly seen in grain flow deposits (Bertran & Texier 1999).

6.2.2 Primary Talus sedimentology

The lack of faunal particles within the P.T. sediments places the analytical emphasis on the sedimentological data in order to provide as much detail as possible on the condition and nature of the source deposits. Table 6.7 presents the sedimentological summary for the two samples taken. The data presented were yielded from samples that were taken from 10cm below the talus surface and 30cm below the talus surface from the eastern wall of the excavation. The P.T. deposit is considered to be homogeneous and reflects a single facies. For this reason, only two samples were processed to minimise cost and processing time. The remaining samples are available if more detailed analysis is deemed necessary. The two samples chosen represent both a shallow level and the deepest point of the excavation. Any intra-deposit trends should be identifiable from these relatively distance sampling points.

				Particle Size		
Art No.	**Sample location**	**Munsell**	**Hydrology %**	**% Clay (<2µm)**	**% Silt (2µm - 63µm)**	**% Sand (> 63µm)**
215	Facies 0 - 10 cm	5 YR 4/3	2.31	3.489	38.591	57.92
217	Facies 0 - 30 cm	5 YR 4/3	3.70	4.086	37.168	58.747

Table 6.7 EC1 Primary Talus sedimentological summary. Depths are taken relative to the deposit surface.

The summary data supports the stratigraphic observations, in that the deposit is homogeneous in particle size distribution and hydrology. The relative proportions of particle size class and water content change by less than 1% between sample points. What is noteworthy is the general dryness of the sediments. The relatively low sediment moisture content is most likely due to the low water retention potential of sandy sediments (Brady 1999). The proportions of the particle size classes are markedly different to the other investigated deposits. The particle size distribution curves will be discussed in the following section. It is clear, however, that there is very little change with depth in the proportions of size class, indicating an absence of, or negligible level of sediment sorting. The sediments of *Facies 0* have settled into their current state and unless the sediments are re-distributed through erosion or collapse the grading pattern will remain the same. The *Facies 0* sorting pattern, or lack of, is unlike the S.T. deposit, where the regular grading system would most likely change during the settling of sediments through the interstitial areas creating an inverse system. *Facies 0* is unlike the MH1 T2 deposit, where the settling process is ongoing but has resulted in an inversely graded facies. *Facies 0* also contains the smallest proportion of clay found in the local deposits (3.5%) and by a significant amount the highest proportion of sand (58%).

XRF

Table 6.8 presents the results of the XRF analysis. A single sample was processed due to the homogeneity of the deposit, this sample was taken from the sedimentological sample at the base of the excavation 30cm below the P.T. surface. The chemical composition of the sediments are significantly different to all the other investigated deposits. Chi^2 analysis on the relative proportions within the deposits shows that $p = 0.000$ for all deposits when compared to *Facies 0*. The discrepancies are found within all the chemicals tested, most of the minor contributors (Al_2O_3, FeO, Fe_2O_3, Na_2O, K_2O, TiO_2, P_2O_5) represent less than half the respective proportions in the P.T. deposit. Cr_2O_3, on the other hand represents double the quantity found in any of the other deposits. The most significant

differences can be found in the proportions of silica and calcium. The silica proportion represents less than half the quantity found in the other deposits (30.74% vs. 75% mean for the other investigated deposits). In contrast, there is almost ten times the calcium in *Facies 0* when compared to the mean calcium proportions in the other investigated deposits (58.97% vs. 6.95% mean for the other investigated deposits). The *Facies 0* sediments are clearly allogenic but the sediments have been heavily modified by the diagenic processes of calcification. The excavated sediments, although now 'soft', derive from a heavily calcified source. Interestingly, the calcium content of the *Facies 0* sediments is higher than the 'hard' breccia of certain parts of M4. Samples taken from both the red and brown breccia show a broad range of calcium contents, ranging from 33% to 75% in Member 4 brown breccia and between 47% and 55% in the red breccia (M. Sutton *in progress*). Within the Silberberg Grotto M2 sediments, the calcium contents range between 23% and 49% across 18 samples (M. Sutton, in progress). It can be seen that even within those sediments considered to be heavily calcified the calcium content can vary greatly, suggesting level of calcification is dependent on localised calcium carbonate deposition. It can be suggested from the high level of calcium still in the P.T. sediments that a combination of diagenic processes is taking place. Firstly, during the development of the P.T. deposit the breccia blocks tumbled down the slope and broke down into finer grains. These finer grains have remained calcified during the deposition and settling of the deposit. Secondly, de-calcification has further broken the blocks down but not yet leached out the calcium from the sediments. The lack of progress of the *in situ* decalcification process is no doubt influenced by the general lack of water in the vicinity and the lack of water holding potential of the sediments themselves.

SiO2	Fe2O3	FeO	MnO	MgO	CaO
30.74	0.25	1.95	0.45	1.86	58.97

TOTAL
99.98

Al2O3	Na2O	K2O	TiO2	P2O5	Cr2O3	NiO
3.64	0.04	0.31	0.27	1.49	0.0040	0.0020

Table 6.8 EC1 Primary Talus XRF result.

Particle size

Figure 6.20 presents the particle size distribution of the EC1 P.T. sediments. Figure 6.21 presents the combined particle size distribution curves for both samples on the same axis. As can be seen, both levels of the deposit show a similar dominance of the larger grains (sand), and a corresponding decrease in silts and finally a small proportion of clays. The graphs do not show any distinct grading pattern within the P.T. deposit. When a closer look is taken at the relative volumes of the constituent Gaussian curves (Table 6.9), which allow a greater resolution on the distribution of particle size, there are clear differences between the two samples. The greatest difference can be found in the distribution of the larger particles, namely within the sand-sized class. The upper sample shows that 21% of the particles fall into the largest of the sand-sized range (coarse sand, >1000µm). Coarse sand particles measuring >1000µm are almost missing from the lower sample (0.02%), with the majority of large particles represented by medium to fine sands measuring between 300µm and 500µm. The absence of the largest sand-sized particles in the lower sediments perhaps indicates a very slight filtration pattern occurring within the sediments, with the smaller sand grains moving down through the sediments during the breakdown of breccia blocks, leaving the largest sand grains in the upper part of the deposit. The Chi^2 statistical comparison of the area occupied by the de-convoluted curves on each sample show that the two distributions are significantly different ($p = 0.000$). The de-convoluted curves for all samples are presented in Appendix 2.

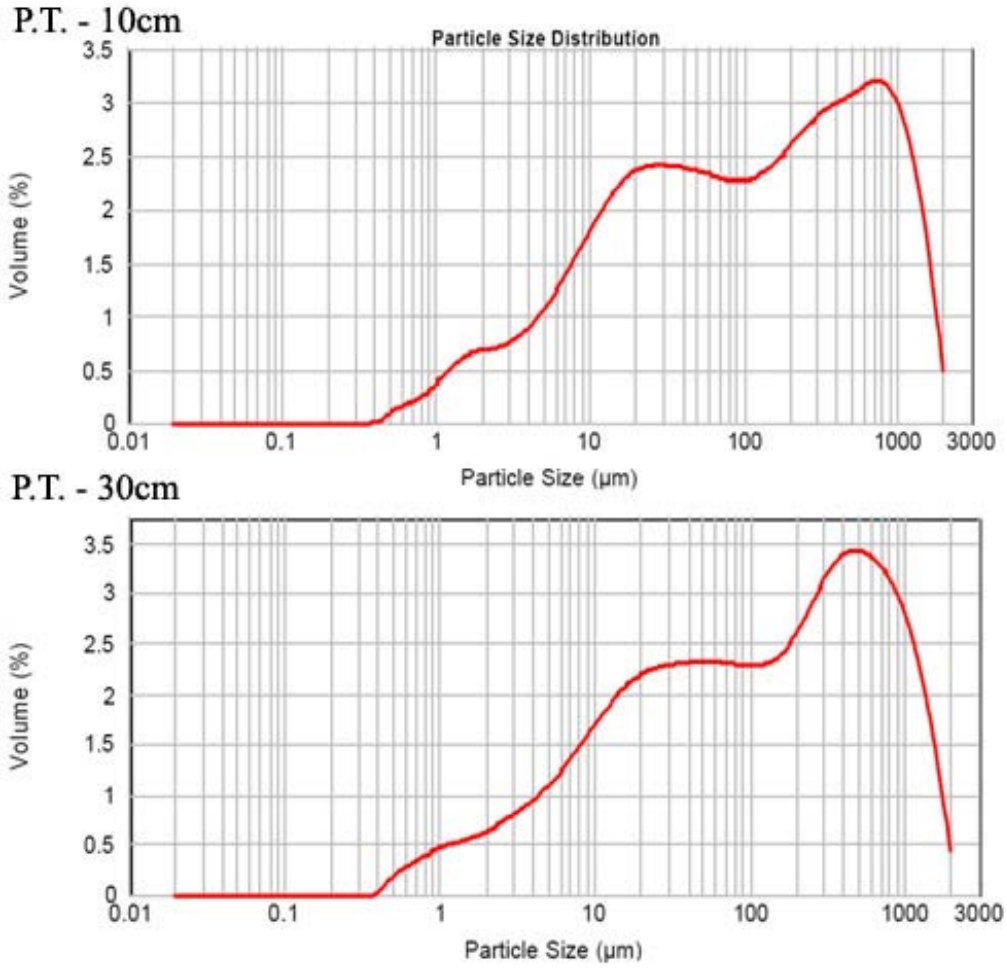


Figure 6.20 P.T. particle size distribution curves for two samples taken at top of the deposit and base of the excavation.

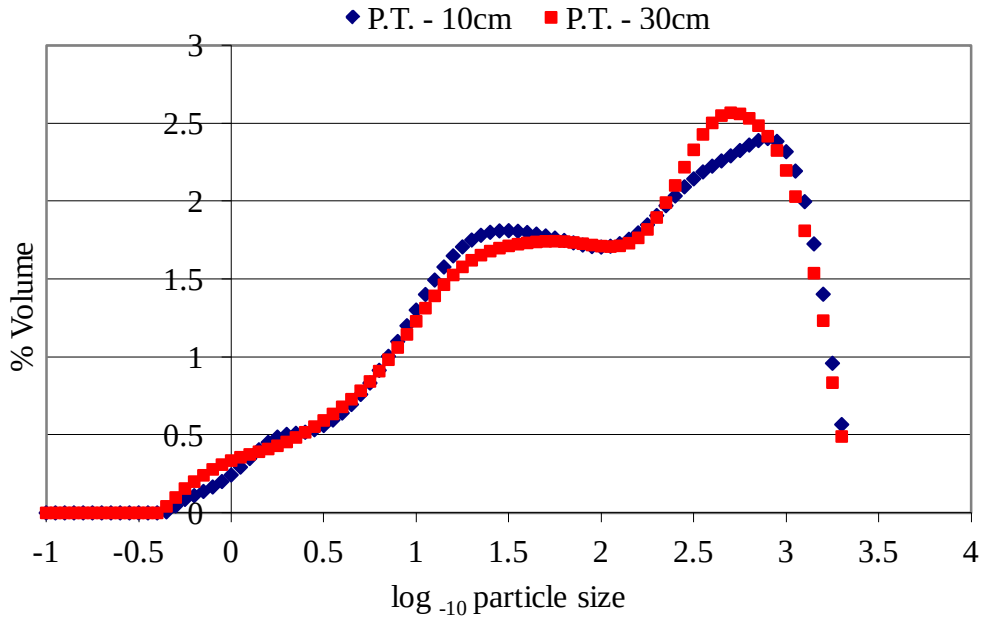


Figure 6.21 P.T. combined particle size distribution curves.

	Curve 1	Curve 2	Curve 3	Curve 4	Curve 5	Total
P.T. - 10cm	3.754	16.794	39.278	18.736	21.439	100.0
P.T. - 30cm	3.156	25.642	27.012	44.170	0.020	100.0

Table 6.9 P.T. relative constituent Gaussian curve volumes. The figures represent the volume as a percentage of the whole sample distribution curve. The Primary Talus particle size distribution curves could be de-convoluted into 5 Gaussian curves.

6.2.3 Primary Talus discussions

It is clear from the stratigraphy that the P.T. deposit was formed rapidly from the abrupt movement or surge of large amounts of mixed but generally dry sediments from a collapse event in the source deposit. The lack of water and rapidity of the accumulation without substantial levels of falling of the sediments qualifies the deposit as a grain flow type. It can also be suggested that, given the narrow nature of the EC1 passage opening, the sediments entering the passage could only have done so from a relatively restricted area in a similar fashion to the S.T. deposit or the Silberberg Grotto derived sediments preserved in the false floors (See Section

6.1 for a description). The stratigraphic features suggest the deposit formed from a deposit: with a very low fossil representation; that was heavily calcified; that had numerous filling episodes interstratified with capping flowstones; that had a high level of active speleothem deposition; that was probably a primary sedimentation deposit, in that the deposit received direct ingresses of fine surface sediments in slope wash events; that had relatively high levels of infiltrating water; that collapsed whilst the majority of sediments were still calcified; that does not correlate to any of the deposits preserved in the MH1 talus.

The last point is significant, in that no similar horizon or depositional features can be found within the nearby MH1 talus. The upper, S.T. deposit is similar to the T2 deposit, and both formed at a roughly contemporaneous time from the overflowing Name Chamber Far Western Talus. The Primary Talus, which must have developed from the movement of sediments in a similar area (in the restricted catchment area of the narrow EC1 passage), differs greatly in sedimentological and fabric attributes to the other investigated deposits. No similar sediments have been found within the Name Chamber either. There is only one known facies in the possible supply area that contains a similar suite of features, and that is the lower facies found in the Silberberg M2 deposit. From the description made by Clarke (2006) (provided within the Background chapter) and from personal inspection, the lower facies is bone-poor, loosely consolidated, clast-rich calcified talus with reddish sediment inter-bedded with calcite layers and dark-brown calcified mudstone. The lower facies lies directly below the M2 upper facies and above Member 1 sediments. Clarke suggests that deposition of the M2 lower facies seems to have been cyclical, providing hiatuses in sedimentation and allowing flowstone growth. Like the M2 upper facies, the lower facies also represents a primary sedimentation deposit.

The M2 lower facies and *Facies 0* share a very similar suite of features, the major difference being that the Primary Talus represents a secondary sedimentation deposit accumulated from a collapse or rapid accumulation event. In the introduction to the EC1 site, the false floors were described and shown to be associated to the M2 deposit which exits the Silberberg grotto in a number of

places. Two of those exits supplied sediments from the M2 upper facies directly into the EC1 passage accumulating in a steeply sloping talus. Within the Silberberg Grotto M2 deposit, both recognised facies represent primary sedimentation deposits. The lower facies lies directly beneath the upper facies with no recognisable transitional disconformities so must have accumulated before the upper facies. It stands to reason that if the M2 upper facies exited the Silberberg Grotto into the EC1 passage then the same exits could have been in operation during the accumulation of the lower facies, accumulating sediments via a collapse/surge episode into the EC1 passage prior to the M2 upper facies developing on top of the lower facies. Unfortunately, without sampling more of the P.T. deposit, it remains unknown from which Silberberg Grotto opening the sediments derive. Continuing work by Clarke and Bruxelles strives to identify the exact opening responsible for the accumulation of the M2 deposit, which will help clarify the infilling patterns of the Silberberg Grotto and in turn clarify the source of the P.T. sediments.

6.3 STK-EC1 Conclusions

The investigation of the EC1 talus represented the second part of the research into the central underground deposit confluence in the far eastern Milner Hall. The first part of this research was accomplished through the investigation of the MH1 talus. The EC1 passage represents the alternative destination for sediments deriving from the Silberberg Grotto or Name Chamber. The importance of the EC1 deposits lies in the discovery of M2 sediments not found within the Milner Hall but integral to the formation of the M2 deposit. The absence of the M2 lower facies from a stratigraphic sequence documenting the sediments exiting the Silberberg Grotto would have been incomplete or required sound stratigraphic explanation. The stratigraphic sequence and proposed associations to source deposits are represented in Figure 6.22. In the case of the EC1 sequence the stratigraphy does not conform to the laws of archaeological stratigraphy and therefore requires a more flexible approach to representation. In order for the Harris Matrix to be used to depict cave stratigraphy, an indication of stratigraphic

unconformity has been included and is described in Section 3.2 and shown in Figure 4.2. In the case of the EC1 sequence, the S.T. is younger than the overlying sediments which are separated by an erosion surface, this relationship is indicated by a broken vertical line and downward facinfg arrow. The first deposit to fill into the EC1 passage was the collapse/surge from the M2 deposit lower facies. The M2 upper facies sediments then built more gradually onto the basal unit. The M2 upper facies sediments were then heavily calcified into the EC1 passage and remnants form the false floors. Increased localised water movement undercut the M2 upper facies sediments, forming the lower passage and creating the smooth, flat, highly consolidated erosion surface on the P.T. The lower passage was then filled with younger sediment deriving mostly from surges of sediment from the Name Chamber into the far eastern Milner Hall at a much later date.

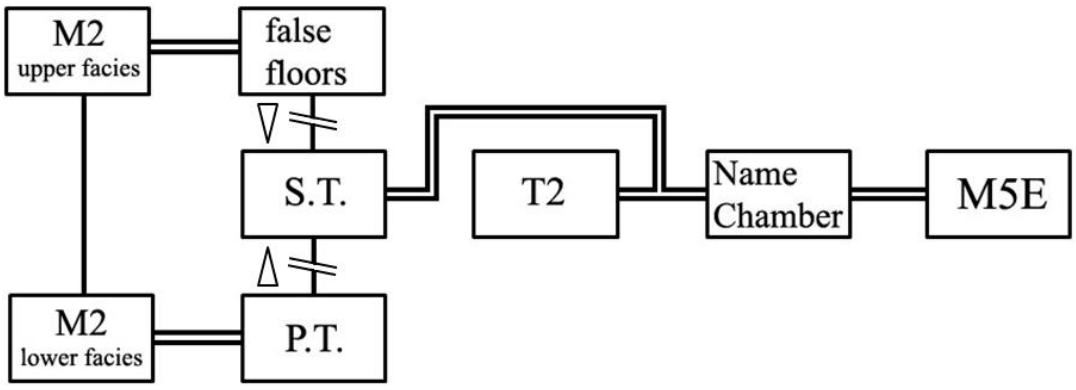


Figure 6.22 Harris Matrix representation of the EC1 stratigraphic sequence.

CHAPTER 7 RESULTS: STK-MH2

The location of the STK-MH2 deposit has been indicated in Figure 1. Two sampling areas were chosen, MH2a and MH2b. The minor pilot sampling excavation was called MH2a and the more significant excavation focussing on the main vertical face was called MH2b, the excavation plan has been illustrated in Chapter 3 (Figure 3.3). Figure 7.1 presents a schematic plan of the STK-MH2 deposit and the immediate vicinity. The location and deposit was first briefly described by Wilkinson (1983): "the 50-m long north wall of Gallery A in the Tourist Cave (now known as the Milner Hall) consists of a debris mass which has descended into the gallery" (pp. 519). The vertical face currently spans only 25m of the northern wall. Wilkinson describes a larger deposit to that seen today, but the reason for this is unknown. All work has been supervised by a researcher since 1966. The STK-MH2 deposit is represented by a large truncated vertical face of a previously expansive talus deposit which occupied a large area of the north-western Milner Hall. The deposit accumulated in a southerly direction from an opening in the roof almost directly above the truncated face. The sediments accumulated down and against the southern face of a very large *in situ* dolomite column. The talus deposit spread in a steep-sided cone across the passage called 'Gallery A' (Wilkinson 1983). Previously the deposit spanned across Gallery A, as indicated by remnants of the talus found on the southern wall of Gallery A, opposite the main body of the deposit. The original opening has been blocked by the growth of the deposit to the height of the chamber (about 12m), and the exact location of the opening on the surface, was not found. The relative location of the opening to the Name Chamber and Silberberg Grotto suggests the opening would have been close to the current western extremity of the Lincoln Cave system, to the north-west of the main Sterkfontein surface excavation. The truncated vertical surface spans the entire width of the deposit and has exposed both distal lateral edges and the main body of the deposit. The majority of the talus has been removed during the mining and subsequent tourist activity. The possible dumping areas of the removed sediments are the lake (20-30m and 3m below to the west),

the passages behind the northern wall, and across the floor of the Milner Hall to level the public access areas.

Several generations of flowstone growth can be found on various areas of the deposit, with the most intact flowstone bodies being found on the eastern area of the talus. In the central to eastern area of the deposit a combination of factors including a thick flowstone and heavily calcified sediments have facilitated the preservation of the eastern lateral and distal termination of the deposit. At the western end of the talus, the mining and installation of tourist infrastructure at the lake edge has been more destructive and has left only a small remnant of the original lateral termination. Several small passages weave behind the main deposit body and northern wall of the Milner Hall (Figure 7.1). These passages have received varying quantities of sediments during the development of the STK-MH2 deposit but have also been heavily disturbed by mining, with large quantities of fractured dolomite and chert, and breccia blocks being dumped on the floors of the passages. The compromised nature of the material within the passages reduces the validity of sampling due to the high potential of anthropogenic mixing from a number of sources both from within the STK-MH2 area and from beyond. The exposed vertical face of the deposit formed the focus on the investigation as it provided opportune areas for sampling and assessment of exposed stratigraphic profiles. STK-MH2 lies a significant distance from the eastern Milner Hall deposits and no stratigraphic connection is apparent so no relative depositional chronology could be proposed. This means that a representative faunal sample is needed to provide the most relevant comparative information. The western distal lateral portion was investigated but not sampled due to a relative dearth of fauna and clastic material suitable for analysis. Sedimentological analyses focussed on the main vertical profile of the deposit main body to provide insight into the intra-deposit sedimentological variation. The differing levels of calcification found within the STK-MH2 deposit precluded the recovery of detailed fabric data as heavy-duty excavation methods were necessary for the removal of faunal samples.

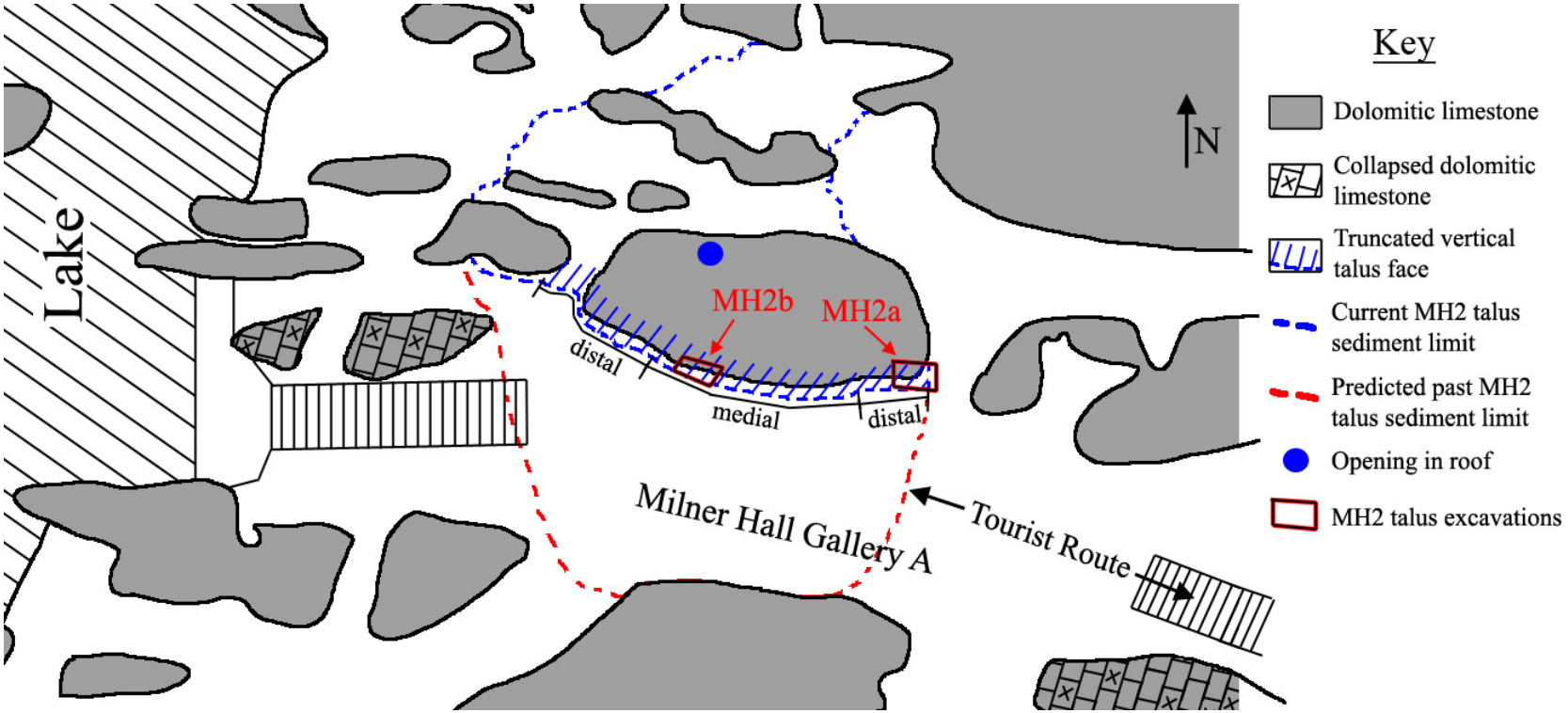


Figure 7.1 Schematic plan of the STK-MH2 location and immediate vicinity. Current STK-MH2 sediment limits are shown in blue dashed line.

7.1 STK-MH2 Stratigraphy

Figure 7.1 shows the location of the STK-MH2 talus, including the identifiable limit of the current STK-MH2 sediments. It provides a predicted past limit to the south, based on the presence of breccia remnants found on the opposite wall of Gallery A. The anthropogenically distributed sediments are easy to identify in that they are characterised by pebble to boulder-sized, angular blocks of chert and/or dolomite and breccia blocks. This rubble is distributed haphazardly on the floor within the passages, sometimes within passages that have no naturally accumulating breccia within them.

The naturally accumulating sediments in the passage network to the north of the main talus body have been cemented into the many faults in the walls with thick filling flowstone forms. The intricacy of the passages and the great number of small apertures promoting sediment distribution into the area make tracking each individual breccia component impossible. It is also an unnecessary task given that the STK-MH2 sediments are the only allogenic sediments filling this area of the Milner Hall and the direct stratigraphic association of the passages to the main deposit body makes the provenance clear. The naturally accumulating passage sediments are generally heavily calcified fine-grained sediments, laced with filling flowstone with only small and infrequent clasts and small (<50mm) faunal particles. Despite the close proximity to the original entrance (mostly <5m), the filtration process that acts on the sediments as they spread through small openings and around intricate passageways produces fine-grained matrix that may be considered similar to a distal facies. Receptacle morphology plays a significant role in particle distribution patterns.

The truncated face, accumulated against the northern wall of Gallery A, represents the main body of the deposit, with the greatest proportion of sediments filling in a southerly direction into Gallery A. The truncated face exposes a broad vertical section presenting the transverse morphology of two deposits, named the Primary Infill and Secondary Infill, in order of deposition. Both deposits form as secondary sedimentation deposits, accumulating through a small aperture high in the roof of the western Milner Hall from deposits within another chamber closer

to the surface. The relative position of the STK-MH2 deposit in relation to the MH1 area relates to a significant difference in distance on the landscape. The position of the upper chamber has not yet been located. The relative position of the opening and upper chamber can be suggested if one uses the Name Chamber Feeding shaft as a geological reference point (opening in square R/57 in M5E, see Clarke 1994a) associated to the surface and the lower deposits. The STK-MH2 deposit lies just over 40m to the north-west of the Feeding Shaft, placing the STK-MH2 deposit close to the western extremity of the Lincoln Cave system, and away from the breccia exposed in the Sterkfontein surface excavation. The proximity to the Lincoln Cave system and the vertical nature of the entrance do provide initial suggestions that the sediments may derive from the Lincoln Cave, and not the established Sterkfontein deposits. Thus far, no sedimentological analysis has been conducted on the Lincoln Cave system. Pilot excavations did yield a taphonomic interpretation and taxonomic representation (Reynolds *et al*. 2003, 2007). The faunal assemblage from the Lincoln Cave will be included in the comparison with the STK-MH2 assemblage.

The majority of analysis was conducted on the Primary Infill, which represents the initial and largest body of sediment and provided the greatest opportunity for access, sampling and study. The main sampling points for the Primary Infill were chosen based on degree of calcification, fossil yield and preservation, clast proportions and accessibility. Two areas where chosen. The main excavation (MH2b) took the form of a geotrench style excavation placed in the western medial portion of the Primary Infill in order to sample the greatest possible extent of the Primary Infill vertical face (see Figure 3.3 for a schematic plan of the MH2b excavation). Two trenches were cut into the truncated face. The trenches were stepped eastwards across the face to avoid heavily calcified pockets of sediment that would hinder sampling but were associated by a discrete stratum. Analysis was based on the yielded faunal sample, stratigraphic observation and six sediment samples taken at regular intervals up the profile to the surface of the Primary Infill. The second excavation (MH2a) sampled the eastern lateral termination (Figure 7.2). The majority of the medial portions of the talus were heavily calcified with the lateral portions showing highly variable levels of

diagenesis, from uncalcified to heavily calcified. Throughout much of the deposit frequent pockets of heavily calcified sediments were found, making *in situ*, accurate excavation problematic.

The Secondary Infill forms a relatively thin bed (ranging between 50cm – 1m) forming directly onto the Primary Infill surface. The Secondary Infill represents a significant depositional episode and in this way differs from the strata found within the Primary Infill boundaries. The Secondary Infill has been capped by a thick and extensive flowstone. Unfortunately, the Secondary Infill was only sampled by a small pilot profile to clarify the relationship to the Primary Infill. Due to the generally difficult access of the STK-MH2 vertical face and the heavily calcified nature of most of the lower Secondary talus sediments, faunal and sedimentological sampling was not carried out. Based on an isolated sampling point, the Secondary Infill can be classed as a deposit within the main STK-MH2 depositional sequence but not as a distinct facies. Classification as a distinct facies would require proof of distinctive sedimentological characteristics or sediment source, neither of which is apparent from the pilot sample. The stratigraphy of the Secondary Infill is likely to be analogous to the Primary Infill in that both deposits have accumulated from the same source into the same receptacle through similar depositional processes. Each infill is discussed below.

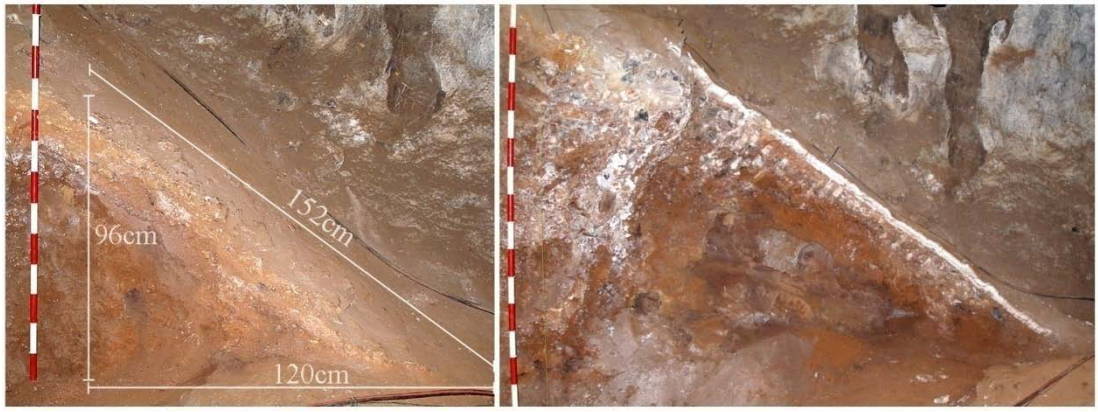


Figure 7.2 Primary Infill excavation point MH2a. The left photograph shows the eastern lateral termination of the Primary Talus prior to excavation with the intended dimensions of the excavation. The right photograph shows the same area post-excavation. Exposure of the northern wall can clearly be seen together with the heavily calcified nature of the upper levels of the deposit creating a 'hard cap' characterised by infiltrating white calcium carbonate. The range staff segments measure 10cm.

7.2 The Primary Infill Stratigraphy

The truncated vertical face of the STK-MH2 talus preserves a large proportion of the transverse section of the Primary Infill. The Primary Infill sediments were the first to enter this part of the Milner Hall and did so from an opening high in the roof of the chamber. The longitudinal medial and distal portions of the Primary Infill reached across Gallery A, but now only the proximal portion remains. The removal of the medial and distal portions of the deposit has left an opportunity to observe the transverse sorting trends within the proximal portion of an aven-fed talus deposit. The transverse portions of a talus can be split into two main facies, a medial and a lateral facies. The position and extent of the transverse portions of the Primary Infill are shown in Figure 7.1. Figure 7.3 shows a schematic diagram of a transverse section of the proximal portion of an aven-fed talus with the relative positions of the discussed transverse facies. It should be noted that the transverse facies pattern discussed may be limited to the proximal portion of an aven-fed grain flow talus. Longitudinal sorting and elongation of the talus is a progressive process that changes the transverse and longitudinal facies attributes with increasing distance from sediment source. The rock fall accumulation

process demonstrated in the proximal medial transverse facies would most likely develop the morphology of a dry grain flow deposit further from the sediment source.

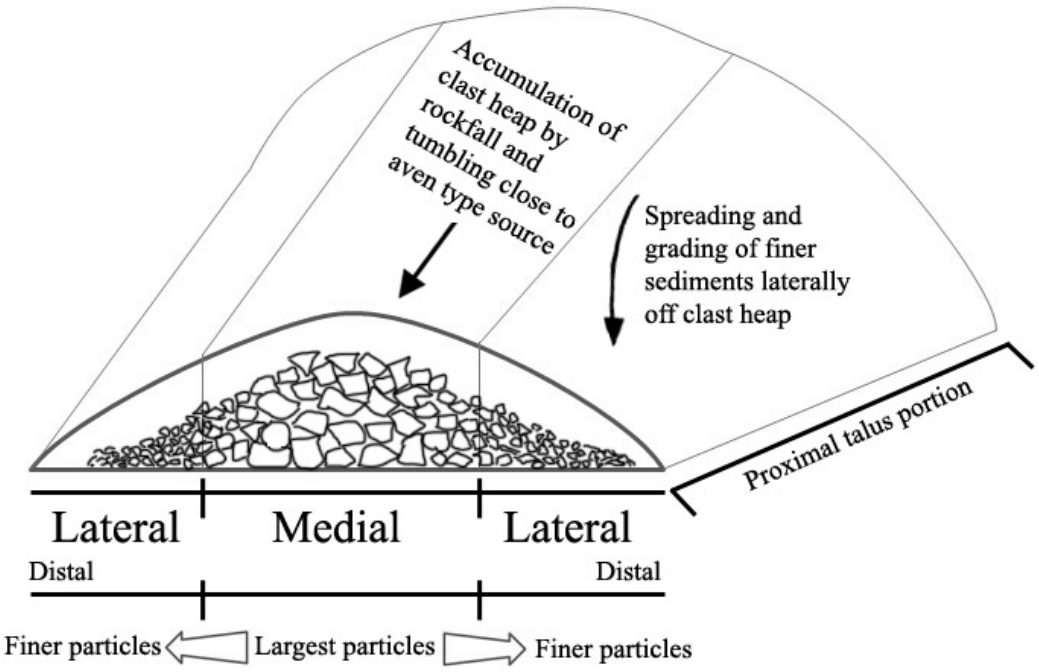


Figure 7.3 Transverse section of a proximal portion of a talus slope developed under an aven-type opening.

The Primary Infill transverse medial facies can be described as a diamicton. The eastern medial facies is characterised by massive, unconsolidated and unsorted clast-supported matrix with numerous interstitial voids, most remaining unfilled by sediments. The interstitial voids are often occupied by aragonite and calcite crystal growth. The interstitial voids in the upper 50cm of the facies are frequently filled with filling flowstone. The clasts range in size from <50mm to >500mm, show no sorting and are often imbricated at the base of the deposit. Many of the clasts are angular with sharp fracture edges but show little rounding, suggesting a lack of post-depositional movement after initial fracture caused by the fall from the opening. The eastern upper areas of the medial portion are heavily calcified

with flowstone filling all the interstitial voids, creating an extremely hard breccia. The surrounding matrix is silt loam in texture and ungraded.

The transverse medial facies indicates the major mode of accumulation of sediments in this area of the talus as being through a continuous rock fall process. This would be expected for the main reception area of a deposit developed from a high but close opening in the ceiling. Finer sediments may be spread over the top but are generally distributed to the lateral portions, creating a lateral grading pattern. With time the interstitial voids may be filled with finer sediments and/or infiltrating speleothem. This trend is observable in the STK-MH2 section, several aven-fed dry grain flow deposits at Sterkfontein and within other Cradle sites (Pers. Obs.). In flume tests conducted by Major (1997), the development of this trend is observed in a number of his experimental debris-flow deposits. It seems this facies may not always develop and may be limited to the proximal portion of the talus, particularly in cases where an aven-type opening accumulated clasts in a rock fall, tumbling process. In these cases the largest clasts are deposited immediately under and in front of the opening forming a clast dominated heap in the transverse medial facies. Fossil preservation within this clast heap is very poor and pieces are frequently crumbling and fragmented beyond identification. Fossil preservation increases towards the more lateral portions of the transverse profile, as clast proportions drop and sediments are accumulated in a more gradual sediment flow process.

The lateral facies are dominated by laterally graded finer particles (sands, silts and clays with little or no clasts). Lateral grading of sediments is analogous to longitudinal grading away from a source, in that finer particles and those with greater transport potential are distributed further. Lateral facies sediments often develop stratification and possibly horizontal grading systems as water may aid the distribution of the sediments to the margins of the deposit.

A number of transverse facies relationships can be observed from an extensive transverse profile of a talus. The nature of these relationships can provide insight into the influences on deposit formation. The first is the position and relative proportions of the transverse facies and the second is the spatial distribution and

relative extent of the transitions of those facies. Both features in the Primary Infill are discussed below.

The position and relative proportions of the transverse facies can provide an insight into the direction of the main sediment flow when the rest of the deposit has been removed. In the Primary Infill the transverse medial portion of the deposit is distributed to the south to south-east of the opening with a greater proportion of the medial facies being represented to the east. The greatest proportion of clasts, and therefore the main reception area for the falling and tumbling rock is towards the eastern end of the medial portion. This suggests the Primary Infill deposit developed in a south-easterly direction from the opening, the rest of the deposit developing in a fan, spreading in a southerly direction towards the lake. The south-easterly direction of deposition may be due to the shape of the opening and the direction of sediment flow in the above chamber, or due to the shape of the underlying column which may have directed flow in this direction. Due to the steep gradient of the upper talus slope, the height and closed nature of the opening and the heavily concreted nature of the upper sediments, neither area was accessible for sampling. The proportion and relative size of the transverse lateral facies of the Primary Infill section also provides indications of the formation influences.

The spread of finer particles is more highly influenced by the topography of the receptacle than by the large clast dominated colluvium forming the base of the talus. In Gallery A, there is a gradual but definite slope running in a westerly direction, towards the lake from the eastern Milner Hall area. The set of steps running eastwards, up from the lake, demonstrates the increasing gradient with the proximity to the permanent water (see Figure 7.1). The current STK-MH2 sediment limits, shown in Figure 7.1, demonstrate a development of the finer sediments towards the lake, or down slope. The same can be seen in the truncated section of the Primary Infill, the lateral facies to the east (upslope), representing a smaller proportion of the talus than the western lateral facies (down slope). The morphology of the distal terminations also differs between the eastern and western lateral facies. The upslope (eastern) distal lateral edge (shown in the right image

of Figure 7.2) terminates in an abrupt fashion with a more obtuse terminating angle and steeper slope gradient, a result of the finer particles accumulating onto an inclining slope, hindering the spread of sediments. In contrast, the western distal termination of the Primary Infill feathers out gradually, the spread of sediments aided by the declining slope beneath. The western distal portion also displays a greater degree of stratification, with multiple lenses of fine, sorted sediments suggesting the presence of water in the deposition of the sediments towards the lake. The greater influence of water in the western side of the talus over the eastern side is expected, given the slope of the Milner Hall floor and the proximity to the water-table. Very few clasts and only microfauna specimens are found within the western distal portion sediments. As a result of the regular contact with water the western lateral facies has remained uncalcified in comparison to the eastern facies which is heavily calcified.

The spatial distribution and relative extent of the transitions of the transverse facies indicates the Primary Infill dominant sediment flow patterns. As well as a proportionally larger, more clearly stratified western lateral facies, the preferential flow of sediment down slope has created a more gradual lateral grading of the medial facies from east to west. Clast sizes and associated voids become increasingly small and the matrix to clast proportion increases in a westerly direction from the medial facies. The medial facies matrix gradually grades from heavily clast dominated with very little fine sediment in the eastern portion, to a matrix-supported sediment with few clasts and only <20mm faunal fragments and microfauna in the western portion. The western medial facies then grades into the western lateral facies. The boundary between the medial and lateral facies is gradual and spans over 2m. The eastern medial facies grades into a matrix-supported sediment more abruptly and occurs within one metre. The narrow matrix-supported section of the medial facies then grades abruptly into the eastern lateral facies within 50cm.

The majority of the Primary Infill sediments are likely to have accumulated in one or more collapse events followed by minor, cyclical sedimentation dropping material in from the chamber above. This is indicated by a dearth in internal

stratigraphy or bedding planes through most of the medial clast-supported sediments and a capping bed of finer sediments. In the upper finer, capping sediments there are a number of discrete consolidated surfaces at different levels of the profile that suggest two smaller episodes of deposition developing towards the end of the Primary Infill deposition. No sedimentological differences could be found between the strata suggesting that the ridges represent short hiatuses within the main Primary Infill sequence. These ridges are also contained within the main Primary Infill boundary, supporting the inference that they represent strata within the main Primary Infill sequence, not necessarily distinct deposits. Their appearance towards the end of the deposition of the Primary Infill suggests a more cyclical deposition and may suggest a changing shape of the chamber above supplying the sediments. Figure 7.4 presents a schematic diagram of the grading pattern seen in the vertical face of the Primary Infill.

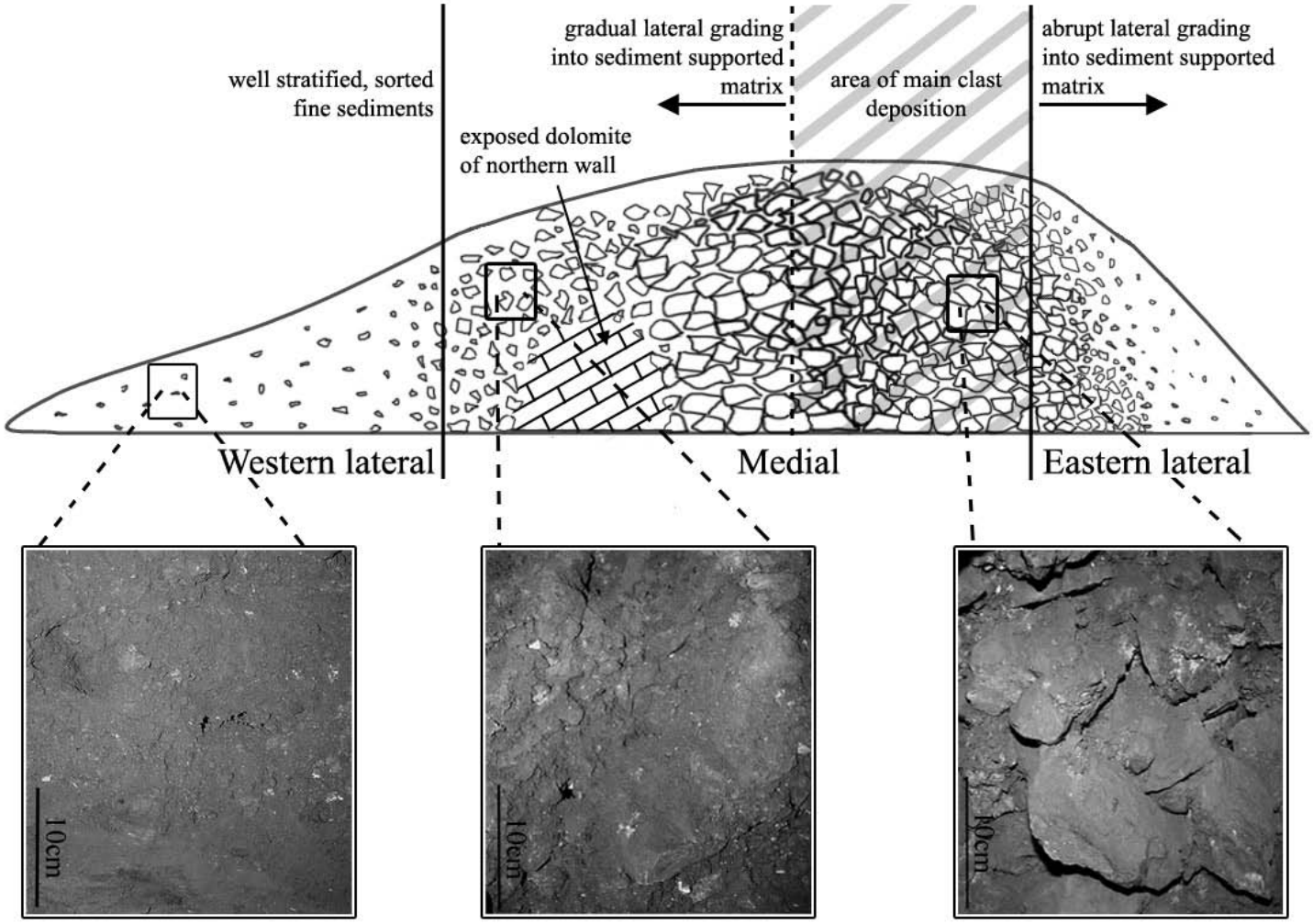


Figure 7.4 Schematic diagram of the vertical face of the Primary Infill. Diagram is not to scale.

The excavation of a hyena coprolite from the upper levels of the main MH2b trench suggests the probability of a shallower entrance to the upper chamber, above the Milner Hall and feeding the MH2 area. This upper chamber may have been accessible to carnivores and facilitated recurrent sedimentation from slope wash events instead of perpetual collapse of material. There are also numerous generations of flowstone growth capping both the Secondary and Primary taluses suggesting a cyclical depositional process with marked hiatuses in deposition. Within the episodes of deposition, accumulation of material may have been rapid as suggested by the unconsolidated nature of the finer sediments and the unsorted, randomly orientated clasts and large proportions of interstitial voids in clast-dominated areas. The sediments occasionally found filling the interstitial spaces are also ungraded indicating a lack of fluid interaction. Flowstone growth also seems to have been prompt within the depositional hiatuses, with speleothem filling the interstitial voids before the finer sediments had settled into them. Towards the eastern end of the medial portion and the eastern lateral portion of the Primary Infill, the flowstone has infiltrated the sediments and cemented them into extremely hard breccia. The extent of this hard breccia does not reach through to the base of the deposit, however, and creates a 'hard cap' representing the upper 50cm of the deposit. The sediments beneath this 'hard cap' are significantly softer, and although the voids within the sediments contain aragonite and calcium crystals, the matrix has not been extensively calcified. On the right hand side of the excavation, the white heavily calcified sediments can clearly be seen.

7.2.1 Primary Infill sedimentology

As mentioned briefly in the introduction, the sedimentological samples taken from the Primary Infill derive from the main profile excavation which runs from the floor of the Milner Hall to just below the surface of the Primary Infill at the transverse western medial facies where the clast-supported medial facies transitions into the more lateral matrix-supported zone. The six samples were subjected to hydrology and particle size analysis, but unfortunately XRF and fabric analysis could not be conducted. Fabric analysis was not carried out due to

the partially calcified nature of the sediments in the Primary Infill. These sediments required the use of comparatively heavy excavation techniques, which means that fossils cannot be extracted *in situ* and precludes the use of faunal material as fabric indicators. Also, the area chosen for excavation, with the highest potential for yielding a representative faunal assemblage, contained no clasts large enough to provide fabric data. Those areas that have built directly onto the dolomite column yield characteristic signatures, indicating a mixing of decayed dolomitic secondary minerals (authigenic) and allogenic sediments.

Table 7.1 presents the sedimentological summary for the Primary Infill. The samples are placed in order of depth from the Primary Infill surface (Sample 6), which was taken from 3.80m above the floor of the Milner Hall to the base (Sample 1). The first three samples were taken from the lower trench (see Figure 3.3 for schematic plan of the MH2b excavation) and the remaining three samples were taken from the upper trench. The colour of the sediments can be used as an indication of high quantities of dolomite in the lower parts of the deposit, with the first two samples being classed as Very Dark Grey and excavated from an area of the deposit in direct contact with the outer decayed layer of the northern dolomite wall. Interestingly, despite the similarities in colour and context, these two samples are significantly different in terms of hydrology. The deepest sample, as expected, contains the highest proportion of moisture. Sample 2 was taken 50cm above Sample 1, from a very similar context, and shows a great reduction in moisture without a correspondingly radical change in particle size proportions. Both these first samples derive from sediments dominated by authigenic material and fall into the silt loam soil texture. The upper sample in the first excavation trench (Sample 3) tested the first sediments with a recognisable component of allogenic material as indicated by the presence of microfauna fossils. Sample 3 shows a significant rise in moisture content and an 8% rise in clay content with a corresponding 6% drop in sand content. Silt content remains close to the underlying Sample 2 proportions and the sediment texture for Sample 3 still falls into the silt loam class. All the samples above Sample 3 are all fossiliferous and are considered to be dominated by allogenic material. The samples above Sample 3 also show a clear inverse grading system with silt proportions dropping by 21%

and sand proportions rising 30% with increasing distance from the floor. Figure 7.5 presents a histogram of the sediment class proportions yielded from the STK-MH2 profile. Although all samples are classed by the US department of Agriculture as silt loams, the range of sediment textures changes distinctly. Moisture content through the allogenic material is very low considering the proximity of the site to the water-table. The most likely reason for the dry nature of the middle to upper areas of the deposit is the increasing proportion of sand in the sediments, thereby reducing the moisture holding capacity of the matrix. The particle size distribution curves for each sample and the associated constituent Gaussian curves are presented in Appendix 2 Figures 2.13 onwards. Statistical comparison of the relative volumes of the constituent curves show Samples 1 and 2 are significantly similar with a p values of 0.774, whereas Samples 3, 4, 5 and 6 show no statistical similarities with the lower two samples, showing p value of <0.05. Within the allogenic sediments of the Primary Infill, Sample 4 is significantly different to Sample 3 (p = <0.05), this is expected given that the greatest change within the Primary Infill sediments is between Samples 3 and 4. Sample 4, however, is statistically similar to both Samples 5 and 6 (p = 0.999 and p = 0.263 respectively).

				Particle Size		
Art No.	**Facies**	**Munsell**	**Hydrology %**	**% Clay (<2µm)**	**% Silt (2µm - 63µm)**	**% Sand (> 63µm)**
6	WM	2.5 YR 3/4	1.18	4.075	50.692	45.233
5	WM	2.5 YR 3/4	1.35	4.408	63.752	31.84
4	WM	5 YR 3/3	0.60	5.424	64.538	30.038
3	WM	7.5 YR 4/2	13.25	14.245	71.513	14.243
2	WM	7.5 YR 3/1	1.19	6.2	73.504	20.297
1	WM	7.5 YR 3/1	22.99	7.911	73.569	18.52

Table 7.1 Primary Infill sedimentological summary. 'WM' refers to the western medial portion of the Primary Infill transverse section.

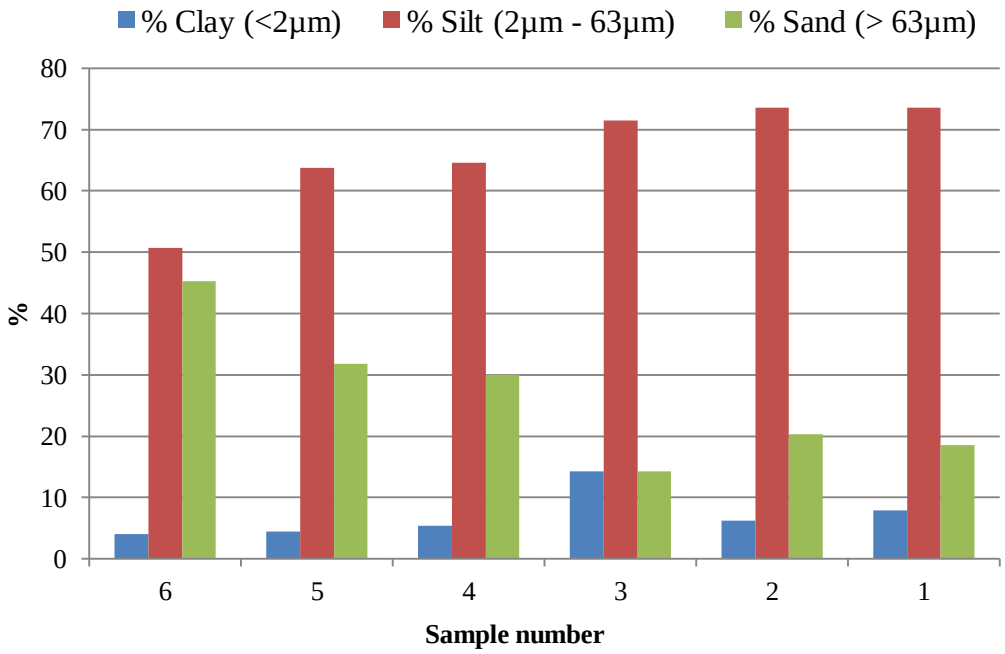


Figure 7.5 Primary Infill basic particle size classes for the STK-MH2 site profile. Depth of sample runs left to right, Sample 1 representing the base of the Milner Hall floor.

The colour of the sediments gets progressively lighter with distance from the base from a Dark Brown (Munsell 7.5YR 4/2) at Sample 3 to Brown (2.5YR 3/4) at samples 5 and 6. Lightening in sediment colour may suggest a decrease in authigenic sediment contribution, although a number of diagenic processes may cause sediment discolouration. Identification and quantification of relative contributions of authigenic secondary minerals is difficult without chemical analysis of the sediments.

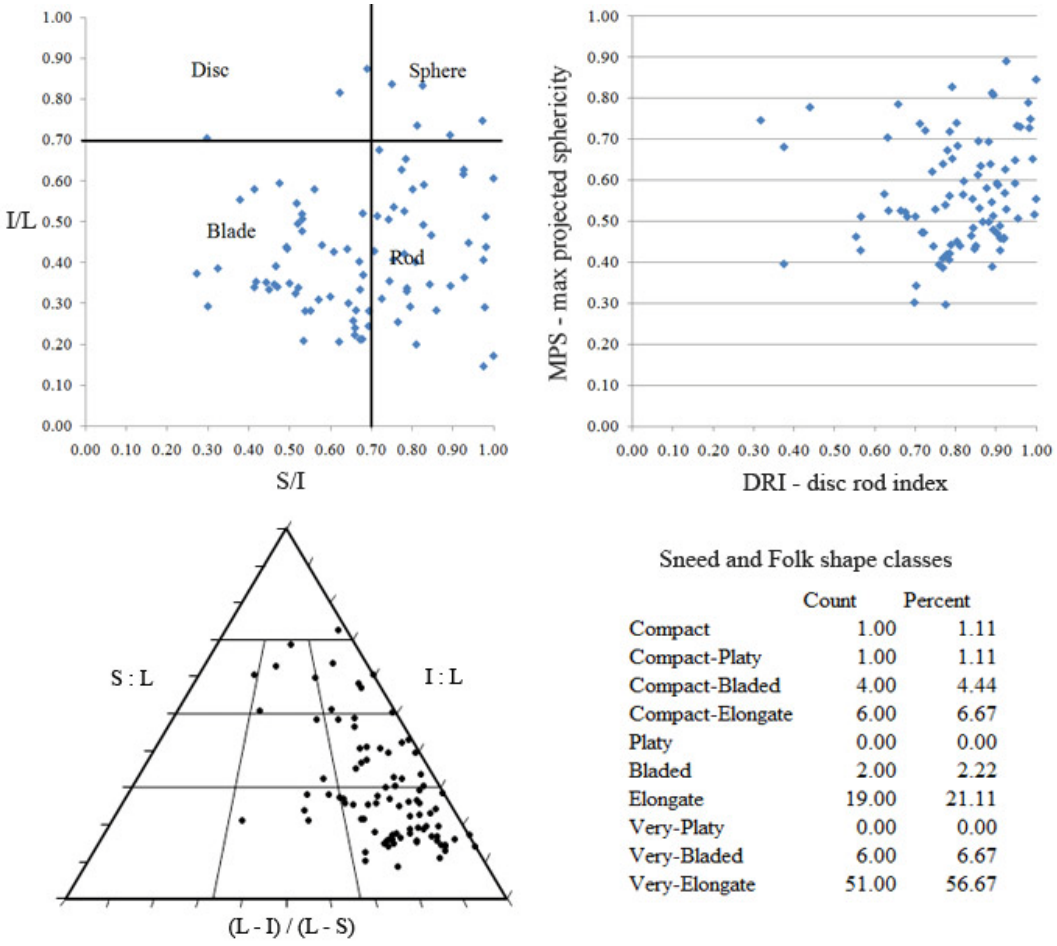
Even if one disregards sediment colour from the analysis and focuses on the hydrology and particle size class proportions, there is a basic trend that can be seen from the sampling of the Primary Infill. The two deeper samples represent the layer of decayed dolomite closest to the wall against which the Primary Infill developed. The removal of large proportions of the talus has exposed the sediments that formed directly against the wall as well as the wall itself, the surface of which has decayed into secondary minerals or ‘cave earth’. Sample 3 represents the lowest of the preserved allogenic sediments that have formed

against the wall. From the accumulation of silts and water in this level it can be inferred that Sample 3 represents the basal level of the Primary Infill and a natural barrier hindering vertical movement of sediments and water into the underlying cave earth. The relative dryness of Sample 2 supports the suggestion that moisture could not move through the Sample 3 sediments. From Sample 3 onwards, the Primary Infill assumes an inverse grading system with relatively stable clay content. It can be further inferred from the formation processes and sedimentology that the inverse grading system seen in the Primary Infill could be the result of a combination of depositional and post-depositional processes. The development and lateral movement of sediments from the main depositional area, in the eastern medial section of the talus, would have seen the smaller components of sediment moved first, thereby developing the lateral areas of the deposit with both a lateral and inverse vertical grading system. The unconsolidated nature of the 'unsettled' matrix has further allowed the vertical movement of water and fines towards the base of the deposit.

7.2.2 Primary Infill particle shape

The two sampling points of the Primary talus allow the investigation of lateral grading patterns on fossil distribution. MH2a and MH2b have sampled the lateral areas of the Primary Infill that have been subjected to positive grading of clasts away from the clast-supported medial facies into matrix-supported lateral areas. Figures 7.6 and 7.7 present the particle shape models for the MH2b and MH2a Primary Infill excavations respectively. MH2b is presented through the analyses first because it derives from the main excavation. The two samples are shown separately to allow the identification of differing shape distribution trends in the respective parts of the deposit. Both assemblages show similarities in that they are generally dominated by elongate forms, with over 75% of elements fitting into the elongate or very elongate Sneed & Folk class. In the MH2b geo-trench excavation there is a significantly higher proportion of compact shapes, 13.3% of elements fall into the compact Sneed & Folk (1958) classes. The spread through the particle shape models is broader within the MH2b assemblage. The Zingg diagram plots a

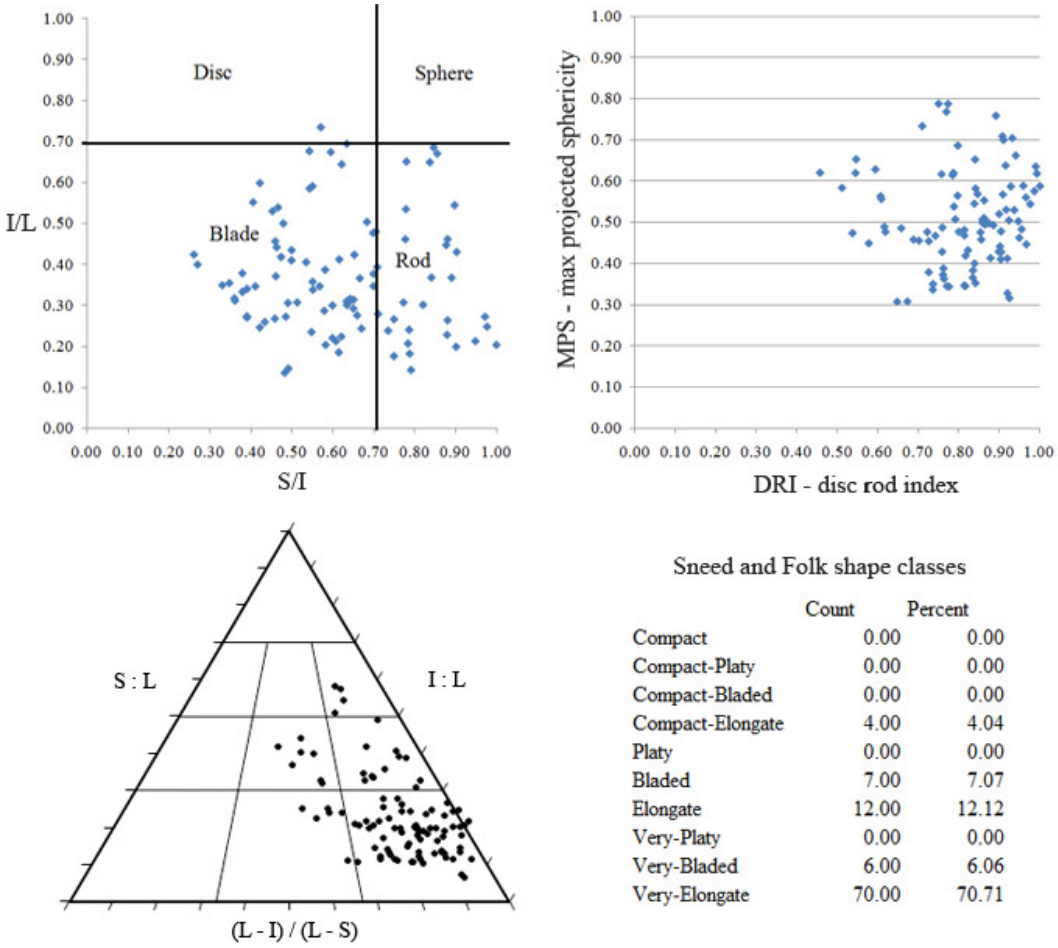
number of elements in the spherical forms, with the rest of the assemblage falling equally between the rod and blade shapes. The MPS vs. DRI scatter plot supports the Zingg diagram in the dominance of rod and blade shaped elements and presents a broad distribution through these areas, with a smaller component falling into the spherical shaped category. The MH2b Sneed & Folk ternary scatter plot corroborates the pattern seen in the other two models. In comparison, in the MH2a assemblage, only 4% falls into the compact classes and a more concentrated distribution is found within the particle shape scatter plots. None of the particle shape diagrams show any compact or spherical shaped elements. Notably, the MPS vs. DRI scatter plot, which has been established to be particularly sensitive to sphericity, shows no spherical/compact shaped elements within the MH2a assemblage. The Zingg model shows a clear dominant distribution of element shapes in the bladed forms than any other shape. The reason for these differences in particle shape distribution is a difference in skeletal element distribution between the two assemblages. MH2b has a larger proportion of bovid and equid teeth, particularly incisors and molars which maintain their compact shape through fragmentation. The two assemblages contain the same number of dental pieces, but different numbers of molars, incisors and fragments. MH2a contains a higher proportion of dental fragments. MH2a on the other hand, contains a larger proportion of rib elements, which, upon fragmentation maintain a generally bladed shape with decreasing elongation ratio. The higher proportion of ribs and rib fragments in the MH2a accounts for the Zingg diagram's concentrated representation of bladed forms, as is to be expected given the sensitivity to blade-shaped particles.



Sneed and Folk shape classes

	Count	Percent
Compact	1.00	1.11
Compact-Platy	1.00	1.11
Compact-Bladed	4.00	4.44
Compact-Elongate	6.00	6.67
Platy	0.00	0.00
Bladed	2.00	2.22
Elongate	19.00	21.11
Very-Platy	0.00	0.00
Very-Bladed	6.00	6.67
Very-Elongate	51.00	56.67

Figure 7.6 Primary Infill particle shape indices from excavation MH2b.



Sneed and Folk shape classes

	Count	Percent
Compact	0.00	0.00
Compact-Platy	0.00	0.00
Compact-Bladed	0.00	0.00
Compact-Elongate	4.00	4.04
Platy	0.00	0.00
Bladed	7.00	7.07
Elongate	12.00	12.12
Very-Platy	0.00	0.00
Very-Bladed	6.00	6.06
Very-Elongate	70.00	70.71

Figure 7.7 Primary Infill particle shape indices from excavation MH2a.

The Voorhies groups for both assemblages are presented in Figure 7.8. It is clear from the relative proportions of element types that both assemblages represent a mixture of elements possessing different transport potentials. Both assemblages show significant proportions of both easily and hardly mobile elements, suggesting the sites have not experienced a significant level of winnowing or sorting. The presence of a proportionately high number of bovid teeth in the MH2b assemblage produces the relatively high number of compact shapes in the particle shape models. Based on their shape, teeth are suggested to possess high transport potential by Frostick & Reid (1983). Voorhies (1969), however, considers bovid dentition to be more difficult to mobilise (by water) despite the

more compact/spherical shape, and consequently teeth contribute significantly to the Group II and III component. In a similar situation, the high proportion of ribs in the MH2a assemblage accounts for the increased representation of bladed forms in the particle shape models.

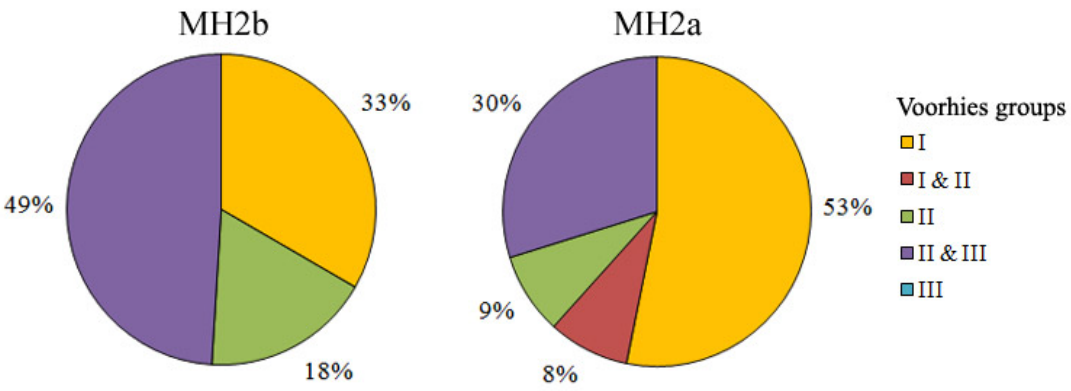


Figure 7.8 Voorhies groups for the MH2b and MH2a assemblages.

Frostick & Reid (1983) consider ribs to be one of the least mobile of elements and so would interpret the particle shape models to suggest a lag-type deposit. The same elements are considered by Voorhies to possess high transport potential and are placed within Group I. Interpretation of a wealth of ribs in the assemblage, based on the Voorhies interpretation, would be the opposite to Frostick & Reid's interpretation of the same assemblage. This contradiction is most pertinent when dealing with assemblages of teeth and ribs, which seem to have conflicting transport potentials in different flow mediums. The contradictions in the interpretation of different element abundances identified above relate to a lack of experimental work on faunal particle behaviour in sediment flow processes. The general trend of the deposits remains the same, however, in that a mixture of elements is present in both sites, although in different specific proportions, suggesting a lack of sorting at these sites. The particle shape models show that both assemblages are dominated by elongate forms, the result of high levels of

fragmentation more than sediment sorting. It is inferred from particle shape or element type that these sites have experienced limited sorting processes. Particle dimensions are another influential attribute on transport and will be discussed in the following section. It is perhaps most relevant that the sites sample areas close to the transverse medial facies, and sorting levels in these areas are not recognisable. More distal lateral portions of the talus may contain more diagnostic elements and particle shape profiles. The eastern lateral termination, or site MH2a, may just be too close to the medial facies, the distance not being sufficient to develop a grading based on the preferential movement of fossils.

7.2.3 Primary Infill faunal assemblage profile

Table 7.2 and Figure 7.9 present the size profile data for the faunal assemblages yielded from the two Primary Infill excavations. Stratigraphically, the Primary Infill was supplied by the re-distribution of sediments that had entered through a single aperture in the roof, thereby representing a single assemblage. The assemblage was then split either side of the medial facies through the spread of sediments into the Milner Hall. Any significant differences in assemblage characteristics between the excavation sites can be identified as a result of either post-depositional processes or secondary sedimentation processes but are not representative of differences in the source assemblage. The assemblages are considered both individually and as a combined assemblage representative of the whole Primary Infill. All Primary Infill faunal analysis is treated in this fashion to allow the recognition of differences in data in different parts of the deposit as well as to provide an assessment of the patterns for the entire deposit. The trend seen in both assemblages is a dominance of material measuring <50mm. This pattern has been seen in all of the other investigated deposits. It has been demonstrated that this pattern can manifest itself through a number of different processes. In the case of the Primary Infill, the restricted particle size profile is a result of fragmentation due to the depositional processes involved in the accumulation of the fauna, namely through rock fall from a high opening in the roof and dry grain flow spreading the sediments to the lateral margins.

The MH2b assemblage mean particle maximum dimension is 40.4mm with a mode of 26.0mm, a median of 37.5mm and a StdDev of 13.6. The smallest particle measures 18.5mm maximum dimension and the largest measures 77.0mm. In terms of particle size (the mean of the three dimensional measurements), the minimum for the MH2b assemblage is 3.0, the maximum 31.0, and the mean of 12.1 with a StdDev of 7.8. The assemblage can be considered highly restricted with 77.5% of the specimens measuring <50mm and no specimens measuring over 80mm.

Max	Summary					
Length	MH2	%	MH2a	%	Combined	%
<10mm	0	0.0	0	0.0	0	0.0
<20mm	1	1.1	1	1.0	2	1.1
20-29mm	20	22.5	38	38.4	58	30.9
30-39mm	30	33.7	30	30.3	60	31.9
40-49mm	18	20.2	20	20.2	38	20.2
50-59mm	10	11.2	3	3.0	13	6.9
60-69mm	6	6.7	1	1.0	7	3.7
70-79mm	4	4.5	2	2.0	6	3.2
80-89mm	0	0.0	1	1.0	1	0.5
90-99mm	0	0.0	1	1.0	1	0.5
>100mm	0	0.0	2	2.0	2	1.1
Total	89	-	99	-	188	100.0
Total %	47.3	-	52.7	-	100.0	

Table 7.2 Primary Infill faunal assemblage size profiles for both excavation sites.

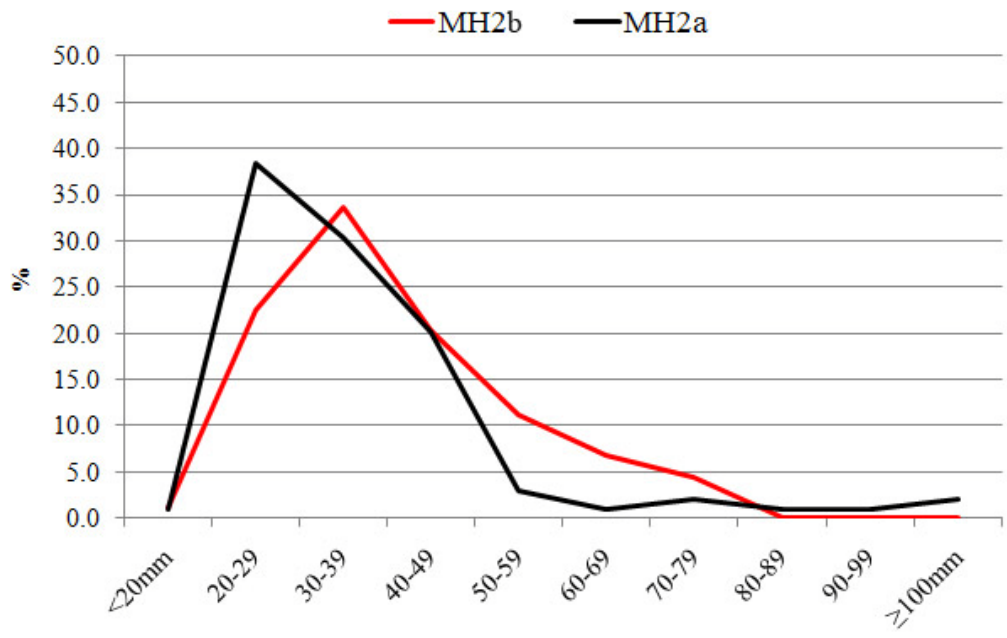


Figure 7.9 Assemblage size profiles for both Primary Infill excavation sites.

The MH2a assemblage mean particle maximum dimension is 37.4mm with a mode of 29.5mm, a median of 32.0mm and a StdDev of 16.9. The smallest particle measures 19.5mm maximum dimension and the largest measures 112.0mm. In terms of particle size (the mean of the three dimensional measurements), the minimum for the MH2a assemblage is 10.5, the maximum 52.6 with a mean of 19.5 and a StdDev of 7.8. The assemblage can be considered highly restricted with 90% of the specimens measuring <50mm, the remaining 10% (n = 10) are spread evenly through the larger size classes than is seen in the MH2b assemblage. Both assemblages have similar size profile distributions, and can be considered representative of the Primary Infill secondary sedimentation deposit. As a combined assemblage, the Primary Infill is characterised by an 83% dominance of <50mm material and 62% falling into the <40mm classes. The high restriction of the size profile is demonstrated by the low standard deviation value of 15.4. The Primary Infill size profile is a result of both the primary sedimentation process and the resedimentation processes which have accumulated the sediments into the Milner Hall. The combination of processes has inflicted extensive fragmentation levels on the assemblages. The excavation of elements

deriving from large (size class three) bovids and equids illustrates the extent of fragmentation affecting the Primary Infill assemblage.

The lack of material measuring below 10mm is a result of the heavier duty excavation methods needed to sample the sediments within the Primary Infill and does not reflect the same collection bias, as all sediment was sieved and processes for microfauna and fragments. The dearth of <20mm material can be considered a valid depositional feature of the samples. The T1 deposit (in the MH1 sequence), for example, yielded a 36% proportion of <20mm fossil material. The relatively high quantity of microfauna observable in the eastern distal facies may indicate the destination of the 10-20mm material. Stratigraphically this would be feasible but would need confirmation through sampling.

The two sites yielded a comparable sample of faunal material. MH2a, which sampled the eastern lateral termination of the Primary Infill, yielded 10 more pieces than the geo-trench excavation MH2b. The MH2a excavation samples a significantly smaller volume of sediment than the MH2b excavation. One could suggest that given the relative sizes of the excavations, MH2a contained a higher density of faunal specimens. The relative fossil yields do provide some data concerning the spread of sediments and fauna. The western portion of the talus has clearly received the majority of the sediments as they spread from the medial facies to the lateral areas. This process would facilitate the accumulation of a greater proportion of specimens in this area. However, the spread of specimens into a larger receptacle also creates a lower number of specimens in a given volume. MH2a has received a smaller proportion of sediments and specimens but has accumulated them into a relatively small area creating a higher fossil yield. Given the size of the Primary Infill and the removal of the majority of the deposit through anthropogenic activity, the fossil yield sampled by the two excavations cannot be considered representative of the primary sedimentation deposit.

7.2.4 Primary Infill faunal analysis

A total of 188 fossils was recovered from the Primary Infill from both excavation sites. The relative fossil abundance at each site has already been discussed. All fossils recovered were identifiable to element type, the most basic level of identification and five specimens were not identifiable to skeletal portion and are classed as (?). One specimen is classed as 'other' and represents a single coprolite which was excavated from the STK-MH2 site. This specimen represents 1% of the MH2b assemblage and 0.5% of the entire Primary Infill assemblage. Coprolites, not being fossilised animal bone are not included in the element analysis but must be included as a distinct faunal by-product and evidence of hyaena activity around the caves. The fauna has been analysed for stratigraphic information in the same way as the other investigated deposits. The data from each site is provided before the combined assemblages are considered as one representative collection. The taphonomic analysis was undertaken separately as slightly different goals called for slightly different focus. The taphonomic analysis methodology is described in detail in Chapter 3.

Skeletal element representation

Figure 7.10 and Tables 7.3, 7.4 and 7.5 show the distribution of skeletal element type and body portion representation respectively. The processes of faunal accumulation and preservation in primary sedimentation deposits are complicated (Brain 1981) and fall under the discipline of taphonomy. The patterns recognised in taphonomy as diagnostic of certain bone accumulation processes are not necessarily preserved through multiple phases of resedimentation, or if they are can be significantly dispersed. The processes of different sediment gravity flows, longitudinal and lateral grading can affect the preservation and distribution of faunal material, also affecting any taphonomic interpretation based on small samples of affected specimens. It follows that stratigraphic data can be yielded from inter-deposit or intra-site comparisons, without specific knowledge of the original assemblage make-up or the taphonomic accumulation agent. In the case

of the Primary Infill, two assemblages have been excavated from different areas of the same deposit, the comparison of the relative abundances of faunal evidence can provide an indication of the association of the two collections.

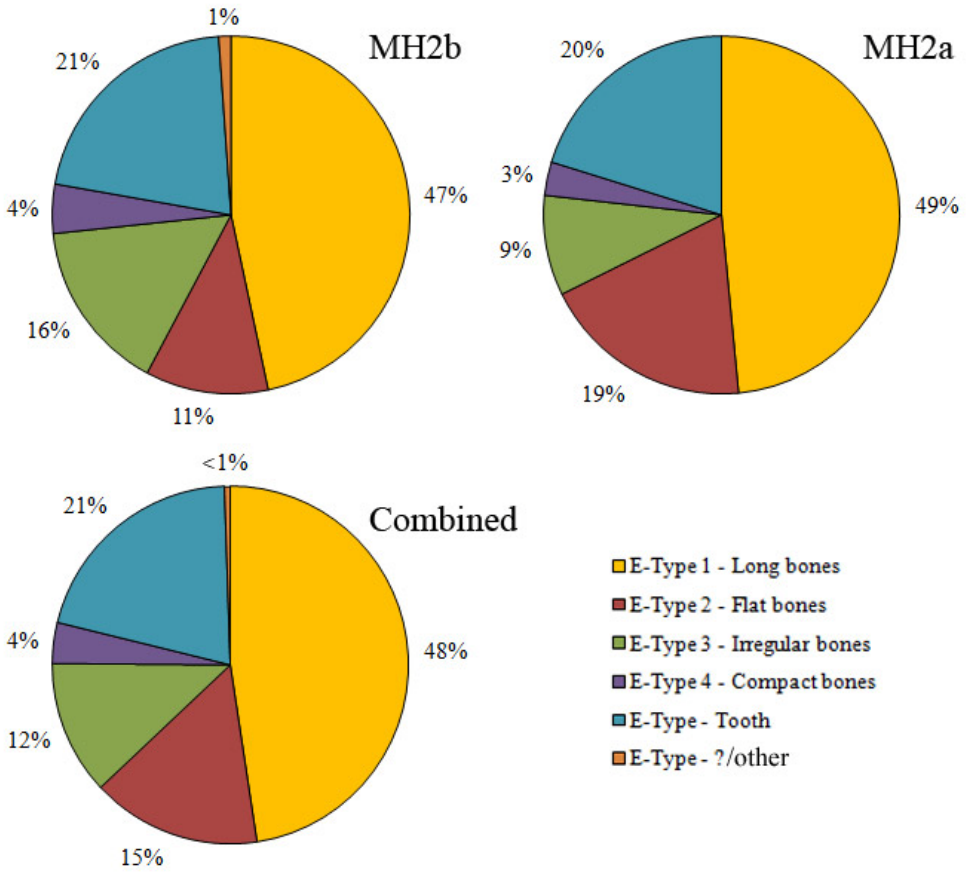


Figure 7.10 Skeletal element type representation for Primary Infill.

Max Length	Fossils						
	Appendicular	Axial	Podial	Tooth	?/other	Total	%
<19.9mm	0	0	1	0	0	1.0	1.1
20-29.9mm	11	6	2	1	0	20.0	22.5
30-39.9mm	15	8	0	5	1/1	30.0	33.7
40-49.9mm	7	3	2	6	0	18.0	20.2
50-59.9mm	3	6	0	1	0	10.0	11.2
60-69.9mm	3	0	0	3	0	6.0	6.7
70-79.9mm	1	1	0	2	0	4.0	4.5
80-89.9mm	0	0	0	0	0	0.0	0.0
90-99.9mm	0	0	0	0	0	0.0	0.0
>100mm	0	0	0	0	0	0.0	0.0
Total	40	24	5	18	2	89.0	100.0
Total %	44.9	27.0	5.6	20.2	2.2	100.0	

Table 7.3 MH2b skeletal portion distribution summary.

Max Length	Fossils						
	Appendicular	Axial	Podial	Tooth	?	Total	%
<19.9mm	0	0	0	1	0	1.0	1.0
20-29.9mm	19	8	1	7	3	38.0	38.4
30-39.9mm	17	5	2	5	1	30.0	30.3
40-49.9mm	7	9	0	4	0	20.0	20.2
50-59.9mm	2	0	0	1	0	3.0	3.0
60-69.9mm	0	0	1	0	0	1.0	1.0
70-79.9mm	0	1	1	0	0	2.0	2.0
80-89.9mm	0	0	0	1	0	1.0	1.0
90-99.9mm	1	0	0	0	0	1.0	0.0
>100mm	1	1	0	0	0	2.0	0.0
Total	47	24	5	19	4	99.0	100.0
Total %	47.5	24.2	5.1	19.2	4.0	100.0	

Table 7.4 MH2a skeletal portion distribution summary.

Max Length	Fossils						
	Appendicular	Axial	Podial	Tooth	?/other	Total	%
<19.9mm	0	0	1	1	0	2.0	1.1
20-29.9mm	30	14	3	8	3	58.0	30.9
30-39.9mm	32	13	2	10	2/1	60.0	31.9
40-49.9mm	14	12	2	10	0	38.0	20.2
50-59.9mm	5	6	0	2	0	13.0	6.9
60-69.9mm	3	0	1	3	0	7.0	3.7
70-79.9mm	1	2	1	2	0	6.0	3.2
80-89.9mm	0	0	0	1	0	1.0	0.5
90-99.9mm	1	0	0	0	0	1.0	0.5
>100mm	1	1	0	0	0	2.0	1.1
Total	87	48	10	37	6	188.0	100.0
Total %	46.3	25.5	5.3	19.7	3.2	100.0	

Table 7.5 Combined skeletal portion distribution summary for the Primary Infill.

It is immediately noticeable that the two assemblages have similar element abundance profiles, as was seen in the particle size distribution and the particle shape distribution. In the skeletal element type proportions, the two profiles are not exactly the same but both are dominated by long bones and dental elements (contributing 68% for MH2b and 69% for MH2a); compact bones also provide similar contributions accounting for 4% on MH2b and 3% in MH2a. The largest dissimilarity is an 8% difference in abundance of flat bones. Flat bones constitute only ribs and rib fragments which are relatively easy to identify. The relative wealth of ribs in the MH2a assemblage has already been highlighted in the particle shape analysis and is represented in the MH2a flat bone proportion. In the body portion abundances the two assemblages show a similar trend with a dominance of appendicular elements, followed by axial elements and then dental elements. The breakage of long bones creates a large number of shaft fragments which tend to maintain their elongate shape despite the resultant size. To test the similarities between the assemblages Chi^2 analysis was carried out on the distributions through classes. The result was that the assemblages are statistically similar with a p value of 0.718. The parallels that have been identified throughout the different analyses demonstrate the mutual source for the sediments and allow the combined assemblages to be considered representative of the Primary Infill.

Any significant element transport or grading process inflicted on either of the sites would have altered certain predictable facets of the assemblage, creating discrepancies in the relative proportions, shapes and size profiles. The similarities between the two assemblages are expected and fit the accumulation scenario for the Primary Infill. Sampling of more distal portions of the transverse section may yield assemblages that have been more affected by the lateral grading process.

Bone breakage

Figures 7.11, 7.12 and 7.13 present the breakage data for the Primary Infill. The dominance of specimens showing four breaks, the maximum level of fragmentation possible, serves to illustrate the high fragmentation levels of the faunal assemblage. Both sites from the Primary Infill show a similar pattern of fragmentation with over 60% of specimens having at least three broken edges. This is contrasted by the low proportion of complete specimens. The complete specimens are not included in the following breakage analysis. The single unbroken bone from the MH2b site is represented by a small bovid (size class 1) podial element measuring 25.5mm in maximum dimension. Podial elements are considered relatively dense, robust bones (Lyman 1984) and often escape destruction. The small size of the podial element also contributes to the potential for preservation. Likewise, the two specimens to escape fracture in the MH2a assemblage are two 1st phalanges, one from a large bovid (size class 3) (measuring 64.5mm maximum dimension) and the other from a medium sized carnivore (measuring 29.5mm maximum dimensions). The survival of the large bovid phalanx can be considered a result of a combination of fortune and the high relative density of the respective element. These specimens are the only fossils to remain unbroken and represent only 1.5% of the total Primary Infill assemblage. From the breakage data it is evident that almost no element escaped fragmentation. The greatest degree of fragmentation relative to original element size has been inflicted on those elements deriving from large ungulates. These generally large bones, have been broken down to an average maximum dimension of 39mm. The high levels of breakage inflicted on larger elements produces large

quantities of shaft fragments, which dominate both the shape profile of the assemblage and the element type representation profile. The rock fall deposition into the medial clast-supported facies is likely to be responsible for a large proportion of the breakage, before faunal remains were distribution to the medial and lateral portions of the talus.

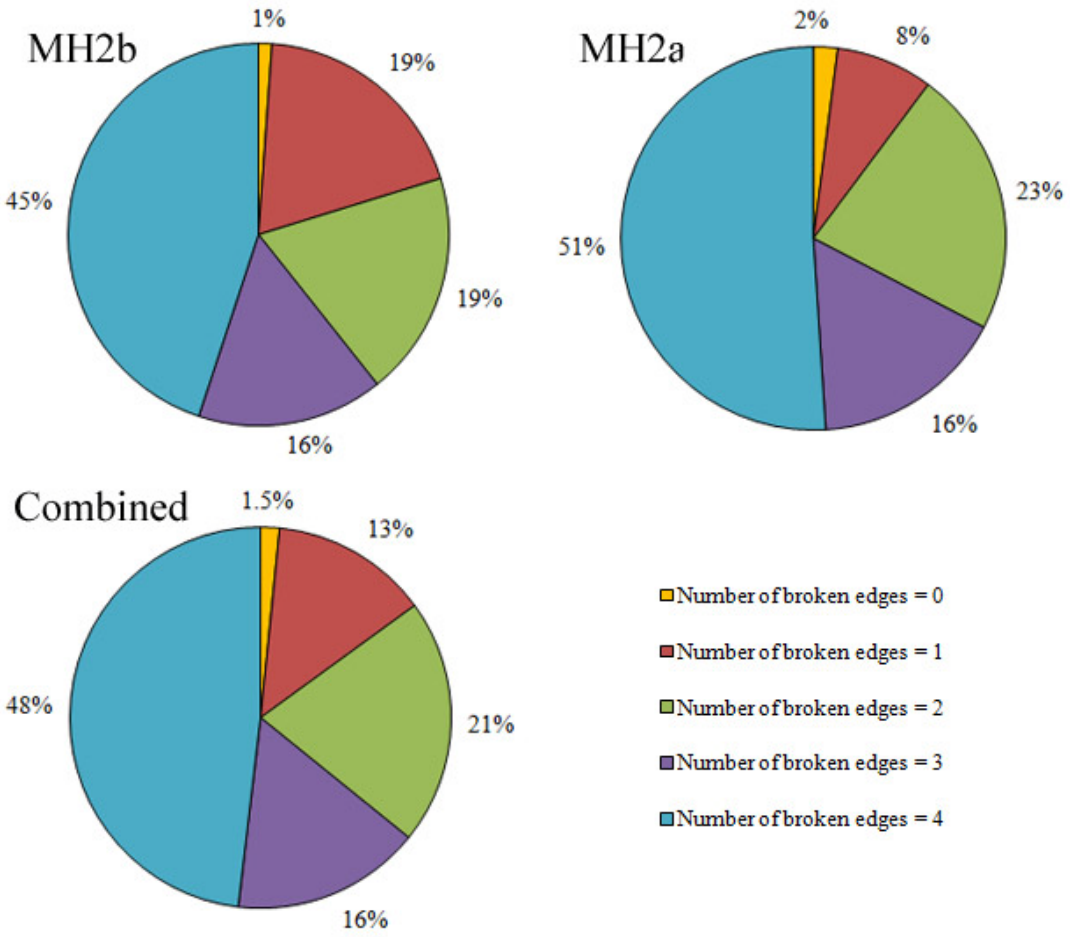


Figure 7.11 Numbers of broken edges on Primary Infill fossil material.

Figure 7.12 presents the break type data for the Primary Infill. The assemblages from both excavation sites and the combined Primary Infill assemblage are presented. Sawtooth break types and perpendicular break angles dominate the assemblages from the two excavation sites and ultimately the whole Primary

Infill. 61% of all specimens in the MH2a assemblage show at least one saw tooth break. This compares closely to the MH2b assemblage which shows 70% of all specimens show at least one sawtooth break type. The assemblage break type data show two dominant components, the specimens with only sawtooth break types, and the specimens with a combination of break types. The next largest contributing proportion is the specimens with only smooth break types. This proportion shows the greatest variation between the MH2b and MH2a assemblages, representing a 15% greater proportion in the MH2a collection. This relates to a 12% difference in proportion of specimens showing at least one smooth break type. The lack of evidence suggesting a significant difference in the levels of post-depositional breakage between the two sites precludes this process as responsible for this difference. Sample size must again be considered as playing a role in the minor differences shown between the assemblages. The major trend remains the same both within the individual assemblages and as a combined Primary Infill representative collection. A large proportion of the assemblage has been broken after fossilisation, as 66% of the assemblage has had at least one break carried out after fossilisation and presumably after primary deposition. Prior to this 1st phase of post-depositional breakage, the assemblage was significantly fragmented whilst still fresh, producing a high proportion of smooth, perpendicular and acute break types. The subsequent major resedimentation produced the dominant break type representation eradicating a proportion of the pre-fossilisation breakage evidence but maintaining the general trend of perpendicular break angles (Figure 7.13). The dominance of perpendicular break angles both pre- and post-fossilisation attests to the development of secondary breakage patterns perpetuating components of the original breakage characteristics, i.e. secondary breakage attributes will be in some part determined by the primary breakage patterns. As was seen in the T2 assemblage, the first breakage process created a signature that has been preserved despite subsequent major breakage.

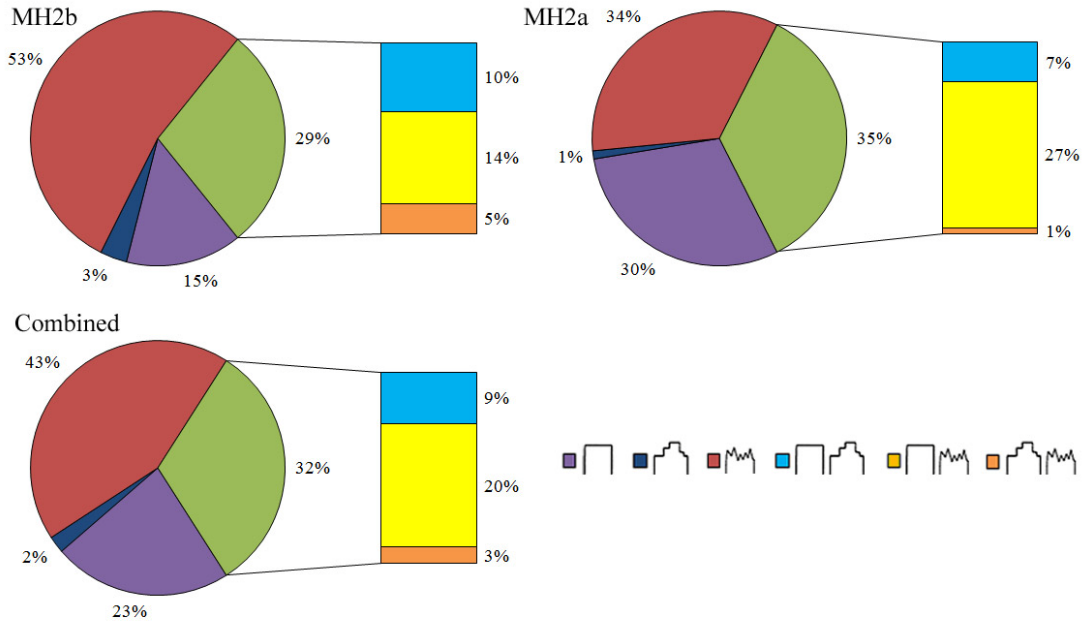


Figure 7.12 Break types for the Primary Infill.

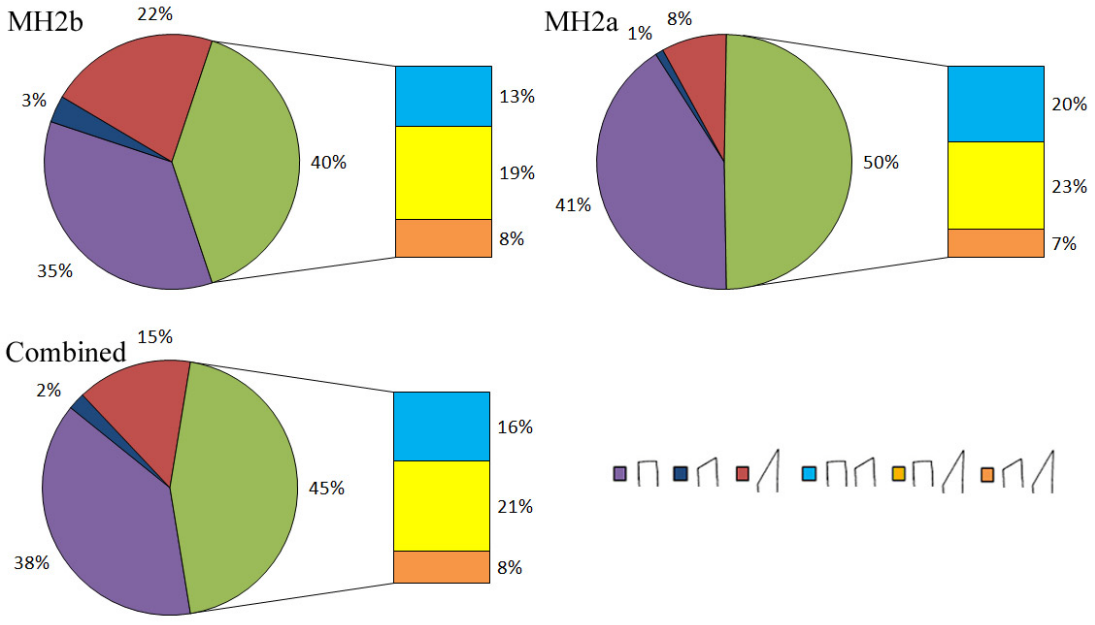


Figure 7.13 Break angles for the Primary Infill.

Bone condition

The bone condition data for the T2 fauna is shown in Figure 7.14. Both the MH2b and the MH2a assemblages show analogous bone condition data and as such can be considered as a single, unified Primary Infill assemblage. From this assemblage it is clear that the general condition of the bone is good with 88% of the assemblage classed as either fresh or slightly weathered (equivalent to Behrensmeyer's stages 0, 1, 2 and 3). There are no specimens that are classed as very weathered (Behrensmeyer's stage 5) and only 10% (n = 19) that can be classed as weathered (Behrensmeyer's stage 4). This pattern suggests that the majority of faunal specimens was deposited into the cave and buried relatively quickly without much time exposed to weathering processes on the surface. As discussed in the Chapter 3, sub-surface weathering rates are assumed to be much lower than surface weathering rates but are generally unknown (Lyman 1994), and this is especially true for karst environments. In the case of the Primary Infill, post-depositional bone surface weathering seems to have affected the bone to a small degree, preserving the condition of the bone surface through multiple resedimentation phases and extensive post-fossilisation breakage. Bearing in mind the recognised issues with the tempo at which the weathering processes work, it is prudent to suggest that the Primary Infill fauna was deposited quickly into the cave in a fresh condition and sustaining some level of breakage during this primary sedimentation. The fauna was then fossilised prior to the attritional affects of re-distribution. There is, however, a component of the Primary Infill assemblage (10%) which suggests some bones may have entered the cave after a significant period of time exposed on the surface as indicated by the 16% of weathered elements.

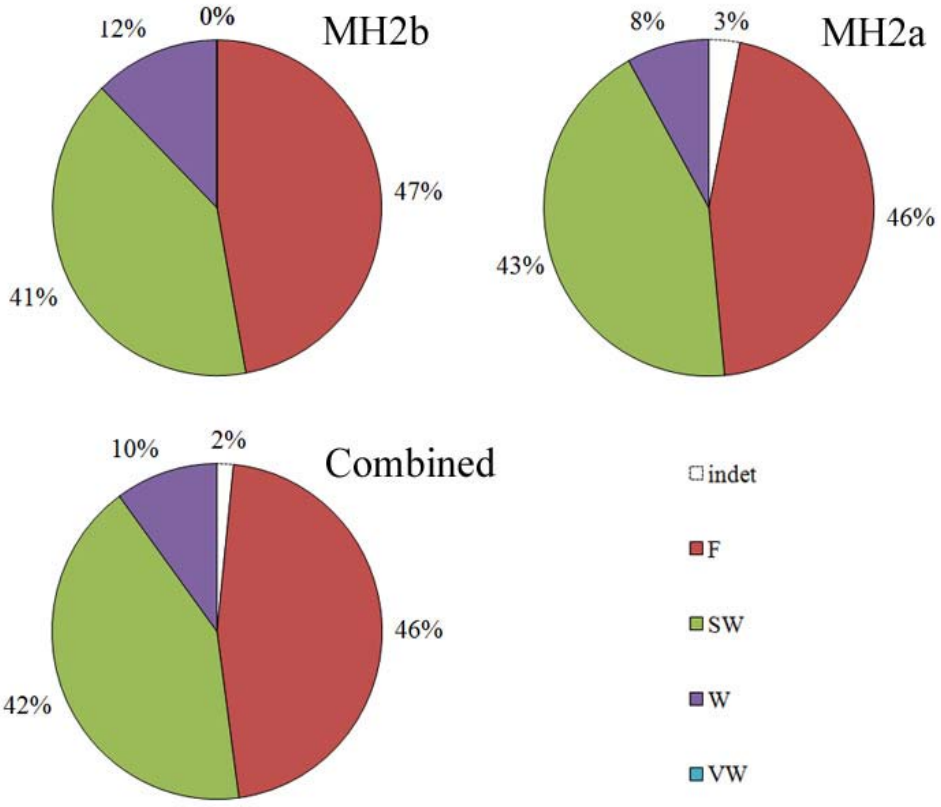


Figure 7.14 Bone condition for the Primary Infill.

7.2.5 Primary Infill taxonomy

The high levels of fragmentation and low representation of taxonomically unidentifiable specimens makes the taxonomic list small. The MH2b and MH2a samples are presented separately before the whole Primary Infill is interpreted.

In the MH2b assemblage, the genus *Equus* was identified and one specimen could be identified to family level, Cercopithecidae of a *Papio* size. Only *Procavia antique* could be identified to species level. The presence of these species is unremarkable for the Cradle sites. The significance of the presence of *Equus* has been discussed in Section 3.6. The presence of *Procavia antiqua* is unremarkable and is discussed in the T1 taxonomic analysis. The Old World monkey (Cercopithecidae) specimens also appear many of the Cradle sites including: Kromdraai A and B; Coopers D; Swartkrans Lower Bank, Hanging Remnant, Member 2 and 3 (de Ruiter *et al.* 2008) and Drimolen (Keyser *et al.* 2000).

Indeterminate monkey species are not useful as temporal indicators as they are be found in a temporally broad range of deposits including M2 (T. Pickering *et al*. 2004a), M4 (Kibii 2007) and M5E (T. Pickering 1999), but have not yet been found in the Lincoln Cave.

The MH2a assemblage yields a similar taxonomic representation. The non-bovid taxonomic list is still very small due to the sample size and includes *Equus* and *Procavia antiqua* both of which were identified in the MH2b assemblage. The third species was identifiable within the MH2a assemblage, the Felid *Caracal caracal*.

The non-bovid species represented in the combined MH2b and MH2a assemblages are commonly found in many of the Cradle sites and most, with exception of *Equus,* are found in a temporally broad spectrum of deposits. *Equus* is considered to have arrived in East Africa 2.3Ma (Churcher & Richardson 1978; Berger *et al*. 2002, Brugal *et al*. 2003) and in South Africa after, and is associated with deposits around the Cradle of 2Ma or younger (See Section 3.6 for discussion). The presence of both *Caracal caracal*, Cercopithecidae and *Equus* may suggest a more open landscape environment with a proximity to more closed shelter. It is likely that the deposit has been intensely time averaged and so palaeoenvironmental interpretations not be considered reliable. It could be said at the time of death of each specimen certain environmental conditions may have prevailed, it may be, however, that each specimen represents a burial time thousands of years apart. The process of time-averaging can be caused in the primary sedimentation deposit as a result of the great periods of accumulation time, or by the mixing of sediments during resedimentation.

7.2.6 Primary Infill taphonomy

Table 7.6 presents the bovid skeletal element data for the MH2b excavation. The presence of large bovids in the assemblage has been mentioned earlier in the analysis to indicate the high level of fracture suffered by the elements during multiple episodes of deposition. All major body parts are represented from

vertebrae through to the tarsals in size class two and three bovids. As can been seen from the MNI data, the small sample size has allowed the recognition of only a single specimen. What is evident is that most elements of the size class two and three bovid skeletons are present, indicating that all body parts of these specimens must have been deposited. Unfortunately, the small sample size does make suggestions of bone accumulation agents tentative. With a greater sample size, patterns would emerge regarding the abundance of certain elements which could suggest either carnivore or natural, death trap accumulation. The presence of a hyaena coprolite does suggest there was a denning site within the catchment area of the cave, most likely the upper cave itself. In terms of bone surface modification, one rib element with tooth scoring and another with rodent gnawing marks have been identified.

Skeletal part	Size 1	Size 2	Size 3
Skull		1/1/1	
Thoracic		1/1/1	1/1/1
Lumbar			4/3/1
Rib			1/1/1
Humerus		1/1/1	3/2/1
Radius	1/1/1	1/1/1	1/1/1
Unciform			1/1/1
Metacarpal		1/1/1	
Femur			1/1/1
Tibia		1/1/1	
Astragalus			1/1/1
Navicular-cuboid		1/1/1	
Metatarsal			1/1/1
Phalanx III		1/1/1	
Upper LBS		3/1/1	
Intermediate LBS			
Metapodial		3/1/1	4/1/1

Table 7.6 Primary Infill MH2b site skeletal element representation of bovid taxa. NISP/MNE/MNI data is given for each cell in columns two through four. LBS: Long Bone Shaft.

In the case of MH2a and MNI of four *Equus* specimens could be accounted for based on the abundance of premolar specimens. Table 7.7 presents the skeletal element representation of bovid taxa, again the small sample size allows only classification to bovid size class. The evident pattern is similar to that seen in the MH2b assemblage in that more elements are represented from size class two and size class three bovid than the smallest size class one. All major parts of the body are represented, with the skull, appendicular and podial elements all present. The relatively large number of rib fragments in the MH2a assemblage has been discussed already. In terms of bone surface modification, one waterlogged, rotten specimen, one LBS specimen with tooth pits and two specimens with attrition consistent with rolling and abrasion were found.

When the two assemblages are combined, and considered as a single representative sample of the Primary Infill, the same general trend is seen in that within the Bovidae, all body proportions of size class two and size class three are found, meaning that the whole skeleton was likely to have been deposited in a single event. The likelihood that these specimens represent the same individual is very small and it is more probable that the broad representation of elements relates to the accumulation agent. The bone surface modification data indicates a component of either hunted or scavenged fauna being consumed within the catchment of the cave opening, followed by rodent activity and an element of pre-fossilisation movement that damaged the cortex of several specimens. The presence of rotten bone suggests a pooling of water in the cave prior to diagenesis. This is not an uncommon situation within cave recesses but the bone would need to be standing for a significant amount of time to cause such bone modification. The high levels of post-fossilisation breakage have removed much of the evidence preserved on the edges of bone, precluding the identification of digestive corrosion modification (Andrews 1990) and general fresh bone breakage data which may yield information regarding the timing of the breakage in relation to death. The small samples sizes of the sub-assemblages and of the combined Primary Infill assemblage unfortunately precluded confident interpretations of the faunal accumulation agent but some diagnostic taphonomic indicators, like the

coprolite, were excavated allowing at least suggestions to be made of a contributing primary sedimentation condition.

Skeletal part	Size 1	Size 2	Size 3
Skull		1/1/1	1/1/1
Thoracic	2/1/1		
Indet. vertebra		1/1/1	
Rib		6/3/1	
Humerus			2/1/1
Radius			2/2/2
Ulna			1/1/1
Metacarpal			
Femur			
Tibia		1/1/1	1/1/1
Phalanx I			1/1/1
Intermediate			

Table 7.7 Primary Infill MH2a site skeletal element representation of bovid taxa. NISP/MNE/MNI data is given for each cell in columns two through four. LBS: Long Bone Shaft.

7.3 The Secondary Infill Stratigraphy

The Secondary Infill takes the form of a relatively small, narrow tongue-shaped deposit which forms over part of the western and central medial portion of the Primary Infill. The deposit has lost the terminal longitudinal portion during the truncation of the STK-MH2 talus. The Secondary Infill longitudinal limits were probably just beyond the proximal section of the Primary Infill. The more distal reaches of the Secondary Infill are heavily calcified, with the more proximal areas being softer and decalcified. The more proximal area is where the pilot profile sampled the Secondary Infill to take advantage of the softer sediments. Figure 7.15 shows the Secondary Infill morphology in relation to the Primary Infill. The arrows depict the sediment flow direction for the different deposits. The aspect of the photograph implies that the surface of the Primary Infill is flat, but this is not accurate. At this point of the talus the surface of the Primary Infill is almost

horizontal east to west, but is sloping in a southerly direction, away from the northern wall, and towards the camera, at an angle of 31°. The base line of the Secondary Infill illustrates the gradient of the Primary Infill surface. As discussed in Section 2.5.1 and depicted in Figure 2.10, the morphology of subsequent infilling sediments into the same receptacle is heavily influenced by the surface topography of the preceding deposit. The surface morphology of the Primary Infill has significantly influenced the development pattern of the following Secondary Infill. The eastern transverse gradient of the Primary Infill surface rapidly steepens towards the eastern lateral facies, creating two gradients. One slope runs in a southerly direction (longitudinal to the sediment flow) and the other increasingly steep gradient slopes east (transverse to the flow direction) from a shallow 18° to 34° at the eastern termination. The Secondary Infill develops across these slopes, and the sediments gravitate in a south easterly direction, towards the rapidly steepening slope of the eastern lateral facies.

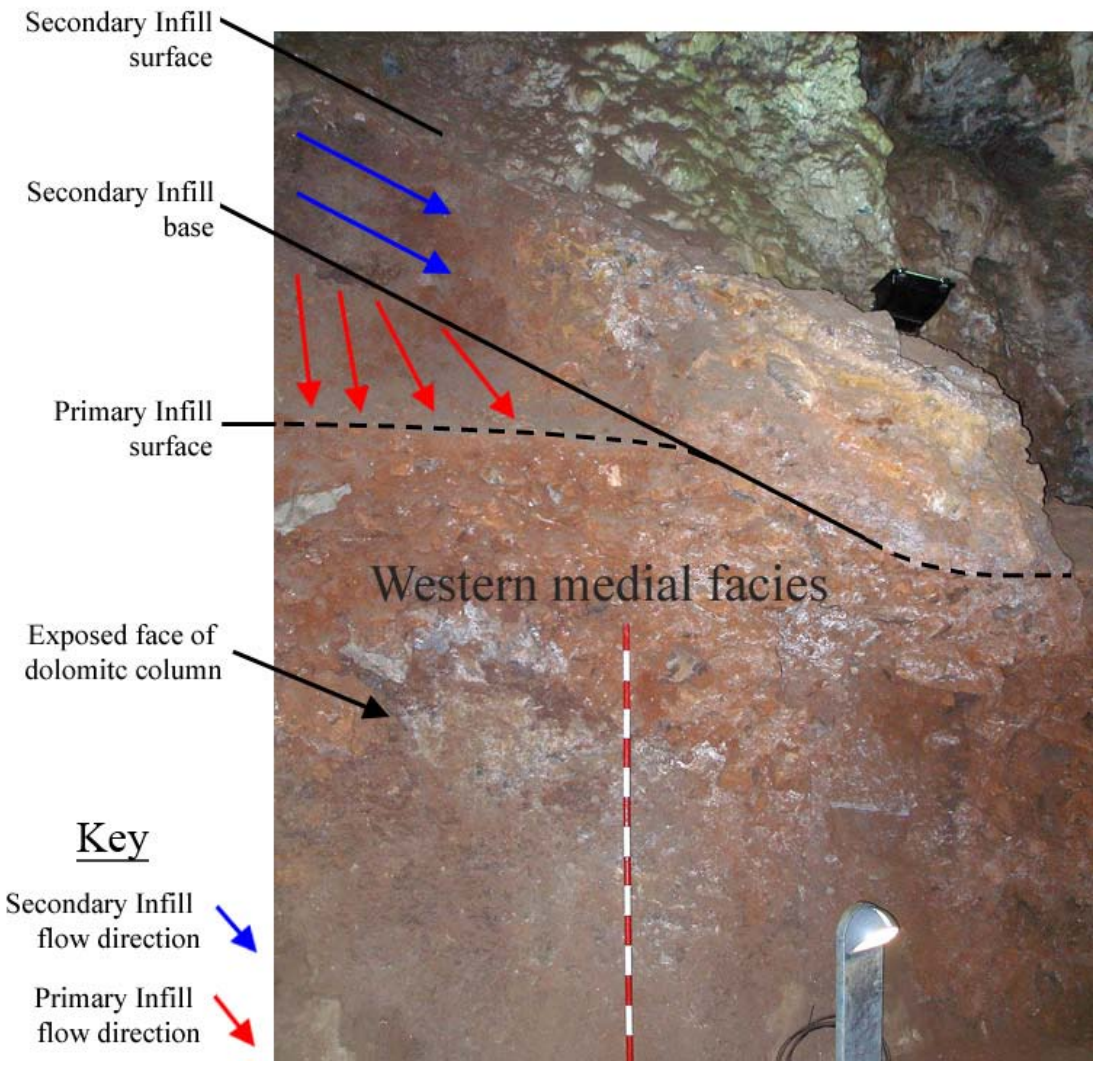


Figure 7.15 STK-MH2 truncated profile showing the western medial facies, the Primary Infill surface and the Secondary Infill boundaries. The arrows represent the different sediment flow directions in each deposit. The range staff segments measure 10cm.

The pilot profile exposed in the proximal reaches of the Secondary Infill allowed an initial assessment of the sediments to be made. Despite the fossiliferous nature of the sediments, no faunal sample was collected. The Secondary Infill sediments can be described as follows:

Dark reddish brown (2.5YR 3/4), unconsolidated matrix-supported silt loam. The deposit is clast-rich (30-40% clasts) containing a wide size range (20mm - >100mm) of angular blocks of dolomite and chert. The clasts are randomly

orientated, often directly associated but rarely imbricated, and show minimal battering. The sediments are heavily calcified towards the distal portion of the deposit and capped by a flowstone of 5-10cm in thickness. Sediments at the proximal portion of the deposit are decalcified and unconsolidated below the flowstone. The matrix is rich in fossil material ranging in size from 20mm to >100mm. No archaeological material was recovered. Interstitial voids are generally filled with sediments but some contain aragonite and calcite crystals.

The Secondary Infill sediments are very similar to the transverse western medial sediments of the Primary Infill and differentiation between the two deposits by observation only is difficult without the surface remnants as depositional boundary indicators. The similarities suggest a comparable mode of accumulation and movement of the sediments. The Secondary Infill merely represents a short-term depositional episode which has subsequently been capped by a flowstone which has covered both the Secondary Infill and then accumulated to the east, down the eastern lateral slope, to cover the eastern lateral portion of the Primary Infill.

7.4 STK-MH2 Conclusions

Both the Primary and Secondary infills have accumulated through the same process and from the same source. The Secondary Infill represents a minor flow of sediments across the main Primary Infill surface in a south-easterly direction. The shape and direction is heavily influenced by the shape on the underlying Primary Infill. The analogous formation processes classify the Secondary Infill as a later episode of the MH2 development and not necessarily a distinct deposit or facies. The inaccessibility of the 'soft' Secondary Infill prohibited sediment or faunal sampling. The Primary Infill represents a large sediment body that once spread across Gallery A in the western Milner Hall. The removal of the medial and distal portions of the talus has left a large vertical surface of the truncated talus deposit. The proximal part of the talus, which formed directly against the northern wall is the only part available for investigation. The exposed transverse

facies, contained within the proximal truncated face, do allow the examination of the morphological attributes which indicate the formation dynamics shaping the MH2 deposit. The lateral stratigraphy of the deposit and lateral grading systems of the Primary Infill have been influenced by the flow direction of sediments falling and tumbling into the cave, and the gradient of the Milner Hall dipping towards the nearby lake. A number of sediment gravity flow types can be identified within the medial and lateral facies of the transverse section and provides an interesting analogy for longitudinal grading systems that are rarely sampled. The matrix-supported part of the Primary Infill shows a distinct inverse grading system which has developed out of the diamicton representing the lateral medial clast heap.

Most of the faunal assemblage was deposited swiftly from the landscape in a fresh condition and incurred a component of damage whilst still in a pre-fossilised condition. Size class two and three bovids were deposited as whole specimens. A minor component of the assemblage seems to have been exposed on the surface for a longer period of time and has suffered damage from carnivores and rodent and waterlogged sediments. The excavation of a hyena coprolite suggests a denning site was nearby. The two primary accumulation signals and the sedimentological evidence could be interpreted as reflecting the changing shape of the upper chamber opening. At first, the entrance provided a death-trap situation in which animals were deposited as whole specimens and incurred breakage during deposition into the cave. The major mode of accumulation of the sediments into the upper chamber was rock fall from a high aven-type opening. The cave entrance then developed into a more sloped opening allowing the habitation of small felids, and hyaenas and rodents which brought bone in from the surrounding landscape. This change introduced sediment more gradually, forming the roughly bedded levels within the finer sediments seen in the upper levels of the Primary Infill. The bone breakage data indicates the majority of breakage has been inflicted post-fossilisation, during the re-distribution of the sediments. It can be suggested from the depositional processes accumulating the sediments, that the same rock fall tumbling process would have contributed a significant amount to that breakage pattern. The tendency of fossil bone surface to be resistant to post-fossilisation damage has been identified in the other investigated deposits. It

seems most post-fossilisation damage focuses the breakage on the specimen edges. Because no upper chamber has been linked to the supply of the MH2 deposit, understanding the levels of sediment movement prior to deposition into the Milner Hall is difficult. Numerous phases of re-distribution around the upper chamber may have occurred inflicting an added generation of breakage.

The taxonomic representation within the Primary Infill is unclear when it comes to comparisons with the nearby deposits. The Lincoln Cave, for instance, has yielded *Equus* and small, indeterminate felids of the same size as the Caracal (Reynolds *et al*. 2007). M5W has yielded *Cercopithecus* and *Procavia antiqua* (Reynolds *et al*. 2007). The absence of a clear taxonomic signal is not surprising given the small sample size. The assemblage within the Lincoln Cave, however, is also not large and so also may not be fully representative. What can be said is that the Primary Infill is of a relatively young age as the inclusion of *Equus* indicates. The time-averaging issues related to secondary sedimentation deposits also prevent suggestions of palaeoecological conditions during primary sedimentation.

In summary, the formation history of the STK-MH2 deposit can be deciphered but only from the point at which sediments entered the Milner Hall. The processes influencing the morphology of the deposit have been discussed above. What has not been possible, with the exception of tentative suggestions based on stratigraphy and taphonomy, is the identification of the source deposit's history. The sediments and fauna contained within the STK-MH2 deposit are not traceable at present. Until an upper chamber related to the Milner Hall can be identified, the association to the main Sterkfontein surface deposits or the Lincoln Cave remains impossible. The age of the deposit, although younger than 2Ma, cannot be refined as no diagnostic temporal indicators were found other than *Equus*. Stratigraphically the distance the STK-MH2 deposit resides from the main Sterkfontein members and the proximity to the Lincoln Cave makes the latter the most likely source for the sediments. No breccias have yet been tracked from the Sterkfontein system west of M5W. The Lincoln Cave, however, extends >10m further west, placing the westerly extremity of the system almost over the MH2

area. A larger faunal assemblage would, hopefully provide greater taxonomic resolution.

CHAPTER 8 SUMMARY AND DISCUSSION

Figure 8.1 presents a schematic plan view of the central underground area and each respective investigation area. The features that have been discussed at length in the analysis and are pertinent to the formation history of the focus sites are also indicated.

8.1 The Eastern Milner Hall

The research presented in this thesis has investigated deposits spanning the entire depositional history of the Sterkfontein caves. The Milner Hall represents one of the lowest parts of the caves and has been receiving sediments from around the cave since the system started to open to the surface. The central position of the eastern Milner Hall, with respect to the surface exposed deposits and the other subterranean deposit, has ensured that sediments deriving from many deposits have gradually been worked down and into this area. It is probable that those sediments deriving from the M5E (Member 5 East) area of the surface exposed deposits includes small quantities of M4 (Member 4) material that derived from close to the opening of Name Chamber Feeding Shaft on the surface, as suggested by Avery *et al*. (2010). Including T4, a total of five deposits has accumulated into two talus slopes in the eastern Milner Hall area. T4 (Talus 4) is the basal unit of the STK-MH1 excavation (Milner Hall 1) and represents one of the earliest primary sedimentation deposits of allogenic derivation to have accumulated into the Sterkfontein caves. Those currently recognised deposits that have contributed to the eastern Milner Hall include both facies identified within Member 2, the deeper portions of the M5E Oldowan deposit, and possibly some M4 sediments. The deposits have been accumulated either through early primary sedimentation accumulation or through secondary sedimentation redistribution. This area has accumulated the highest density of temporally diverse deposits yet found at Sterkfontein. Two areas where excavated in an attempt to clarify the depositional history of the central underground deposits. Named STK-MH1 and STK-EC1,

both sites focus on talus slopes that have formed directly under the main confluence of the Name Chamber and Silberberg Grotto. The justification for the placement of each excavation is discussed in Chapter 1. The STK-MH1 excavation (Figure 8.1) sampled a large talus slope that has spread from the confluence point into the eastern area of the main chamber of the Milner Hall. The excavation uncovered 4 deposits. These were named T1 through T4 based on their order of deposition. T2, T3 and T4 represent unmixed deposits deriving from different chambers and areas during distinct time periods. T1 represents a heavily mixed, disturbed deposit created through the blasting and removal of a large stalactite at the top of the MH1 slope during the years of mining at Sterkfontein.

The STK-EC1 excavation (Elephant Chamber 1) sampled a relatively small talus which is contained within a long, tall and narrow passage (called the EC1 passage) which opens, in the east, at the top of the MH1 talus and beneath the M2 (Member 2) Hanging Remnant (Figure 8.1). The passage is split into and upper and lower passage by two false floors. The false floors are made up of heavily cemented fine-grained sediment and represent remnants of the surface of a previous deposit filling the passage. The EC1 excavation uncovered two distinct deposits. The first deposit, named Secondary Talus (S.T.), derived from the Name Chamber Far Western Talus in a single surge of sediments. The second deposit, named the Primary Talus (P.T.), accumulated much earlier and represents a collapse or rapid surge of material exiting the Silberberg Grotto during the deposition of the M2 lower facies. The stratigraphic sequence describing the full history of deposition into the eastern Milner Hall is presented below.

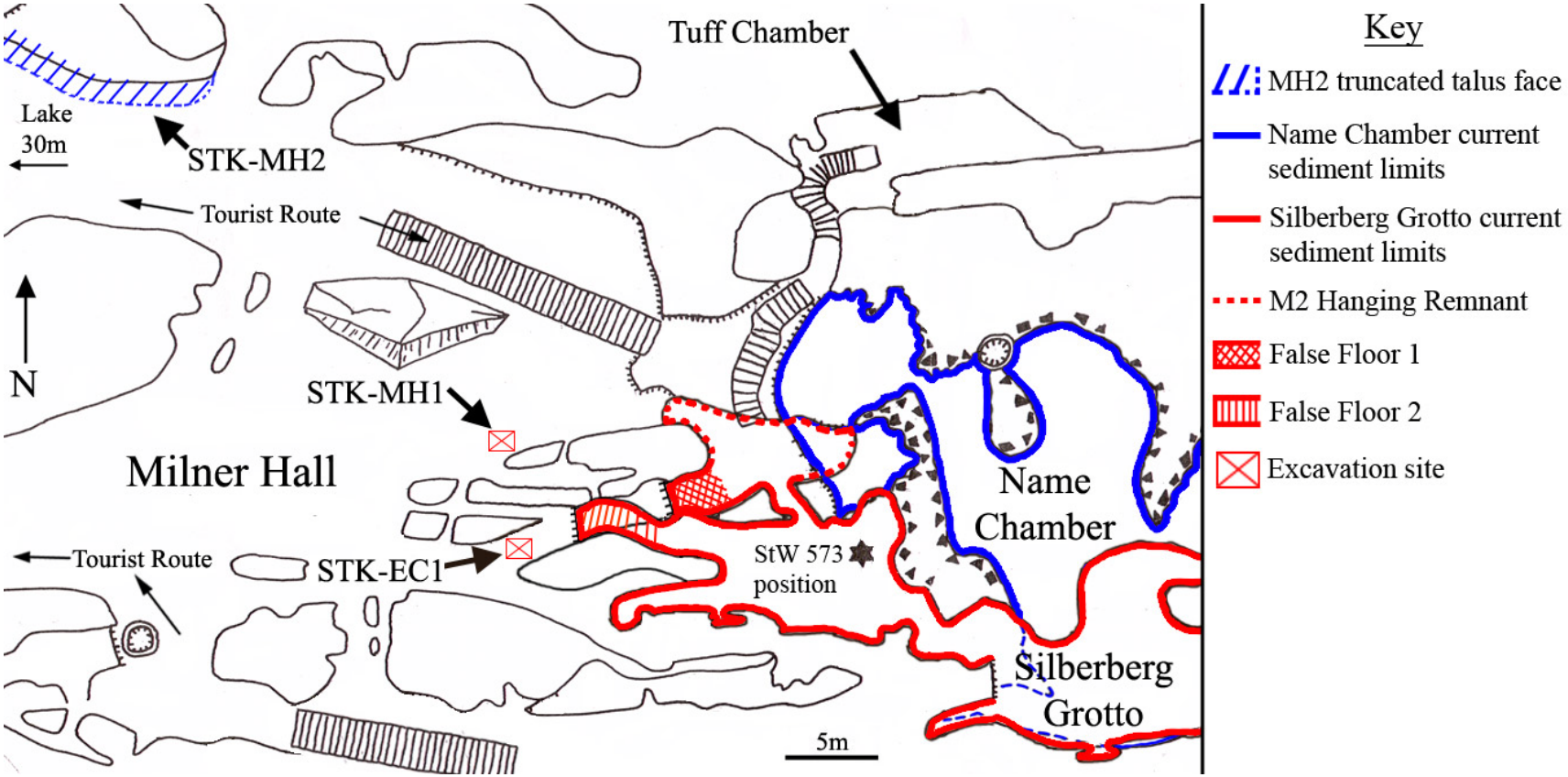


Figure 8.1 Schematic plan of the Sterkfontein central underground area, positions of relevant chambers and investigated areas. Each site investigated is indicated. Adapted from Martini *et al*. (2003).

1. The earliest allogenic sediments deposited into the karst system were accumulated through numbers of small apertures. Water moving through the early cave system brought those sediments to the lowest area of the caves, depositing them in the shallows and margins of the water-table. Low levels of vadose breakdown occasionally deposited ceiling and wall-derived debris into the deposit. Fluctuations in the water-table consolidated the sediments and blurred the internal stratigraphy but sustained a high sediment moisture content precluding calcification. This deposit constitutes the T4 deposit.
2. An aven-type opening developed in the roof of the Silberberg Grotto "in the vicinity of the stalagmite boss [forming against the southern wall of the Silberberg Grotto]" (Clarke 2006, pp. 117). This entrance allowed the deposition of the M2 lower facies sediments. These sediments formed an extensive talus deposit in a westerly direction from the opening, filling into the deeper areas of the Silberberg Grotto (Clarke 2006). Deposition was cyclical with many periods of flowstone development. The presence of mudstone and different forms of travertine suggest regular ingresses of fresh water and a high rate of localised speleothem growth. A collapse event that may have coincided with the further opening of the M2 entrance caused a rapid surge or collapse of the M2 lower facies through one of the north-western exits into the EC1 passage, creating the Primary Talus (P.T.) deposit.
3. Within the Silberberg Grotto the enlarged entrance facilitated the deposition of larger quantities of allogenic clastic material and fauna (Clarke 2006). The aven-type opening acted as a death-trap for carnivores and monkeys (T. Pickering 2004a, Clarke 2006). These sediments constitute the M2 upper facies. The earliest phases of sedimentation deposited these sediments from the Silberberg Grotto into the far eastern Milner Hall and gradually developed the T3 deposit. T3 accumulated into the margins of the water-table and built in many hyperconcentrated sediment flows directly on top of the T4 deposit. The weight of the T3 sediments caused the soft sediment deformation features seen at the T3 T4

contact. The fluctuation of the water-table during the T3 deposition caused a cyclical wetting and drying of the sediments. The continued deposition of the M2 upper facies built an enormous talus that filled most of the eastern Milner Hall and filled the EC1 passage. Close to the end of the M2 upper facies deposition the StW 573 specimen was deposited.

4. Deposition of the M2 upper facies then ceased and the main body of the M2 upper facies was eventually heavily calcified and capped by an extensive flowstone emanating from the area of the boss stalagmite in the Silberberg Grotto (Clarke 2006, 118) and spreading out the north-western exits to the Silberberg Grotto. The deepest portions of the M2 upper facies in the Milner Hall (T3) remained uncalcified due to the continued presence of permanent fresh water and the high clay content of the sediments.
5. Extensive ingresses of fresh water into the Silberberg Grotto then facilitated the collapse seen in the StW 573 specimen breccia and developed pools of fresh water, creating calcite lips on the capping flowstones, shelfstones and botryoidal calcite (Clarke 2006). The increased movement of water into the Silberberg Grotto, and probably through the eastern Milner Hall at the same time, caused the erosion of the medial part of the M2 upper facies deposit in the Milner Hall and the undercutting of the M2 upper facies sediments filling the EC1 passage. This erosive episode shaped both the M2 Hanging Remnant and the EC1 false floors into the forms seen now. The erosive waters also formed the erosion surfaces which have shaped the surfaces of the T3 and P.T deposits.
6. The spaces left by the erosion and transportation of the M2 upper facies sediments were filled considerably later on, from the surges of sediment caused by the over-steepening of more recent talus deposits accumulating within the Name Chamber. The Name Chamber sediments themselves, have been redistributed from the above M5E deposit (Stratford 2008). The dry grain flows emanating from the Name Chamber and forming the Far Western Talus spread across the far eastern Milner Hall, covering the T3

deposit (forming T2) and also filled into the EC1 lower passage, directly onto the P.T. deposit, forming the Secondary Talus (S.T.) deposit.

7. Mining of a large stalactite which also formed in the space left by the erosion of the M2 upper facies violently redistributed a large amount of allogenic sediments that filled the far eastern Milner Hall, forming a mixed, heavily fragmented deposit (T1) directly onto the T2 deposit. The proximity of the M2 Hanging Remnant and the Far Western Talus sediments makes it likely that T1 contains sediment from both.

Figure 8.2 presents the full stratigraphic sequence for the eastern Milner Hall and the area known as the ‘underground central deposits’ in an adjusted Harris Matrix format. When the MH1 (Milner Hall 1) and EC1 (Elephant Chamber 1) stratigraphic sequences are amalgamated, each of the locally found deposits and facies is represented in the sequence.

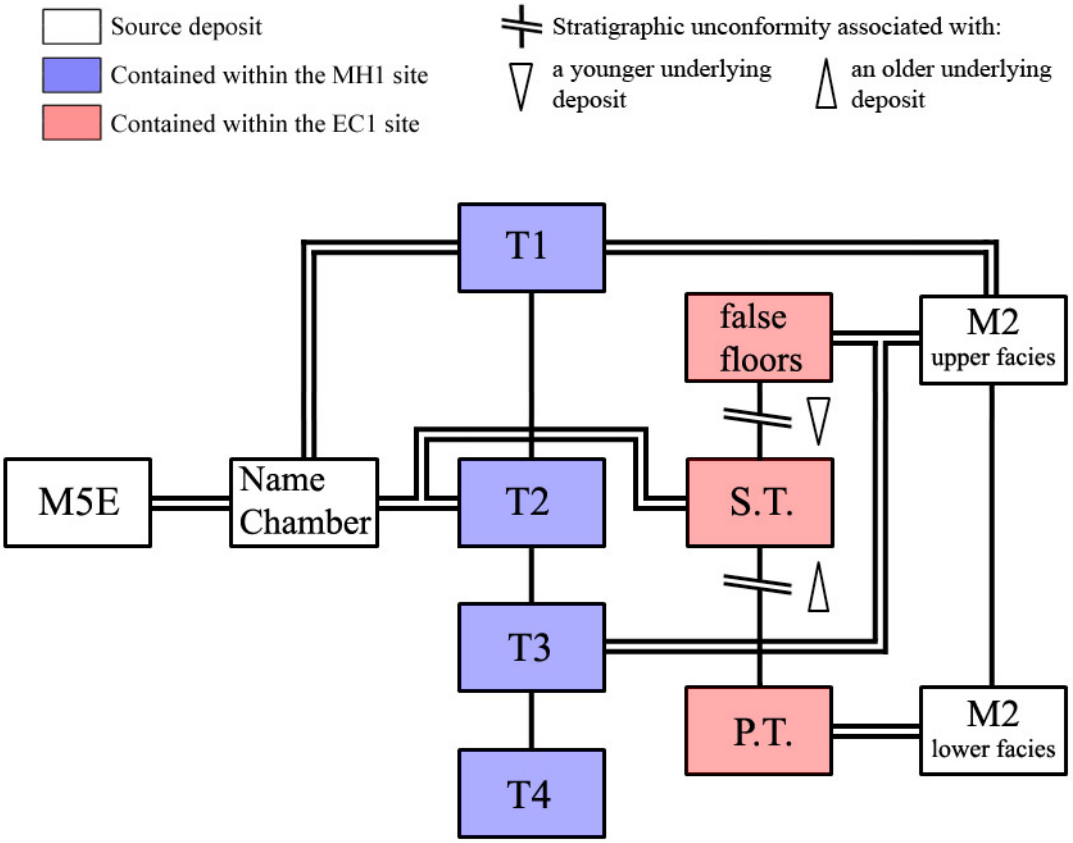


Figure 8.2 Harris Matrix representation of the eastern Milner Hall stratigraphic sequence.

8.2 STK-MH2

The STK-MH2 (Milner Hall 2) site was excavated to clarify the formation history and source of the sediments that constitute the large truncated talus deposit located in the north-western end of the Milner Hall (Figure 8.1). The deposit, which can be split into two main depositional episodes (named the Primary Infill and Secondary Infill), has formed as a secondary sedimentation deposit under an opening high in the roof almost directly above the truncated vertical face. The formation history of the STK-MH2 deposit can be deciphered only from the point at which sediments entered the Milner Hall. The underlying topography of the cave floor has heavily influenced the flow direction and shape of the accumulation sediments, a process evident in all of the investigated deposits. What has not been possible, with the exception of tentative suggestions based on stratigraphy and

taphonomy, is the identification of the history of the deposit's source or sources. The sediments and fauna contained within the STK-MH2 deposit are not traceable at present. Until an upper chamber can be identified above the Milner Hall, the association to the main Sterkfontein surface deposits or the Lincoln Cave remains impossible. The age of the deposit, although younger than 2.3Ma, cannot be refined as no diagnostic temporal indicators were found other than *Equus*. Stratigraphically, the STK-MH2 deposit resides closer to the Lincoln Cave system in the north-west of the site than to the main Sterkfontein members. Based on the proximity to the Lincoln Cave system and the probability that connections to the subterranean chambers were active (see Reynolds *et al*. 2007), I would hypothesise that this is the most likely source for the sediments. The depths of the Lincoln Cave deposits are still unknown and should be investigated in the future to clarify the connections between the two cave systems. A larger faunal assemblage would, hopefully provide greater taxonomic resolution.

8.3 Final Discussion

The processual questions regarding the stratigraphy of the investigated deposits have been addressed in the preceding analyses. The stratigraphic sequence, although complicated and representing the most deposit-dense area of the Sterkfontein caves, has been successfully clarified through the use of a multidisciplinary approach. Identification of primary vs. secondary sedimentation deposits and characterisation of their respective flow dynamics and morphologies allowed tangible deposit boundaries and sediment sources to be proposed. These stratigraphic proposals were substantiated and supported by a host of sedimentological, faunal and archaeological examinations.

The primary theoretical question concerned the role of sediment flow dynamics on faunal particle modification, distribution and, ultimately, representation. Taphonomic analysis and most comparative analyses based on animal remains rely on abundance of faunal attributes and recognition of patterns relating to bone modification, which allow interpretations of the primary depositional context.

Faunal analyses, in this study, are generally limited because of the small proportion of assemblages appropriate for examination. The majority of information derives from elements identifiable to specific element and taxa. This immediately produces issues of sample representativeness, as was demonstrated by the subsamples of the T1 assemblage. In addition to the sampling problem, the complex site formation processes make interpretations very difficult.

The patterns found through the examination of the excavated material and the bone breakage tests suggest a complicated relationship exists between bone and shape, breakage, diagenesis, transport and ultimately distribution through the deposit. What is indicated is that increasing breakage levels reduce the size and change the shape of most skeletal elements, thereby affecting the transport potential. Some elements maintain their general shape (shaft bones and ribs) through multiple levels of breakage, and some bones change radically (dentition) in the intermediate stages of breakage. All bones become more transportable, enabling vertical movement through sediments or promoting further longitudinal movement within a flow process. It may be suggested that longitudinal grading effects on faunal particles diminish with increasing breakage levels. Or, in the context of slope deposits, the effects of longitudinal grading diminish with distance from the source. Essentially, one finds a mixing of elements at a distal location that may have been separated at a more proximal location, due to a shape-averaging process induced by breakage. This was demonstrated in T3, which was developed gradually in many hyperconcentrated flows creating a longitudinally graded deposit over a significant distance. At the terminal portion of the deposit, the vertebrae, which were relatively large and complete, were joined by many smaller shaft fragments originally belonging to large, immobile but vulnerable long bones. The EC1 deposit shows a similar trend but within a grain flow process. The terminal portion, dominated by smaller bone fragments, had a few much larger spherical bones which had been pushed to the snout with the larger clasts during the sediment surge. It would be interesting to sample the element type, shape and size representation at the medial portions of both hyperconcentrated and grain flow deposits. Grading systems sort particles based on shape and size, two factors that are associated with the vulnerability of bones.

As a hypothesis, I would expect to find larger, fragmented pieces of more immobile elements (e.g. bovid mandible) together with complete pieces with more intermediate transport potentials (e.g. humerus and pelvis), in the medial areas.

What is unclear is the exact role of particle shape in different sediments as transport media. One of the recurrent issues encountered with regards to faunal particle transport is the discrepancy between the work of Frostick & Reid (1983) and Voorhies (1969). There are undoubtedly differences between sediment and water as transport media, but I consider that Frostick & Reid used the incorrect model to interpret faunal particle shape and therefore misinterpreted the transport potential of many elements. Experimental work using a selection of shape indices would clarify the role of particle shape in sedimentary flows. It may be that a new shape model needs to be developed to account for the wider range of shapes represented by faunal particles in comparison to geological particles. Using the measurement system adopted in this research such a model is possible.

Sedimentology and accumulation processes are clearly integral to the integrity, preservation and representation of faunal particles. Understanding the site formation context prior to excavation, or from small test pits, would allow one to predict (depending on the sediment flow type and sedimentology) where samples should be taken in order to recover the most representative sample and complete assemblage possible. The extremities of the talus will evidently accumulate different faunal material in different states of modification. It is prudent to sample all portions of the deposit to allow confident fauna-based interpretations. If multiple samples cannot be excavated (which is commonly the case for logistical reasons), recognition of biased assemblages and accounting for them is essential.

The multidisciplinary approach used in this research has been justified by the wealth of corroborating information yielded. This information has inspired many further questions concerning the relationship between sediments, fossils and caves. The approach has been limited in its effective resolution by issues inherent to different disciplines, which were not entirely satisfied by the excavation practices used, and by the time constraints imposed on the research. These issues centre around faunal sample size. The taxonomic and taphonomic analyses require

large samples of fossils to produce statistically confident inferences. The interpretations based on faunal analyses have far reaching repercussions based on the high value given to these forms of data. When faunal remains constitute the only analytical approach to a deposit, misinterpretations of the assemblage, provoked by unrecognised stratigraphic complications, have potentially severe consequences for future research. Excavation of 'soft' sediments allowed the use of *in situ*, accurate, but consequently slow methods with relatively low fossil yields. These more accurate excavation methods allowed detailed fabric analyses to be carried out and *in situ* fossil mapping to assess density and distribution, which greatly improve stratigraphic resolution and understanding. As this research was primarily concerned with stratigraphy, with the faunal analysis being used to support this data, the slower but more accurate excavation techniques were chosen and pursued wherever possible. Clearly there has to be a balance struck between stratigraphic resolution and sample size for taphonomic and taxonomic resolution. The balance of resolution required and respective data value depends on the scientist and the scientist's research focus. This does not, however, justify singular approaches to complex problems that involve a wide variety of processes. The balance of relative data value, and associated sampling and excavation methods, should be seriously considered prior to excavation to avoid any loss of important information that may only be realised after excavations have been completed.

References

Abrahams, A.D., Parsons, A. J., Cooke, R.U. & Reeves, R.W. 1984. Stone movement on hillslopes in the Mo-jave Desert, California: a 16-year record. *Earth Surface Processes and Landforms* 9(5): 365-370.

Abrahams, A.D., Parsons, A.J. & Hirsh, P.J. 1985. Hillslope Gradient-Particle Size Relations: Evidence for the Formation of Debris Slopes by Hydraulic Processes in the Mojave Desert. *The Journal of Geology* 93(3): 347-357.

Abrahams, A.D., Soltyka, N., Parsons, A.J. & Hirsh, P.J. 1990. Fabric Analysis of a Desert Debris Slope: Bell Mountain, California. *The Journal of Geology* 98(2): 264-272.

Ahler, A.S. 1989. Mass analysis of flaking debris: studying the forest rather than the trees. In: Henry, D.O. & Odell, G.H. (Eds.), *Alternative Approaches to Lithic Analysis. Archaeological Papers of the American Anthropological Association.* 85-118. American Anthropological Association.

Akerman, H.J. 1984. Notes on Talus Morphology and Processes in Spitsbergen. *Geografiska Annaler Series A, Physical Geography* 66(4): 267-284.

Albjar, G., Rehn, J. & Stromquist, L. 1979. Notes on Talus Formation in Different Climates. *Geografiska Annaler Series A, Physical Geography* 61(3/4): 179-185.

Allen, J.R.L. 1985. *Principles of Physical Sedimentology*. Chapman & Hall.

Andrefsky, Jr. W. 2001. Emerging directions in debitage analysis. In: Andrefsky, Jr. W. (Ed.), *Lithic Debitage: Context, Form, Meaning*. 1-14. University of Utah Press: Salt Lake City.

Andrefsky, Jr. W. 2006. The application and misapplication of mass analysis in lithic debitage studies. *Journal of Archaeological Science* 20: 1-11.

Andrews, P. 1990. *Owls, Caves and Fossils*. Natural History Museum and University of Chicago Press: Chicago, Illinois.

Arroyo, A.B.M., Ruiz, M.D.L., Bernanbeu, G.V., Román, R.S., Morales, M,R,G. & Straus, L.G. 2008. Archaeological implications of human-derived manganese coatings: a study of blackened bones from El Mirón Cave, Cantabrian, Spain. *Journal of Archaeological Science* 35: 801-813.

Austin, R.J. 1999. Technological characterization of lithic waste-flake assemblages: multivariate analysis of experimental and archaeological data. *Lithic Technology* 24: 53-68.

Avery, D.M. 2001. The Plio-Pleistocene vegetation and climate of Sterkfontein and Swartkrans, South Africa, based on micromammals. *Journal of Human Evolution* 41: 113-132.

Avery, D.M., Stratford, D.J. & Sénégas, F. 2010. Micromammals and the formation of the Name Chamber at Sterkfontein, South Africa. *Geobios* 43: 379-387.

Bamford, M. 1999. Pliocene woods from an early hominid cave deposit, Sterkfontein, South Africa. *South African Journal of Science* 95: 231-237.

Bárdossy, G. 1982. Karst Bauxites. Bauxite Deposits on Carbonate Rocks. *Developments in Economic Geology* 14: 441.

Bárdossy, G. & Aleva, G.J.J. 1990. *Lateritic Bauxites*. Elsevier: Amsterdam.

Bar-Matthews, M., Ayalon, A., Matthews, A., Sass, E. & Halicz, L. 1996. Carbon and oxygen isotope study of the active water–carbonate system in a karstic Mediterranean cave: implications for palaeoclimate research in semiarid regions. *Geochimica et Cosmochimica Acta* 60: 337-347.

Bar-Matthews, M., Ayalon, A. & Kaufman, A. 1997. Late Quaternary paleoclimate in the Eastern Mediterranean region from stable isotope

analysis of speleothems at Soreq Cave, Israel. *Quaternary Research* 47: 155-168.

Barrett, L., Gaynor, D., Rendall, D., Mitchell, D. & Henzi, S.P. 2004. Habitual cave use and thermoregulation in chacma baboons (*Papio hamadryas ursinus*). *Journal of Human Evolution* 46(2): 215-222.

Behrensmeyer, A.K. 1978. Taphonomic and ecological information from bone weathering. *Palaeobiology* 4: 150-162.

Behrensmeyer, A.K. 1983. Patterns of natural bone distribution on recent land surfaces: implications for archaeological site formation. In: Clutton-Brock, J. & Grigson, C. (Eds.), *Animals and archaeology: 1. hunters and their prey*. 93-106. British Archaeological Reports International.

Behrensmeyer, A.K. 1990. Transport – Hydrodynamics: bones. In: Briggs D.E.G & Crowther, P.R. (Eds.), *Palaeobiology: a synthesis*. 232-235. Oxford Blackwell Scientific Publications. Oxford.

Behrensmeyer, A.K., Kidwell, S.M. & Gastaldo, R.A. 2000. Taphonomy and Palaeobiology. *Palaeobiology* 26(4): 103-147.

Benn, D.I. & Ballantyne, C.K. 1993. The description and representation of particle shape. *Earth Surface Processes and Landforms* 18: 665-672.

Berger, L.R. & Clarke, R.J. 1995. Eagle involvement in accumulation of the Taung child fauna *Journal of Human Evolution* 29: 275-299.

Berger, L.R., Lacruz, R. & de Ruiter, D.J. 2002. Brief Communication: Revised Age Estimates of *Australopithecus*- Bearing Deposits at Sterkfontein, South Africa. *American Journal of Physical Anthropology* 119: 192-197.

Berger, L.R. & Lacruz, R. 2003. Preliminary report on the first excavations at the new fossil site of Motsetse, Gauteng, South Africa. *South African Journal of Science* 99(3): 279-282.

Berger, L.R., de Ruiter, D.J., Steininger, C.M. & Hancox, J. 2003. Preliminary results of excavations at the newly investigated Coopers D deposit, Gauteng, South Africa. *South African Journal of Science* 99: 276-278.

Bertran, P. & Texier, J-P. 1995. Fabric Analysis: Application to Palaeolithic Sites. *Journal of Archaeological Science* 22: 521-535.

Bertran, P. & Texier, J-P. 1999. Facies and microfacies of slope deposits. *Catena* 35: 99-121.

Bertran, P., Hetu, B., Texier, J-P. & van Steijn, H. 1997. Fabric characteristics of subaerial slope deposits. *Sedimentology* 44: 1-16.

Bishop, L.C., Pickering, T., Plummer, T. & Thackeray, F. 1999. Palaeoenvironmental setting for the Oldowan industry at Sterkfontein. Paper presented at the *XVth International Congress of the International Union for Quaternary Research, The Environmental Background to Hominid Evolution in Africa,* August, Durban.

Bones, J.G. 1973. Process and Sediment Size Arrangement on High Arctic Talus, Southwest Devon Island, N.W.T., Canada. *Arctic and Alpine Research* 5(1): 29-40.

Brady, N.C. 1999. *The Nature and Properties of Soils* (12th ed.). Prentice-Hall: Upper Saddle River, New Jersey.

Brain, C.K. 1958. The Transvaal Ape-man-bearing Cave Deposits. *Transvaal Museum Memoir No. 11.* Pretoria.

Brain, C.K. 1974. Some suggested procedures in the analysis of bone accumulations from southern African Quaternary sites. *Annuals of the Transvaal Museum* 29: 1-8.

Brain, C.K. 1981. *The hunters or the hunted?* University of Chicago Press: Chicago.

Brain, C.K. 1993. Swartkrans: A cave's chronicle of early man. *Transvaal Museum Monograph. Pretoria: Transvaal Museum.*

Brink, A.B.A. & Partridge, T.C. 1965. Transvaal karst: some considerations of development and morphology. *South African Geographical Journal* **47**: 11-34.

Broom, R. 1936. A new fossil anthropoid skull from South Africa. *Nature* 138: 486-488.

Broom, R. 1945a. Age of the South African ape-men. *Nature* 155: 389-390.

Broom, R. 1945b. A new primitive hyaena from Sterkfontein. *South African Museum Association Bulletin* 3: 273.

Broom, R. 1947. Discovery of a New Skull of the South African Ape-Man, Plesianthropus. *Nature* 159: 672-672.

Broom, R. & Schepers, G.W.H. 1946. The South African fossil ape-men, the *Australopithecinae*. *Transvaal Museum Memoir No. 2*. Pretoria.

Broom, R., Robinson, J.T. & Schepers, G.W. 1950. Sterkfontein apeman, *Plesianthropus*. *Transvaal Museum Memoir No. 4*. Pretoria.

Brugal, J.P., H. Roche, H. & Kibunjia, M. 2003. Faunes et paléoenvironnements des principaux sites archéologiques plio-pléistocènes de la formation de Nachukui (Ouest-Turkana, Kenya), *Comptes Rendus Palevol* **2:** 675-684.

Bunn, H.T. 1982. *Meat eating and human evolution: studies on the diet and subsistence patterns of Plio-Pleistocene hominids in East Africa*. Ph.D. Dissertation, University of California, Berkley. Ann Arbour.

Butzer, K.W. 1981. Cave sediments, Upper Pleistocene stratigraphy, and Mousterian facies in Cantabrian Spain. *Journal of Archaeological Science* 8: 133-183.

Cañón-Tapia, E. & Chávez-Álvarez, J. 2004. Theoretical aspects of particle movement in flowing magma: implications for the anisotropy of magnetic susceptibility of dykes. *Geological Society, London, Special Publications* 238: 227-249.

Carlson, K.J. & Pickering, T.R. 2003. Intrinsic qualities of primate bones as predictors of skeletal element representation in modern and fossil carnivore feeding assemblages. *Journal of Human Evolution* 44: 431-450.

Carrión, J.S. & Scott, L. 1999. Twentieth century changes in montane vegetation in the eastern Free State, South Africa, derived from palynology of hyrax dung middens. *Journal of Quaternary Science* 14(1): 1-16.

Chandler, R.J. 1973. The Inclination of Talus, Arctic Talus Terraces, and Other Slopes Composed of Granular Materials. *The Journal of Geology* 81(1): 1-14.

Churcher, C.S. & Richardson, M.L. 1978. Equidae. In: Maglio, V.J. & Cooke. H.B.S. (Eds.), *Evolution of African Mammals*. 379-422. Cambridge: Harvard University Press.

Clarke, J. & Kietzke, K.K. 1967. Paleoecology of the Lower Nobular Zone, Brule Formation, in the Big Badlands of South Dakota. In: Clarke, J., Beerbower, J.R. & Kietzke, K.K. (Eds.), *Oligocene sedimentation, stratigraphy, and paleoclimatology in the Big Badlands of South Dakota*. 111-137. Fieldiana Geology Memoir.

Clarke, R.H. & McIntyre, D.B. 1951. A macroscopic method of fabric analysis: *American Journal of Science* 249: 755-768.

Clarke, R.J. 1985. Early Acheulean with *Homo habilis* at Sterkfontein. In: Tobias, P. V. (Ed.), *Hominid Evolution: Past, Present, and Future*. 287-298. Alan R. Liss: New York.

Clarke, R.J. 1988. Habiline handaxes and paranthropine pedigree. *World Archaeology* 20: 1-12.

Clarke, R.J. 1989. A new *Australopithecus* cranium from Sterkfontein and its bearing on the ancestry of *Paranthropus.* In: Grine, F. (Ed.), *Evolutionary History of the 'Robust' Australopithecines.* 285-292. Aldine de Gruyter: New York.

Clarke, R.J. 1994a. On some new interpretations of Sterkfontein stratigraphy. *South African Journal of Science* 90: 211-214.

Clarke, R.J. 1994b. Advances in understanding the craniofacial anatomy of South African early hominids. In: Corruccini, R.S. & Ciochon, R.L. (Eds.), *Integrative Paths to the Past: Essays in Honor of F. Clark Howell.* 205-222. Prentice Hall: New Jersey.

Clarke, R.J. 1998. First ever discovery of a well-preserved skull and associated skeleton of *Australopithecus. South African Journal of Science* 94: 460-463.

Clarke, R.J. 2002. On the unrealistic 'Revised age estimates' for Sterkfontein. *South African Journal of Science* 98: 415-419.

Clarke, R.J. 2006. A deeper understanding of the stratigraphy of Sterkfontein fossil hominid site. *Transactions of the Royal Society of South Africa* 61(2): 111-120.

Clarke, R.J. 2008. Latest information on Sterkfontein's *Australopithecus* skeleton and a new look at *Australopithecus*. *South African Journal of Science* 104: 443-449.

Cooke, H.B.S. 1938. The Sterkfontein bone breccia: a geological note. *South African Journal of Science* 35: 204-208.

Cooke, H.B.S. 1974. Plio-Pleistocene deposits and mammalian faunas of eastern and southern Africa. *Proceedings of 5th Congress on the Neogene of the Mediterranean* BRGM, Paris. 78(1): 99-108.

Cooke, H.B.S. 1991. *Dinofelis barlowi* (Mammalia, Carnivora, Felidae) cranial material from Bolt's Farm, collected by the University of California African Expedition. *Palaeontologia Africana* **28:** 9-21.

Corey, A.T. 1949. *Influence of shape on the fall velocity of sand grains*. M.Sc. Dissertation. A & M College. Colorado.

Costa, J.E. 1984. Physical geomorphology of debris flows. In: Costa, J.E. & Fleisher, P.J. (Eds.), *Developments and Applications of Geomorphology*. 268-317. Springer: Berlin & New York.

Coussot, P. & Meunier, M. 1996. Recognition, classification and mechanical description of debris flows. *Earth-Science Reviews* 40(3-4): 209-227.

Coyne, M.S. & Thompson, J.A. 2006. *Fundamental Soil Science.* Thomson Delmar Learning.

Cukrowska, E.M., McCarthy, T.S., Pole, S., Backwell, L. & Steininger, C. 2005. The chemical removal of manganese dioxide coatings from fossil bones from the Cradle of Humankind, South Africa. *South African Journal of Science* 101: 101-103.

Culling, W.E.H. 1963. Soil creep and the development of hillside slopes. *The Journal of Geology* 71(2): 127-161.

Curnoe, D. 2002. Fossil human taxonomic hypotheses examined with topology dependent permutation tail probability (T-PTP) tests. *South African Journal of Science* 98: 310-312.

Curnoe, D. & Tobias, P.V.T. 2006. Description, new reconstruction, comparative anatomy, and classification of the Sterkfontein StW 53 cranium, with discussions about the taxonomy of other southern African early Homo remains. *Journal of Human Evolution* 50: 36-77.

Dart, R.A. 1948. The Makapansgat proto-human *Australopithecus prometheus*. *American Journal of Physical Anthropology* 6: 259-284.

Dart, R.A. 1955. The first *Australopithecine* fragment from the Makapansgat Pebble Culture stratum. *Nature* 176: 170-171.

Dart, R.A. 1959. The first *Australopithecine* cranium from the Pink Breccia at Makapansgat. *American Journal of Physical Anthropology* 17: 77-82.

Dasgupta, P. 2003. Sediment gravity flow – the conceptual problems. *Earth-Science Reviews* 62: 265-281.

Delson, E. 1984. Cercopithecid biochronology of the African Plio-Pleistocene: correlation among eastern and southern hominid-bearing localities. *Courier Forschungsinstitut Senckenberg* 69: 199-218.

Dirks, P.H.G.M., Kibii, J.M., Kuhn, B.F., Steininger, C., Churchill, S.E., Kramers, J.D., Pickering, R., Farber, D.L., Mériaux, A-S., Herries, A.I.R., King, G.C.P. & Berger, L.R. 2010. Geological Setting and Age of *Australopithecus sediba* from Southern Africa. *Science* 328: 205-207.

Draper, D. 1898. Meeting of the geological Society of South Africa, 12th July 1897. *Transactions of the Geological Society South Africa* 3: 63.

Eisenhart, W.L. 1974. *The fossil cercopithecoids of Makapansgat and Sterkfontein*. BA. Dissertation. University of the Witwatersrand.

Elton, S. 2000. *Ecomorphology and evolutionary biology of African cercopithecoids: providing the ecological context for hominin evolution*. Ph.D. Dissertation, University of Cambridge.

Elton, S. 2001. Locomotor and habitat classifications of *cercopithecoid* postcranial material from Sterkfontein Member 4, Bolt's Farm and Swartkrans Members 1 and 2, South Africa. *Palaeontologia Africana* 37: 115-126.

Farrand, W.R. 1975. Sediment analysis of a prehistoric rockshelter: The Abri Pataud. *Quaternary Research* 5: 1-26.

Farrand, W.R. 2000. *Depositional history of Franchthi Cave, Fascicle 12*. Indiana University Press: Bloomington and Indianapolis.

Farrand, W.R. 2001. Sediments and stratigraphy in rockshelters and caves: A Personal perspective on principles and pragmatics. *Geoarchaeology: An International Journal* 16(5): 537-557.

Farrand, W.R. & McMahon, J.P. 1997. History of the Sedimentary Infilling of Yarimburgaz Cave, Turkey. *Geoarchaeology: An International Journal* 12(6): 537-565.

Field, A.S. 1999. *An analytical and comparative study of the Earlier Stone Age archaeology of the Sterkfontein Valley*. MSc. Dissertation. University of Witwatersrand.

Fladmark, K.R. 1982. Microdebitage analysis: initial considerations. *Journal of Archaeological Science* 9: 205-220.

Ford, D.C. & Williams, P.W. 2007. *Karst Geomorphology and Hydrology*. Chapman and Hall: London.

Francou, B. 1990. Stratification mechanisms in slope deposits in high subequatorial mountains. *Permafrost and Periglacial Processes* 1: 249-263.

Freedman, L. 1957. The fossil Cercopithecoidae of South Africa. *Annals of the Transvaal Museum* 23: 121-262.

Friedman, G.M. & Sanders, J.E. 1978. *Principles of Sedimentology*. John Wiley, New York.

Frisia, S. & Borsato, A. 2010. Karst. In: Alonso-Zarza, A.M. & Tanner, L.H. (Eds.), *Carbonates in Continental Settings - Facies Environments and Process Volume 62*. 269-319. Elsevier Science.

Frison, G.C. & Todd, L.C. 1986. *The Colby Mammoth Site: Taphonomy and Archaeology of a Clovis Kill in Northern Wyoming*. University of New Mexico Press: Albuquerque.

Frostick, L. & Reid, V. 1983. Taphonomic significance of sub-aerial transport of vertebrate fossils on steep semi-arid slopes. *Lethaia* 16: 157-164.

Gifford, D.P. 1981. Taphonomy and Palaeoecology: a critical review of archaeologies sister disciplines. In: Schiffer, M.B. (Ed.), *Advances in Archaeological Method and Theory 4*. 365-438. Academic Press: New York.

Gillieson, D. 1996. *Caves: Processes, Development, and Management*. Blackwell, Oxford.

Gove, P.B. (Ed.). 1961. *Webster's Third International Unabridged Dictionary*. Riverside Press, Cambridge Massachusetts.

Gow, C.E. 1973. Habitual sheltering in an extensive cave system by baboons near Bredasdorp, South Africa. *South African Journal of Science* **69**: 182.

Gow, N.N. & Lozej, G.P. 1993. Bauxite. *Geoscience Canada* 20: 9-16.

Hand, B.M. 1997. Inverse grading resulting from coarse-sediment transport lag. *Journal of Sedimentary Research* 67(1): 124-129.

Harris, E.C. 1975. The stratigraphic sequence: a question of time. *World Archaeology* 7(1): 109-121.

Harris, E.C. 1979a. The Laws of Archaeological Stratigraphy. *World Archaeology* 11(1): 111-117.

Harris, E.C. 1979b. *Principles of Archaeological Stratigraphy*. Academic Press: London & San Diego.

Heaton, J.L. 2006. *Taxonomy of the Sterkfontein fossil Cercopithecinae: The Papionini of Members 2 and 4 (Gauteng, South Africa).* PhD Thesis. Indiana University.

Hedges, R.E. & Millard, A.R. 1995. Bones and ground-water: toward the modelling of diagenetic processes. *Journal of Archaeological Science* 22: 155-164.

Henning, G.J., Grun, R. & Brunnacker, K. 1983. Speleothems, travertines and paleoclimates. *Quaternary Research* 20: 1-29.

Herries, A.I.R., Curnoe, D. & Adams, J.W. 2009. A multi-disciplinary seriation of early *Homo* and *Paranthropus* bearing palaeocaves in southern Africa. *Quaternary International* 202: 14-28.

Hétu, B., Van Steijn, H. & Bertran, P. 1995. Le rõle des coulées de pierres se`ches dans la génèse d'un certain type d'èboulis stratifiés. *Permafrost and Periglacial Processes* 6: 173-194.

Howell, F.C. 1978. Hominidae. In: Maglio, V. & Cooke H.B.S. (Eds.), *Evolution of African Mammals.* 154–248. Harvard University Press: Cambridge, Massachusetts.

Hughes, A.R. & Tobias, P.V. 1977. A fossil skull probably of the genus *Homo* from Sterkfontein, Transvaal. *Nature* 265: 310-312.

Illenberger, W.K. 1991. Pebble shape (and size): *Journal of Sedimentary Petrology* 61: 756-767.

Johnson, E. 1985. Current developments in bone technology. In: Schiffer, M.B. (Ed.), *Advances in Archaeological Method and Theory*. 157-235. Academic Press: New York.

Kamb, W.B. 1959. Ice petrofabric observations from Blue Glacier, Washington, in relation to theory and experiment. *Journal of Geophysical Research* 54(11): 1891-1909.

Karkanas, P., Kyparissi-Apostolika, N., Bar-Yosef, O. & Weiner, S. 1999. Mineral assemblages in Theopetra, Greece: a framework for understanding diagenesis in a prehistoric cave. *Journal of Archaeological Science* 26: 1171-1180.

Karkanas, P., Bar-Yosef, O., Goldberg, P. & Weiner, S. 2000. Diagenesis in prehistoric caves: The use of minerals that form *in situ* to assess the completeness of the archaeological record. *Journal of Archaeological Science* 27: 915-930.

Karkanas, P., Schepartz, L.A., Miller-Antonio, S., Wei, W. & Weiwen, H. 2008. Late Middle Pleistocene climate in southwestern China: Inferences from the stratigraphic record of Panxian Dadong Cave, Guizhou. *Quaternary Science Reviews* 27: 1555-1570.

Kavalieris, I. & Martini, J. 1976. Structural control of some Western Transvaal caves. *South African Journal of Science* 72: 308-309.

Keyser, A.W., Menter, C.G., Moggi-Cecchi, J., Pickering, T.R. & Berger, L.R. 2000. Drimolen: a new hominid-bearing site in Gauteng, South Africa. *South African Journal of Science* 96: 193-197.

Kibii, J. 2000. *The macrofauna from Jakovec Cavern, Sterkfontein*. M.Sc. Dissertation. University of the Witwatersand.

Kibii, J. 2004. *Comparative taxonomic, taphonomic and palaeoenvironmental analysis of 4-2.3 million year old Australopithecine cave infills at Sterkfontein*. Ph.D. Dissertation, University of Witwatersrand.

Kibii, J.M. 2007. Taxonomy, Taphonomy and Palaeoenvironment of Hominid and Non-Hominid Primates from the Jakovec Cavern, Sterkfontein. *The South African Archaeological Bulletin* 62(186): 90-97.

Kidwell, S.M., Fürsich, F.T. & Aigner, T. 1986. Conceptual Framework for the Analysis and Classification of Fossil Concentrations. *PALAIOS* 1(3): 228-238.

Kos, A.M. 2001. Stratigraphy, sedimentary development and palaeoenvironmental context of a naturally accumulated pitfall cave deposit from south-eastern Australia. *Journal of Earth Sciences* 48: 621-632.

Kos, A.M. 2003a. Pre-burial taphonomic characterisation of a vertebrate assemblage from a pitfall cave fossil deposit in southeastern Australia. *Journal of Archaeological Science* 30: 769-779.

Kos, A.M. 2003b. Characterisation of post-depositional taphonomic processes in the accumulation of mammals in a pitfall cave deposit from southeastern Australia. *Journal of Archaeological Science* 30: 781-796.

Krumbein, W.C. 1941. Measurement and geological significance of shape and roundness of sedimentary particles. *Journal of sedimentological research* 11(2): 64-72.

Krumbein, W.C. 1942. Settling-velocity and flume behaviour of non-spherical particles. *Transactions of the American Geophysical Union* 23: 621-633.

Kuczumowa, A., Cukrowska, A.E., Stachniuk, A., Gawęda, R., Mroczka, R., Paszkowicz, W., Skrzypiec, K., Falkenberg, R. & Blackwell, L. 2010. Investigation of chemical changes in bone material from South African fossil hominid deposits. *Journal of Archaeological Science* 37: 107-115.

Kuman, K. 1994a . The archaeology of Sterkfontein: past and present. *Journal of Human Evolution* 27: 471-495.

Kuman, K. 1994b. The archaeology of Sterkfontein: preliminary findings on site formation and cultural change. *South African journal of Science* 90: 215-219.

Kuman, K. 1996. The Oldowan industry from Sterkfontein: raw materials and core forms. In: Pwiti, G. & Soper, R. (Eds.), *Aspects of African Archaeology: Papers from the 10th Congress of the Panafrican Association for Prehistory and Related Studies*. 139-146. University of Zimbabwe Press: Harare.

Kuman, K. 1997. Recent findings on the archaeology of Sterkfontein. *Four million years of hominid evolution, proceedings of a congress in honour of Dr. Mary Leakey*, Arusha, Tanzania.

Kuman, K. 1998. The earliest South African industries. In: Petraglia, M.D. & Korisettar, R. (Eds.), *Early Human Behaviour in Global Context. The Rise and Diversity of the Lower Palaeolithic Record*. 108-132. Routledge: London and New York.

Kuman, K. 2003. Site formation in the early South African Stone Age sites and its influence on the archaeological record. *South African Journal of Science* 99: 251-254.

Kuman, K. 2007. The Earlier Stone Age in South Africa: site context and the influence of cave studies. In: Pickering, T.R., Schick, K. & Toth, N. (Eds.), *Breathing Life into Fossils: Taphonomic Studies in Honour of C.K. (Bob) Brain*. 181-198. Stone Age Institute Press: Bloomington, Indiana.

Kuman, K. & Clark, R.J. 2000. Stratigraphy, Artefact Industries and Hominid associations, Member 5. *Journal of Human Evolution* 38: 827-847.

Kuman, K., Field, A.S. & McNabb, J. 2005. La Préhistoire ancienne de l'Afrique méridionale: contribution des sites à hominidés d'Afrique du Sud. In: Sahnouni, M. (Ed.), *Les Cultures Paléolithiques en Afrique*. 53-82. Artcom/Errance : Paris.

Kuman, K. & Field, A.S. 2009. The Oldowan Industry from Sterkfontein Caves, South Africa. In: Schick, K. & Toth, N. (Eds.), *The Cutting Edge: Approaches to the Earliest Stone Age*. Stone Age Institute Press: Bloomington, Indiana.

Latham, A.G. 1999. Cave Breccias and Archaeological Sites. *Capra* 1.

Lee-Thorp, J., Thackeray, J.F. & van der Merwe, N. 2000. The hunters and the hunted revisited. *Journal of Human Evolution* 39: 565-576.

Lenoble, A. & Bertran, P. 2004. Fabric of Palaeolithic levels: methods and implications for site formation processes. *Journal of Archaeological Science* 31: 457-469.

Leyland, R.C., Witthüser, K.T. & van Rooy, J.L. 2008. *Vulnerability Maing in Karst Terrains, Exemplified in the Wider Cradle of Humankind World Heritage Site*. WRC REPORT NO. KV 208/08.

Lisle, R.J. 1976. Some Macroscopic Methods of Fabric Analysis. *Journal of Geology* 84(2): 225-235.

Longwell, C.R., Flint, R.F. & Sanders, J.E. 1969. *Physical Geology*. Wiley and Sons. New York

Lowe, D.R. 1975. Water escape structures in coarse-grain sediments. *Sedimentology* 22: 157-204.

Lowe, D.R. 1976. Grain flow and grain flow deposits. *Journal of sedimentary research* 46(1): 188-199.

Lowe, D.R. 1979. Sediment gravity flows: their classification and some problems of application to natural flows and deposits. In: Doyle, L.J. & Pilkey, O.H. (Eds.), *Geology of the Continental Slopes* 27: 75-82. Special Publication, Society of economic Palaeontologists and Mineralogists: Tucson, Oklahoma.

Lowe, D.R. 1982. Sediment gravity flows: II. Depositional models with special reference to the deposits of high density turbidity currents. *Journal of Sedimentary Petrology* 52(1): 279-297.

Luyt, C.J. 2001. *Revisiting palaeoenvironments of hominid-bearing Plio-Pleistocene sites: new isotopic evidence from Sterkfontein.* M.Sc. Dissertation, University of Cape Town.

Luyt, C.J. & Lee-Thorp, J.A. 2003. Carbon isotope ratios of Sterkfontein fossils indicate a marked shift to open environments *c.* 1.7 Myr ago. *South African Journal of Science* 99: 271-273.

Lyman, R.L. 1984. Bone Density and Differential Survivorship of Fossil Classes. *Journal of Anthropological Archaeology* 3: 255-299.

Lyman, R.L. 1994. *Vertebrate Taphonomy*. Cambridge University Press: Cambridge.

MacNeish, R.S. & Libby, J.G. 2003. *Pandejo Cave*. University of New Mexico Press: Mexico.

Major, J.J. 1997. Depositional Processes in Large-Scale Debris-Flow Experiments. *The Journal of Geology* 105(3): 345-366.

Major, J.J. 1998. Pebble orientation on large, experimental debris flows. *Sedimentary Geology* 117: 151-164.

Marais, E.N. 1939. *My Friends the Baboons*. Methuen: London.

Mark, D.A. 1973. Analysis of axial orientation data, including till fabrics. *Geological Society of America Bulletin* 84: 1369-1374.

Marshall, L.G. 1989. Bone modification and the "laws of burial". In: Bonnichsen, R. & Sorg, M.H. (Eds.), *Bone modification.* 7-24. University of Maine Centre for the Study of the First Americans: Orono.

Martini, J. & Kavalieris, I. 1978. Mineralogy of the Transvaal caves. *Transvaal Geological Society, South Africa* 81: 47-54.

Martini, J., Wilinger, P.E., Moen, H.F.G. & Keyser, A. 2003. Contribution to the Speleology of Sterkfontein cave, Gauteng province, South Africa. *International Journal of Speleology* 32: 43-49.

Mason, R.J. 1957. The Transvaal Middle Stone Age and Statistical Analysis. *The South African Archaeological Bulletin* 12(48): 119-137.

Mason, R.J. 1962a. *Prehistory of the Transvaal.* Witwatersrand University Press: Johannesburg.

Mason, R.J. 1962b. The Sterkfontein stone artefacts and their maker. *South Africa Archaeological Bulletin* 17: 109.

Mason, R.J. 1976. The earliest artefact assemblages in South Africa. *Proceeding of the IXth Congress U.I.S.P.P., Nice*.

McGrew, W.C., McKee, J.K. & Tutin, C.E.G. 2003. Primates in caves: two new reports of *Papio spp*. *Journal of Human Evolution* **44**: 521-526.

McKee, J.K. 1991. Palaeoecology of the Sterkfontein hominids: a review and synthesis. *Palaeontologia Africana* 28: 41-51.

McKee, J.K. 1996. Faunal evidence and Sterkfontein Member 2 foot bones of an early hominid. *Science* 271: 521-524.

McSaveney, E.R. 1971. The surficial fabric of rockfall talus. In: Coates, D. R. (Ed.), *Quantitative Geomorphology: Some Aspects and Applications.* Annual Geomorphology Symposium. 181-198. State University of New York.

McSaveney, E.R. 1972. The surficial fabric of rockfall talus. In: Morisawa, M. E. (Ed.), *Quantitative Geomorphology: Some Aspects and Applications.* 181-197. Publications in Geomorphology. Binghamton, New York.

Melton, M. 1965. Debris-Covered Hillslopes of the Southern Arizona Desert: Consideration of Their Stability and Sediment Contribution. *The Journal of Geology* 73(5): 715-729.

van der Merwe, N.J., Thackeray, J.F., Lee-Thorp, J.A. & Luyt, J. 2003. The carbon isotope ecology and diet of Australopithecus africanus at Sterkfontein, South Africa. *Journal of Human Evolution* 44: 581-597.

Mills, H.H. 1984. Clast orientation in Mount St. Helens debris flow deposits: North Fork Toutle River, Washington. *Journal of Sedimentary Petrology* 54(2): 626-634.

Morin, R.H. 2006. Negative correlation between porosity and hydraulic conductivity in sand-and-gravel aquifers at Cape Cod, Massachusetts, USA. *Journal of Hydrology* 316(1): 43-52.

Mosher, D.C., Moran, K. & Hiscott, R.N. 1994. Late Quaternary sediment, sediment mass flow processes and slope stability on the Scotian Slope, Canada. *Sedimentology* 41: 1039-1061.

Muzikar, P. & Granger, D. 2006. Combining cosmogenic, stratigraphic, and paleomagnetic information using a Bayesian approach: General results and an application to Sterkfontein. *Earth and Planetary Science Letters* 243: 400-408.

Nemec, W. & Kazanci, N. 1999. Quaternary colluvium in west-central Anatolia: sedimentary facies and palaeoclimatic significance. *Sedimentology* 46: 139-170.

Nichols, R.J., Sparks, R.S.J. & Wilson, C.J.N. 1994. Experimentation in the fluidization of layered sediments and the formation of water escape structures. Sedimentology 41: 233-253.

Nieuwenhuijzen, M.E. & Van Steijn, H.1990. Alpine debris flows and their sedimentary properties. A case study from the French Alps. *Permafrost and Periglacial Processes* 1: 111-128.

Oakey, R.J., Green, M., Carling, P.A., Lee, M.W.E., Sear, D.A. & Warburton, J. 2005. Grain-shape analysis – A new method for determining representative particle shapes for populations of natural grains. *Journal of Sedimentary Research* 75: 1065-1073.

Oakley, K. 1955. Fire as a Palaeolithic tool and weapon. *The Prehistoric Society* 4: 36-48.

Obanawa, H. & Matsukura, Y. 2006. Mathematical modelling of talus development. *Computers & Geosciences* 32: 1461-1478.

Ogola, C. 2009. *The Sterkfontein western breccias: stratigraphy, fauna and artefacts*. Ph.D. Dissertation. University of the Witwatersrand. Johannesburg.

Onac, B.P. 2003. Cave Minerals. In: Culver, B. & White, W.B. (Eds.), *Encyclopaedia of Caves*. Academic Press, New York.

Onac, B.P. & Vereş, D.S. 2003. Sequence of secondary phosphates deposition in a karst environment: Evidence from Măgurici Cave, Romania. European Journal of Mineralogy 15: 741-745.

O'Regan, H.J. 2007. A revision of the Carnivora from Member 5, Sterkfontein, South Africa, based on a re-assessment of published material and site stratigraphy. *Annals of the Transvaal Museum* 44: 209-214.

O'Regan, H.J. & Menter, C.G. 2009. Carnivora from the Plio-Pleistocene hominin site of Drimolen, Gauteng, South Africa. *Geobios* 42: 329-350.

O'Regan, H.J. & Reynolds, S.C. 2009. An ecological reassessment of the South African carnivore guild: a case study from member 4, Sterkfontein, South Africa. *Journal of Human Evolution* 57(3): 212-222.

Osborne, R.A.L. 2001. Petrography of lithified cave sediment. *Proceedings of the 13th International Congress of Speleology, Brasilia* 1: 101-104.

Osborne, R.A.L. 2002. Cave breakdown by Vadose Weathering. *International Journal of Speleology* 31(1): 37-53.

Parsons, J.D., While, K.X. & Simoni, A. 2001. Experimental Study of the Grain-Flow, Fluid-Mud Transition in Debris Flows. *The Journal of Geology* 109(4): 427-447

Partridge, T.C. 1978. Re-appraisal of lithostratigraphy of Sterkfontein hominid site. *Nature* 275: 282-286.

Partridge, T.C. 1982. The chronological positions of the fossil hominids of southern Africa. *Proceedings of 1st International Congress on Human Palaeontology* 2: 617-675. Centre National de la Recherche Scientifique: Paris.

Partridge, T.C. 2002. Were Heinrich Events forced from the southern hemisphere? *South African Journal of Science* 98: 43-36.

Partridge, T.C. 2005. Dating of the Sterkfontein hominids: progress and possibilities. *Transactions of the Royal Society of South Africa* 60(2): 107-109.

Partridge, T.C. & Watt, I.B. 1991. The stratigraphy of the Sterkfontein hominid deposit and its relationship to the underground cave system. *Palaeontologia Africana* 28: 35–40.

Partridge, T.C., Shaw, J., Heslop, D. & Clarke, R.J. 1999. The new hominid skeleton from Sterkfontein, South Africa: age and preliminary assessment. *Journal of Quaternary Science* 14: 293-298.

Partridge, T.C., Latham, A.G. & Heslop, D. 2000. Appendix on magnetostratigraphy of Makapansgat, Sterkfontein, Taung and Swartkrans. In: Partridge, T.C. & Maud, R.R. (Eds.), *The Cenozoic of Southern Africa. Oxford Monographs on Geology and Geophysics 40.* 126-129. Oxford University Press.

Partridge, T.C., Granger, D.E., Caffee, M.W. & Clarke, R.J. 2003. Lower Pliocene hominid remains from Sterkfontein. *Science* 300: 607-612.

Patterson, L.W. 1990. Characteristics of bifacial-reduction flake-size distribution. *American Antiquity* 55: 550-558.

Perez, F.L. 1989. Talus fabric and particle morphology on Lassen Peak, California: *Geografiska Annaler Series A- Physical Geography* 71: 43-57.

Perez, F.L. & Yin, Z.Y. 1988. The measurement of girdle strength in particle fabrics. *Journal of Sedimentary Research* 58(4): 756-757.

Pickering, R., Kramers, J.D., Partridge, T.C. & Venneman, T.M. 2006. U–Pb dating of speleothems from Sterkfontein Cave, South Africa. *Goldschmidt Conference Abstracts.* 492.

Pickering, R., Kramers, J.D. & Partridge, T.C. 2010. U–Pb dating of calcite–aragonite layers in speleothems from hominin sites in South Africa by MC-ICP-MS. *Quaternary Geochronology* 5(5): 544-558.

Pickering, R. & Kramers, J.D. 2010. Re-appraisal of the stratigraphy and determination of new U-Pb dates for the Sterkfontein hominin site, South Africa. *Journal of Human Evolution* 59: 70-86.

Pickering, T.R. 1999. *Taphonomic interpretations of the Sterkfontein early hominid site (Gauteng, South Africa) reconsidered in the light of recent evidence*. Ph.D. Dissertation. University of Wisconsin.

Pickering, T.R., White, T. & Toth, N. 2000. Brief communication: cutmarks on a Plio-Pleistocene hominid from Sterkfontein, South Africa. *American Journal of Physical Anthropology* 111(4): 579-584.

Pickering, T.R., Clarke, R.J. & Heaton, J.L. 2004a. The context of Stw 573, an early hominid skull and skeleton from Sterkfontein Member 2: taphonomy and paleoenvironment. *Journal of Human Evolution* 46: 277-295.

Pickering, T.R., Clarke, R.J. & Moggi-Cecchi, J. 2004b. The role of carnivores in the accumulation of the Member 4 Hominid assemblage. *American Journal of Physical Anthropology* 125: 1-15.

Pickering, T.R., Donínquez-Rodrigo, M., Egeland, C.P. & Brain, C.K. 2004c. Beyond leopards: tooth marks and the contribution of multiple carnivore taxa to the accumulation of the Swartkrans Member 3 fossil assemblage. *Journal of Human Evolution* 46: 595-604.

Pickering, T.R., Egeland, C.P., Dominguez-Rodrigo, M., Brain, C.K. & Schnell. A.G. 2008. Testing the ‘‘shift in the balance of power’’ hypothesis at Swartkrans, South Africa: Hominid cave use and subsistence behaviour in the Early Pleistocene. *Journal of Anthropological Archaeology* 27: 30-45.

Pilo, L.B., Auler, A.S., Neves, W.A., Wang, X., Cheng, H. & Edwards, R.L. 2005. Geochronology, Sediment Provenance, and Fossil Emplacement at Sumidouro Cave, a Classic Late Pleistocene/Early Holocene Paleoanthropological Site in Eastern Brazil. *Geoarchaeology: An International Journal* 20(8): 751-764.

Pleurdeau, D. 2006. Human Technical Behaviour in the African Middle Stone Age. The lithic assemblage of Porc-Epic Cave (Dire-Dowa, Ethiopia). *African Archaeological Review* 22 (4): 177-197.

Postma, G. 1983. Water escape structures in the context of a depositional model of a mass flow dominated conglomerate fan-delta (Abrioja Formation, Pliocene, Almeria Basin, Spain). *Sedimentology* 30: 91-103.

Postma, G. 1986. Classification for sediment gravity-flow deposits based on flow conditions during sedimentation. *Geology* 14: 291-294.

Price, G.D., Valdes, P.J. & Sellwood. B.W. 1997. Prediction of modern bauxite occurrences: implications for climate reconstruction. *Palaeogeography, Palaeoclimatology, Palaeoecology* 131: 1-13.

Pruetz, J.D. 2001. Use of caves by savanna chimpanzees (*Pan troglodytes verus*) in the Tomboronkoto region of southeastern Senegal. *Pan Africa News* **8:** 26-28.

Quinif, Y., Genty, D. & Maire, R. 1994. Les spéléothèmes: un outil perfomant pour les études paléoclimatiques. *Bulletin Societé Géologique France* 165: 603-612.

Reed, K.E. 1997. Early hominid evolution and ecological change through the African Plio-Pleistocene. *Journal of Human Evolution* 32: 289-322.

Reineck, H.E. & Singh, I.B. 1980. *Depositional Sedimentary Environments*. Springer-Verlag.

Reynolds, S.C., Clarke, R.J. & Kuman, K. 2007. The view from the Lincoln Cave: mid to late Pleistocene fossil deposits from Sterkfontein hominid site, South Africa. *Journal of Human Evolution* 53(3): 260-271.

Reynolds, S.C., Vogel, J.C., Clarke, R.J. & Kuman, K.A. 2003. Preliminary results of excavations at Lincoln Cave, Sterkfontein, South Africa. *South African Journal of Science* 99: 286-288.

Robinson, J.T. 1957. Occurrence of stone artefacts with *Australopithecus* at Sterkfontein (Parts 1 and 2). *Nature* 180: 521-524.

Robinson, J.T. 1962. Sterkfontein stratigraphy and the significance of the Extension Site. *South African Archaeological Bulletin* 17: 87-107.

Robinson, J.T. 1997. The discovery of the 'Mrs. Ples' skull specimen. *South African Journal of Science* 93(4): 160-164.

de Ruiter, D.J. & Berger, L.R. 2000. Leopards as Taphonomic Agents in Dolomitic Caves - Implications for Bone Accumulations in the Hominid-bearing Deposits of South Africa. *Journal of Archaeological Science* 27: 665-684.

de Ruiter, D.J., Sponheimer, M. & Lee-Thorp, J.A. 2008. Indications of habitat association of *Australopithecus robustus* in the Bloubank Valley, South Africa. *Journal of Human Evolution* 55: 1015-1030.

Sancho, C., Peñab, J-L., Mikkanc, R. & Oscára, C. 2004. Yves Quinif Morphological and speleothemic development in Brujas Cave (Southern Andean Range, Argentine): palaeoenvironmental significance. *Geomorphology* 57: 367-384.

Sanders, D., Ostermann, M. & Kramers, J. 2008. Quaternary carbonate-rocky talus slope successions (Eastern Alps, Austria): sedimentary facies and facies architecture. *Facies - International Journal of Paleontology, Sedimentology and Geology* 55(3): 345-373.

Sass, O. & Krautblatter, M. 2007. Debris flow-dominated and rockfall-dominated talus slopes: Genetic models derived from GPR measurements. *Geomorphology* 86: 176-192.

Schellmann, W. 1994. Geochemical differentiation in laterite and bauxite formation. *Catena* 21: 131-143.

Schuldenrein, J. 2001. Stratigraphy, Sedimentology, and Site Formation at Konispol Cave, Southwest Albania. *Geoarchaeology: An International Journal* 16(5): 559-602.

Schwarcz, H.P., Grun, R. & Tobias, P.V. 1994. ESR dating of the australopithecine site of Sterkfontein, South Africa. *Journal of Human Evolution* 26: 175-181.

Shahack-Gross, R., Bar-Yosef, O. & Weiner, S. 1997. Black-Coloured Bones in Hayonim Cave, Isreal: Differentiating Between Burning and Oxide Staining. *Journal of Archaeological Science* 24: 439-446.

Shipman, P., Bosler, W. & Davis, K.L. 1981. Butchering of giant geladas at an Acheulian site. *Current Anthropology* 22: 257-268.

Shott, M.J. 1994. Size and Form in the analysis of Flake Debris: Review and recent Approaches. *Journal of Archaeological Method and Theory* 1(1): 69-110.

Sillen, A. & Parkington, J. 1996. Diagenesis of Bones from Eland's Bay Cave**.** *Journal of Archaeological Science* 23: 535-542.

Sillen, A., Hall, G., Richardson, S. & Armstrong, R. 1998. 87Sr/86Sr ratios in modern and fossil food-webs of the Sterkfontein Valley: Implications for early hominid habitat preference. *Geochimica et Cosmochimica Acta* 62(14): 2463-2473.

Simons, J.W. 1966. The presence of leopard and a study of the food debris in the leopard lairs of the Mount Suswa caves, Kenya. *Bulletin of the Cave Exploration Group East Africa* 1: 5-69.

Skinner, J.D. & Chimimba, C.T. 2005. *The Mammals of the Southern African Sub-region*. Cambridge University Press.

Sneed, E.D. & Folk, R.L. 1958. Pebbles in the lower Colorado River, Texas: a study in particle morphogenesis. *Journal* of *Geology* 66: 114-150.

Sponheimer, M. Lee-Thorp, J. de Ruiter, D.J., Smith, J.M., van der Merwe, M.J., Reed, K., Grant, C.C., Ayliffe, L.K., Robinson, T.F., Heidelberger, C. & Marcus, W. 2003. Diets of Southern African Bovidae: Stable Isotope Evidence. *Journal of Mammology* 84: 471-479.

Sponheimer, M., Lee-Thorp, J., de Ruiter, D., Codron, D., Codron, J., Baugh, A.T. & Thackeray, F. 2005. Hominins, sedges, and termites: new carbon isotope data from the Sterkfontein valley and Kruger National Park. *Journal of Human Evolution* 48: 301-312.

Stahle, D.W. & Dunn, J.E. 1982. An analysis and application of the size distribution of waste flakes from the manufacture of bifacial tools. *World Archaeology* 14: 84-97.

Stratford, D.J. 2008. *A Study of Newly Discovered Lithics from Earlier Stone Age deposits at Sterkfontein, Gauteng Province, South Africa*. M.Sc. Dissertation, University of Witwatersrand.

Stratford, D.J., Bruxelles, L. & Clarke, R.J. In prep. *New interpretations of the Name Chamber. Submitted to Journal of Human Evolution.*

Stiles, D. & Partridge, T.C. 1979. Results of recent archaeological and palaeoenvironmental studies at the Sterkfontein Extension Site. *South African Journal of Science* 75: 346-352.

Sullivan, III.A.P. & Rozen, K.C. 1985. Debitage Analysis and Archaeological Interpretation. *American Antiquity* 50(4): 755-779.

Tankard, A.F. & Schweitzer, F.R. 1976. Textural analysis of cave sediments: Die Kelders, Cape Province, South Africa. In: Davidson, D.A. & Shackley, M.L. (Eds.), *Geoarchaeology, earth science and the past*. 289-316. Westview Press: Boulder, Colorado.

Tanner, L.H. & Hubart, J.F. 1991. Basalt breccias and conglomerates in the Lower Jurassic McCoy Brook Formation, Fundy Basin, Nova Scotia: differentiation of talus and debris-flow deposits. *Journal of Sedimentary Petrology* 61(1): 15-27.

Tardy, Y., Kobilsek, B. & Paquet, H. 1991. Mineralogical composition and geographical distribution of Africa and Brazilian periatlantic laterites. The influence of continental drift and tropical paleoclimates during the past 150 million years and implications for India and Australia. *Journal of African Earth Science* 12: 283-295.

Taylor, G., Truswell, E.M., McQueen, K.G. & Brown, M.C.1990. Early Tertiary palaeogeography, landform evolution, and palaeoclimates of the Southern Monaro, N.S.W., Australia. *Palaeogeography, Palaeoclimatology and Palaeoecology* 78: 109-134.

Thackeray, J.F., Sénégas, F. & Laden, G. 2005. Manganese dioxide staining on hominid crania from Sterkfontein and Swartkrans: possible associations with lichen. South Africa. *South African Journal of Science* 101: 28-35.

Tobias, P.V. 1978. The earliest Transvaal members of the genus *Homo* with another look at some problems of hominid taxonomy and systematics. *Zeitschrift fur Morphologie und Anthropologie* 69: 225-265.

Tobias, P.V. 1979. The Silberberg Grotto, Sterkfontein, Transvaal, and its importance in palaeo-anthropological research. *South African Journal of Science* 75: 161-164.

Tobias, P.V. 1997a. Some little known chapters in the early history of the Makapansgat fossil hominid site. *Palaeontologia Africana* 33: 67-79.

Tobias, P.V. 1997b. Makapansgat. In: Spencer, F. (Ed.), *Encyclopaedia of the History of Physical Anthropology, VII.* 634-636. Garland Publishing Inc: New York.

Tobias, P.V., Clarke, R.J. & White, H. 1993. *27th Annual Report of the Palaeoanthropology Research Unit.* University of the Witwatersrand. Johannesburg.

Turner, A. 1987. New fossil carnivore remains from the Sterkfontein hominid site (Mammalia: Carnivora). *Annuals of the Transvaal Museum* 34: 319-347.

Turner, A. 1997. Further remains of Carnivora (Mammalia) from the Sterkfontein hominid site. *Palaeontologia Africana* 34: 115-126.

Ungar, P.S. & Teaford, M.F. 1996. Preliminary examination of non-occlusal microwear in anthropoids: implications for the study of fossil primates. *American Journal of Physical Anthropology* 100: 101-113.

Verruijt, A. 2010. *Soil Mechanics*. Delft University of Technology.

Villa, P. & Mahieu, E. 1991. Breakage patterns on human long bones. *Journal of Human Evolution* 21: 27-48.

Vogel, H-J., Hoffmann, H. & Roth, K. 2005a. Studies of crack dynamics in clay soil I: Experimental methods, results, and morphological quantification. *Geoderma* 125: 203-213.

Vogel, H-J., Hoffmann, H., Leopold, A. & Roth, K. 2005b. Studies of crack dynamics in clay soil II: A physically-based model for crack formation. *Geoderma* 125**:** 213-223.

Voorhies, M. 1969. *Taphonomy and population dynamics of an early Pliocene vertebrate fauna, Knox County, Nebraska.* University of Wyoming Contributions to Geology Special Paper. No. 1. Laramie.

Vrba, E.S. 1974. Chronological and ecological implications of the fossil Bovidae at the Sterkfontein *Australopithecine* site. *Nature* 250: 19-23.

Vrba, E.S. 1975. Some evidence of chronology and palaeoecology of Sterkfontein, Swartkrans and Kromdraai from the fossil Bovidae. *Nature* 254: 301-304.

Vrba, E.S. 1976. The fossil bovidae of Sterkfontein, Swartkrans and Kromdraai. *Transvaal Museum Pretoria Memoirs* 21.

Vrba, E.S. 1982. Biostratigraphy and chronology based particularly on Bovidae of southern hominid-associated assemblages. *Proceedings of 1st International Congress on Human Palaeontology* 2: 707-752. Centre National de la Recherche Scientifique, Paris.

Vrba, E.S. 1985. Ecological and adaptive changes associated with early hominid evolution. In: Delson, E. (Ed.), *Ancestors, the Hard Evidence*. 63-71. Alan R. Liss: New York.

Vrba, E.S. 1995. The fossil record of the African antelopes (Mammalia, Bovidae) in relation to human evolution and paleoclimate. In: Vrba, E.S., Denton, G.H., Partridge, T.C. & Burckle, L.H. (Eds.), *Paleoclimate and Evolution with emphasis on human origins*. 385-424. Yale University Press: Boston.

Walker, J., Cliff, R.A., Partridge, T.C. & Latham, A.G. 2004. Research into U-Pb dating of 'Little Foot'. *Abstract for 2004 Geocongress of the Geological Society of South Africa.*

Walker, J., Cliff, R.A. & Latham, A.G. 2006. U-Pb isotopic age of the StW573 hominid from Sterkfontein, South Africa. *Science* 314: 1592-1594.

Ward, W. H. 1945. The stability of natural slopes: *Geography Journal* 105: 170-197.

Weiner, S., Traub, W. & Elster, H. 1989. The molecular structure of bone and its relation to diagenesis. *Applied Geochemistry* 4: 231-232.

Wells, L.H. 1973. Baboons sheltering in caves. *South African Journal of Science* 69: 279.

White, W.B. 2007. Cave sediments and palaeoclimate. *Journal of Cave and Karst Studies* 69(1): 76-93.

Wilkinson, M.J. 1973. *Sterkfontein cave system: evolution of a karst form*. M.A. thesis, University of the Witwatersrand, Johannesburg.

Wilkinson, M.J. 1983. Geomorphic perspectives on the Sterkfontein *Australopithecine* breccias. *Journal of Archaeological Science* 10: 515-529.

Wilkinson, M.J. 1985. Lower-lying and possibly older fossilferous deposits at Sterkfontein. In P. V. Tobias (Ed.), *Hominid Evolution: Past, Present and Future*. 165-170. New York, Alan R. Liss.

Wolpoff, M.H. 1996. *Human Evolution*. Knopf: New York.

Woodward, J.C. 1997a. Late Pleistocene rockshelter sedimentation at Klithi. In: G.N. Bailey (Ed.), *Klithi: Palaeolithic settlement and Quaternary landscapes in northwest Greece (1)*. 361-376. McDonald Institute for Archaeological Research: Cambridge.

Woodward, J.C. 1997b. Late Pleistocene rockshelter sedimentation at Megalakkos. In: G.N. Bailey (Ed.), *Klithi: Palaeolithic settlement and*

Quaternary landscapes in northwest Greece (2). 377-394. McDonald Institute for Archaeological Research: Cambridge.

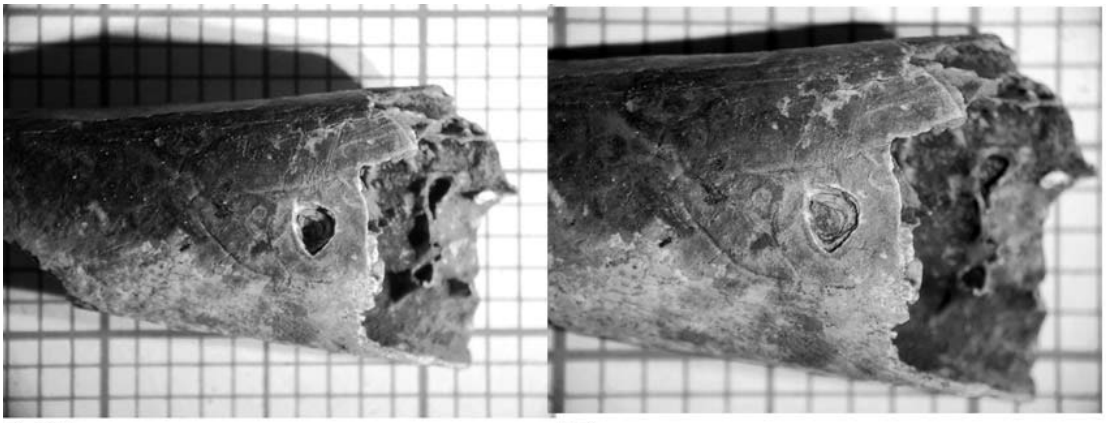
Write, R. & Anderson, B. 1982. The importance of sediment gravity flow to sediment transport and sorting in the glacial marine environment: Eastern Weddell Sea, Antarctica. *Geological Society of American Bulletin* 93: 951-963.

Zingg, T. 1935. Beitrag zur Schotteranalyse. *Schweizerische Mineralogische und Petro-graphische Mitteilungen* 15: 38-140.

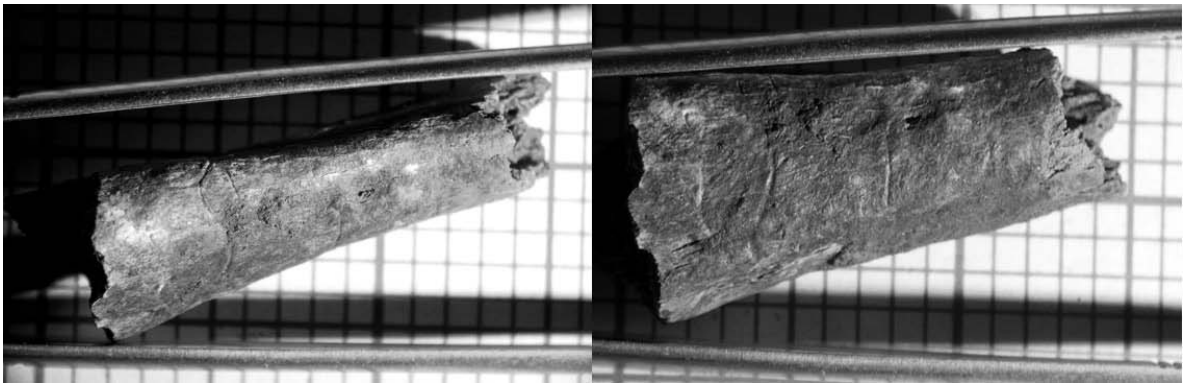
Appendix 1 Diagnostic faunal modification images

Figure Number	Art Number	Type	Example of:	Magnification & photograph details
1.1	216 - T3	BSM	Tooth pitting	0.67, 1.0
1.2	192 - T3	BSM	Root etching	0.67
1.3	185 - T3	BSM	Notched Rib	macro canon
1.4	206 - T3	Condition	Fresh Bone	0.67, 1.0
1.5	191 - T3	Condition	Weathered	macro canon
1.6	219 - T3	Condition	Weathered	0.67, 1.0
1.7	208 - T3	Condition	Superb fossilisation	macro canon
1.8	177 - T3	Break type	Smooth perpendicular break; fresh stepped	macro, both ends & break types
1.9	149 - T3	Break type	Obtuse Fresh Bone break	macro canon
1.10	235 - T3	Break type	Stepped sawtooth break	macro canon
1.11	152 - T2	Condition/BT	Slightly weathered	0.67; macro for break detail
1.12	160 - T2	Condition	Weathered	1.0
1.13	121 - T1	BSM	Knawing marks	0.67, 1.5
1.14	196 - T1	BSM	Knawing marks	0.67
1.15	226 - T1	BSM	Large pitting	0.67, 1.0
1.16	259 - T1	Condition	Slightly weathered	0.67
1.17	206 - T3; 152	Condition	Fresh, SW and VW single shot comparison	macro canon
1.18	191 - T1	Artefact	Quartz complete flake	macro, ventral & dorsal faces
1.19	283 - T1	Artefact	Quartz incomplete flake	macro, ventral & dorsal faces
1.20	244 - T1	Artefact	Quartzite complete flake	macro, ventral & dorsal faces
1.21	134 - T1	Artefact	Quartzite incomplete flake	macro, ventral & dorsal faces
1.22	110 - T2	Artefact	Quartz complete flake	macro, ventral & dorsal faces
1.23	101 - T3	Artefact	Quartz flake fragment	macro, ventral & dorsal faces
1.24	124 - T3	Artefact	Core	macro, both sides, platform
1.25	146 - MH2	Coprolite	Coprolite	macro, three sides

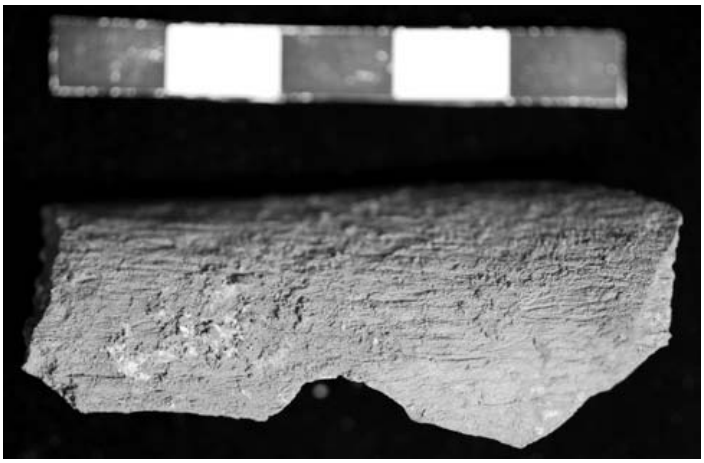
Microscope: Olympus SZ61 zoom stereo microscope
Microscope camera: Olympus Camedia C-5060 5.1MP with 5.7-22.9mm wide zoom lense
Macro camera: Canon EOS 400D with compact-macro 18-50mm lense



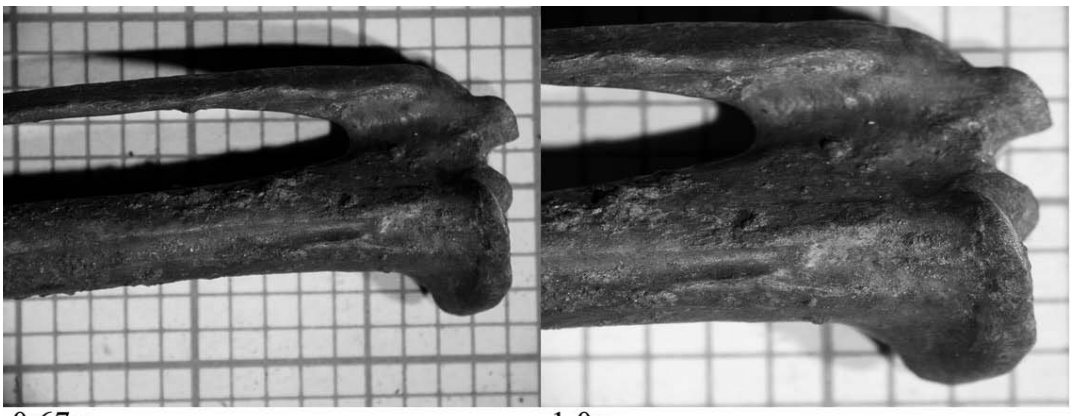
Appendix Figure 1.1 Art. 216 – T3. Tooth pitting example.



Appendix Figure 1.2 Art. 192 – T3. Root etching example.



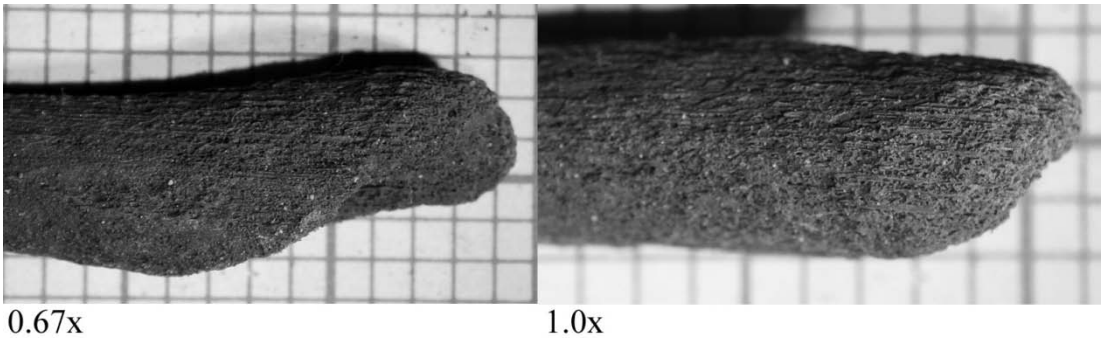
Appendix Figure 1.3 Art. 185 – T3. Notching example.



Appendix Figure 1.4 Art. 206 – T3. Fresh bone example.



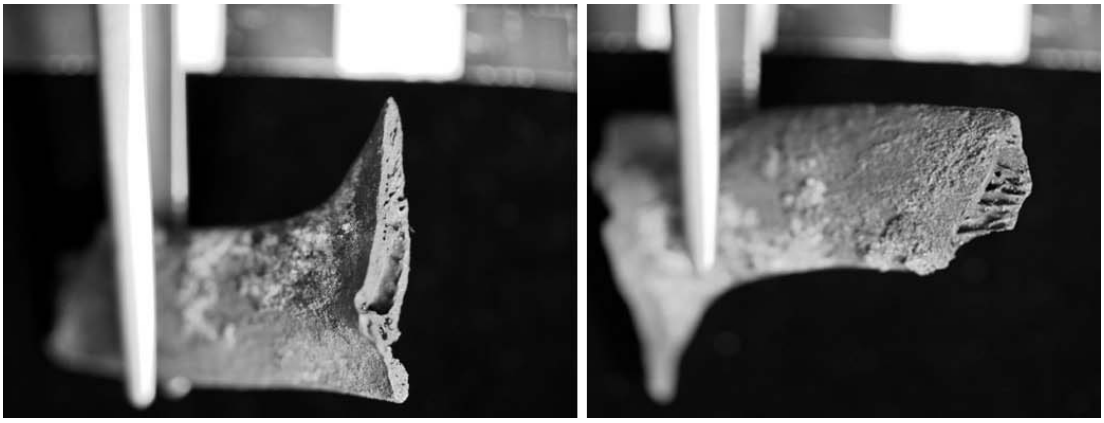
Appendix Figure 1.5 Art. 191 – T3. Weathered bone example. Notice the obtuse sawtooth breakage



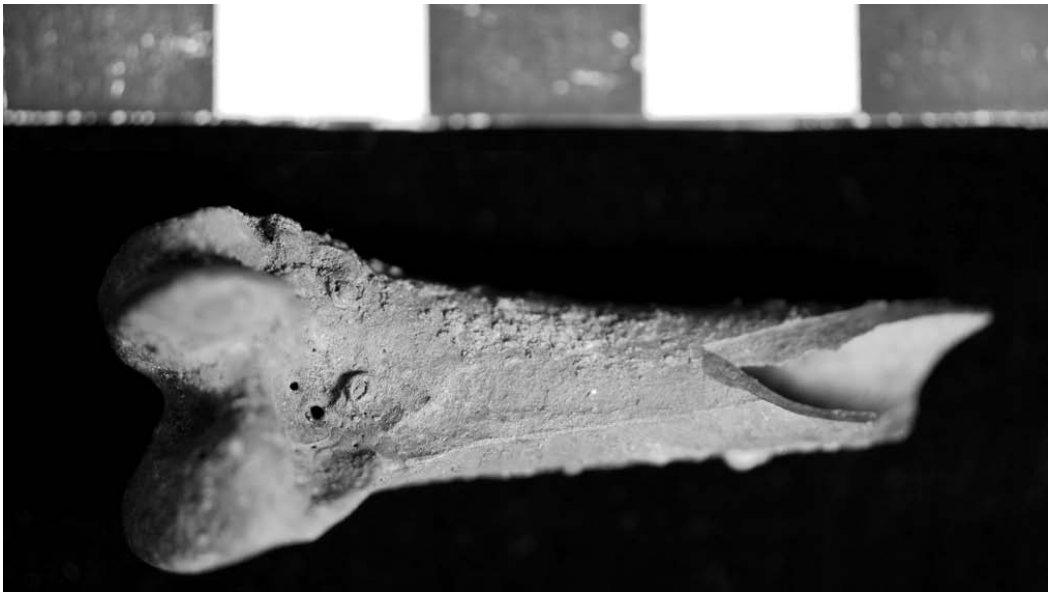
Appendix Figure 1.6 Art. 219 – T3. Weathered bone example.



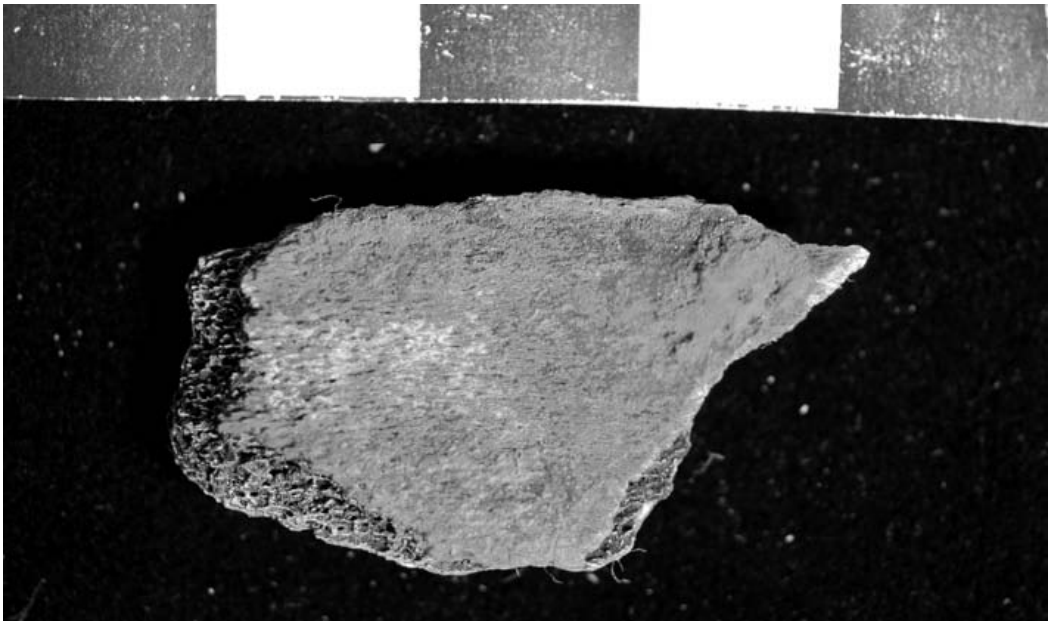
Appendix Figure 1.7 Art. 208 – T3. Exceptional fossilisation detail.



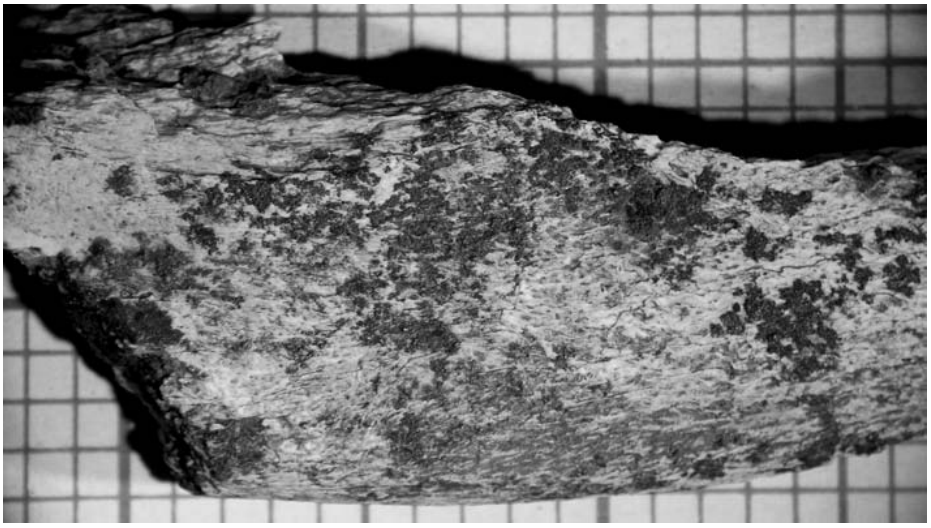
Appendix Figure 1.8 Art. 177 – T3. Smooth perpendicular break and a fresh stepped break.



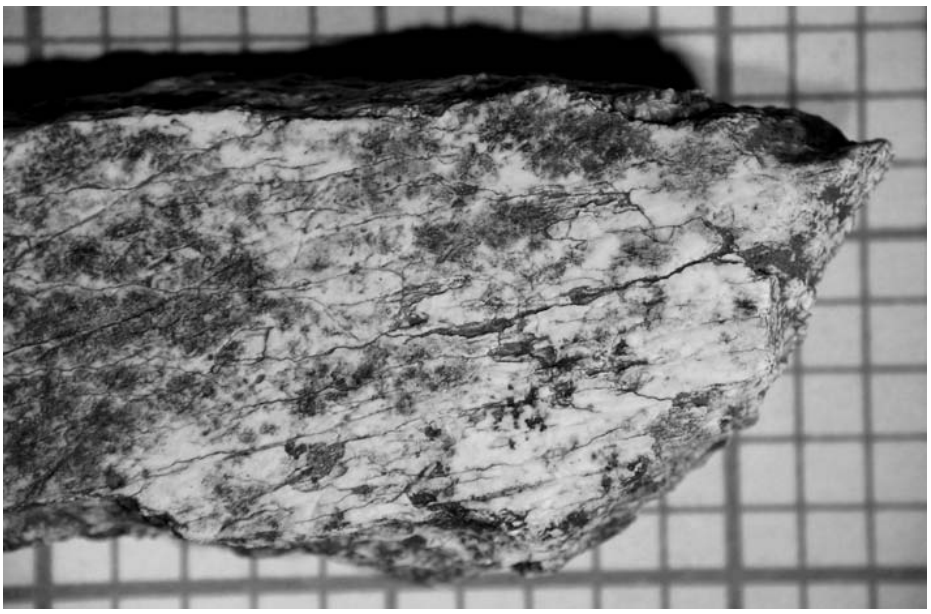
Appendix Figure 1.9 Art. 149 – T3. Obtuse angled fresh break.



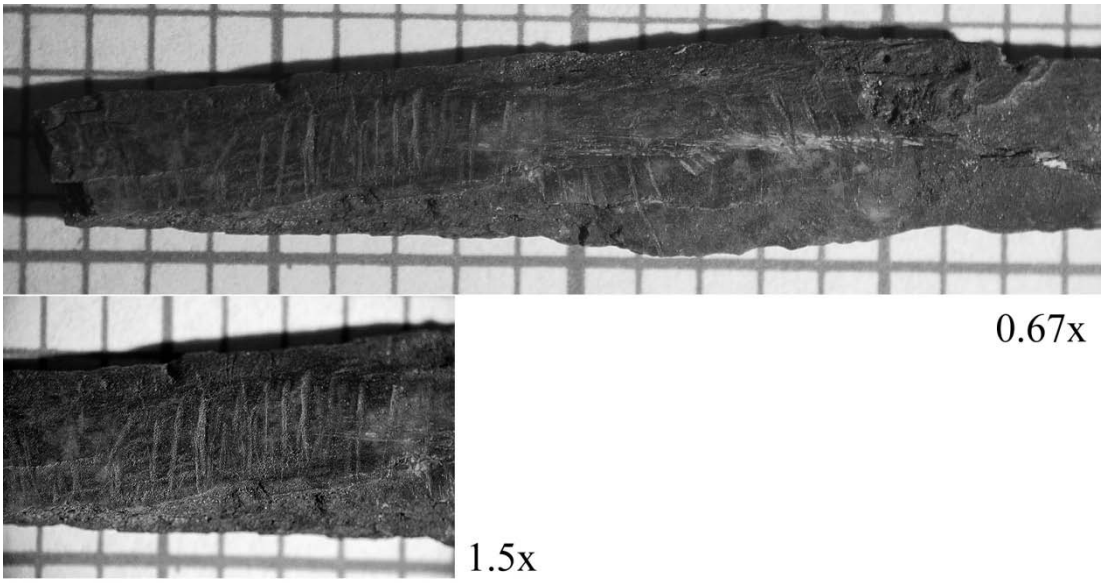
Appendix Figure 1.10 Art. 235 – T3. Stepped sawtooth break. The left edge is the example.



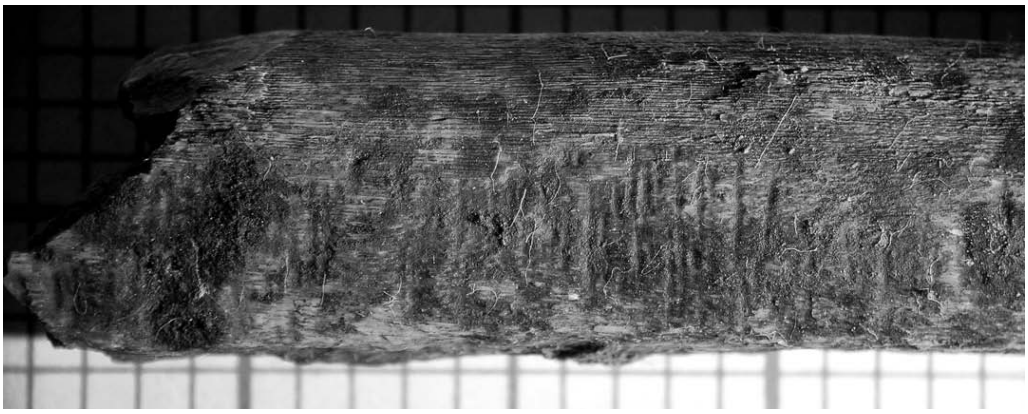
Appendix Figure 1.11 Art. 152 – T2. Slightly weathered bone example. 0.67x magnification.



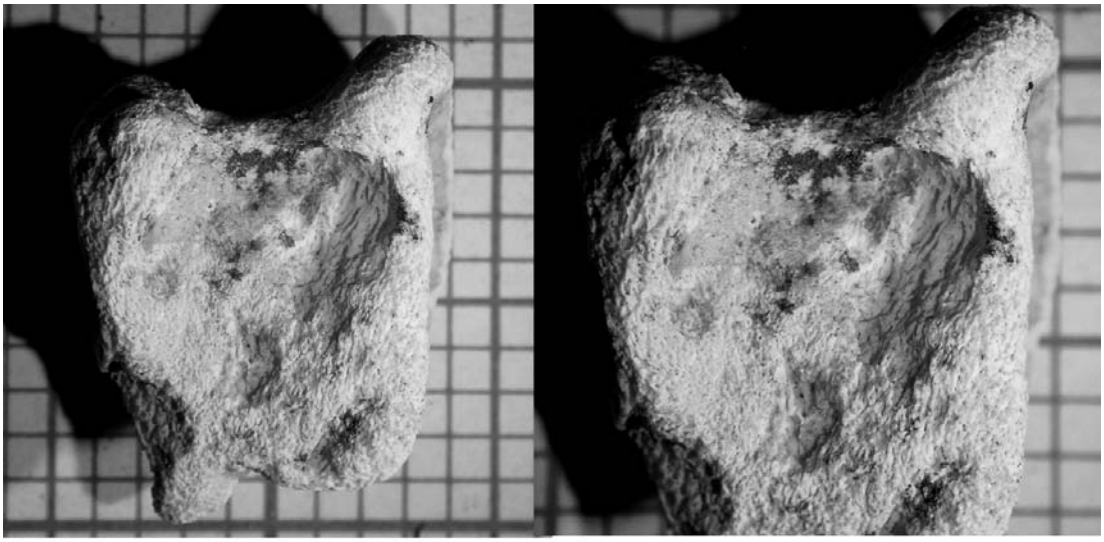
Appendix Figure 1.12 Art. 160 – T2. Weathered bone example. 1.0x magnification.



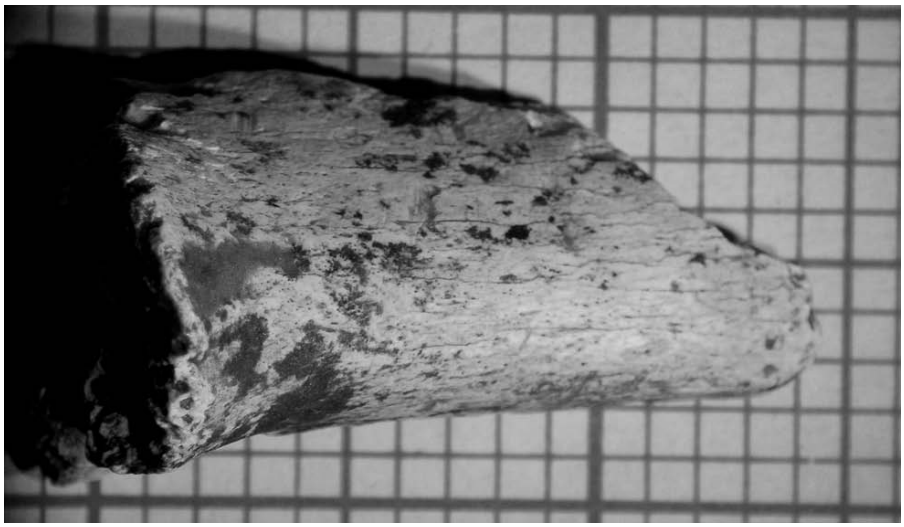
Appendix Figure 1.13 Art. 121 – T1. Rodent knawing modification.



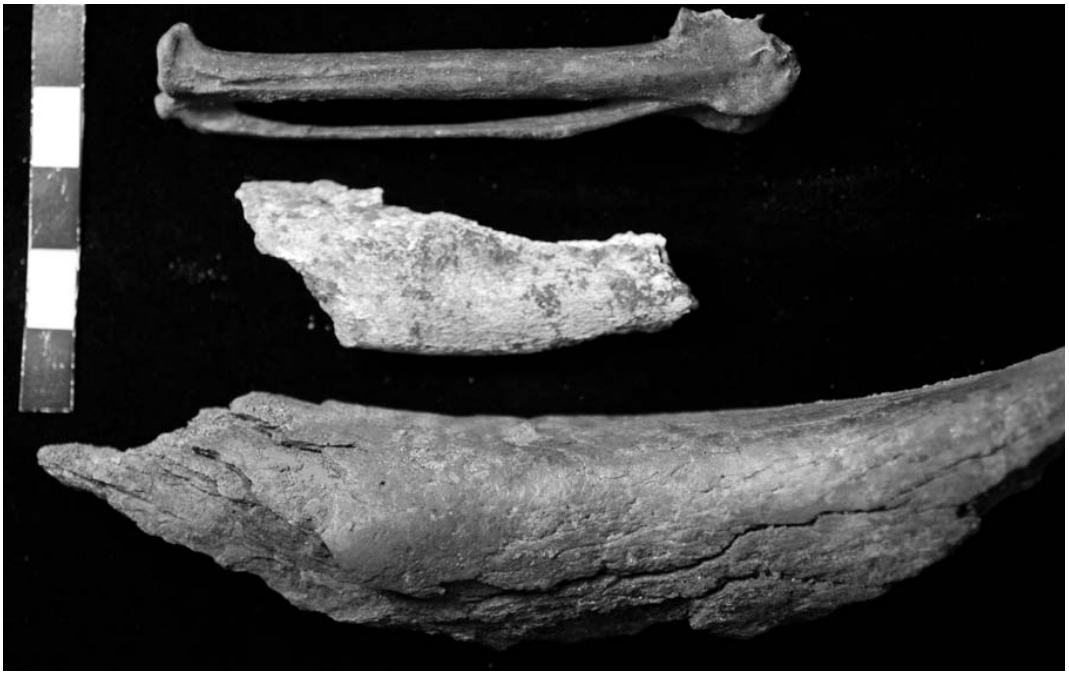
Appendix Figure 1.14 Art. 196 – T1. Rodent knawing modification. 0.67x magnification.



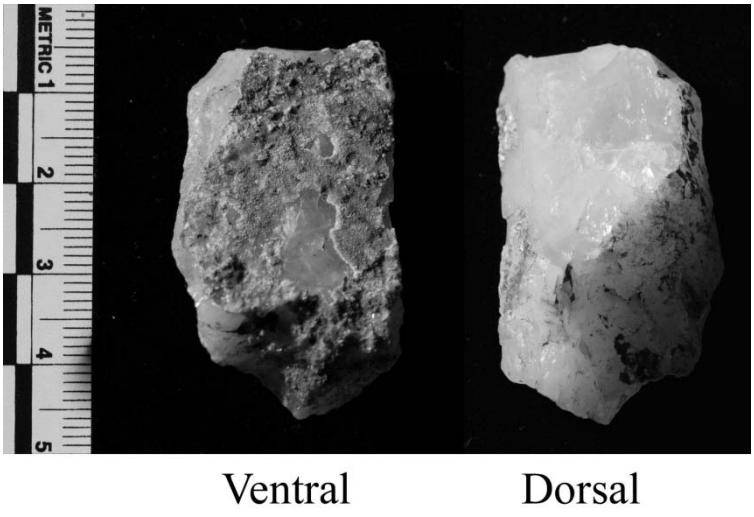
Appendix Figure 1.15 Art. 226 – T1. Large pitting modification example.



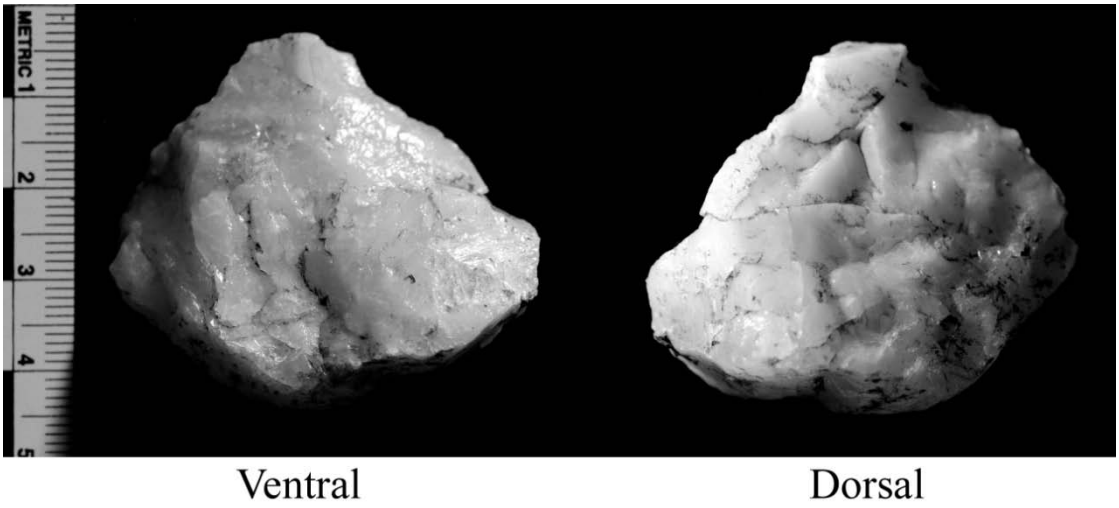
Appendix Figure 1.16 Art. 259 – T1. Slightly weathered bone example.



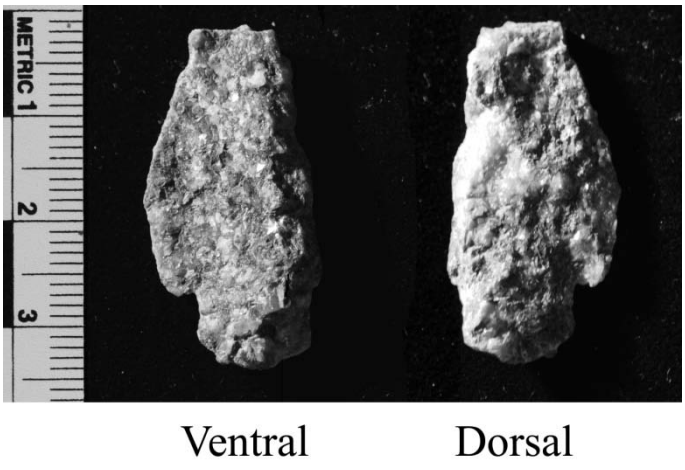
Appendix Figure 1.17 Art. 206 – T3. Fresh bone example; Art. 152 – T2. Slightly weathered bone example; Art. 191 – T3. Weathered bone example.



Appendix Figure 1.18 Art. 191 – T1. Quartz complete flake. Platform is facing towards the top of the picture.



Appendix Figure 1.19 Art. 283 – T1. Quartz incomplete flake. Platform is facing towards the top of the picture.



Appendix Figure 1.20 Art. 244 – T1. Quartzite complete flake. Platform is facing towards the top of the picture.



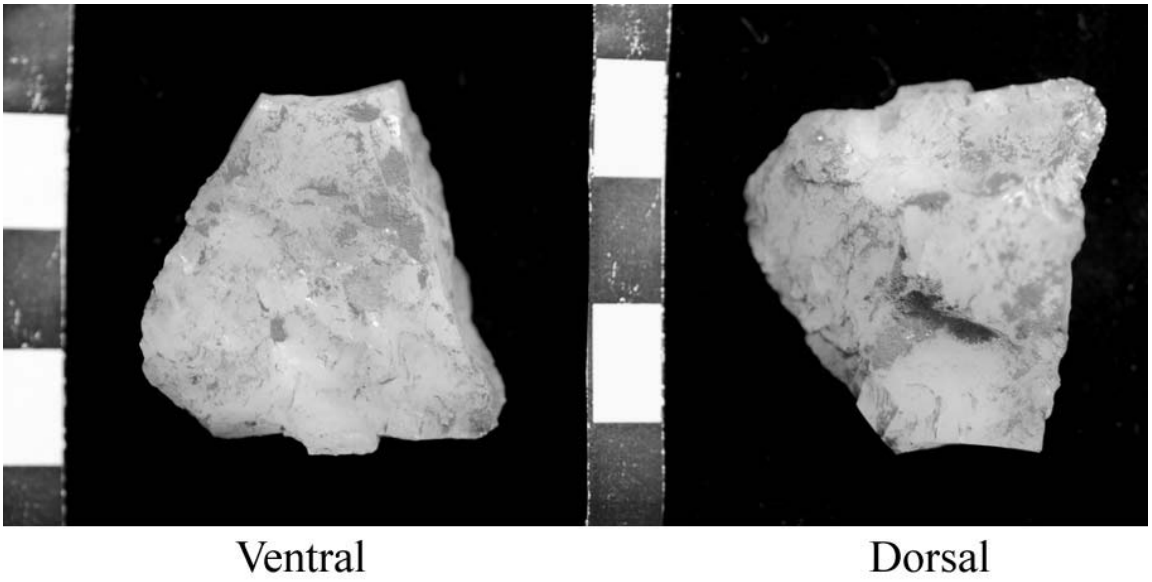
Ventral Dorsal

Appendix Figure 1.21 Art. 134 – T1. Quartzite incomplete flake. Platform is facing towards the top of the picture.

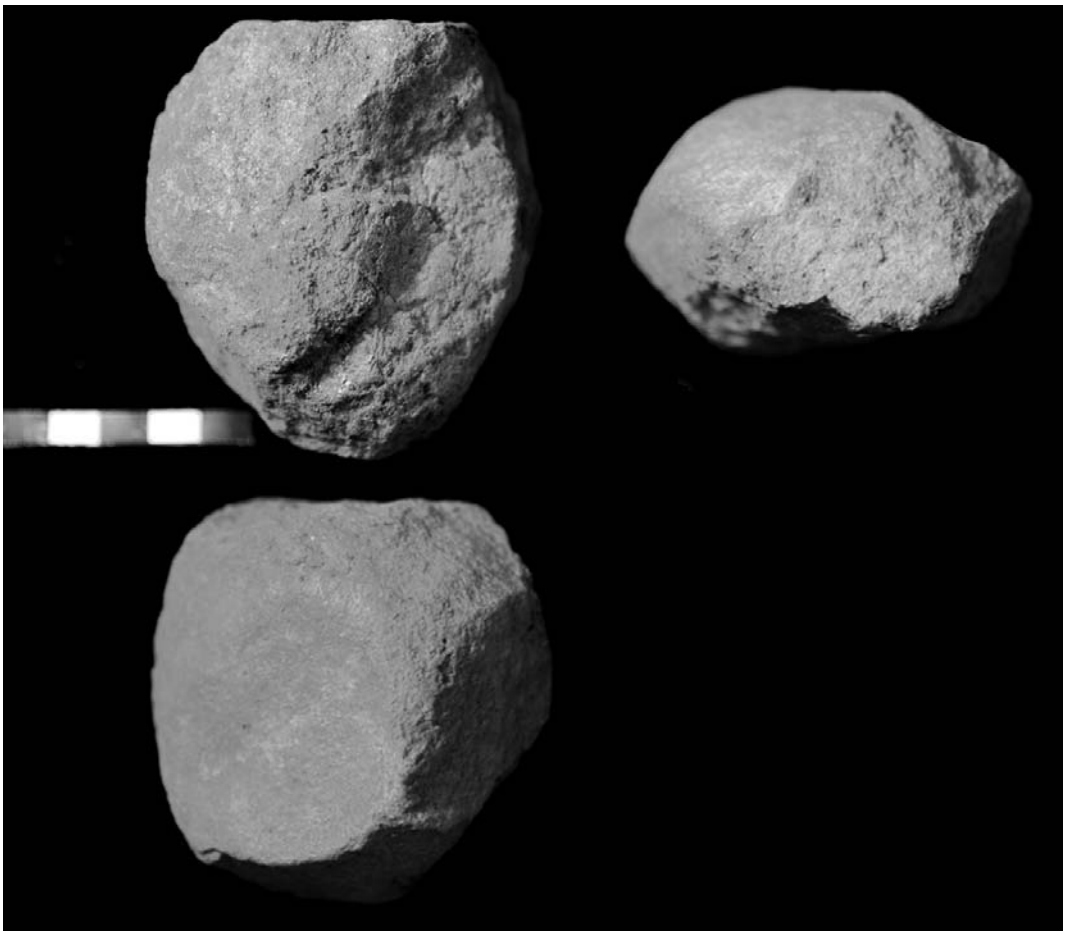


Ventral Dorsal

Appendix Figure 1.22 Art. 110 – T2. Quartz complete flake. Platform is facing towards the top of the picture.

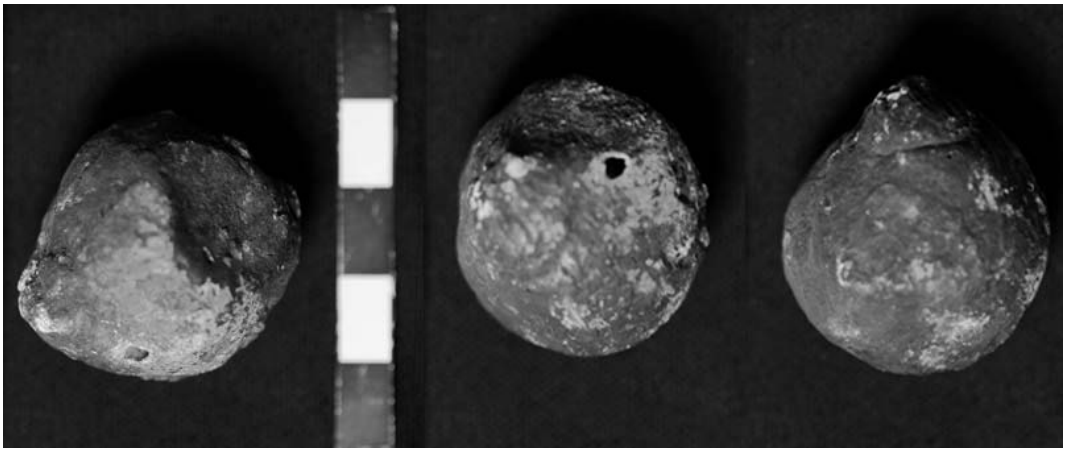


Appendix Figure 1.23 Art. 101 – T3. Quartz flake fragment.



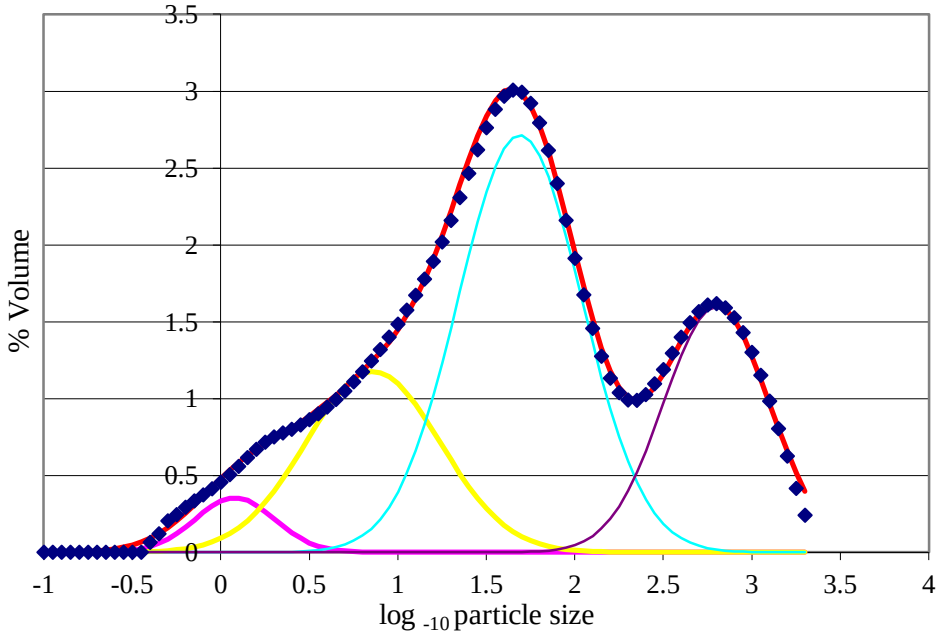
Appendix Figure 1.24 Art. 124 – T3. Quartzite casual core. The left upper image shows the main flake scar surface and platform facing the top, a clear point of percussion can be seen in the middle

of the platform. The right upper image shows the striking platform from which all 3 scars derive. The left lower image shows the cortex surface which covers the majority of the piece.



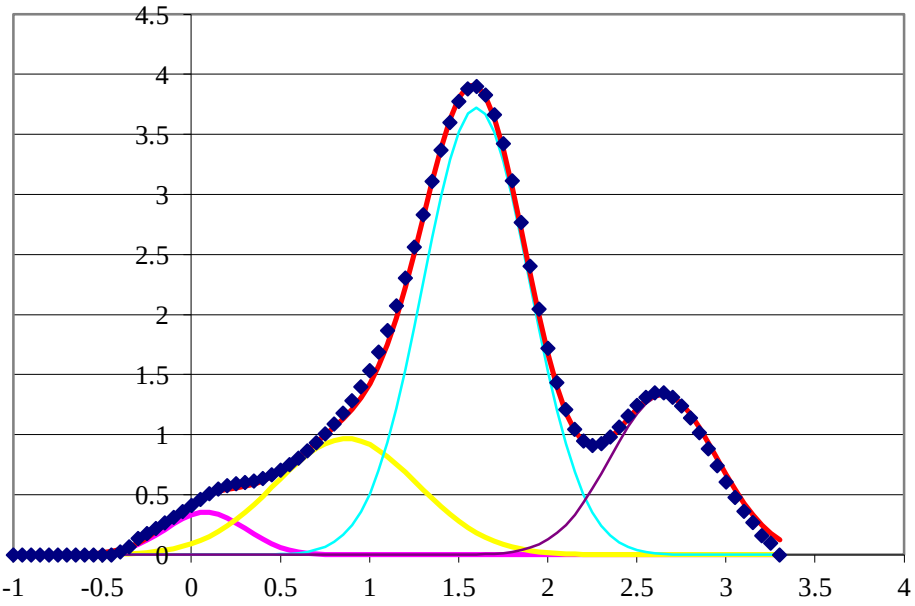
Appendix Figure 1.25 Art. 146 – MH2. Hyena coprolite.

Appendix 2 Deconvoluted Particle Size Distribution Curves



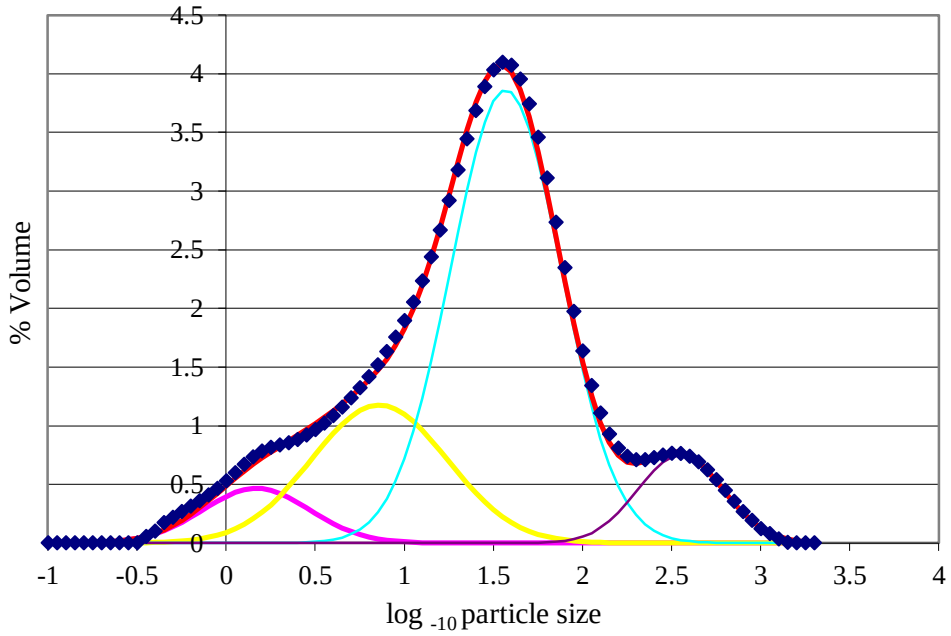
	Curve 1	Curve 2	Curve 3	Curve 4
T2 0-5cm	2.990	25.911	47.835	23.265

Appendix Figure 2.1 STK MH1 T2 0 – 5cm



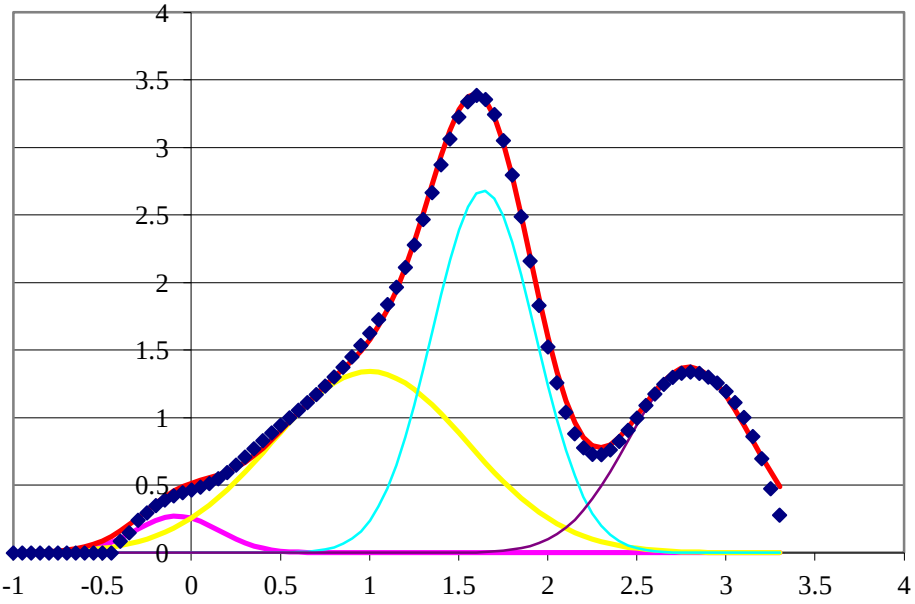
	Curve 1	Curve 2	Curve 3	Curve 4
T2 30-40cm	4.033	19.565	56.475	19.927

Appendix Figure 2.2 STK MH1 T2 30 – 40cm



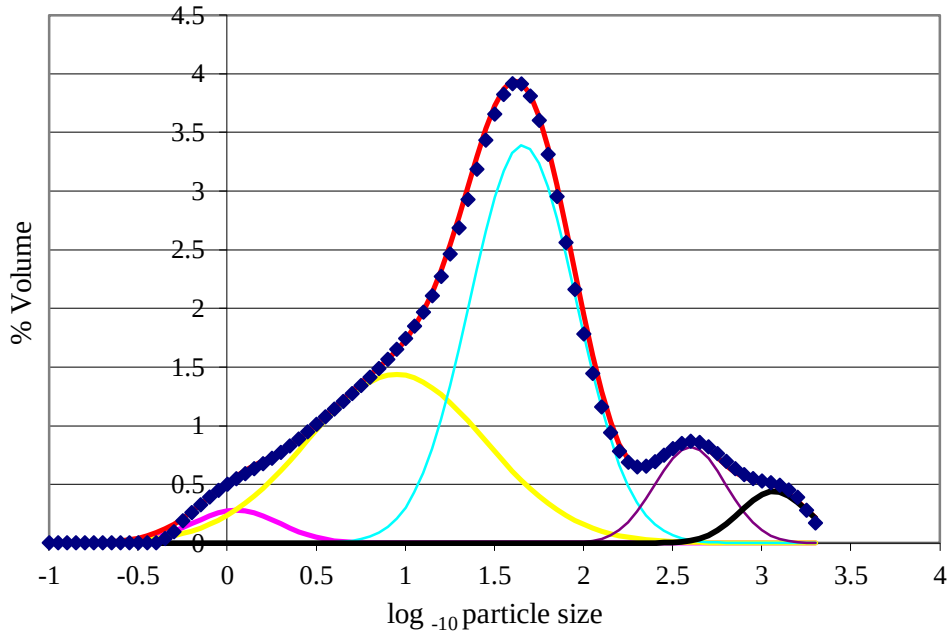
	Curve 1	Curve 2	Curve 3	Curve 4
T2 50-60cm	7.114	22.766	60.979	9.141

Appendix Figure 2.3 STK MH1 T2 50 – 60cm



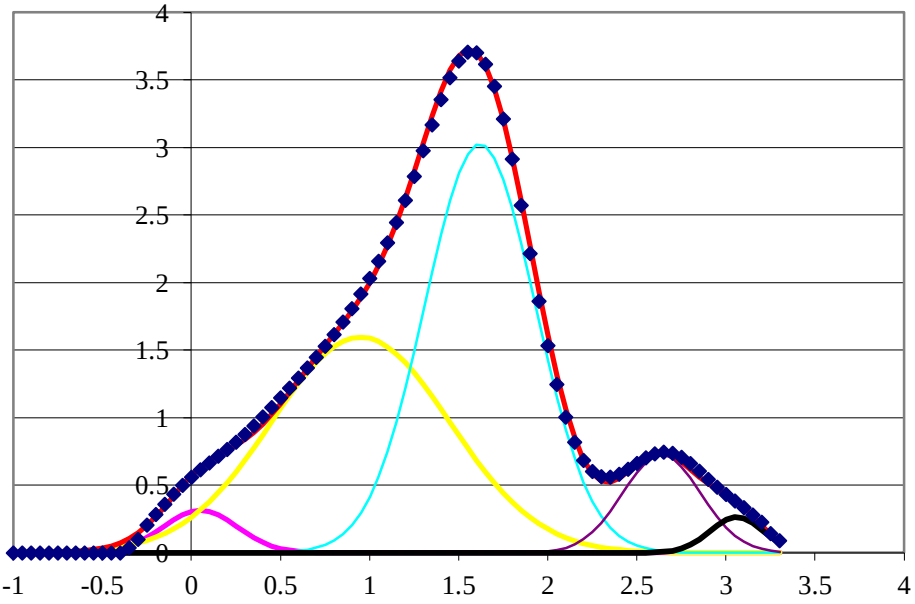
	Curve 1	Curve 2	Curve 3	Curve 4	Curve 5
T3 5-10cm	3.149	36.407	38.375	22.050	0.020

Appendix Figure 2.4 STK MH1 T3 5 – 10cm



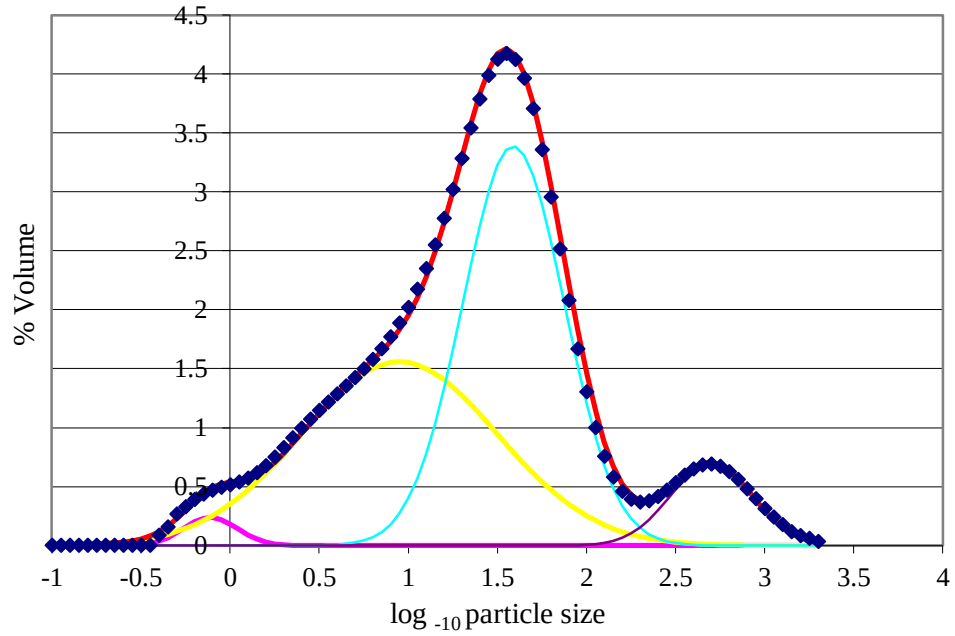
	Curve 1	Curve 2	Curve 3	Curve 4	Curve 5
T3 30-40cm	3.319	35.147	49.791	8.004	3.738

Appendix Figure 2.5 STK MH1 T3 30 – 40cm



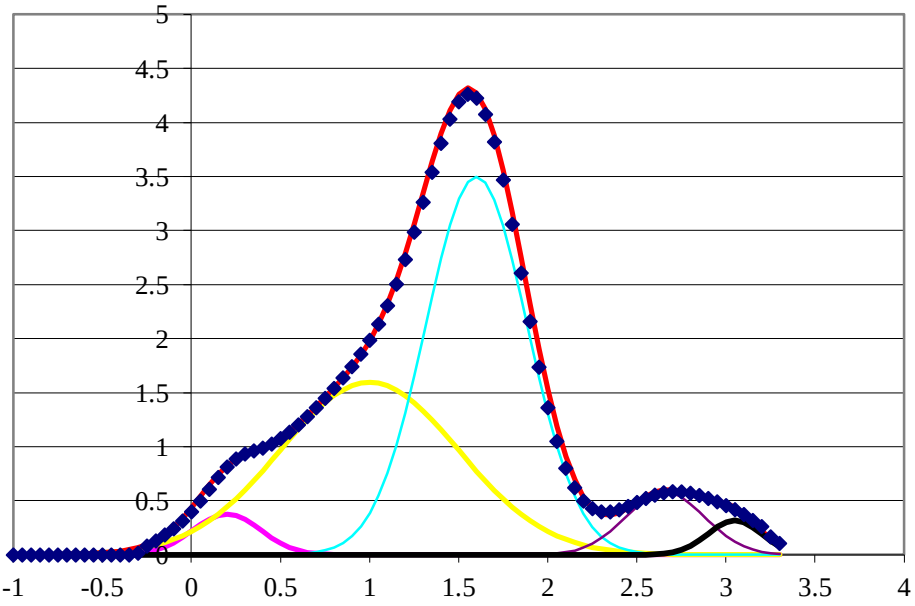
	Curve 1	Curve 2	Curve 3	Curve 4	Curve 5
T3 -125cm	3.292	39.913	46.898	7.975	1.921

Appendix Figure 2.6 STK MH1 T3 – 125cm



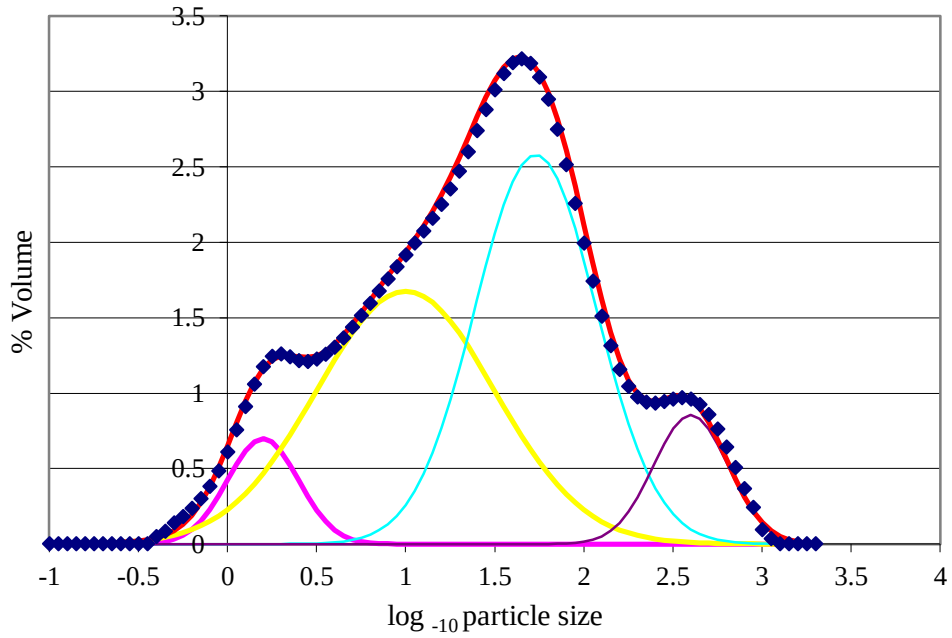
	Curve 1	Curve 2	Curve 3	Curve 4	Curve 5
T4 - 10cm	1.779	42.492	47.829	7.880	0.020

Appendix Figure 2.7 STK MH1 T4 – 10cm



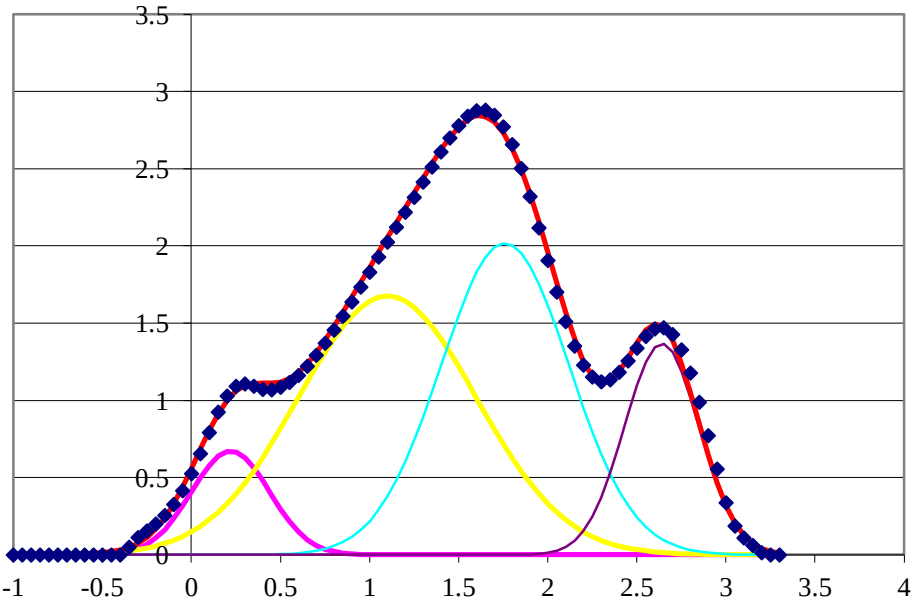
	Curve 1	Curve 2	Curve 3	Curve 4	Curve 5
T4 - 75cm	3.518	39.095	48.869	6.248	2.270

Appendix Figure 2.8 STK MH1 T4 – 75cm



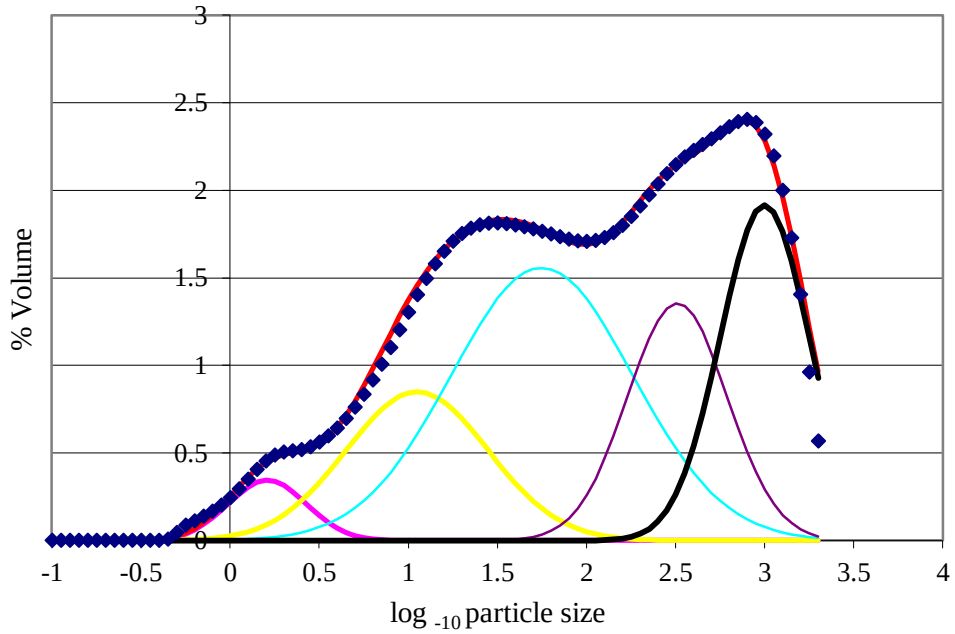
	Curve 1	Curve 2	Curve 3	Curve 4
S.T. - 10cm	6.862	41.178	43.138	8.821

Appendix Figure 2.9 STK EC1 Secondary Talus – 10cm



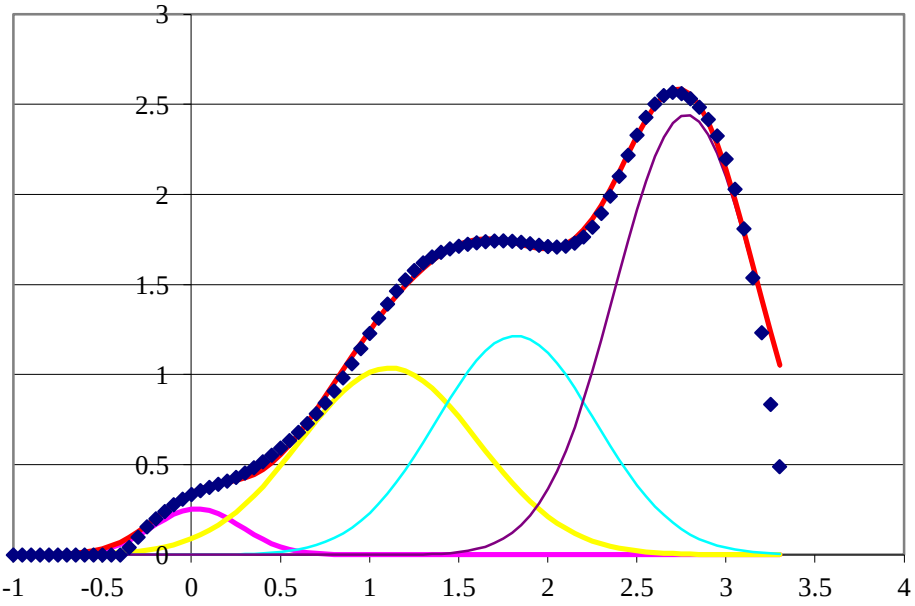
	Curve 1	Curve 2	Curve 3	Curve 4
S.T. - 30cm	7.385	41.920	36.330	14.365

Appendix Figure 2.10 STK EC1 Secondary Talus – 30cm



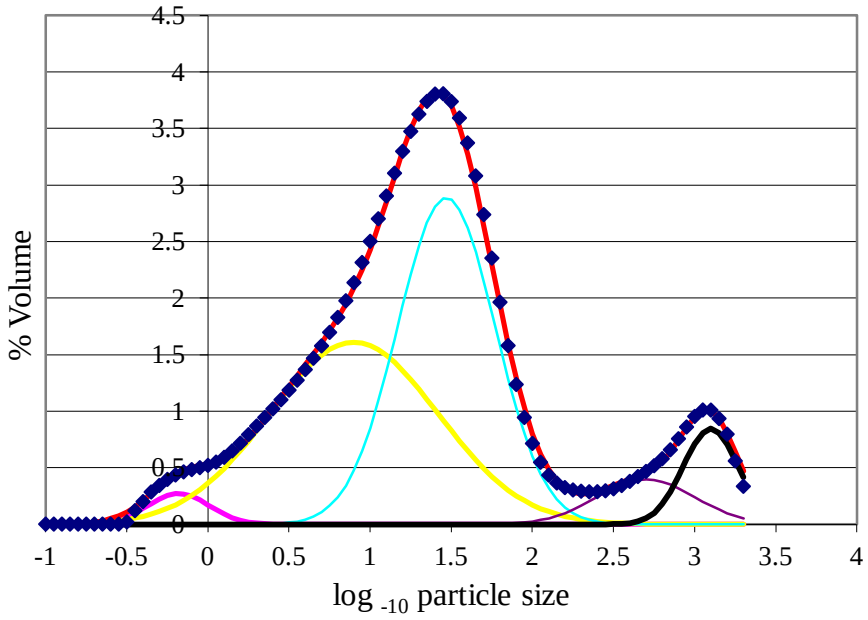
	Curve 1	Curve 2	Curve 3	Curve 4	Curve 5
P.T. - 10cm	3.754	16.794	39.278	18.736	21.439

Appendix Figure 2.11 STK EC1 Primary Talus – 10cm



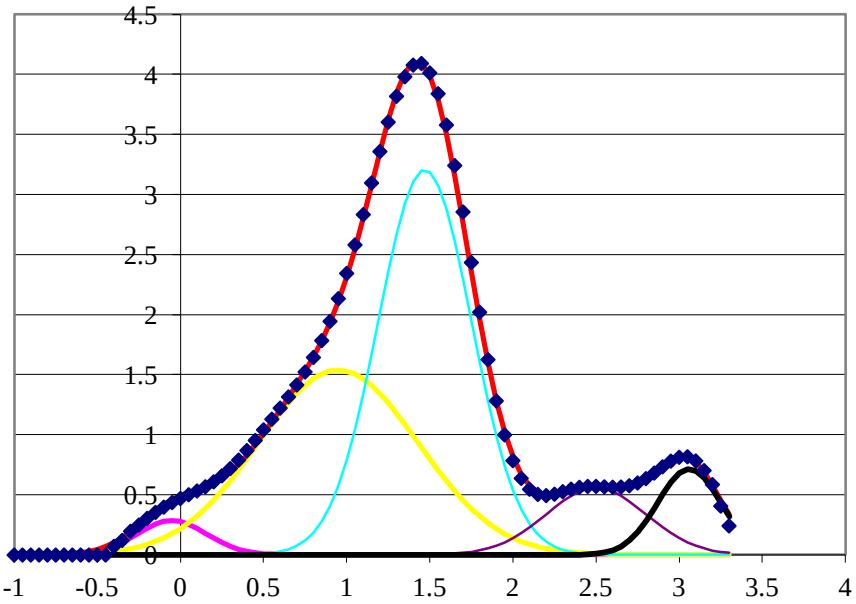
	Curve 1	Curve 2	Curve 3	Curve 4	Curve 5
P.T. - 30cm	3.156	25.642	27.012	44.170	0.020

Appendix Figure 2.12 STK EC1 Primary Talus – 30cm



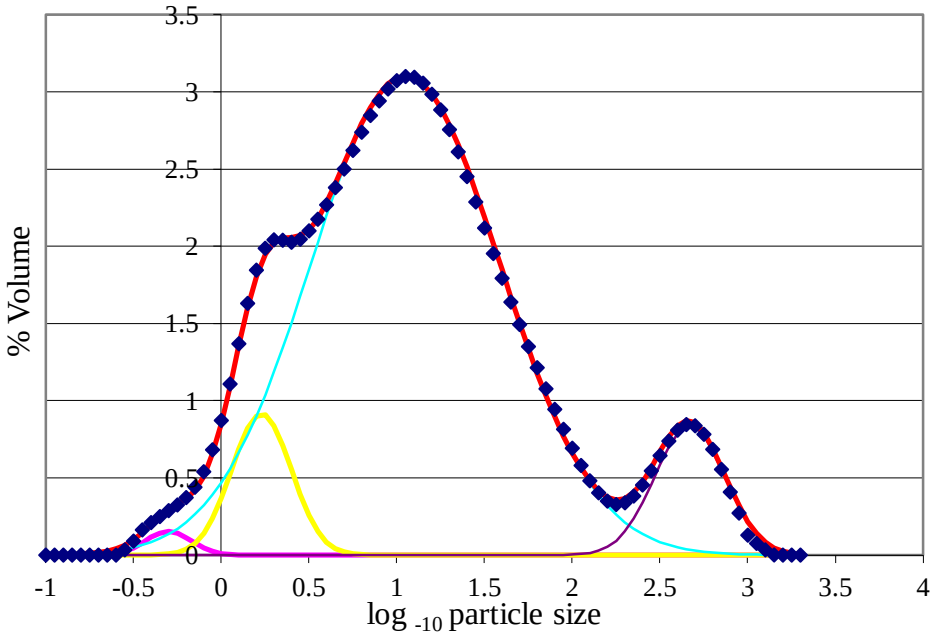
	Curve 1	Curve 2	Curve 3	Curve 4	Curve 5
Sample 1	2.589	41.818	43.212	5.864	6.516

Appendix Figure 2.13 STK MH2 Sample 1



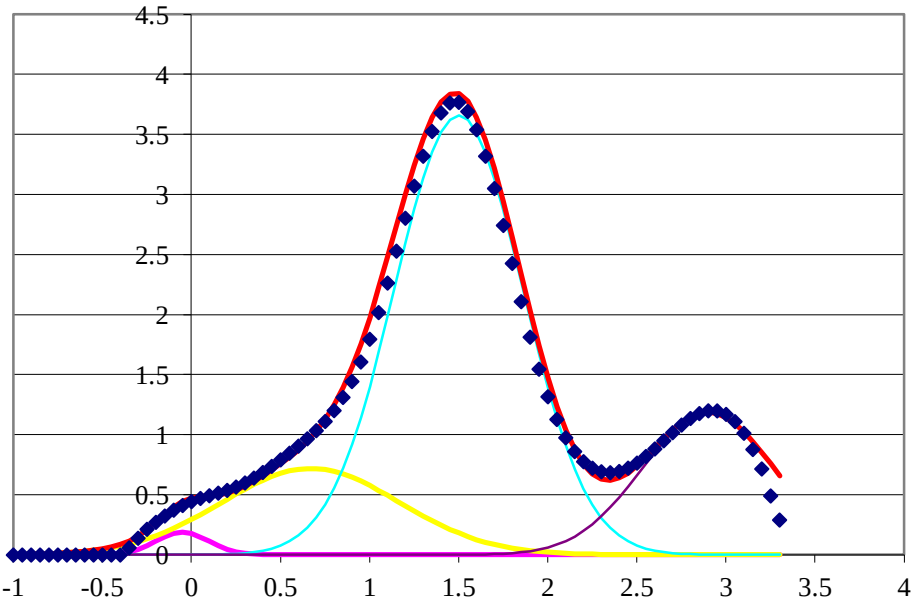
	Curve 1	Curve 2	Curve 3	Curve 4	Curve 5
Sample 2	3.011	37.137	45.167	8.406	6.278

Appendix Figure 2.14 STK MH2 Sample 2



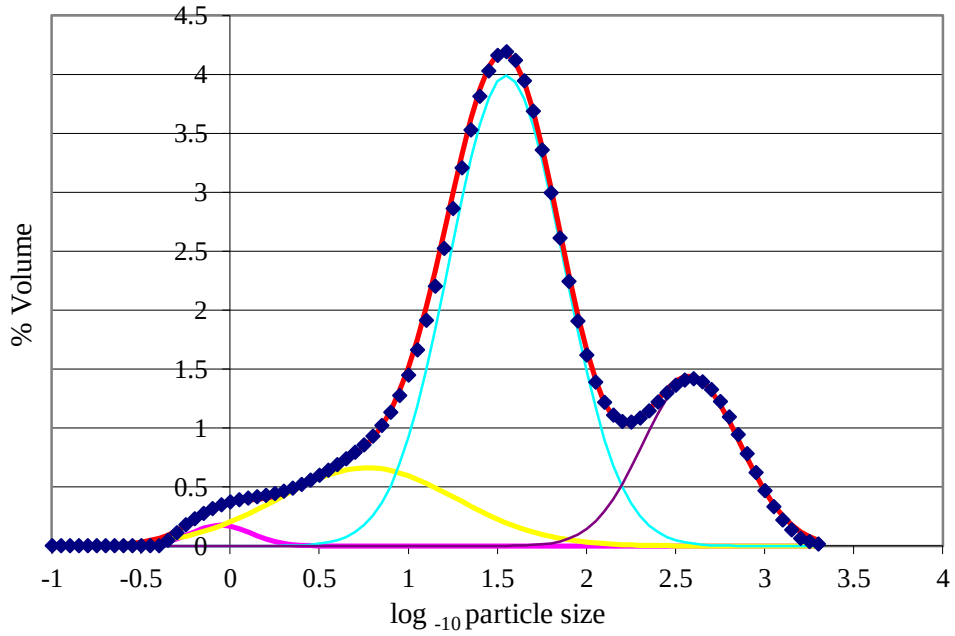
	Curve 1	Curve 2	Curve 3	Curve 4	Curve 5
Sample 3	0.989	7.706	82.991	8.295	0.020

Appendix Figure 2.15 STK MH2 Sample 3



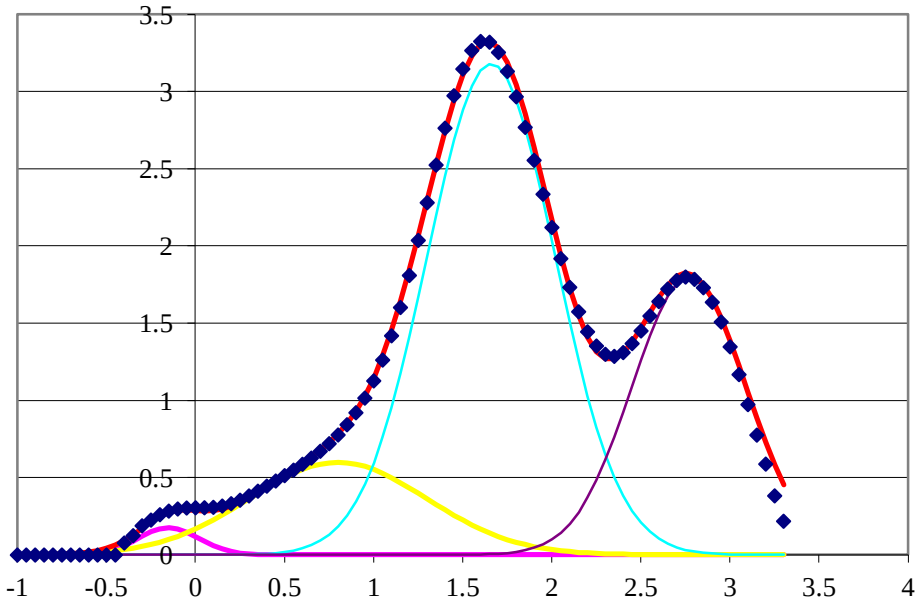
	Curve 1	Curve 2	Curve 3	Curve 4	Curve 5
Sample 4	1.337	17.196	63.050	18.398	0.020

Appendix Figure 2.16 STK MH2 Sample 4



	Curve 1	Curve 2	Curve 3	Curve 4	Curve 5
Sample 5	1.476	16.331	62.963	19.211	0.020

Appendix Figure 2.17 STK MH2 Sample 5



	Curve 1	Curve 2	Curve 3	Curve 4	Curve 5
Sample 6	1.478	14.773	56.529	27.201	0.020

Appendix Figure 2.18 STK MH2 Sample 6